



# University of HUDDERSFIELD

## University of Huddersfield Repository

Al-Tameemi, Wafaa

Studying the Mechanisms of Chemotherapy-Induced Alopecia and the Effect of Cooling using in Vitro Human Keratinocyte Models

### Original Citation

Al-Tameemi, Wafaa (2017) Studying the Mechanisms of Chemotherapy-Induced Alopecia and the Effect of Cooling using in Vitro Human Keratinocyte Models. Doctoral thesis, University of Huddersfield.

This version is available at <http://eprints.hud.ac.uk/id/eprint/32611/>

The University Repository is a digital collection of the research output of the University, available on Open Access. Copyright and Moral Rights for the items on this site are retained by the individual author and/or other copyright owners. Users may access full items free of charge; copies of full text items generally can be reproduced, displayed or performed and given to third parties in any format or medium for personal research or study, educational or not-for-profit purposes without prior permission or charge, provided:

- The authors, title and full bibliographic details is credited in any copy;
- A hyperlink and/or URL is included for the original metadata page; and
- The content is not changed in any way.

For more information, including our policy and submission procedure, please contact the Repository Team at: [E.mailbox@hud.ac.uk](mailto:E.mailbox@hud.ac.uk).

<http://eprints.hud.ac.uk/>



*University of*  
**HUDDERSFIELD**

**Studying the mechanisms of  
chemotherapy-induced alopecia and the effect  
of cooling using in vitro human keratinocyte  
models**

**Wafaa Al-Tameemi**

**A thesis submitted in partial fulfilment of the  
requirements for the degree of Doctor of Philosophy**

**The University of Huddersfield  
School of Applied Sciences**

**March 2017**

## Abstract

Chemotherapy-induced alopecia (CIA) is widely regarded as the most traumatic side effect associated with cancer treatment and the associated stress can be detrimental to overall outcomes. Yet there has been little research into its pathobiology and no pharmaceutical intervention is available. CIA is caused by chemotherapy-mediated damage of the rapidly dividing cells of the hair follicle and although it is normally reversible, on regrowth the hair is often different in colour and/or texture and only grows gradually. The only effective treatment for CIA currently available is scalp cooling. It has been hypothesised that scalp cooling works by a combination of vasoconstriction, a reduction in the metabolic rate and/or reduced drug uptake by cells in the hair bulb.

The ability of cooling to protect from CIA has been clinically demonstrated for years yet, to date, no cell biology is available to support its cytoprotective effects. The overall aim of this work was to for the first time provide a systematic investigation of the effects of cooling on chemotherapy-induced toxicity in human cells. The work established cellular models to determine the efficacy of cooling in rescuing from toxicity, investigate the temperature conditions providing maximal rescue and understand not only the mechanisms responsible for drug-mediated cytotoxicity, but also the way in which cooling regulates such mechanisms. Various human keratinocyte models were established, including normal (epidermal, NHEK, and follicular, HHFK) cells and adapted HaCaT (HaCaTa) cells. Viability, cell cycle and apoptosis assays were used, alongside Reactive Oxygen Species (ROS) detection, mitochondrial integrity assays and Western blotting, as well as functional pharmacological inhibition experiments. A panel of chemotherapy drugs commonly used in the clinic were employed, including doxorubicin, docetaxel and active metabolite of cyclophosphamide, 4-hydroxy-cyclophosphamide (4-OH-CP) and 5-FU, whilst a series of temperature conditions were tested, including 22°C as well as more severe cooling, particularly 18°C and 14°C (and even extreme cooling at 10°C).

This study showed that cooling dramatically reduces or completely prevents the cytotoxic effects of docetaxel (T), doxorubicin (A), 5-FU (F) and particularly 4-OH-CP (C); however, optimal rescue was observed in conjunction with mono-therapy treatments (and substantial rescue with dual therapies, e.g. AC), whereas combinatorial treatment (TAC) showed relatively poor response to cooling, in agreement with clinical observations. Importantly, the work demonstrated that lowering the temperature below the widely accepted 22°C threshold, even by a small number of degrees (e.g. 18°C), resulted in significantly improved or even complete cytoprotection, a striking observation strongly suggesting that the scalp temperature achieved clinically is of critical importance in dictating the success of head cooling in CIA prevention.

The panel of chemotherapy drugs tested caused differential effects on keratinocyte cell cycle progression and drug-mediated cell cycle arrest was significantly attenuated by cooling. Notably, cooling alone appeared to decelerate cell cycle progression, providing evidence for metabolic effects. More importantly, protective pre-conditioning (PPC) achieved either by growth factor removal or pharmacological inhibition of EGFR activation enhanced the cytoprotective effects of cooling and significantly reduced the effects of the chemotherapy drugs. As the ability of PPC to enhance protection from drug cytotoxicity could be attributed to its propensity to regulate the cell cycle progression, the work provided evidence that one mechanism *via* which cooling cytoprotects might be due to its ability to decelerate cell cycle progression.

Disruption of mitochondrial membrane potential and elevation of ROS indicated the activation of an apoptotic pathway, which was confirmed by cell death-specific assays that confirmed a mitochondrial apoptotic pathway, as evident by plasma membrane disruption, caspase activation and DNA fragmentation. Importantly, cooling at a variety of temperatures (but mainly at or below 18°C) attenuated drug-mediated apoptosis. To further investigate the precise mechanisms of growth arrest and/or cytotoxicity, activation/regulation of critical intracellular signalling mediators was investigated at the protein level. The majority of the drugs used induced activation of p53 and subsequent induction of p53-inducible mediators such as p21, as well as pro-apoptotic mediators associated with the mitochondrial pathway, such as Bak, PUMA and Noxa, whilst induction of pro-apoptotic FasL and Bid cleavage was detected, suggesting possible cross-talk with the extrinsic apoptotic pathway. Strikingly, cooling attenuated or blocked in a time- and, more importantly, temperature-dependent fashion induction of these pro-apoptotic mediators (an effect that became more marked as the temperature was reduced from 37°C, to 22°C, 18°C and 14°C); these results have provided for the first time a more detailed mechanistic explanation for the cytoprotective effects of cooling.

As ROS appeared to be important in cytotoxicity, the hypothesis raised was that the cytoprotective effect of cooling might be enhanced *via* co-treatment with an antioxidant (e.g. NAC), aimed at enhancing the cytoprotective capacity of cooling at sub-optimal temperatures (such as 26°C). The findings presented here suggested that cooling plus topical treatment with antioxidants might represent a promising approach to improve the cytoprotective effects without compromising the anticancer effects of chemotherapy.

Overall, despite their reductive nature, these *in vitro* models have provided experimental evidence for the ability of cooling to rescue from chemotherapy drug-mediated toxicity and shown that the choice of temperature may be critical in determining the efficacy of cooling in the clinic. This, whilst generating a novel combinatorial approach that has the potential to significantly enhance the ability of scalp cooling to protect against CIA in the clinic.

# Contents

<b>CHAPTER 1: INTRODUCTION .....</b>	<b>1</b>
1.1 An introduction to hair and the hair follicle (HF) .....	2
1.1.1 HF structure.....	2
1.1.2 HF morphogenesis .....	5
1.1.3 The hair growth cycle and its phases .....	8
1.2 Chemotherapy .....	14
1.2.1 Classification of chemotherapy drugs.....	15
1.2.2 Molecular targets of chemotherapeutic drugs.....	18
1.2.3 The mechanisms of apoptosis in HF in normal conditions and under pathological circumstances.....	20
1.2.4 Chemotherapy-induced HF apoptosis .....	24
1.3 Alopecia.....	25
1.3.1 Types of alopecia .....	25
1.4 Chemotherapy-induced alopecia (CIA).....	26
1.4.1 Pathophysiology of CIA .....	29
1.4.2 Experimental models of CIA .....	30
1.4.3 Treatment options for CIA.....	33
1.5 Thesis aims .....	41
<b>CHAPTER 2: MATERIALS AND METHODS.....</b>	<b>42</b>
2.1 General.....	43
2.1.1 Suppliers.....	43
2.1.2 Disposable plasticware .....	43
2.1.3 Stock solutions .....	43
2.1.4 Safe handling of cytotoxic (chemotherapy) drugs .....	43
2.2 Reagent.....	45
2.2.1 Primary antibodies.....	45
2.2.2 Secondary antibodies .....	46
2.2.3 Pharmacological agonists and antagonists.....	47
2.3 Tissue culture .....	48
2.3.1 General.....	48
2.4 Cell culture.....	48
2.4.1 Normal human epidermal keratinocytes (NHEK) and Human hair follicular keratinocytes (HHFK) .....	48
2.4.2 HaCaT cell line .....	49
2.4.3 HaCaT adaptation to serum-free medium (HaCaTa).....	49
2.4.4 Cell maintenance.....	49
2.4.5 Cryo-preservation and recovery of cell lines.....	50
2.5 Assessment of cell growth .....	50
2.6 Observation of cell viability by microscopy .....	51
2.7 Assessment of the role of temperature conditions on chemotherapy-mediated cytotoxicity .....	52
2.7.1 (A) NHEK cells challenged with the following three TAC regimes: .....	52
2.7.2 (B) HaCaTa cells challenged with the following three TAC regimes:.....	52
2.7.3 (C) HaCaTa cells challenged with the following three ACT regimes:.....	53
2.7.4 (D) HaCaTa cells challenged with the following three FAC regimes:.....	53
2.8 Functional inhibition experiments .....	53
2.9 Supplement starvation.....	53
2.10 Detection of cell growth, death (apoptosis) and reactive oxygen species (ROS) production .....	54
2.10.1 General.....	54
2.10.2 Detection of cell death using the CytoTox-Glo™ assay.....	54
2.10.3 Detection of apoptosis using caspase-3/7 assays .....	55
2.10.4 Detection of apoptosis using the DNA fragmentation ELISA .....	56
2.11 SDS-PAGE and Immunoblotting (Western Blotting) .....	58
2.11.1 General.....	58
2.11.2 Protein extraction.....	58
2.11.3 Protein Quantification .....	58
2.11.4 SDS-Polyacrylamide gel Electrophoresis (SDS-PAGE) .....	59

2.11.5	Electrophoretic membrane transfer .....	60
2.11.6	Membrane immunolabelling and visualisation using the Li-Cor Odyssey system.....	61
2.11.7	Membrane stripping and re-probing.....	61
2.11.8	Detection of Reactive oxygen species using H <sub>2</sub> DCFDA .....	61
2.12	Flow Cytometry.....	63
2.12.1	Background .....	63
2.12.2	Detection of the mitochondrial membrane potential.....	63
2.12.3	Detection of oxidative stress.....	65
2.12.4	Cell cycle analysis by propidium iodide (PI) labelling .....	65
2.13	Statistical analysis .....	66

**CHAPTER 3: EFFECT OF CANCER CHEMOTHERAPY DRUGS ON THE VIABILITY OF HUMAN**

**KERATINOCYTE CELL LINES AND THE EFFECT OF COOLING ON DRUG-MEDIATED CYTOTOXICITY ..... 67**

3.1	Background .....	68
3.2	Chapter Aims.....	70
3.3	The effect of chemotherapy drugs on normal human epidermal keratinocyte viability and the role of cooling on drug-mediated cytotoxicity.....	71
3.4	The cytotoxicity of chemotherapy drugs on human hair follicular keratinocytes and the effect of cooling on drug-mediated effects .....	73
3.5	The effect of the combinatorial chemotherapy treatment TAC on normal human keratinocyte growth and the role of cooling .....	75
3.6	Chemotherapy drug-mediated effects on HaCaT keratinocyte viability and the role of cooling .....	77
3.7	Adaptation of HaCaT keratinocytes to low-calcium, serum-free culture conditions and investigation of the role of cooling in chemotherapy drug-induced effects in the adapted cells .....	82
3.8	The effect of the combinatorial TAC chemotherapy treatment on HaCaTa cell viability and the role of cooling .....	88
3.9	Investigations into the differences in keratinocyte cytotoxicity caused between TAC <i>versus</i> ACT combinatorial regimes .....	90
3.10	Effects of dual drug chemotherapy exposure and the impact of cooling in combinatorial drug-induced cytotoxicity .....	94
3.11	The importance of temperature (cooling conditions) in determining the efficacy of cooling in protecting from chemotherapy drug-mediated cytotoxicity.....	95
3.12	Summary .....	99
3.13	Discussion .....	100
3.13.1	Development of <i>in vitro</i> models to study chemotherapy drug-induced cytotoxicity and assess the effect of cooling .....	102
3.13.2	The effects of cooling on drug-mediated cytotoxicity .....	102
3.13.3	The effects of cooling on combinatorial therapy .....	103

**CHAPTER 4: THE EFFECTS OF CHEMOTHERAPY DRUGS AND COOLING ALONE OR IN**

**COMBINATION ON THE HUMAN KERATINOCYTE CELL CYCLE ..... 108**

4.1	Background .....	109
4.1.1	Effects of chemotherapeutic agents on the cell cycle .....	109
4.1.2	Effects of hypothermic conditions on the cell cycle.....	110
4.2	Cell cycle analysis .....	111
4.3	Effects of the epidermal growth factor receptor pathway (EGFR) inhibitor in chemotherapy induced cytotoxicity .....	111
4.4	Chapter Aims.....	112
4.5	Cell cycle analysis in HaCaTa cells using flow cytometry .....	113
4.5.1	Flow cytometric analysis of human keratinocytes following treatment with chemotherapy drugs.....	115
4.5.2	The impact of reducing temperature on untreated cultured cells .....	119
4.5.3	The effects of cooling in the prevention of the changes in the cell cycle induced by chemotherapy drugs.....	121
4.6	Short-term starvation protects HaCaTa cells against chemotherapy drugs .....	148
4.7	Cytoprotective role of the PD153035 against chemotherapy drug-mediated toxicity in HaCaTa cells.....	150
4.7.1	Cell cycle analysis after growth inhibition .....	158

4.8	Summary .....	161
4.9	Discussion .....	164
4.9.1	Role of cooling on the effect of chemotherapy drugs on cell cycle progression and cytotoxicity .....	164
4.9.2	Effects of low temperature (cooling) on cell cycle distribution in human keratinocytes .....	166
4.9.3	Time and temperature dependence of cytotoxic agent-induced cell cycle arrest and apoptosis under cooling conditions .....	167

**CHAPTER 5: THE EFFECT OF COOLING ON CHEMOTHERAPY DRUG-MEDIATED CELL DEATH INDUCTION, MITOCHONDRIAL MEMBRANE POTENTIAL DISRUPTION AND REACTIVE OXYGEN SPECIES GENERATION .....**

<b>SPECIES GENERATION .....</b>	<b>170</b>	
5.1	Background .....	171
5.1.1	Reactive oxygen species .....	171
5.1.2	Apoptosis mechanisms of HF under pathological conditions .....	172
5.1.3	Measurement of intracellular ROS and mitochondrial membrane integrity .....	173
5.1.4	Use of JC-1 dye for mitochondrial membrane potential detection .....	175
5.2	Apoptosis assays for the detection of cell death induced by chemotherapeutic agents on human keratinocytes .....	176
5.3	Chapter Aims .....	177
5.4	Optimisation of the JC-1 assay for the detection of changes in mitochondrial membrane potential ( $\Delta\Psi_m$ ) .....	178
5.5	Cytoprotective role of cooling against chemotherapy drug-induced $\Delta\Psi_m$ disruption in HaCaTa cells .....	183
5.5.1	Effects of 4-OH-CP on $\Delta\Psi_m$ and role of cooling .....	183
5.5.2	Effects of docetaxel on $\Delta\Psi_m$ and role of cooling .....	186
5.5.3	Effects of doxorubicin on $\Delta\Psi_m$ and role of cooling .....	189
5.6	Cytoprotective role of cooling against chemotherapy drug-induced $\Delta\Psi_m$ disruption in NHEK cells .....	192
5.7	Cytoprotective role of cooling against chemotherapy drug-induced $\Delta\Psi_m$ disruption in HHFK cells .....	195
5.8	Optimization of the H2DCFDA assay for the detection of intracellular Reactive Oxygen Species .....	198
5.9	Effect of cooling on chemotherapy drug-induced ROS .....	207
5.9.1	Influence of temperature on ROS production induced by doxorubicin in HaCaTa cells .....	207
5.9.2	Influence of temperature on ROS production by 4-OH-CP in HaCaTa cells .....	209
5.9.3	ROS production mediated by docetaxel and effects of cooling .....	211
5.10	Detection of chemotherapy drug mediated HaCaTa cell death using the CytoTox-Glo assay and assessment of the effect of cooling .....	212
5.11	Detection of chemotherapy drug-induced activation of caspases-3/7 using the SensoLyte assay and assessment of the effect of cooling .....	217
5.12	Detection of DNA fragmentation after HaCaTa cell exposure to chemotherapeutic drugs and assessment of the role of cooling .....	220
5.13	Summary .....	223
5.14	Discussion .....	225
5.14.1	Cytoprotective properties of cooling against chemotherapy drug-induced mitochondrial damage .....	225
5.14.2	Effects of cooling on chemotherapy drug-induced ROS generation in HaCaTa cells .....	227
5.14.3	Chemotherapy drug-induced apoptosis in HaCaTa cells is attenuated by cooling .....	228

**CHAPTER 6: INVESTIGATIONS ON THE EFFECTS OF COOLING ON THE ACTIVATION AND FUNCTIONAL INVOLVEMENT OF KEY INTRACELLULAR MEDIATORS IN CHEMOTHERAPY DRUG-MEDIATED APOPTOSIS IN HUMAN KERATINOCYTES .....**

<b>232</b>	<b>232</b>	
6.1	The selective induction of apoptosis as a therapeutic strategy .....	233
6.2	Control of DNA damage responses by p53: regulation of cell cycle and induction of apoptosis .....	233
6.3	Mechanisms of action of the Bcl-2 family members .....	234
6.4	Hypothesis and Specific Aims .....	235
6.5	Regulation of p53 activation in human keratinocytes after chemotherapy drug treatment at 37°C and the effect of cooling .....	237
6.6	The p53 inhibitor pifithrin- $\alpha$ (PFT- $\alpha$ ) .....	243

6.7	Regulation of p21 in response to chemotherapy drug treatment and the effects of cooling	249
6.8	Regulation of PUMA protein in response to chemotherapy drug treatment and the effects of cooling .....	255
6.9	Regulation of Noxa protein expression in response to chemotherapy drug treatment and the effects of cooling.....	260
6.10	Regulation of pro-apoptotic Bak protein in response to chemotherapy drug treatment and the effects of cooling.....	264
6.11	Changes in Bax protein expression following chemotherapy drug treatment and the effects of cooling .....	269
6.12	Regulation of Fas ligand (FasL) in response to chemotherapy drug treatment and the effects of cooling.....	273
6.13	Effect of functional blockade of FasL/Fas interaction on drug-mediated apoptosis in HaCaTa cells.....	277
6.14	Expression of TRAIL ligand in response to chemotherapy drug treatment and the effects of cooling .....	279
6.15	Changes in Bid protein in response to chemotherapy drugs treatment and the effects of cooling .....	281
6.16	Summary .....	285
6.17	Discussion .....	289
6.17.1	Cooling reduces p53 activation and subsequent p21 induction triggered by chemotherapy drug treatment .....	289
6.18	Cooling attenuates induction of p53-dependent pro-apoptotic BH3-only proteins PUMA and Noxa .....	291
6.18.1	Effects of cooling on the expression of pro-apoptotic proteins Bax and Bak .....	292
6.18.2	Investigation on possible cell death signalling cross-talk in apoptosis induction and the effects of cooling.....	293
 <b>CHAPTER 7: THE EFFECT OF ANTIOXIDANT-MEDIATED BLOCKADE OF ROS IN COOLING-INDUCED CYTOPROTECTION: COMBINATORIAL TREATMENT WITH N-ACETYL-CYSTEINE (NAC) AND COOLING PROTECTS AGAINST CHEMOTHERAPY DRUG CYTOTOXICITY .....</b>		<b>296</b>
7.1	Oxidative stress and cellular antioxidant mechanisms.....	297
7.2	N-acetyl-cysteine (NAC) and its antioxidant properties.....	297
7.3	Chapter Aims.....	299
7.4	Optimisation (titration) of NAC .....	300
7.5	Determining the efficacy of combination of cooling and NAC in protecting from chemotherapy drug-mediated cytotoxicity .....	303
7.6	Investigations on the ability of NAC to enhance protection from chemotherapy drug-mediated cytotoxicity under sub-optimal cooling conditions .....	307
7.7	Effect of combination of cooling and NAC treatment on AC and TAC-mediated cytotoxicity in HaCaTa cells .....	311
7.8	Summary .....	316
7.9	Discussion .....	318
7.9.1	The chemoprotective agent and antioxidant N-acetylcysteine (NAC) blocks chemotherapy drug-induced cell death and enhances the cytoprotective effect of cooling .....	318
 <b>CHAPTER 8: CONCLUDING REMARKS .....</b>		<b>321</b>
8.1	Future work.....	322

## Figures

Figure 1-1 The mature human HF .....	4
Figure 1-2 The morphogenesis of the HF .....	7
Figure 1-3 The hair cycle .....	11
Figure 1-4 Molecular control of apoptosis in the distinct HF compartments.....	13
Figure 1-5 Chemotherapy drugs and their point of action in the cell cycle.....	19
Figure 1-6 The main mechanisms of apoptotic cell death.....	23
Figure 2-1 The structure of MTS tetrazolium and its reaction product .....	51
Figure 2-2 The principle of the CytoTox-Glo™ assay .....	55
Figure 2-3 proteolytic cleavage of Ac-DEVD-AFC substrate.....	56
Figure 2-4 Principle of DNA fragmentation assay .....	57
Figure 2-5 Precision plus Protein standard.....	59
Figure 2-6 Single sandwich.....	60
Figure 2-7 Conversion of non-fluorescent dye DCFH-DA in the fluorescent dye DCF by ROS .....	62
Figure 2-8 Mechanism of action of the JC1 dye.....	64
Figure 2-9 Change in the cell cycle were determined by PI staining.....	66
Figure 3-1 Cytoprotective role of cooling against chemotherapy drug-mediated toxicity in NHEK cells .....	72
Figure 3-2 Cytoprotective role of cooling against chemotherapy drug-mediated toxicity in HHEK cells .....	74
Figure 3-3 Effect of cooling on TAC-mediated cytotoxicity in NHEK cells.....	76
Figure 3-4 Cytoprotective role of cooling against chemotherapy drug-mediated toxicity in HaCaT cells .....	78
Figure 3-5 Microscopic observation of cooling-mediated cytoprotection of HaCaT cells from chemotherapy drug-mediated toxicity.....	81
Figure 3-6 Establishment of the HaCaTa cell line and assessment of its phenotypic and growth characteristics.....	84
Figure 3-7 Cytoprotective role of cooling against chemotherapy drug-mediated toxicity in HaCaTa cells .....	85
Figure 3-8 Microscopic observation of cooling-mediated cytoprotection of HaCaT cells from chemotherapy drug-mediated toxicity.....	86
Figure 3-9 Cytoprotective role of cooling against Fluorouracil (5FU)-mediated toxicity in HaCaTa cells .....	87
Figure 3-10 Effect of cooling on TAC-mediated cytotoxicity in HaCaTa cells .....	89
Figure 3-11 Effect of cooling on ACT and TAC-mediated cytotoxicity in HaCaTa cells .....	91
Figure 3-12 Effect of cooling on modified ACT-mediated cytotoxicity in HaCaTa cells.....	92
Figure 3-13 The ability of cooling to protect from combined therapy FAC (5FU, doxorubicin and cyclophosphamide)-mediated cytotoxicity in HaCaTa cells .....	93
Figure 3-14 Effect of cooling on dual drug-mediated cytotoxicity in HaCaTa cells.....	94
Figure 3-15 The role of temperature on the efficacy of cooling in protecting from chemotherapy drug-mediated cytotoxicity .....	96
Figure 3-16 The role of cooling in protecting from 5-fluorouracil (5-FU)-mediated cytotoxicity .....	97
Figure 3-17 The role of 'severe cooling' conditions on the ability of cooling to protect from chemotherapy drug-mediated cytotoxicity .....	98
Figure 3-18 Proposed mechanisms of action of scalp cooling.....	101
Figure 4-1 Representative cell cycle analysis of unsynchronised proliferating HaCaTa cells in culture.....	114
Figure 4-2 Cell cycle analysis of HaCaTa cells after 36h chemotherapeutic drug treatment .....	117
Figure 4-3 Summary of independent replicate experiments for cell cycle analysis of HaCaTa cells after 36h chemotherapeutic drug treatment.....	118
Figure 4-4 Effects of cooling at 22°C vs physiological temperature on HaCaTa cell cycle distribution .....	120
Figure 4-5 Cell cycle analysis of HaCaTa cells after 0h chemotherapeutic drug treatment at 22°C and 37°C.....	125
Figure 4-6 Cell cycle analysis of HaCaTa cells after 1h chemotherapeutic drug treatment at 22°C and 37°C.....	127
Figure 4-7 Cell cycle analysis of HaCaTa cells after 2h chemotherapeutic drug treatment at 22°C and 37°C.....	129

Figure 4-8 Summary of independent replicate experiments for cell cycle analysis of HaCaTa cells after 2h chemotherapeutic drug treatment.....	130
Figure 4-9 Cell cycle analysis of HaCaTa cells after 4h chemotherapeutic drug treatment at 22°C and 37°C.....	131
Figure 4-10 Summary of independent replicate experiments for cell cycle analysis of HaCaTa cells after 4h chemotherapeutic drug treatment.....	132
Figure 4-11 Cell cycle analysis of HaCaTa cells after 8h chemotherapeutic drug treatment at 22°C and 37°C.....	133
Figure 4-12 Summary of independent replicate experiments for cell cycle analysis of HaCaTa cells after 8h chemotherapeutic drug treatment.....	134
Figure 4-13 Cell cycle analysis of HaCaTa cells after 24h chemotherapeutic drug treatment at 22°C and 37°C.....	135
Figure 4-14 Summary of independent replicate experiments for cell cycle analysis of HaCaTa cells after 24h chemotherapeutic drug treatment.....	136
Figure 4-15 Cell cycle analysis of HaCaTa cells after 2h chemotherapeutic drug treatment at 22°C and 37°C.....	142
Figure 4-16 Summary of independent replicate experiments for cell cycle analysis of HaCaTa cells after 2h chemotherapeutic drug treatment at 18°C.....	143
Figure 4-17 Cell cycle analysis of HaCaTa cells after 36h chemotherapeutic drug treatment at 18°C and 37°C.....	144
Figure 4-18 Summary of independent replicate experiments for cell cycle analysis of HaCaTa cells after 36h chemotherapeutic drug treatment at 18°C.....	145
Figure 4-19 Cytoprotective role of cooling and short-term starvation protects against chemotherapy drug-mediated toxicity in HaCaTa cells.....	149
Figure 4-20 Viability of HaCaTa cells after incubation with the tyrosine kinase inhibitor PD 153035	152
Figure 4-21 Cytoprotective role of 2h pre-treatment by PD153035 against chemotherapy drug-mediated toxicity in HaCaTa cells.....	153
Figure 4-22 Cytoprotective role of 24h pre-treatment by PD153035 against chemotherapy drug-mediated toxicity in HaCaTa cells.....	154
Figure 4-23 Cytoprotective role of cooling + PD153035 against doxorubicin-mediated toxicity in HaCaTa cells.....	155
Figure 4-24 Cytoprotective role of cooling + PD153035 against 4-OH-CP-mediated toxicity in HaCaTa cells.....	156
Figure 4-25 Cytoprotective role of cooling + PD153035 against docetaxel-mediated toxicity in HaCaTa cells.....	157
Figure 4-26 Effects of EGFR signalling pathway inhibition by PD153035 vs removal of growth factors (starvation) on HaCaTa cell cycle distribution.....	159
Figure 5-1 The principle of ROS detection using H2DCFDA .....	174
Figure 5-2 The principle of the fluorescent JC-1 dye .....	175
Figure 5-3 Optimisation of JC-1 dye assay at 37°C.....	179
Figure 5-4 Summary of optimisation of JC-1 concentration at 37°C .....	180
Figure 5-5 Preliminary experiments on detection of chemotherapy drug-induced $\Delta\Psi_m$ loss using JC-1 and the effect of cooling in HaCaTa cells.....	181
Figure 5-6 Summary of replicate preliminary experiments on detection of chemotherapy drug-induced $\Delta\Psi_m$ loss using JC-1 and the effect of cooling .....	182
Figure 5-7 Cooling inhibits 4-OH-CP- induced $\Delta\Psi_m$ loss in HaCaTa cells.....	184
Figure 5-8 Summary of independent replicate experiments on the role of cooling in 4-OH-CP-mediated disruption of $\Delta\Psi_m$ in HaCaTa cells.....	185
Figure 5-9 Cooling inhibits docetaxel induced $\Delta\Psi_m$ loss in HaCaTa cells .....	187
Figure 5-10 Summary of independent replicates experiments the role of cooling in inhibits docetaxel disruption of the $\Delta\Psi_m$ in HaCaTa cells .....	188
Figure 5-11 Cooling inhibits doxorubicin induced $\Delta\Psi_m$ loss in HaCaTa cells .....	190
Figure 5-12 Summary of independent replicates experiments the role of cooling in inhibits doxorubicin disruption of the $\Delta\Psi_m$ in HaCaTa cells .....	191
Figure 5-13 Cooling inhibits chemotherapy drugs-induced $\Delta\Psi_m$ loss in NHEK cells .....	193
Figure 5-14 Summary of independent replicates experiments the role of cooling in inhibits chemotherapy drugs disruption of the $\Delta\Psi_m$ in NHEK cells .....	194
Figure 5-15 Cooling inhibits chemotherapy drugs-induced $\Delta\Psi_m$ loss in HHFK cells.....	196
Figure 5-16 Summary of independent replicates experiments the role of cooling in inhibits chemotherapy drugs, disruption of the $\Delta\Psi_m$ in HHFK cells.....	197

Figure 5-17 Microtiter plate-based spectrophotometric detection of ROS levels after H2DCFDA staining in HaCaTa cells treated with doxorubicin .....	199
Figure 5-18 Time-dependent ROS production measured by flow cytometry analysis using H2DCFDA after treatment with doxorubicin in HaCaTa cells.....	200
Figure 5-19 ROS levels measured by flow cytometry analysis after drug treatment with and without H2DCFDA reagent in HaCaTa cells.....	201
Figure 5-20 ROS induction determined using 2.5 and 5 $\mu$ M [H2DCFDA] in HaCaTa Cells .....	202
Figure 5-21 Time-dependent reactive oxygen species (ROS) production measured by flow cytometry analysis after treatment with 4-OH-CP and 5 and 10 $\mu$ M [H2DCFDA] in HaCaTa cells .....	203
Figure 5-22 Time-dependent reactive oxygen species (ROS) production measured by flow cytometry analysis after treatment with 4-OH-CP and 5 $\mu$ M [H2DCFDA] in HaCaTa cells.	204
Figure 5-23 Time-dependent reactive oxygen species (ROS) production measured by flow cytometry analysis after treatment with docetaxel and 5 $\mu$ M [H2DCFDA] in HaCaTa cells	205
Figure 5-24 Time-dependent reactive oxygen species (ROS) production measured by flow cytometry analysis after treatment with docetaxel and 5 $\mu$ M [H2DCFDA] in HaCaTa cells	206
Figure 5-25 Temperature-dependent reactive oxygen species (ROS) production after treatment with doxorubicin in HaCaTa cells.....	208
Figure 5-26 Temperature-dependent reactive oxygen species (ROS) production after treatment with 4-OH-CP in HaCaTa cells .....	210
Figure 5-27 Temperature-dependent reactive oxygen species (ROS) production after treatment with docetaxel in HaCaTa cells.....	211
Figure 5-28 Detection of the cytoprotective role of cooling against chemotherapy drug-mediated cell death in HaCaTa cells after 24h using CytoTox-Glo .....	214
Figure 5-29 Detection of the cytoprotective role of cooling against chemotherapy drug-mediated cell death in HaCaTa cells after 48h using CytoTox-Glo .....	215
Figure 5-30 Detection of cytoprotective role of cooling against 5-fluorouracil (5-FU)-mediated toxicity in HaCaTa cells after 48h using CytoTox-Glo.....	216
Figure 5-31 The role of cooling in caspase-3/7 activation induced by chemotherapy drugs in HaCaTa cells after 24h using the SensoLyte assay .....	218
Figure 5-32 The role of cooling in caspase-3/7 activation induced by chemotherapy drugs in HaCaTa cells after 48h using the SensoLyte assay .....	219
Figure 5-33 The effect of cooling on DNA fragmentation induced by chemotherapy drugs in HaCaTa cells after 24h using the DNA fragmentation assay.....	221
Figure 5-34 The role of cooling in the inhibition of DNA fragmentation induced by chemotherapy drug in HaCaTa cells after 48h using the DNA fragmentation assay.....	222
Figure 6-1 The role of temperature on the regulation of P-p53 expression in response to 4-OH-CP in HaCaTa cells .....	239
Figure 6-2 The role of temperature on the regulation of P-p53 expression in response to 4-OH-CP in primary keratinocytes.....	240
Figure 6-3 The role of temperature on the regulation of P-p53 expression in response to doxorubicin in HaCaTa cells.....	241
Figure 6-4 The role of temperature on the regulation of P-p53 expression in response to docetaxel in HaCaTa cells.....	242
Figure 6-5 Viability of HaCaTa cells after incubation with Pifithrin- $\alpha$ (PFT- $\alpha$ ) .....	244
Figure 6-6 Protection against 4-OH-CP drug cytotoxicity by lower concentrations of PFT- $\alpha$ in HaCaTa .....	245
Figure 6-7 : Protection against 4-OH-CP drug cytotoxicity by PFT- $\alpha$ in HaCaTa cells.....	246
Figure 6-8 Protection against doxorubicin drug cytotoxicity by PFT- $\alpha$ in HaCaTa cells.....	247
Figure 6-9 Protection against doxorubicin drug cytotoxicity by lower concentrations of PFT- $\alpha$ in HaCaTa cells .....	248
Figure 6-10 The role of temperature on the regulation of p21 expression in response to 4-OH-CP in HaCaTa cells .....	251
Figure 6-11 The role of temperature on the regulation of p21 expression in response to 4-OH-CP in primary keratinocytes.....	252
Figure 6-12 The role of temperature on the regulation of p21 expression in response to doxorubicin in HaCaTa cells .....	253
Figure 6-13 The role of temperature on the regulation of p21 expression in response to docetaxel in HaCaTa cells .....	254

Figure 6-14 The role of temperature on the regulation of PUMA expression in response to 4-OH-CP in HaCaTa cells .....	256
Figure 6-15 The role of temperature on the regulation of PUMA expression in response to 4-OH-CP in NHEK cells.....	257
Figure 6-16 The role of temperature on the regulation of PUMA expression in response to doxorubicin in HaCaTa cells.....	258
Figure 6-17 The role of temperature on the regulation of PUMA expression in response to docetaxel in HaCaTa cells.....	259
Figure 6-18 The role of temperature on the regulation of Noxa expression in response to 4-OH-CP in HaCaTa cells .....	261
Figure 6-19 The role of temperature on the regulation of Noxa expression in response to doxorubicin in HaCaTa cells.....	262
Figure 6-20 The role of temperature on the regulation of Noxa expression in response to docetaxel in HaCaTa cells.....	263
Figure 6-21 The role of temperature on the regulation of Bak expression in response to 4-OH-CP in HaCaTa cells .....	265
Figure 6-22 The role of temperature on the regulation of Bak expression in response to 4-OH-CP in primary keratinocytes.....	266
Figure 6-23 The role of temperature on the regulation of Bak expression in response to doxorubicin in HaCaTa cells.....	267
Figure 6-24 The role of temperature on the regulation of Bak expression in response to docetaxel in HaCaTa cells .....	268
Figure 6-25 The role of temperature on the regulation of Bax expression in response to 4-OH-CP in HaCaTa cells .....	270
Figure 6-26 The role of temperature on the regulation of Bax expression in response to doxorubicin in HaCaTa cells.....	271
Figure 6-27 The role of temperature on the regulation of Bax expression in response to docetaxel in HaCaTa cells .....	272
Figure 6-28 The role of temperature on the regulation of FasL expression in response to 4-OH-CP in HaCaTa cells .....	274
Figure 6-29 The role of temperature on the regulation of FasL expression in response to doxorubicin in HaCaTa cells.....	275
Figure 6-30 The role of temperature on the regulation of FasL expression in response to docetaxel in HaCaTa cells.....	276
Figure 6-31 Effect of the blocking anti-FasL antibody NOK1 on drug-mediated apoptosis.....	278
Figure 6-32 The role of temperature on the regulation of TRAIL expression in response to chemotherapy drugs in HaCaTa cells.....	280
Figure 6-33 The role of cooling on Bid cleavage (tBid formation) in response to 4-OH-CP in HaCaTa cells.....	282
Figure 6-34 The role of cooling on Bid cleavage (tBid formation) in response to doxorubicin in HaCaTa cells.....	283
Figure 6-35 The role of cooling on Bid cleavage (tBid formation) in response to docetaxel in HaCaTa cells.....	284
Figure 7-1 Titration of NAC on HaCaTa cells.....	301
Figure 7-2 Protection against chemotherapy drug cytotoxicity by NAC .....	302
Figure 7-3 Cytoprotective role of combination of cooling and NAC treatment against chemotherapy drug-mediated toxicity in HaCaTa cells at 37°C and 22°C.....	304
Figure 7-4 Cytoprotective role of combination of cooling and NAC treatment against chemotherapy drug-mediated toxicity in HaCaTa cells at 37°C and 18°C.....	305
Figure 7-5 Cytoprotective role of combination of cooling and NAC treatment against high concentrations of 4-OH-CP at 37°C and 22°C.....	306
Figure 7-6 Cytoprotective role of combination of cooling and NAC against chemotherapy drug-mediated toxicity in HaCaTa cells at 37°C and 26°C.....	308
Figure 7-7 Cytoprotective role of combination of cooling and NAC against doxorubicin-mediated toxicity in HaCaTa cells at 37°C and 26°C .....	309
Figure 7-8 Cytoprotective role of combination of cooling and NAC against chemotherapy drug-mediated toxicity in HaCaTa cells at 37°C and 24°C.....	310
Figure 7-9 Effect of combination of cooling and NAC on AC-mediated cytotoxicity in HaCaTa cells at 37°C and 22°C.....	312

Figure 7-10 Effect of combination of cooling and NAC on AC-mediated cytotoxicity in HaCaTa cells at 37°C and 18°C .....	313
Figure 7-11 Effect of combination of cooling and NAC on AC-mediated cytotoxicity in HaCaTa cells at 37°C and 26°C .....	314
Figure 7-12 Effect of combination of cooling and NAC on TAC-mediated cytotoxicity in HaCaTa cells at 37°C and 26°C .....	315
Figure 8-1 Molecular mechanisms of cooling mediated cytoprotection against chemotherapy drug-mediated toxicity.....	321

## Tables

Table 1-1 List of anticancer compounds and their mechanism of action .....	17
Table 1-2 Cytotoxic agents known to induce alopecia .....	28
Table 1-3 : Post infusion cooling times (PICTs).....	40
Table 2-1 Primary antibodies.....	45
Table 2-2 Secondary antibodies.....	46
Table 2-3 Agonists & antagonists.....	47
Table 4-1 Cell cycle distribution of HaCaTa cells between control (untreated cells) and cells treated with doxorubicin.....	138
Table 4-2 Distribution of HaCaTa cells between cell cycle phases in control (untreated cells) and treated with docetaxel .....	139
Table 4-3 Distribution of HaCaTa cells between cell cycle phases in control (untreated cells) and treated with 4-OH-CP .....	140
Table 4-4 Distribution of HaCaTa cells between cell cycle phases in control (untreated cells) and treated at at 37°C and 18°C .....	147

## Abbreviations

°C.....	Grad Celcius
4-OH-CP.....	4-hydroxycyclophosphamide
µL.....	Micro litre
APAF1.....	Apoptotic protease activating factor 1
Bad .....	Bcl-XL/bcl-2 associated death promoter homolog
Bak .....	Bcl-2 homologous antagonist/killer
Bax .....	Bcl-2-associated X protein
Bcl-2 .....	B-cell lymphoma 2
Bcl-x .....	Bcl-2 homolog X protein from avian lymphocyte development
Bcl-xL .....	longer alternatively spliced form of Bcl-x
Bcl-xS .....	Shorter alternatively spliced form of Bcl-x
Bid .....	Bax-like BH3 protein
Bik .....	Bcl-2 interacting killer
Bim .....	Bcl-2 interacting mediator of cell death
BP.....	Bovine pituitary extract
BPE.....	Bovine pituitary extract
BrdU .....	5-bromo-2'-deoxyuridine
CAD.....	Caspase activated DNase
CARD.....	Caspase activation and recruitment domain
Caspase.....	Cysteiny aspartic acid-protease
Cat#.....	Catalogue number
CCCP.....	Carbonyl cyanide m-chlorophenyl hydrazone
CIA.....	Chemotherapy-induced alopecia
CO <sub>2</sub> .....	Carbone dioxide
Con.....	Control
Cyto-c.....	Cytochrome c
DD.....	Death domain
DISC.....	Death inducing signalling complex
DMEM.....	Dulbecco's modified Eagle's medium
DMSO.....	Dimethyl Sulphoxide
DNA.....	Deoxyribonucleic acid
DNase.....	Deoxyribonuclease
Doce.....	Docetaxel
Doxo.....	Doxorubicin
EDTA.....	Ethylineamide
EGFR.....	Epidermal growth factor receptor
ELISA.....	Enzyme-linked immunosorbent assay
ER.....	Endoplasmic reticulum
FADD.....	Fas-associated death domain
FasL.....	Fas Ligand
FBS.....	Foetal Bovine Serum
GSH.....	Glutathione
H <sub>2</sub> DCFDA.....	6-carboxy-2,7 dichloro dihydrofluorescein diacetate
H <sub>2</sub> SO <sub>4</sub> .....	Sulphuric acid
HF.....	Hair follicle
HHFK.....	Human Hair Follicular Keratinocytes
JC-1.....	5,5',6,6'-Tetrachloro-1,1',3,3'-Tetramethyl-enzimidazolyl carbocyanine Iodide
kDa.....	kilo Dalton
KSFM.....	KSFM medium with complete supplements
LG.....	L-glutamine
min.....	Minutes
MOMP.....	Mitochondrial outer membrane permeabilization
NAC.....	N-acetyl cysteine
NF-κB.....	NF-κB (nuclear factor kappa-light-chain-enhancer of activated B cells)
NHEK.....	Normal Human Epidermal Keratinocytes
Noxa.....	BH3-only member of the Bcl-2 family
OMM.....	Outer mitochondrial membrane
PBS.....	Phosphate buffer saline

PFT- $\alpha$ .....	Pifithrin $\alpha$
PI.....	Propidium iodide
PPC.....	protective pre-conditioning
PUMA.....	P53-Up-regulated Modulator of Apoptosis
PVDF.....	Poly Vinylidene difluoride membrane
Redox.....	Reduction-oxidation
RFU.....	Relative Fluorescence Units
RLU.....	Relative luminescence Unit
ROS.....	Reactive Oxygen Species
SDS-AGE.....	Sodium dodecyl sulfate polyacrylamide gel electrophoresis
supps.....	Supplements
T.....	Time post treatment
TRAIL.....	TNF-related apoptosis inducing ligand
UV.....	Ultra violet
$\Delta\Psi_m$ .....	mitochondrial membrane potent
$\mu\text{g}$ .....	Micro gram
$\mu\text{M}$ .....	Micro molar

## List of publications

### Publications that are part of this thesis:

- Al-Tameemi, W., Dunnill, C., Hussain, O., Komen, M. M., van den Hurk, C. J., Collett, A., & Georgopoulos, N. T. (2014). Use of in vitro human keratinocyte models to study the effect of cooling on chemotherapy drug-induced cytotoxicity. *Toxicology in Vitro* 28 (8), 1366-1376.
- Collett, A., Al-Tameemi, W., Dunnill, C., Hussain, O., & Georgopoulos, N. T. (2014). The role of scalp cooling in the prevention of chemotherapy induced alopecia. *European Journal of Clinical and Medical Oncology* 65-69.

### Publications that are not part of this thesis:

- Airley, R., McHugh, P., Evans, A., Harris, B., Winchester, L., Buffa F., Al-Tameemi, W., Leek, R., Harris, A. L. (2014). Role of carbohydrate response element-binding protein (ChREBP) in generating an aerobic metabolic phenotype and in breast cancer progression. *British Journal of Cancer* 110 (3), 715-723.

## **Acknowledgements**

Thank you God for every blessing you have given me. The long sleepless and stressful moments have now ended because of the strength and hope I have been given from you lord... After four years of thesis, it is time for me to say loud and clear: "Research is sacrifice and patience"

First, I would like to thank my supervisors Dr. Nikolaos Georgopoulos for the direction, patience, useful advice and support throughout my PhD journey.

Also, I would like to thank Dr. Andrew Collett for his advices.

I am also forever grateful to Professor Rob Brown for all his support and encouragement.

I would like to thank my parents and brothers to whom I dedicate this thesis. Words cannot justify how much I appreciate everything they have done and continue to do for me. Your constant support, guidance, inspiration and love has helped me grow as a person not only in my work, yet in life itself. Without their support, I would have not been where I am today and reach so far to my scientific dreams.

May God bless you all, once again thank you very much everyone for all the love, prayer and motivation.

## **Dedication**

I dedicate this thesis to my beloved parents, my brothers and sisters for their endless love and support.

Wafaa Al-Tameemi

## **CHAPTER 1: Introduction**

## 1.1 An introduction to hair and the hair follicle (HF)

The HF is a multicellular, self-renewing, tubular cavity located in the layers of the skin. The HF has been classified as a mini-organ, due to consisting of broad cell type diversity, ranging from epithelial to mesenchymal and neural crest cells. Furthermore, it has its own immune system and hormonal milieu (Schmidt-Ullrich and Paus, 2005; Paus, 2011). The HF produces the hair shaft, which is commonly referred to as 'hair' (Paus *et al.*, 1999). Hair covers the majority of the human body, at an estimated total of around 5 million hairs, of which approximately 80,000 to 150,000 are located on the scalp (Krause and Foitzik, 2006). In adult humans, there are two types of morphologically distinct HFs. These are: 1) vellus follicles, which contain short, fine, light-coloured, barely visible hair, such as that found on the bodies of children and adult women and 2) terminal follicles, which assemble thick and pigmented hair (Paus *et al.*, 1999; Whiting, 2004). Hair plays an critical role in protecting the skin and various internal cavities against external factors, including sunlight and dust, and also thermo-regulates the body (Winters, 2002).

### 1.1.1 HF structure

Human skin comprises of three layers: the epidermis, the dermis and the subcutis. Each layer has a unique structure and function. The epidermis is largely composed of cells migrating to the skin surface and includes an array of sub-layers, with the order of layers from deepest to the most superficial being the stratum basal, spinosum, granulosum, lucidum and corneum (Mihm *et al.*, 1976; Odland 1991). The dermis is comprised of dense, irregular connective tissue, blood vessels, oil and sweat glands, lymph vessels, nerves endings and the HF, with the layer dominating the mechanical behaviour of the skin overall. The dermis is distinguished into two additional layers, with the upper layer called the papillary dermis and the lower layer being the reticular dermis (Parish 2011). The subcutis is the skin's innermost layer, consisting of loose connective tissue and lobules of fat. The subcutis acts as a conduit for nerves and blood vessels, while also serving the function of body temperature regulation (Odland 1991; Douglas *et al.*, 2004).

Skin-associated structures (skin appendages) consist of the HF, hair shaft, sebaceous gland, apocrine sweat gland, and arrector pili muscle, which are known collectively as a pilo-sebaceous unit (Figure 1-1). The hair shaft and its manufacturing apparatus, the HF, make up one entity (Widelitz *et al.*, 2006). The hair shaft of the human terminal hair is composed of three concentric parent layers. These are, from externally to internally, the cuticle, cortex and cord (medulla) (Paus and Cotsarelis, 1999; Whiting,

2004). The hair growth cycle comprises three distinct phases: active growth (anagen), apoptosis-driven regression (catagen) and rest (telogen). The structure of the HF reflects the different stages of its growth cycle. The anagen VI HF morphology, is most commonly invoked to describe adult hair human (Paus and Cotsarelis, 1999).

HFs in anagen consist of three anatomical segments, which are from distal to proximal: the infundibulum, isthmus and inferior segment (Figure 1-1). The infundibulum is a funnel-shaped cavity through the epidermis that allows for an opening for the hair shaft. The lower part of the infundibulum is defined by an opening of a duct from the sebaceous gland, through which, sebum is excreted into the HF and from here it spreads across the skin surface (Schneider *et al.*, 2009; Whiting, 2004). The isthmus extends from the duct of the sebaceous gland to the exertion of the arrector pili muscle (Ronald *et al.*, 2004). The only function currently attributed to the arrector pili muscle, is the contraction under stress such as low temperature and fear (Sevadjan, 1985). The isthmus and the infundibulum contain very few dividing cells (Cotsarelis, 2006).

Below the isthmus is the bulge region, which is a specialised compartment of the outer root sheath; here the epithelial stem cells (also known as follicular trochanter cells) (Winters, 2002) and melanocytic stem cells reside that differentiate into the hair bulb matrix, epidermal and sebaceous gland regions. In the event of stem cell damage, loss of hair shaft production is likely to occur, resulting in conditions including permanent alopecia (Randall and Botchkareva, 2008).

The HF is separated from the surrounding dermis by dermal cylinder sheaths, also referred to as follicular sheaths, consisting of concentric layers of cells that surround the HF (Zillikens, 2010). The sheath is composed of an external and internal layer known as the outer root sheath (ORS) and the inner root sheath (IRS). The ORS starts from the matrix cells and extends to the entry level of the sebaceous duct (Schneider *et al.*, 2009). The innermost cuticle layer of the IRS is interlocked with the cuticle of the hair shaft surface (Krause and Foitzik, 2006) and extends from the lower part of the hair bulb to the lower part of the isthmus. In this layer, cornified cells (terminally differentiated keratinocytes) form a rigid, funnel-like structure that surrounds the growing hair enabling its protection (Joshi, 2011). Overall, the IRS is important in determining the appropriate shape, adherence and keratinisation of the growing hair fibre (Piérard *et al.*, 1991; Steffen, 2001). The hair bulb is located in the inferior segment and is the centre of the hair shaft production site. The hair bulb contains hair matrix melanocytes that are scattered between hair matrix keratinocytes and together these surround the dermal papilla. Matrix cells in the lower part of the hair bulb boast a higher mitotic rate compared to those of the upper

segment, as the matrix cells are required to migrate upwards, whilst differentiating into both the hair shaft and IRS (Randall and Botchkareva, 2008). The dermal papilla is an oval mass of specialised fibroblasts that are embedded in an extracellular matrix with extensive vacuolisation (Stenn and Paus, 2001; Tobin *et al.*, 2003; Whiting, 2004). There is an association between the size of the dermal papilla and the size of the HF. Indeed, a larger dermal papilla can create larger HF capable of generating a thicker hair shaft (Legué and Nicolas, 2005; Lemenager *et al.*, 1997).

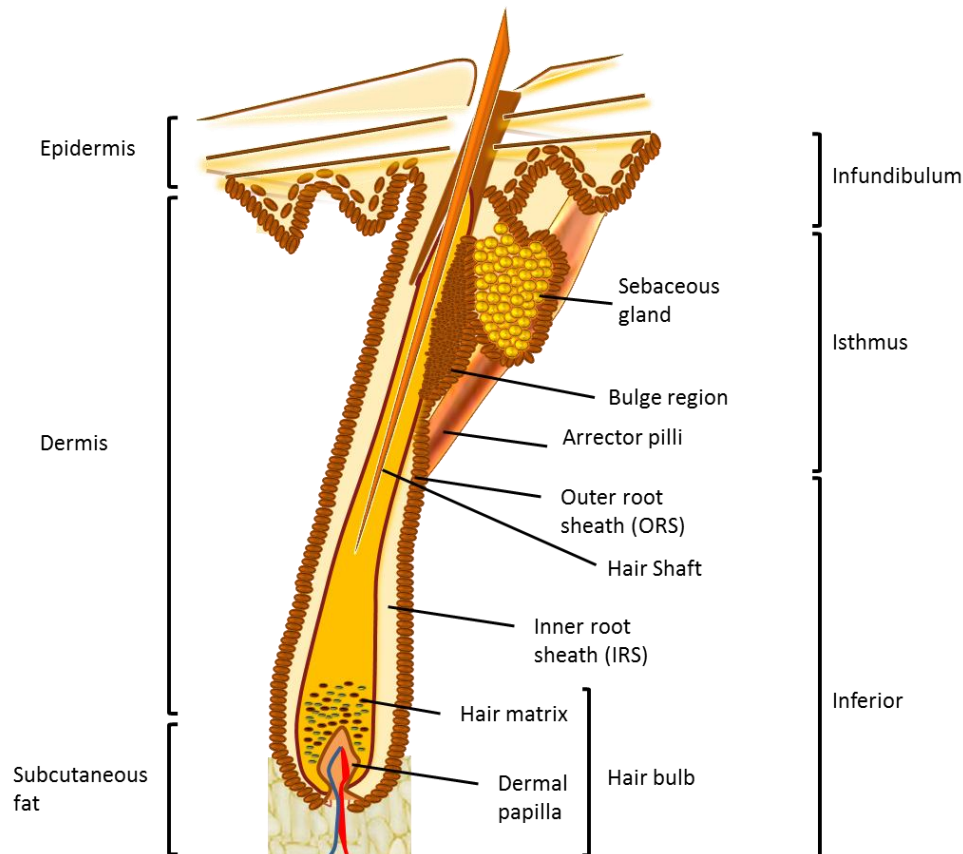


**Figure 1-1 The mature human HF**

The schematic illustrates the structure of the terminal hair anagen in longitudinal section including the hair shaft, bulge region, arrector pili, sebaceous gland, outer root sheath (ORS), inner root sheath (IRS), and the hair bulb that includes the hair matrix keratinocyte compartment and the dermal papilla region. Figure adopted from (Geras, 1990).

### **1.1.2 HF morphogenesis**

The term morphogenesis originates from the Greek words *morphê* (shape) and *genesis* (creation) and is the biological process by which an organism develops its shape. HF development normally requires epithelial–mesenchymal (epidermal keratinocytes and dermal papilla fibroblasts) interactions in utero (during the embryonic stage). This interaction plays a pivotal role in morphogenesis leading to hair shaft production. Different types of HFs have distinct time courses of induction during morphogenesis (Ronald *et al.*, 2004).

Formation of the HF occurs during morphogenesis and budding of the embryonic epidermis forms each HF. This formation requires a series of molecular interactions between the embryonic epidermis and underlying mesenchymal cells (Figure 1-2; Hardy, 1992; Pispá and Thesleff, 2003). Several molecules induce signals specific for cells in the epidermis, including embryonic mesenchymal cells. This involves molecules encoding transcription factors Wnt/LEF-1, Hairless, Sonic hedgehog (Shh) signalling pathways and Notch, in addition to growth factors of the EGF family, FGF, and TGF- $\beta$ . Follicular growth occurs in waves, comprising of a growth phase (anagen), a regression phase (catagen) and a resting phase (telogen). The cellular and molecular mechanisms observed in embryogenesis are often identical to those involved during the hair cycle (Millar, 2002; Schmidt-Ullrich and Paus, 2005).

#### **1.1.2.1 Mesenchymal-epithelial interactions during morphogenesis and HF cycling**

The epithelial and mesenchymal interactions during the hair cycle are directed by a distinct set of molecular signals, which are unique to each phase of the hair cycle (Botchkarev and Kishimoto, 2003). During the telogen phase, inhibitory signals are predominant, maintaining the HF in a quiescent state. However, during the anagen phase several growth stimulatory pathways are activated in the epithelium and in the mesenchyme, the organisation of which is vital for HF formation. The termination of anagen-signalling interactions between the epithelium and the mesenchyme during the catagen phase leads to apoptosis in the HF matrix (Botchkarev and Kishimoto, 2003).

Development of HFs is governed by growth factors triggering a signalling cascade between epithelium and mesenchymal cells to form the connective tissue compartment of the developing HF (Ronald *et al.*, 2004). These signals include Wnt family members (which are ligands acting through their cognate cell surface receptors), TGF- $\beta$ /BMP, Hedgehog (a signalling pathway that transmits information to embryonic cells required for

development), EGF, FGF, Notch (single-pass trans-membrane receptor protein), TNF and neurotrophins (Millar, 2002). There are regulatory interactions between these signalling pathways and cross-talk (as they modulate each other's activities at the extracellular, cytoplasmic or at nuclear level) (Von Bubnoff and Cho, 2001). During the anagen phase, the interaction between the HF epithelium and the mesenchyme increases gradually and peaks in the late anagen HF. Transition from the anagen to the catagen phase is associated with the down-regulation of signalling activity between hair matrix cells and the dermal papilla (Botchkarev and Kishimoto, 2003).

In telogen HFs, the cells are relatively dormant, with low DNA synthesis in the germinative epithelium region of the bulb area (Wilson *et al.*, 1994). In addition, the secondary hair germ and the mesenchymal stem cells form a ball-like cluster with a poorly developed extracellular matrix (Müller-Röver *et al.*, 2001; Young, 1980). Moreover, the basement membrane of the telogen HF is relatively thick and multi-layered, separating epithelial cells of the secondary hair germ and mesenchymal cells of the follicular papilla (Jahoda *et al.*, 1992).

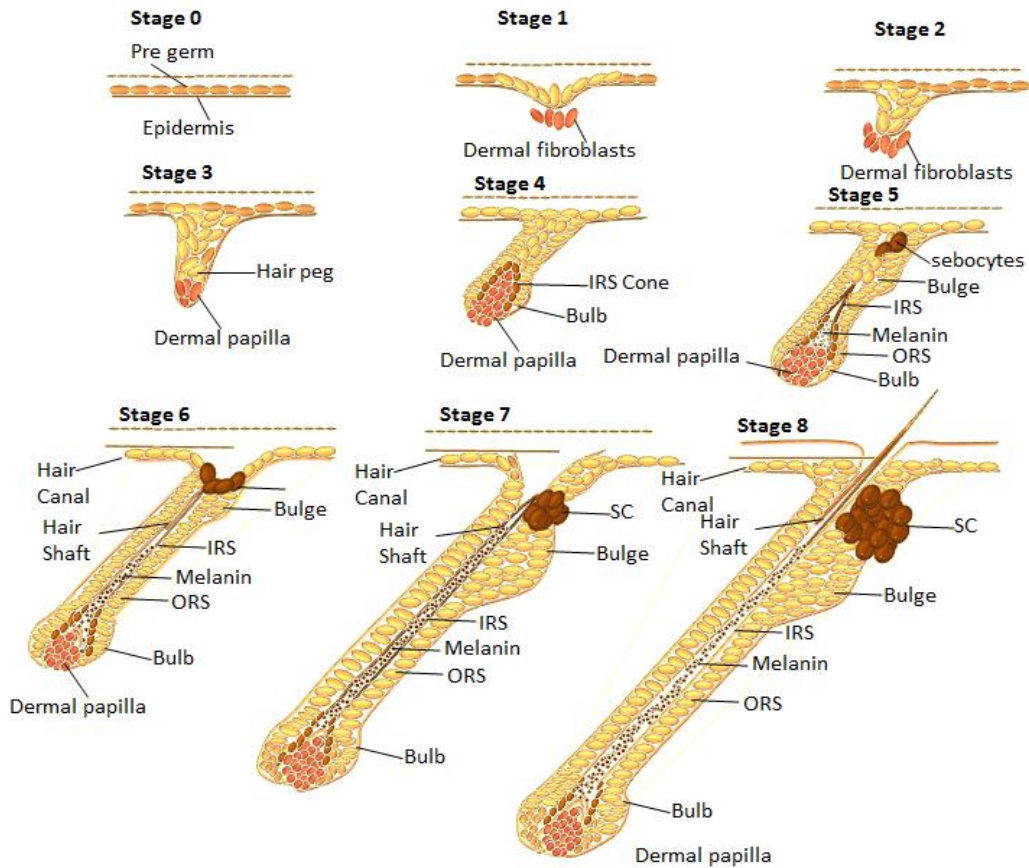


### Figure 1-2 The morphogenesis of the HF

Schematic diagram of the 9 stages of HF morphogenesis. In stage 0 there are no visible morphological signs that HF formation is taking place. HF morphogenesis starts by the initial budding of the embryonic epidermis after a series of molecular interactions between it and the underlying mesenchymal cells. In stage 1, morphogenetic signals derived from the mesenchymal cells, trigger a thickening of the basal layer of epidermis, resulting in the formation of an epidermal placode (the pregerm of the hair) the cells of which elongate. In stage 2 and 3 the cells of the epidermal hair placode proliferate and grow down into the dermis to form the hair peg, which eventually surrounds a cluster of mesenchymal cells known as the germinal matrix. In stage 4, the mesenchymal cells that surround the germinal matrix form the dermal papilla. The dermal papilla is a richly vascularised and innervated structure essential for the effective renewal of hair. The dermal papilla supplies the nutritional elements that allow the growth and differentiation of the keratinocytes. These keratinocytes in the hair bulb migrate upwards and differentiate into the hair shaft and inner root sheath. In stage 5 sebocytes, which are precursors of the apocrine gland, are visible in the distal parts of the HF and the first melanin granules and hair shaft develop above the dermal papilla. In stages 6-7, the HF proliferates and moves downwards into the sub-cutis layer of the skin, the hair shaft then reaches the level of the sebaceous gland and at this point, the hair canal becomes visible in the skin. In stage 8, the HF has all the characteristics of an anagen-phased hair and has reached its maximal length. At the end of this stage the hair shaft begins to emerge through the skin. Figure adopted from (Mcelwee and Hoffmann, 2000; Paus *et al.*, 1999).

### **1.1.3 The hair growth cycle and its phases**

The hair cycle starts immediately following morphogenesis. There are three main phases during the hair growth cycle: the active growth phase (anagen), the transition phase (catagen) and the rest phase (telogen), there is also a shedding phase (exogen). These phases are schematically shown in Figure 1-3 (Paus and Foitzik, 2004).

The process of .. The chronology of HF cycling is from catagen to telogen, to anagen, and returning to catagen. However, the HF alters its normal cycling behaviour in response to damage, such as chemotherapy, so that HF cycling can continue later (Paus and Foitzik, 2004).

#### **1.1.3.1 Anagen**

During anagen, the HF passes through six sub-stages (anagen I-VI), which mainly comprise extensive matrix keratinocyte cell proliferation and differentiation. The matrix keratinocytes differentiate into the keratin rich hair shaft and IRS, with the hair shaft elongating from the bottom causing it to extend upwards (Randall and Botchkareva, 2008). During the anagen phase, several growth stimulatory pathways are activated in the epithelium and mesenchyme and the execution of these is vital for hair fibre formation (Botchkarev and Kishimoto, 2003). In early anagen, the stem cells at the base of the telogen follicle structure also proliferate in a manner that causes them to migrate downward into the dermis, where they begin to differentiate into the hair shaft and IRS. Once the early anagen follicle reaches its predetermined depth, cells reverse their growth direction and progress upward, creating the IRS and the hair shaft. During anagen, the process of the hair shaft pigmentation also occurs by melanogenesis and follicular vascularisation is significantly increased (Slominski *et al.*, 2005). Additionally, numerous growth factors including; insulin like growth factor-1 (IGF-1), keratinocyte growth factor (FGF7), stem cell factor (SCF) and hepatocyte growth factor (HGF) are secreted by dermal papilla fibroblasts to maintain active proliferation and differentiation of the hair matrix keratinocytes (Botchkarev and Kishimoto, 2003; Rudman *et al.*, 1997).

The human scalp hair remains in the anagen phase for approximately 2 to 6 years (Paus and Foitzik, 2004) and typically up to 80-85% of HFs are in this phase at single period of time (Randall and Botchkareva, 2008). During anagen, the interactions between the HF epithelium and the mesenchyme increase, reaching its highest in the follicles during late anagen. Consequently, the dermal papilla combines within the centre of the epithelial hair bulb. During anagen, the HF is sensitive to its environment and therefore, this needs to be carefully controlled to allow normal hair growth. For example, sudden

stress, including psychological or metabolic, can instigate a large number of anagen follicles to move to the telogen phase, where hair falls out and alopecia may be accelerated (Phillips *et al.*, 1986). The normal transition of the anagen phase to catagen is associated with the down-regulation in the signalling exchange between hair matrix cells and the dermal papilla (Botchkarev and Kishimoto, 2003). Due to the termination of signalling interactions between the epithelium and the mesenchyme during the progressive catagen phase, apoptosis in the HFs matrix cells begins (Botchkarev and Kishimoto, 2003).

### **1.1.3.2 Catagen**

For reasons currently unknown to science, following anagen a regressive phase of the hair cycle occurs, known as catagen, during which, the HF ceases production. Catagen can be subdivided into eight stages and is characterised by apoptosis in the lower two thirds of the HF, including the matrix keratinocytes IRS cells and ORS cells, leading to the overall regression of the hair bulb and isthmus. In addition, apoptosis of the hair matrix melanocytes occurs, thus causing cessation of melanin production and hair pigmentation (Slominski *et al.*, 2005). One dictator of HF apoptosis is the hairless gene, which controls apoptosis across the various HF compartments. In the absence of hairless protein, the HF is destroyed the first time it enters the catagen (Zillikens, 2010). This process may also be triggered by the withdrawal of dermal papilla delivered growth factors, or by death inducing signals derived from immunocytes (Brajac *et al.*, 2003; Ryan and Christiano, 2004). Catagen leads to the separation of the dermal papilla from the hair bulb and the upward movement of the HF with the IRS beginning to shorten and leaves the ORS. Collectively, this results in the formation a specialised structure known as the hair club (Randall and Botchkareva, 2008; Rudman *et al.*, 1997). In the later stages of catagen, the dermal papilla develops into a cluster of quiescent cells, located near the regressing HF matrix cells. After its formation, the hair club moves from the subcutis to the dermis/subcutis edge to maintain contact with the distal portion of the HF matrix cells, including the hair bulge. In addition, follicle compartments are reduced in size by 70%, although they can regenerate in the next hair cycle after the appropriate growth stimulation (Randall and Botchkareva, 2008). In total, this phase lasts between 7-14 days, with approximately 2% of scalp HFs estimated to be in catagen at any one time (Randall and Botchkareva, 2008).

### **1.1.3.3 Telogen**

Following catagen, the HF enters telogen, a phase where no major structural changes occur (Randall and Botchkareva, 2008) and where the HF is about half of its

maximum length. During this stage, below the secondary hair germ, the mesenchymal stem cells form a ball-like cluster with a poorly developed extracellular matrix (Müller-Röver *et al.*, 2001; Young, 1980). The basement membrane of the telogen HF is relatively thick and multi-layered, separating the epithelial cells of the secondary hair germ and the mesenchymal cells of the dermal papilla (Couchman and Gibson, 1985; Geraghty *et al.*, 2014). At the lower end of the HF, the club-shaped hair shaft can remain as a distinct structure within the follicular canal for several months, although it can now be depilated much more easily compared to its preceding stages. During the telogen phase, epithelial-mesenchymal interactions serve to deliver dominant inhibitory signals to maintain the HF in a quiescent state (Botchkarev and Kishimoto, 2003). Telogen phased cells have low rates of DNA synthesis in the germinative parts of the epithelium around the bulb region (Wilson *et al.*, 1994). Although there is no significant change in synthesis of DNA, RNA or of the anagen proteins, the expression of a cell cytoskeletal protein keratin 14 remains driven (Bowden *et al.*, 1998), thus telogen is not fully classified as a phase of dormancy. At their cycle end, the end of the telogen phase, a new anagen phase begins by sending signals from the dermal papilla to the follicle. These signals trigger the activity of stem cells and recruit those who are going to grow down, forcing the follicle to lengthen and wrap the dermal papilla. Immediately after the signal has been sent, the vascular endothelial growth factor (VEGF) activates the number and growth of blood vessels in the papilla and start producing a new line of hair, during which, three other proteins are involved: the Insulin-like growth factor (IGF1), keratinocyte growth factor (KGF), and telomerase RNA component (TERC) (Blanpain *et al.*, 2004; Oh and Smart, 1996; Tumber *et al.*, 2004). Telogen HFs can be activated through mechanical depilation or in some cases pharmacologically (Müller-Röver *et al.*, 2001) through the use of cyclosporine A and FK506 compounds that stimulate a return to anagen (Blume-Peytavi *et al.*, 2008; Spencer and Callen, 1987). It has been estimated that 10-15% of HFs are in the telogen phase and that it lasts for at least 3-4 months (Botchkareva *et al.*, 2001; Randall and Botchkareva, 2008).

#### **1.1.3.4 Exogen**

The 'shedding' of the hair shaft at the end of the telogen phase is known as exogen and occurs when the hair shaft is shed from the telogen follicle, resulting in the formation of a new hair shaft from the next cycle in the HF canal (Higgins *et al.*, 2009; Milner *et al.*, 2002; Stenn *et al.*, 1998).

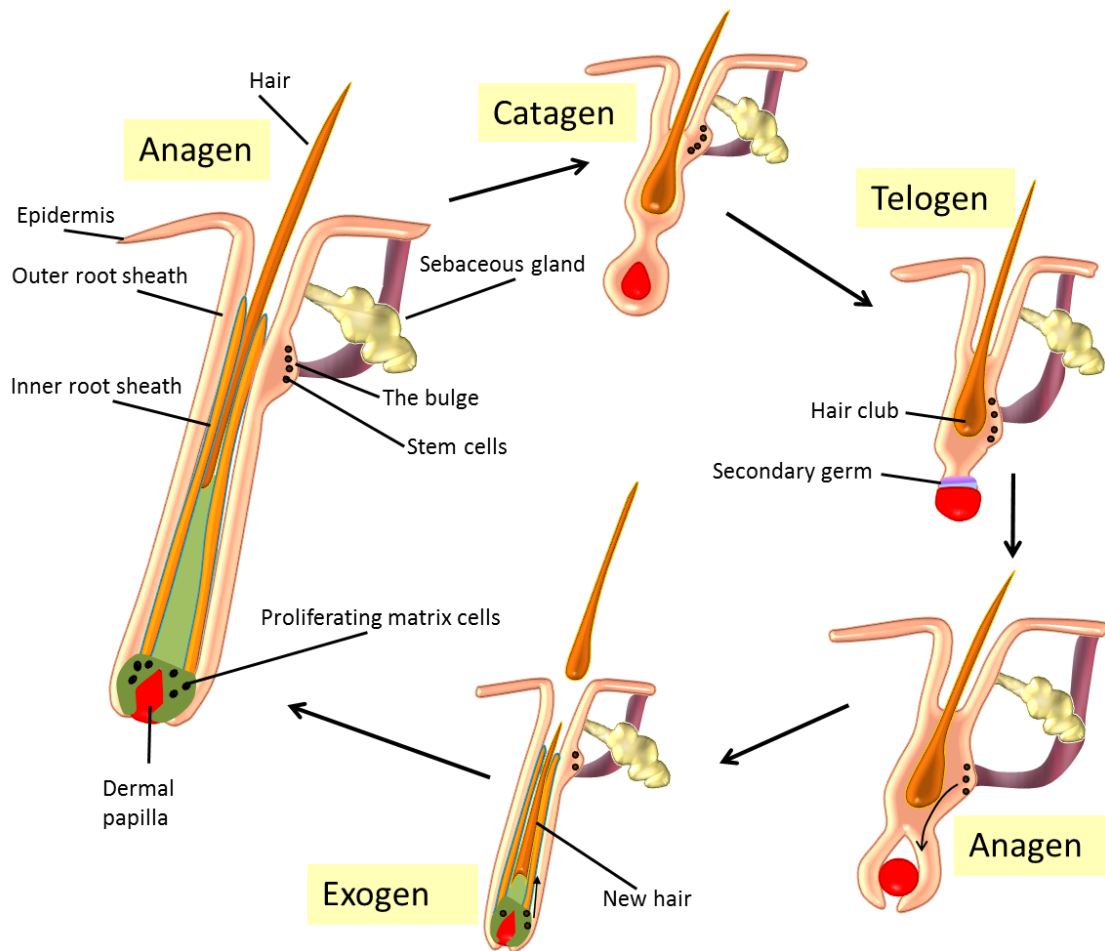


**Figure 1-3 The hair cycle**

Schematic diagram of the three main phases of hair cycle: growth phase (anagen), dystrophic phase (catagen), an extremely shortened resting phase (telogen) and the shedding phase (exogen). In anagen, the hair bulb is located deep inside the skin and then grow towards the skin surface; matrix cells in the hair bulb have high mitotic activity. Catagen is a phase activated when the anagen phase is complete, the follicle no longer produces hair, and it undergoes involution. Cell division stops and in the apoptosis-driven process the follicle retracts to the surface. Telogen is the resting phase, during which the hair shaft is removed. In telogen, epidermal stem cells of the HF, which are located in an area just above the hair bulb, will migrate deep to the bulb to reactivate a new phase anagen hair. Exogen is the shedding phase during which the old hair is shed. Adopted from (Schneider *et al.*, 2009).

### **1.1.3.5 Regulation of HF growth and survival**

Growth factors and associated pathways that specifically regulate epidermal cells have been shown to include transcription factors LEF-1, Hairless, the Shh signalling pathway, Wnt, Notch, EGF/FGF and TGF- $\beta$ . The cellular and molecular mechanisms observed in HF morphogenesis appear undistinguishable to those involved during the hair cycle (Millar, 2002; Schmidt-Ullrich and Paus, 2005). Other factors important in HF growth include cathepsin L, an enzyme involved in the initiation of protein degradation and an important regulator of keratinocyte and melanocyte differentiation in HF morphogenesis and the Hairless protein, which is an important transcription factor that orchestrates follicular regeneration, whilst the anti-apoptotic proteins Bcl-2 and survivin are equally important mediators of growth by inhibiting cell death (Figure 1-4) (Botchkareva *et al.*, 2006a; Tobin *et al.*, 2002). Survivin, an inhibitor of apoptosis is expressed in the proliferative keratinocytes of the anagen hair matrix and the ORS, and its expression is reduced during catagen progression (Botchkareva *et al.*, 2006b).

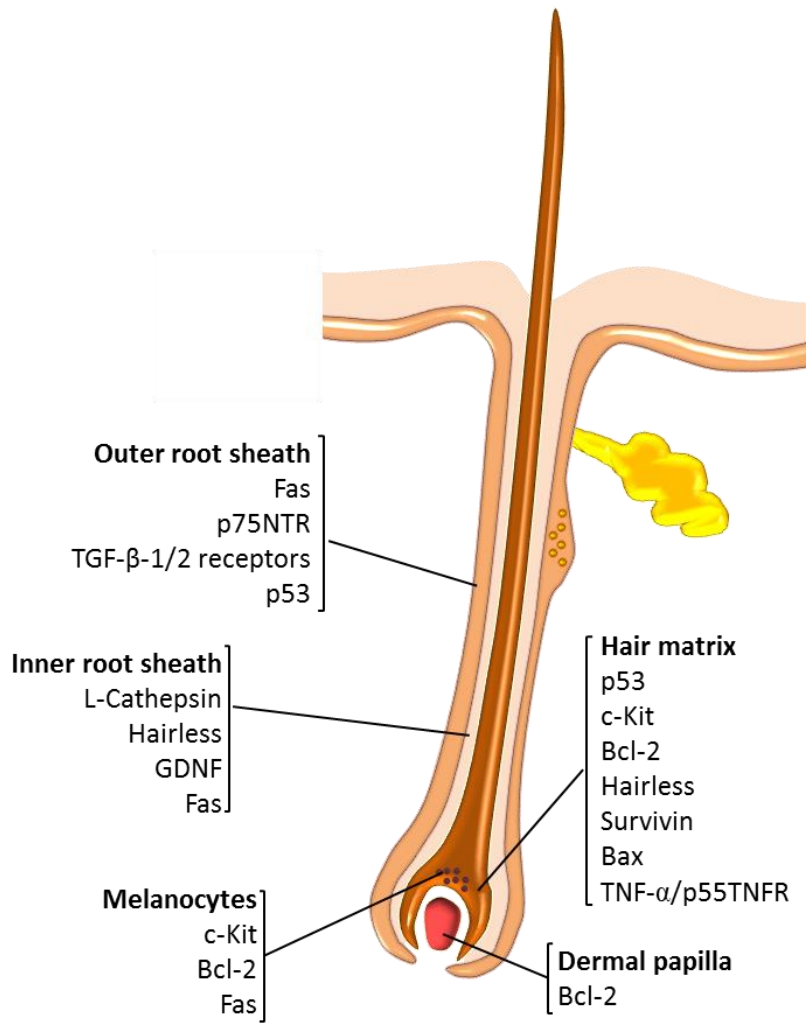


**Figure 1-4 Molecular control of apoptosis in the distinct HF compartments**

The diagram illustrates the expression pattern of pro-apoptotic (e.g. Fas, p53, Bax) and anti-apoptotic (Bcl-2, Survivin) molecules in the different HF compartments. Adopted from (Randall and Botchkareva, 2008).

## 1.2 Chemotherapy

The term chemotherapy is now synonymous with anticancer drug therapy and can be defined as the use of compounds/drugs with the aim of destroying rapidly dividing cells by targeting DNA, RNA, protein synthesis, or a combination of these. Since the Food and Drug Administration (FDA) approved mechlorethamin in 1949 for the treatment of non-small cell lung cancer, more than 100 chemotherapy agents have been approved for cancer treatment in the United States (Payne *et al.*, 2006). In contrast to surgery and radiation therapy, which are directed at the primary tumour in a local manner, chemotherapy is a systemic treatment and as such, it targets both primary and metastatic tumour cells (Symonds and Foweraker, 2006). Generally, chemotherapeutic agents are administered intravenously; however, some are administered orally (or topically). The distribution of any given drug within the body depends on many factors such as blood flow to the different organs, drug diffusion, protein binding, tissue penetration and lipid solubility, but in general, drugs with extensive tissue penetration (e.g. doxorubicin) or high lipid solubility tend to exhibit prolonged elimination phases due to the slow release of drugs from tissue (Tannock and Hill, 1998).

Most chemotherapy drugs are administered at close to the maximum tolerated dose (MTD) and administration is relative to the body's surface area, as it is suggested that this standardises the pharmacokinetics to normalise for physiological factors, such as cardiac output, body fat, and size, and as such the standard dosage units are mg/m<sup>2</sup> (Tannock and Hill, 1998). The frequency of treatments and the intervals between them also depends on the type of cancer and the treatment regime. Chemotherapy is often administered in cycles that include rest periods so that the body is able to recover from the side effects, by allowing production of new cells in healthy tissues (Tannock and Hill, 1998). Clinical trials have suggested that most cancers cannot be cured with a single chemotherapy agent and that a combination of these offers the optimal way to manage cancer (Trigg and Flanigan-Minnick, 2011). The advantages of such combinations are: i) they provide maximal cancer cell death within the range of tolerated toxicity; ii) cells in different phases of the cycle will be targeted; and iii) there is a reduced chance of the cells developing some form of drug resistance (Lilenbaum *et al.*, 2005). Normal cells such as HF keratinocytes, intestinal epithelial cells and bone marrow cells, also divide rapidly and thus are affected by the cytotoxic properties of most chemotherapy, resulting in off-target side-effects (Skeel and Khleif, 2011). In the case of bone marrow toxicity, this is associated with neutropenia, thrombocytopenia and anaemia. Damage to the alimentary canal results in oral mucositis, nausea, vomiting and diarrhoea and keratinocyte damage

causes chemotherapy-induced alopecia (CIA), and nail bed damage (Symonds and Foweraker, 2006).

### **1.2.1 Classification of chemotherapy drugs**

Common drugs used for chemotherapy are classified based on their chemical structure and mechanism of action, as discussed in detail below (Table 1-1).

#### **1.2.1.1 Alkylating agents**

Alkylating agents were the first compounds identified as potential anti-cancer agents and there are different classes including: nitrogen mustards (e.g. cyclophosphamide), nitrosoureas (e.g. streptozocin), alkyl sulfonates (e.g. busulfan), triazines (e.g. dacarbazine and temozolomide) and ethylenimines (e.g. thiotepa and Altretamine) (Tannock and Hill, 1998). Alkylating agents work by various mechanisms: 1) alkyl group attachment to DNA bases, 2) crosslinks formation between single DNA atoms or between two different DNA molecules and 3) prompting mispairing of nucleotides i.e. mutation induction (Trigg and Flanigan-Minnick, 2011).

#### **1.2.1.2 Platinum-based heavy metal alkylators**

Platinum-based heavy metal alkylators are one of the most beneficial groups of anticancer agents and thus are traditionally the favoured choice therapy for testicular, urothelial, and lung cancers (Pinedo and Schornagel, 1996). The first member identified called cisplatin, acts by cross-linking DNA and as this is irreparable, cells undergo apoptosis (Trigg and Flanigan-Minnick, 2011). However, normal cell toxicities limit the clinical application of cisplatin, although this has been partly alleviated through the introduction of the less toxic alternative carboplatin (Symonds and Foweraker, 2006).

#### **1.2.1.3 Antimetabolites**

Antimetabolites are drugs that interfere with nucleotide metabolism, which results in RNA and particularly DNA synthesis inhibition. Therefore, they are predominantly specific to cells in S phase, causing abnormal nucleotide insertion obstructing transcription and translation, or manufacturing DNA that requires resection and repair. This class encompasses 5-fluorouracil (5-FU), 6-mercaptopurine (6-MP) and capecitabine (Takimoto and Calvo, 2008; Trigg and Flanigan-Minnick, 2011).

#### **1.2.1.4 Anti-microtubular agents**

Anti-microtubular agents are compounds that bind to tubulin, the integral protein involved in this process preventing the formation of new cells through mitotic process.

These include taxanes (e.g. paclitaxel and docetaxel), epothilones (e.g. ixabepilone) (Diana and Vahdat, 2008) and vinca alkaloids (e.g. vinblastine, estramustine) (Takimoto and Calvo, 2008; Trigg and Flanigan-Minnick, 2011).

### **1.2.1.5 Topoisomerase inhibitors**

DNA topoisomerases are ubiquitous nuclear enzymes that help facilitate unwinding of the DNA double helix, which allows for DNA replication and RNA transcription. There are two types topoisomerase -I and -II (Takimoto and Calvo, 2008) and inhibitors of these ultimately prevent DNA repair, leading to cell death. Examples of topoisomerase I inhibitors are topotecan and irintecan, and of topoisomerase II are etoposide and teniposide (Trigg and Flanigan-Minnick, 2011).

### **1.2.1.6 Anticancer antibiotics**

Anticancer antibiotics are derived from the bacterial species *Streptomyces* and essentially function as antibiotics within cancer cells (Payne and Miles, 2008). The most important family of this drug class are the anthracyclines (e.g. doxorubicin and epirubicin), but some non-anthracyclines such as bleomycin and mitomycin-C are used clinically. These drugs interfere with enzymes involved in DNA replication, but also take effect in all phases of the cell cycle (Payne and Miles, 2008; Symonds and Foweraker, 2006). Common to all anthracyclines, doxorubicin intercalates within the strands of DNA and this inhibits the progression of the topoisomerase II which prevents the unwinding and the replication of DNA (Trigg and Flanigan-Minnick, 2011). These compounds consequently also lead to the formation of the free radicals such as reactive oxygen species (ROS) (Takimoto and Calvo, 2008). The specific molecular target of many of the anticancer antibiotics is unknown, however two possibilities have been proposed: a) the binding to DNA that prevents its replication and thus cell division and b) the inhibition of mRNA formation preventing protein synthesis (Trigg and Flanigan-Minnick, 2011).

### **1.2.1.7 Miscellaneous agents**

This category includes drugs that act in a number of different ways and also for those that have an unknown mechanism (Trigg and Flanigan-Minnick, 2011). An example is L-asparaginase, a non-essential amino acid required by both normal and malignant cells, however certain cells such as leukaemic cells cannot synthesize asparagine, in which case the administration of L-asparaginase results in asparagine depletion, causing damage cells that have a high dependency on it, or those that may already contain a low concentration (Mccredie *et al.*, 1973).

<b>Anticancer compound type</b>		<b>Generic name</b>
<b>Alkylating agents</b>	Nitrogen mustard derivatives	Mechlorethamine, Melphalan, Ifosfamide, Cyclophosphamide
	Nitrosoureas	Carmustine (BiCNU)
	Heavy metal alkylators	Cisplatin, Carboplatin, Oxaliplatin
	Other	Dacarbazine, Temozolomide
<b>Antimetabolites</b>	Pyrimidine analogues	Gemcitabine, 5-Fluorouracil, Cytarabine, Capecitabine
	Purine analogues	Mercaptopurine (6-MP)
	Folic acid antagonists	Methotrexate (MTX), Pemetrexed
<b>Mitotic/spindle inhibitors and plant alkaloids</b>		Paclitaxel, Docetaxel, Ixabepilone, Vinblastine, Vincristine, Vinorelbine
<b>Topoisomerase inhibitors</b>		Irinotecan (CPT-11), Topotecan, Etoposide
<b>Antitumor antibiotics</b>		Mitoxantrone, Dactinomycin, Doxorubicin, Epirubicin, Bleomycin
<b>Signal transduction inhibitors</b>		Cetuximab, Trastuzumab, Erlotinib, Bevacizumab Sorafenib, Imatinib, Dasatinib, Temsirolimus
<b>Hormonal agents</b>		Tamoxifen
<b>Epigenetic agents</b>		Vorinostat, Azacitidine
<b>Immunomodulators</b>		Interferon alpha-2a and alpha-2b Rituximab
<b>Miscellaneous agents</b>		Lenalidomide, Bexarotene, Tretinoin, Arsenic trioxide, Asparaginase, Bortezomib

**Table 1-1 List of anticancer compounds and their mechanism of action**

Adapted from (Trigg and Flanigan-Minnick, 2011)

### **1.2.2 Molecular targets of chemotherapeutic drugs**

Chemotherapeutic drugs primarily target DNA synthesis and the proteins critical for normal mitosis by targeting specific stages of the cell cycle, as explained below and summarised in Figure 1-5 (Nicolson and Conklin, 2008). The G1 phase, for actively dividing cells, is the longest and most varied stage, and where most anabolism and cell growth occurs. However, there are few known drugs clinically tested that are able to target G1 apart from rapamycin (Symonds and Foweraker, 2006). S phase follows G1 and is characterised by rapid DNA replication, following this, the cells enter G2 when the mitotic apparatus is formed (Alkan *et al.*, 2014). M phase, or mitosis, is the culmination of the S and G2 phases, during which there is a succession of prophase chromosome condensations and the subsequent breakdown of the nuclear membrane, meta-phase depolymerisations and polymerisation. Furthermore, microtubule formation occurs leading to chromosome localisation and equatorial division (Halliwell, 2014). The cells then enter anaphase, which is defined by the polar migration of the chromosomes and then finally, telophase, when cell division occurs (Halliwell, 2014). Drugs that target certain parts of the cell cycle will be discussed with the specific class of drugs in the following section.

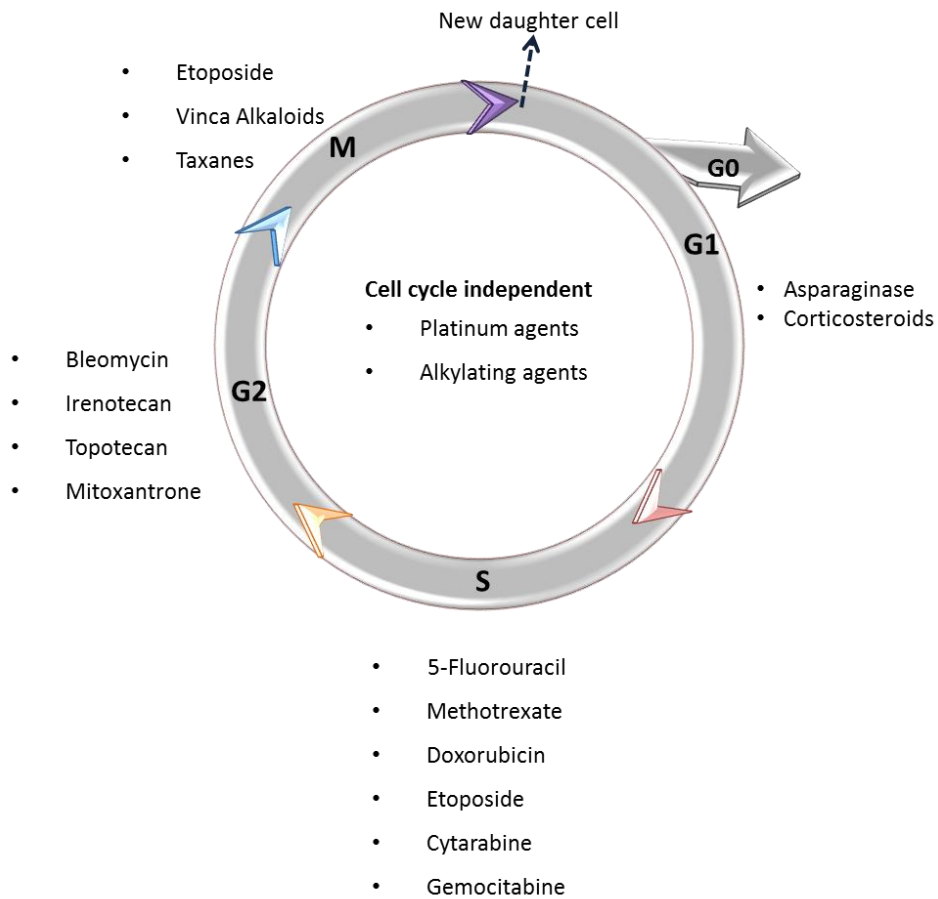


**Figure 1-5 Chemotherapy drugs and their point of action in the cell cycle**

The diagram is a schematic representation of the cell cycle and its phases, illustrating the point of action during the cell cycle for a number of chemotherapy drugs commonly used in clinics. It should be noted that although all drugs are denoted as linked with specific cell cycle stages, there is often a phase-overlap as some chemotherapy agents may target more than one phase (and/or overlapping phases) of the cell cycle, whilst others act on cells irrespective of the phase they are in (cell cycle independent). G0: the cell is out of cycle (quiescence); G1: the cell prepares for division and produces a variety of proteins required for DNA replication; S: DNA double-stranded breaks induced by topoisomerase enzymes, DNA replication takes place; G2: the cell prepares the components that make up the spindle required during mitosis; M: nuclear division, chromosome separation, and cytokinesis to ultimately separate the dividing cell into two new daughter cells. Adopted from (Symonds and Foweraker, 2006)

### **1.2.3 The mechanisms of apoptosis in HF in normal conditions and under pathological circumstances**

Programmed cell death is, particularly within all tissue structures with high proliferation and differentiation rate, strongly characterised (Paus *et al.*, 1993; Zakeri and Lockshin, 2002). It is dependent on genetically encoded signals or cellular activity within the dying cell and provides a cascade of events that induce cell death (Fink and Cookson, 2005). In the biology of the skin, apoptotic pathways have an important place, serving to maintain the homeostasis of the skin. The differentiation of keratinocytes is a unique form of apoptosis, leading to the presence of the typical stratification of the skin and tissue functioning as a termination. At the end of this process of transformation (Magerl *et al.*, 2001) is the formation of corneocytes (terminally differentiated keratinocytes). Apoptosis plays a role in the development of the skin and skin appendages (skin-associated structures) and a central role in the spontaneous HF regression (catagen) (Lindner *et al.*, 1997).

Apoptosis is a form of genetically programmed cell death, which is controlled enzymatically by proteolytic enzymes with a cysteine residue in the catalytic site (these enzymes are therefore called caspases) (Boatright and Salvesen, 2003; Lavrik *et al.*, 2005). The process leads to morphological condensation and fragmentation of the nuclear DNA in the cell nucleus, the condensation of cytoplasm and for the encapsulation of cell components, which have been described as being apoptotic bodies (Fink and Cookson, 2005).

The mechanism of apoptosis is well studied for the eukaryotes (Lockshin and Zakeri, 2004; Oltvai and Korsmeyer, 1994). Apoptosis can be triggered both *in vivo* and *in vitro* (Aurelian, 2005; Mcgregor *et al.*, 1997). Causes for the apoptosis can be loss of growth factors or cell-cell contacts, specific cell-substrate interactions, changes in cytokine expression, as well as the effect of neurotrophins, hormones, and various exogenous noxious factors (Krajewski *et al.*, 1994; Raj *et al.*, 2006). Moreover, external factors that stimulate apoptosis include UV light, X-rays, extreme temperature, toxins, lytic viruses and toxic chemicals, including drugs such as cyclophosphamide, doxorubicin, 5-fluorouracil, vincristine, methotrexate, cis-platinum. Under such influences, the phenomenon of oncosis also occurs (Fink and Cookson, 2005; Majno and Joris, 1995). Oncosis or accidental cell death with swelling of the nucleus, mitochondria and the cytoplasm and karyolysis (Majno and Joris, 1995), making it the morphological contrast to apoptosis. Oncosis is often a result of ischemia (Jaeschke and Lemasters, 2003) and can occur (and

be enhanced by) toxic influences, in particular, through the application of chemotherapeutic agents (Selleri *et al.*, 2004).

There are two major pathways that lead to apoptosis: the extrinsic (death receptor-mediated), the intrinsic (mitochondrial) (Figure 1-6). The extrinsic pathway of apoptosis is regulated by TNF receptor (TNFR) members such as Fas, TNFRI and TRAIL-RI/TRAIL-RII, which are referred to as 'death' receptors and contain a death domain which plays a specific role in cell apoptosis and these receptors are activated by their cognate ligands (Ashkenazi and Dixit, 1998; Danial and Korsmeyer, 2004). This leads to activation of initiator caspase-8 and effector caspase-3 progresses the definitive death of the cell. Negative induction (the intrinsic pathway) is initiated by loss of an inhibitor and activation of pro-apoptotic factors. The process is the active involvement of mitochondria and caspase-9 (Schultz and Harrington Jr, 2003). Finally, both mechanisms lead to the activation of effector caspases 3, 6 and 7, the cleavage of a wide variety of substrates in a cytosol, including deoxyribonuclease, which is responsible for the cleavage the nuclear DNA (Schultz and Harrington Jr, 2003).

The intrinsic pathway is controlled by members of the Bcl-2 family, which have been divided as inhibitors (e.g., bcl-2) (Petros *et al.*, 2004; Van Gurp *et al.*, 2003) and pro-apoptosis such as Bax, Bak, puma Noxa and Bid, characterised by the release of cytochrome c from mitochondria (Van Gurp *et al.*, 2003). Cytochrome c will form an apoptosome with the Apaf-1 and caspase-9 (Li *et al.*, 2000a). Extracellular and intracellular signals through radiation, oxidative stress, and DNA damage due to chemical substance exposure may cause a malfunction of the mitochondria and put the intrinsic mechanism in motion (Raj *et al.*, 2006; Schultz and Harrington Jr, 2003). Zamzami *et al.*, (1995) reported that an early step in apoptosis was a reduction in mitochondrial membrane potential (Zamzami *et al.*, 1995). It is generally believed that factors such as p53 and Nur77 / TR3 / NGFB-1 diffuse from the nucleus to the mitochondria and cytochrome c and continue induce apoptosis *via* the induction of PUMA and Noxa (Fridman and Lowe, 2003; Li *et al.*, 2000a).

Apoptosis is a natural part of the hair cycle and has been studied intensively using both *in vivo* and *in vitro* models (Lindner *et al.*, 1997; Peters *et al.*, 2005; Soma *et al.*, 1998). Apoptosis takes place within all structural components of the HF, with the exception of DP fibroblasts (Botchkareva *et al.*, 2006a) and is a normal process in the reformation of HF architecture, particularly it acts as a mediator for catagen (Botchkarev, 2003; Lindner *et al.*, 1997; Payne *et al.*, 2006). Among the factors with established pro-apoptotic effect of the HF are the neurotrophins of the nerve growth factor (NGF) family,

transforming growth factor (TGF)  $\beta$  1 and 2, the DR Apo-1 / Fas, DR3 / DR4, L-Catepsin, hairless, p53, TNF- $\alpha$  / TNFR p55, FGF-5, and the acting pro-apoptotic members of the Bcl-2 family (Bax, Bak, *etc*) (Botchkareva *et al.*, 2006a). The apoptotic processes within the HF are controlled by caspase-1, caspase-3, caspase-4, and caspase-7 (Botchkareva *et al.*, 2006a; Lindner *et al.*, 1997; Soma *et al.*, 1998).

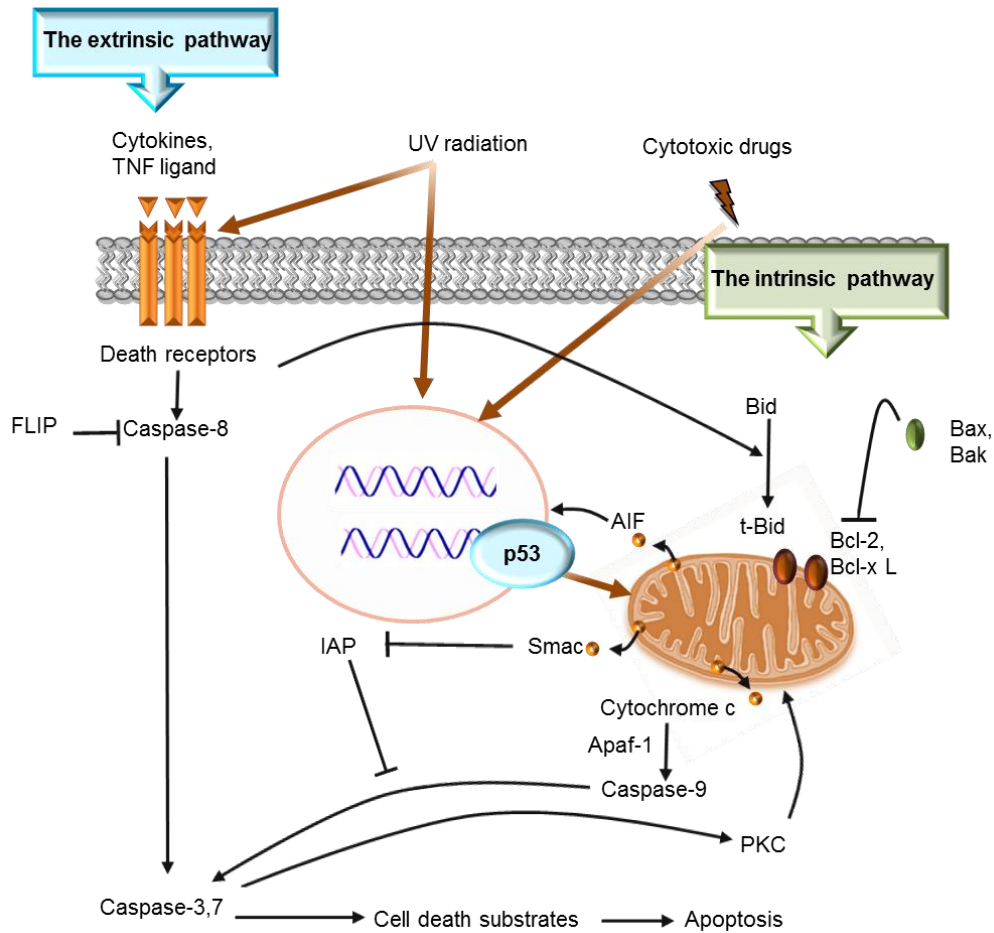


**Figure 1-6 The main mechanisms of apoptotic cell death**

Apoptosis may be triggered by the extrinsic (TNF receptor-mediated) pathway by specific ligand-receptor interaction or *via* the intrinsic (mitochondrial) pathway in response to different types of stress (e.g. genotoxic stress). Both the extrinsic and intrinsic pathways can lead to disruption of mitochondrial outer membrane potential or MOMP. MOMP is controlled by the pro-apoptotic Bcl-2 family proteins Bak and Bax (as well as or voltage dependant anion channels or VDACs – not shown), which facilitate the release of cytochrome c, SMAC/DIABLO or apoptosis inducing factor (AIF) into the cytoplasm. Once in the cytoplasm, cytochrome c mediates the formation of the apoptosome (*via* Apaf-1 engagement), which activates caspase-9 and in turn caspase-3/7 resulting in apoptotic death. SMAC/DIABLO binds to inhibitors of apoptosis (IAPs) and blocks their capacity to attenuate caspase activation and thus promotes apoptosis. AIF translocates from the mitochondrial intermembrane space to the nucleus where it interacts with Endo G to initiate DNA fragmentation Adopted from (Raj *et al.*, 2006).

#### 1.2.4 Chemotherapy-induced HF apoptosis

As described previously, many anticancer agents such as cyclophosphamide, doxorubicin and cisplatin induce DNA damage (Müller *et al.*, 1998). During this process, the transcription factor and tumour suppressor protein p53 plays a critical role in cell protection and apoptosis induction. Specifically, DNA damage can break the p53-MDM2 interaction leading to p53 phosphorylation, which turns p53 into a gene expression enhancer (Moll and Petrenko, 2003). In this situation, p53-induces the expression of the pro-apoptotic genes Fas, Bax, insulin-growth factor receptor type I and insulin like growth factor binding protein 3, IGFBP3 and can also down-regulate anti-apoptotic proteins such as Bcl-2 (Lindner *et al.*, 1997). In light of the fact that many of these proteins can be located in hair follicular cells, it appears that this pathway plays a significant role in regulating hair production. In adult mice, p53 has been shown to be essential in the regulation of the HF response to DNA damage by cyclophosphamide. In p53 knockout mice, hair loss was not observed and the HF remained cycling (Botchkarev *et al.*, 2000). In addition, it was shown in the same study that the TNFR “death” receptor Fas plays a key role in mediating the cytotoxic response as it was shown that Fas knockout mice had significant protection from chemotherapy-induced alopecia (CIA) caused by cyclophosphamide (Botchkarev *et al.*, 2000), although this may be unique to cyclophosphamide. Furthermore, the report highlighted that in response to cyclophosphamide DNA damage induction, the hair matrix cells growth arrested in G<sub>1</sub> via binding and inactivation of the CDK2/cyclin E complex, which is known to be regulated by both p21 and p53. Thus p53 may induce p21 leading to inhibition of G<sub>1</sub>/S cell cycle progression (Botchkarev, 2003).

Several studies suggest p53 mediates apoptosis following growth factor withdrawal without DNA damage in hematopoietic cells and neurons (Gottlieb and Oren, 1998), yet whether this applies to the HF remains unclear. The p53 protein is up-regulated and co-localises with apoptotic cells in the HF during catagen. Furthermore, p53 deficiency in HF leads to a decrease in Bax and IGFBP3, and an increase in Bcl-2 protein expression (Botchkarev *et al.*, 2001). In addition, it has been suggested that oxidative damage of mitochondrial DNA (Bodo *et al.*, 2007) and inhibition of endothelial proliferation of the vascular network surrounding the HF can cause chemotherapy-induced alopecia (Amoh *et al.*, 2007). Moreover, Fas and c-kit signalling is involved in HF melanocyte apoptosis and both proteins are up-regulated after cyclophosphamide treatment (Sharov *et al.*, 2003). It is worth noting that approximately 50% of cancers are p53 negative, and thus the stimulation of this pathway may not kill tumour cells, however,

as the HFs are more likely to express p53 they may be more sensitive to some chemotherapy drugs than cancerous cells.

#### **1.2.4.1 Reactive oxygen species (ROS) in hair follicular apoptosis**

Reactive oxygen species (ROS) are a group of molecules, which contain an oxygen atom with an unpaired electron, making them highly unstable, very reactive, and damaging to other molecules as they remove their electrons. Cells utilise ROS as a second messenger for a number of processes, however at high concentrations ROS cause cell stress and loss of normal function, thus, as a protective mechanism, cells have evolved to become apoptotic in such conditions. N-acetyl-cysteine (NAC) is a potent ROS scavenger, which can provide protection from CIA in animal models and thus it appears that ROS may have a role in CIA (Simon *et al.*, 2000). In addition, a range of chemotherapeutic drugs have been shown to induce ROS *via* various mechanisms, including phosphorylation of the NADPH oxidase system member and by impacting on mitochondrial function. Agents shown to augment ROS production to apoptotic levels include anthracyclines (e.g. doxorubicin, epirubicin), alkylating agents (e.g. cyclophosphamide), and platinum-based drugs (e.g. cisplatin, carboplatin and oxaliplatin) (Nicolson and Conklin, 2008). Interestingly, it is these agents that induce alopecia at a greater frequency and severity than most of other drugs, indicating that there could be a strong relationship between ROS production and CIA (Simon *et al.*, 2000).

### **1.3 Alopecia**

Historically, even ancient as Rome, people were admired for thick, well-groomed hair, as this was associated with male masculinity or female beauty and femininity. By contrast, hairlessness was degrading or humiliating and it has been documented that a concerned Julius Caesar combed his thinning hair over the crown of his head to try to cover his balding scalp. In the modern era, as it has in the past, a lack of hair, or even more so hair loss (alopecia), reflects a significant degree of personal importance. The term alopecia came from the Greek "alopex," which means, "fox." This is because a fox often undergoes alopecia during the course of skin pathology (Joss *et al.*, 1988; Schmidt, 1994; Wagner and Bye, 1979).

#### **1.3.1 Types of alopecia**

There are two types of alopecia; congenital and acquired (Phillips *et al.*, 1986). Congenital alopecia is a genetic predisposition to hair loss and therefore is more frequently observed in the population. Acquired alopecia is not genetically predisposed,

but rather is progressively augmented only by factors that may include iron deficiency, endocrine disorders, androgenic disorders, skin infectious agents, physical damage, inflammation, autoimmunity (Schmidt, 1994), smoking (Trüeb, 2003), stress (Tallon *et al.*, 2010), chemotherapy and/or radiotherapy (Organization, 1979; Van Den Hurk *et al.*, 2012b), genetic mutations (Epstein Jr and Lutzner, 1969), and systemic disease (Sevadjian, 1985). Regardless of the primary cause, the pathophysiology of alopecia results in the cessation of hair shaft production and hair loss.

#### **1.4 Chemotherapy-induced alopecia (CIA)**

Hair loss induced by chemotherapy compromises patients' quality of life and can negatively impact body image, sexuality and self-esteem, as well as depriving patients of their privacy (Hesketh *et al.*, 2004). CIA is often a particular burden for those with young children, of who have reported that CIA is the most traumatising aspect of treatment, despite the previously mentioned complications (Forrest *et al.*, 2006). Collectively, these issues mean that CIA is often one of the most emotionally difficult side effects and female patient feedback has implied that some find losing their hair more difficult to accept than the loss of their breast (Pickard-Holley, 1995). These factors are believed to negatively impact on therapeutic outcome, as severe stress and depression can be linked to a weakening of the immune system, a key factor in cancer survival and prevention (Spiegel and Giese-Davis, 2003). Moreover, strikingly, a report revealed that up to 8% of female patients may refuse chemotherapy for fear of CIA (Hesketh *et al.*, 2004; Tierney *et al.*, 1992). Although most of the research on the emotional effects of CIA have been conducted on females, the research that has been undertaken in males, indicates that at least for younger males, the impact of CIA is the same as that experienced by females (Hilton *et al.*, 2008). Considerable efforts have been expended in order to treat other side effects of chemotherapy, but the pathobiology of CIA has been overlooked (Paus, 2006) and to date, there are no efficacious drug-based treatments available for its management (Luanpitpong and Rojanasakul, 2012).

The HF is particularly sensitive to chemotherapy because up to 90% of their cell population are in the active growth phase, anagen (Batchelor, 2001). The mitotic rate of the matrix keratinocytes is reported to be greater than that of cancer cells (Paus *et al.*, 2013) thus they are especially targeted by cell replication-targeting agents. Moreover, as mentioned previously there is a high blood perfusion around the hair bulb (supplied by the dermal papilla) leading to an increased drug accumulation in all the HF cell populations, with drug concentration and toxicity invariably linked. CIA usually begins 2-4 weeks after chemotherapy and is complete within 1-2 months (Batchelor, 2001). The varying degrees

and severity of CIA depends on the type of chemotherapy drug, dose, route of administration and treatment schedule (Table 1-2) (Luanpitpong and Rojanasakul, 2012). High intravenous doses usually cause more rapid and extensive hair loss, whereas oral therapy (despite administration at a higher total dosage) is likely to cause less severe alopecia (Wilkes, 1996). CIA extent is classified using a WHO classification system and is as follows; grade 0 implies no hair loss, grade 1 is minor, grade 2 is moderate but with wig requirement grade 3 is severe with wig requirement and grade 4 is complete hair loss (Organization, 1979). Alopecia occurs at an estimated incidence of >60% for alkylating agents (e.g. cyclophosphamide), >80% for anti-microtubular agents (e.g. docetaxel), 60-100% for topoisomerase inhibitors (e.g., doxorubicin), and 10-50% for antimetabolites (e.g., 5-fluorouracil and leucovorin) (Trüeb, 2010). Severe alopecia was reported after treatment with daunorubicin, adriamycin, vincristine, ifosfamide and etoposide (Table 1-2) (Batchelor, 2001). Yun and colleagues found that alkylating agents produced the most alopecia, followed by inhibitors of topoisomerase and vinca alkaloids. No significant differences in the pattern of alopecia relating to age, associated symptoms, or chemotherapeutics combinations were observed (Yun and Kim, 2007). High doses of cyclophosphamide and busulfan have been reported to produce irreversible damage to the HF and concurrent alopecia in approximately half of patients (Tosti et al., 2005). As expected, combination therapies consisting of two or more CAs produce a higher incidence and more severe CIA compared to mono-therapy (Luanpitpong and Rojanasakul, 2012). For instance, severe CIA has been reported after treatment with the drug combination fluorouracil-epirubicin-cyclophosphamide (FEC) and also docetaxel, particularly in patients with breast cancer (Kluger *et al.*, 2012). Stem cells of HFs are normally not affected irreversibly, as evidenced by hair regrowth 3-6 months after discontinuation of antineoplastic chemotherapy in the majority of cases when the normal hair cycle begins and new hair production occurs (Batchelor, 2001; Oshima *et al.*, 2001). Permanent CIA or incomplete regrowth, though rare, has been reported after 6 months, thus acute damage to the stem cells is possible. In permanent CIA there is a large decrease in the total number of HF (Cotsarelis *et al.*, 1990; Tosti *et al.*, 2005; Tran *et al.*, 2000).

More common or severe CIA		Less common or severe CIA	
Bleomycin	Cyclophosphamide	Amscarine	Busulfan
Cytarabine	Cisplatin	Carmusine	Chlorambucil
Dacarbazine	Dactinomycin	Carboplatin	Epirubicin
Docetaxel	Doxorubicin	Gemcitabine	Hydroxyurea
Etoposide	Fluorouracil	Interleukin-2	Melphalan
Idarubicin	Ifosfamide	Mercaptopurine	Methotrexate
Interferon- $\alpha$	Irinotecan	Mitomycin C	Mitoxantrone
Mechlorethamine	Nitrosoureas	Procarbazine	Teniposide
Paclitaxel	Thiotepa	Vinorelbine	Busulfan
Topotecan	Vinblastine	Amscarine	Chlorambucil
Vincristine	Vindesine	Carmusine	

**Table 1-2 Cytotoxic agents known to induce alopecia**

Adapted from (Apisarnthanarax and Duvic, 2003; Cline, 1984)

### 1.4.1 Pathophysiology of CIA

Chemotherapeutic agents often induce CIA by interfering with the transition between the stages of the HF development, stimulating follicular dystrophy or the induction of premature follicle regression (Paus *et al.*, 1994), which is triggered by a number of different mechanisms based on the precise mechanism of action of the chemotherapy drug used (Trüeb, 2009a; Trüeb, 2009b; Yeager and Olsen, 2011). Telogen effluvium occurs when a larger proportion of hairs in anagen progress prematurely into the telogen phase, for example cyclophosphamide causes CIA by this mechanism (Patel *et al.*, 2014). This results in an increase in diffuse hair shedding over the scalp causing significant hair thinning, with this being reportedly more distressing to the patient than complete hair loss (Olsen, 2011). Lower concentrations of cyclophosphamide, methotrexate or doxorubicin can promote the HF into the catagen phase, without significant changes in HF morphology, but this also produces visible hair loss (telogen effluvium) (Kligman, 1961). Anagen effluvium is the most common kind of CIA, because at a given time up to 90% of scalp hair is in anagen and occurs within days to few weeks after the administration of cytotoxic agents (Olsen, 2011) and it is stimulated by alkylating agents, antimetabolites, vinca alkaloids, topoisomerase inhibitors, anthracyclines and taxanes (Espinosa *et al.*, 2003; Yun and Kim, 2007). In contrast, telogen effluvium has a latency period of months. The high doses of cytotoxic agents leads to change the HF morphology to dystrophic anagen and cause a localised transition from anagen to telogen with a subsequent release of telogen hairs and the hair loss is usually subclinical involving less than 50% of hairs (Trüeb, 2009b).

Scalp HFs are more affected by chemotherapy drugs than other terminal HFs, for example those of the eyebrows, eyelashes, beard, auxiliary and pubic hairs that are variably affected (Paus & Cotsarelis, 1999). HFs across various regions of the body have variable durations of anagen. For example, scalp HFs stay in the anagen stage for 2-6 years and ultimately produce long hairs, whereas actively growing eyebrow follicles remain in the anagen stage for between 2-3 months. In the HFs of eye lashes, this stage lasts between 30 and 45 days, producing short hairs (Thibaut *et al.*, 2010; Valeyrie-Allanore *et al.*, 2007). Furthermore, in terms of eyelash HFs, only around 40% of the upper lashes and 15% of the lower lashes are in the anagen phase at any point, whereas for scalp hair, 80-85% are undergoing the anagen phase (Thibaut *et al.*, 2010). Eyebrow and eyelash HFs maintain the slowest hair growth rate for any area of the body. As a consequence of increased mitotic activity, anagen follicles are the most vulnerable to toxic effects. Therefore, regions with the greatest proportion of anagen follicles, for example the scalp, are traumatised more severely by noxious events compared with regions

comprising a lower proportion of anagen follicles, for example the eyelashes (Patel & Tosti, 2014; Remesh, 2012).

#### **1.4.1.1 Permanent alopecia induced by chemotherapeutic drugs**

Few studies have explored the histology of irreversible CIA (Tosti *et al.*, 2005; Tran *et al.*, 2000) despite the psychological impact. In most cases, HF stem cells appear to be largely unaffected by chemotherapy agents, demonstrated by hair regrowth 3-6 months post-treatment (Tallon *et al.*, 2010). However, some cases have been reported as an absence of or incomplete hair regrowth after 6 months of completion of chemotherapy (Dorr, 1998). High doses of cyclophosphamide and busulfan may produce irreversible damage to the HF and alopecia occurs in approximately half of patients after receiving these drugs (Tosti *et al.*, 2005). Permanent alopecia also has been reported after treatment with combinatorial drugs FEC (fluorouracil /epirubicin /cyclophosphamide) and docetaxel in patients with breast cancer (Kluger *et al.*, 2012). Hair loss after FEC treatment is observed with a moderate or intense androgenic-like pattern (Kluger *et al.*, 2012).

All the permanent alopecia cases showed that there was a severe decrease in the total number of HFs (Tallon *et al.*, 2010), however, no inflammation or fibrosis was exhibited. Permanent alopecia was observed in another study, which was assessed by a 4-mm punch biopsy. This was taken from the frontal scalp; studies of this biopsy showed a reduction in anagen HFs and the presence of multiple linear aggregates of basaloid epithelium. Another study highlighted that in cases of permanent alopecia the density of the HF reduced, however, the number of vellus hairs were increased (Prevezas *et al.*, 2009). This was similar to telogen HFs however, they differed in structure with a more slender and branched arrangement with no hair shaft (Tallon *et al.*, 2010).

#### **1.4.2 Experimental models of CIA**

CIA remains an important unmet clinical challenge and as such, there is a need to develop robust experimental models of CIA so that new treatment strategies can be developed. Currently there are no ideal pre-clinical models, however, a number of very useful experimental approaches have been developed.

##### **1.4.2.1 Animal models**

Difficulties obtaining scalp biopsies from patients undergoing chemotherapy treatment means that little is known about the true mechanisms of apoptosis and hair loss caused by chemotherapy. Research into CIA has thus heavily exploited the use of animal models, usually neonatal rats or adult mice (Luanpitpong and Rojanasakul, 2012).

However, one fundamental difference exists in the hair growth pattern between humans and rodents as human HF growth cycles occur in a mosaic pattern, with each follicle having its own growth cycle, which behaves independently of its follicle neighbours. In contrast, rodents HFs grow in a wave pattern, starting from the head moving towards the tail. Also in adult mice, HFs are mostly in the telogen phase and only 10% are in the anagen, compared to 90% of follicles on a normal human (Luanpitpong and Rojanasakul, 2012).

#### **1.4.2.1.1 Newborn and young rat models**

As CIA occurs when HFs are in anagen, animal models would require a synchronised induction of HFs into the anagen phase. One way of simulating this is the use of young rat or mice models after the physical depletion of hair as this causes all HFs to re-start their growth in anagen (Wikramanayake *et al.*, 2012). A second technique, established by Hussein and colleagues is the new born rat CIA model (Hussein *et al.*, 1990). Seven to eight day-old rats exhibit spontaneous anagen hair growth for approximately a week, and this has been used to test the effect of several chemotherapeutic agents; arabinoside, doxorubicin, cyclophosphamide, and etoposide. It was reported that alopecia occurred within one week after the initially administered dose and the severity of CIA was dependent on the category of drug infused (Hussein *et al.*, 1990). The advantage of this model is the rapid and obvious onset of hair follicular CIA. The disadvantage is that the HFs are in their first cycle and, as such, they have a different structure and expression of growth factors compared to mature HFs. Furthermore, HFs in the newborn rat lack pigmentation, which is known to limit the effect of drugs on melanocytes (Jimenez and Yunis, 1992b). Thus, this model may be used to demonstrate that chemotherapeutic drugs damage HFs in anagen, but these data cannot be directly extrapolated to man. Following high dose administration of cyclophosphamide, rats show a mitotic reduction in the hair bulb cells, which led to narrowing of the hair shaft and its breakage, thus showing how cytotoxic cyclophosphamide is to the HF (Patel *et al.*, 2014).

#### **1.4.2.1.2 Adult mouse model**

To overcome some of the limitations of newborn and young models, the adult C57BL-6 mouse model was developed by Paus and colleagues (Paus *et al.*, 1994). The advantage of this model is that the hair shafts are well pigmented and thus their response to chemotherapy agents is more comparable to humans. In addition, the stage of hair growth cycle can be identified by the skin colour, as it is pink during the telogen phase, and in anagen, it turns black (Paus *et al.*, 1994). In this model, administration of cyclophosphamide caused dose dependent mild or severe CIA (Paus *et al.*, 1994). Mild

drug-induced toxicity results in a longer than normal anagen phase which initiates a dystrophic anagen response. By contrast, if chemotherapy induces severe toxic effects, HFs are transitioned into a dystrophic catagen (Bodo *et al.*, 2007; Bodo *et al.*, 2009), and although this is caused by greater toxicity, HFs recover faster from dystrophic catagen than dystrophic anagen (Paus *et al.*, 2013).

#### **1.4.2.1.3 Xenografts of human skin samples into nude mice**

Due to the different properties of the human and rodent HF, a method of grafting human skin on to nude mice has been developed (Manning *et al.*, 1973). This potentially powerful model has been used to study CIA as it has the advantages of a whole animal model whilst at the same time allowing the unique physiology of the human scalp HF to be studied (Manning *et al.*, 1973). After grafting human scalp skin onto a mouse the hairs are initially shed within a month, but the hair regrows over the next few months (Neste *et al.*, 1991). This model has been used to study the HF biology and also the effects that chemotherapy has on human HFs (Domashenko *et al.*, 2000) and thus represents a useful *in vivo* tool for studying CIA (Kyoizumi *et al.*, 1998).

#### **1.4.2.2 Non-animal (*ex vivo* and *in vitro*) culture models**

##### **1.4.2.2.1 Organ culture model**

Due to the limitations of animal models discussed above, a system of human HF cultured *ex vivo* was developed by Bodo *et al* and has been utilised for the study of CIA (Bodo *et al.*, 2007). In this model, human HFs in anagen phase were micro-dissected from excess normal human scalp skin obtained from healthy adults undergoing routine face-lift surgery. In a previous study, these human HFs were treated with 4-OH-CP, the active metabolite of cyclophosphamide, and this treatment was shown to reduce matrix keratinocyte proliferation as well as induce apoptosis (Bodo *et al.*, 2007). Therefore, this model represents a potentially powerful tool for the study of CIA in a well-controlled *in vitro* environment whilst maintaining the *in vivo* characteristics of human HFs.

##### **1.4.2.2.2 Cell culture models**

Commercially available cultured primary normal human epidermal keratinocytes (NHEK) and, more rarely normal hair follicular keratinocytes (HHFK), have been used as a model to study chemotherapy-induced damage and apoptosis in skin cells. NHEK are isolated from juvenile foreskins and maintain many of the characteristics of the tissue from which they are derived and have been used as a model to study various aspects of skin physiology. This population of cells is similar to the matrix keratinocytes of the HF, which are damaged by chemotherapy and causing CIA *in vivo*, thus the rationale for this model

is that there is some reciprocation of the clinical scenario. Studies have exploited these finite NHEK and HHFK cultures to examine the effects of commonly used chemotherapy drugs, in particular doxorubicin, docetaxel and the active metabolite of cyclophosphamide (4-OH-CP), as well as combinations of these such as TAC and FAC (Deyrieux and Wilson, 2007; Janssen *et al.*, 2008; Janssen *et al.*, 2007).

A well-established, immortalised human keratinocyte cell line, HaCaT, has also been used to study CIA (Liu *et al.*, 2012; Luanpitpong *et al.*, 2011). As the HaCaT cell line is spontaneously immortalised, it can be cultured in serum-containing media indefinitely. Mitotic or oncogenic mutations are not responsible for the immortalised HaCaT phenotype (Boukamp *et al.*, 1988), but the p53 gene is known to have a UV-specific mutation in both alleles (Lehman *et al.*, 1993). A fundamental difference between NHEK/HHFK and HaCaT is their cell culture conditions; HaCaT cells are cultured in standard, bovine serum-containing medium containing ~2mM calcium (physiological levels), whereas NHEK and HHFK cells are cultured in Keratinocyte Serum Free Medium (KSFM), which contains EGF and BPH and ~0.09 mM calcium (Georgopoulos *et al.*, 2010). The concentration of extracellular calcium has a major effect on keratinocyte growth and differentiation because calcium induces terminal differentiation, specific structural changes, cell cycle withdrawal and induction of terminal differentiation (Boelsma *et al.*, 1999).

### **1.4.3 Treatment options for CIA**

Since the 1970s, there have been numerous attempts to prevent chemotherapy-induced hair loss by means of mechanical, physical, and pharmacological intervention (Grevelman and Breed, 2005; Sredni *et al.*, 1996) and these are discussed below.

#### **1.4.3.1 Pharmacological prevention**

Several classes of pharmacological agents with different mechanisms of action have been evaluated in animal models of CIA; these include drug-specific antibodies, hair growth cycle modifiers, cytokines and growth factors, antioxidants, cell cycle or proliferation modifiers and inhibitors of apoptosis. Their potential applications and limitations have been reviewed previously (Wang *et al.*, 2006) and are briefly discussed below.

##### **1.4.3.1.1 Drug-specific antibodies**

To reduce the severity of doxorubicin-induced alopecia in the neonatal rat model, antibodies to doxorubicin and other anthracycline agents incorporated in liposomes have been explored. Topical administration of these anti-anthracyclines prevented doxorubicin

induced CIA in 31 of 45 rats (Balsari *et al.*, 1994). The limitation to this strategy is that it would require a range of antibodies to prevent alopecia caused by the different drugs usually used in chemotherapy.

#### **1.4.3.1.2 Hair growth cycle modifiers**

Immunosuppressive immunophilin ligands such as cyclosporine, are used in the treatment of autoimmune disease and post-organ transplantation, however, these drugs also induce anagen and inhibit the catagen phase of the hair cycle leading to hair growth activity in several normal and pathogenic alopecia conditions (Taylor *et al.*, 1993). Neonatal rats and mice have been used to investigate the effects of cyclosporine on CIA. Topical application of cyclosporin protected against local alopecia induced by cyclophosphamide, cytosine arabinoside and etoposide in rats (Hussein *et al.*, 2009). Another immunomodulator, AS101, has shown a reduction in the severity of alopecia in patients treated with a combination therapy of carboplatin and etoposide (Sredni *et al.*, 1996). Topical minoxidil is used for the treatment of male pattern baldness and modifies hair cycle dynamics by shortening the telogen hair phase, thus facilitating anagen phase and encouraging hair growth (Duvic *et al.*, 1996). Several studies have examined the effect of minoxidil on CIA. In a rodent model, local application of minoxidil protected against CIA induced by arabinosylcytosine, but showed no protection to doxorubicin and cyclophosphamide-induced CIA (Hussein, 1995). In a clinical study in breast cancer patients, minoxidil has been shown to speed recovery from CIA, but does not prevent it (Duvic *et al.*, 1996).

#### **1.4.3.1.3 Cytokines and growth factors**

Interleukin 1 (IL-1), which plays a role in the regulation of inflammatory and immune responses to infections and ImuVert, a biological response modifier with immune stimulatory properties, derived from the bacterium *S. marcescens* have both been reported to protect rats from CIA induced by cell cycle-specific agents, namely; cytosine arabinoside and doxorubicin, but not from cell cycle-nonspecific agents such as cyclophosphamide (Jimenez *et al.*, 1992). Both ImuVert and IL-1 induce the release of multiple cytokines or growth factors and it has been suggested that the action of ImuVert is *via* IL-1 (Hussein, 1993). Screening of various cytokines and growth factors has found that acidic fibroblast growth factor (aFGF) and epidermal growth factor (EGF) protect from CIA, but again, only if induced by cell cycle specific agents (Jimenez and Yunis, 1992a).

#### **1.4.3.1.4 Cell cycle or proliferation modifiers**

As previously stated, rapid cell proliferation in HFs during anagen and the lack of cancer cell selectivity of anticancer agents is the main factor for CIA. Hence, one approach to protect against the CIA is to inhibit cell proliferation in order to decrease the sensitivity of HFs to chemotherapy (Davis *et al.*, 2001). An example of this method is the administration of calcitriol (1,25-dihydroxyvitamin D3) that has multiple effects on keratinocytes; it stimulates cell differentiation, inhibits DNA synthesis and leads to G0/G1 cell cycle arrest (Kobayashi *et al.*, 1998; Wang *et al.*, 2006). Therefore, it is probable that calcitriol induces changes in keratinocyte proliferation and/or terminal differentiation, subsequently altering cellular susceptibility to apoptosis. It has been shown that calcitriol protects neonatal rats from alopecia induced by cyclophosphamide, etoposide and a combination of cyclophosphamide and doxorubicin (Jimenez and Yunis, 1992b). Furthermore, in the adult mouse model, it was demonstrated that calcitriol could enhance the normal pigmented hair shaft regrowth and reduce apoptosis in the hair bulb, however, it failed to prevent or retard hair loss after the administration of cyclophosphamide (Paus *et al.*, 1996; Schilli *et al.*, 1998).

Cyclin-dependent kinase 2 (CDK2) plays a key role from G1 phase to late G2 phase of the cell cycle. Inhibitors of CDK2, by inhibiting the progression from late G1 phase into S phase, reduce the sensitivity of HFs to chemotherapy agents and inhibits apoptosis induced by etoposide, 5-fluorouracil, taxol, cisplatin and doxorubicin. In neonatal rats, topical application of a CDK2 inhibitor reduced etoposide mediated hair loss by 50% at the site of application and by 33% in CIA induced by of doxorubicin and cyclophosphamide (Davis *et al.*, 2001).

#### **1.4.3.2 Physical intervention**

##### **1.4.3.2.1 Scalp tourniquets**

Scalp tourniquets are special bands that tightly fit the scalp region with the aim of occluding the superficial blood flow to reduce the amount of drug delivered to the HFs (O'brien *et al.*, 1970). Scalp tourniquets are applied when the plasma drug levels are at their peak, i.e. from the last 10 min of infusion to 10 min after the cessation of drug administration (Maxwell, 1980). Tourniquets have achieved a small to moderate degree of rescue from CIA induced by vincristine, cyclophosphamide, and doxorubicin. However, it is no longer recommended due to the high pressure applied resulting in patient discomfort (Maxwell, 1980; Wang *et al.*, 2006).

### **1.4.3.2.2 Scalp (head) cooling**

#### **1.4.3.2.2.1 The principle of scalp cooling and its proposed mechanism(s) of action**

Scalp cooling throughout the administration of chemotherapy drugs in most cases reduces CIA in patients undergoing anticancer chemotherapy (Protiere *et al.*, 2002) since it was introduced in the 1970s at a few hospitals in the Netherlands (Grevelman and Breed, 2005). The methods for application of scalp cooling and the clinical evidence for its efficacy in preventing CIA will be discussed in subsequent sections.

Several hypotheses have been proposed to explain how scalp cooling reduces CIA. Firstly, cooling causes rapid vasoconstriction, which has been shown to reduce blood flow in the scalp significantly and perfusion can be reduced to even 20-40% of normal levels (Janssen *et al.*, 2007); thus it has been suggested that this will result in less chemotherapeutic drug perfusing to the dermal papilla (Bülow *et al.*, 1985). A second hypothesis is that, as the general rate of drug diffusion across a plasma membrane is reduced at cooler temperatures (due to low kinetic energy) and also as membrane lipid fluidity is lower (thus impacting on diffusion), consequently less chemotherapy drug would enter HF cells overall (Lane *et al.*, 1987). In addition, some drugs may enter cells *via* active transport mechanisms (for instance doxorubicin) which would equally be reduced by cooling. Moreover, as cell division is an energy-requiring metabolic process, it is highly likely that its enzyme-dependent reactions are slowed down by cooling. Indeed, it has been reported that temperature can particularly affect the G1 and S phases of the cell cycle (Watanabe and Okada, 1967) and this could be especially important for drugs that target specific phases of the cell cycle, such as mitosis-targeting microtubule-destructive drugs. In support, it has been shown that doxorubicin-induced damage to DNA is reduced at lower temperatures (Vichi *et al.*, 1989). Finally, a general decrease in the metabolic activity of the cells in the HF could cause a reduction in the cytotoxicity of chemotherapy drugs as a range of cellular processes slow (Bülow *et al.*, 1985). In practice, it is likely that a combination(s) of several (or all) of these methods have a role in reducing CIA.

#### **1.4.3.2.2.2 Scalp cooling using cool caps**

Initially cooling of the scalp was achieved using crushed ice in a plastic bag fixed into position with elasticated bandages (Guy *et al.*, 1982). However, because heat from the head rapidly warms the ice packs, these need to be replaced regularly, which is time consuming, and does not maintain a consistently reduced temperature (Katsimbri *et al.*, 2000). The number of countries and hospitals using scalp cooling has increased substantially mainly following the introduction of improved commercially available

products. One uses a refrigerated cryogel cap, which is placed in a freezer at -25°C before being fitted to the head (e.g. Penguin cold cap) (Katsimbri *et al.*, 2000). However, because of the very low initial temperature, these gel-caps are reported to be uncomfortable, and although they are better than the use of ice packs, they still thaw rapidly and must be changed regularly (approximately every 20 min) in order to maintain a consistently reduced scalp temperature. Thus, several changes are required during most standard chemotherapy perfusion protocols (Katsimbri *et al.*, 2000). The most recent development to scalp cooling is the use of a refrigerated unit that circulates a refrigerant solution through a specially designed close-fitting cooling cap.

#### **1.4.3.2.3 Modern scalp cooling devices**

Refrigeration unit-fitted machines, designed to circulate liquid refrigerant through a cooling cap, are the modern day choice in scalp cooling. These caps are available in a range of sizes to ensure a suitable fit as patient head sizes (and shapes) vary (e.g. Paxman PSC system) (Massey, 2004). This modern type of application offers several advantages. The coolant flow achieves and maintains a constant, reduced scalp temperature throughout drug infusion without the need for cap replacement/re-application. This reduces medical staff burden and also, because the caps are not cooled to such unnecessarily low temperatures and they are not as heavy, they are overall more comfortable. Studies examining the Paxman Coolers Orbis head cooling device have shown that 18°C can be consistently achieved in the scalp of patients throughout the course of chemotherapy infusion, and most patients tolerate this intervention very well, with the majority indicating either low or moderate levels of discomfort (Komen *et al.*, 2013b). Advantageously, throughout its application, only the outer part of the scalp to a depth of 2 cm is affected with no subsequent alteration of core temperature, thus posing no risk of hypothermia (Janssen *et al.*, 2005).

#### **1.4.3.2.4 Efficacy of cooling in protecting from drug-mediated toxicity**

##### **1.4.3.2.4.1 Clinical evidence for the efficacy of scalp cooling in cancer patients**

Scalp (head) cooling (or scalp hypothermia) is currently the only technique for which there is clinical evidence-based efficacy for CIA reduction (Breed *et al.*, 2011). Numerous clinical studies have demonstrated that the efficacy of scalp cooling can range from 0-90% depending on the chemotherapy agent and cooling technique used (Grevelman and Breed, 2005).

Auvinen *et al.*, (2010) showed that scalp cooling resulted in a significant reduction in CIA with a 100% of patients maintaining their hair after doxorubicin treatment, 83.3%

after docetaxel, 76.5% after FEC (5-fluorouracil, epirubicin and cyclophosphamide) and 78% after docetaxel together with FEC (Auvinen *et al.*, 2010). A larger and prospective multi-centre study conducted by van den Hurk *et al.*, (2012) explored the effect of scalp cooling on hair preservation in 1411 chemotherapy patients between 2006 and 2009 (Van Den Hurk *et al.*, 2012c). The data were collected by the Dutch scalp-cooling registry, the mean age of the subjects was 53 (18-81 years), with 86% having treatment for breast cancer and 96% of these being female. Treatments varied depending on the different stages and progression of the cancer and consisted of the following: 5-fluorouracil, epirubicin, cyclophosphamide, the combinatorial regimes FEC and TAC (doxorubicin, docetaxel and cyclophosphamide), plus several different anthracyclines and taxanes (given as monotherapy or combination). Patients in the study used the Paxman PSC-1, PSC-2 or ORBIS scalp cooling devices, the median number of chemotherapy and cooling sessions was four (Van Den Hurk *et al.*, 2012c). The results were evaluated by questionnaires, with patients scoring their own hair loss according to a WHO scale (outlined in previous sections) (Organization, 1979). The best results were obtained following monotherapy treatments, for instance taxanes such as docetaxel (75 mg/cm<sup>2</sup>) or paclitaxel (70-90 mg/cm<sup>2</sup>) with 94% and 81%, respectively, of patients not requiring a wig or some form of head cover. The results were less impressive in the case of the TAC combo-therapy, even when used at low doses, as only 8% of patients did not require a form of head cover (Van Den Hurk *et al.*, 2012c). Overall, ~50% of all 1411 scalp-cooled patients did not use head covering at the time of their last round of chemotherapy treatment. Moreover, van den Hurk *et al.*, (2010) have reported that besides the specific chemotherapy protocol, other factors can have an influence on the use of head cover, such as patient age (generally it is higher in those over 50), gender, ethnicity, hair length, quantity, waving, colouring, dyeing and wetting before scalp cooling (Van Den Hurk *et al.*, 2012c). The duration of cooling further influences the protection provided by scalp cooling, thus where possible the timing of cooling periods should be based on the drug pharmacokinetics (Tollenaar *et al.*, 1994). However, in the case of combination therapies, the plasma half-life of a number of drugs would have to be considered and thus the optimal duration of scalp cooling has not been systematically addressed. In most studies, the pre-cooling time (i.e. the time between the start of scalp cooling and the administration of chemotherapy) is between 5 and 30 min to ensure that the scalp is cool when the drugs reach the HFs (Anderson *et al.*, 1981; Johansen, 1985; Lemenager *et al.*, 1997). Another equally important consideration during scalp cooling is the period of time necessary to maintain cooling following completion of drug administration (infusion). Routinely, the cap remains in place during the administration of the chemotherapy drugs and also for a period after this, referred to as the post-infusion cooling time (or PICT), which allows the

drug concentration to drop below toxic levels before the HFs warm up. Although until recently, a 90 min PICT was recommended to ensure maximal efficacy, van den Hurk *et al.*, (2012) specifically examined the effect of post infusion scalp cooling time in reducing CIA after docetaxel treatment and found that better results were obtained by reducing PICT from 90 min to 45 min (Table 1-3) (Van Den Hurk *et al.*, 2012a). This is presumably because once the plasma concentration of docetaxel drops below toxic levels, the warming of the scalp allows any drug that has accumulated during the course of chemotherapy to be more rapidly 'flushed out' of the scalp. This study indicates that some optimisation of cooling protocols might be required to improve the efficacy for different chemotherapy regimens (Van Den Hurk *et al.*, 2012c). In line with this, very recently, a study by Kemon *et al.*, (2016) has reported that even a 20 min PICT is as effective and tolerable as the 45 min period (Komen *et al.*, 2016). Therefore, both of these studies represent potentially significant improvements in the scalp cooling protocols.

It should be noted that in the past, some concern was raised as to whether scalp cooling could be associated with a higher incidence of scalp metastasis, however no studies provide any near statistical evidence for a positive correlation between metastasis and scalp cooling (Lemieux *et al.*, 2011). Lemieux *et al.*, (2009) found a very low incidence of scalp metastases (Lemieux *et al.*, 2009). Additionally, studies that have been conducted to specifically address this issue in patients with breast cancer firstly, confirmed that scalp metastasis occurs very rarely, with an incidence between 0.03% and 3% in individuals that did not receive cooling, and that this is no different to that for individuals who received scalp cooling 0.04–1% (Van Den Hurk *et al.*, 2013). In most cases reported so far, scalp metastases after scalp cooling were not the first metastatic site and the scalp metastasis observed might then only be the result of widespread metastatic disease and unrelated to scalp cooling. Finally, all these observations are further supported by studies demonstrating that use of scalp cooling has no effect on the breast cancer patient survival (Lemieux *et al.*, 2015).

#### **1.4.3.2.2.4.2 Evidence for a cytoprotective role of cooling from *in vitro* models**

Previous studies by Janssen *et al.*, (2008), was shown using NHEK cells treated with doxorubicin that cytoprotection could be achieved at 26 and 22°C and cooling to 10°C had no further effect on cell protection. Based on those observations, it was proposed that with the optimal temperature for scalp cooling being approximately 20-22°C, a further decrease in temperature would be unnecessary and would only result in potential patient discomfort (Janssen *et al.*, 2008). Interestingly, this 'cut off' point in the protective effect of cooling at ~20°C has been shown to occur for doxorubicin at both the level of the cell

membrane (Lane *et al.*, 1987) and damage to DNA (Vichi *et al.*, 1989). The finding that lowering the temperature further results in improved cytoprotection suggests that the scalp temperature achieved in cancer patients may be critical in determining the success of scalp cooling in CIA prevention (Janssen *et al.*, 2008). Collectively, these *in vitro* studies have provided evidence that, despite their reductive nature, such culture models provide clinically relevant data and may thus be useful in understanding the mechanisms of human CIA as well as designing novel strategies to counteract the cytotoxic effects of chemotherapy drugs in the clinic.

	PICT (min)	Number	% no wig or head cover
<b>Observational</b>	90	53	81
<b>Randomised</b>	90	38	79
	45	38	95

**Table 1-3 : Post infusion cooling times (PICTs)**

Use of wig or head cover in scalp-cooled patients after treatment with docetaxel with different PICTs. \*p00.04 (90 vs 45 min). Adapted from (Van Den Hurk *et al.*, 2012a).

## 1.5 Thesis aims

Despite the available clinical evidence, for a positive effect of cooling and direct protection from CIA, the mechanisms by which cooling protects remain not understood. The overall the aim of this work was to for the first time establish *in vitro* models to study the effect of cooling in chemotherapy drug induced cytotoxicity and to provide a detailed understanding at the cellular level of the biological mechanisms involved.

### More specifically:

- **Chapter 3:** Establish *in vitro* culture models for the study of chemotherapy-induced cytotoxicity; these models involved the use of normal human keratinocytes and the non-finite cell line HaCaT; investigate the effect of cooling on cell growth after treatment with a panel of representative chemotherapy drugs used in cancer chemotherapy (and combinations thereof) and establish whether the *in vitro* data are in agreement with clinical observations.
- **Chapter 4:** Investigate the effects of cooling on HaCaTa cell cycle and the distribution of cell cycle phase at cooling conditions in the presence or absence of chemotherapy drugs.
- **Chapter 5:** Investigate the effect of chemotherapy drugs on mitochondrial membrane potential and the influence of cooling; study the effect of chemotherapy drugs in the context of oxidative stress (reactive oxygen species, ROS) and the effects of cooling on ROS induction. Detect chemotherapy drug-mediated cell death using appropriate apoptosis assays and assess the effect of cooling.
- **Chapter 6:** Investigations on the effects of cooling on the activation and functional involvement of key intracellular mediators in chemotherapy drug-mediated apoptosis in human keratinocytes.
- **Chapter 7:** Investigations on the effect of antioxidant-mediated blockade of ROS in cooling-mediated cytoprotection.

## **CHAPTER 2: Materials and Methods**

## **2.1 General**

All practical work was carried out in the School of Applied Sciences, at the University of Huddersfield.

### **2.1.1 Suppliers**

Commercial suppliers and manufacturers are indicated at the first mention of the reagent or equipment in the text. A comprehensive list of all suppliers is provided in Appendix I.

### **2.1.2 Disposable plasticware**

Sterile and non-sterile plasticware was obtained from different suppliers (Sarstedt, Fisher Scientific, Greiner Bio-One or Alpha Laboratories). Non-sterile, disposable plasticware was sterilised by autoclaving in a Prior Clave/London Autoclave at 121°C under pressure for 15 min and then left to dry at room temperature.

### **2.1.3 Stock solutions**

All chemical reagents were either of analytical or tissue culture grade as appropriate for the experiment and were supplied by Sigma Aldrich unless otherwise stated. General laboratory stock solutions were prepared in the laboratories with deionised water (dH<sub>2</sub>O). All solutions, which were used in tissue culture, were prepared with ultra-pure water from a LabStar Ultra Violet purification unit. Heat stable solutions were sterilised by autoclaving at 121°C for 15 min. Otherwise, to ensure lack of microbial contamination, stock solutions were filter sterilised using Acrodisc (VWR) low-protein binding Tuffryn® HT syringe filters with a pore size of 0.2 µm. Recipes for all stock solution can be found in Appendix II.

### **2.1.4 Safe handling of cytotoxic (chemotherapy) drugs**

Cytotoxic drugs were handled with extreme care at all times to reduce any risk of exposure, as these drug can be absorbed through the skin and acute exposure can cause severe cytotoxicity such as nausea and vomiting, abdominal pain, headache and long period exposure can cause reproductive losses and cancer later in life. As part of standard cell culture procedures, all work involving use of cytotoxic drugs was carried whilst wearing disposable nitrile gloves, particularly when dealing with concentrated

stocks and drug-related excess/waste material. A particular amount of each drug was utilised in this work for each experiment, with the drugs adopted comprising of the following: doxorubicin (Sigma Cat # D1515-10MG), which was dissolved in water; docetaxel (Sigma Cat # 01885-5MG-F), which was dissolved in DMSO, as well as cyclophosphamide (4-OH-CP) (supplied by Niomech, Germany), which was also dissolved in DMSO. Following the dissolution procedures, aliquots of each of these drugs were stored in the dark at 4°C for ~1 week. Additional aliquots of each dissolved drug were also stored in the dark at -20°C, as a means of long-term storage over a period of 12 months. Subsequently, the potency of each of the drugs following storage was tested. Such analysis revealed that there was no loss of potency among any of the drugs when tested, whether they were stored at 4°C or when stored at -20°C.

## 2.2 Reagent

### 2.2.1 Primary antibodies

Primary antibodies used in this study are listed in Table 2-1. These antibodies were aliquoted and stored as recommended by the manufacturer until required. Working stocks were diluted in Tris buffered saline (TBS; Appendix II) with 0.1% (v/v) Tween (TWEEN® 20; Sigma Aldrich) and stored at 4°C. When blocking buffers were included in the antibody dilutions, these were specified under 'dilution'.

Antigen	Catalogue no/ Clone	Host	Supplier (product of)	Dilution	Application	MW (kDa)
BAX	2282-MC-100 (YTH-2D2)	Ms	R&D systems (Trevigen)	1:1000 in TBS 0.1% TWEEN® 20	WB	23
Bak	AF816	Rb	R&D systems	1:1000 in TBS 0.1% TWEEN® 20	WB	28
TRAIL	3219	Rb	NEB (CST)	1:1000 in TBS 0.1% TWEEN® 20	WB	28
FasL	4273	Rb	NEB (CST)	1:1000 in TBS 0.1% TWEEN® 20	WB	26, 40
Bid	2002	Rb	NEB (CST)	1:1000 in TBS 0.1% TWEEN® 20	WB	15-22
P53	9284	Rb	NEB (CST)	1:1000 in TBS 0.1% TWEEN® 20	WB	53
Puma	4976	Rb	NEB (CST)	1:1000 in TBS 0.1% TWEEN® 20	WB	23
Noxa	ALX-804-408-C100	Ms	ENZO	1:1000 in TBS 0.1% TWEEN® 20	WB	11
P21	2946	Ms	NEB (CST)	1:1000 in TBS 0.1% TWEEN® 20	WB	21
$\beta$ actin Clone AC15	A5441-2mL	Ms	Sigma	1:20,000 in TBS 0.1% TWEEN® 20	WB	42

**Table 2-1 Primary antibodies**

A list of all primary antibodies used in this study, their catalogue number, host origin, supplier or manufacturer, optimal dilution, type of blocking buffer and the range of their applications is shown here. (Abbreviations - WB: Western blotting, NEB: New England BioLabs, CST: Cell Signalling Technologies).

### 2.2.2 Secondary antibodies

For visualisation of primary monoclonal antibody binding in Western blotting, the molecular probe Alexa Fluor® 680 Goat anti-mouse IgG antibody was used (Invitrogen Cat # A21057). Detection of polyclonal antibodies (all rabbit immunoglobulins) was achieved using the Goat anti-Rabbit IgG IRDYE800 antibody (Tebu-bio Cat # 039611-132-122). Fluorochrome conjugated secondary antibodies were titrated prior to use and are listed in Table 2-2.

Antigen	Catalogue no/ Clone	Host	Supplier (product of)	Dilution	Application
Mouse IgG	A21057	Rb	Invitrogen	1:10,000 in TBS 0.1% TWEEN® 20	WB
Rabbit IgG	039611-132-122	Goat	Tebu-bio	1:10,000 in TBS 0.1% TWEEN® 20	WB

**Table 2-2 Secondary antibodies**

All secondary antibodies used in this study, their catalogue number, host, origin, supplier or manufacturer, optimal dilution, type of blocking buffer and the range of their applications are listed (Symbols - WB: Western blotting). Fluorescence detection at wavelengths 680nm and 800nm was performed using the Licor Odyssey Infra-red imaging system. When not in use, antibodies were stored in the dark at 4°C.

### 2.2.3 Pharmacological agonists and antagonists

Pharmacological agonists and antagonists (Table 2-3) were reconstituted in either tissue culture grade dimethyl sulphoxide (DMSO; Sigma) or sterile distilled water (dH<sub>2</sub>O) according to the manufacturer's instructions. These were stored in single-use aliquots at -20°C as recommended. Prior to use, all compounds were titrated using the cell viability assay (CellTiter 96® AQueous One Solution Cell Proliferation Assay; Promega, UK, Cat # G3581) to determine the effective and non-toxic dosage. All reagents used in this study were purchased from the indicated supplier.

Compound	Target	Supplier	Stock concentration	Effective concentration
Staurosporine	Protein Kinases	Sigma	100 µM	5 µM
NOK1	FasL (CD95L)	Gift of Prof Yagita, Japan	1 mg	100 µg
MR106	Control Ab for anti-FasL labelling	Gift of Prof Yagita, Japan	1 mg	100 µg
N-acetyl L-cysteine (NAC)	ROS	Sigma	20 mM (culture media)	0.625 mM
Pifithrin-α hydrobromide	P53	Santa Cruz Biotechnology	1000 µg/mL	1 µg/mL
PD153035 hydrochloride	Epidermal Growth Factor Receptor (EGFR)	Sigma	5 mg	3 µM

**Table 2-3 Agonists & antagonists**

Agonists and antagonists used in this study, their target molecule, the supplier, the stock and effective concentrations are shown. \*NB. NAC reacts with the CellTiter MTS substrate and has to be removed and washed before addition of the MTS reagent.

## **2.3 Tissue culture**

### **2.3.1 General**

All tissue culture work was undertaken using aseptic techniques within a HEPA filtration CellGard class II biological safety cabinet (NUAIRE). Prior to and after use, internal working areas within the hood were disinfected using 70% (w/v) ethanol (Fisher). To do so, 99% ethanol was diluted appropriately (150mL: 350mL) with autoclaved dH<sub>2</sub>O. Internal hood spillages were disinfected using Mikrozid® (Gompel Healthcare Cat # 32644) and this was also used for monthly routine disinfection of the safety cabinet. Any unwanted cells, exhausted media or solutions were aspirated into a large conical flask containing 10% (w/v) Virkon and were then left for a minimum of 30 min before being decanted and washed into sewage.

All cell culture reagents were of tissue culture grade and were from Sigma unless otherwise stated. To separate cells from solution, cell suspensions were centrifuged for 5 min at 1500 rpm using a Hettich Zentrifugen Universal 320 bench top centrifuge. Cell counts were performed from cell suspensions using a Marienfield Neubauer improved bright line haemocytometer before cells were seeded at the required cell density. When cells were not being manipulated they were kept in an Iso class 5 Nuaire Autoflow direct heat, CO<sub>2</sub> incubator with a HEPA filtration system at 37°C in a 5% CO<sub>2</sub> humidified atmosphere (incubator contained dH<sub>2</sub>O supplemented with Sigma clean (Sigma Cat # S5525-40Z). Cultured cells were routinely observed by phase contrast microscopy using an EVOS XL (PeqLab) inverted microscope at x100 magnification.

## **2.4 Cell culture**

### **2.4.1 Normal human epidermal keratinocytes (NHEK) and Human hair follicular keratinocytes (HHFK)**

Neonatal human epidermal keratinocytes (HEKn), referred to in this study as normal human epidermal keratinocytes (NHEK), were obtained from Life Technologies (supplied by Fisher Scientific) and were cultured in keratinocyte serum free medium (KSFM) (Gibco, Life Technologies Cat # 17005-034) supplemented with epidermal growth factor (EGF) and bovine pituitary extract (BPE) (Gibco, Life Technologies Cat # 10450-013) as recommended by the manufacturer. Human hair follicular keratinocytes (HHFK) were purchased from ScienCell Research Laboratories (supplied by Caltag MedSystems) and were cultured in

Keratinocyte Medium kit (ScienCell Cat # 2101) according to the manufacturer's recommendations.

#### **2.4.2 HaCaT cell line**

As a model for human proliferating keratinocytes were HaCaT cells was purchased from Cell Line Services (CLS). The HaCaT cells are a transformed, spontaneously immortalised, tumorigenic cell line (Boukamp *et al.*, 1988). HaCaT cells possess mutation in both alleles of the p53 gene (Lehman *et al.*, 1993).

HaCaT cells were grown in DMEM medium (DMEM Sigma cat # D6546-6X500ML) 10% fetal calf serum FBS (FCS Biosera Cat # S1810/500) with 1% L-Glutamine (Sigma Cat # G7513-100ML). Cells were maintained in T75 flasks with 12-14mL medium or T25 flasks in 5mL medium and were incubated at 37°C under 5% CO<sub>2</sub>. Cells were sub-cultured every 3-4 days, when they were 80-95% confluent. At all times cell lines were cultured in the above mentioned medium and incubated at 37°C in 5% CO<sub>2</sub> unless otherwise stated. For all experiments, HaCaT cells were used at passages 1–15 to ensure maximal proliferative capacity.

#### **2.4.3 HaCaT adaptation to serum-free medium (HaCaTa)**

A sequential adaptation methodology was followed to switch the culture conditions of HaCaT cells from a serum-supplemented to a serum-free, low calcium medium (KSFM). This involved culture and passaging whilst gradually reducing the proportion of standard culture medium DMEM/10% FBS (DMEM complete, DMEMc) and replacing it with KSFM/EGF/BPE (KSFM complete, KSFMc) and lasted a period of six passages. Briefly, this involved: medium-change of cells (p1) from DMEMc to 3:1 (v/v) DMEMc:KSFMc medium and passage (p2); medium-change to 1:1 (v/v) DMEMc:KSFMc followed by passage (p3); medium change to 1:3 (v/v) DMEMc:KSFMc and passage in this medium (p4), medium-change to 1:9 (v/v) DMEMc:KSFMc (p4) and passage (p5); final medium-change to KSFMc and subsequent passage (p6). After this, HaCaT cells had fully adapted to the new culture medium and were named HaCaTa. Adapted HaCaT (HaCaTa) cells (see below) were cultured in the same medium as NHEK cells. For all experiments, HaCaTa cells were used at passages 9–15 to ensure maximal proliferative capacity.

#### **2.4.4 Cell maintenance**

For all experiments, NHEK and HHFK cells were used at passages 1–3 to ensure maximal proliferative capacity. All cells were routinely cultured at 37°C in a humidified atmosphere of 5% CO<sub>2</sub>, whereas for cooling experiments the temperature was altered as

indicated. Cells were passaged at approximately 80–90% confluence by removing media, washing with 0.1% (w/v) EDTA in phosphate buffered saline PBS (without Ca<sup>2+</sup> and Mg<sup>2+</sup>) (Invitrogen Cat # 14200-067) to aid disaggregation; this was carried out for 15 min for HaCaT cells and for 2 min for HaCaTa, HHFK, and NHEK cell lines. Cells were lifted using trypsin–EDTA solution (Sigma Cat # T41474-20mL) in Ca<sup>2+</sup> and Mg<sup>2+</sup> free Hanks-balanced salt solution (HBSS, Sigma Cat # H9394-6X500ML) until cells detached from the culture flasks. In the case of NHEK, HHFK and HaCaTa cells the trypsin was inactivated using trypsin inhibitor (Sigma Aldrich Cat #T6522-100MG) then cells were centrifuged at 1200 rpm for 5 min. The supernatant was aspirated, and the cells gently resuspended in fresh medium. For routine maintenance and experiments, NHEK and HHFK cells were cultured in Primaria™ (Scientific Laboratory Supplies) or Cell Plus (Sarstedt) plasticware, whereas original and adapted HaCaT cells were maintained in standard plasticware (Sarstedt).

#### **2.4.5 Cryo-preservation and recovery of cell lines**

Cells were cryo-preserved and kept in liquid nitrogen in a Statebourne storage dewar at -196°C. For cryopreservation of cell lines, cultures were collected as for passaging (as explained in section 2.4.4) and collected by centrifugation. The cell pellet was re-suspended in the appropriate ice-cold growth medium supplemented with 10% (v/v) FBS and 10% (v/v) dimethylsulphoxide (DMSO) at a cell density not less than 1x10<sup>6</sup> cells/mL. Cells were aliquoted in a total of 1-1.5mL into polypropylene cryovials (Sarstedt) and then transferred to an ice-cold Nalgene “Mr Frosty” (Fisher) containing 250mL of isopropanol (Fisher) to control the cooling rate to 1°C per minute. Cells were then placed within a -80°C freezer for 4-6h prior to transfer to liquid nitrogen. Cells were recovered by thawing rapidly at 37°C, before 5-10mL of pre-warmed growth medium was added. Cells were centrifuged at 1500 rpm for 5 min; after that the media aspirated and fresh media were added then incubated at 37°C in a 5% CO<sub>2</sub> humidified atmosphere.

### **2.5 Assessment of cell growth**

The effect of chemotherapy drugs on keratinocyte cell growth and viability was determined by measuring cell biomass (the mass of living biological organisms in a specific area at a given time (Gold *et al.*, 1997)). Cell biomass was measured using the CellTiter 96® AQueous One cell proliferation assay (Promega Cat # G3580) and following the manufacturer’s instructions. The CellTiter 96® AQueous One Solution Cell Proliferation assay involves the use of the MTS tetrazolium (yellow) which is reduced to a formazan derivative (brown colour) by respiring cells (Figure 2-1). The observed change in color is proportional to the total number of viable/proliferating cells. Keratinocytes cells lines (HaCaT,

HaCaTa, HHFK and NHK) were seeded into 96 well plates in 6 replicate wells for each condition and then left to adhere overnight before the addition of culture medium containing chemotherapy drugs, with or without pharmacological agonists or inhibitors. Following treatment of cells as described above, 20  $\mu$ L of reagent (CellTiter reagent) was added to each well and plates were incubated at 37°C in 5% CO<sub>2</sub> conditions for 4h. Total levels of formazan formation, which corresponds to relative cell biomass, was assessed using a FLUOstar OPTIMA (BMG Labtech) plate reader at a wavelength of 492 nm following background subtraction. Percentage (%) cell biomass was calculated using the formula: (Abs T/Abs C) x 100, where 'Abs T' is absorbance value for drug-treated cells and 'Abs C' corresponds to the absorbance value for controls cultures.

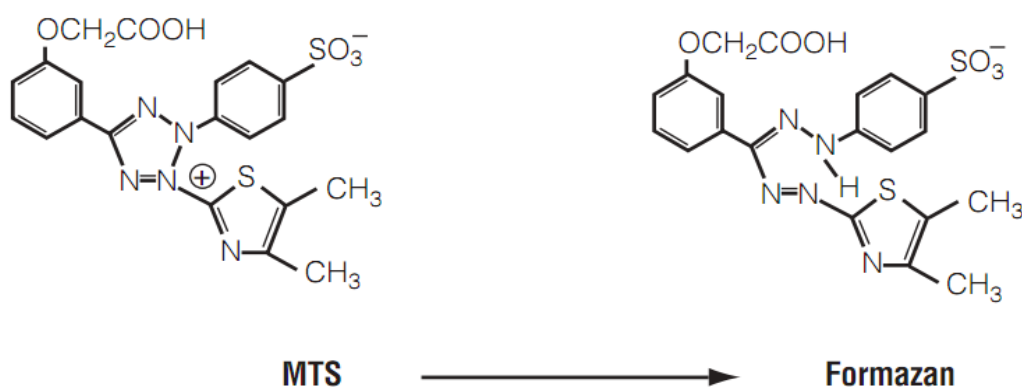


**Figure 2-1 The structure of MTS tetrazolium and its reaction product**

This assay is a colorimetric method containing only one solution reagent. The tetrazolium compound includes 3-(4,5-dimethylthiazol-2-yl)-5-(3-carboxymethoxyphenyl)-2-(4-sulfophenyl)-2H-tetrazolium, inner salt: MTS and also contains phenazine ethosulfate (PES), which uses as an electron coupling reagent that can bind with MTS to form a constant solution. This reagent can be reduced by cells into coloured product, which is soluble in the medium, which is known as formazan. The amount of formazan produced is directly proportional to the number of living/viable cells.

## 2.6 Observation of cell viability by microscopy

In addition to CellTiter assays, cell viability was also routinely monitored by phase contrast microscopy. In particular, HaCaTa cells were seeded at 5 x 10<sup>3</sup> cells per well in 96-well tissue culture plates, whilst HaCaTa cells were seeded in 10 cm tissue culture dishes at 9 x 10<sup>5</sup> cells per dish. Test cultures were treated at 37°C or 22°C, 18°C and 14°C with the indicated drug concentrations alongside negative controls (as described above) and cells were incubated at 37°C for the indicated time period observed at 100x and 200x magnification.

## **2.7 Assessment of the role of temperature conditions on chemotherapy-mediated cytotoxicity**

Keratinocytes were seeded into 96-well tissue culture plates at a density of  $5 \times 10^3$  (HaCaT and HaCaTa) or  $7.5 \times 10^3$  (NHEK and HHFK) cells per well – optimal density for each cell type was determined by pre-titration experiments – and incubated for 24h at 37°C. For individual drugs treatment experiments, cells were subjected to a range of concentrations of docetaxel (Sigma Cat # 01885-5MG-F), doxorubicin (Sigma Cat # D1515-10MG) and 4-hydroxycyclophosphamide (4-OH-CP), the active metabolite of cyclophosphamide (supplied by Niomech, Germany) and 5- fluorouracil (5-FU) (Sigma Cat # F6627-1G), for a period of 2h at 37°C (control conditions) or under cooling conditions (22°C, 18°C or 14°C) in the appropriate culture medium and as detailed in the Results. Solvent (DMSO) controls (representing the maximal amount of DMSO that corresponded to the highest drug concentration) were included in all experiments. Following treatment, drugs were removed; cells washed twice using PBS by careful aspiration and fresh culture medium added. Cultures were then incubated at 37°C for 72h before cell growth was assessed (below). For combinatorial TAC, ACT and FAC therapy experiments, sequential treatment with docetaxel (T), doxorubicin (A) and 4-OH-CP the active metabolite of cyclophosphamide (C) and 5- fluorouracil (F) was carried out, with the exact concentration of each drug being dependent on the cell type (as explained in the main text). In particular:

### **2.7.1 (A) NHEK cells challenged with the following three TAC regimes:**

- (a) Docetaxel 0.05 µg/mL (2h), doxorubicin 3 µg/mL (1h), and 4-OH-CP 25 µg/mL (1h), termed 'TAC'.
- (b) Docetaxel 0.05 µg/mL (2h), doxorubicin 3 µg/mL plus docetaxel 0.005 µg/mL (1h), 4-OH-CP 25 µg/mL plus doxorubicin 0.3 µg/mL (1h), termed 'TAC (+10%)'.
- (c) Docetaxel 0.05 µg/mL (2h), doxorubicin 3 µg/mL plus docetaxel 0.05 µg/mL (1h), 4-OH-CP 25 µg/mL plus doxorubicin 3 µg/mL (1h), termed 'TAC (+100%)'.

### **2.7.2 (B) HaCaTa cells challenged with the following three TAC regimes:**

- (a) Docetaxel 0.01 µg/mL (2h), doxorubicin 0.3 µg/mL (1h), and 4-OH-CP 5 µg/mL (1h), termed 'TAC'.
- (b) Docetaxel 0.01 µg/mL (2h), doxorubicin 0.3 µg/mL plus docetaxel 0.001 µg/mL (1h), 4-OH-CP 5 µg/mL plus doxorubicin 0.03 µg/mL (1h), termed 'TAC (+10%)'.

(c) Docetaxel 0.01 µg/mL (2h), doxorubicin 0.3 µg/mL plus docetaxel 0.01 µg/mL (1h), 4-OH-CP 5 µg/mL plus doxorubicin 0.3 µg/mL (1h), termed 'TAC (+100%)'.

(d) Docetaxel 0.01 µg/mL (1.5h), doxorubicin 0.3 µg/mL plus docetaxel 0.01 µg/mL (1.5h), 4-OH-CP 5 µg/mL plus doxorubicin 0.3 µg/mL (1.5h), termed 'TAC (+10% incubation time for each drug 1.5h)'.

### **2.7.3 (C) HaCaTa cells challenged with the following three ACT regimes:**

(a) Doxorubicin 0.3 µg/mL (1.5h), 4-OH-CP 5 µg/mL plus doxorubicin 0.03 µg/mL (1.5h), docetaxel 0.01 µg/mL (1.5h) plus 4-OH-CP 0.5 µg/mL termed 'ACT (+10% with 1.5h incubation time)'.

(b) Doxorubicin 0.3 µg/mL (1h), 4-OH-CP 5 µg/mL plus doxorubicin 0.03 µg/mL (1h), docetaxel 0.01 µg/mL (2h) plus 4-OH-CP 0.5 µg/mL termed 'ACT (+10% with 1.5h incubation time)'.

### **2.7.4 (D) HaCaTa cells challenged with the following three FAC regimes:**

(b) 5FU 25 µg/mL (1.5h), doxorubicin 0.3 µg/mL plus 5FU 2.5 g/mL (1.5h), 4-OH-CP 5 µg/mL plus doxorubicin 0.03 µg/mL (1h), termed 'FAC (+10%)'.

Cells were then washed and medium was replaced as described above, before cell growth was assessed 72h later.

## **2.8 Functional inhibition experiments**

For functional inhibition experiments involving biological (NOK-1) or pharmacological (NAC, Pifithrin-α hydrobromide and PD153035 (Epidermal Growth Factor Receptor (EGFR)) antagonists, the appropriate concentration of inhibitor was added to culture for the indicated period of time before cytotoxic drug treatment. The inhibitor was then removed, and drug added as a 2x concentration with 2x concentration of inhibitor. Cells were incubated either for 2h or for 72h with this drug-inhibitor combination, after which time cell viability was determined using the CellTiter assay.

## **2.9 Supplement starvation**

Cells were seeded at a density of  $9 \times 10^5$  in petri dishes one day prior to treatment. Cells were carefully washed with sterile PBS three times and then incubated in KSFM media without supplements for 24h, after which time cells were treated with cytotoxic drugs for 2h.

After that, the cells were washed and incubated with fresh medium, then CellTiter and cell cycle analysis experiments were performed.

## **2.10 Detection of cell growth, death (apoptosis) and reactive oxygen species (ROS) production**

### **2.10.1 General**

Previously published guidelines regarding the use and interpretation of assays for monitoring cell death (Galluzzi *et al.*, 2009) have recommended that a minimum of two assays are utilised for the detection of cell apoptosis. The current research made use of a cell proliferation assay (MTS CellTiter) in addition to three apoptosis detection-specific assays; (a) CytoTox-Glo, (b) Anaspec Caspase-3/7 and (c) DNA fragmentation.

These assays were based on measurement of absorbance, fluorescence, or luminescence. 96-well Nunc white, tissue culture treated plates (Fisher Cat # TKT-186-010C) were used for luminescence-(CytoTox-Glo) and fluorescence (Anaspec Caspase-3/7)-based assays, 96-well Costar transparent tissue treated culture plates (Fisher Cat # TKT-186-010C) for absorbance (CellTiter), and 96-well ELISA microplates (Greiner bio one Cat # 655101) for ELISA (DNA fragmentation).

### **2.10.2 Detection of cell death using the CytoTox-Glo™ assay**

The CytoTox-Glo assay is based on detection of the activity of a proprietary, specific protease normally present inside cells. During apoptosis, as the cell membrane is compromised the protease is released and it cleaves the AAF-Glo™ substrate, thus generating a luminescence signal (Figure 2-2). The intensity of the luminescence signal indicates the degree of apoptotic cells in a population. Before the experiment, all reagents were thawed at room temperature and all components mixed to ensure homogeneity. The CytoTox-Glo™ cytotoxicity reagent was prepared by transferring the contents of one bottle of assay buffer to the AAF-Glo™ substrate bottle, and then mixed to ensure homogeneity.

Cells were treated with 4-OH-CP, doxorubicin, and docetaxel as described (in section 2.7) and after 2h cells were washed and fresh drug- free medium were added and then cells were incubated for 24h and 48h, before 50 µL CytoTox-Glo substrate were added. Luminescence was detected using a FLUOstar OPTIMA (BMG Labtech) plate reader, following calibration of the reader using the Gain function on the MARS software to ensure the measurements were taken within the dynamic range of the instrument. The plates were kept away from light and left at RT for 15 min before measurements were taken. Data was

acquired using MARS software (BMG Labtech) and analysed by Microsoft Excel. To calculate percentage cell death the equation used was (treated cells RLU / control RLU), where RLU indicates relative luminescence units.

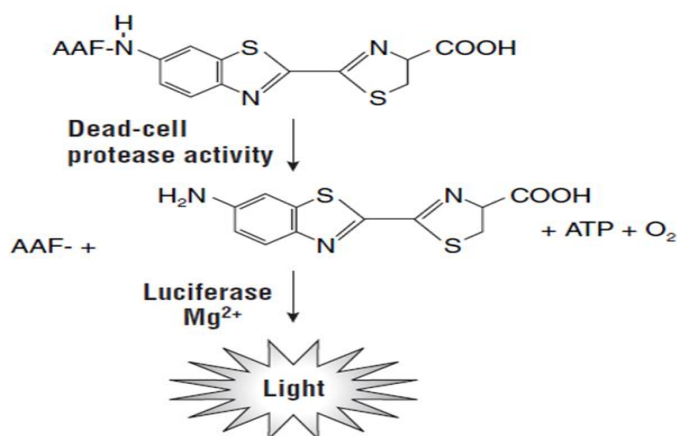


**Figure 2-2 The principle of the CytoTox-Glo™ assay**

The first cleavage of luminogenic AAF-Glo™ substrate occurs by dead-cell protease activity and the second cleavage, and a substrate for luciferase (aminoluciferin) is released resulting in the luciferase-mediated production of light.

### 2.10.3 Detection of apoptosis using caspase-3/7 assays

The activation of caspases-3/7 is a well-established feature of cell apoptosis. caspases-3 and -7 target a specific amino acid sequence located on many proteins, which leads to overall cell demise by an organised apoptotic event. The activation of caspases-3/7 was determined using the SensoLyte® Homogenous AFC caspase-3/7 substrate (Anaspec Cat # 71114, supplied by Cambridge Bioscience). The assay utilises the cleavage of the recognition sequence of caspase-3/-7 that is Asp-Glu-Val-Asp (DEVD). The SensoLyte® Homogeneous AFC Caspase-3/7 assay kit uses Ac-DEVD-AFC as the fluorogenic indicator for assaying caspase-3/7 activity. Upon caspase-3/7-mediated cleavage, Ac-DEVD-AFC generates the AFC fluorophore, which has bright blue fluorescence and can be detected at Excitation / Emission = 380nm/500nm. The degree of production of the strongly fluorescent fluorophore is relative to total levels of caspase-3/7 activation as shown in Figure 2-3.

Cells were treated with 4-OH-CP, doxorubicin and docetaxel in 96-well plates as described (in section 2.7) before the addition of 50 µL SensoLyte® Homogenous AFC caspase-3/7 substrate. Fluorescence was measured using a FLUOstar OPTIMA (BMG Labtech) plate reader using Excitation/Emission 355nm/520nm filters, following calibration of the reader using the Gain function on the MARS software to ensure the measurements were

taken within the dynamic range of the instrument. The plates were kept away from light and left at room temperature (RT) overnight after which fluorescence measurements were taken. To account for the activity of caspase-3/7 after treating with chemotherapeutic drugs, the cell these were cultured alone (without treatment) and their relative fluorescent units (RFU) subtracted from the treated cells (as explained in section 2.7).

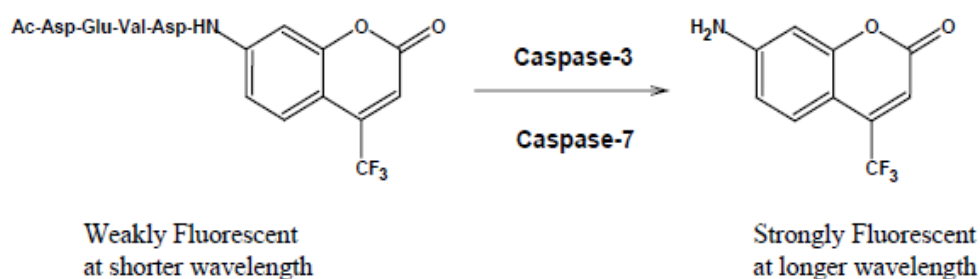


### Figure 2-3 proteolytic cleavage of Ac-DEVD-AFC substrate

The amount of fluorescent product generated is proportional to the amount of caspase-3/7 cleavage activity present in the sample. Cleavage of the weakly fluorescent caspase-3/7 Ac-DEVD-aminoluciferin substrate Z-DEVD by caspase-3/7 to create the strongly fluorescent compound.

#### 2.10.4 Detection of apoptosis using the DNA fragmentation ELISA

The fragmentation of DNA is often a hallmark of apoptosis and the DNA fragmentation ELISA assay uses 5-bromo-2'-deoxyuridine (BrdU) specific antibodies to detect BrdU-labelled fragments of DNA. Greater amounts of fragmented DNA labelled with BrdU represent a greater number of cells that have undergone apoptosis (the principle of the assay is schematically illustrated in Figure 2-4).

Exponentially growing cells were loaded with the DNA labelling agent BrdU for 2h at a concentration of 10  $\mu$ M according to the manufacturer's instructions. Cells were then seeded in 96-well plates and incubated overnight. Then the cells were treated with 7.5  $\mu$ g/mL 4-OH-CP, 0.5  $\mu$ g/mL doxorubicin, 0.05  $\mu$ g/mL docetaxel and 5  $\mu$ M staurosporine as positive control as described (in section 2.7) and then cells were incubated for 24 and 48h. An ELISA plate (96 well flat bottom MTP) (Fisher Scientific Cat # E951040308) was coated with an anti-DNA antibody and then blocked to remove any non-specific binding sites. After washing of the ELISA plate to remove any blocking buffer, supernatants from cell cultures were added; these may contain DNA fragments pulsed with BrdU. The labelled fragments of DNA stick to the plate *via* the anti-DNA antibody and then a secondary, enzyme-linked antibody that specifically recognises BrdU was added. Finally, an enzyme TMB substrate was added

which is converted into a blue colour by the secondary, enzyme-linked antibody. The increased amount of colour change is relative to the amount of secondary antibody bound to BrdU labelled fragments of DNA. TMB substrate (High Sensitive) detects horseradish peroxidase (HRP) activity when TMB substrate is reacted with peroxidase, a soluble blue reaction product is obtained. Dilute sulphuric acid (H<sub>2</sub>SO<sub>4</sub>) was used to stop the reaction after sufficient colour change, and following this, a deep yellow colour represented the degree of cell apoptosis. The plates were used to measure absorbance using a 455-10nm filter on a FLUOstar OPTIMA (BMG Labtech) plate reader. Data was acquired using MARS software and analysed by Microsoft Excel. Staurosporine-treated cells were used as positive control (5 μM).

**Fold of DNA fragmentation = Treated cells / control (staurosporine)**

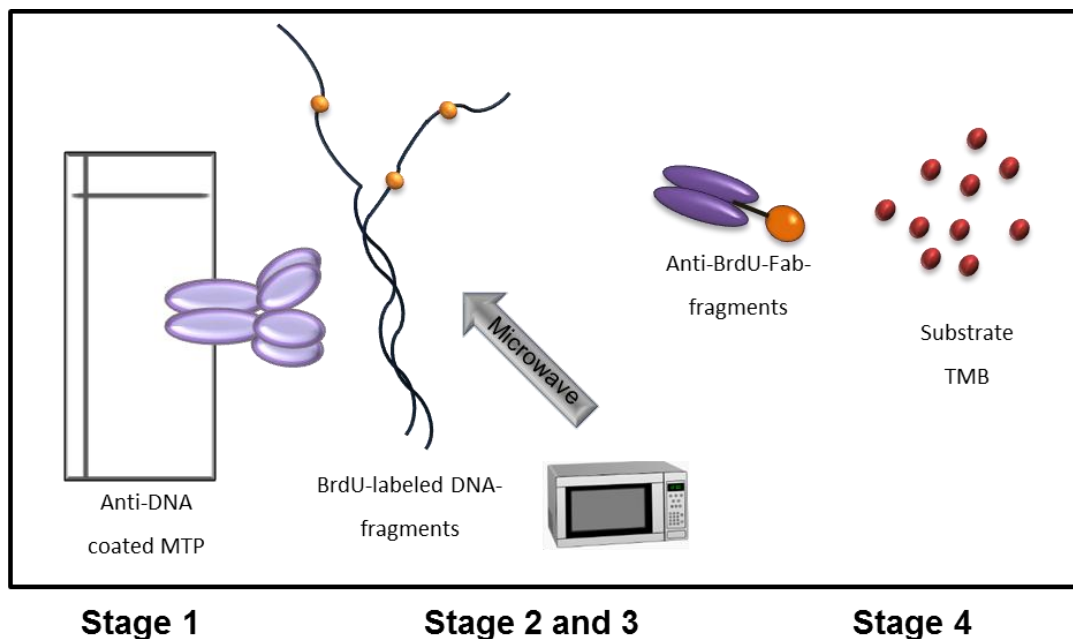


**Figure 2-4 Principle of DNA fragmentation assay**

Microtiter plate was coated with anti-DNA antibody. Brdu-labelled fragments of DNA from supernatants were fixed by denaturing using a microwave (500watt for 5 min). This was followed by a secondary antibody labelling (anti-BrdU-Fab). The plate was incubated 90 min at room temperature and substrate was added. Following yellow colour formation, sulphuric acid was added to stop the reaction.

## **2.11 SDS-PAGE and Immunoblotting (Western Blotting)**

### **2.11.1 General**

Western blotting is a powerful technique widely used in different fields in biological research to detect specific proteins in whole cell lysates. Under denaturing conditions, proteins are size-fractionated using SDS-PAGE, a form of gel electrophoresis.

SDS-PAGE separation was performed under denaturing conditions due to the addition of SDS (sodium dodecyl sulfate). SDS is a strong detergent having a long hydrophobic hydrocarbon tail and a negatively charged end. By binding to proteins, SDS prevents protein folding and imparts a net negative charge, so all proteins migrate towards the anode. This means that only the molecular weight of the protein is the factor of separation. Proteins separated by this method are then transferred onto a membrane, which has high protein binding affinity. Stably bound to a membrane, size fractionated and denatured proteins are detected using epitope specific primary antibodies. A near-infrared (NR) fluorophore conjugated secondary antibody raised against the primary antibody is then added to the membrane and the membrane is scanned using an infrared scanner.

### **2.11.2 Protein extraction**

Cells treated with chemotherapeutic drugs and non-treated (control) cells were grown in 10cm<sup>2</sup> culture dishes and lysed *in situ*. Culture medium was aspirated and cell sheets were washed 2x in ice-cold PBS to remove any excess proteins. 20 µL of ice-cold 2x sodium dodecyl sulphate (SDS) buffer (Appendix III) containing 2 mg/mL DTT and 0.2% (v/v) protease inhibitor cocktail set 3 (Calbiochem) was pipetted onto the cell monolayer and the cells were scraped using a cell scraper (Fisher Cat # FB55199) into a lysate. The solution was then transferred to a chilled micro-centrifuge tube kept on ice. Samples were sonicated using an ultrasonic probe (Sonics Vibra cell) for 10-second bursts (until the lysate showed froth like consistency) and it was then cooled on ice for 30 min. The lysates were centrifuged at 12,000-14000g at 4°C for 30 min to pellet the insoluble material, before aliquoting the supernatant and storing at -20°C.

### **2.11.3 Protein Quantification**

The protein concentration of each sample was determined using a Coomassie protein reagent assay kit (Pierce Cat # PN23236). Samples were diluted 4:46 in dH<sub>2</sub>O and 10 µL was aliquoted in quadruplicates into a transparent 96-well flat bottomed plate. A seven point standard curve of 0-1 mg/mL (0, 25, 125, 250, 500, 750 1000 µg/mL) BSA (Cat # PN23208)

was included on each plate. 200  $\mu\text{L}$  of ambient temperature coomassie reagent was added to each well and mixed gently by pipetting. The absorbance was then measured using a FLUOstar OPTIMA (BMG Labtech) plate reader at Abs 595 nm against a  $\text{dH}_2\text{O}$  control. MARS analysis software 2.0 (BMG Labtech) was used to plot a standard curve for the BSA and to estimate the protein concentration for each lysate (Appendix III).

#### 2.11.4 SDS-Polyacrylamide gel Electrophoresis (SDS-PAGE)

20  $\mu\text{g}$  of protein lysate was made up to 13  $\mu\text{L}$  with  $\text{dH}_2\text{O}$  then this was totalled to 20  $\mu\text{L}$  by the addition of 5  $\mu\text{L}$  4x lithium dodecyl sulphate sample buffer (LDS; Invitrogen Cat # NP0007) and 2  $\mu\text{L}$  of 10x reducing agent (500 mM Dithiothreitol) (Invitrogen Cat#NP0009). The sample was denatured by heating for 10 min in a  $70^\circ\text{C}$  water bath. 10-well NuPAGE™ Novex electrophoresis pre-cast gels (Invitrogen Cat # NP0321) were placed into an Xcell Surelock™ mini-cell upright electrophoresis tank (Invitrogen). 200mL and 600mL of 1x NuPAGE™ MES SDS running buffer (Invitrogen Cat # NP0002) was poured into the inner and outer chambers, respectively. 200  $\mu\text{L}$  of NuPAGE™ antioxidant (Invitrogen Cat # NP0005) was added to the inner chamber prior to loading of the samples. 5  $\mu\text{L}$  of All-Blue Precision Plus Protein™ standard (Bio-Rad Cat # 161-0373) was loaded alongside the samples as a marker of protein size (Figure 2-5) and gel was run at 200V for 35 min.

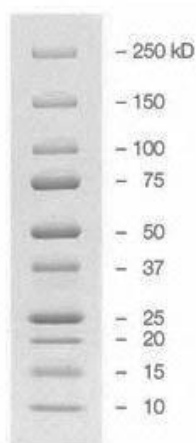


**Figure 2-5 Precision plus Protein standard**

All Blue standards are a mixture of ten blue-stained recombinant proteins (10–250 kDa), including three reference bands (25, 50, and 75 kDa).

### 2.11.5 Electrophoretic membrane transfer

Electrophoretically-separated proteins were transferred onto Immobilon-FL™ polyvinylidene difluoride membrane (PVDF; Millipore) using an Xcell II™ blot module (Invitrogen). PVDF membranes were dipped in methanol, rinsed in dH<sub>2</sub>O and then soaked in 0.5x “Towbin” transfer buffer with 20% (v/v) methanol along with the required number of blotting pads and Whatman™ filter paper (Fisher). The gel membrane sandwich was assembled cathode to anode as follows; 2x blot pads, filter paper, gel, PVDF membrane, filter paper and 2x blot pads (Figure 2-6). The blot module was secured into the Xcell SureLock™ Mini-Cell and filled with transfer buffer. The outer chamber was filled with ice-cold dH<sub>2</sub>O and the transfers were performed on ice at 25V for 2h.

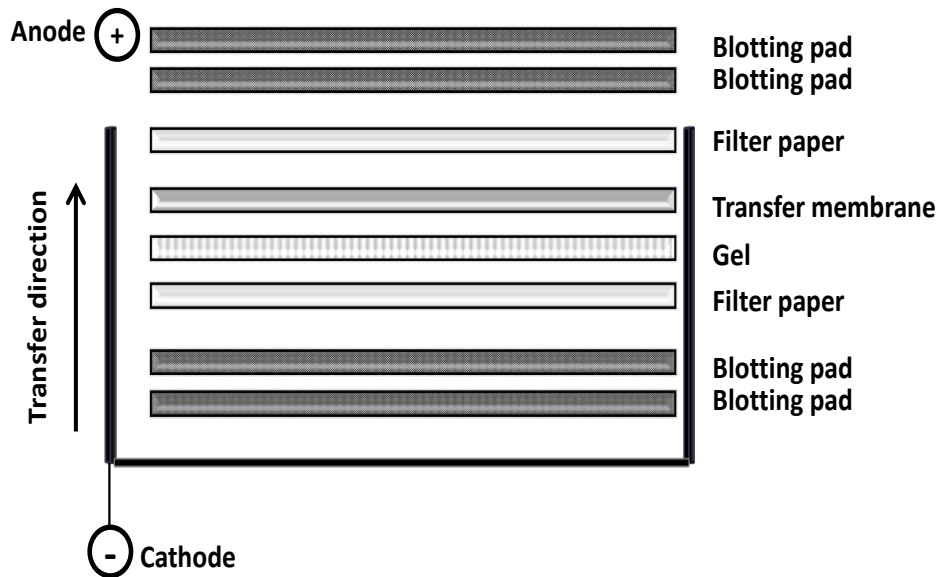


**Figure 2-6 Single sandwich**

The diagram illustrates protein transfer during immunoblotting.

### **2.11.6 Membrane immunolabelling and visualisation using the Li-Cor Odyssey system**

To minimise non-specific binding, membranes were blocked in 50:50 (v/v) Odyssey blocking buffer (Li-Cor Cat # 927-4000): 10 mM TBS pH 7.6 at ambient temperature on a plate rocker for 1h. Membranes were then probed with 5-8mL of pre-titrated primary antibody diluted in TBS+0.1% (v/v) Tween-20. All primary antibody incubations were performed on a rocking platform overnight at 4°C. Membranes were then washed 3x for 5 min in TBS+0.1% (v/v) Tween-20 prior to addition of 10mL appropriate infra-red secondary antibodies (Table 2-2) for 1h at ambient temperature on a rocker. Membranes were washed as for primary antibody and then washed 3x for 5 min with TBS prior to visualization using an Odyssey™ Infra-red Imaging system (Li-Cor). Densitometry was performed using Image Studio 4.0 software and protein expression was normalised relative to  $\beta$ -actin (housekeeping control protein).

### **2.11.7 Membrane stripping and re-probing**

PVDF Membranes were incubated in 5mL of 1x western blot recycling reagent (Autogen Bioclear) for 20-30 min at ambient temperature on an orbital shaker. Membranes were then washed in TBS, re-blocked with 50:50 (v/v) Odyssey blocking buffer: TBS.

### **2.11.8 Detection of Reactive oxygen species using H<sub>2</sub>DCFDA**

6-carboxy-2', 7'-dichlorodihydrofluorescein diacetate (H<sub>2</sub>DCFDA) (Invitrogen Cat # c2938) is a cell permeable, chemically reduced, acetylated form of fluorescein used as an indicator for reactive oxygen species (ROS) in cells. This non-fluorescent molecule is readily converted into a green-fluorescent form when the acetate groups are removed by intracellular esterases and ROS-associated oxidation within the cell. As it is oxidation sensitive, H<sub>2</sub>DCFDA was reconstituted in oxygen-free conditions (in a nitrogen environment) before aliquoting and storage at -80°C, as recommended by the manufacturer (Figure 2-7).

Cells were treated with chemotherapeutic drugs as described in section 2.7. Thereafter, cells were first washed with PBS to remove any culture medium and were then treated with 5  $\mu$ M of H<sub>2</sub>DCFDA in pre-warmed (37°C) PBS for 30 min 37°C in 5% CO<sub>2</sub>. The reduced forms of the substrate lack any fluorescence until acetyl groups are removed by intracellular esterases and oxidation is occurring in the cell. When this occurs, the charge of the molecule makes much less likely to leave the cell and it emits detectable fluorescence. Following treatment with H<sub>2</sub>DCFDA for the indicated time periods, fluorescence was measured on a FLUOstar OPTIMA (BMG Labtech) plate reader at excitation 485 nm/

emission 520 nm, following calibration of the reader using the gain function on the MARS software to ensure the measurements were taken within the dynamic range of the instrument.

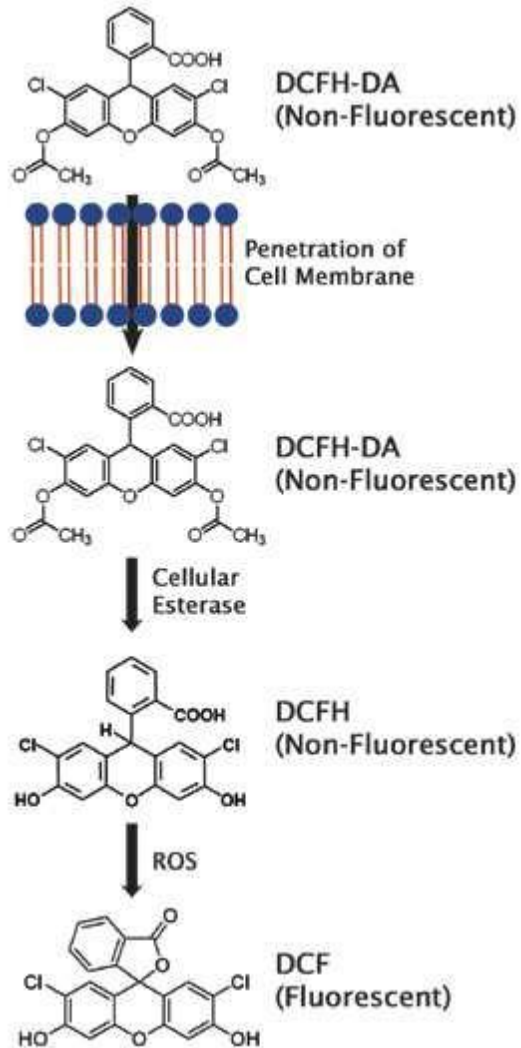


**Figure 2-7 Conversion of non-fluorescent dye DCFH-DA in the fluorescent dye DCF by ROS**

<http://www.cellbiolabs.com/reactive-oxygenspecies-ros-assay>

## 2.12 Flow Cytometry

### 2.12.1 Background

Flow cytometry is used to analyse the chemical/physical characteristics of particles and cells, and has several applications, including quantification of specific cellular proteins and detection of dead or alive cells. The particles/cells are detected by movement at high speed by exposure to a laser beam, and a computer analyses their characteristics and properties.

### 2.12.2 Detection of the mitochondrial membrane potential

One of the early events in apoptosis is the depolarisation of electrochemical gradient of the inner mitochondrial membrane, providing a valuable indicator of the cells' health and functional status (Perelman *et al.*, 2012).

Mitochondrial membrane potential was measured using the MitoProbe™ JC-1 Assay Kit (Life Technologies Ltd. Cat # M34152). This assay contains 5', 6, 6'- tetrachloro-1, 1', 3, 3'-tetraethyl-benzimidazolylcarbocyanine iodide (JC-1). JC-1 dye is a lipophilic dye that accumulates and is dependent on the mitochondrial membrane potential in the mitochondria. At a low membrane potential, mitochondria take up very little of the dye and the dye remains in its monomeric green fluorescent form. A high mitochondrial membrane potential leads to the accumulation of JC-1 and formation of so-called J-aggregates that emit red fluorescence (Smiley *et al.*, 1991). The degree of mitochondrial depolarisation is determined by fluorescence measurements using flow cytometry (Figure 2-8). Differences in membrane potential are established by a shift in the fluorescence emission from green to red in depolarised mitochondria to polarised (Cossarizza *et al.*, 1993; Smiley *et al.*, 1991). The events can be visualised by flow cytometry using scatter diagrams ("dot plots"), where each cell appears as a point in a two-dimensional x / y diagram. Different cell populations can be detected depending on size (FSC) and granularity (SSC) and marking ("gating") can be employed. The state of the mitochondrial membrane potential was determined by staining keratinocyte cells with JC-1. The events in the green fluorescence channel (fluorescence of JC-1 monomers) were plotted on the x-axis against the red fluorescence channel (J-aggregates) on the y-axis. Comparisons were made with non-treated cells (negative controls) and cells treated with carbonyl cyanide m-chlorophenyl hydrazine (CCCP) as a positive control (Bortoletto *et al.*, 2004; Cossarizza *et al.*, 1993).

Cells were treated with chemotherapeutic drugs as in section 2.7. Following this, cells were stained with JC-1 according to the manufacturer's protocol and analysed using

subsequent flow cytometry. Cells were washed with EDTA for approximately 2 min and collected after incubation with 1x Trypsin-EDTA for approximately 3 min. Then cells were centrifuged at 1200 rpm for 5 min and resuspended in medium. Living-control cells were left untreated and damage-control cells were treated with 1  $\mu\text{L}$  CCCP (included in the MitoProbe™ JC-1 Assay Kit) 5 min before staining to induce mitochondrial membrane depolarisation. Then 10  $\mu\text{L}$  of JC-1 (of final concentration 2  $\mu\text{M}$ ) was added to medium. Cells were incubated at 37°C with 5%  $\text{CO}_2$  and 95% air for 30 min. JC-1 fluorescence at  $\sim 525$  nm (JC-1 “green”) and  $\sim 590$  nm (JC-1 “red” or “J-aggregates”) was determined for each sample. Cellular fluorescence was determined 12h, 24h, 36h and 48h after treatment by flow cytometry and for each sample, a minimum of 20,000 events was recorded. JC-1 fluoresces green when the mitochondrial potential is lost as they are depolarised in the dead cells. However, in living cells with intact mitochondria (mitochondrion is polarised) JC-1 is reduced and forms aggregates, which are detected by red fluorescence. Cells were acquired on an EasyCyte (Guava) flow cytometer and data were analysed by Cyte 26 Guava software (Millipore).

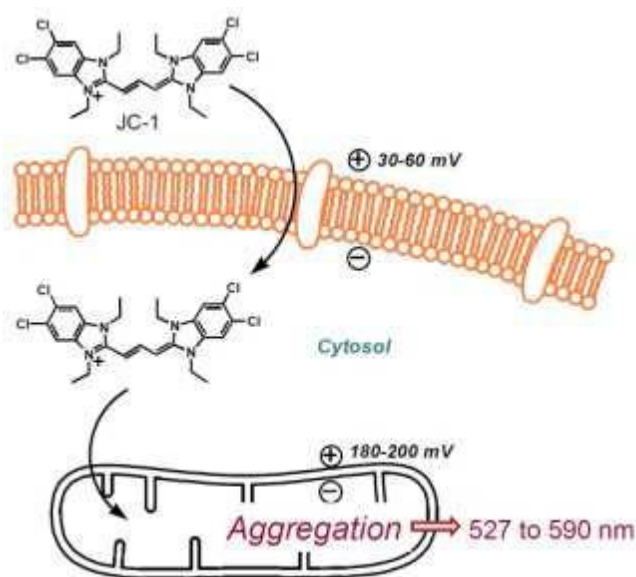


**Figure 2-8 Mechanism of action of the JC1 dye**  
<http://lcbim.epfl.ch/research>

### **2.12.3 Detection of oxidative stress**

In addition to spectrophotometry (section 2.11.8), intracellular reactive oxygen species (ROS) were detected by H<sub>2</sub>DCFDA dichlorodihydrofluoresceine-diacetate (Invitrogen Cat # c2938) using flow cytometry. Cells were seeded and left to adhere overnight, after which, cells were treated with the target compound (4-OH-CP, doxorubicin and docetaxel) for 2h (as optimised). The culture medium was aspirated and cells washed twice with PBS at room temperature. 5  $\mu$ M of H<sub>2</sub>DCF-DA (optimised by pre-titration experiments) was diluted in PBS or Phenol Red-free/serum-free medium. Treatments were performed for no more than 30 min at 37°C. Then the PBS containing H<sub>2</sub>DCF-DA was aspirated and the samples were washed twice with PBS. Cells were then harvested using Trypsin/EDTA, centrifuged at 1200 rpm for 5 min, supernatants removed, the pellets washed once in 500  $\mu$ L PBS, centrifuged and resuspended in cold PBS, then kept on ice until acquisition. Flow cytometry was performed in the green fluorescence channel. Data were collected from at least 10,000 cells per treatment/condition. Treated cells in which induction of ROS occurred demonstrated a shift to green fluorescence that was detected by flow cytometry.

### **2.12.4 Cell cycle analysis by propidium iodide (PI) labelling**

In culture, cells are asynchronous populations, i.e. a mixed population of cells in all four distinct cell cycle phases G<sub>0</sub>/G<sub>1</sub>, S, G<sub>2</sub> and M phases. Cell cycle analysis is used to determine the relative cellular DNA content, which enables discrimination between the different phases of the cell cycle. Cell cycle measurement and distribution were performed by flow cytometry using propidium iodide (PI) (Sigma Cat # P4170), which is an intercalating agent and a fluorescent molecule that can be used to stain DNA. PI binds to DNA by intercalating between the bases, forming complexes with double stranded DNA and RNA. RNase is used in cell cycle analysis to ensure that the PI staining is DNA-specific.

Cells were treated with chemotherapeutic drugs as in section 2.7 and incubated for the indicated periods. Cells were harvested and thoroughly resuspended in solution (ensuring single cell suspension), and cells were washed twice in ice-cold PBS. The pellet was resuspended by the addition of ice-cold 70% ethanol, and then the samples were incubated for 1.5h on ice or overnight at 4°C (at this stage samples could be kept at 4°C for ~1 week). Then the fixed cells were centrifuged at 1500 rpm for 5 min at 4°C. The ethanol was aspirated and the cells pellet were washed with PBS and centrifuged at 1500 rpm for 5 min at 4°C. The residual PBS was removed and the cell pellet was resuspended gently in 200  $\mu$ g/mL PBS containing RNase (Sigma Cat # R4875). Following this, 20  $\mu$ g/mL of PI in

PBS was added and incubated for 30 min at 37°C. The samples were analysed by flow cytometry to determine PI (red staining) in the FL2 (yellow) channel. In total, three independent experiments were conducted. Guava cell cycle analysis software was used following sample acquisition on a Guava easyCyte™ system (Millipore) (Figure 2-9).

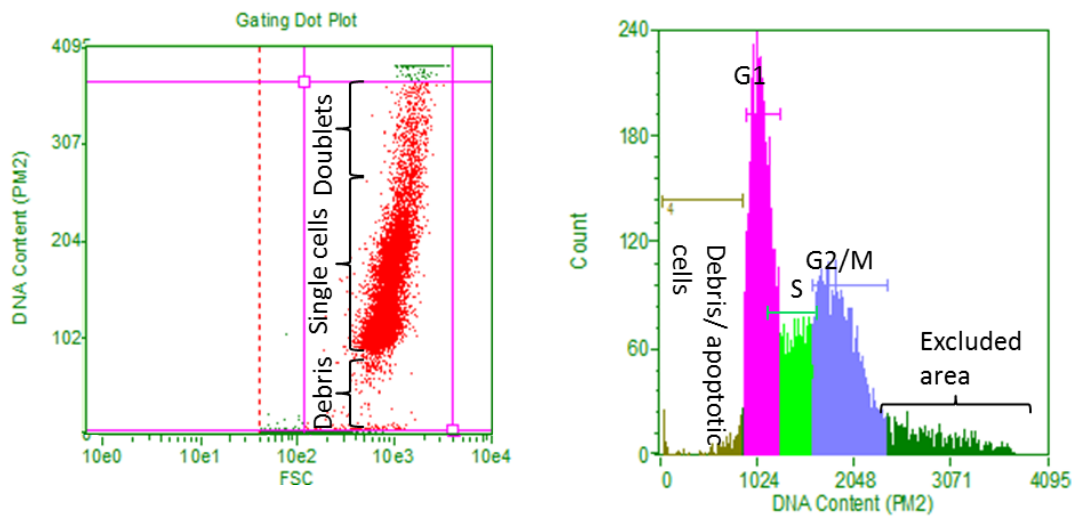


**Figure 2-9 Change in the cell cycle were determined by PI staining**

## 2.13 Statistical analysis

Data analysis was carried out using Excel® (Microsoft) and most results presented as the mean of all replicates (minimum 5-6), with error bars representing  $\pm$  the standard error of mean (S.E.M.). Statistical analysis was performed using Minitab 16 statistical software. Two tailed, paired, or unpaired t-tests were used to compare two sample means with levels of significance cited in the text. Comparisons were assumed to be biologically significant where  $*, p < 0.05$ .

**CHAPTER 3: Effect of cancer chemotherapy drugs on the viability of human keratinocyte cell lines and the effect of cooling on drug-mediated cytotoxicity**

### 3.1 Background

Chemotherapy-induced alopecia (CIA) is the most common and distressing side effect of anticancer chemotherapy (Wang *et al.*, 2006) and the anxiety caused by the prospect of CIA can cause patients to even refuse treatment in certain cases (Münstedt *et al.*, 1997). Thus development of an effective CIA preventative regime represents an important challenge in oncology (Paus *et al.*, 2013). CIA occurs due to damage to the HFs, which comprise various cell types including hair matrix keratinocytes, which represent the most rapidly dividing HF cell subset that contributes to HF structure and function and in particular hair generation (Roh *et al.*, 2005). As chemotherapeutic drugs such as taxanes (e.g. docetaxel), alkylating agents (e.g. cyclophosphamide) and anthracyclines/DNA intercalating agents (e.g. doxorubicin) target cancer cells due to their rapid division rate, these drugs also target the matrix keratinocytes and induce their apoptosis, which results in hair loss (Paus *et al.*, 2013).

Currently the only available preventative treatment for CIA is head (scalp) cooling. Scalp cooling (or scalp hypothermia) during the administration of chemotherapy drugs can substantially reduce hair loss (Protiere *et al.*, 2002) and has been used since the 1970s (Dean, 1979). Clinically it has been shown that scalp cooling can substantially reduce the incidence of hair loss in response to individual drugs, including cyclophosphamide, doxorubicin and cisplatin (Breed *et al.*, 2011; Van Den Hurk *et al.*, 2012c). However, for combined treatment regimes, such as sequential treatment with docetaxel (taxotere), doxorubicin (adriamycin) and cyclophosphamide (clinically also referred to as TAC), scalp cooling has limited reported efficacy (Grevelman and Breed, 2005). Despite the fact that scalp cooling can be effective, its overall mechanism of action is not fully understood.

In order to improve the efficacy of scalp cooling, particularly in the case of combinatorial drug treatments that do not respond well to cooling (such as TAC), it is necessary to achieve a better understanding of the cellular mechanisms that underlie drug-induced cytotoxicity and study the effects of cooling in this context. Several experimental *in vivo* models have been used to help understand CIA; however, rodent-based models demonstrate inherent physiological and practical limitations (Paus *et al.*, 2013). *Ex vivo* models, such as those established by Paus and colleagues that are based on isolation and culture of human HFs, represent an elegant model for studying cyclophosphamide-induced CIA (Bodo *et al.*, 2007). A more reductive model to study chemotherapy drug-induced cytotoxicity involves the use of human neonatal epidermal keratinocytes cultured *in vitro* and a previous report has provided some, though limited, evidence for an effect of culture

temperature on the cytotoxicity of doxorubicin on such cells (Janssen *et al.*, 2008). The principle behind the use of human epidermal keratinocytes is that they are maintained under culture conditions that render them highly proliferative, thus resembling (in terms of growth characteristics) the rapidly dividing population of native matrix keratinocytes. However, because of the finite nature of such primary cultures, the well-characterised cell line HaCaT, that shows similar characteristics and cell behaviour to normal keratinocytes ((Deyrieux and Wilson, 2007); and references therein), has also been used to study drug-induced cytotoxicity (Luanpitpong *et al.*, 2011).

## 3.2 Chapter Aims

- Establish biological models that will allow the study of chemotherapy drug-induced cytotoxicity *in vitro*. The *in vitro* models established included: a) normal human epidermal keratinocytes (NHEK), b) human hair follicular keratinocytes (HHFK), c) the keratinocyte cell line HaCaT and d) HaCaT derivatives that were gradually adapted to culture conditions identical to those for NHEK cells (serum-free and low-calcium medium).
- Examine the cytotoxicity of a panel of commonly used chemotherapeutic modalities and the effect of temperature on cytotoxicity
- Perform systematic investigations on the optimal culture temperature (cooling conditions), which achieve optimal rescue from drug induced cytotoxicity after administration of a panel of chemotherapeutic agents.
- Examine the cytotoxicity and ability of cooling to cytoprotect for combinations of chemotherapy drugs (such as TAC, TCA, FAC, and AC).

### **3.3 The effect of chemotherapy drugs on normal human epidermal keratinocyte viability and the role of cooling on drug-mediated cytotoxicity**

A single, and very limited, study has previously addressed the effect of chemotherapy drugs on normal human epidermal keratinocytes (NHEKs) and examined the effect of cooling conditions on doxorubicin-mediated cytotoxicity on NHEKs (Janssen *et al.*, 2008). NHEK cells were cultured in low calcium (0.09 mM) serum-free medium, under conditions where they adopt a highly-proliferative basal, non-differentiated phenotype. In this work for the first time the cytotoxic effect of a panel of three routinely used cancer chemotherapy drugs were assessed (Grevelman and Breed, 2005), in particular the taxane docetaxel, the anthracycline doxorubicin and the alkylating agent cyclophosphamide, all of which are associated with CIA. Because *in vivo* cyclophosphamide requires enzymatic conversion to its active form 4-hydroxy-cyclophosphamide (4-OH-CP), was used in our study and as previously described elsewhere (Bodo *et al.*, 2007).

The effect of each of these drugs over a wide range of concentrations at standard culture temperature 37°C and, to mimic cooling conditions, at 22°C was examined. This was primarily because it has been suggested by various studies that a scalp temperature of 22°C or less is required for hair preservation (Komen *et al.*, 2013a) and also it was the temperature previously tested *in vitro* by Janssen *et al.* (2008). As shown in Figure 3-1, all three drugs caused increasing cytotoxicity (indicated by loss of viability) in NHEKs in a dose-dependent fashion, although in the case of docetaxel the maximum relative loss of cell biomass was ~75%. Also the results confirmed that the decrease in biomass was the result of active induction of cell death (apoptosis) using apoptosis detection assays (not shown). Interestingly, and despite the fact that these drugs act *via* different molecular mechanisms, cooling dramatically rescued cells from cytotoxicity for all three compounds (Figure 3-1, upper panels), with the observation for doxorubicin being in agreement with previous studies (Janssen *et al.*, 2008). The ability of cooling to protect from cytotoxicity was striking for several, mid-range drug concentrations, particularly for doxorubicin and 4-OH-CP; in fact for some drug doses cell biomass returned from below 20% to nearly 100% of the control value (Figure 3-1, lower panel).

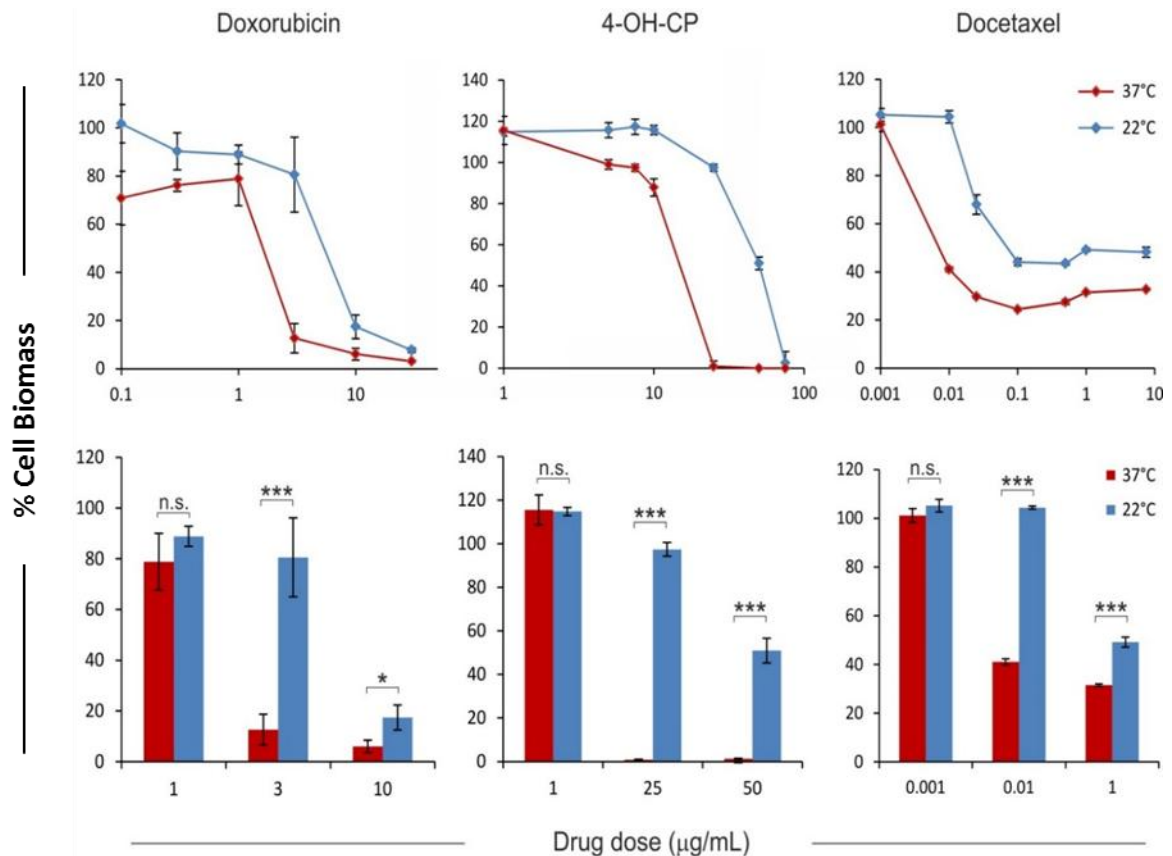


**Figure 3-1 Cytoprotective role of cooling against chemotherapy drug-mediated toxicity in NHEK cells**

NHEK cells (passages 1–3) were seeded in 96 well plates at 7500 cells/well in KSFM medium and were incubated overnight at 37°C/5% CO<sub>2</sub>. NHEK cells were treated for 2h with a range of concentrations of doxorubicin, 4-OH-CP, and docetaxel at 37°C and 22°C (representing normal and cooling conditions, respectively) compared with vehicle control (cells treated with medium containing DMSO, in which the reagent was dissolved). The solvent represents the maximum amount of DMSO corresponding to the highest drug concentration). The drugs were then removed, wells were rinsed with PBS to remove any traces of drug and cultures incubated for a further 72h, and after which 20 µL of CellTiter 96® AQueous One solution was added to the wells and plates were incubated at 37°C in 5% CO<sub>2</sub> for a total of four hours. Absorbance was measured spectrophotometrically at a wavelength of 492nm and % cell biomass was calculated as described in Materials and Methods (Chapter 2). Representative results from the dose response curves (upper panels) are also shown in bar graph form (lower panels) for clarity and presentation of statistical significance. Data points correspond to mean % cell biomass (±S.E.M.) for three independent biological experiments, each consisting of 6–8 technical replicates. n.s., non-significant; \*,  $p < 0.05$ ; \*\*\*,  $p < 0.001$ .

### **3.4 The cytotoxicity of chemotherapy drugs on human hair follicular keratinocytes and the effect of cooling on drug-mediated effects**

A potential weakness of our approach of using 'generic' keratinocytes of epidermal origin is that such cells, despite their ability to grow as a basal, highly-proliferative cell population (thus mimicking in terms of their growth characteristics the rapidly-dividing population of native matrix keratinocytes), they are not specifically isolated from the HF area. To circumvent this limitation, we used the only Human Hair Follicular Keratinocyte (HHFK) cultures currently commercially available (see Materials and Methods section 2.7). Upon routine culture and observation, HHFK cells showed virtually identical morphological and growth properties to NHEK cells (not shown). When the effects of doxorubicin and 4-OH-CP were tested, as with keratinocytes of epidermal origin. The data showed that both drugs caused a dose-dependent cytotoxicity in HHFKs and cooling dramatically rescued HHFK cells from this significantly (Figure 3-2), the response of cells under cooling conditions was strikingly similar to that observed for NHEK cells for these drugs (Figure 3-1). Therefore, these experiments confirmed the validity of our approach of using NHEK cells as a representative keratinocyte *in vitro* model.

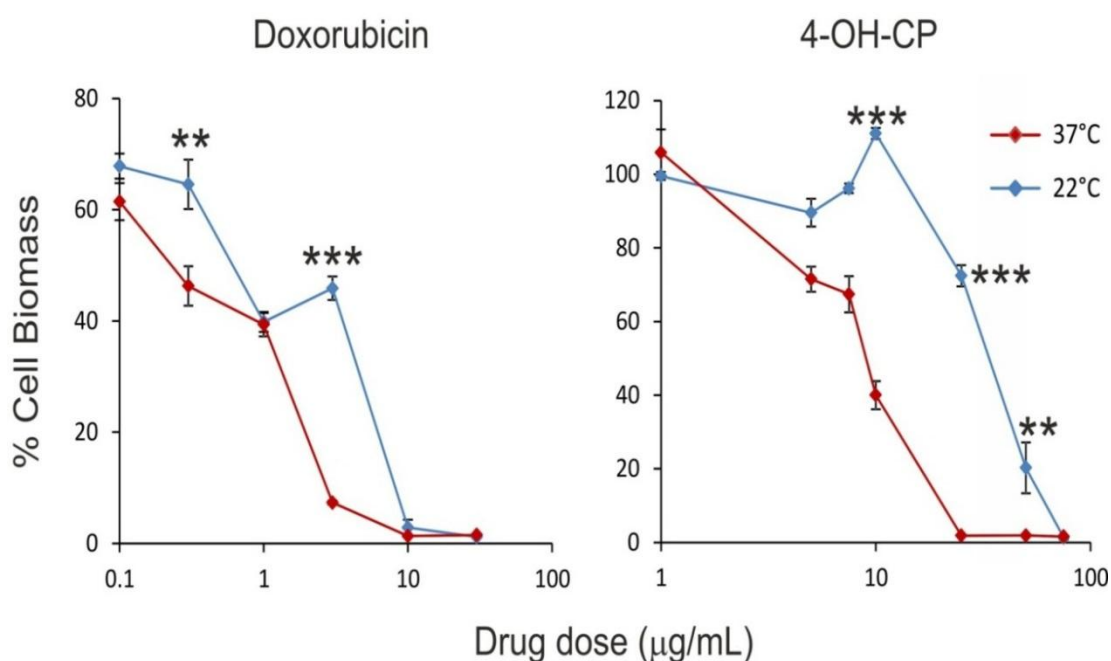


**Figure 3-2 Cytoprotective role of cooling against chemotherapy drug-mediated toxicity in HHFK cells**

HHFK cells (passages 1–3) were seeded in 96 well plates at 7500 cells/well in KSM medium and were incubated overnight at 37°C/5% CO<sub>2</sub>. HHFK cells were treated for 2h with a range of concentrations of doxorubicin and 4-OH-CP at 37°C and 22°C (representing normal and cooling conditions, respectively) compared with vehicle control (cells treated with medium containing DMSO, in which the reagent was dissolved). The solvent represents the maximum amount of DMSO corresponding to the highest drug concentration). The drugs were then removed, wells were rinsed with PBS to remove any traces of drug and cultures incubated for a further 72h, and after which 20 µL of CellTiter 96® AQueous One solution was added to the wells and plates were incubated at 37°C in 5% CO<sub>2</sub> for a total of four hours. Absorbance was measured spectrophotometrically at a wavelength of 492nm and % cell biomass was calculated as described in Materials and Methods (Chapter 2). Representative results from the dose response curves (upper panels) are also shown in bar graph form (lower panels) for clarity and presentation of statistical significance. Data points correspond to mean % cell biomass (±S.E.M.) for three independent biological experiments, each consisting of 6–8 technical replicates. \*\*,  $p < 0.01$ ; \*\*\*,  $p < 0.001$ .

### **3.5 The effect of the combinatorial chemotherapy treatment TAC on normal human keratinocyte growth and the role of cooling**

Having shown that cooling can protect keratinocytes from cytotoxicity caused by docetaxel, and particularly doxorubicin and cyclophosphamide, the combinatorial drug therapy TAC in this context was investigated. Clinical data demonstrate that, although scalp cooling provides good protection from CIA caused by these drugs when applied as monotherapies in the clinic (an observation mirrored by our *in vitro* findings), scalp cooling is less effective for patients undergoing the combinatorial use of these drugs, i.e. TAC therapy (Grevelman and Breed, 2005; Van Den Hurk *et al.*, 2012c).

To test for the first time *in vitro* the potential cytotoxic effect of the TAC regimen and assess the influence of cooling, cells were treated with docetaxel (T), doxorubicin (A) and 4-OH-CP (C) as detailed in Materials and Methods section 2.7.1. One approach ('TAC') involved sequential treatment with the individual drugs at doses for which significant or maximal *in vitro* rescue was achieved by cooling when each drug was tested separately (Figure 3-1). In an attempt to simulate drug exposure *in vivo* (as during TAC therapy infusion not all the previous drug would be expected to be cleared systemically by the time the subsequent drug is infused), two modifications of this protocol were also employed (as outlined in detail in section 2.7.1). Specifically, following initial treatment (T), cells were exposed to each subsequent drug (A and C) whilst being also supplemented with 10% (denoted 'TAC (+10%)') or 100% (denoted 'TAC (+100%)') of the previous drug. As shown in Figure 3-3, combinatorial treatment at 37°C resulted in nearly complete loss of NHEK biomass for all three TAC protocols. Notably, upon cooling (22°C), although substantial (in some cases 100%) rescue was previously observed for individual drug treatments (Figure 3-1), only a modest degree of cytoprotection was observed following the 'TAC' and 'TAC (+10%)' treatments. By contrast, cooling provided little detectable rescue from the extensive cytotoxicity observed following 'TAC (+100%)' treatment (Figure 3-3).

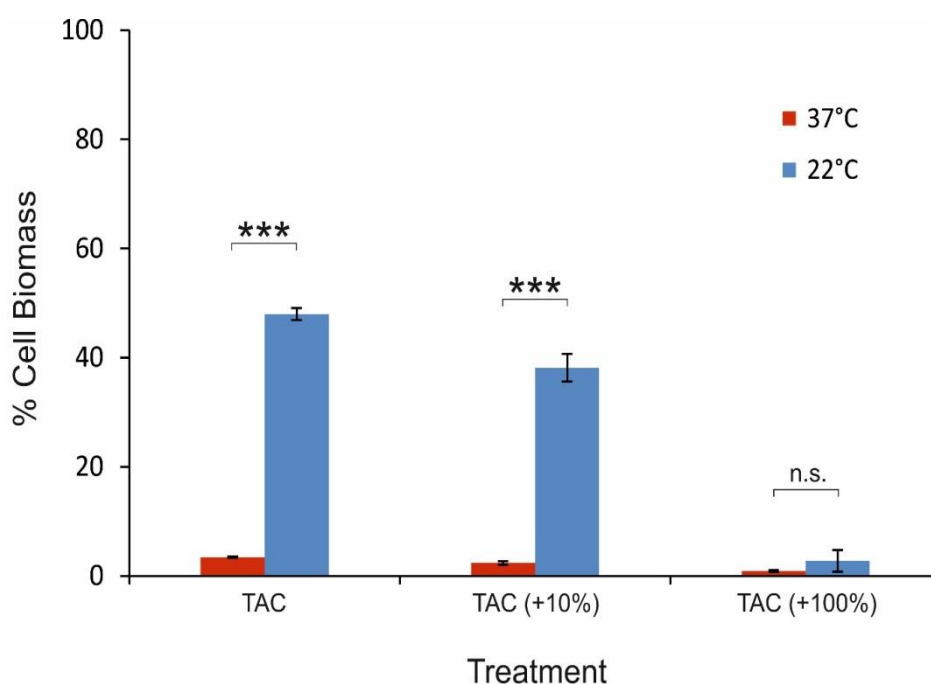


**Figure 3-3 Effect of cooling on TAC-mediated cytotoxicity in NHEK cells**

NHEK cells (passages 1–3) were seeded in 96 well plates at 7500 cells/well in KSM medium and were incubated overnight at 37°C/5% CO<sub>2</sub>. NHEK cells were treated with the combinatorial drug protocols ‘TAC’, ‘TAC (+10%)’ or ‘TAC (+100%)’ at 37°C and 22°C (representing normal and cooling conditions, respectively) compared with vehicle control (cells treated with medium containing DMSO, in which the reagent was dissolved). The solvent represents the maximum amount of DMSO corresponding to the highest drug concentration). The drugs were then removed, wells were rinsed with PBS to remove any traces of drug and cultures incubated for a further 72h, after which 20 µL of CellTiter 96® AQueous One solution was added to the wells and plates were incubated at 37°C in 5% CO<sub>2</sub> for a total of four hours. Absorbance was measured spectrophotometrically at a wavelength of 492nm and % cell biomass was calculated as described in Materials and Methods (Chapter 2). Representative results shown in bar graph form for clarity and presentation of statistical significance. Data points correspond to mean % cell biomass (±S.E.M.) for three independent biological experiments, each consisting of 6–8 technical replicates. n.s., non-significant; \*\*\*,  $p < 0.001$ .

### **3.6 Chemotherapy drug-mediated effects on HaCaT keratinocyte viability and the role of cooling**

Our observation that by using cooling conditions highly-proliferative, cultured normal keratinocytes (a) could be efficiently rescued from chemotherapy drug-induced cytotoxicity, yet (b) could only be protected to a limited degree from combinatorial TAC treatment, are concordant with the data reported in the clinic (Grevelman and Breed, 2005). However, the finite nature of these cells (NHEK and HHFK cells display a decrease in proliferative potential by passages 5–6 and senesce soon after) poses a significant experimental obstacle. Therefore the well-characterised, immortalised, non-malignant human keratinocyte line HaCaT was exploited, as it shows characteristics and behaviour similar to normal keratinocytes (Boukamp *et al.*, 1988) and has been used to study drug-induced cytotoxicity (Luanpitpong *et al.*, 2011).

Similarly to our studies using NHEK cells, the effect of the same panel of chemotherapy drugs on HaCaT cell growth and examined the potential protective role of cooling by comparing treatments at 37°C and, to mimic cooling conditions, at 22°C were assessed. Upon morphological examination, there was a clear correlation between drug concentration and number of phase-bright, non-adherent, apoptotic/dead cells; however, under cooling conditions there was a noticeable reduction in dead cell numbers for all three drugs, and particularly in the case of doxorubicin and 4-OH-CP. These observations are illustrated in Figure 3-4, which shows representative phase contrast photomicrographs of HaCaT cultures 72h after treatment with doxorubicin, 4-OH-CP and docetaxel at both temperature conditions. When the role of cooling over a wide range of drug concentrations using cell biomass assays was assessed, data showed that, in agreement with our NHEK experiments, cooling conditions provided significant and consistent protection against cytotoxicity (Figure 3-5). However, the observed cooling-mediated rescue from drug cytotoxicity, although occurring over a wide range of drug doses, was noticeably less dramatic in HaCaT (Figure 3-5) than in NHEK (Figure 3-1) and HHFK cells (Figure 3-2).

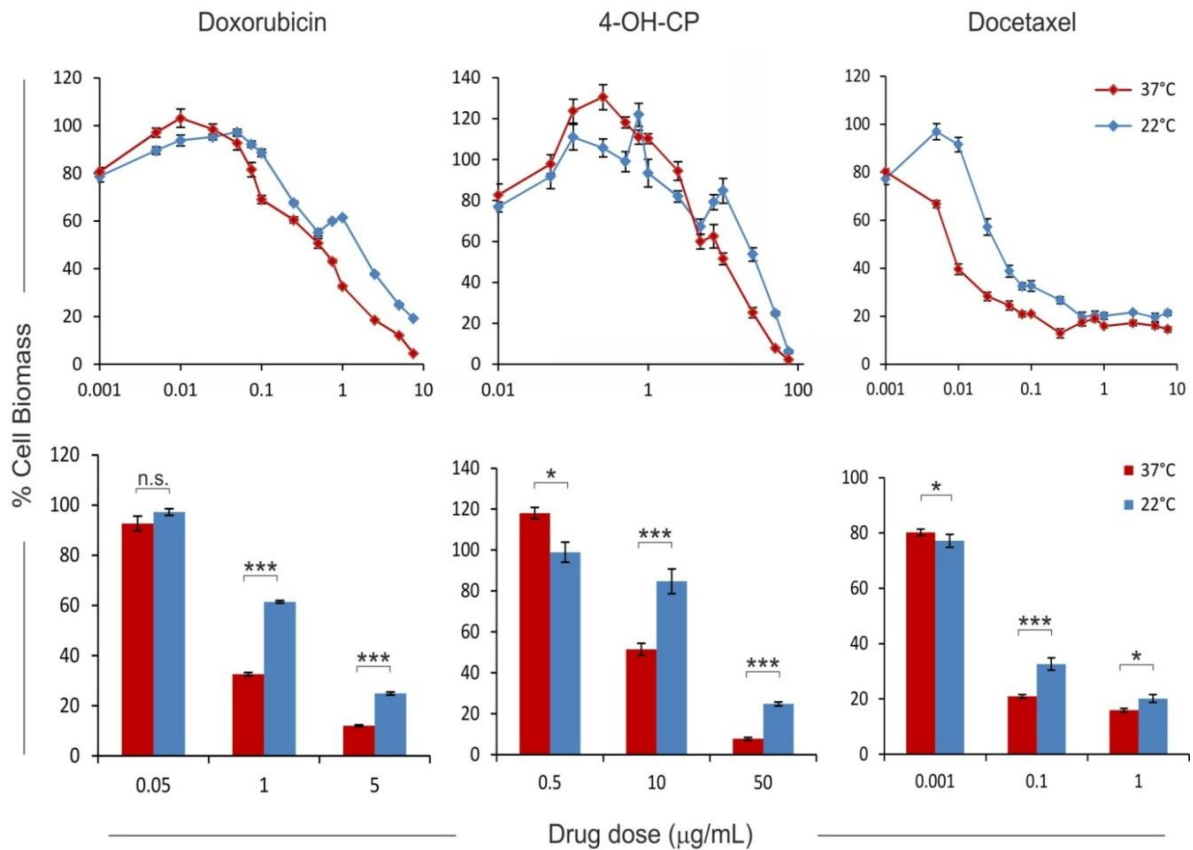
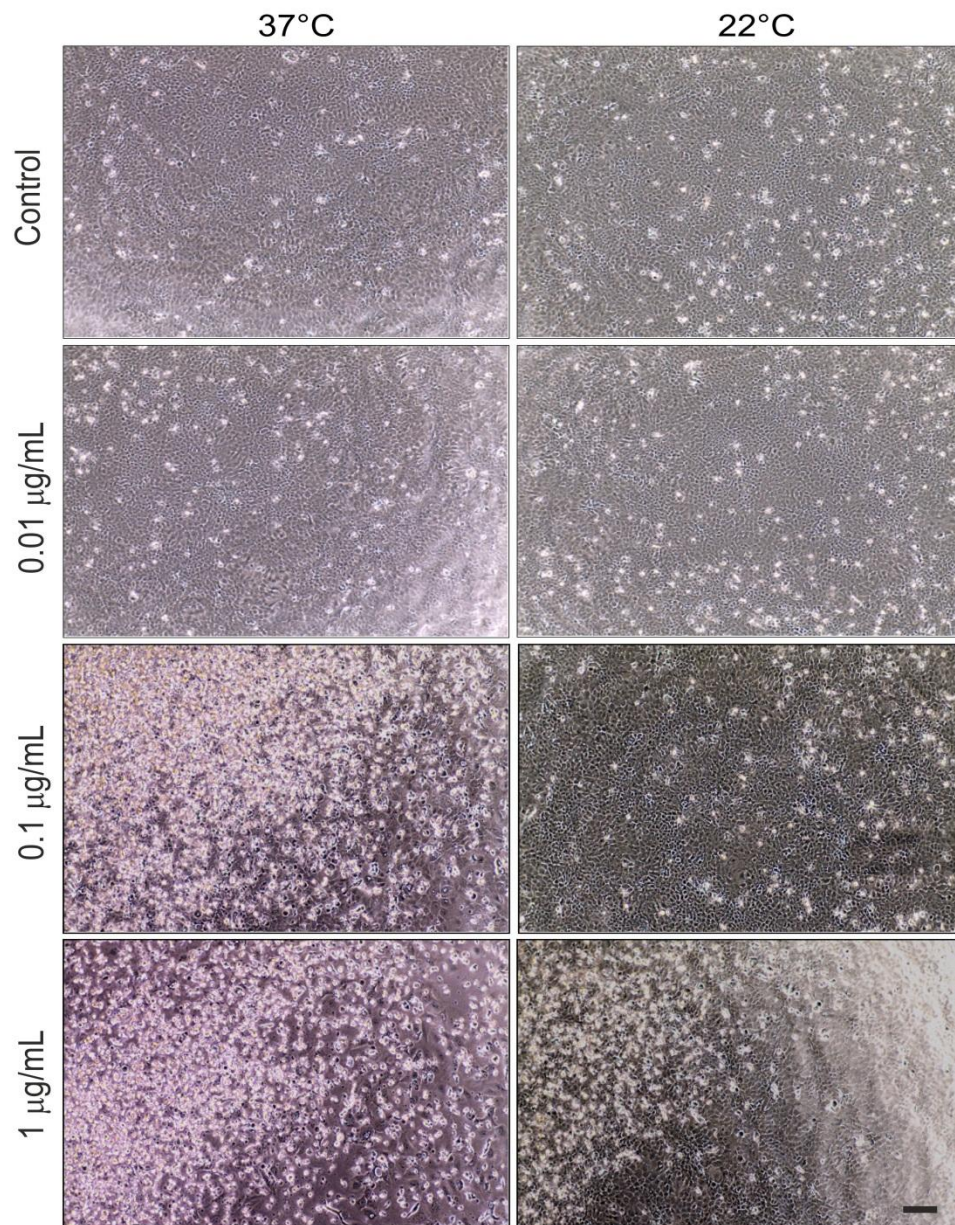


**Figure 3-4 Cytoprotective role of cooling against chemotherapy drug-mediated toxicity in HaCaT cells**

HaCaT cells were seeded in 96 well plates at 5000 cells/well in DMEM medium supplemented with 5% FBS and 1% LG were incubated overnight at 37°C/5% CO<sub>2</sub>. HaCaT cells were treated for 2h with a range of concentrations of doxorubicin, 4-OH-CP, and docetaxel at 37°C and 22°C (representing normal and cooling conditions, respectively) compared with vehicle control (cells treated with medium containing DMSO, in which the reagent was dissolved). The solvent represents the maximum amount of DMSO corresponding to the highest drug concentration). The drugs were then removed, wells were rinsed with PBS to remove any traces of drug and cultures incubated for a further 72h, after which 20 µL of CellTiter 96® Aqueous One solution was added to the wells and plates were incubated at 37°C in 5% CO<sub>2</sub> for a total of four hours. Absorbance was measured spectrophotometrically at a wavelength of 492nm and % cell biomass was calculated as described in Materials and Methods (Chapter 2). Representative results from the dose response curves (upper panels) are also shown in bar graph form (lower panels) for clarity and presentation of statistical significance. Data points correspond to mean % cell biomass (±S.E.M.) for three independent biological experiments, each consisting of 6–8 technical replicates. n.s., non-significant; \*,  $p < 0.05$ ; \*\*\*,  $p < 0.001$ .

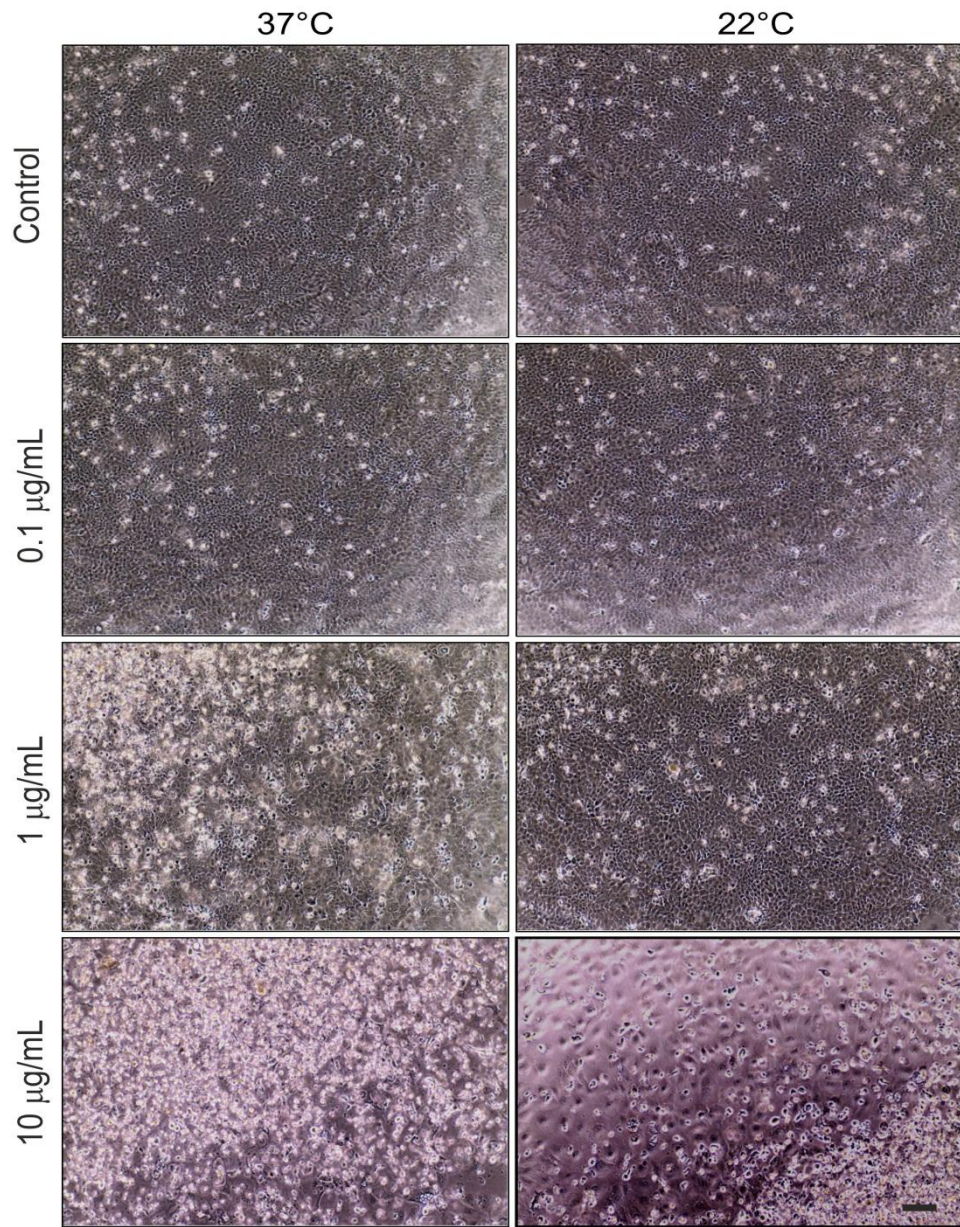
A

Doxorubicin



B

4-OH-CP



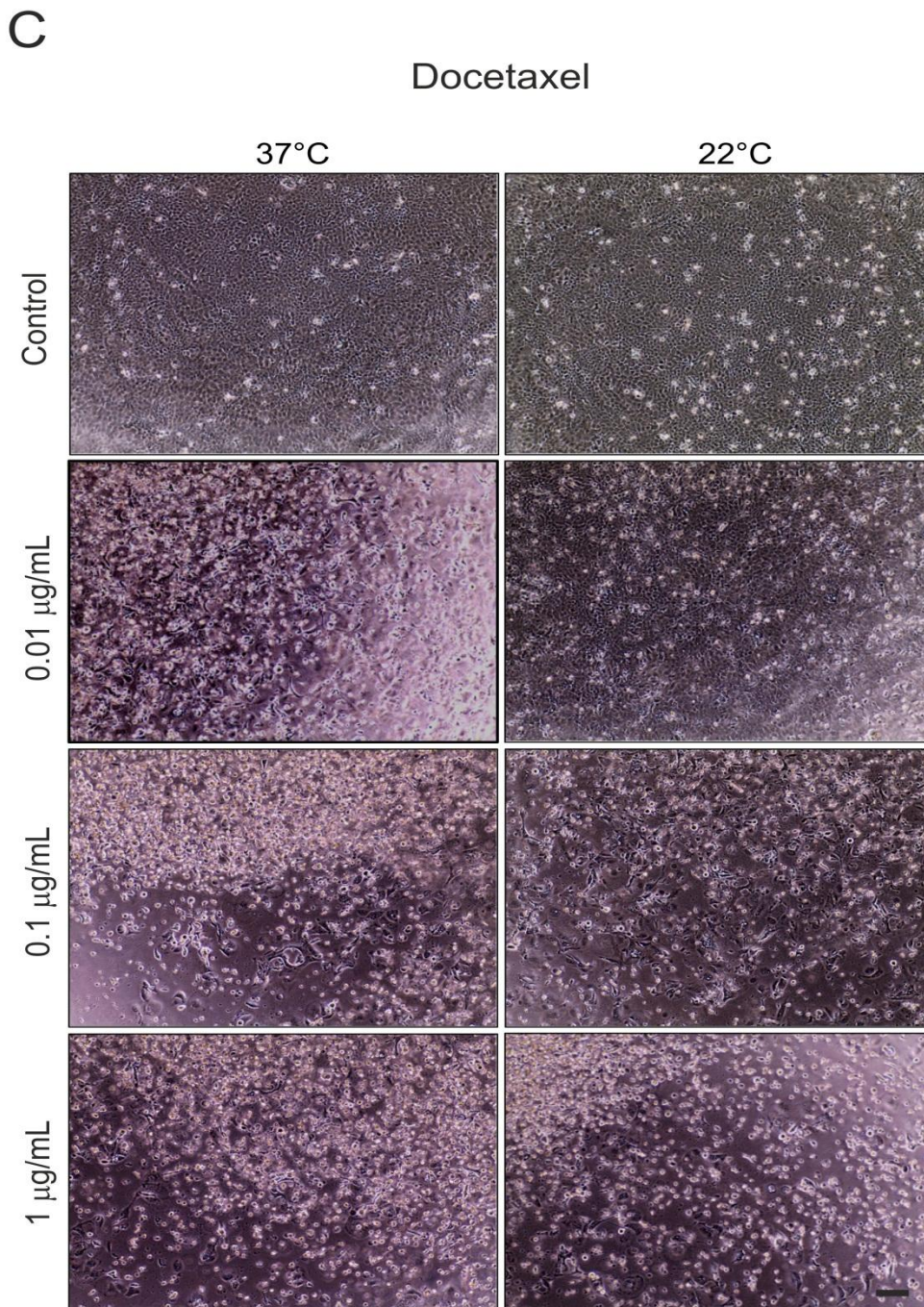


**Figure 3-5 Microscopic observation of cooling-mediated cytoprotection of HaCaT cells from chemotherapy drug-mediated toxicity**

HaCaT cells were treated with the indicated doses of doxorubicin (A), 4-OH-CP (B) and docetaxel (C) at 37°C and 22°C. Solvent alone-treated (control) HaCaT cultures served as negative controls. Phase contrast light microscopy was used to assess the viability of control and drug-treated cultures and representative photomicrographs are provided from two independent series of experiments. The presence of non-adherent, phase-bright cells following drug treatment was indicative of drug-mediated cytotoxicity. Phase contrast images were obtained using an EVOS XL core inverted microscope and at x100 magnification.

### **3.7 Adaptation of HaCaT keratinocytes to low-calcium, serum-free culture conditions and investigation of the role of cooling in chemotherapy drug-induced effects in the adapted cells**

The differences in the ability of cooling to protect primary NHEK and HFFK cells *versus* the HaCaT cell line from drug-induced cytotoxicity, with NHEK showing a far more pronounced 'response' to cooling, prompted us to investigate the possibility of adapting the HaCaT cell line to culture conditions identical to those of NHEK. A previous study has reported that reduction of calcium levels in serum-containing culture medium allows HaCaT cells to adopt a more basal, less differentiated phenotype (Deyrieux and Wilson, 2007), consistent with the important role of calcium in mediating keratinocyte differentiation. In order to render the HaCaT cell model more closely representative to primary cells, HaCaT cells were adapted to grow in both low calcium (0.09 mM) and serum-free conditions (KFSM medium) by sequential medium adaptation and passage, as described in detail in section 2.4.3 and this new cell line was named HaCaTa.

Figure 3-6A shows representative phase contrast photomicrographs of fully adapted HaCaTa cells during routine maintenance in comparison to the original HaCaT cell line as well as primary NHEK. By observing all three cell types at different culture densities (low, medium and high), it was apparent that HaCaTa cells exhibited a phenotype that was more representative of that of NHEKs. At low/medium densities (Figure 3-6A), upper and middle panels), HaCaT cells were less phase-bright, formed strong cell contacts and showed a clear tendency to form colonies; by contrast, HaCaTa cells were very phase-bright and showed reduced tendency to form cell contacts. The similarity of HaCaTa cells to NHEK was even more pronounced when cultures approached full confluence (Figure 3-6A, lower panels); at such density HaCaTa remained phasebright and were nearly indistinguishable from NHEK cultures. More importantly, when the proliferation rate of the HaCaTa derivative to the HaCaT line was compared, cell biomass assays demonstrated that adapted cells grew much more rapidly than the parental cell line, with HaCaTa showing a nearly 50% higher proliferation rate (Figure 3-6B), which was comparable to that of early-passage NHEK cells (not shown).

Then the response of the HaCaTa line to the same panel of chemotherapy drugs (above) and using the cooling regime (22°C) previously tested for HaCaT (and NHEK) cells was investigated. As shown in Figure 3-7, cooling during drug treatment provided consistent and significant protection from drug-mediated cytotoxicity for nearly all concentrations tested for doxorubicin, 4-OH-CP and, though to a lesser extent, docetaxel. Importantly, however, unlike our findings with HaCaT cells (Figure 3-4), the cytoprotection observed for HaCaTa

cells resembled more closely that seen with NHEK, with the results for 4-OH-CP (Figure 3-7) being particularly similar to those observed with NHEK (Figure 3-1). In support of our quantitative assays, phase-contrast microscopic observation of HaCaTa cells treated with 4-OH-CP at 37°C *versus* 22°C showed clear, cooling-mediated protection against drug-mediated cytotoxicity (Figure 3-8). Furthermore, the response of the HaCaTa line to 5-Fluorouracil (5-FU) and using the same cooling regime (22°C) was investigated. 5-FU is an anticancer drug that belongs to the family of drugs called antimetabolites and it is the most commonly used drug as first-line chemotherapy for various stages of colorectal cancer (Chansky *et al.*, 2005). Alopecia occurs at an estimated reported incidence of 10-50% after treatment with 5-FU (Batchelor, 2001). As shown in Figure 3-9 cooling during drug treatment provided a significant protection from 5-FU-mediated cytotoxicity for nearly all concentrations tested.

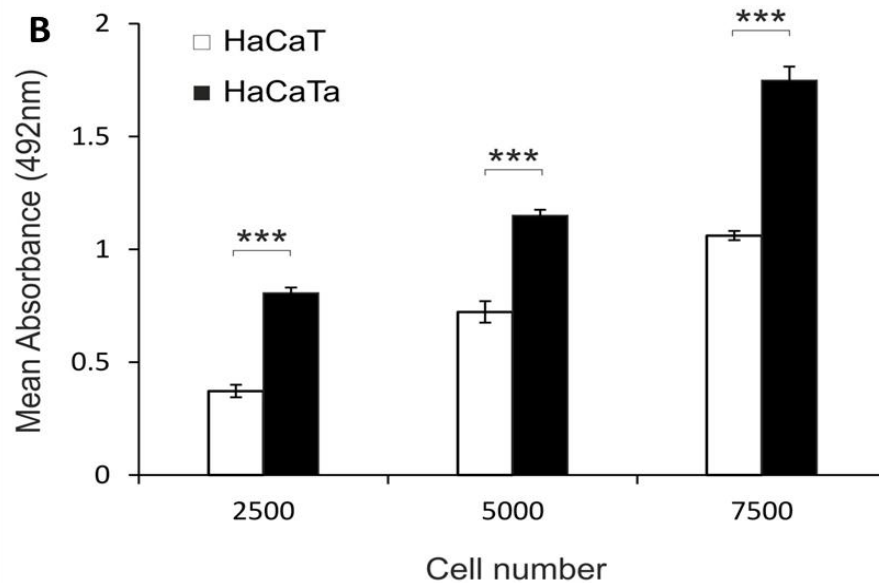
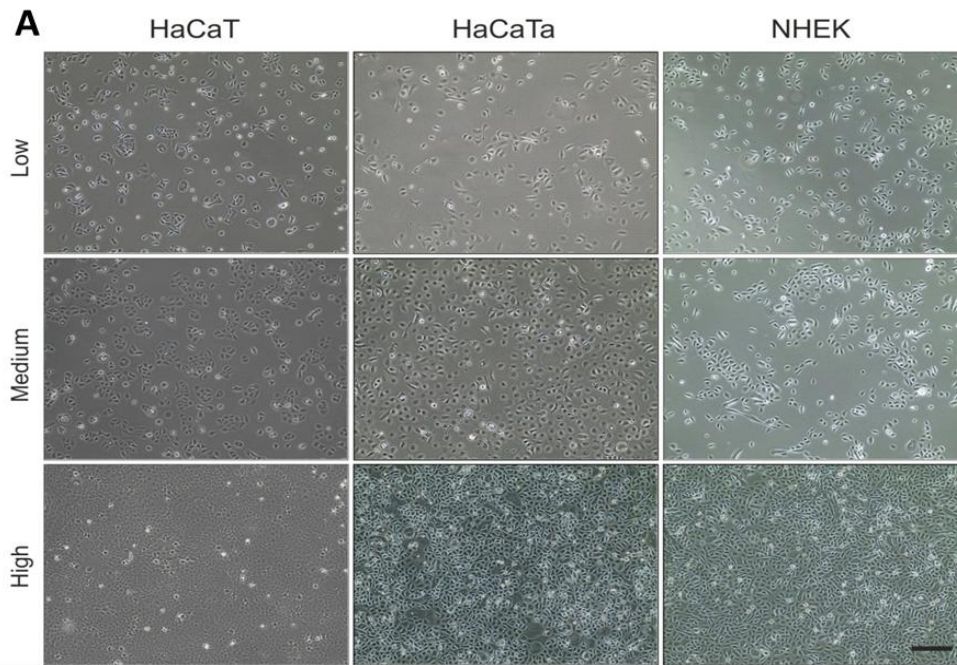


**Figure 3-6 Establishment of the HaCaTa cell line and assessment of its phenotypic and growth characteristics**

**(A)** The HaCaTa cell line was derived as described in the text and detailed in Section 2.4.3. HaCaTa derivatives, the original cell line HaCaT and primary NHEK cells at increasing cell densities ('Low', 'Medium' and 'High') under routine culture conditions were examined by Phase contrast images were obtained using an EVOS XL core inverted microscope and at x100 magnification and representative photomicrographs are provided. **(B)** Adapted HaCaTa and the original HaCaT cell line were seeded at the indicated cell densities ('Cell number' represents number of cells seeded per well) before cell growth was assessed 72h later on the basis of total cell biomass as described in section 2.7. Bars correspond to mean absorbance at 492 nm ( $\pm$ SD) for three independent biological experiments, each consisting of 6–8 technical replicates. \*\*\*,  $p < 0.001$ .

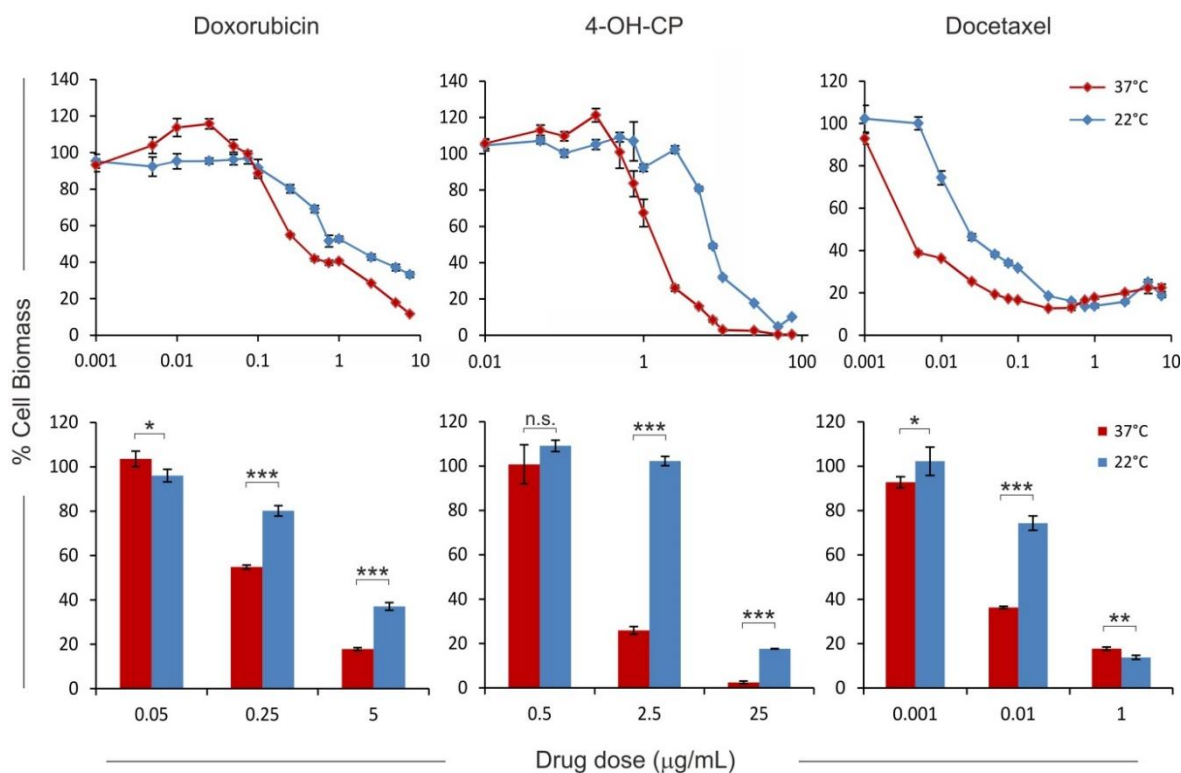


**Figure 3-7 Cytoprotective role of cooling against chemotherapy drug-mediated toxicity in HaCaTa cells**

HaCaTa cells were seeded in 96 well plates at 5000 cells/well in KFSM medium and were incubated overnight at 37°C/5% CO<sub>2</sub>. HaCaTa cells were treated for 2h with a range of concentrations of doxorubicin, 4-OH-CP, and docetaxel at 37°C and 22°C (representing normal and cooling conditions, respectively) compared with vehicle control (cells treated with medium containing DMSO, in which the reagent was dissolved). The solvent represents the maximum amount of DMSO corresponding to the highest drug concentration). The drugs were then removed, wells were rinsed with PBS to remove any traces of drug and cultures incubated for a further 72h, and after which 20 µL of CellTiter 96® AQueous One solution was added to the wells and plates were incubated at 37°C in 5% CO<sub>2</sub> for a total of four hours. Absorbance was measured spectrophotometrically at a wavelength of 492nm and % cell biomass was calculated as described in Materials and Methods (Chapter 2). Representative results from the dose response curves (upper panels) are also shown in bar graph form (lower panels) for clarity and presentation of statistical significance. Data points correspond to mean % cell biomass (±S.E.M.) for three independent biological experiments, each consisting of 6–8 technical replicates. n.s., non-significant; \*,  $p < 0.05$ ; \*\*,  $p < 0.01$ ; \*\*\*,  $p < 0.001$ .

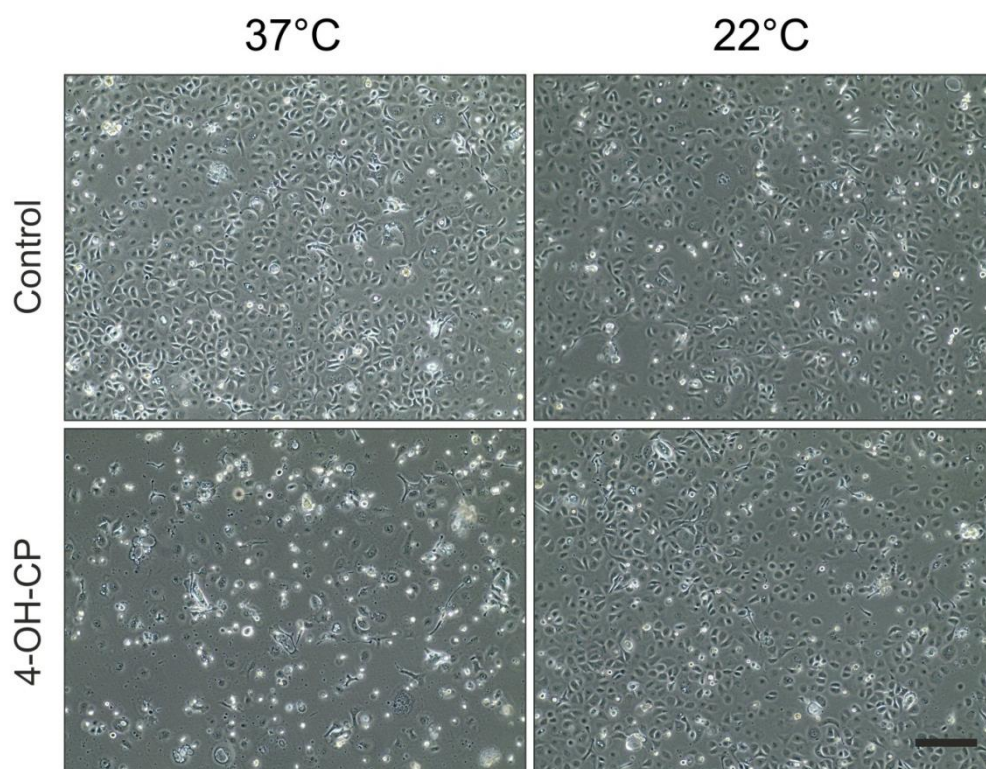


**Figure 3-8 Microscopic observation of cooling-mediated cytoprotection of HaCaT cells from chemotherapy drug-mediated toxicity**

HaCaTa cells were seeded in 10cm dishes and treated with 7.5  $\mu\text{g}/\text{mL}$  of 4-OH-CP at 37°C and 22°C as described in the section 2.7. Solvent alone-treated (control) HaCaTa cultures served as negative controls. Phase contrast images were obtained using an EVOS XL core inverted microscope at x100 magnification to assess the viability of control and drug-treated cultures 36h post-treatment and representative photomicrographs from two independent experiments are provided.

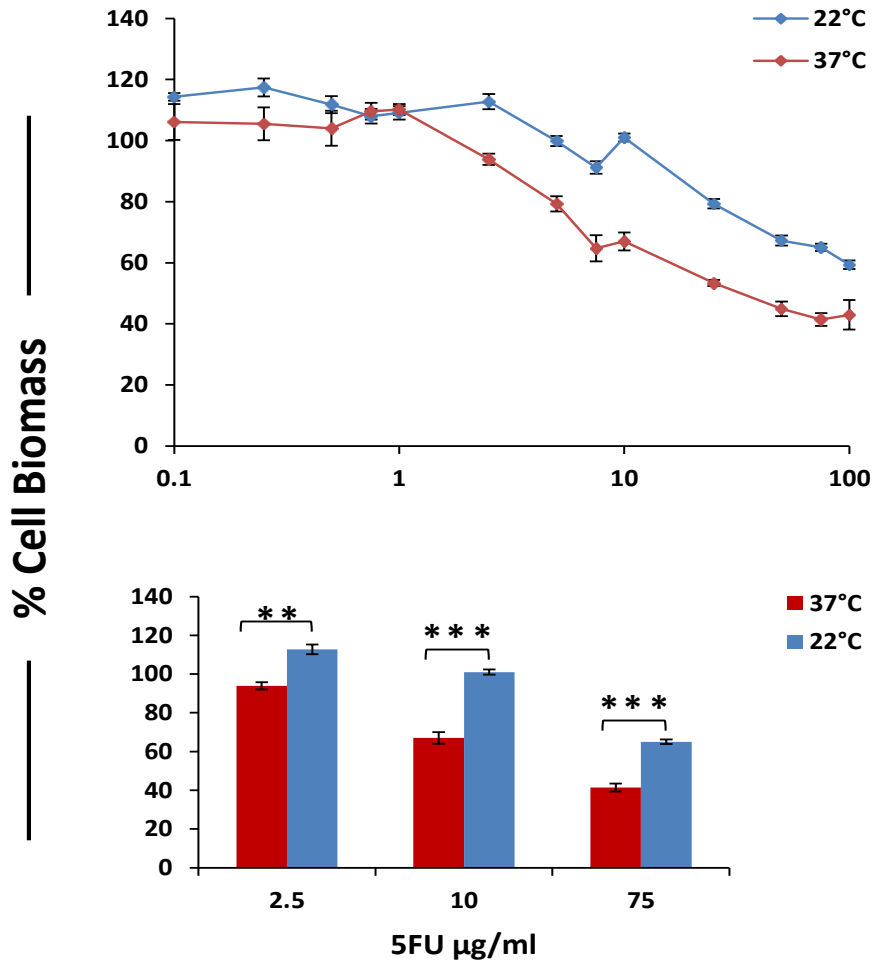


**Figure 3-9 Cytoprotective role of cooling against Fluorouracil (5FU)-mediated toxicity in HaCaTa cells**

HaCaTa cells were seeded in 96 well plates at 5000 cells/well in KSFM medium and were incubated overnight at 37°C/ 5% CO<sub>2</sub>. HaCaTa cells were treated for 2h with a range of concentrations of Fluorouracil (5FU) at 37°C and 22°C (representing normal and cooling conditions, respectively) compared with vehicle control (cells treated with medium containing DMSO, in which the reagent was dissolved). The solvent represents the maximum amount of DMSO corresponding to the highest drug concentration). The drugs were then removed, wells were rinsed with PBS to remove any traces of drug and cultures incubated for a further 72h, after which 20 µL of CellTiter 96® AQueous One solution was added to the wells and plates were incubated at 37°C in 5% CO<sub>2</sub> for a total of four hours. Absorbance was measured spectrophotometrically at a wavelength of 492nm and % cell biomass was calculated as described in Materials and Methods (Chapter 2). Representative results from the dose response curves (upper panels) are also shown in bar graph form (lower panels) for clarity and presentation of statistical significance. Data points correspond to mean % cell biomass (±S.E.M.) for three independent biological experiments, each consisting of 6–8 technical replicates. \*\*,  $p < 0.01$ ; \*\*\*,  $p < 0.001$ .

### **3.8 The effect of the combinatorial TAC chemotherapy treatment on HaCaTa cell viability and the role of cooling**

Our observations of TAC indicated that, unlike the parental cell line, HaCaTa cells closely resembled NHEK in their responses to chemotherapy drugs and in the extent of their protection by cooling, the effect of combinatorial treatment TAC on HaCaTa were tested. To do so, the previously tested three treatment regimes were followed, i.e. TAC, 'TAC (+10%)' and 'TAC (+100%)' and the drug concentrations chosen were doses that corresponded to the maximal observed cytoprotection upon cooling in HaCaTa cells (Figures 3-7 and 3-8). As shown in Figure 3-10, treatment with all TAC protocols caused substantial loss of cell growth, which was particularly evident following treatment using the 'TAC (+100%)' protocol. In concordance with our findings with NHEKs (Figure 3-2), some, though modest, cytoprotection by cooling was observed for the 'TAC' and 'TAC (+10%)' treatments (30–35% relative biomass). Moreover, cooling provided even less rescue from the extensive cytotoxicity observed following 'TAC (+100%)' treatment (Figure 3-10).

Collectively, our findings demonstrated that HaCaTa cells showed results that closely resembled those obtained with NHEK (and HHFK) cultures, attesting to the suitability of HaCaTa for our studies. Therefore, a large proportion of subsequent experiments performed in this thesis involved use of HaCaTa cells; however, where appropriate, important biological findings were confirmed using NHEK (and/or HHFK) cultures (see subsequent sections and chapters).

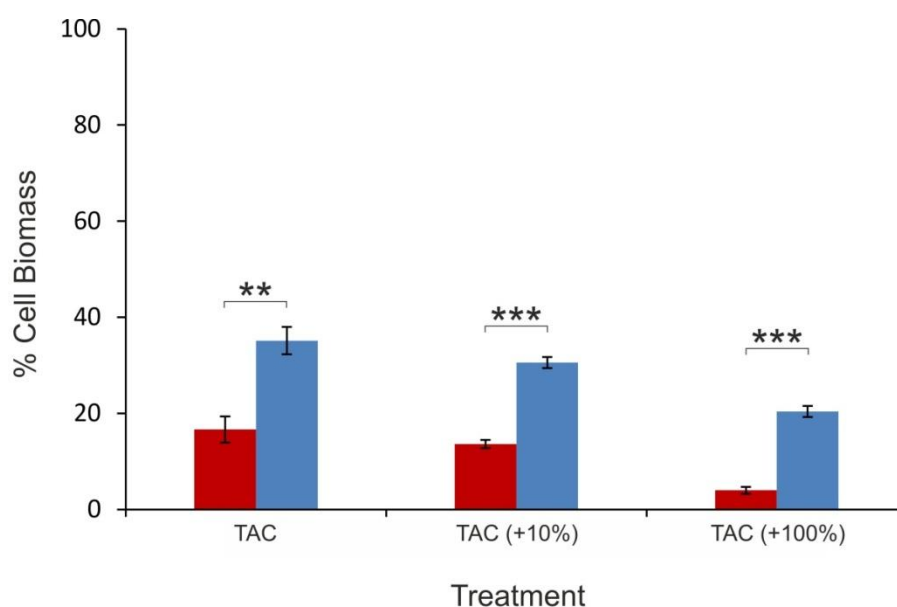


**Figure 3-10 Effect of cooling on TAC-mediated cytotoxicity in HaCaTa cells**

HaCaTa cells were seeded in 96 well plates at 5000 cells/well in KFSM medium and were incubated overnight at 37°C/5% CO<sub>2</sub>. HaCaTa cells were treated with the combinatorial drug protocols 'TAC', 'TAC (+10%)' or 'TAC (+100%)' at 37°C and 22°C (representing normal and cooling conditions, respectively) compared with vehicle control (cells treated with medium containing DMSO, in which the reagent was dissolved). The solvent represents the maximum amount of DMSO corresponding to the highest drug concentration). The drugs were then removed, wells were rinsed with PBS to remove any traces of drug and cultures incubated for a further 72h, after which 20 µL of CellTiter 96® AQueous One solution was added to the wells and plates were incubated at 37°C in 5% CO<sub>2</sub> for a total of four hours. Absorbance was measured spectrophotometrically at a wavelength of 492nm and % cell biomass was calculated as described in Materials and Methods (Chapter 2). Representative results shown in bar graph form for clarity and presentation of statistical significance. Data points correspond to mean % cell biomass (±S.E.M.) for three independent biological experiments, each consisting of 6–8 technical replicates. \*\*,  $p < 0.01$ ; \*\*\*,  $p < 0.001$ .

### **3.9 Investigations into the differences in keratinocyte cytotoxicity caused between TAC versus ACT combinatorial regimes**

Combinatorial therapy holds the potential for enhanced anticancer activity compared with monotherapy, as mentioned previously in chapter 1. However, the effectiveness of this approach is more strongly associated with side effects such as alopecia. After establishing an *in vitro* system to assess the effects of a specific treatment sequence for the TAC (*via* sequential treatment with docetaxel, doxorubicin, and 4-OH-CP), only a modest degree of cytoprotection was observed following ‘TAC’ treatments in agreement with clinical observations. There are many different modes of cytotoxic action for anticancer drugs, hypothetically these drugs produce various degrees of cytotoxicity depending on administered sequences (Rowinsky *et al.*, 1993). Both TAC and ACT are types of combinatorial chemotherapies for breast cancer. However, so far there has been no study that compares ACT and TAC (Buyukhatipoglu *et al.*, 2015) and it appears that different hospitals treat breast patients with these three drugs in different orders, resulting in various degrees of CIA (Paxman personal communication). Therefore, in this study, the TAC and ACT combinatorial regimes were investigated and their effects on HaCaTa cells were compared. The combinations of drugs with different duration periods of administration (cell treatment period) were tested and the effect of cooling was assessed in comparison to physiological temperature. HaCaTa cells were treated with a combination of doxorubicin, 4-OH-CP, and docetaxel ‘ACT’ and ‘TAC’ for 1.5h for each drug compared with TAC (see section 2.7.3). Data showed that there was no increase in the viability of the cells that were treated with ACT when compared to TAC treatments (Figure 3-11).

Istomin *et al.* showed that the drug exposure time and concentration are important *in vitro* and *in vivo* (Istomin *et al.*, 2008). Therefore, it is important to compare the combined therapy of ACT in equal treatment conditions at different drug exposure times for each drug and the impact of cooling. To test for the first time *in vitro* the cytotoxic effect of the ‘ACT’ at different drug exposure duration and assess the influence of cooling as detailed in section 2.7.1. As shown in Figure 3-12, there was no effect observed as a result of drug sequence or duration of treatment on drug effectiveness, and biomass at both 37°C and 22°C. Furthermore, the effect of cooling on HaCaTa cells treated with FAC combinatorial regimes (5-FU, doxorubicin and cyclophosphamide) was investigated. As shown in Figure 3-13, HaCaTa cells were exposed to the combination drug FAC, and cooling showed almost 50% increase in cell biomass and improved the relatively modest protection observed when

compared with FAC at 37°C, which is in agreement with the clinical data (Van Den Hurk *et al.*, 2012c).

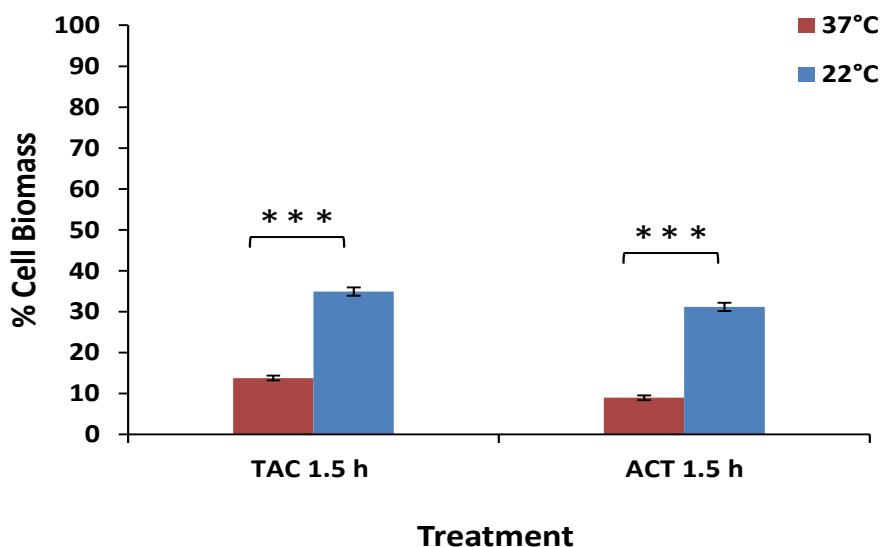


**Figure 3-11 Effect of cooling on ACT and TAC-mediated cytotoxicity in HaCaTa cells**

HaCaTa cells were seeded in 96 well plates at 5000 cells/well in KFSM medium and were incubated overnight at 37°C/5% CO<sub>2</sub>. HaCaTa cells were treated with the combinatorial drug protocols 'TAC (+10%) compared ACT (+10%) for treatment 1.5h for each drug at 37°C and 22°C (representing normal and cooling conditions, respectively) compared with vehicle control (cells treated with medium containing DMSO, in which the reagent was dissolved). The solvent represents the maximum amount of DMSO corresponding to the highest drug concentration). The drugs were then removed, wells were rinsed with PBS to remove any traces of drug and cultures incubated for a further 72h, and after which 20 µL of CellTiter 96@ AQueous One solution was added to the wells and plates were incubated at 37°C in 5% CO<sub>2</sub> for a total of four hours. Absorbance was measured spectrophotometrically at a wavelength of 492nm and % cell biomass was calculated as described in Materials and Methods (Chapter 2). Representative results shown in bar graph form for clarity and presentation of statistical significance. Data points correspond to mean % cell biomass (±S.E.M.) for three independent biological experiments, each consisting of 6–8 technical replicates. \*\*\*,  $p < 0.001$ .

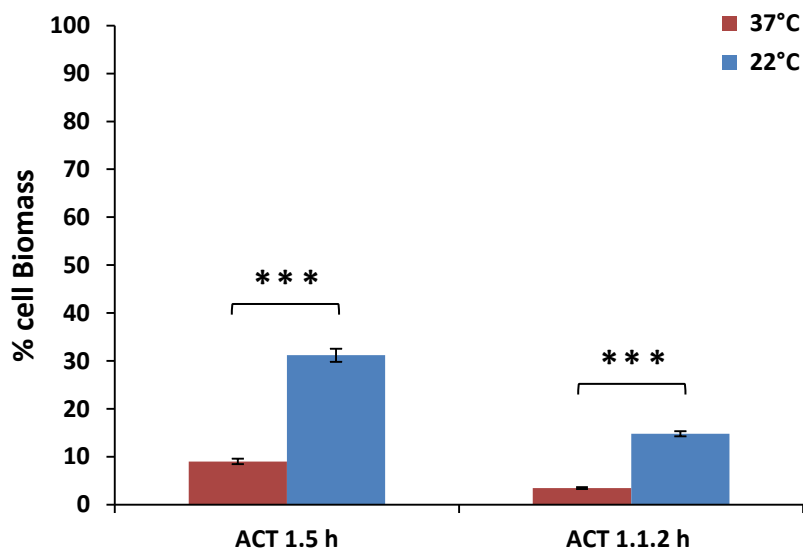


**Figure 3-12 Effect of cooling on modified ACT-mediated cytotoxicity in HaCaTa cells**

HaCaTa cells were seeded in 96 well plates at 5000 cells/well in KSFM medium and were incubated overnight at 37°C/5% CO<sub>2</sub>. HaCaTa cells were treated with the combinatorial drug protocols ACT (+10%) for treatment 1.5h for each drug and ACT 1.1.2h (1h doxorubicin, 1h 4-OH-CP and 2h docetaxel) at 37°C and 22°C (representing normal and cooling conditions, respectively) compared with vehicle control (cells treated with medium containing DMSO, in which the reagent was dissolved. The solvent represents the maximum amount of DMSO corresponding to the highest drug concentration). The drugs were then removed, wells were rinsed with PBS to remove any traces of drug and cultures incubated for a further 72h, after which 20 µL of CellTiter 96® AQueous One solution was added to the wells and plates were incubated at 37°C in 5% CO<sub>2</sub> for a total of four hours. Absorbance was measured spectrophotometrically at a wavelength of 492nm and % cell biomass was calculated as described in Materials and Methods (Chapter 2). Representative results shown in bar graph form for clarity and presentation of statistical significance. Data points correspond to mean % cell biomass (±S.E.M.) for three independent biological experiments, each consisting of 6–8 technical replicates. \*\*\*, *p* < 0.001.

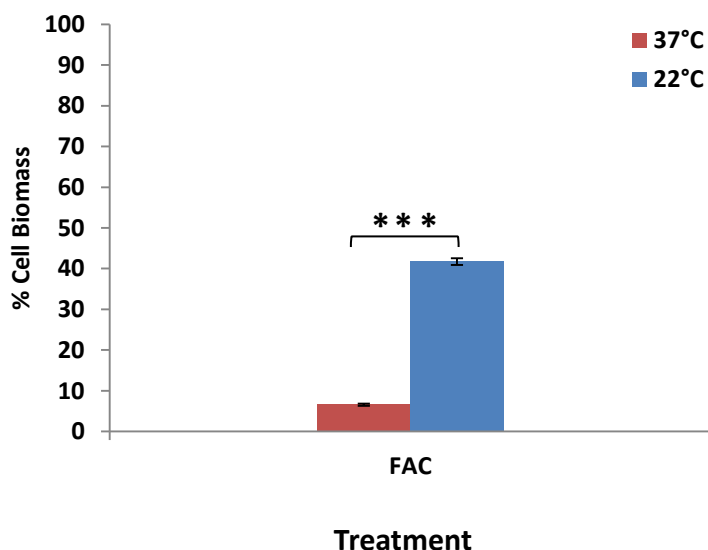


**Figure 3-13 The ability of cooling to protect from combined therapy FAC (5FU, doxorubicin and cyclophosphamide)-mediated cytotoxicity in HaCaTa cells**

HaCaTa cells were seeded in 96 well plates at 5000 cells/well in KSFM medium and were incubated overnight at 37°C/5% CO<sub>2</sub>. HaCaTa cells were treated with the combinatorial drug protocols FAC (+10%) at 37°C and 22°C (representing normal and cooling conditions, respectively) compared with vehicle control (cells treated with medium containing DMSO, in which the reagent was dissolved). The solvent represents the maximum amount of DMSO corresponding to the highest drug concentration). The drugs were then removed, wells were rinsed with PBS to remove any traces of drug and cultures incubated for a further 72h, after which 20 µL of CellTiter 96® AQueous One solution was added to the wells and plates were incubated at 37°C in 5% CO<sub>2</sub> for a total of four hours. Absorbance was measured spectrophotometrically at a wavelength of 492nm and % cell biomass was calculated as described in Materials and Methods (Chapter 2). Representative results shown in bar graph form for clarity and presentation of statistical significance. Data points correspond to mean % cell biomass (±S.E.M.) for three independent biological experiments, each consisting of 6–8 technical replicates. \*\*\*,  $p < 0.001$ .

### 3.10 Effects of dual drug chemotherapy exposure and the impact of cooling in combinatorial drug-induced cytotoxicity

Adriamycin/doxorubicin, cyclophosphamide/Cytoxan (AC) chemotherapy is a common chemotherapy administered to breast cancer patients (Land *et al.*, 2004). Most patients will lose all their hair after AC therapy (Partridge *et al.*, 2001), yet scalp cooling has showed a good ability to prevent or minimise hair loss (Grevelman and Breed, 2005). Therefore, the dual drug chemotherapy AC and its effects was investigated on HaCaTa cells at 37°C vs cooling conditions. Cells were treated with drugs for 1h for each drug and also for 2h with the same drugs. As shown in Figure 3.14, there was significant reduction in cell viability at 37°C for all the groups compared with cell treated at 22°C.

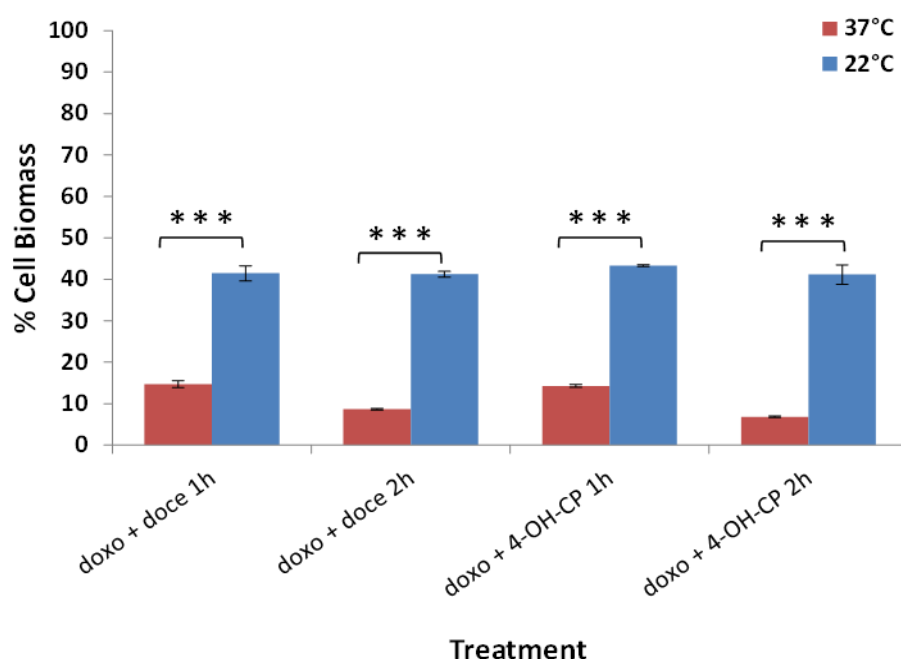


**Figure 3-14 Effect of cooling on dual drug-mediated cytotoxicity in HaCaTa cells**

HaCaTa cells were seeded in 96 well plates at 5000 cells/well in KFSM medium and were incubated overnight at 37°C/5% CO<sub>2</sub>. HaCaTa cells were treated with the combinatorial drug protocols 1h and 2h for each drug see section 2.7.1 at 37°C and 22°C (representing normal and cooling conditions, respectively) compared with vehicle control (cells treated with medium containing DMSO, in which the reagent was dissolved. The solvent represents the maximum amount of DMSO corresponding to the highest drug concentration). The drugs were then removed, wells were rinsed with PBS to remove any traces of drug and cultures incubated for a further 72h, after which 20 µL of CellTiter 96® AQueous One solution was added to the wells and plates were incubated at 37°C in 5% CO<sub>2</sub> for a total of four hours. Absorbance was measured spectrophotometrically at a wavelength of 492nm and % cell biomass was calculated as described in Materials and Methods (Chapter 2). Representative results shown in bar graph form for clarity and presentation of statistical significance. Data points correspond to mean % cell biomass (±S.E.M.) for three independent biological experiments, each consisting of 6–8 technical replicates. \*\*\*,  $p < 0.001$ .

### **3.11 The importance of temperature (cooling conditions) in determining the efficacy of cooling in protecting from chemotherapy drug-mediated cytotoxicity**

It has previously been reported that cooling below 22°C did not provide any further protection against doxorubicin-mediated keratinocyte cytotoxicity, even when the culture temperature was reduced to 10°C during drug treatment (Janssen *et al.*, 2008). Using HaCaTa cells, we tested whether temperature values below 22°C could provide further protection against doxorubicin, 4-OHCP and docetaxel, and 5FU. As evident by representative results shown in Figure 3-15 and 3-16, lowering the temperature from 22°C to 18°C and even further to 14°C, resulted incrementally in a better degree of rescue from drug cytotoxicity. Strikingly, cytoprotection was detectable even for the maximal drug doses tested, which had previously resulted in complete loss in cell biomass that was non-recoverable by cooling at 22°C. Decreasing the cooling temperature further to 10°C ('severe cooling') did not provide any significantly better protection than did cooling at 14°C (Figure 3-17). Interestingly, cooling even at 14°C did not substantially improve the relatively modest protection observed for the 'TAC' and 'TAC (+10%)' protocols or the minimal protection from the 'TAC (+100%)' treatment when experiments were performed in either NHEK or HaCaTa cells (data not shown).

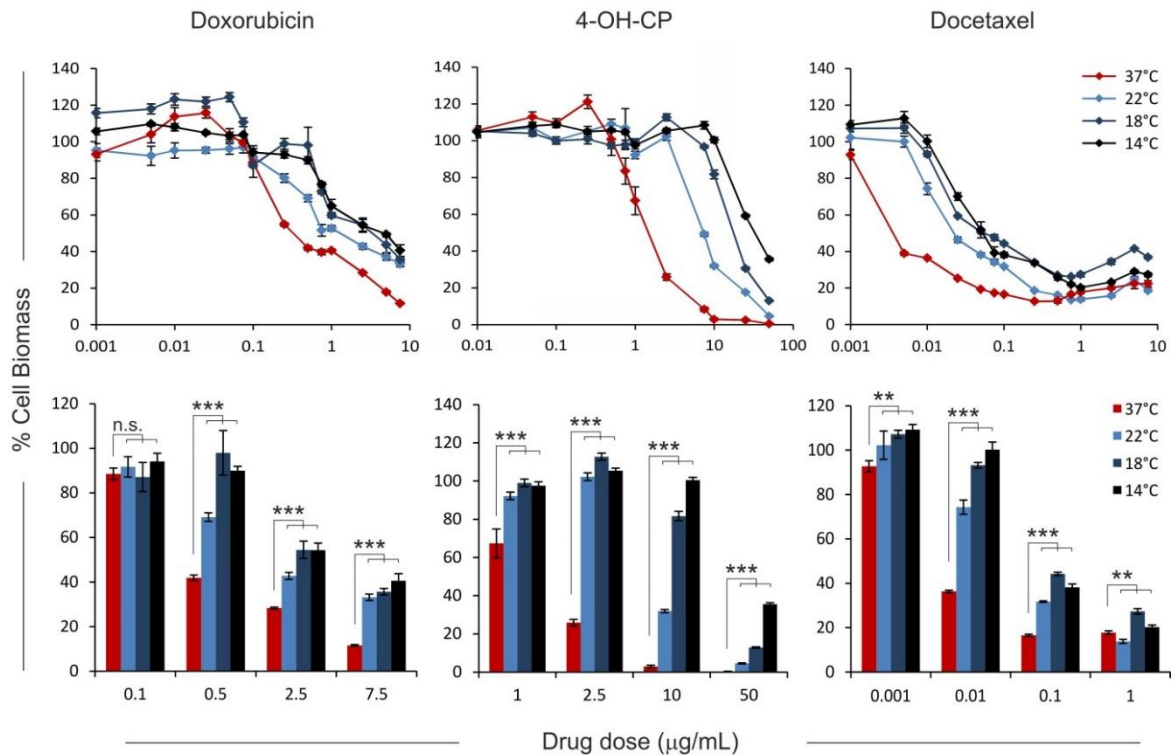


**Figure 3-15 The role of temperature on the efficacy of cooling in protecting from chemotherapy drug-mediated cytotoxicity**

HaCaTa cells were seeded in 96 well plates at 5000 cells/well in KSFM medium and were incubated overnight at 37°C/5% CO<sub>2</sub>. HaCaTa cells were treated for 2h with a range of concentrations of doxorubicin, 4-OH-CP, and docetaxel at 37°C and 22°C, 18°C and 14°C (representing normal and cooling conditions, respectively) compared with vehicle control (cells treated with medium containing DMSO, in which the reagent was dissolved). The solvent represents the maximum amount of DMSO corresponding to the highest drug concentration). The drugs were then removed, wells were rinsed with PBS to remove any traces of drug and cultures incubated for a further 72h, after which 20 μL of CellTiter 96® Aqueous One solution was added to the wells and plates were incubated at 37°C in 5% CO<sub>2</sub> for a total of four hours. Absorbance was measured spectrophotometrically at a wavelength of 492nm and % cell biomass was calculated as described in Materials and Methods (Chapter 2). Representative results from the dose response curves (upper panels) are also shown in bar graph form (lower panels) for clarity and presentation of statistical significance. Data points correspond to mean % cell biomass (±S.E.M.) for three independent biological experiments, each consisting of 6–8 technical replicates. n.s., non-significant; \*\*,  $p < 0.01$ ; \*\*\*,  $p < 0.001$ .

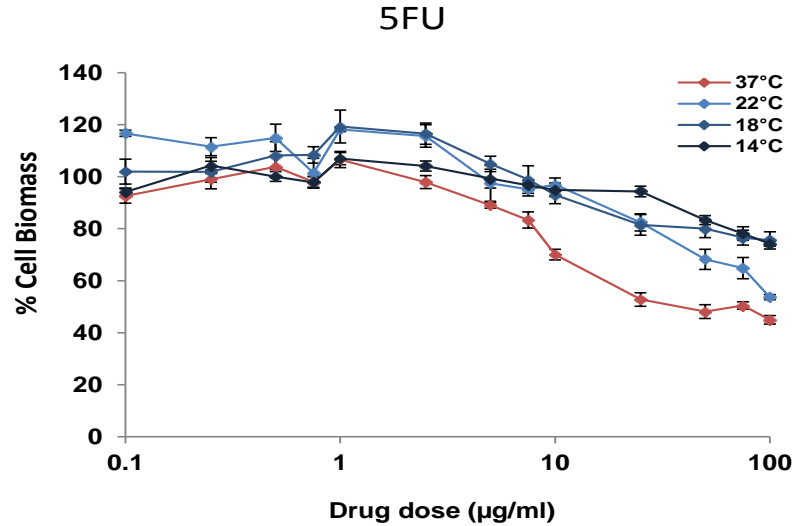


**Figure 3-16 The role of cooling in protecting from 5-fluorouracil (5-FU)-mediated cytotoxicity**

HaCaTa cells were seeded in 96 well plates at 5000 cells/well in KSFM medium and were incubated overnight at 37°C/5% CO<sub>2</sub>. HaCaTa cells were treated for 2h with a range of concentrations of 5-FU at 37°C and 22°C, 18°C and 14°C (representing normal and cooling conditions, respectively) compared with vehicle control (cells treated with medium containing DMSO, in which the reagent was dissolved). The solvent represents the maximum amount of DMSO corresponding to the highest drug concentration). The drugs were then removed, wells were rinsed with PBS to remove any traces of drug and cultures incubated for a further 72h, after which 20 µL of CellTiter 96® AQueous One solution was added to the wells and plates were incubated at 37°C in 5% CO<sub>2</sub> for a total of four hours. Absorbance was measured spectrophotometrically at a wavelength of 492nm and % cell biomass was calculated as described in Materials and Methods (Chapter 2). Representative results from the dose response curves (upper panels) are also shown in bar graph form (lower panels) for clarity and presentation of statistical significance. Data points correspond to mean % cell biomass (±S.E.M.) for three independent biological experiments, each consisting of 6–8 technical replicates.

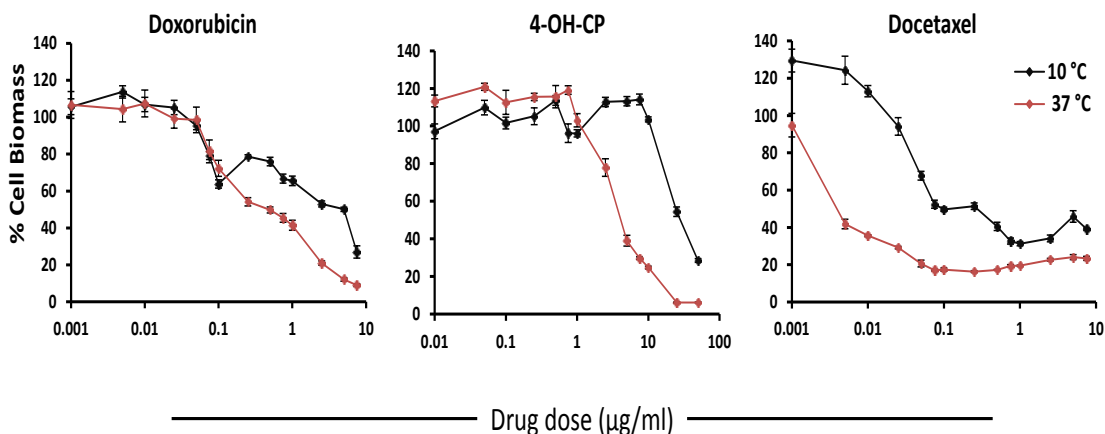


**Figure 3-17 The role of ‘severe cooling’ conditions on the ability of cooling to protect from chemotherapy drug-mediated cytotoxicity**

HaCaTa cells were seeded in 96 well plates at 5000 cells/well in KSFM medium and were incubated overnight at 37°C/5% CO<sub>2</sub>. HaCaTa cells were treated for 2h with a range of concentrations of doxorubicin, 4-OH-CP, and docetaxel at 37°C and 10°C (representing normal and cooling conditions, respectively) compared with vehicle control (cells treated with medium containing DMSO, in which the reagent was dissolved). The solvent represents the maximum amount of DMSO corresponding to the highest drug concentration). The drugs were then removed, wells were rinsed with PBS to remove any traces of drug and cultures incubated for a further 72h, after which 20 µL of CellTiter 96® AQueous One solution was added to the wells and plates were incubated at 37°C in 5% CO<sub>2</sub> for a total of four hours. Absorbance was measured spectrophotometrically at a wavelength of 492nm and % cell biomass was calculated as described in Materials and Methods (Chapter 2). Representative results from the dose response curves (upper panels) are also shown in bar graph form (lower panels) for clarity and presentation of statistical significance. Data points correspond to mean % cell biomass (±S.E.M.) for three independent biological experiments, each consisting of 6–8 technical replicates.

### 3.12 Summary

- The work described in this chapter allowed the establishment of *in vitro* models for the study of the effects of chemotherapy drug-induced cytotoxicity *in vitro* and to assess the role of cooling in protecting from drug-mediated cytotoxicity
- Normal human epidermal keratinocytes (NHEK) and human hair follicular keratinocytes (HHFK) were initially used, as well as the keratinocyte cell line HaCaT and HaCaT cells that were adapted to culture conditions identical to those for NHEK cells (serum-free and low-calcium medium)
- Cooling-mediated rescue from drug cytotoxicity after treatment with a wide range of doxorubicin, 4-OH-CP and docetaxel concentrations, a protection that was noticeably less dramatic in HaCaT cells in comparison to NHEK and HHFK cells.
- For this purpose, and for the first time, HaCaT cells were adapted to grow in both low calcium and serum-free conditions (KSFM medium) by sequential medium adaptation and passage, resulting in the new cell line named HaCaTa. HaCaTa cell proliferation rates were higher than the parental cell line HaCaT line. Furthermore, HaCaTa cells exhibited a phenotype that was more representative of that of NHEKs.
- Cooling dramatically reduced or completely prevented the cytotoxic effects of docetaxel, doxorubicin, 5-FU, and particularly cyclophosphamide. Optimal rescue was observed in conjunction with mono-therapy treatment whilst combinatorial treatment (TAC) showed relatively poor response to cooling, findings that are in agreement with clinical observations.
- There was no impact of changing the sequences of the drugs and duration of the treatment of each drug on effectiveness at both temperature 37°C and 22°C.
- Adriamycin/doxorubicin, cyclophosphamide/Cytoxan (AC) related experiments showed that the cell under cooling conditions showed significantly better viability in comparison to 37C controls.

### 3.13 Discussion

Chemotherapy-induced alopecia (CIA) is the most common and distressing side effect of anticancer chemotherapy (Wang *et al.*, 2006) and due to the fear caused by the prospect of CIA, cancer patients may even refuse treatment in some cases (Münstedt *et al.*, 1997). Therefore, with cancer chemotherapy, still representing the most widely employed therapeutic approach; development of CIA preventative regimes represents an important challenge in oncology (Paus *et al.*, 2013). The only currently available preventative treatment is scalp cooling. Scalp cooling (scalp hypothermia) during administration of chemotherapy drugs can substantially reduce hair loss (Protiere *et al.*, 2002). Clinically it has been shown that scalp cooling can substantially reduce the incidence of hair loss in response to individual drugs, including cyclophosphamide, doxorubicin, and cisplatin (Grevelman and Breed, 2005). However, for combination treatment regimes, such as doxorubicin (Adriamycin) and cyclophosphamide (clinically referred to as AC), and particularly treatment with docetaxel (Taxotere), doxorubicin and cyclophosphamide (clinically known as TAC), and Fluorouracil (5FU), doxorubicin and cyclophosphamide (clinically known as FAC), scalp cooling shows relatively moderate or little reported efficacy (Breed *et al.*, 2011; Van Den Hurk *et al.*, 2012c).

Despite the fact that scalp cooling can be effective, its principal mechanism(s) of action remain not understood and several hypotheses have been raised to explain its role. Firstly, as cooling causes blood vessel vasoconstriction, which dramatically reduces blood flow to the scalp (Janssen *et al.*, 2008), it has been suggested that the less chemotherapeutic drug is 'delivered' to the HFs (Bülow *et al.*, 1985). Another possibility is that the rate of drug diffusion across a plasma membrane may be reduced and thus lower the 'effective' drug dose which can enter the cells (Lane *et al.*, 1987). Finally, as cell division is metabolism-driven, this process could be decelerated by cooling as temperature can particularly affect phases G1 and S (Watanabe and Okada, 1967), which could be particularly important for drugs that target specific phases of the cell cycle, such as microtubule-destructive drugs targeting mitosis. It is possible that cooling involves a combination of these three mechanisms to exert its protective effect (Figure 8-1).

Several experimental *in vivo* models have been used to help understand CIA, however, despite their clear physiological relevance; rodent-based models demonstrate a number of inherent limitations. For instance, in adult mice, HFs are mostly in the telogen phase and only 10% are in the anagen, compared to 90% of follicles on a normal human (Luanpitpong *et al.*, 2012; Paus *et al.*, 2013). For this reason *ex vivo* models have been developed, such as those by Paus (2013) that are based on the isolation and culture of

human HFs, which represent a physiologically-relevant and elegant approach to mimic and study cyclophosphamide-induced CIA (Bodo *et al.*, 2007).

A more reductive *in vitro* culture approach involves studying chemotherapy drug-induced cytotoxicity using primary normal human epidermal keratinocytes (NHEK). The principle behind the use of such keratinocytes is that they are maintained under culture conditions that render them highly-proliferative, thus resembling the rapidly-dividing population of native matrix keratinocytes. Using such primary NHEKs, a previous report has provided evidence, that doxorubicin induces NHEK cytotoxicity over a range of concentrations (Janssen *et al.*, 2008). Another *in vitro* approach has used the well-characterised cell line HaCaT, which shows similar characteristics and cell behaviour to normal keratinocytes (Deyrieux *et al.*, 2007). These cells have been used to study chemotherapy drug-induced keratinocyte cytotoxicity and such studies provided evidence on cisplatin-induced cytotoxicity by demonstrating Reactive Oxygen Species (ROS) -mediated mechanisms that induce Bcl-2 down-regulation, Bax up-regulation and subsequent induction of apoptosis (Luanpitpong *et al.*, 2011).

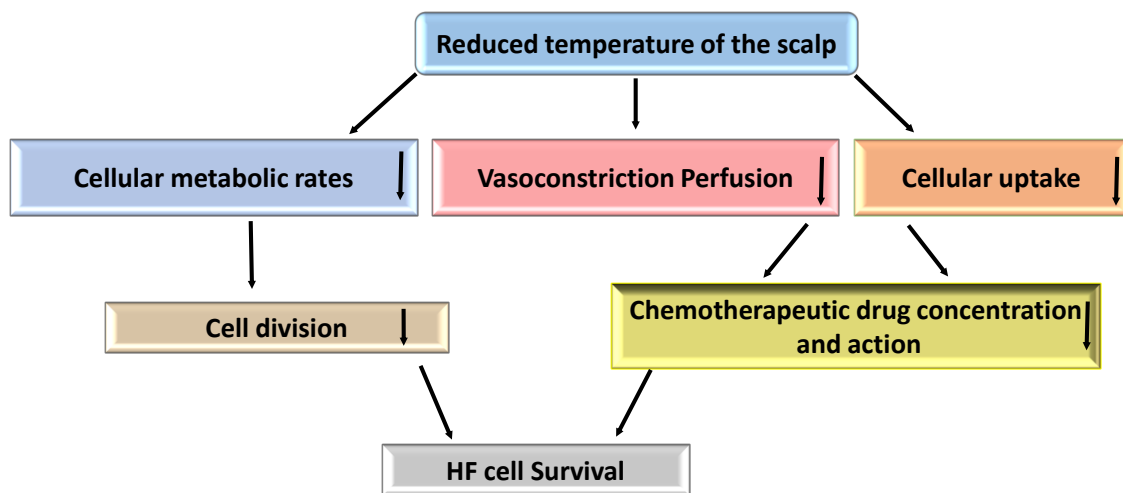


**Figure 3-18 Proposed mechanisms of action of scalp cooling**

### **3.13.1 Development of *in vitro* models to study chemotherapy drug-induced cytotoxicity and assess the effect of cooling**

This study focused on the biological effects of cooling (hypothermia) following chemotherapy drug-treated *in vitro* in keratinocyte cells and demonstrated the protective effect of cooling at the cellular level. The study for the first time examined the cytotoxicity of a panel of chemotherapeutic modalities, including doxorubicin, docetaxel, and the active metabolite of cyclophosphamide (4-OH-CP), on NHEK cultures and investigated the possible influence of culture temperature on drug-mediated cytotoxicity. Importantly, our study has been the first to test these effects on human hair follicular keratinocytes (HHFKs). Moreover, this study established a derivative of the HaCaT cell line (coined HaCaTa) as an alternative *in vitro* model. The initial temperature choice of 22°C was made to mimic cooling, because (a) at the time our laboratory studies were being performed, the clinical evidence had suggested that 22°C was the temperature the skin reached (on average) in patients during scalp cooling (Komen *et al.*, 2013a), (b) various studies had shown that a scalp temperature of 22°C or less is required for hair preservation (reviewed in (Komen *et al.*, 2013a)) and (c) 22°C was the temperature previously tested *in vitro* (Janssen *et al.*, 2008). However, this thesis systematically examined a series of temperature conditions, that included 22°C as well as more severe cooling, particularly 18°C, 14°C (and even extreme cooling at 10°C). The suitability of our approach has been attested very recently by published evidence (appearing in public databases during the preparation of this dissertation) reporting that lowering the temperature further (from 22°C to 18°C) is associated with improved efficacy of cooling (Komen *et al.*, 2016).

### **3.13.2 The effects of cooling on drug-mediated cytotoxicity**

The results of our study demonstrate that cooling can rescue HaCaTa, NHEK and HHFK cells from drug-mediated cytotoxicity. The cytoprotective effect of cooling was striking for a series of drug concentrations, particularly for doxorubicin and 4-OH-CP where for some doses cell biomass returned from below 20% to nearly 100% of the control value. For doxorubicin, this effect was particularly marked for 3 µg/mL. Interestingly, the maximal plasma concentration ( $C_{max}$ ) following routine infusion with doxorubicin in patients undergoing chemotherapy is reported to be ~2–4 µg/mL (Brunsvig *et al.*, 2007; Itoh *et al.*, 2000; Nabholz *et al.*, 2001). Although measured drug concentrations in the overall circulation may not necessarily correspond to those in the HFs, our finding that even at this maximal concentration cooling can fully protect from cytotoxicity at 22°C, explains the success of head cooling in preventing CIA clinically. We also show for the first time that both the active metabolite of cyclophosphamide, 4-hydroxy-cyclophosphamide (4-OH-CP) and docetaxel

induce dose-dependent cytotoxicity in human keratinocytes, an effect, which is consistent with the association of these drugs with CIA clinically. The dose-dependence of this toxicity is also in agreement with a number of clinical reports that slower infusion speeds which will lead to a reduced  $C_{max}$  cause less severe CIA (Breed *et al.*, 2011). More importantly, our findings that cooling can rescue from cytotoxicity are in concordance with clinical observations that scalp cooling significantly reduces the incidence of CIA following treatment with these drugs (Van Den Hurk *et al.*, 2012c).

### **3.13.3 The effects of cooling on combinatorial therapy**

Having demonstrated that exposure to individual chemotherapeutic drugs caused dose-dependent toxicity in human keratinocytes of both epidermal and follicular origin and that this could be significantly attenuated by cooling, we examined the response to the combinatorial TAC therapy (T = taxotere/docetaxel, A = adriamycin/doxorubicin, C = cyclophosphamide/ Cytoxan). This regimen is being increasingly used in early stage breast cancer, but almost always results in CIA and it has been reported that head cooling has very limited success in preventing TAC-mediated CIA, with ~90% of patients exhibiting CIA despite using scalp cooling (Breed *et al.*, 2011). Treatment of cells *in vitro* to mimic clinical administration of TAC (or FAC) posed challenges. One challenge was the choice of concentration of each chemotherapy drug. Equally, as drugs are administered sequentially in the clinic, it would be expected (based on published pharmacokinetic data) that following administration of the first drug, infusion of the next drug would take place whilst the previous drug may still be present at high concentrations in the blood. Also, the infusion of these three drugs takes place in different time periods during TAC treatment; often this involves docetaxel for 60 min followed by doxorubicin for 15 min and cyclophosphamide for 15 min (Van Den Hurk *et al.*, 2012c). However, precise timings and the order of administration can vary between different clinics.

In an attempt to incorporate these parameters and make the *in vitro* TAC treatment as relevant as possible, we adopted three approaches. In all cases, cells were treated with chemotherapy drug doses for which significant or maximal *in vitro* rescue was observed when each drug was tested individually. The first approach ('TAC') involved sequential treatment with the individual drugs. The other two approaches involved initial treatment with the first drug (T), followed by treatment with each subsequent drug (A and C) whilst being also supplemented with either 10% (denoted 'TAC (+10%)') or 100% (denoted 'TAC (+100%)') of the previous drug. The use of 'TAC (+100%)' aimed at addressing the scenario where infusion with the second or third drug would take place whilst the previous drug was still present in maximal concentration. The rationale behind the 'TAC (+10%)' protocol was

based on the reported observation that the plasma levels of doxorubicin and docetaxel fall on average by approximately 10-fold within 1–2h post-infusion in comparison to the  $C_{max}$  (Brunsvig *et al.*, 2007; Itoh *et al.*, 2000; Nabholz *et al.*, 2001). Interestingly, all three TAC protocols tested caused significant toxicity to NHEKs and HaCaTa cells at 37°C consistent with the high levels of CIA reported for individuals undergoing TAC therapy in the clinic (Van Den Hurk *et al.*, 2012c). Upon cooling to 22°C in NHEK cell, and in HaCaTa cells the TAC regimen was tested at 22°C and the sub-optimal temperature 26°C, data showed that despite some degree of cytoprotection, and although the drug concentrations used had previously ‘responded’ to cooling in individual treatment experiments, following combinatorial treatment the protection observed was modest at 22°C. Interestingly, 26°C showed improved, though relatively modest, cell viability compared to at 22°C.

Of note, despite observing a cell biomass between 40% and 50% for the TAC only and TAC (+10%) protocols, we found little detectable rescue following treatment with the TAC (+100%) protocol, suggesting that this may represent the protocol that more appropriately reflects cytotoxicity *in vivo*. It is most striking that, despite the assumptions made when constructing the TAC protocols for cell treatment *in vitro*, our observations reflect the clinically reported inability of cooling to attenuate TAC-mediated toxicity that results in CIA. Also in support of these findings, is the observation that, in addition to the TAC protocols reported in the results section, when we tested further possible alternatives as TAC treatments (for instance by altering drug treatment duration and/or a drug sequence (ACT protocol)) our results remained unchanged.

Due to the finite nature of NHEK and HHEK cells, we explored the possibility of using the well-characterised, immortalised, non-malignant human keratinocyte line HaCaT for our studies, as HaCaT cells show characteristics and behaviour similar to normal keratinocytes (Boukamp *et al.*, 1988; Deyrieux and Wilson, 2007; Inui *et al.*, 2000; Itami *et al.*, 1995). They adopt a phenotype similar to cell sub-populations of the human HF (Inui *et al.*, 2000) and have been used to study drug-induced (Luanpitpong *et al.*, 2011) or ROS-mediated (Liu *et al.*, 2012) cytotoxicity. At 37°C, the response of HaCaT cells to docetaxel was similar to that in NHEK and HHEK. However, for both doxorubicin and 4-OH-CP, although the general pattern of toxicity was similar, qualitatively there were some clear differences. HaCaT cells were somewhat more drug-sensitive than primary keratinocytes.

Interestingly, we observed that low concentrations of doxorubicin and 4-OH-CP stimulated an overall increase in biomass compared to controls in HaCaT a response also observed for 4-OH-CP in NHEK and HHEK cells (Figures 3-1 and 3-2). This increase in cell growth in sub-lethal concentrations of otherwise cytotoxic drugs have been reported

previously in different cell types by our laboratory and by others (Kayamba *et al.*, 2013; Paus *et al.*, 2013).

Cooling HaCaT cells to 22°C during drug exposure produced a general reduction in the toxicity of the drugs, however, this was less dramatic than NHEK cells and at no concentration was the nearly 100% cell rescue that we had observed with NHEK for singularly administered drugs replicated. These findings indicated that HaCaT cells do not represent an appropriate *in vitro* model for investigations on the role of cooling in modulating chemotherapy drug-induced cytotoxicity.

The reduced efficacy of cooling in HaCaT compared to NHEK and HHFK cells, led us to hypothesise that the differences in responses may be due to the lower proliferative capacity and the more differentiated phenotype of HaCaT compared to NHEK. HaCaT cells are routinely cultured in standard, serum-containing medium, whereas NHEK are maintained in Keratinocyte Serum Free Medium (KSFM), which contains a low calcium concentration (~0.09 mM) – in comparison to physiological (~2 mM) calcium (Georgopoulos *et al.*, 2010). The concentration of extracellular calcium has a profound role as a switch between epithelial growth and differentiation of keratinocytes, as calcium induces terminal differentiation, including specific structural changes, cell cycle withdrawal, and induction of terminal differentiation-related genes (Boelsma *et al.*, 1999). It has previously been reported that reducing the level of calcium in the culture media of HaCaT cells resulted in a more proliferative/basal and less differentiated phenotype evident by the reduction of molecular differentiation markers, such as K1 and involucrin (Deyrieux and Wilson, 2007).

When HaCaT cells were adapted to grow in low calcium (0.09 mM), serum-free conditions, the new cell line (HaCaTa) was phenotypically very similar to NHEKs and exhibited higher proliferation rates than HaCaT cells that were comparable to those of early-passage NHEKs. More importantly, when we tested the effects of the panel of chemotherapy drugs and the capacity of cooling to protect from cytotoxicity, the results with the HaCaTa cell line closely resembled our observations with NHEKs, as exemplified by the results using 4-OH-CP. When we tested the different TAC protocols on these cells and examined the ability of cooling to protect, again the findings with the HaCaTa cells were in concordance with those for NHEKs, as only modest cytoprotection by cooling was observed for the 'TAC' and 'TAC (+10%)' treatments and cooling provided even less rescue from the extensive cytotoxicity observed following the 'TAC (+100%)' protocol. Therefore, this novel, low-calcium and serum-free condition-adapted HaCaTa cell line represents an *in vitro* model that more closely resembles NHEKs whilst, due to its immortal nature, it has the advantage of maintaining a proliferative phenotype over an extended number of passages and was

therefore used extensively in this work for investigating the influence of cooling on chemotherapy drug-induced cytotoxicity.

Previous *in vitro* studies by Janssen *et al.*, (2008) have reported that reducing culture temperatures below 22°C did not provide any further protection against doxorubicin-induced cytotoxicity in NHEKs (Janssen *et al.*, 2008). Using the HaCaTa line as a model, our study demonstrated that further reduction of culture temperature to 18°C and 14°C provided significantly more cytoprotection (than that at 22°C) for all drugs tested, and resulted in particularly marked rescue from 4-OH-CP, doxorubicin-induced cytotoxicity and 5-FU. One possibility for the discrepancy between our findings and those of Janssen *et al.*, (2007) could be that those studies used NHEKs whereas in our experiments we used the HaCaTa line. However, this possibility was excluded by demonstrating that lowering the culture temperature below 22°C in experiments where NHEK cells were exposed to all three drugs employed in this study also resulted in improved cytoprotection (Chapter 4) (an observation also confirmed using HHFKs as well). A more likely explanation for the difference in observations is that in the studies by Janssen *et al.*, (2008) the cell density used in all cell biomass measurement experiments was substantially lower than those we used in our studies. It is possible that this could result in much higher cellular stress during drug treatment that could 'mask' the real potential of cooling in rescuing from cytotoxicity (Janssen *et al.*, 2008).

Our finding that lowering the temperature further results in improved cytoprotection implies that the scalp temperature that is achieved clinically may be important in dictating the success of head cooling in CIA prevention. Despite the lack of appropriate clinical data to formally demonstrate the precise temperature conditions that determine the efficacy of cooling, it has been suggested by various studies that a scalp temperature of 22°C or less is required for hair preservation during chemotherapy (Gregory *et al.*, 1982) and reviewed in (Komen *et al.*, 2013a), and as mentioned above. Recently published evidence reported that 18°C temperature in the scalp is associated with improved efficacy of cooling in comparison to 22°C (Komen *et al.*, 2016). Moreover, we have evidence that a scalp temperature <18°C can be achieved during cooling with commercially available scalp cooling devices such as the Paxman scalp cooling device (Hussain and Georgopoulos, unpublished data), not all subjects undergoing scalp cooling achieve this potentially critical temperature threshold. Thus, the ability to reach a temperature low enough to achieve cytoprotection may hold the key in determining the success of scalp cooling in preventing CIA in the clinic. Nevertheless, the lack of improvement in protecting from TAC-mediated cytotoxicity despite cooling at even lower temperatures indicates that for treatment types that do not respond well, further cooling alone might not provide an effective solution. Understanding the mechanisms of cooling-

mediated cytoprotection may therefore provide novel avenues for combinatorial intervention in the future, and this was a main driver in the mechanisms investigated in this study.

**CHAPTER 4: The effects of chemotherapy drugs and cooling alone or in combination on the human keratinocyte cell cycle**

## 4.1 Background

The cell cycle is the fundamental means by which every living entity divides and multiplies. The cell cycle is divided into four main phases: G1 phase (Gap phase 1) where the nucleus has the two complementary strands of DNA; S-phase (synthesis) during which DNA replication takes place, and G2 phase (Gap phase 2) preceding mitosis (M phase). Some cells are either not in an active cycle (post-mitotic) or have become quiescent enter a resting phase known as G0; during this time when the cell receives a mitotic signal it can re-enter G1 phase (Pardee, 1989). In order to preserve the stability of the genome in response to cellular damage there are monitoring mechanisms (checkpoints) that will arrest the cycle at either G1/S or G2/M. Which provides additional time for cells to activate repair processes to remove any damage before DNA replication; alternatively, if damage is excessive and/or repair cannot occur, cell death by apoptosis can be stimulated (Hartwell and Kastan, 1994). Cell division is a complex, finely tuned mechanism. In each cell cycle phase, the cell monitors both its own growth as well as the external conditions. If these are unfavourable then growth arrest or cell cycle arrest is initiated (Sunley and Butler, 2010).

The distribution of cells at different stages of the cycle determines cell growth rates and usually S phase percentage reflects the quantity of multiplying cells. Cancers tend to have a higher percentage of S phase cells than that of normal tissues. Furthermore, more aggressive cancer types have a higher proportion of cells in the S phase compared to less aggressive tumours (Braylan *et al.*, 1980; Evan and Vousden, 2001).

### 4.1.1 Effects of chemotherapeutic agents on the cell cycle

Since many chemotherapy drugs are only effective on actively dividing cells and not those that are in a quiescent or dormant stage (and out of cycle), cell cycle analysis is important in helping to understand their mechanism of action. DNA damage by chemotherapeutic agents disrupts the cell cycle and slows down or halts the reproduction of dividing cells until DNA repair is completed (Gligorov and Lotz, 2004).

Many chemotherapeutic drugs interfere with cellular metabolism and trigger apoptosis (Reed, 1997). It has been shown that different degrees of stress can have a variety of effects on cells. Mild stress can trigger repair mechanisms, which can aid in cell survival. Low or moderate stress (damage) activates apoptosis; extremely high stress overwhelms apoptosis and leads to necrosis. An unregulated catastrophic mode of cell death occurs when the cell is intensely damaged or stressed. Chemotherapeutic drug treatment can induce apoptosis, indicating that cells initiate a controlled suicide in which the cell passes through different phases and eventually fragmentation (DNA) in cells is observed, thus

apoptosis is a means that can allow an organism to eliminate damaged cells in an orderly fashion (Reed, 1997).

Chemotherapeutic drugs can be classified as cell cycle specific and non-specific drugs. Some chemotherapeutic agents specifically affect dividing cells during one or more phases of the cell cycle, by triggering arrest either in G1/S or G2/M phases; for example docetaxel acts on cells in G2 and M phases by exhibiting high affinity to  $\beta$ -tubulin and targeting centrosome organization (Gligorov and Lotz, 2004). By contrast docetaxel has minimal effects on cells in G1 phase and as a result there is an accumulation of the cells in G2/M phase (Gligorov and Lotz, 2004). Doxorubicin induces G2/M arrest in cell cycle progression (Tyagi *et al.*, 2002). Other drugs, such as cyclophosphamide, may affect dividing cells in all phases of the cycle, and as such are non-cell cycle specific (Alkan *et al.*, 2014).

#### **4.1.2 Effects of hypothermic conditions on the cell cycle**

For cells to proliferate they need both stimulating and progression factors (Rozengurt, 1986) to enter the cycle. If one or more of these factors is thermally labile then non-optimal temperature might be leading to the rate of its loss being greater than its enzymatic production and as a result of that the cell cycle will be affected (Dewey, 1987). Cold treatment (cooling) has been divided into five categories; mild (35-33°C), moderate (31-29°C), low (24-20°C), very low (20°C) and hypothermia (10-4°C) (Pardi *et al.*, 2004; Shibano *et al.*, 2002).

In 1956, Cheveremont found that in primary embryo skeletal muscle cell cultures after 24h incubation at 16-20°C the number of cells undergoing mitosis dropped to zero. However, after 3h of warming at physiological temperature (37°C) cells were dividing 2-3 times faster than the non-cooled cells (Chevremont, 1956). The explanation provided for this was that the cells continue to progress through the cell cycle until they arrest at late G2. As might be expected, all phases of the cell cycle of mammalian cells are inhibited at temperatures lower than 10°C (severe hypothermia) (Rieder and Cole, 2002). Culturing CHO (Chinese Hamster Ovary) cells at 30-35°C have been shown to demonstrate reduction in the number of cells in G1 or S phase, whilst maintaining higher cell viability (Sunley and Butler, 2010). In addition, after reducing the temperature of cultured cells to 16-20°C, rewarming has been found to increase the rate of cell division by 2-3 fold compared to non-cooled controls (Rieder and Cole, 2002). Despite these reports, relatively little is still known about the effects of cooling on the cell cycle although. It has been shown that cell cycle progression is temperature sensitive (Rieder and Cole, 2002); and although there is some evidence that culturing cells at a reduced temperature can protect from apoptotic agents (Sakurai *et al.*, 2005), it remains

unknown if cooling can modulate (prevent) the effects of chemotherapy drugs on the cell cycle.

## **4.2 Cell cycle analysis**

Flow cytometry is a conventional, fast, and simple technique for determining the relative DNA content of the cell by using a fluorochrome such as propidium iodide (PI) intercalated into the DNA and thus enables discrimination between the various phases of the cell cycle. As mentioned above cell cycle divides into phases G<sub>0</sub>/G<sub>1</sub>, S, and G<sub>2</sub>/M. The distinction between G<sub>0</sub> (quiescent) and G<sub>1</sub> (preparation phase DNA synthesis), and between G<sub>2</sub> (preparation for mitosis) and M (mitosis) is not possible because the DNA content is the same. The technique can, nevertheless, track the distribution of cells in other phases of the cycle and thus determine how cells respond to various stimuli or the addition of cytotoxic drugs. Moreover, during apoptosis, cell cycle analysis can highlight a subG<sub>0</sub>/G<sub>1</sub> peak (located just before the peak G<sub>0</sub>/G<sub>1</sub>) indicating cell populations with fragmented DNA, which is used to determine the proportion of cells in apoptosis since one of the hallmarks of apoptotic death is DNA fragmentation (Kajstura *et al.*, 2007). Fluorochromes, such as PI, are useful markers binding to DNA as the amount of PI bound to DNA is relatively proportional to the amount of cellular DNA content. Because PI forms complexes with double stranded DNA and also with RNA and thus can stain both DNA and RNA, for cell cycle analysis cells must be treated with RNase to ensure that PI staining is DNA-specific (Riccardi and Nicoletti, 2006).

## **4.3 Effects of the epidermal growth factor receptor pathway (EGFR) inhibitor in chemotherapy induced cytotoxicity**

Human skin is composed of three layers the epidermis, the dermis and the subcutis; in the epidermis, keratinocytes are the predominant cell type constituting 90% of all cells. These cells proliferate in the basal layer of the epidermis and undergo differentiation and migration, to the most external layer of the skin. Epidermal growth factor receptor (EGFR) is mainly expressed by undifferentiated, proliferating keratinocytes in the basal layers of the epidermis as well as in the ORS of HFs (Hansen *et al.*, 1997). The HF matrix keratinocytes represent highly proliferative cells and thus these cells are especially targeted by anti-cell replicative agents (Paus *et al.*, 2013). EGFR is a cell membrane growth factor receptor (receptor tyrosine kinase, or RTK) and is a target for anticancer drugs (Ge *et al.*, 2012). Previous studies showed that EGFR signalling might be involved in cyclophosphamide-induced alopecia because EGFR signals anagen HFs to enter catagen (Bichsel *et al.*, 2013). In addition, Bichsel *et al.*, (2013) suggested a topical inhibition of signals downstream from

EGFR for protection from CIA (Bichsel *et al.*, 2013). Therefore, because “artificial” deceleration of cell growth by blockade of the cell cycle would be expected to reduce the cytotoxic effects of chemotherapy drugs, “protective pre-conditioning” (PPC) by pharmacological inhibition of EGFR signalling might represent an efficient strategy to reduce the effects of chemotherapy drugs in the HFs.

#### **4.4 Chapter Aims**

Understanding the mechanisms regulating cell cycle progression in response to drug treatment at physiological temperature and cooling is vital for elucidating pathways responsible for the protection cooling provides against drug toxicity. Using such analyses, investigating the response to a range of temperatures could help to optimise cooling as a method to protect against chemotherapy induced cell damage. The overall aim of the work described in this chapter was to investigate *in vitro* the effects of both cooling and chemotherapy drugs on the cell cycle and using this cell cycle analysis to determine whether cooling ameliorates the effects of cytotoxic drugs on the cell cycle of human keratinocytes. Furthermore, pharmacological inhibition of EGFR signalling (using the well characterised antagonist PD153035) was employed to assess whether EGFR signalling blockade could reduce the cytotoxic effects of chemotherapy and thus if PD153035 combined with cooling could provide higher protection than cooling alone.

**Specifically the aims of the work in this chapter were to:**

- Explore the effects of cooling on HaCaTa cell cycle and the distribution of cell cycle phases at cooling conditions
- Investigate the effects of chemotherapeutic agents (4-OH-CP, doxorubicin, and docetaxel) on HaCaTa cell cycle at physiological temperatures and to compare with cooling conditions / low temperatures (22°C and 18°C).
- Evaluate the ability of the EGFR tyrosine kinase inhibitor PD153035 to suppress cell cycle progression and reduce cytotoxicity induced by chemotherapy drugs in HaCaTa cells with and without cooling, as a strategy to enhance the effects of cooling by PPC.

## 4.5 Cell cycle analysis in HaCaTa cells using flow cytometry

Initially, cell cycle analysis of untreated HaCaTa cells grown under standard culture conditions 36h after seeding was carried out. The distribution of cells in different phases of the cell cycle was determined by flow cytometry after labelling with PI as detailed in the methods section 2.12.4. Figure 4-1 shows representative data from such analysis, including dot plots (for doublet discrimination) and histograms (to visualise and quantify the proportion of cells in the different cell cycle phases). The different stages of the cell cycle are clearly denoted, including the G1 phase of the cell cycle ( $2n$  DNA content), in the middle the S phase peak, and the right-hand peak represents cells in G2/M phase having ( $4n$  DNA content) just before mitosis. The apoptotic cells, which is represented by the subG0/G1 population is seen to the left of the G1 peak (Figure 4-1).

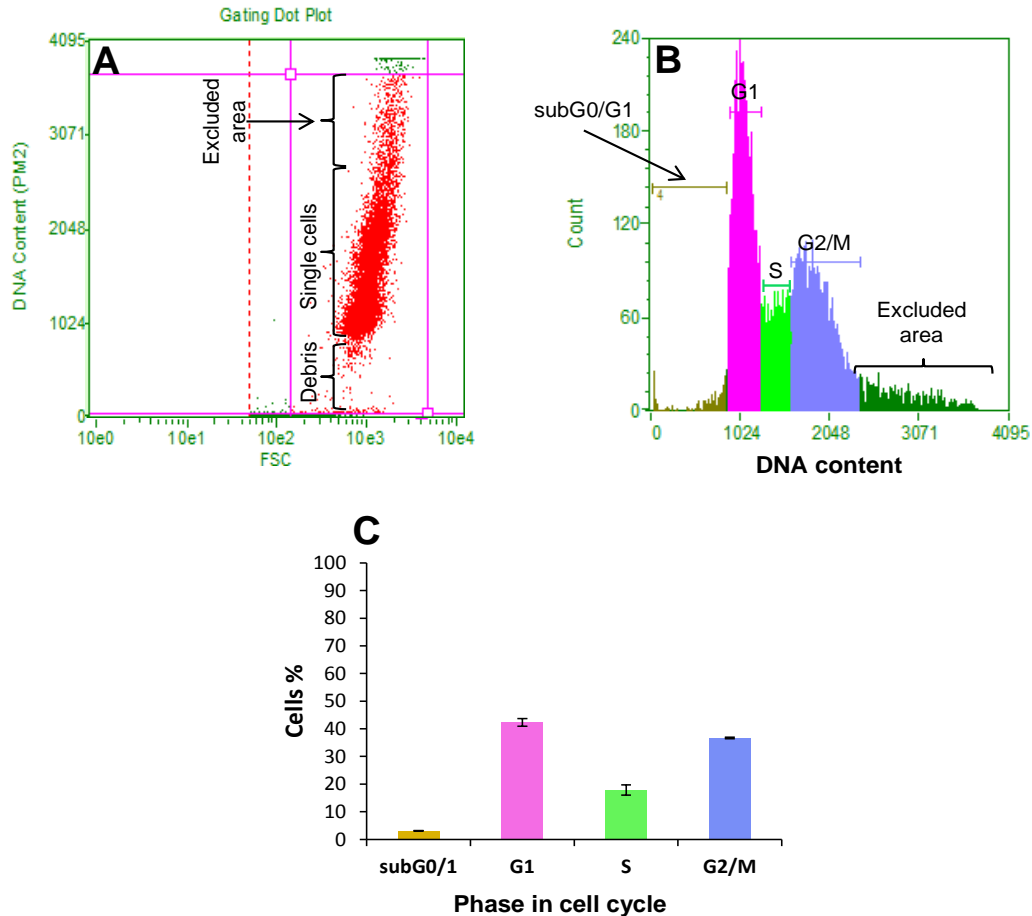


**Figure 4-1 Representative cell cycle analysis of unsynchronised proliferating HaCaTa cells in culture**

$9 \times 10^5$  HaCaTa cells were harvested and fixed in 70% ethanol, DNA stained with PI and cells acquired by flow cytometry for cell cycle analysis using the Guava cell cycle assay software module. **A)** Representative plot from a set of three experiments, showing “gating” to distinguish cells of interest from cells in apoptosis (subG0/G1) and to discriminate doublets. **B)** The gated data (from A) is used to plot the histogram, which shows the percentage of cells in G1, S, G2/M, and subG0/G1. **C)** Percentages of cells in G1 (42.3%), S (17.9%), G2/M (36.7%) and subG0/G1 (3.1%) phases are shown as bar graphs and are presented as mean % ( $\pm$ S.E.M.) from three independent biological experiments, each consisting of 2 technical replicates.

#### **4.5.1 Flow cytometric analysis of human keratinocytes following treatment with chemotherapy drugs**

Several studies have shown that exposure of cell lines to chemotherapy drugs induces cell arrest *in vitro* (Jordan and Wilson, 2004; Senderowicz, 2002). In order to better characterise the cytotoxic effects of the chemotherapy drugs used in this study, and to determine whether these drugs elicited alterations in cell cycle progression, cell cycle analysis was performed. The effects of chemotherapeutic drugs on HaCaTa cell cycle distribution were examined using PI labelling and flow cytometry as above. HaCaTa cells were treated with 0.5 µg/mL doxorubicin, 0.01 µg/mL docetaxel, and 7.5 µg/mL 4-OH-CP (Figure 4-2 and 4-3). These drug concentrations were selected for analysis because they were the concentrations at which cooling demonstrated the greatest relative rescue of cells compared to the toxicity observed at 37°C. To quantify cell cycle distribution, both attached and floating cells were collected and analysed.

After treatment with doxorubicin, cell cycle analysis was performed 36h later and cells clearly accumulated in G2/M phase 75.7% ( $\pm$  2.1) compared with the control cells 36.7% ( $\pm$  1.8). This was accompanied by a decreased G1 cell population of the treated cells in comparison with control cells. Furthermore, the subG0/G1 phase of cells treated with doxorubicin increased compared with control (Figure 4-2A 4-2B). Doxorubicin acts by intercalating between the paired bases in DNA, as a result, cells in the S phase are most sensitive to doxorubicin treatment, due to the fact that the DNA is uncoiled at this phase for DNA replication (Barlogie *et al.*, 1976). Yet, interestingly, rather than showing an increase in S phase, as shown in Figure 4-2A, that the cells were accumulated in G2/M after 36h.

Results for cells treated with docetaxel showed that the percentage of cells in G2/M phase after 36h increased to 45.5% ( $\pm$  0.5) compared to 36.7% ( $\pm$  1.8) for the controls (Figure 4-2C). There was a corresponding decrease in cells in the G1 and S phases. In addition, there was a striking increase in the subG0/G1 fraction 28.3% ( $\pm$  1.2) in cells treated with docetaxel compared to untreated control cells 3.1% ( $\pm$  0.3). The detection of a subG0/G1 peak is a specific marker of apoptosis, which is evidence that cells arrest at G2/M and underwent crisis, leading to irreversible arrest and subsequent activation of apoptosis.

Upon treatment HaCaTa cells with 7.5 µg/mL 4-OH-CP there was a substantial accumulation of cells in the S phase 74.8% ( $\pm$  0.4) compared with the control 17.9% ( $\pm$  1.4); this was accompanied by a significant decrease in the percentage of cells in the G1 and G2/M phases (Figure 4-2D). These data suggested that effects of the 4-OH-CP on the proliferation of HaCaTa cells involved a block during the S phase. All cell cycle analysis

results from independent experiments are summarised in Figure 4-2 as bar graphs which allows direct comparison of the percentage of cells in each sample / treatment for controls (untreated cells) and drug (doxorubicin, docetaxel and 4-OH-CP)-treated cells. Cell cycle analysis revealed significant changes in the percentage of treated cells compared with the control cells (untreated cells) in subG0/G1, G1, S and G2/M phase of the cell cycle.

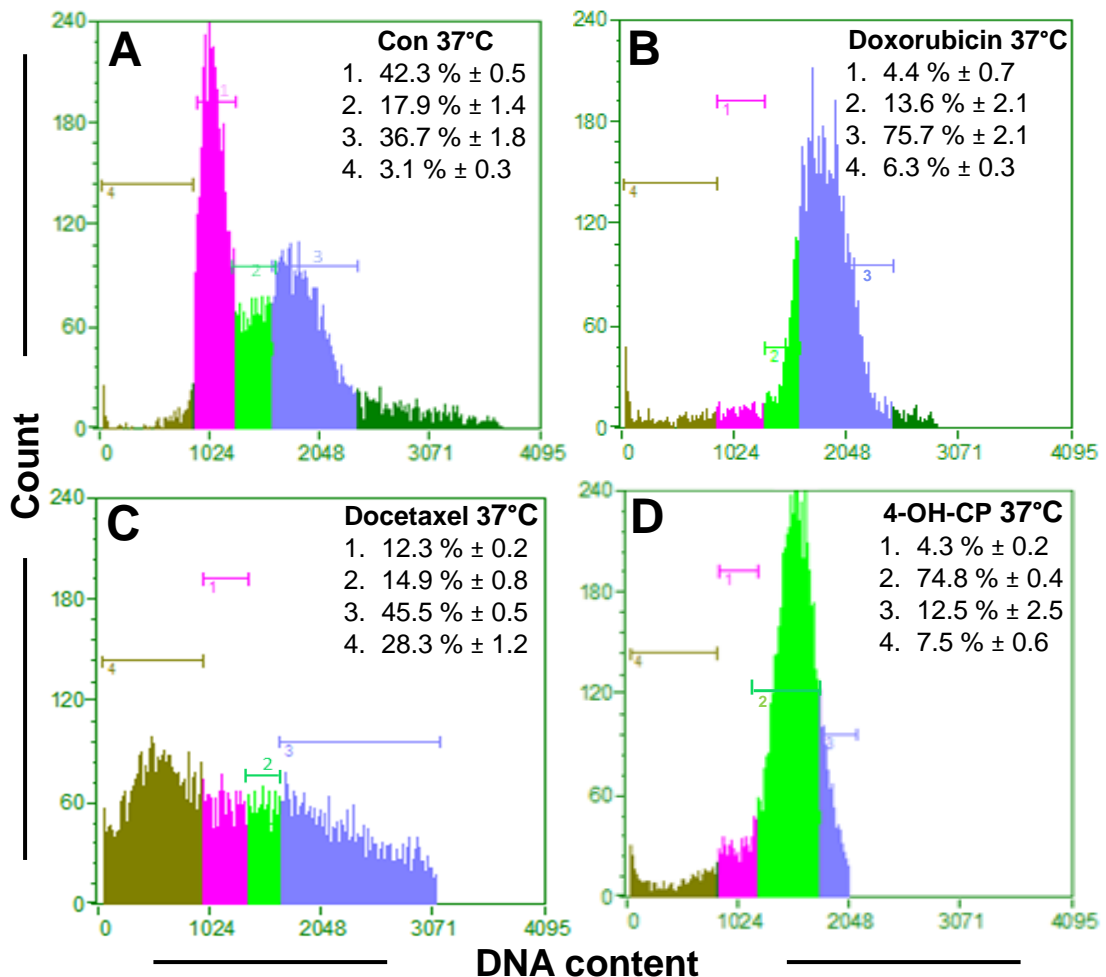


**Figure 4-2 Cell cycle analysis of HaCaTa cells after 36h chemotherapeutic drug treatment**

9x10<sup>5</sup> HaCaTa cells were cultured in 10 cm<sup>2</sup> dishes in complete KSFM medium and cells were incubated overnight at 37°C / 5% CO<sub>2</sub>. Cells were treated with 0.5 µg/mL doxorubicin, 0.01 µg/mL docetaxel and 7.5 µg/mL 4-OH-CP for 2h at 37°C compared with vehicle control (cells treated with medium containing DMSO, in which the reagent was dissolved). The solvent represents the maximum amount of DMSO corresponding to the highest drug concentration). The drugs were then removed; dishes were rinsed with PBS to remove any traces of drug and cultures incubated in fresh medium. Both attached and floating cells were harvested after 36h and fixed in 70% ethanol and DNA stained with PI. 10,000 cells were acquired on a Guava EasyCyte flow cytometer and results analysed using GuavaSoft software. Results represent plots of one set of triplicates experiments and the distribution and percentage of cells in subG1/G0, G1, S, and G2/M phases of the cell cycle are indicated. Percentages of cells in each cell cycle phase distribution means values were determined and indicated in each pane from three independent biological experiments, each consisting of 2 technical replicates. Regions 1, 2, 3 and 4 on each panel represent G0/G1, S, and G2/M and subG0/G1 phase of the cell cycle, respectively.

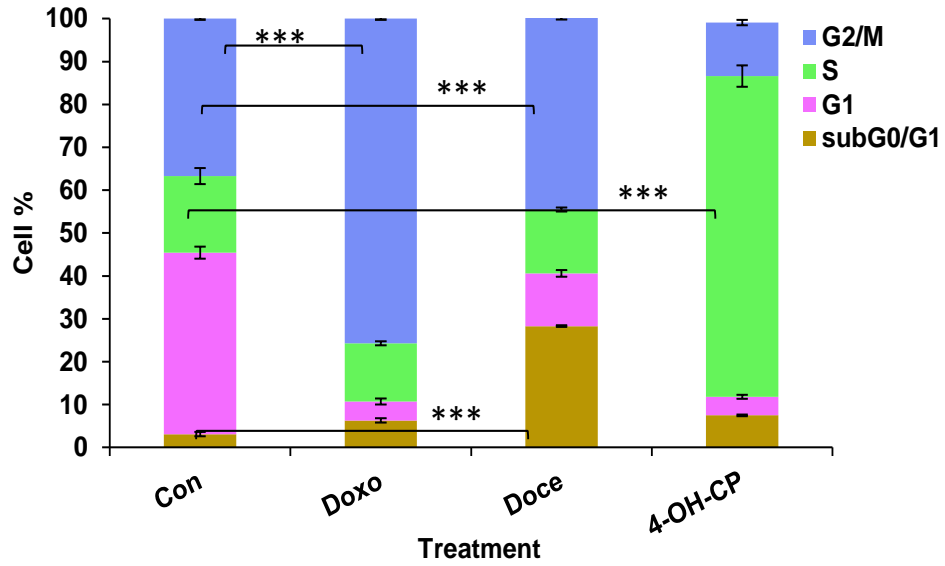


**Figure 4-3 Summary of independent replicate experiments for cell cycle analysis of HaCaTa cells after 36h chemotherapeutic drug treatment**

Bar graph summarises data obtained from three independent biological experiments, each consisting of 2 technical replicates performed as described in Figure 4-2. Bars represent mean values of % of cells ( $\pm$ S.E.M.) \*\*\*,  $p < 0.001$ .

#### **4.5.2 The impact of reducing temperature on untreated cultured cells**

Cooling may lead to short term reversible cell cycle arrest in cell culture, suggesting that cooling might be a way to achieve selective toxicity of chemotherapeutic agents for cells (Matijasevic, 2001). We hypothesised that it might be possible that the cytoprotective effect of cooling against chemotherapy-induced toxicity was due to its ability to reduce cell proliferation rates. The present study thus tested the influence of cooling on cell cycle distribution in HaCaTa cells at 37°C and 22°C, representing the physiological temperature and cooling conditions, respectively, and with and without chemotherapeutic agents.

To understand whether cooling can protect from cytotoxicity of chemotherapy drugs by altering the effects of these drugs on the cell cycle, we first investigated the effects of cooling alone on cultured human keratinocytes. These experiments involved reduction of the culture temperature to 22°C and 18°C in HaCaTa cells in order to determine cell cycle distribution after cold exposure for 2h as well as the time required for cell cycle recovery following rewarming at 37°C. Initially the effect of 22°C in HaCaTa cell cycle distribution was examined. HaCaTa cells were incubated at 22°C for 2h, the percentage of cells in each phase of the cycle was G1 phase 52.9% ( $\pm$  2.1), S phase 27.2% ( $\pm$  0.9) and G2/M phase 16.9% ( $\pm$  0.5) compared to 41.7% ( $\pm$  0.5), 22.4% ( $\pm$  1.8), and 32.8% ( $\pm$  1.4) at 37°C, respectively. Therefore, clearly this analysis showed an increase in the G1 and S phase populations and a reduction of cell entry into G2/M. Importantly, there was no significant difference in subG0/G1 between cells at 22°C 3.1% ( $\pm$  0.1) and 37°C 3.3% ( $\pm$  0.3) confirming that cooling is not detrimental (toxic) to the cells (Figure 4-4A and B). Thus, exposure of cells to 22°C appeared to “slow down” entry to the cell cycle and causing a reduction in cell proliferation rate evident by the increase in G1 and S phase peaks and reduction in G2/M phase (Figure 4-4C).

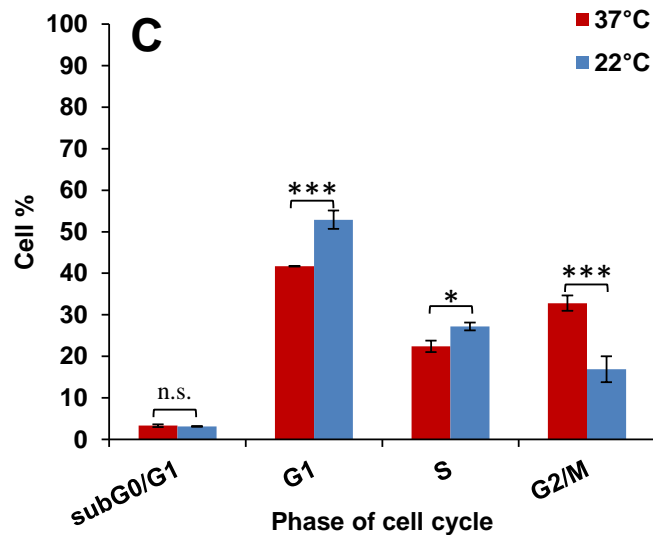
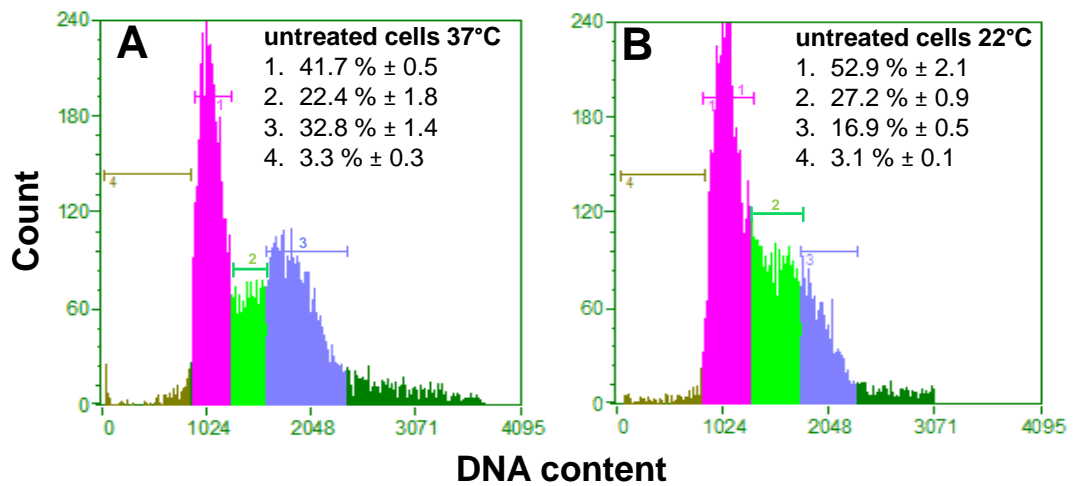


**Figure 4-4 Effects of cooling at 22°C vs physiological temperature on HaCaTa cell cycle distribution**

9x10<sup>5</sup> HaCaTa cells were cultured 10 cm<sup>2</sup> dish in KSFM medium and cells were incubated overnight in 37°C / 5% CO<sub>2</sub>. Cells were incubated for 2h at 22°C and 37°C as a control. Both attached and floating cells were harvested and fixed in 70% ethanol, DNA stained with PI. 10,000 cells were acquired on a Guava EasyCyte flow cytometer and results analysed using GuavaSoft software. Results representative plots of one set of triplicates experiments and the distribution percentages of cells in each cell cycle phase distribution means values were calculated from triplicate experiments. Regions 1, 2, 3 and 4 on each panel represent G0/G1, S, and G2/M and subG0/G1 phase of the cell cycle, respectively. **A)** Control cells at 37°C **B)** Cells incubated at 22°C **C)** Bars correspond to mean (±S.E.M.) from three independent biological experiments, each consisting of 2 technical replicates. n.s., non-significant; \*,  $p < 0.05$ ; \*\*\*,  $p < 0.001$ .

### 4.5.3 The effects of cooling in the prevention of the changes in the cell cycle induced by chemotherapy drugs

Understanding the mechanisms *via* which cooling may modulate the cell cycle in cells treated with chemotherapy drugs is essential for defining the mechanisms behind the cytoprotective effect of cooling from chemotherapy drug-induced cytotoxicity. The distributions of cells in individual cell cycle phases at different time points were investigated in order to a) perform a time course study to follow up cell cycle distribution changes following a 2h drug treatment, b) determine if cooling can prevent the changes in the cell cycle distribution caused by individual drugs and c) investigate what is the required time length for each individual drug needed for cell cycle distribution to return to a normal pattern, by comparing cell cycle analysis data for 37°C *versus* cooling conditions.

The effects of cooling in cell cycle distribution in HaCaTa cells at various times after chemotherapy drug treatment at 37°C, 22°C or 18°C compared to untreated control cells were investigated. HaCaTa cells were treated with 0.5 µg/mL doxorubicin, 0.01 µg/mL docetaxel, and 7.5 µg/mL 4-OH-CP as previously and cell cycle analysis was performed at various time points post the 2h treatment. Specifically, cell cycle analysis was carried out at 0, 1, 2, 4, 8 and 24h and treated cells were compared with incubation in drug-free medium at 22°C and at 2 and 36h at 18°C (Materials and Methods section 2.12.4).

Tests were performed at 22°C and 37°C in HaCaTa cells treated with doxorubicin, docetaxel and 4-OH-CP at T=0h (post the 2h treatment) (Figures 4-5 and 4-6). In agreement with previous findings (section 3-5), there was a significant change in cell cycle phase distribution in untreated cells post incubation for 2h at 22°C compared with untreated cells at 37°C (Figure 4-4). As shown in Figure 4-5, there was no significant change in cell cycle phase in HaCaTa cells treated with doxorubicin or docetaxel at 37°C (T = 0h) compared with the control (untreated) cells. Cells treated with doxorubicin and docetaxel whilst incubated at 22°C, showed little change in the percentage of cells in different phases of the cell cycle phases compared with the treated cells at 37°C (Figure 4-5 D and F). Cells treated with 4-OH-CP at 22°C showed a decrease in cells in the G1 population 37.5% ( $\pm$  1.7) and an increase in G2/M 42.6% ( $\pm$  1.3) (Figure 4-5G) compared with G1 and G2/M of the control at 37°C 41.7% ( $\pm$  0.6) and 32.8% ( $\pm$  3.9) respectively (Figure 4-5A). However, untreated cells incubated at 22°C followed by rewarming at 37°C were recovered rapidly and returned to the normal cell cycle distribution after (T=1h) (Figure 4-7B). This indicates a correlation between cell growth and temperature and that cell cycle progression is temperature sensitive and reversible.

The second test series was performed comparing the effect of chemotherapeutic drugs on HaCaTa cell cycle (T=1h) post chemotherapy treatment after the cells were incubated at 22°C and 37°C (Figures 4-7 and 4-8). The result showed that in cells treated with doxorubicin at 37°C there was a small reduction in G1 phase compared to 22°C (Figure 4-7A and B). However, for cells treated with 4-OH-CP at 37°C (Figure 4-7G) or 22°C (Figure 4-7H) there was no difference in cell cycle distribution. On the other hand, for cells treated with docetaxel at 37°C, the percentages of cells in G1, S and G2/M were 33.4% ( $\pm$  3.7), 27.1% ( $\pm$  1.4), and 37.3% ( $\pm$  2.6), while at 22°C the corresponding values were 41.7% ( $\pm$  0.7), 21.5% ( $\pm$  0.9) and 34.2% ( $\pm$  0.9) (Figure 4-7E and F). This was compared to the values for untreated control cells at 37°C of 39.8% ( $\pm$  1.2), 21.1% ( $\pm$  2) and 36.6% ( $\pm$  1.2), respectively. In the presence of docetaxel, the depolymerisation of the microtubules is interrupted, which results in stabilization of the microtubules. These results indicate that docetaxel treatment causes cell cycle disturbance more quickly than that which occurs with doxorubicin and 4-OH-CP.

Cell cycle distribution analyses at T=2h is shown in Figures 4-9 and 4-10. Doxorubicin induced a marked increase in the subG0/G1 population at 37°C (Figure 4-9C) and 22°C (Figure 4-9D) which was 6% ( $\pm$  0.2) and 5.3% ( $\pm$  1) respectively compared to controls (untreated cells) 2.8% ( $\pm$  0.5) (Figure 4-9A). The population of G1 in cells treated at 37°C was decreased significantly compared with cells treated at 22°C or controls. Two hours after docetaxel treatment at 37°C the percentage of cells in G1 was decreased significantly to 28.8% ( $\pm$  2.2) in comparison to cells incubated at 22°C 41.3% ( $\pm$  1) and control cells at 37°C 38.7% ( $\pm$  4) (Figure 4-9A). In addition, the percentage of G2/M phase increased to 45.5% ( $\pm$  3.7) for cells at 37°C compared to 22°C 33.9% ( $\pm$  1.9) or the control at 37°C 36.8% ( $\pm$  3).

The results of the cell cycle analysis at T=4h after treatment are shown in Figures 4-11 and 4-12. This data showed that doxorubicin caused cell arrest at G2/M phase at 37°C and unexpectedly at 22°C as well, although G2/M phase at 37°C 39.4% ( $\pm$  3) (Figure 4-11C) was higher than at 22°C 38.2% ( $\pm$  1.2) (Figure 4-11D) compared to the control 34.4% ( $\pm$  0.7). Four hours after docetaxel treatment at 37°C were cells arrested at G2/M 45.1% ( $\pm$  0.1) (Figure 4-11E) compared to treated cells at 22°C 31.3% ( $\pm$  1.8) (Figure 4-11F) or control cells at 37°C this was 34.4% ( $\pm$  0.7) (Figure 4-11A). By contrast, there were significantly fewer cells in G1 after docetaxel treatment at 37°C 20.9% ( $\pm$  1.6) compared to control at 37°C 42.6% ( $\pm$  2.5) but importantly this was almost completely restored for the cells incubated at 22°C 38.9% ( $\pm$  1). This protective effect of cooling also reduced the apoptotic cell population peak (subG0/G1) which was for cells incubated at 37°C 10.8% ( $\pm$  0.3) compared to at 22°C 5% ( $\pm$  0.3).

Cell cycle distributions at T=8h post treatment are provided in Figures 4-13 and 4-14. Cells were treated with doxorubicin and results shown in Figure 4-13 indicate for cells treated at 37°C and 22°C, that G1 phase was significantly less than in control cells (Figure 4-13A). However, the percentages of cells in G2/M after doxorubicin treatment increased significantly at both 37°C and 22°C compared to the control. In cells treated with docetaxel (T=8h) at 37°C, it was observed that 17.3% ( $\pm 0.6$ ) were in the apoptotic subG0/G1 phase (Figure 4-13E) indicating that after mitotic arrest a larger number of cells undergo apoptosis and again cooling to 22°C significantly reduced subG0/G1 to 5.9% ( $\pm 0.1$ ). In addition, the G2/M arrest induced by docetaxel at 37°C was higher than at 22°C 50.1% ( $\pm 1.2$ ) and 35% ( $\pm 3$ ), respectively, indicating that the cytotoxicity of docetaxel was reduced. In addition, there were significantly less G1 cells at 37°C 15.5% ( $\pm 0.7$ ) compared with at 22°C 40.7% ( $\pm 0.6$ ). By contrast with earlier time points, there were significant changes in cell cycle distribution after treatment with 4-OH-CP at both 37°C and 22°C (Figure 4-11G and H) with the percentage of subG0/G1 at 37°C 15.6% ( $\pm 1.8$ ) was significantly higher than, at 22°C 6.6% ( $\pm 0.2$ ). This was accompanied by a significantly lower number of G2/M cells after treatment at 37°C 20.3% ( $\pm 0.8$ ) compared with at 22°C 36.5% ( $\pm 2.2$ ).

Experiments on cell cycle distribution at T=24h post treatment are summarised in Figures 4-15 and 4-16. Experiments involving treatment with doxorubicin (T=24h) showed that many cells appeared to be arrested at the S and G2/M phase at both 37°C (Figure 4-15C) and at 22°C (Figure 4-15D). As shown in Figure 4-15, at T=24h after treatment with docetaxel at 37°C higher percentages of cells are in subG0/G1 and G2/M phase was observed compared to the cells treated at 22°C. These results suggest that docetaxel at 37°C is able to stimulate cell death (indicated by the increase in subG0/G1) and this may be the result of increased G2/M arrest; reducing the temperature to 22°C clearly reduced these effects. In cells treated with 4-OH-CP, at 37°C there was a distinct peak representing a cell population arrested in S phase (Figure 4-15G), with 55.1% ( $\pm 3.2$ ) of cells being in S phase compared to 18.4% ( $\pm 2.8$ ) at 22°C (Figure 4-15H) and compared to control cells 23.5% ( $\pm 2.7$ ) (Figure 4-15A). Cells maintained 16% ( $\pm 2.8$ ) at 37°C were in G1 compared to 32.5% ( $\pm 0.7$ ) at 22°C, which was significantly reduced compared with the control cells at both 37°C 42.6 ( $\pm 0.7\%$ ) and 22°C 43.7% ( $\pm 0.7$ ). On the other hand, cells in the G2/M population increased to 46.6% ( $\pm 4$ ) at 22°C and this was reduced to 25.4% ( $\pm 0.4$ ) at 37°C. This compares to 30.7% ( $\pm 1.6$ ) for control cells (Figure 4-15A). These findings support results presented in chapter 3 that temperatures lower than the physiological temperature protect cells from 4-OH-CP cytotoxic effects.

Collectively, the above results indicate that treatment of HaCaTa cells with chemotherapy drugs at 37°C altered cell cycle progression at different phases according to

the mechanism of action of these drugs (Morgan, 2003). However, treating the cells under cooling conditions inhibited the effects of the chemotherapy drugs and reduced induced apoptosis (indicated by the observed reduction in the percentage of subG0/G1 cells).

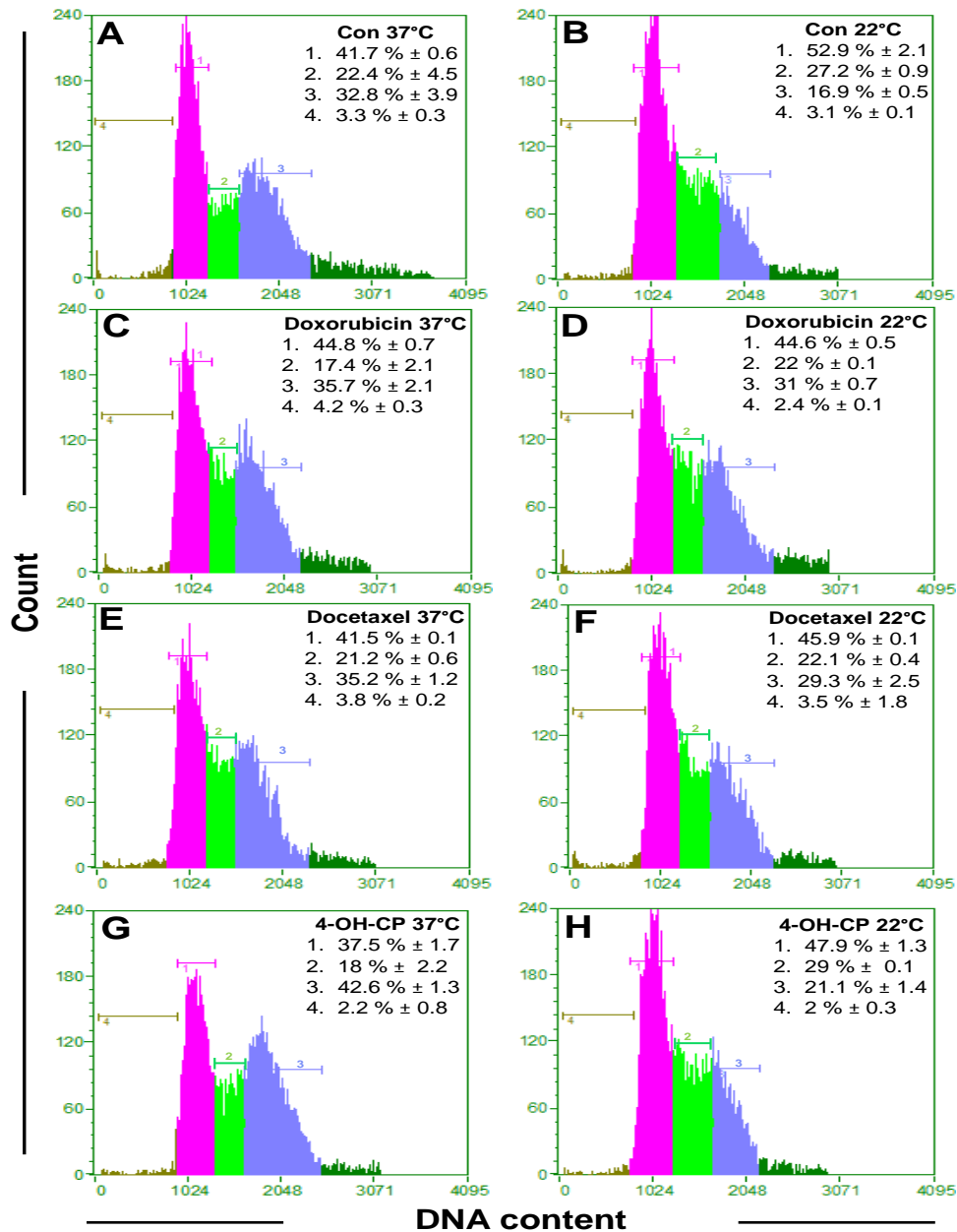


**Figure 4-5 Cell cycle analysis of HaCaTa cells after 0h chemotherapeutic drug treatment at 22°C and 37°C**

9x10<sup>5</sup> HaCaTa cells were cultured in 10 cm<sup>2</sup> dishes in KSFM medium and cells were incubated overnight in 37°C / 5% CO<sub>2</sub>. HaCaTa cells were treated with 0.5 µg/mL of doxorubicin (Doxo), 0.01 µg/mL docetaxel (Doce), and 7.5 µg/mL 4-OH-CP for 2h at 37°C and 22°C compared with vehicle control (cells treated with medium containing DMSO, in which the reagent was dissolved). The solvent represents the maximum amount of DMSO corresponding to the highest drug concentration). The drugs were then removed; dishes were rinsed with PBS to remove any traces of drug and cultures incubated in fresh medium. Both attached and floating cells were harvested after 0h and fixed in 70% ethanol, DNA stained with PI. 10,000 cells were acquired on a Guava EasyCyte flow cytometer and results analysed using GuavaSoft software. Results representative plots of one set of triplicate experiments and the distribution and percentage of cell cycle in subG0/G1, G1, S, and G2/M phase of the cell cycle are indicated. Percentages of cells in each cell cycle phase distribution mean values were calculated from three independent biological experiments, each consisting of 2 technical replicates. Regions 1, 2, 3 and 4 on each panel represent G0/G1, S, and G2/M and subG0/G1 phase of the cell cycle, respectively.

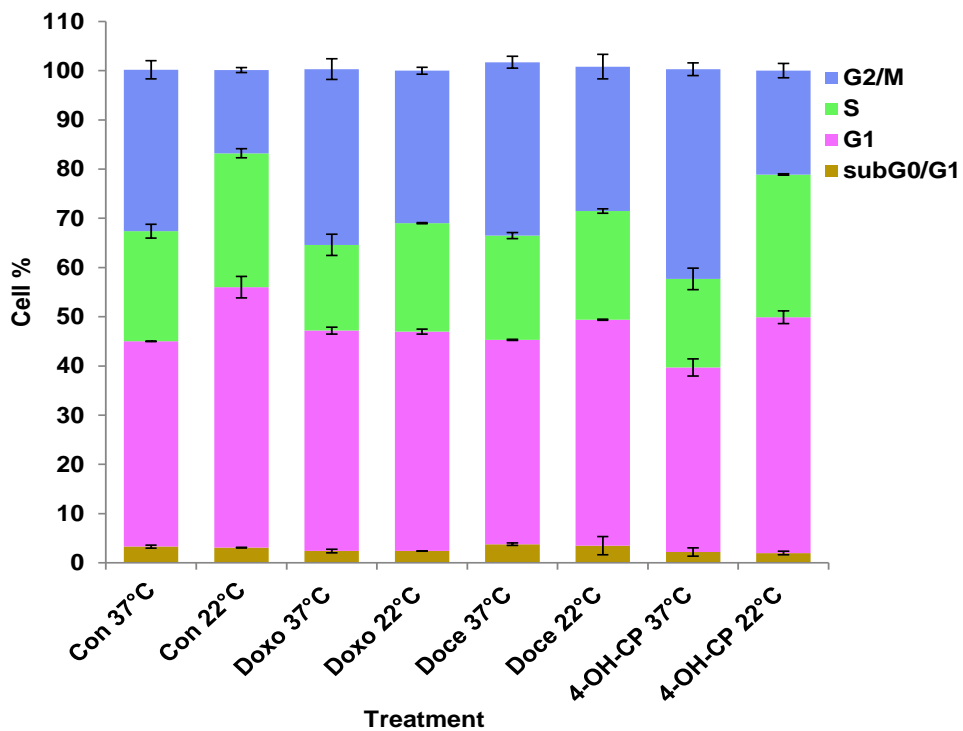


**Figure 4-1 Summary of independent replicate experiments for cell cycle analysis of HaCaTa cells after 0h chemotherapeutic drug treatment**

Bar graph summarises data obtained from three independent biological experiments, each consisting of 2 technical replicates as in Figure 4-2. Bars represent mean values of % of cells ( $\pm$ S.E.M.).

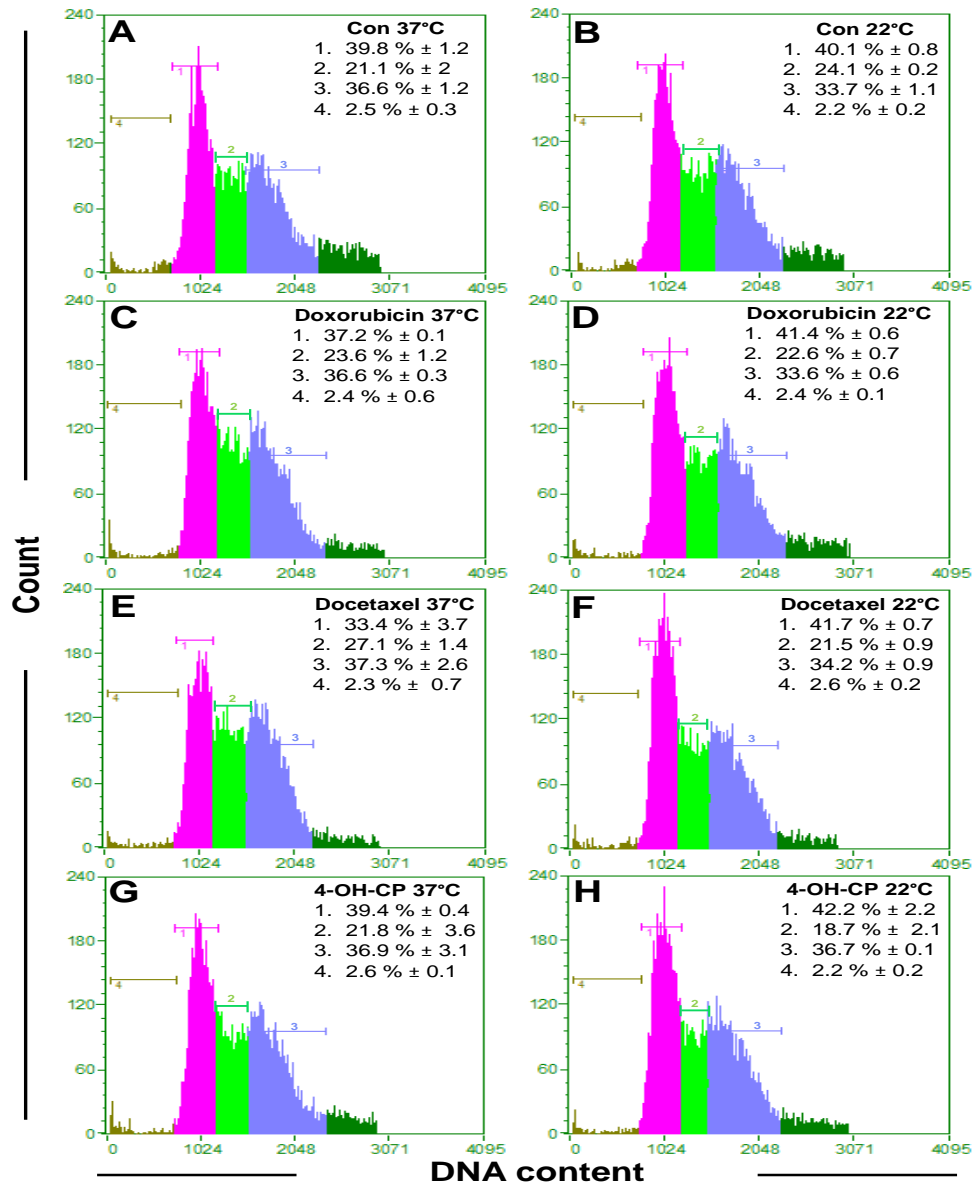


**Figure 4-6 Cell cycle analysis of HaCaTa cells after 1h chemotherapeutic drug treatment at 22°C and 37°C**

$9 \times 10^5$  HaCaTa cells were cultured in 10 cm<sup>2</sup> dishes in KSFM medium and cells were incubated overnight in 37°C / 5% CO<sub>2</sub>. HaCaTa cells were treated with 0.5 µg/mL of doxorubicin (Doxo), 0.01 µg/mL docetaxel (Doce), and 7.5 µg/mL 4-OH-CP for 2h at 37°C and 22°C compared with vehicle control (cells treated with medium containing DMSO, in which the reagent was dissolved). The solvent represents the maximum amount of DMSO corresponding to the highest drug concentration). The drugs were then removed; dishes were rinsed with PBS to remove any traces of drug and cultures incubated in fresh medium. Both attached and floating cells were harvested after 1h and fixed in 70% ethanol, DNA stained with PI. 10,000 cells were acquired on a Guava EasyCyte flow cytometer and results analysed using GuavaSoft software. Results representative plots of one set of triplicate experiments and the distribution and percentage of cell cycle in subG0/G1, G1, S, and G2/M phase of the cell cycle are indicated. Percentages of cells in each cell cycle phase distribution mean values were calculated from three independent biological experiments, each consisting of 2 technical replicates. Regions 1, 2, 3 and 4 on each panel represent G0/G1, S, and G2/M and subG0/G1 phase of the cell cycle, respectively.

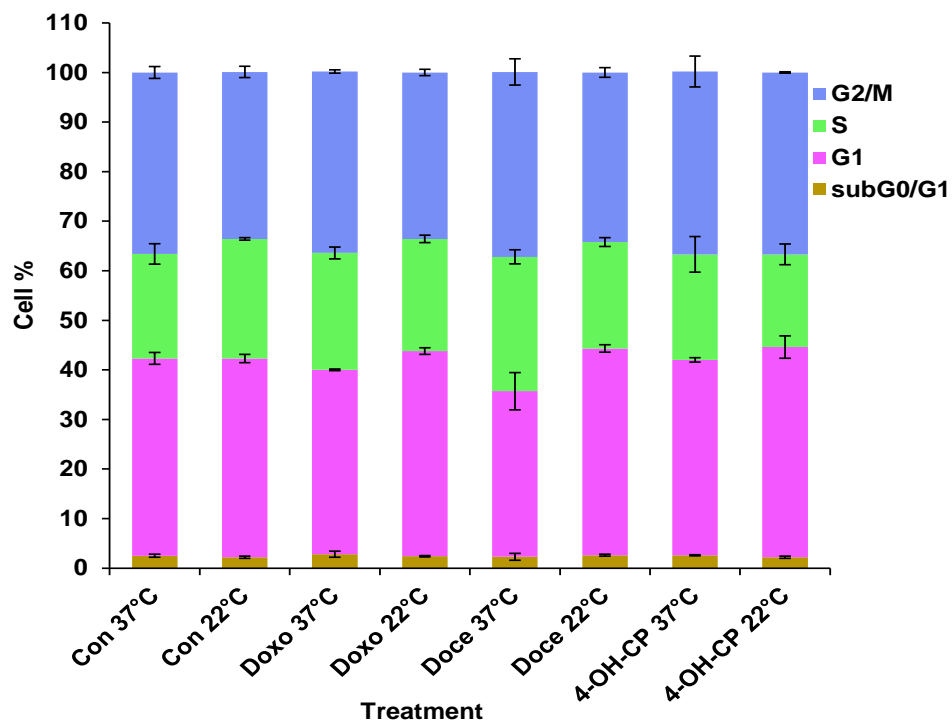


**Figure 4-2 Summary of independent replicate experiments for cell cycle analysis of HaCaTa cells after 1h chemotherapeutic drug treatment**

Bar graph summarises data obtained from three independent biological experiments, each consisting of 2 technical replicates as in Figure 4-7. Bars represent mean values of % of cells ( $\pm$ S.E.M.)

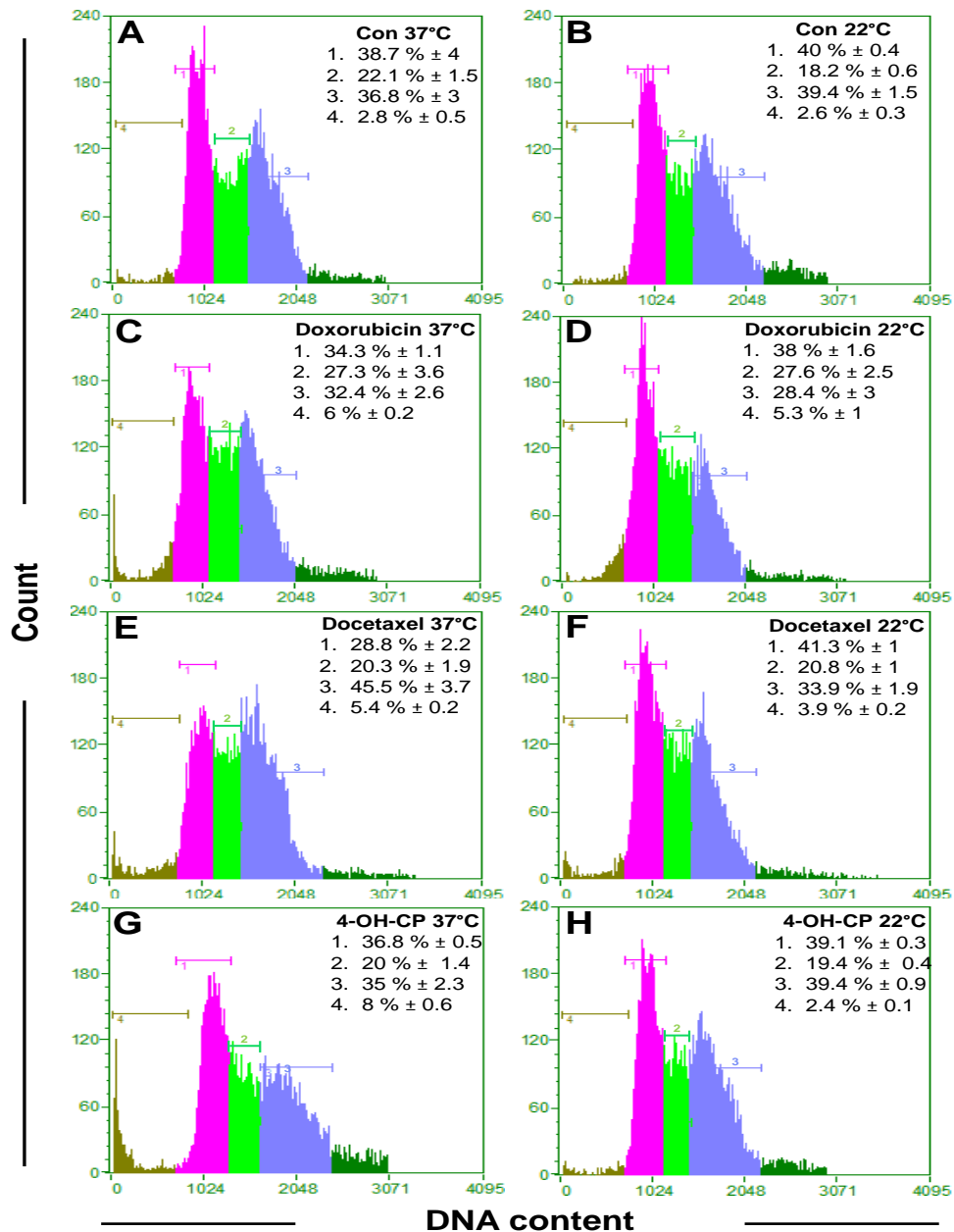


**Figure 4-7 Cell cycle analysis of HaCaTa cells after 2h chemotherapeutic drug treatment at 22°C and 37°C**

$9 \times 10^5$  HaCaTa cells were cultured in 10 cm<sup>2</sup> dishes in KSFM medium and cells were incubated overnight in 37°C / 5% CO<sub>2</sub>. HaCaTa cells were treated with 0.5 µg/mL of doxorubicin (Doxo), 0.01 µg/mL docetaxel (Doce), and 7.5 µg/mL 4-OH-CP for 2h at 37°C and 22°C compared with vehicle control (cells treated with medium containing DMSO, in which the reagent was dissolved). The solvent represents the maximum amount of DMSO corresponding to the highest drug concentration). The drugs were then removed; dishes were rinsed with PBS to remove any traces of drug and cultures incubated in fresh medium. Both attached and floating cells were harvested after 2h and fixed in 70% ethanol, DNA stained with PI. 10,000 cells were acquired on a Guava EasyCyte flow cytometer and results analysed using GuavaSoft software. Results representative plots of one set of triplicate experiments and the distribution and percentage of cell cycle in subG0/G1, G1, S, and G2/M phase of the cell cycle are indicated. Percentages of cells in each cell cycle phase distribution mean values were calculated from three independent biological experiments, each consisting of 2 technical replicates. Regions 1, 2, 3 and 4 on each panel represent G0/G1, S, and G2/M and subG0/G1 phase of the cell cycle, respectively.

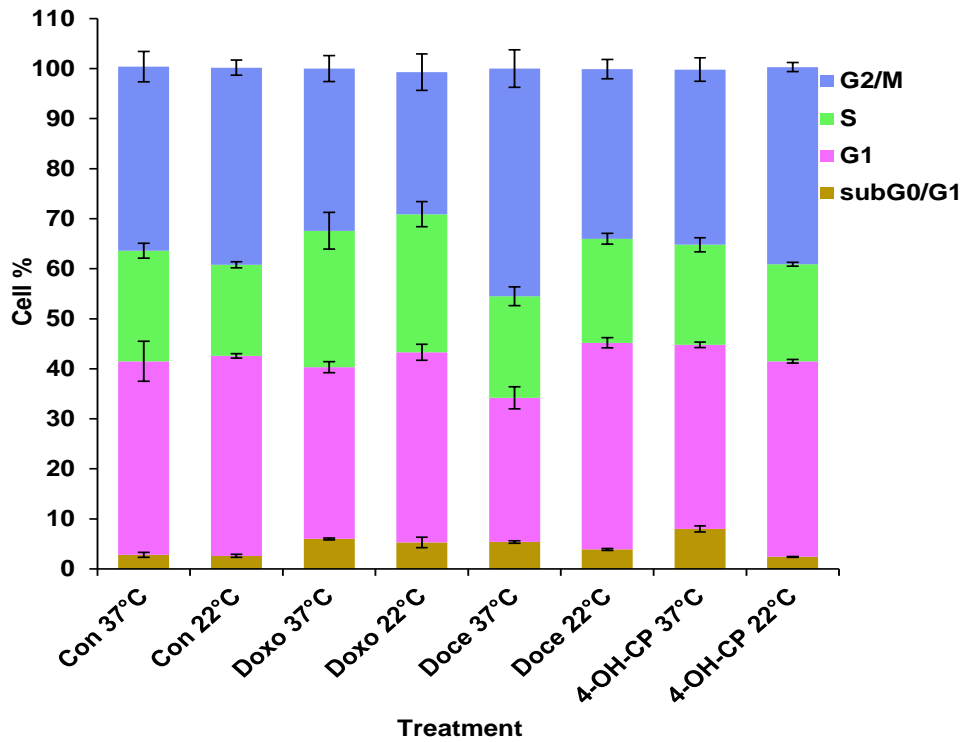


**Figure 4-8 Summary of independent replicate experiments for cell cycle analysis of HaCaTa cells after 2h chemotherapeutic drug treatment**

Bar graph summarises data obtained from three independent biological experiments, each consisting of 2 technical replicates as in Figure 4-9. Bars represent mean values of % of cells ( $\pm$ S.E.M.).

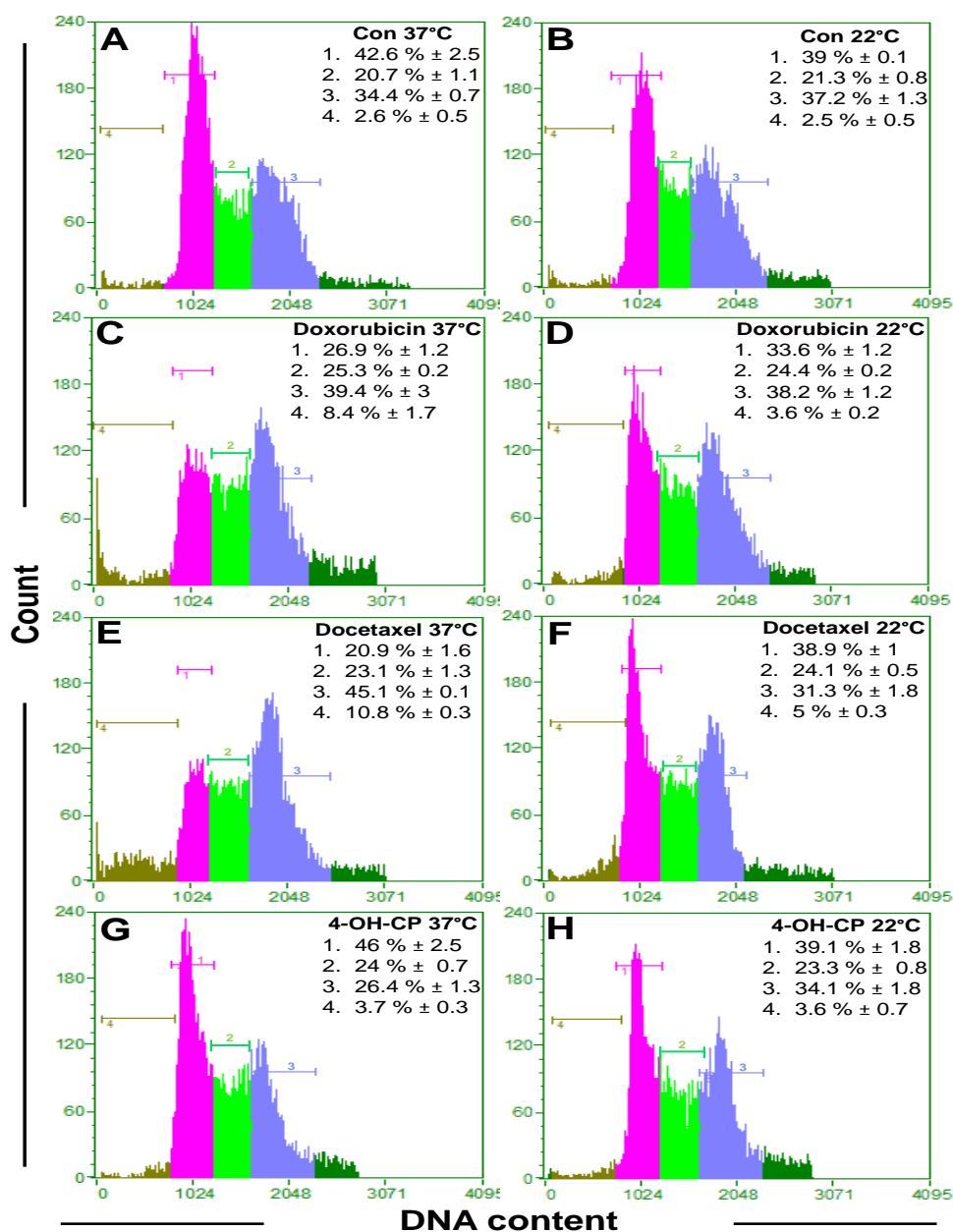


**Figure 4-9 Cell cycle analysis of HaCaTa cells after 4h chemotherapeutic drug treatment at 22°C and 37°C**

$9 \times 10^5$  HaCaTa cells were cultured in 10 cm<sup>2</sup> dishes in KSFM medium and cells were incubated overnight in 37°C / 5% CO<sub>2</sub>. HaCaTa cells were treated with 0.5 µg/mL of doxorubicin (Doxo), 0.01 µg/mL docetaxel (Doce), and 7.5 µg/mL 4-OH-CP for 2h at 37°C and 22°C compared with vehicle control (cells treated with medium containing DMSO, in which the reagent was dissolved). The solvent represents the maximum amount of DMSO corresponding to the highest drug concentration). The drugs were then removed; dishes were rinsed with PBS to remove any traces of drug and cultures incubated in fresh medium. Both attached and floating cells were harvested after 4h and fixed in 70% ethanol, DNA stained with PI. 10,000 cells were acquired on a Guava EasyCyte flow cytometer and results analysed using GuavaSoft software. Results representative plots of one set of triplicates experiments and the distribution and percentage of cell cycle in subG1, G1, S, and G2/M phase of the cell cycle are indicated. Percentages of cells in each cell cycle phase distribution mean values were calculated from three independent biological experiments, each consisting of 2 technical replicates. Regions 1, 2, 3 and 4 on each panel represent G0/G1, S, and G2/M and subG0/G1 phase of the cell cycle, respectively.

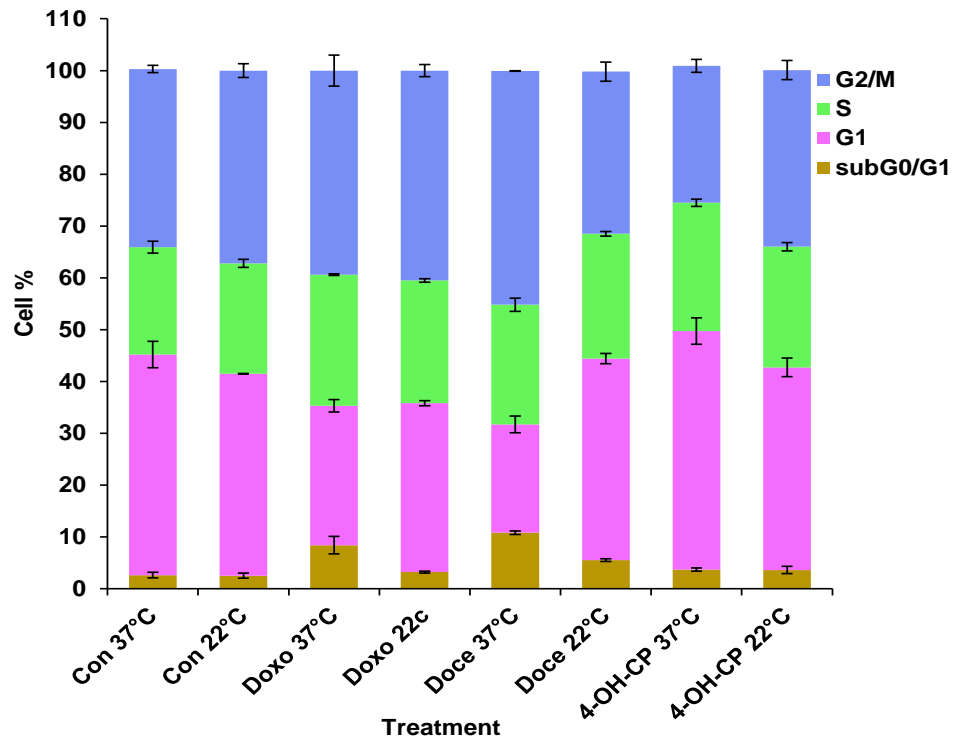


**Figure 4-10 Summary of independent replicate experiments for cell cycle analysis of HaCaTa cells after 4h chemotherapeutic drug treatment**

Bar graph summarises data obtained from three independent biological experiments, each consisting of 2 technical replicates as in Figure 4-11. Bars represent mean values of % of cells ( $\pm$ S.E.M.).

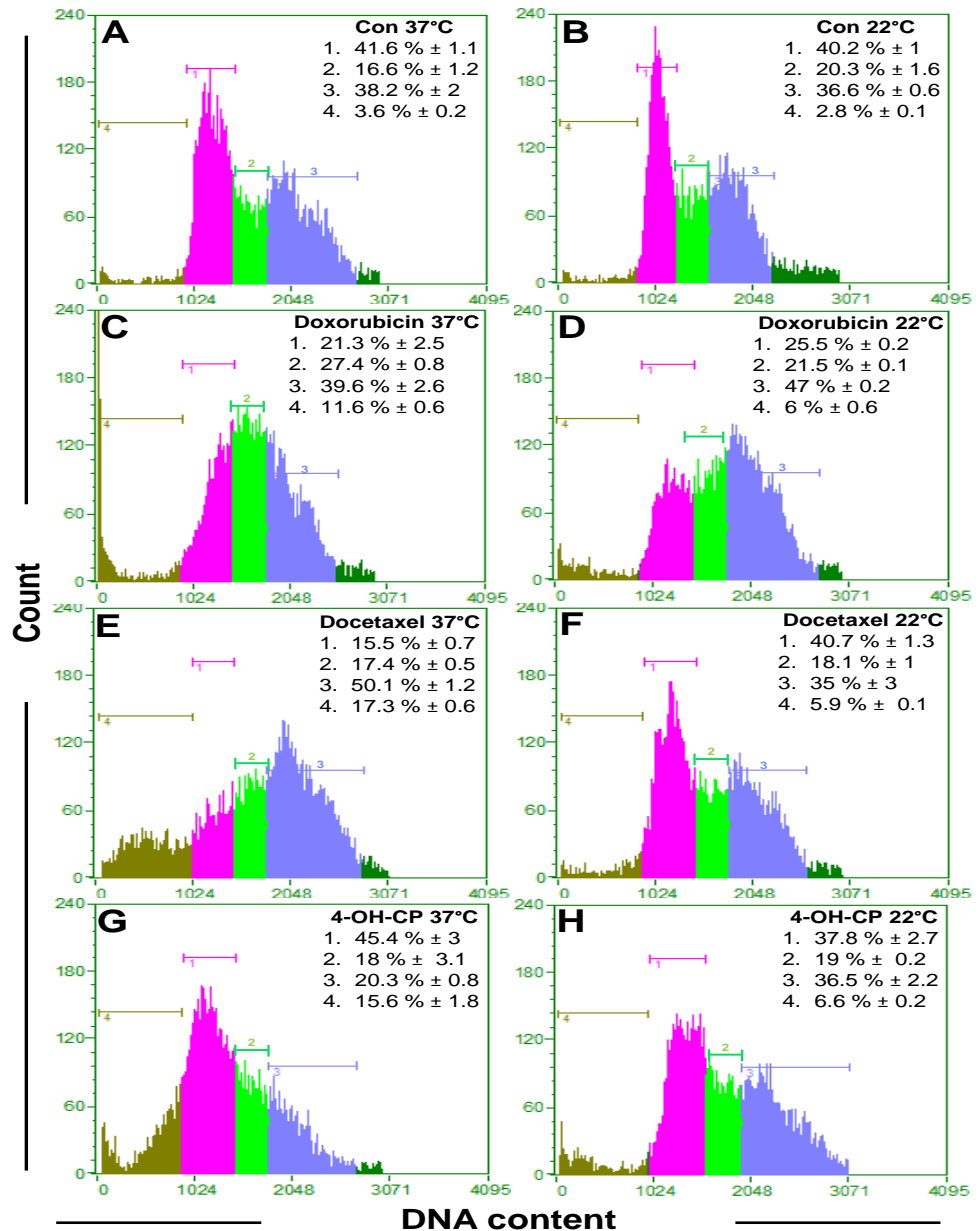


**Figure 4-11 Cell cycle analysis of HaCaTa cells after 8h chemotherapeutic drug treatment at 22°C and 37°C**

$9 \times 10^5$  HaCaTa cells were cultured in 10 cm<sup>2</sup> dishes in KSFM medium and cells were incubated overnight in 37°C / 5% CO<sub>2</sub>. HaCaTa cells were treated with 0.5 µg/mL of doxorubicin (Doxo), 0.01 µg/mL docetaxel (Doce), and 7.5 µg/mL 4-OH-CP for 2h at 37°C and 22°C compared with vehicle control (cells treated with medium containing DMSO, in which the reagent was dissolved). The solvent represents the maximum amount of DMSO corresponding to the highest drug concentration). The drugs were then removed; dishes were rinsed with PBS to remove any traces of drug and cultures incubated in fresh medium. Both attached and floating cells were harvested after 8h and fixed in 70% ethanol, DNA stained with PI. 10,000 cells were acquired on a Guava EasyCyte flow cytometer and results analysed using GuavaSoft software. Results representative plots of one set of triplicate experiments and the distribution and percentage of cell cycle in subG1, G1, S, and G2/M phase of the cell cycle are indicated. Percentages of cells in each cell cycle phase distribution mean values were calculated from three independent biological experiments, each consisting of 2 technical replicates. Regions 1, 2, 3 and 4 on each panel represent G0/G1, S, and G2/M and subG0/G1 phase of the cell cycle, respectively.

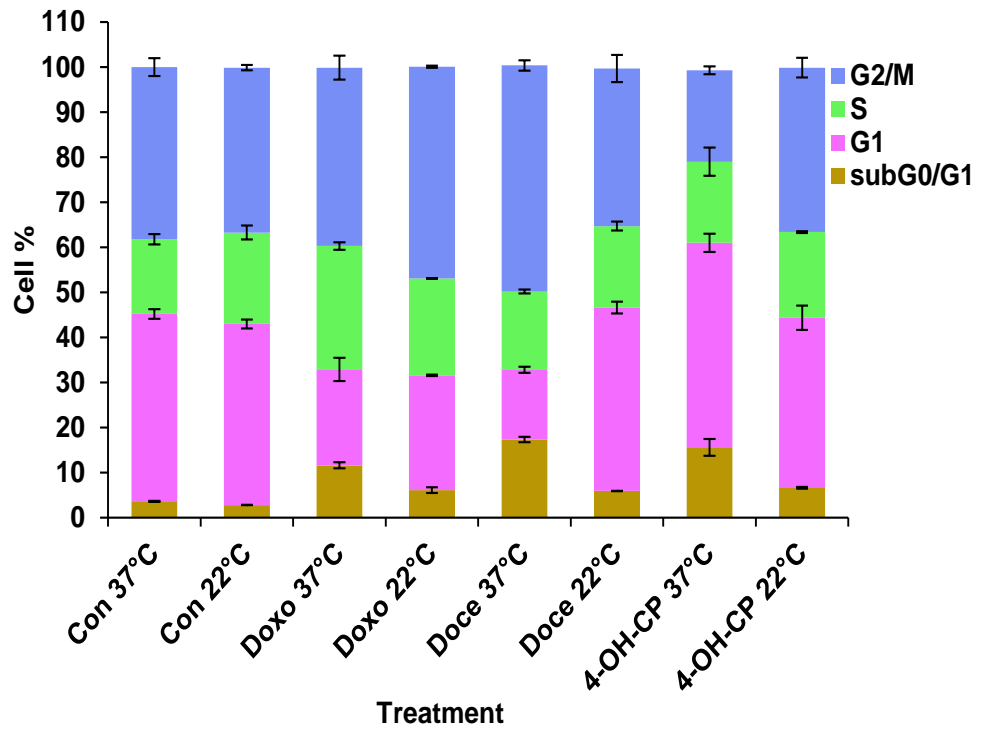


**Figure 4-12 Summary of independent replicate experiments for cell cycle analysis of HaCaTa cells after 8h chemotherapeutic drug treatment**

Bar graph summarises data obtained from three independent biological experiments, each consisting of 2 technical replicates as in Figure 4-13. Bars represent mean values of % of cells ( $\pm$ S.E.M.).

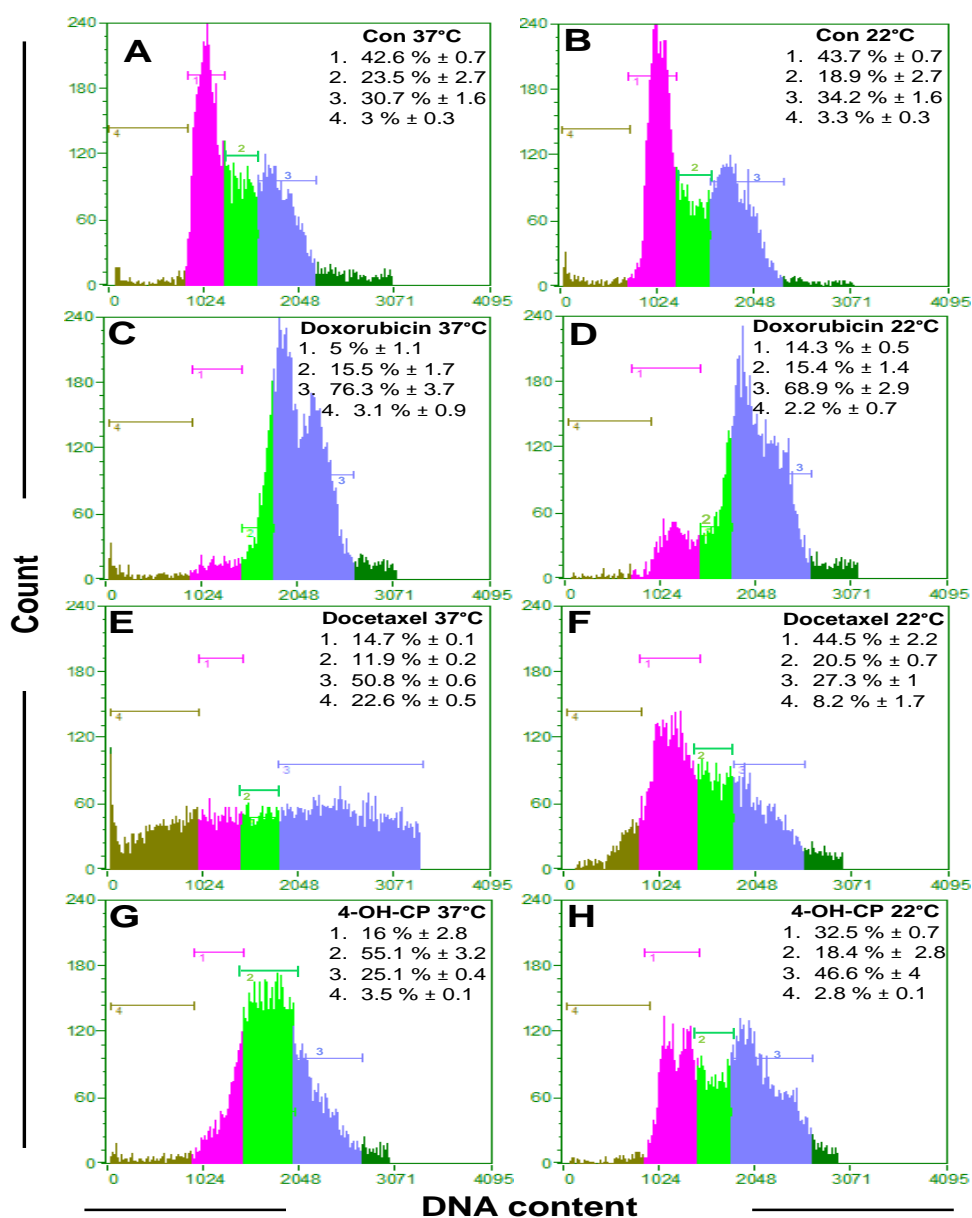


**Figure 4-13 Cell cycle analysis of HaCaTa cells after 24h chemotherapeutic drug treatment at 22°C and 37°C**

$9 \times 10^5$  HaCaTa cells were cultured in 10 cm<sup>2</sup> dishes in KFSM medium and cells were incubated overnight in 37°C / 5% CO<sub>2</sub>. HaCaTa cells were treated with 0.5 µg/mL of doxorubicin (Doxo), 0.01 µg/mL docetaxel (Doce), and 7.5 µg/mL 4-OH-CP for 2h at 37°C and 22°C compared with vehicle control (cells treated with medium containing DMSO, in which the reagent was dissolved). The solvent represents the maximum amount of DMSO corresponding to the highest drug concentration). The drugs were then removed; dishes were rinsed with PBS to remove any traces of drug and cultures incubated in fresh medium. Both attached and floating cells were harvested after 24h and fixed in 70% ethanol, DNA stained with PI. 10,000 cells were acquired on a Guava EasyCyte flow cytometer and results analysed using GuavaSoft software. Results representative plots of one set of triplicate experiments and the distribution and percentage of cell cycle in subG1, G1, S, and G2/M phase of the cell cycle are indicated. Percentages of cells in each cell cycle phase distribution mean values were calculated from three independent biological experiments, each consisting of 2 technical replicates. Regions 1, 2, 3 and 4 on each panel represent G0/G1, S, and G2/M and subG0/G1 phase of the cell cycle, respectively.

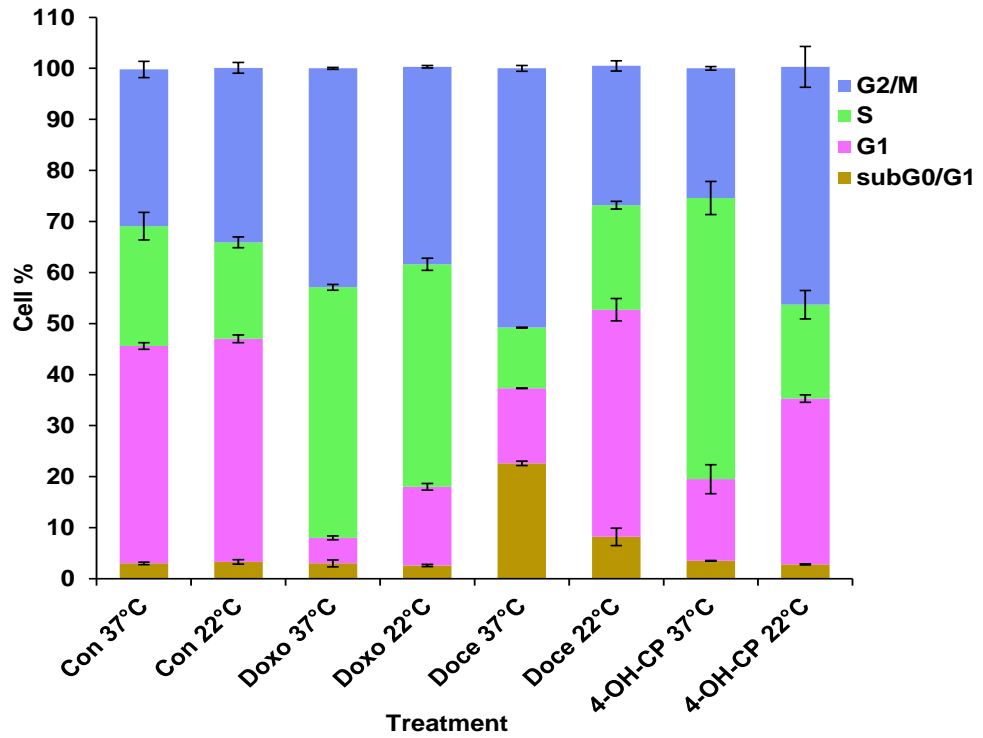


**Figure 4-14 Summary of independent replicate experiments for cell cycle analysis of HaCaTa cells after 24h chemotherapeutic drug treatment**

Bar graph summarises data obtained from three independent biological experiments, each consisting of 2 technical replicates as in Figure 4-15. Bars represent mean values of % of cells ( $\pm$ S.E.M.).

Moreover, results in this chapter have shown that untreated (non-drug-treated) cells at 22°C at different time points after treatment (0–36h) quickly return to exponential growth when re-warmed to 37°C and the cell cycle returns to the normal phase distribution after 1h compared to the control cells at 37°C (Figure 4-7B). Data showed that there was no significant difference between the controls (non-drug-treated cells) at 22°C after 1h of re-warming to 37°C and non-drug-treated cells incubated at 37°C. For this reason, for comparison between treated and non-treated control, we will use control at 37°C. These data suggested that the cell cycle progression is temperature sensitive and returns to normal when the temperature increases to physiological temperature (37°C); thus proliferation changes induced by cooling are reversible and there was a significant correlation between cell growth rate and temperature.

Tables 4-1, 4-2, and 4-3 summarize all flow cytometric data obtained for HaCaTa cells treated with doxorubicin, docetaxel and 4-OH-CP, to permit comparison of flow cytometric data at 37°C and 22°C for each drug in a simple and understandable fashion. These tables summarise cell cycle progression analysis at different time point and statistical analysis of cell cycle phase distribution shown in Figures 4-5 to 4-16.

0.5 µg/mL doxorubicin								
Time-point	G0/G1 %		S %		G2/M %		subG0/G1 %	
	37°C	22°C	37°C	22°C	37°C	22°C	37°C	22°C
Con	39.8% ± 1.2	40.1% ± 0.8	21.1% ± 2	24.1% ± 0.2	36.6% ± 1.2	33.7% ± 1.1	2.5% ± 0.3	2.2 ± 0.2
0h	44.8% ± 0.7	44.6% ± 0.5	17.4% ± 2.1	22% ± 0.1	35.7% ± 2.1	31% ± 0.7	4.2% ± 0.3	2.4 ± 0.1
1h	37.2% ± 0.1	41.4% ± 0.6	23.6% ± 1.2	22.6% ± 0.7	36.6% ± 0.3	33.6% ± 0.6	2.4% ± 0.6	2.4 ± 0.1
2h	34.3% ± 1.1	38% ± 1.6	27.3% ± 3.6	27.6% ± 2.5	32.4% ± 2.6	28.4% ± 3	6% ± 0.2	5.3 ± 1
4h	26.9% ± 1.2	33.6% ± 1.2	25.3% ± 0.2	24.4% ± 0.2	39.4% ± 3	38.2% ± 1.2	8.4% ± 1.7	3.6 ± 0.2
8h	21.3% ± 2.5	25.5% ± 0.2	27.4% ± 0.8	21.5% ± 0.1	39.6% ± 2.6	47% ± 0.2	11.6% ± 0.6	6 ± 0.6
24h	5% ± 1.1	14.3% ± 0.5	15.5% ± 1.7	15.4% ± 1.4	76.3% ± 3.7	68.9% ± 2.9	3.1% ± 0.9	2.2 ± 0.7

**Table 4-1 Cell cycle distribution of HaCaTa cells between control (untreated cells) and cells treated with doxorubicin**

The table summarizes the percentage mean values ± S.E.M of each cell cycle phase in HaCaTa cells treated with 0.5 µg/mL of doxorubicin at 37°C and 22°C (representing normal and cooling conditions, respectively) compared with vehicle control (cells treated with medium containing the solvent in which the reagent was dissolved) at various time-point (0, 1, 2, 4, 8, and 24h). Data points were obtained from three independent biological experiments, each consisting of 2 technical replicates.

0.01 µg/mL docetaxel								
Time-point	G0/G1 %		S %		G2/M %		subG0/G1 %	
	37°C	22°C	37°C	22°C	37°C	22°C	37°C	22°C
Con	39.8% ± 1.2	40.1% ± 0.8	21.1% ± 2	24.1% ± 0.2	36.6% ± 1.2	33.7% ± 1.1	2.5% ± 0.3	2.2% ± 0.2
0h	41.5% ± 0.1	45.9% ± 0.1	21.2% ± 0.6	22.1% ± 0.4	35.2% ± 1.2	29.3% ± 2.5	3.8% ± 0.2	3.5% ± 1.8
1h	33.4% ± 3.7	41.7% ± 0.7	27.1% ± 1.4	21.5% ± 0.9	37.3% ± 2.6	34.2% ± 0.9	2.3% ± 0.7	2.6% ± 0.2
2h	28.8% ± 2.2	41.3% ± 1	20.3% ± 1.9	20.8% ± 1	45.5% ± 3.7	33.9% ± 1.9	5.4% ± 0.2	3.9% ± 0.2
4h	20.9% ± 1.6	38.9% ± 1	23.1% ± 1.3	24.1% ± 0.5	45.1% ± 0.1	31.3% ± 1.8	10.8% ± 0.3	5% ± 0.3
8h	15.5% ± 0.7	40.7% ± 1.3	17.4% ± 0.5	18.1% ± 1	50.1% ± 1.2	35% ± 3	17.3% ± 0.6	5.9% ± 0.1
24h	14.7% ± 0.1	44.5% ± 2.2	11.9% ± 0.2	20.5% ± 0.7	50.8% ± 0.6	27.3% ± 1	22.6% ± 0.5	8.2% ± 1.7

**Table 4-2 Distribution of HaCaTa cells between cell cycle phases in control (untreated cells) and treated with docetaxel**

The table summarizes the percentage mean values ± S.E.M of each cell cycle phase cell populations of HaCaTa cells were treated with 0.01 µg/mL of docetaxel at 37°C and 22°C (representing normal and cooling conditions, respectively) compared with vehicle control (cells treated with medium containing the solvent in which the reagent was dissolved) at various time-point (0, 1, 2, 4, 8, and 24h). Data points obtained from three independent biological experiments, each consisting of 2 technical replicates.

7.5 µg/mL 4-OH-CP								
Time-point	G0/G1 %		S %		G2/M %		subG0/G1 %	
	37°C	22°C	37°C	22°C	37°C	22°C	37°C	22°C
Con	39.8% ± 1.2	40.1% ± 0.8	21.1% ± 2	24.1% ± 0.2	36.6% ± 1.2	33.7% ± 1.1	2.5% ± 0.3	2.2% ± 0.2
0h	37.5% ± 1.7	47.9% ± 1.3	18% ± 2.2	29% ± 0.1	42.6% ± 1.3	21.1% ± 1.4	2.2% ± 0.8	2% ± 0.3
1h	39.4% ± 0.4	42.2% ± 2.2	21.8% ± 3.6	18.7% ± 2.1	36.9% ± 3.1	36.7% ± 0.1	2.6% ± 0.1	2.2% ± 0.2
2h	36.8% ± 0.5	39.1% ± 0.3	20% ± 1.4	19.4% ± 0.4	35% ± 2.3	39.4% ± 0.9	8% ± 0.6	2.4% ± 0.1
4h	46% ± 2.5	39.1% ± 1.8	24% ± 0.7	23.3% ± 0.8	26.4% ± 1.3	34.1% ± 1.8	3.7% ± 0.3	3.6% ± 0.7
8h	45.4% ± 3	37.8% ± 2.7	18% ± 3.1	19% ± 0.2	20.3% ± 0.8	36.5% ± 2.2	15.6% ± 1.8	6.6% ± 0.2
24h	16% ± 2.8	32.5% ± 0.7	55.1% ± 3.2	18.4% ± 2.8	25.1% ± 0.4	46.6% ± 4	3.5% ± 0.1	2.8% ± 0.1

**Table 4-3 Distribution of HaCaTa cells between cell cycle phases in control (untreated cells) and treated with 4-OH-CP**

The table summarizes the percentage mean values ± S.E.M of each cell cycle phase cell populations of HaCaTa cells were treated with 7.5 µg/mL of 4-OH-CP at 37°C and 22°C (representing normal and cooling conditions, respectively) compared with vehicle control (cells treated with medium containing the solvent in which the reagent was dissolved) at various time-point (0, 1, 2, 4, 8, and 24h). Data points obtained from three independent biological experiments, each consisting of 2 technical replicates.

#### **4.5.3.1 Determining the efficacy of cooling in protecting from chemotherapy drug-mediated cytotoxicity**

The results of this study showed that lowering the temperature below 22°C results in improved cytoprotection against chemotherapy drug-mediated keratinocyte cytotoxicity (Chapter 3). Another key finding was that cooling at 22°C protected from chemotherapy drug induced cell cycle arrest in HaCaTa cells. To investigate whether temperature values below 22°C could provide further protection against cell cycle arrest induced by doxorubicin, 4-OH-CP and docetaxel cell, cycle analysis was performed at 18°C.

To compare the cell cycle phase distribution of HaCaTa at 37°C and 18°C, two different sets of experiments were performed, i.e. 2h and 36h at the 18°C post 2h treatment with chemotherapeutic drugs. As shown by the DNA content histograms in Figure 4-17 and 4-19, the effects of doxorubicin on cell cycle distribution were significantly reduced at 18°C compared with at 22°C, evident by representative results shown in T=2h (Figures 4-17 and 4-18) and T=36h (Figures 4-19 and 4-20). The most striking results were observed in Figure 4-17F, where cell cycle distribution after docetaxel at 18°C was close to that of the untreated control cells compared with cells treated at 37°C and 22°C. These results provided strong evidence that lowering the temperature from 22°C to 18°C, dramatically protected cells further from cytotoxicity.

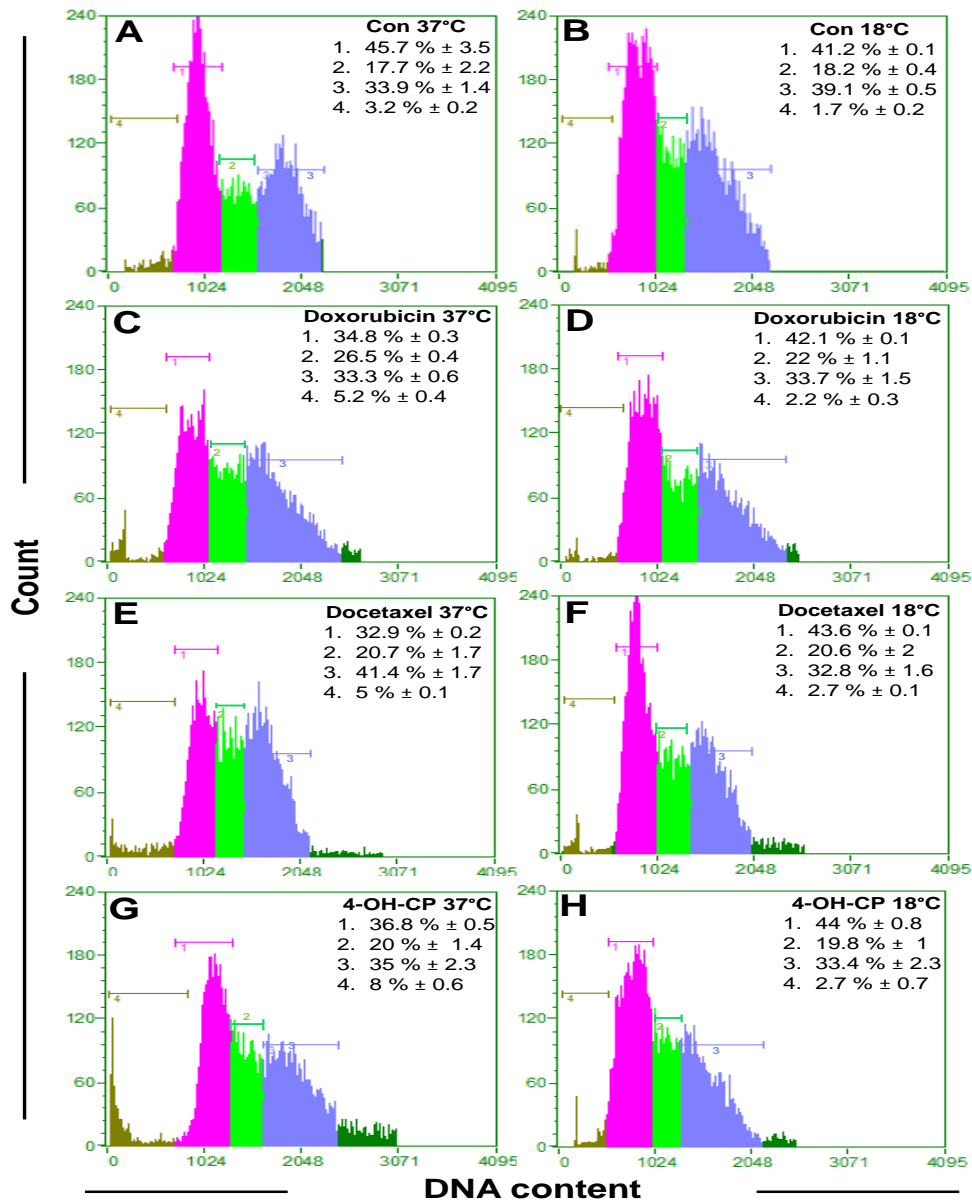


**Figure 4-15 Cell cycle analysis of HaCaTa cells after 2h chemotherapeutic drug treatment at 22°C and 37°C**

9x10<sup>5</sup> HaCaTa cells were cultured in 10 cm<sup>2</sup> dishes in KSFM medium and cells were incubated overnight in 37°C / 5% CO<sub>2</sub>. HaCaTa cells were treated with 0.5 µg/mL of doxorubicin (Doxo), 0.01 µg/mL docetaxel (Doce), and 7.5 µg/mL 4-OH-CP for 2h at 37°C and 22°C compared with vehicle control (cells treated with medium containing DMSO, in which the reagent was dissolved). The solvent represents the maximum amount of DMSO corresponding to the highest drug concentration). The drugs were then removed; dishes were rinsed with PBS to remove any traces of drug and cultures incubated in fresh medium. Both attached and floating cells were harvested after 2h and fixed in 70% ethanol, DNA stained with PI. 10,000 cells were acquired on a Guava EasyCyte flow cytometer and results analysed using GuavaSoft software. Results representative plots of one set of triplicate experiments and the distribution and percentage of cell cycle in subG1, G1, S, and G2/M phase of the cell cycle are indicated. Percentages of cells in each cell cycle phase distribution mean values were calculated from three independent biological experiments, each consisting of 2 technical replicates. Regions 1, 2, 3 and 4 on each panel represent G0/G1, S, and G2/M and subG0/G1 phase of the cell cycle, respectively.

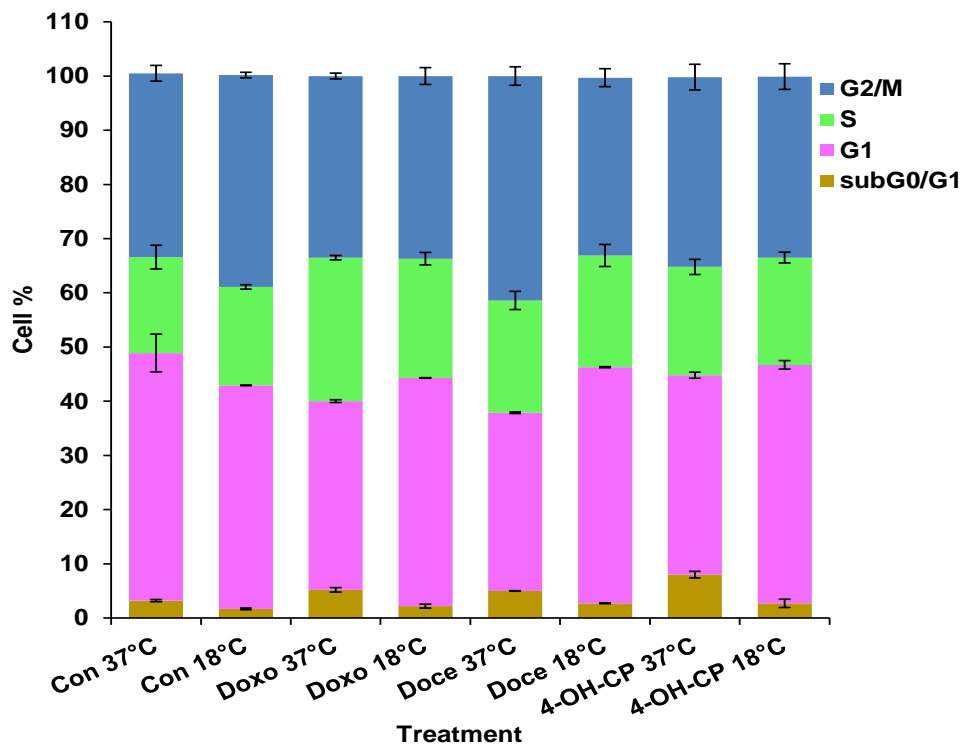


**Figure 4-16 Summary of independent replicate experiments for cell cycle analysis of HaCaTa cells after 2h chemotherapeutic drug treatment at 18°C**

Bar graph summarises data obtained from three independent biological experiments, each consisting of 2 technical replicates as in Figure 4-17. Bars represent mean values of % of cells ( $\pm$ S.E.M.).

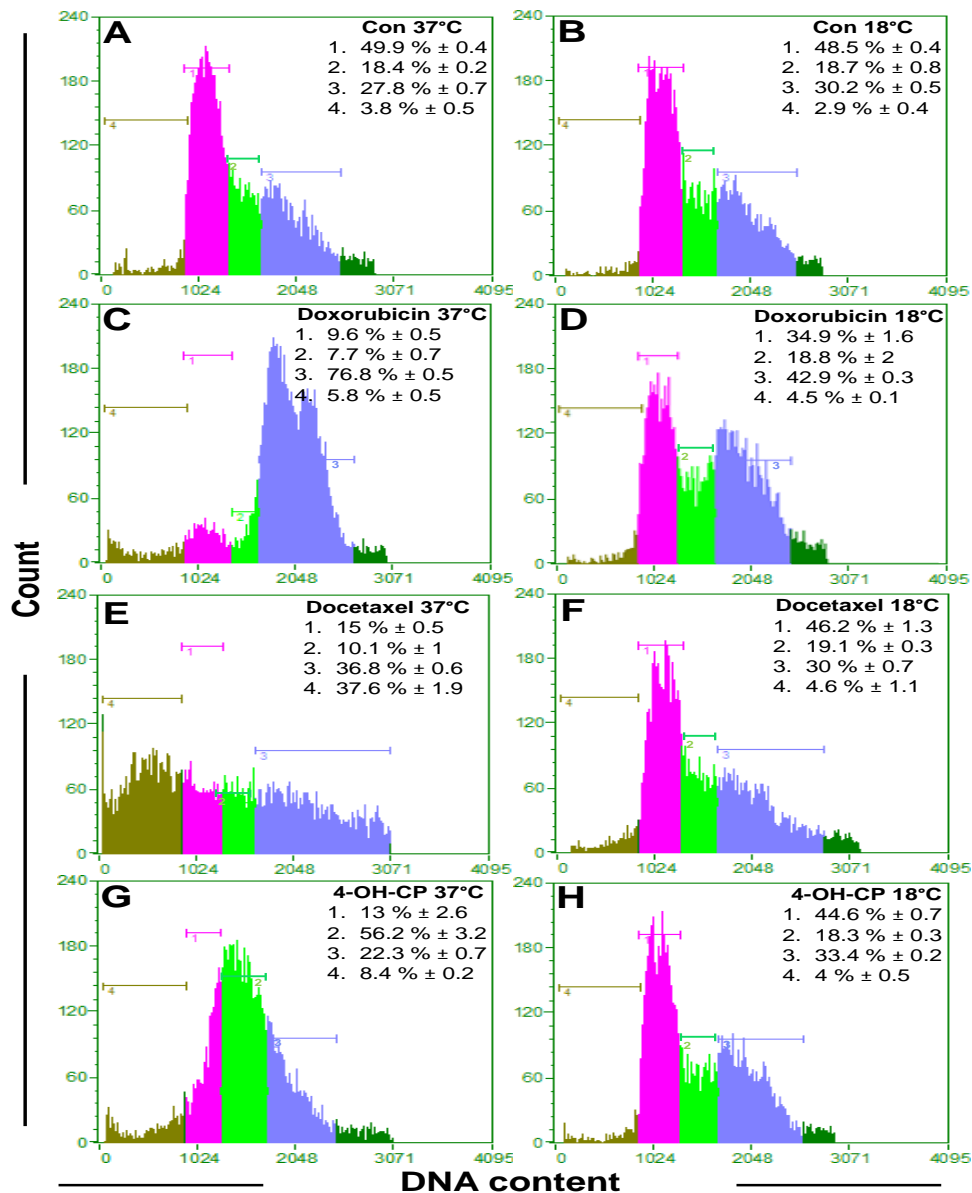


**Figure 4-17 Cell cycle analysis of HaCaTa cells after 36h chemotherapeutic drug treatment at 18°C and 37°C**

$9 \times 10^5$  HaCaTa cells were cultured in 10 cm<sup>2</sup> dishes in KSFM medium and cells were incubated overnight in 37°C / 5% CO<sub>2</sub>. HaCaTa cells were treated with 0.5 µg/mL of doxorubicin (Doxo), 0.01 µg/mL docetaxel (Doce), and 7.5 µg/mL 4-OH-CP for 2h at 37°C and 22°C compared with vehicle control (cells treated with medium containing DMSO, in which the reagent was dissolved). The solvent represents the maximum amount of DMSO corresponding to the highest drug concentration). The drugs were then removed; dishes were rinsed with PBS to remove any traces of drug and cultures incubated in fresh medium. Both attached and floating cells were harvested after 36h and fixed in 70% ethanol, DNA stained with PI. 10,000 cells were acquired on a Guava EasyCyte flow cytometer and results analysed using GuavaSoft software. Results representative plots of one set of triplicate experiments and the distribution and percentage of cell cycle in subG1, G1, S, and G2/M phase of the cell cycle are indicated. Percentages of cells in each cell cycle phase distribution mean values were calculated from three independent biological experiments, each consisting of 2 technical replicates. Regions 1, 2, 3 and 4 on each panel represent G0/G1, S, and G2/M and subG0/G1 phase of the cell cycle, respectively.

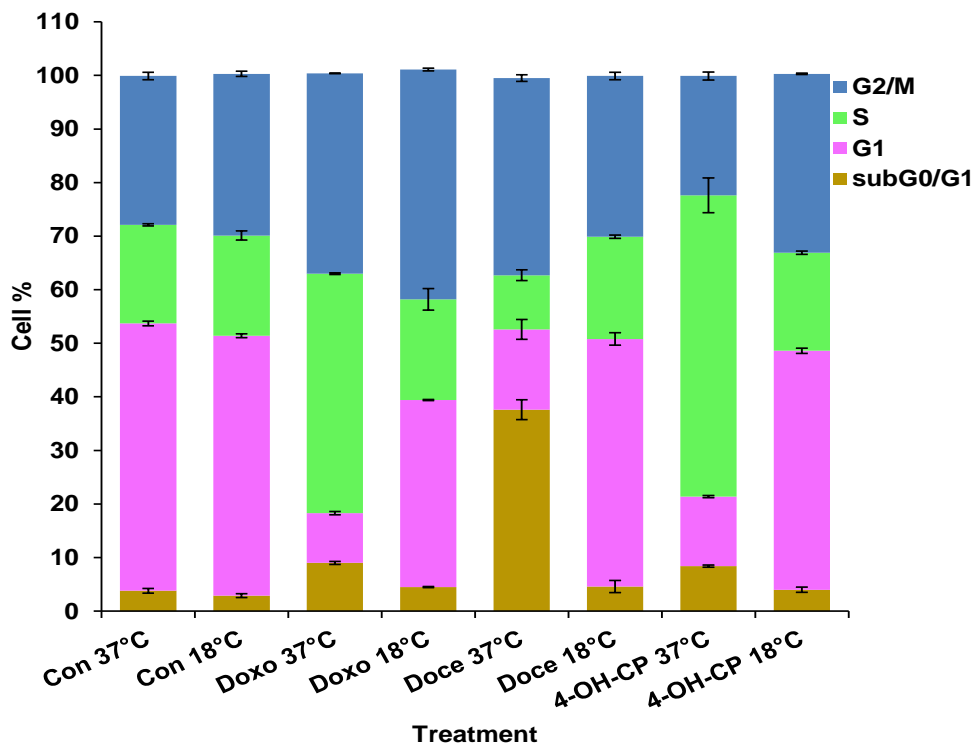


**Figure 4-18 Summary of independent replicate experiments for cell cycle analysis of HaCaTa cells after 36h chemotherapeutic drug treatment at 18°C**

Bar graph summarises data obtained from three independent biological experiments, each consisting of 2 technical replicates as in Figure 4-19. Bars represent mean values of % of cells ( $\pm$ S.E.M.).

For ease of interpretation and to permit easier direct comparisons to be made, data in Figures 4-17 to 4-20 are presented in Table 4-4, which summarizes the flow cytometric data obtained for HaCaTa cells treated with doxorubicin, docetaxel and 4-OH-CP respectively at 37°C and 18°C. These results supported the hypothesis that lowering the temperature from 22°C to 18°C resulted incrementally in a better degree of rescue from drug cytotoxicity.

**A**

0.5 µg/mL doxorubicin								
Time-point	G0/G1 %		S %		G2/M %		subG0/G1 %	
	37°C	18°C	37°C	18°C	37°C	18°C	37°C	18°C
Con	45.7% ± 3.5	41.2% ± 0.1	17.7% ± 2.2	18.2% ± 0.4	33.9% ± 1.4	39.1% ± 0.5	3.2% ± 0.2	1.7% ± 0.2
2h	34.8% ± 0.3	42.1% ± 0.1	26.5% ± 0.4	22% ± 1.1	33.3% ± 0.6	33.7% ± 1.5	5.2% ± 0.4	2.2% ± 0.3
36h	9.6% ± 0.5	34.9% ± 1.6	7.7% ± 0.7	18.8% ± 2	76.8% ± 0.5	42.9% ± 0.3	5.8% ± 0.5	4.5% ± 0.1

**B**

0.01 µg/mL docetaxel								
Time-point	G0/G1 %		S %		G2/M %		subG0/G1 %	
	37°C	18°C	37°C	18°C	37°C	18°C	37°C	18°C
Con	45.7% ± 3.5	41.2% ± 0.1	17.7% ± 2.2	18.2% ± 0.4	33.9% ± 1.4	39.1% ± 0.5	3.2% ± 0.2	1.7% ± 0.2
2h	32.9% ± 0.2	43.6% ± 0.1	20.7% ± 1.7	20.6% ± 2	41.4% ± 1.7	32.8% ± 1.6	5% ± 0.1	2.7% ± 0.1
36h	15% ± 0.5	46.2% ± 1.3	10.1% ± 1	19.1% ± 0.3	36.8% ± 0.6	30% ± 0.7	37.6% ± 1.9	4.6% ± 1.1

**C**

7.5 µg/mL 4-OH-CP								
Time-point	G0/G1 %		S %		G2/M %		subG0/G1 %	
	37°C	18°C	37°C	18°C	37°C	18°C	37°C	18°C
Con	45.7% ± 3.5	41.2% ± 0.1	17.7% ± 2.2	18.2% ± 0.4	33.9% ± 1.4	39.1% ± 0.5	3.2% ± 0.2	1.7% ± 0.2
2h	36.8% ± 0.5	44% ± 0.8	20% ± 1.4	19.8% ± 1	35% ± 2.3	33.4% ± 2.3	8% ± 0.6	2.7% ± 0.7
36h	13% ± 2.6	44.6% ± 0.7	56.2% ± 3.2	18.3% ± 0.3	22.3% ± 0.7	33.4% ± 0.2	8.4% ± 0.2	4% ± 0.5

**Table 4-4 Distribution of HaCaTa cells between cell cycle phases in control (untreated cells) and treated at at 37°C and 18°C**

The table summarizes the percentage mean values ± S.E.M of each cell cycle phase cell populations of HaCaTa cells were treated with **A)** 0.5 µg/mL doxorubicin, **B)** 0.01 µg/mL docetaxel, and **C)** 7.5 µg/mL of 4-OH-CP at 37°C and 18°C (representing normal and cooling conditions, respectively) compared with vehicle control (cells treated with medium containing the solvent in which the reagent was dissolved) at various time-point (2 and 36h). Data points obtained from three independent biological experiments, each consisting of 2 technical replicates.

## 4.6 Short-term starvation protects HaCaTa cells against chemotherapy drugs

Anti-cancer drugs cause different side effects by mediating toxicity to normal cells and tissues, for instance cardiotoxicity and hair loss are associated with doxorubicin and cisplatin (Wang *et al.*, 2004). Thus, decrease of undesired chemotoxicity by selective protection of normal cells without compromising the killing of cancer cells represents a promising strategy to enhance cancer treatment (Safdie *et al.*, 2009). Previous studies showed that short-term fasting could be effective in protecting normal cells and mice but not cancer cells against high dose anticancer drugs (Raffaghello *et al.*, 2008).

We hypothesised that cooling may protect cells from cytotoxic drugs, partly by decreasing the metabolic activity of the cells, which inhibits proliferation (Lemieux, 2012). Thus, we tested whether cooling combined with short-term starvation could enhance the scalp cooling method against chemotherapy drug effects. HaCaTa cells were incubated in supplements (supps)-free medium (KSFM without supplements EGF and bovine pituitary extract BPE)) for 24h. HaCaTa cells were then treated with three concentrations of doxorubicin, docetaxel, and 4-OH-CP at 37°C and 22°C in KSFM with and without supplements then cell viability was assessed as previously.

Data showed that pre-starvation of cells (incubated cells in KSFM without supps) for 24h then treatment with doxorubicin, docetaxel, 4-OH-CP, provided consistent and significant protection from drug-mediated cytotoxicity at 37°C compared with cells incubated and treated at 37°C in KSFM complete with supps (KSFMc) (Figure 4-21). Interestingly, cells at 22°C in KSFMc showed better or similar protection compared to cells treated at 22°C in KSFM without supps (Figure 4-21). These results suggest that starvation can be effective in protecting HaCaTa cells against chemotherapy at physiological temperature but cooling alone protects better. Short-term starvation is more effective to prevent chemotherapy drug toxicity since starved cells switch off signals for growth, however, cooling alone was more effective than exposure the cells to both cooling and starvation.

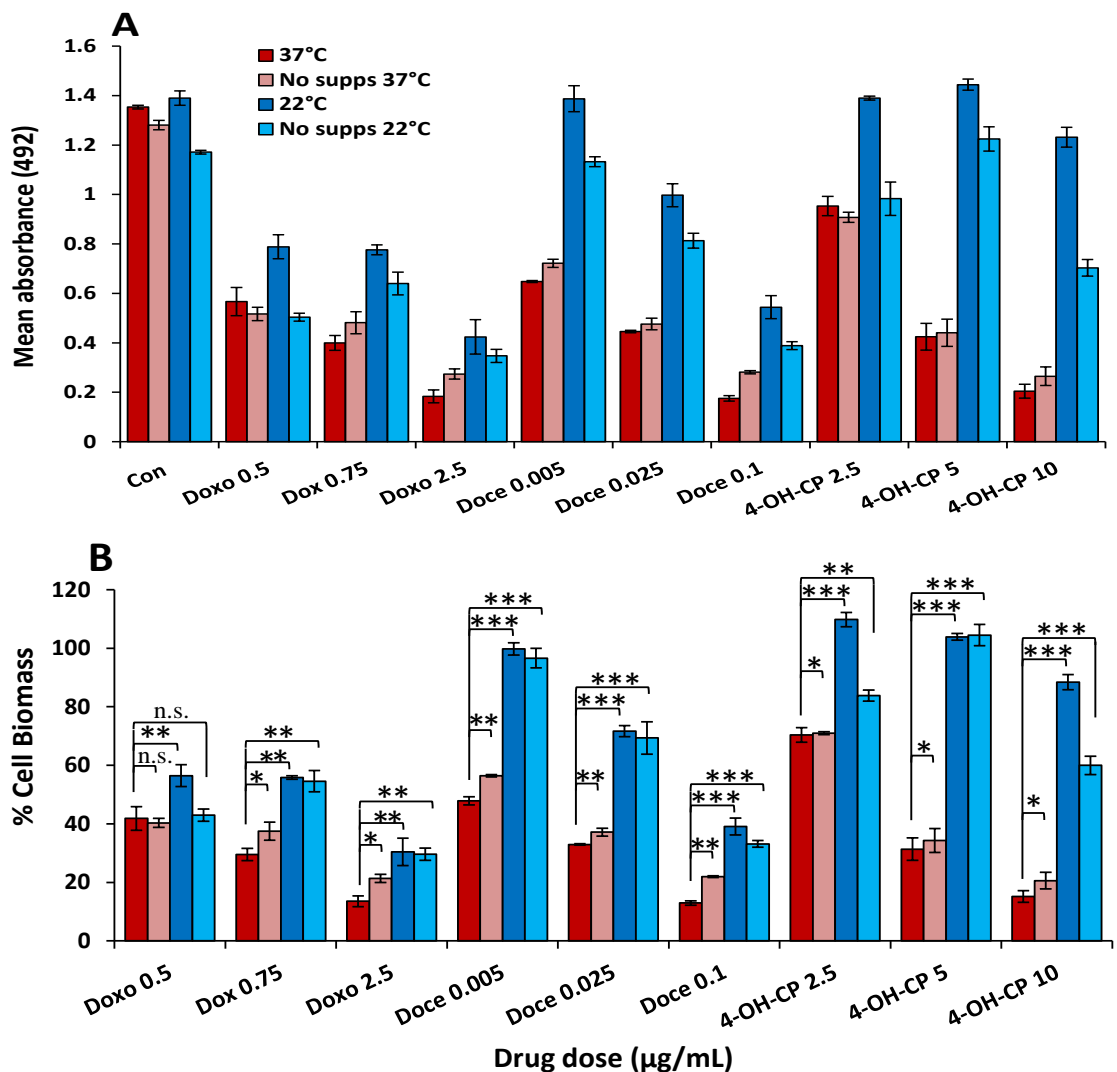


**Figure 4-19 Cytoprotective role of cooling and short-term starvation protects against chemotherapy drug-mediated toxicity in HaCaTa cells**

HaCaTa cells were seeded in 96 well plates at 5000 cells/well in KSFM medium and were incubated overnight at 37°C/ 5% CO<sub>2</sub>. The medium were then removed and HaCaTa cells were incubated in KSFM free supps for 24h, compared with cells incubated in KSFMc. HaCaTa cells were treated for 2h with a range of concentrations of doxorubicin (Doxo), docetaxel (Doce) and 4-OH-CP at 37°C and 22°C (representing normal and cooling conditions, respectively) compared with vehicle control (cells treated with medium containing DMSO, in which the reagent was dissolved). The solvent represents the maximum amount of DMSO corresponding to the highest drug concentration). The drugs were then removed, wells were rinsed with PBS to remove any traces of drug and cultures incubated for a further 72h, and after which 20 µL of CellTiter 96® AQueous One solution was added to the wells and plates were incubated at 37°C in 5% CO<sub>2</sub> for a total of four hours. Absorbance was measured spectrophotometrically at a wavelength of 492nm and % cell biomass was calculated as described in Materials and Methods (Chapter 2). **A**) Absorbance (raw data) were **B**) % cell biomass shown in bar graph are also shown in bar graph form (lower panels) for clarity and presentation of statistical significance. Data points correspond to mean % cell biomass (±S.E.M.) for three independent biological experiments, each consisting of 6–8 technical replicates. n.s., non-significant; \*,  $p < 0.05$ ; \*\*,  $p < 0.01$ ; \*\*\*,  $p < 0.001$ .

**Key:** No supps: KSFM with no supplements  
KSFMc: KSFM medium with complete supplements

## 4.7 Cytoprotective role of the PD153035 against chemotherapy drug-mediated toxicity in HaCaTa cells

EGFR is a receptor tyrosine kinase involved in regulation of apoptosis, and particularly proliferation and angiogenesis (Cole *et al.*, 2005) and it plays an important role in HF homeostasis by acting as an important regulator of cell proliferation. It has thus been suggested that topical inhibition of EGFR signalling might permit protection from CIA (Bichsel *et al.*, 2013). We hypothesised that “artificial” deceleration of cell growth by blockade of the cell cycle may reduce the cytotoxic effects of chemotherapy drugs; i.e. “protective pre-conditioning” (PPC) by pharmacological inhibition of EGFR, might represent a strategy to reduce the effects of chemotherapy drugs and perhaps enhance the cytoprotective effect of cooling. We therefore inhibited the kinase activity of the EGF receptor by the use of the specific EGFR inhibitor PD153035, which is a reversible tyrosine kinase activity inhibitor that inhibits auto-phosphorylation of EGFR and efficiently blocks EGFR signalling as shown by ourselves (Georgopoulos *et al.*, 2014) and others (Bos *et al.*, 1997; Fry *et al.*, 1994; Grunt *et al.*, 2007).

We initially determined the optimal PD153035 concentration to be used in HaCaTa by pre-titration experiments (using inhibitor concentrations in the range of 0.25-10  $\mu\text{M}$ ) and cytotoxicity was determined by measuring cell absorbance (using the CellTiter assay) 72h later (Figure 4-22). Data confirmed that the optimal concentration for PD153035 was 3  $\mu\text{M}$  compared to the control (cells not treated with PD153035). Indeed, HaCaTa cells treated with lower inhibitor concentrations of PD153035 exhibited higher viability than control cells and higher concentrations exhibited increasing cytotoxicity (Figure 4-22).

We ultimately aimed to determine whether PPC using PD153035 could enhance the efficacy of cooling. First, we examined the effect of pre-treatment of HaCaTa cells for 2h with 3 $\mu\text{M}$  of PD153035 on the effects of cytotoxic drugs (doxorubicin, docetaxel, 4-OH-CP) at 37°C. As shown in Figure4-23, there was no significant increase in biomass in cells treated with doxorubicin compared with cells treated with KSM with and without supplements. However, cells treated with docetaxel showed a slightly better protection, but only at low concentrations in cells treated with PD153035. Similar observations were made with cells treated with 4-OH-CP as they too showed a slight increase (Figure 4-23). These data suggested that when EGFR signalling was inhibited for only 2h before drug treatment, the protection from drug toxicity was minimal and only significant for lower drug doses. To examine whether an increase in the pre-treatment time period may offer a better level of protection from cytotoxicity, cells were pre-treated for 24h with PD153035. Interestingly, 24h

pre-treatment with PD153035 exhibited a marked ability to significantly protect cells from cytotoxicity for all three compounds tested (Figure 4-24), which confirmed that PPC could, at least in part, rescue cells from drug toxicity.

We then investigated the effect of combination of PPC and cooling by testing the response of HaCaTa to these chemotherapy drugs at 37°C and 22°C. For each temperature, there were 4 types of pre-treatment conditions: 1) cells treated with KSFMc, 2) cells treated in medium without supps, 3) cells treated with KSFMc + PD153035, 4) cells treated in medium without supps + PD153035. As shown in Figures 4-25 to 4-27, that combination of PD153035 and cooling during chemotherapy drug treatment provided consistent and significant protection from drug-mediated cytotoxicity for nearly all concentrations tested for doxorubicin, 4-OH-CP and, though to a lesser extent, docetaxel.

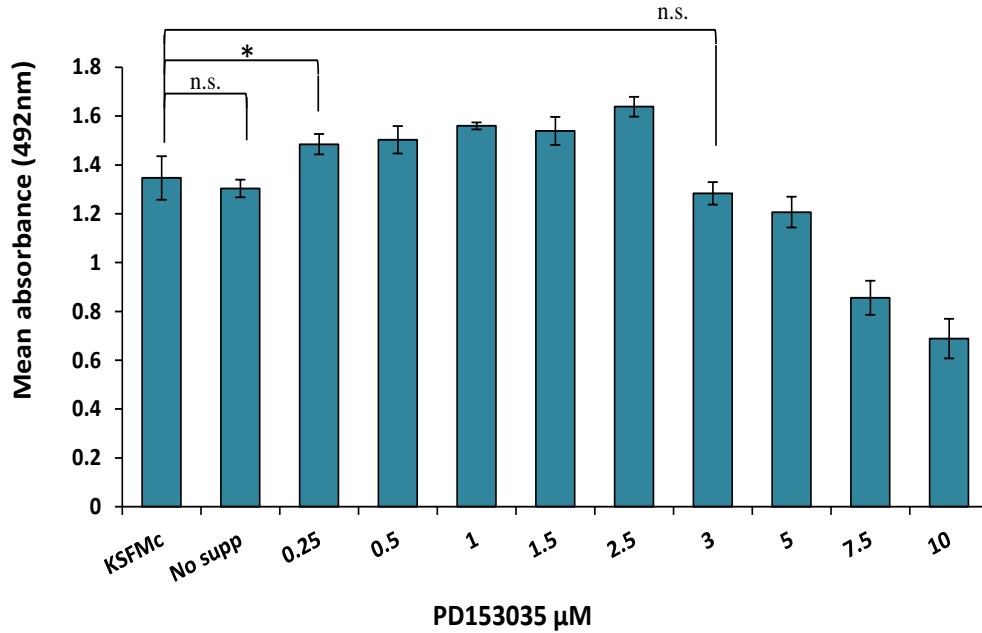


**Figure 4-20 Viability of HaCaTa cells after incubation with the tyrosine kinase inhibitor PD 153035**

HaCaTa cells were seeded in 96 well plates at 5000 cells/well in KSFMc medium and were incubated overnight at 37°C/ 5% CO<sub>2</sub>. HaCaTa cells were incubated with a range of concentrations of the tyrosine kinase inhibitor PD153035; two controls included were cells incubated in KSFMc and cells in No sup medium. After 72h incubation, 20  $\mu\text{L}$  of CellTiter 96® AQueous One solution was added to the appropriate wells and plates were incubated at 37°C in 5% CO<sub>2</sub> for a total of 4hours. Bars correspond to mean absorbance at 492 nm ( $\pm$ S.E.M.) from three independent biological experiments, each consisting of 6-8 technical replicates. n.s., non- significant; \*,  $p < 0.05$ .

**Key:** No supps: KSFMc with no supplement

KSFMc: KSFMc medium complete with all supplements

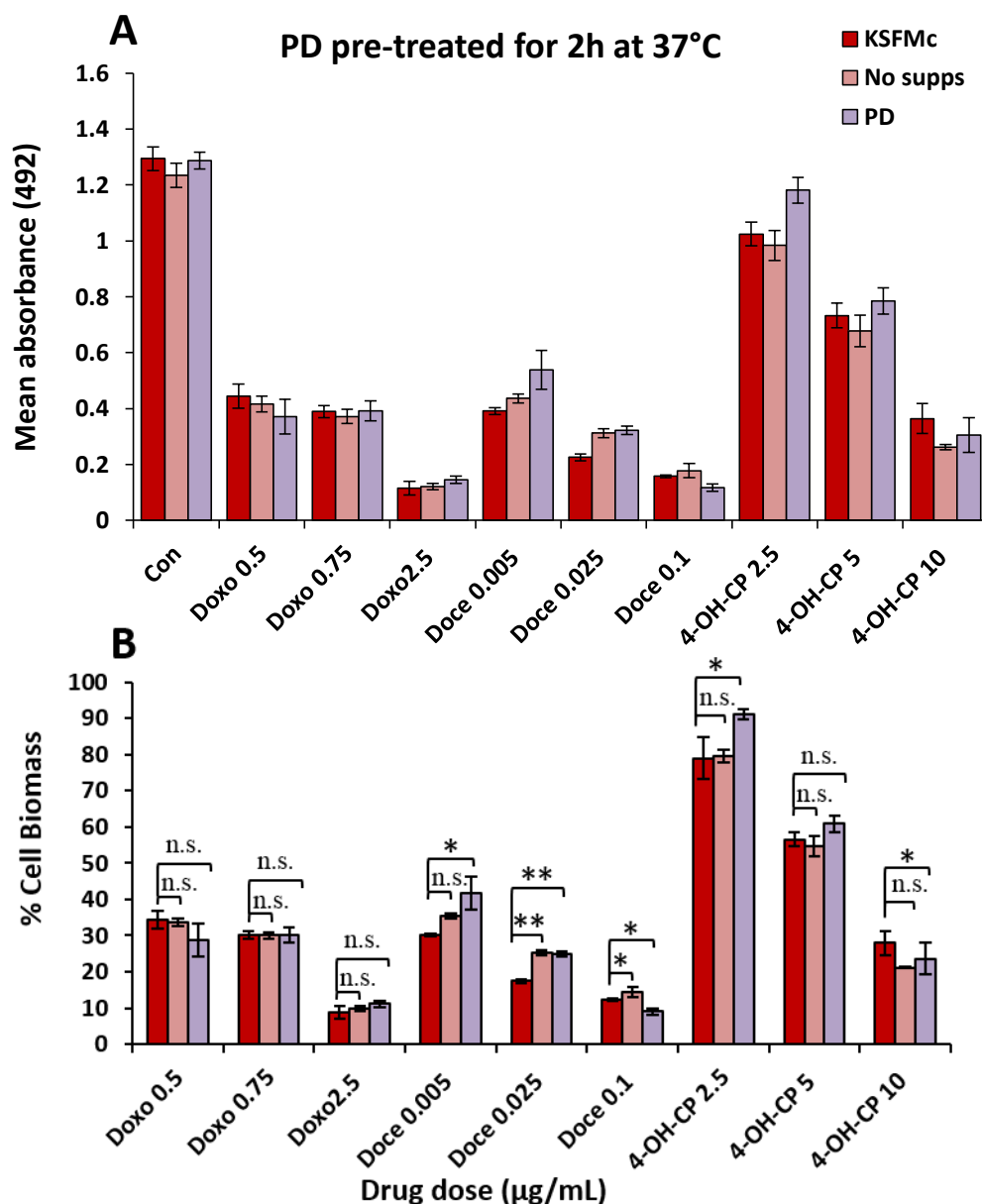


**Figure 4-21 Cytoprotective role of 2h pre-treatment by PD153035 against chemotherapy drug-mediated toxicity in HaCaTa cells**

HaCaTa cells were seeded in 96 well plates at 5000 cells/well in KSFMc medium and were incubated overnight at 37°C/ 5% CO<sub>2</sub>. HaCaTa cells were pre-treated with 3 μM PD153035 or in KSFMc or KSFMc free supps (No supps) for 2h. HaCaTa cells were treated for 2h with (0.5, 0.75, and 2.5 μg/mL) doxorubicin (Doxo), (0.005, 0.025, and 0.1 μg/mL) docetaxel (Doce) and (2.5, 5, and 10 μg/mL) 4-OH-CP, in KSFMc with PD153035, or in KSFMc or KSFMc (No supps) at 37°C compared with vehicle control (cells treated with medium containing DMSO, in which the reagent was dissolved). The solvent represents the maximum amount of DMSO corresponding to the highest drug concentration). The drugs were then removed, wells were rinsed with PBS to remove any traces of drug and cells, which pre-treated incubated with PD153035 and the both other groups were incubate in fresh KSFMc for 72h, after which 20 μL of CellTiter 96® AQueous One solution was added to the wells and plates were incubated at 37°C in 5% CO<sub>2</sub> for a total of four hours. Absorbance was measured spectrophotometrically at a wavelength of 492nm and % cell biomass was calculated as described in Materials and Methods (Chapter 2). Data are presented as **A**) Absorbance (raw data) **B**) % cell biomass shown in a bar graph. Data points correspond to mean % cell biomass (±S.E.M.) from three independent biological experiments, each consisting of 6-8 technical replicates. n.s., non- significant; \*,  $p < 0.05$ .

**Key:** No supps: KSFMc with no supplement  
KSFMc: KSFMc medium with complete supplements

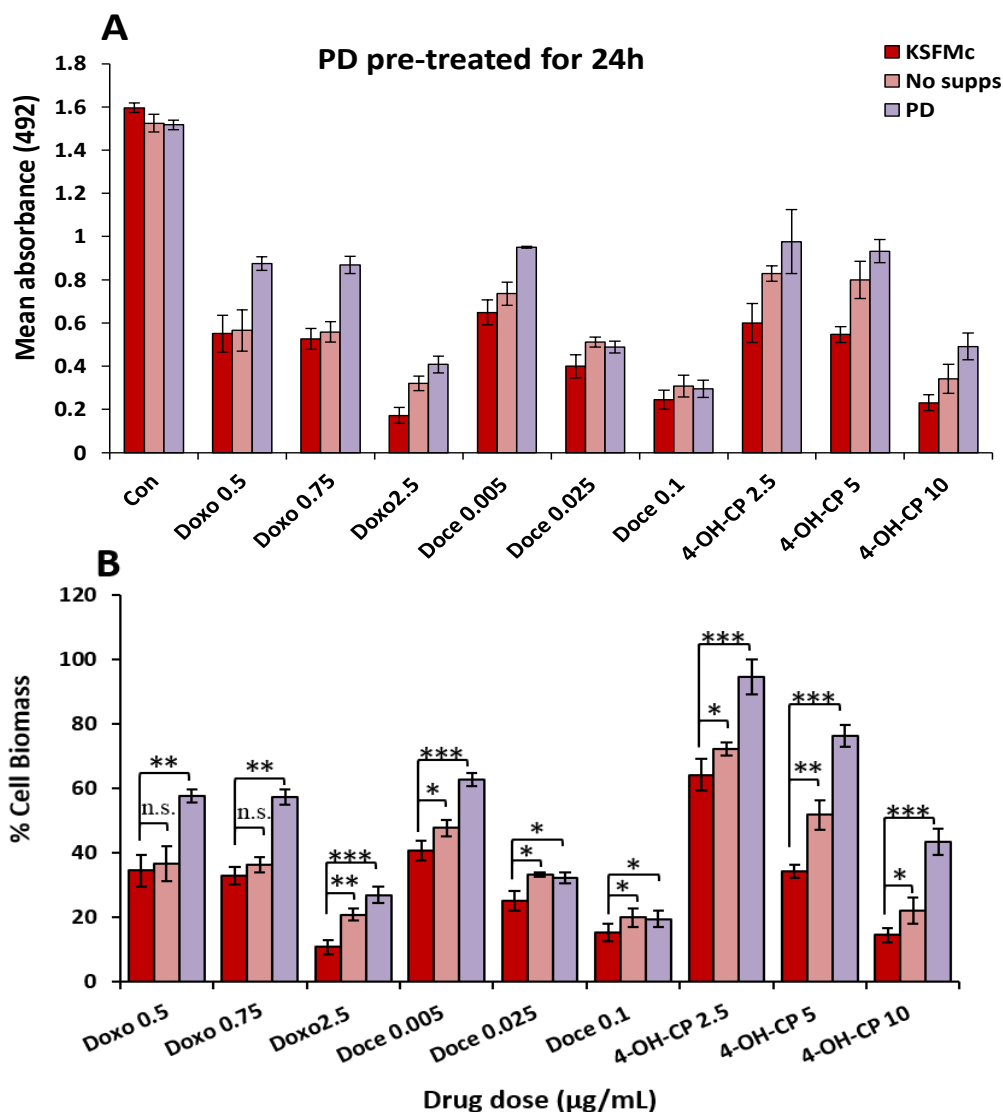


**Figure 4-22 Cytoprotective role of 24h pre-treatment by PD153035 against chemotherapy drug-mediated toxicity in HaCaTa cells**

HaCaTa cells were seeded in 96 well plates at 5000 cells/well in KSFMc medium and were incubated overnight at 37°C/ 5% CO<sub>2</sub>. HaCaTa cells were pre-treated with 3  $\mu\text{M}$  PD153035 or in KSFMc or KSFMc (No sup) for 24h. HaCaTa cells were treated for 2h with (0.5, 0.75, and 2.5  $\mu\text{g/mL}$ ) doxorubicin (Doxo), (0.005, 0.025, and 0.1  $\mu\text{g/mL}$ ) docetaxel (Doce) and (2.5, 5, and 10  $\mu\text{g/mL}$ ) 4-OH-CP, in KSFMc with PD153035, or in KSFMc (No supps) at 37°C compared with vehicle control (cells treated with medium containing DMSO, in which the reagent was dissolved). The solvent represents the maximum amount of DMSO corresponding to the highest drug concentration). The drugs were then removed, wells were rinsed with PBS to remove any traces of drug and cells, which pre-treated incubated with PD153035 and the both other groups were incubated in fresh KSFMc for 72h, after which 20 $\mu\text{L}$  of CellTiter 96® Aqueous One solution was added to the wells and plates were incubated at 37°C in 5% CO<sub>2</sub> for a total of four hours. Absorbance was measured spectrophotometrically at a wavelength of 492nm and % cell biomass was calculated as described in Materials and Methods (Chapter 2). Data is presented as **A**) Absorbance (raw data) **B**) % cell biomass shown in bar graph. Data points correspond to mean % cell biomass ( $\pm$ S.E.M.) from three independent biological experiments, each consisting of 6-8 technical replicates. n.s., non-significant; \*,  $p < 0.05$ ; \*\*,  $p < 0.01$ ; \*\*\*,  $p < 0.001$ .

**Key:** No supps: KSFMc with no supplement  
KSFMc: KSFMc medium with complete supplements

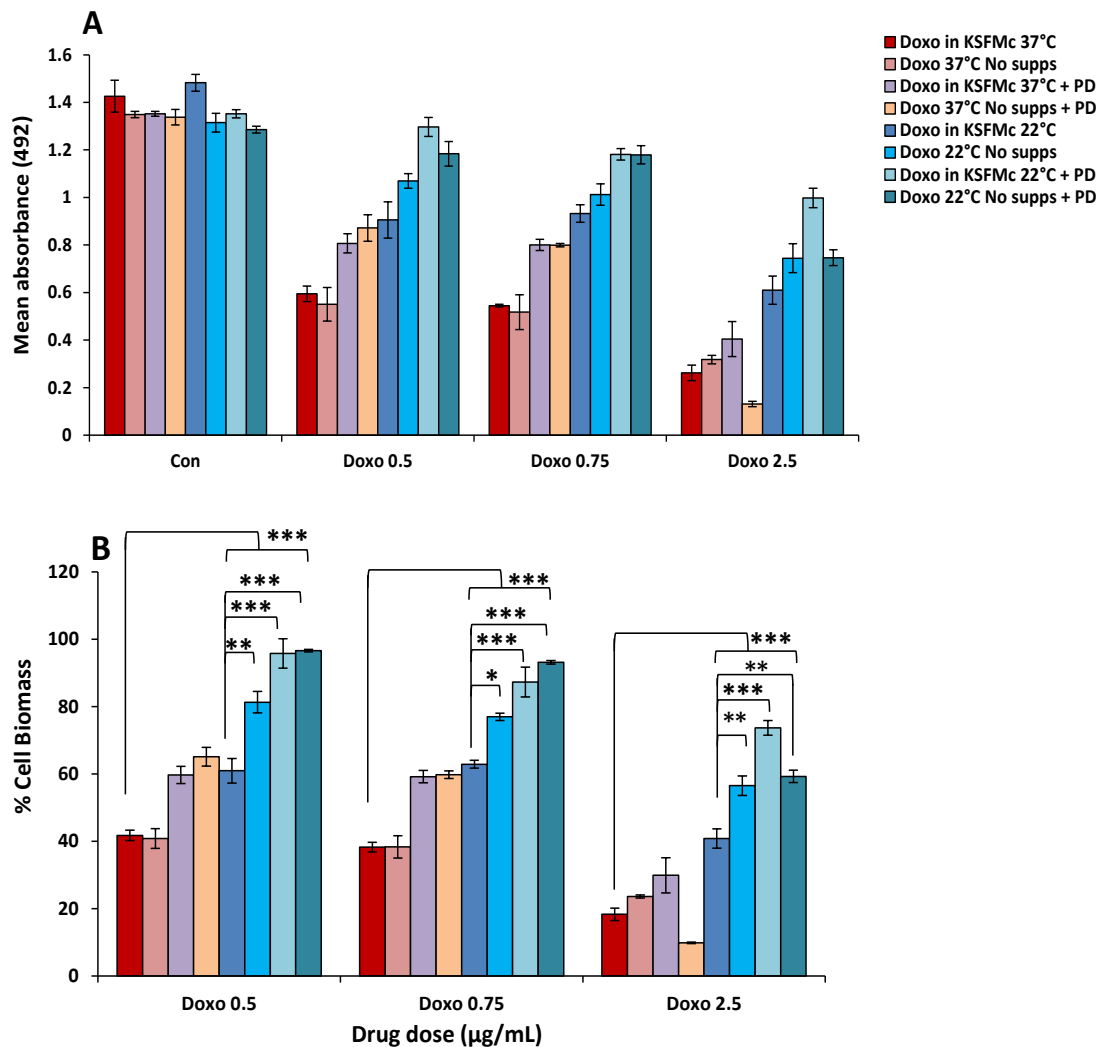


**Figure 4-23 Cytoprotective role of cooling + PD153035 against doxorubicin-mediated toxicity in HaCaTa cells**

HaCaTa cells were seeded in 96 well plates at 5000 cells/well in KSFM medium and were incubated overnight at 37°C/ 5% CO<sub>2</sub>. HaCaTa cells were pre-treated with 3 µM PD153035 or in KSFMc or KSFM (No supps) for 24h. HaCaTa cells were treated for 2h with (0.5, 0.75, and 2.5 µg/mL) doxorubicin (Doxo), in 4 types of medium, 1) KSFMc, 2) KSFM (No supps) 3) KSFMc contained 3 µM PD153035 4) KSFM (No supps) contained 3 µM PD153035 at 37°C and 22°C compared with vehicle control (cells treated with medium containing DMSO, in which the reagent was dissolved). The solvent represents the maximum amount of DMSO corresponding to the highest drug concentration). The drugs were then removed, wells were rinsed with PBS to remove any traces of drug and cells, which pre-treated incubated with PD153035 and the both other groups were incubate in fresh KSFMc. 72h, after which 20 µL of CellTiter 96® AQueous One solution was added to the wells and plates were incubated at 37°C in 5% CO<sub>2</sub> for a total of four hours. Absorbance was measured spectrophotometrically at a wavelength of 492nm and % cell biomass was calculated as described in Materials and Methods (Chapter 2). Data is presented as **A**) Absorbance (raw data) **B**) % cell biomass shown in bar graph. Data points correspond to mean % cell biomass (±S.E.M.) from three independent biological experiments, each consisting of 6-8 technical replicates. \*\*\*,  $p < 0.001$ .

**Key:** No supps: KSFM with no supplement

KSFMc: KSFM medium with complete supplements

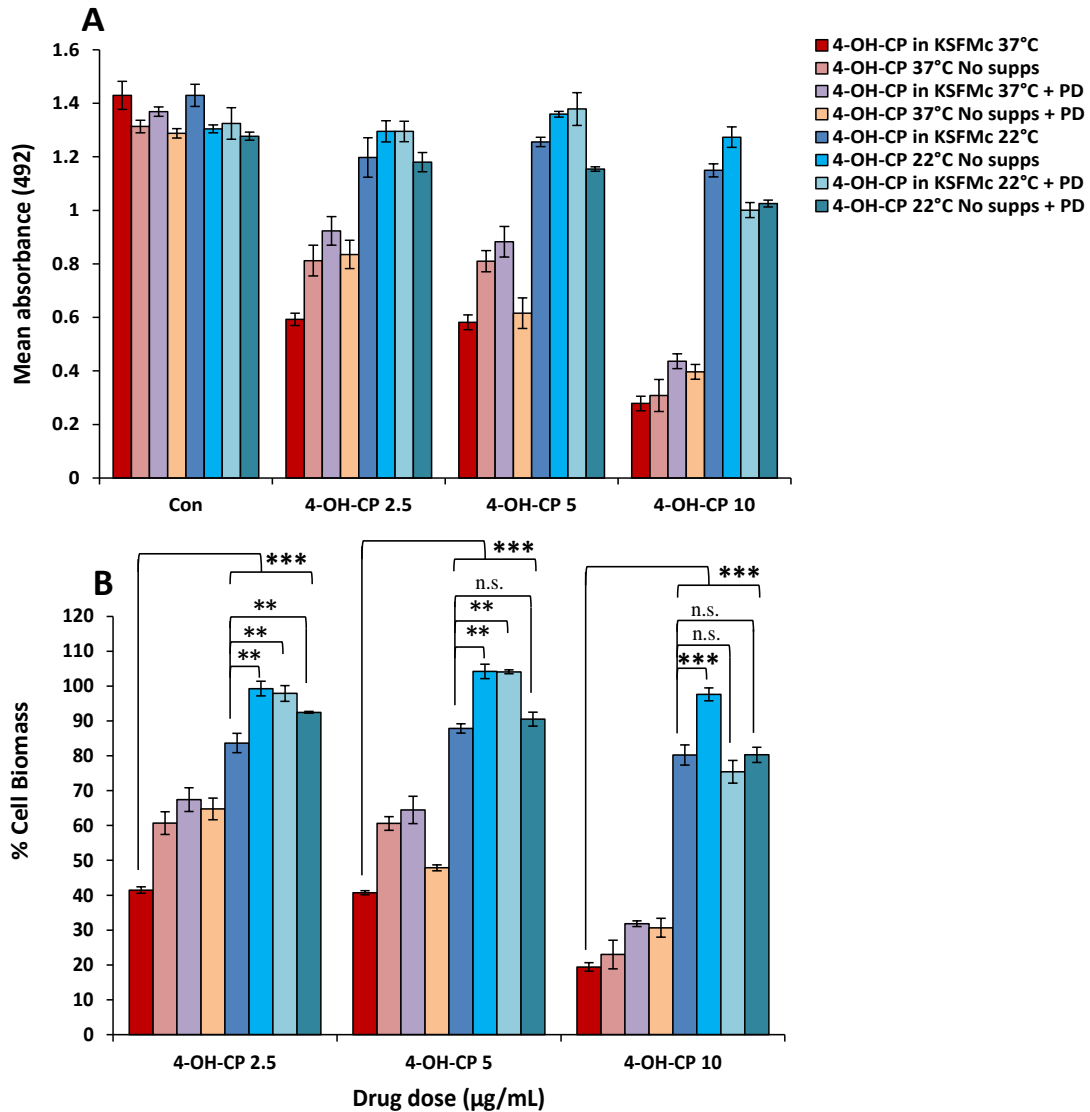


**Figure 4-24 Cytoprotective role of cooling + PD153035 against 4-OH-CP-mediated toxicity in HaCaTa cells**

HaCaTa cells were seeded in 96 well plates at 5000 cells/well in KSFMc medium and were incubated overnight at 37°C/ 5% CO<sub>2</sub>. HaCaTa cells were pre-treated with 3 µM PD153035 or in KSFMc or KSFMc (No supps) for 24h. HaCaTa cells were treated for 2h with (2.5, 5, and 10 µg/mL) 4-OH-CP, in 4 types of medium, 1) KSFMc, 2) KSFMc (No supps) 3) KSFMc contained 3 µM PD153035 4) KSFMc (No supps) contained 3 µM PD153035 at 37°C and 22°C compared with vehicle control (cells treated with medium containing DMSO, in which the reagent was dissolved). The solvent represents the maximum amount of DMSO corresponding to the highest drug concentration). The drugs were then removed, wells were rinsed with PBS to remove any traces of drug and cells, which pre-treated incubated with PD153035 and the both other groups were incubate in fresh KSFMc. 72h, after which 20 µL of CellTiter 96® AQueous One solution was added to the wells and plates were incubated at 37°C in 5% CO<sub>2</sub> for a total of four hours. Absorbance was measured spectrophotometrically at a wavelength of 492nm and % cell biomass was calculated as described in Materials and Methods (Chapter 2). Data is presented as **A**) Absorbance (raw data) **B**) % cell biomass shown in bar graph. Data points correspond to mean % cell biomass (±S.E.M.) from three independent biological experiments, each consisting of 6-8 technical replicates. \*\*\*,  $p < 0.001$ .

**Key:** No supps: KSFMc with no supplement

KSFMc: KSFMc medium with complete supplements



#### 4.7.1 Cell cycle analysis after growth inhibition

As shown in section 4.7, the combination of PD153035 treatment (PPC) and cooling (compared with incubation cells in KSFM with and without supps) showed that there was decrease in HaCaTa cells proliferation after 24h and this resulted in a significant increase in rescue from drug cytotoxicity. We therefore sought to determine whether a) removal of medium supps alone, b) PD153035 treatment alone, or c) combination of medium supps removal and PD153035 and the changes in cell viability observed correlated with changes in cell cycle distribution.

Interestingly, cell proliferation was inhibited by removal of growth factors (supps) as indicated by the observed cell cycle arrest in G0/G1 phase (Figure 4-28). The percentage of the G1 in cells incubated in KSFMc (normal growth medium with full set of supps) was 47.2% ( $\pm 0.5$ ) and this percentage increased to 49.4% ( $\pm 0.4$ ) in cells incubated in KSFM containing bovine pituitary extract (BPE) extract only but no recombinant EGF ligand (Figure 4-28B). This percentage increased further to 53.7% ( $\pm 0.9$ ) when cells were incubated for 24h in KSFM without any supps (Figure 4-28C). In HaCaTa cells treated with 3  $\mu$ M PD153035, the percentage of G1 was 55.0% ( $\pm 0.8$ ) (Figure 4-28D). Importantly, the most dramatic change was observed in cells treated for 24h in KSFM without supps and in the presence of PD153035 inhibitor and the percentage was 63.1% ( $\pm 0.6$ ) (Figure 4-28E). In these groups, the percentage of cells undergoing S phase was reduced from 15.3 ( $\pm 1.3$ ) to 13.5% ( $\pm 1.5$ ), 11.8% ( $\pm 0.5$ ), 10.6% ( $\pm 0.4$ ), and 8.8% ( $\pm 0.7$ ), respectively (Figure 4-28). These findings confirmed that the ability of PPC to enhance protection from drug cytotoxicity could be attributed to its property to regulate the cell cycle.

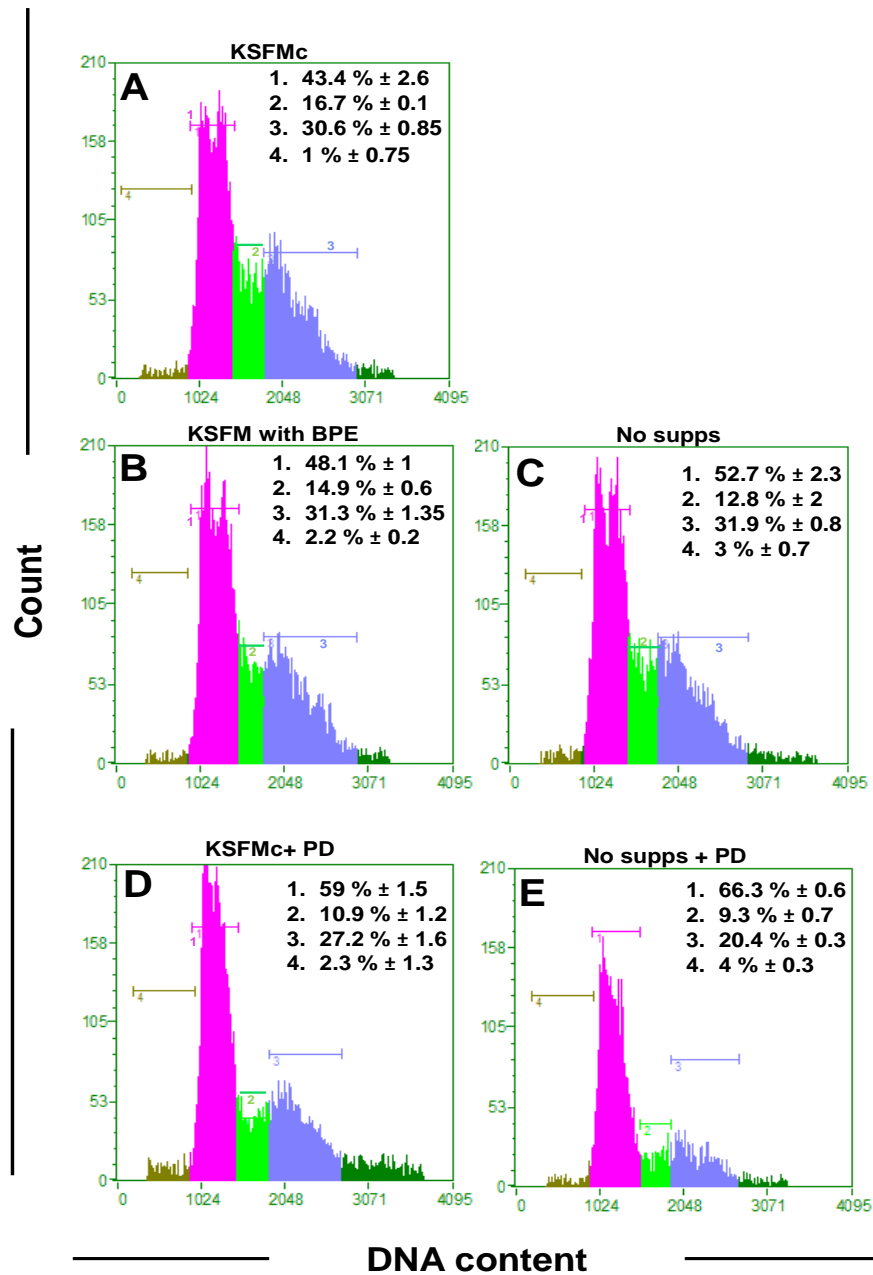


**Figure 4-26 Effects of EGFR signalling pathway inhibition by PD153035 vs removal of growth factors (starvation) on HaCaTa cell cycle distribution**

$9 \times 10^5$  HaCaTa cells were cultured in 10 cm<sup>2</sup> dish in KSFMc and cells were incubated overnight in 37°C / 5% CO<sub>2</sub>. Cells were incubated at 37°C/5% CO<sub>2</sub> for 24h in **A**) KSFMc; **B**) in BPE without EGF; **C**) KSFM (No supps); **D**) KSFMc + PD153035; **E**) in KSFM (No supps) + PD153035. Both attached and floating cells were harvested and fixed in 70% ethanol, DNA stained with PI. 10,000 cells were acquired on a Guava EasyCyte flow cytometer and results analysed using GuavaSoft software. The results represent plots of one set of triplicate experiments and the distribution percentages of cells in each cell cycle phase distribution means values were calculated from three independent biological experiments, each consisting of 2 technical replicates. Regions 1, 2, 3 and 4 on each panel represent G0/G1, S, and G2/M and subG0/G1 phase of the cell cycle, respectively.

**Key:** No supps: KSFM with no supplement  
 KSFMc: KSFM medium with complete supplements  
 BPE: Bovine pituitary extract

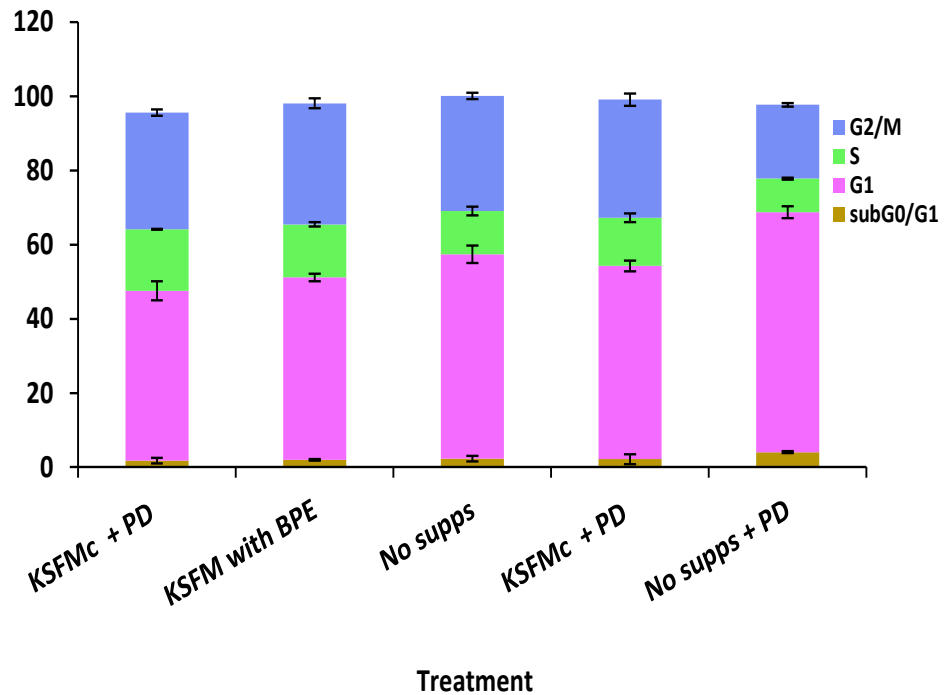


**Figure 4-29 Summary of independent replicate experiments for cell cycle analysis of HaCaTa cells after EGFR signalling pathway inhibition by PD153035 vs removal of growth factors (starvation)**

Bar graph summarises data obtained from three independent biological experiments, each consisting of 2 technical replicates as in Figure 4-28. Bars represent mean values of % of cells ( $\pm$ S.E.M.).

**Key:** No supps: KSFMc with no supplements  
 KSFMc: KSFMc medium with complete supplements  
 BPE: Bovine pituitary extract

## 4.8 Summary

- The main aims of this chapter were to a) identify the influence of the chemotherapy drugs doxorubicin, docetaxel and 4-OH-CP on the cell cycle in HaCaTa using flow cytometry and explore the effects of cooling on cell cycle distribution with and without drugs; and b) to determine whether protective pre-conditioning (PPC) using EGFR signalling blockade could enhance the ability of cooling to rescue cells from drug cytotoxicity.
- The results have demonstrated that cooling cells did not fully block cell progression through G1, S phase or M phases, but we did observe an increase in the G1 phase peak and a decrease in G2/M phase directly after 2h of cooling (T=0h). However, this effect was temporary and reversible as cell cycle distribution returned to normal rapidly (after 1h). This result indicated that perhaps a cell cycle checkpoint is involved triggered by cooling that regulates progression through G1 and cell cycle entry or G2/S transition; alternatively, it could be purely that cell metabolism overall is slowed down due to cooling, resulting in cell cycle deceleration.
- Flow cytometer results demonstrated that chemotherapy drugs induced cell cycle redistribution at 37°C: treatment with doxorubicin arrested the cells in G2/M phases, docetaxel showed a high subG0/G1 population and arrest in G2/M, and 4-OH-CP treatment appeared to arrest cells in S phase.
- When chemotherapy drug-exposed cells treated at 37°C were compared with cells treated at 22°C and 18°C at different time points, it was shown that cooling protects from drug-induced changes in cell cycle distribution. Different drugs (doxorubicin, docetaxel, and 4-OH-CP) responded to cooling in different ways (as expected, based on the different molecular mechanisms that underlie the ability of individual drugs to cause cell cycle changes).
- Importantly, cooling induced the recovery from DNA damage checkpoint arrest when the temperature was reduced from 22°C to 18°C, which is supportive of the findings in Chapter 3, where a further reduction in temperature provided better rescue.
- The effects of 0.5 µg/mL doxorubicin in HaCaTa cells were tested at different time points (0-24h). After 2h at 37°C there was a decreased G1 and an increased G/M phase compared to control cells. However, in cells treated at 22°C there was a decreased G2/M phase. After 4h the result at 37°C and 22°C showed further

decrease in G1 and the increase in both G2/M and subG0/G1 population, but the cells treated at 22°C showed a less subG0/G1 population. After 8h, 37°C conditions showed higher G2/M and subG0/G1 % populations than did 22°C. The results showed that most cells become arrested in G2/M phase at 24h after cells were exposed to doxorubicin and the results showed high peaks in G2/M phase for both temperatures 37°C and 22°C. However, G1 phase at 22°C was slightly higher than G1 at 37°C. When cells were treated with doxorubicin at 18°C they showed better inhibition of doxorubicin effects on cell cycle redistribution.

- A concentration of 0.01 µg/mL docetaxel in HaCaTa cells was able to induce G2/M arrest, starting as early as 1h after treatment at 37°C compared to control and this significantly increased after 4h with an accompanying reduction in the G1 population and this continued to increase up to 24h. This was significantly attenuated when the cells were incubated at 22°C and virtually abolished at 18°C.
- When HaCaTa were exposed to 7.5 µg/mL 4-OH-CP at 37°C there was a significant increase in G1 and decrease of G2/M phase compared to the control between 2 and 8h after treatment. This effect was reduced when the cells, which were treated at 22°C. After 24h in the cells, which were treated at 37°C, proliferation was significantly inhibited *via* induction arrested at the S phases compared to control cells after 24h. In cells treated at 22°C the effects of 4-OH-CP were significantly inhibited and at 18°C the cell cycle distribution was close to the distribution of the control. These findings are compatible with the hypothesis that cyclophosphamide induces DNA cross-links as a result of that cause changes of the cell cycle, and this is inhibited by cooling.
- Moreover, we investigated the responses of HaCaTa cells to starvation as well as EGFR tyrosine kinase inhibitor PD153035 with and without treatment of chemotherapy drugs. We showed that short-term starvation (by incubating cells without supplements) resulted in a higher biomass compared with cells treated with complete KFSM medium (KFSM medium with complete supplements) which provided evidence that the slowing cell growth rate correlates with protection from the cytotoxicity of the chemotherapy drugs. Pre-treatment with the EGFR inhibitor PD153035 significantly protected from drug-mediated cytotoxicity for all compounds tested confirming that PPC could, at least partly, rescue cells from drug toxicity.
- Importantly, combination of PD153035 and cooling during chemotherapy drug treatment provided significant protection from drug-mediated cytotoxicity for nearly

all concentrations tested for doxorubicin, 4-OH-CP and, though to a lesser extent, docetaxel.

- Finally, cell cycle analysis provided evidence that the ability of PPC to enhance protection from drug cytotoxicity could be attributed to its property to regulate the cell cycle distribution.

## 4.9 Discussion

### 4.9.1 Role of cooling on the effect of chemotherapy drugs on cell cycle progression and cytotoxicity

Cell cycle analysis was conducted to evaluate the activity of the chemotherapeutic drugs used in this study (doxorubicin, docetaxel, and 4-OH-CP) and to identify if they induce cell cycle arrest *in vitro*. Once this analysis was complete, the aim was to investigate the effects of cooling in cell cycle changes induced by chemotherapy drugs.

The control apparatus of the cell (also referred to as the 'cell cycle clock') consists of a variety of proteins that monitor the extra- and intracellular environment of the cell and its division status. Monitoring the environment is imperative, as, for example, cells can respond to stress (e.g genotoxic stress). As part of these monitoring mechanisms, there are several checkpoints within the cell cycle at which the cycle can be paused; one of these is the G2/M checkpoint where, if the environmental conditions appear optimal and the cell has reached a particular size and successfully replicated its DNA, will it then proceed into M-phase.

Chemotherapy generally interferes with cell proliferation or directly stimulates death. Some anticancer drugs act only on a particular part or parts of the cell cycle (cell cycle-specific) while others act throughout the cell cycle (cell cycle-nonspecific) (Payne and Miles, 2008). When chemotherapy drugs induce DNA damage, either the cell cycle can be arrested temporarily to allow for DNA repair (Di Leonardo *et al.*, 1994 420) or the cells could be eliminated by apoptosis (Liebermann *et al.*, 1995 421), a decision-making process in which the tumour suppressor p53 is critical.

Doxorubicin is a drug that intercalates the DNA by inserting itself between nucleotide bases and thereby interferes with DNA and RNA synthesis, mainly affecting the cells in S phase due to the formation of DNA adducts that inhibit DNA replication (Swift *et al.*, 2006). In this work, when HaCaTa cells were treated with doxorubicin (0.5 µg/mL) for 2h and cell cycle analysis performed 36h post-treatment, results showed that the cells accumulated in the late S and predominantly G2/M phase (Figure 4-2B). This might be explained by the ability of doxorubicin, following DNA intercalation, to inhibit the enzyme topoisomerase II, which is responsible for replicating the two strands of DNA and thus when inhibited, this prevents the synthesis of nucleic acids (Payne and Miles, 2008; Trigg and Flanigan-Minnick, 2011). At 0.5 µg/mL doxorubicin, cell viability was about 40% at 37°C (Chapter 3); this was the concentration of choice, as higher doses would be expected to induce apoptosis, thus making it difficult to perform cell cycle analysis. These observations are in agreement with previous findings in HCT116 cells where treatment with 1µM dose of doxorubicin for 1h

followed by 72h incubation in drug-free medium caused G2/M arrest (Lüpertz *et al.*, 2010). Treatment with doxorubicin induced DNA damage can result in DNA double-strand breaks, which leads to apoptosis (Kaina, 2003). In our study, keratinocytes arrested in G2/M in response to doxorubicin treatment, which is in agreement with a previous study by Zeng *et al.*, (2000) showing that doxorubicin may cause predominantly G2 phase arrest rather than mitotic arrest in the human breast tumour cell line BCap37 (Zeng *et al.*, 2000). Zeng *et al.*, (2000) suggested that because it is difficult to distinguish between both G2 and M phase in the flow cytometer, as both phases are included in the G2/M peak, the G2/M phase arrest by doxorubicin was predominantly G2 arrest (Zeng *et al.*, 2000). Another study showed that treatment of Swiss 3T3 fibroblasts with doxorubicin arrested the cells at G2/M at 48h post-treatment (Siu *et al.*, 1999).

Docetaxel belongs to a class of cytotoxic drugs that inhibit microtubule depolymerisation, resulting in mitotic arrest, with large cells forming with approximately twice the typical cellular DNA content; these cells are unable to divide into two daughter cells and subsequently undergo 'crisis' and die (apoptosis) (Mooberry, 2011). The results of this study showed that treatment of HaCaTa cells with docetaxel (0.01 µg/mL) at 37°C was able to induce a remarkably high subG0/G1 population and mitotic arrest at 36h post-exposure (Figure 4-2C). Hernandez-Vargas *et al.*, (2007) showed that as low concentrations as 2-4 nM docetaxel induced mitotic arrest followed by apoptosis in breast carcinoma MCF7 and MDA-MB-231 cell lines (Hernández-Vargas *et al.*, 2007). When cells are triggered to undergo apoptosis, genomic DNA is cleaved into small fragments, observed as distinct subG0/G1 peaks by flow cytometry (Kroemer *et al.*, 2009). The detection of a subG0/G1 DNA peak is a specific marker (hallmark) of apoptosis since death by necrosis in most cases does not induce a subG0/G1 peak (Nicoletti *et al.*, 1991). In this work, docetaxel-treated cells showed a greater subG0/G1 population than the other drugs tested. A previous study showed that H134, IGROV-1 and OVCAR-3 cell lines treated with docetaxel accumulated in the G2/M phase and the a prolonged G2/M arrest induced caspase-3 activation, which initiates apoptosis, DNA fragmentation, whilst an increased subG0/G1 population was observed by flow cytometry (Kolfshoten *et al.*, 2002).

Cyclophosphamide is a cell cycle-nonspecific drug and thus acts against cells at any phase of the cycle, including the resting phase (Payne and Miles, 2008). The activated form of cyclophosphamide (4-hydroxycyclophosphamide, 4-OH-CP) is an alkylating agent which adds an alkyl group to DNA, thus blocking DNA replication and arresting cells in S phase (Alkan *et al.*, 2014). The data in this study showed that the cell cycle distribution at 37°C in response to 4-OH-CP treatment induced cells arrest in S phase. This is in agreement with

Schwartz *et al.*, (2001) who showed that 9L tumour cells treated with 4-OH-CP arrested in S phase (Schwartz and Waxman, 2001).

#### **4.9.2 Effects of low temperature (cooling) on cell cycle distribution in human keratinocytes**

The cell cycle is a tightly regulated vital process by which new cells are generated and grow. Here it has been confirmed that temperature is an important factor in regulating cell growth, an effect that was anticipated because the enzymes that control many biochemical reactions need an optimal temperature of around 37°C to function at an optimum rate and thus this may have a general effect on cell growth. The effect of temperature on the cell cycle and viability are not well understood (Ramirez and Mutharasan, 1990) and there have been relatively few studies that have examined this. Two specific aspects investigated in this work, which had not been previously reported, are a) the effect of cooling on the cell cycle of human keratinocytes, and b) the connection between the cell protection caused by cooling and the cell cycle distribution of these cells after treatment with cytotoxic agents.

A series of experiments was designed to determine the effect of cooling on the cell cycle of keratinocytes by using HaCaTa cells at 0, 1, 2, 4, 8 and 24h after treatment (cooling). The flow cytometry data in this study indicate that low temperature affects all parts of the cell cycle phases (Figure 4-3) thus indicating a state of reduced/slow proliferation. Lowering the temperature from 37°C to 22°C for 2h (time point 0h) resulted in a decrease in the number of cells in G2/M phase and accumulation of the cells in G1/S phase compared to control cells at 37°C. These observations suggest that cooling may act specifically on the transition from G1 to S phase and the control point of G2 is affected by temperature. This supports the observation from a previous study-using mouse leukemic and HeLa cells, which showed prolongation of cell cycle at 25°C-33°C and a temporal dilation of the G1 and S phase. HeLa cells were cultured at different temperatures and this was shown to modify all phases of the cell cycle (Rao and Engelberg, 1965) whilst M phase was more sensitive than G1, S, G2 phase to temperature (Rao and Engelberg, 1965). Our data are in agreement with the hypothesis that cooling during drug exposure may decelerate growth rates and thus protect cells from chemotherapy-induced toxicity. However, the specific molecular mechanisms by which cooling decelerates the cell cycle remain unclear and require further future studies.

Interestingly, after the 2h incubation at 22°C, when cell cultures were subsequently re-warmed to physiological temperature 37°C, the mitotic index rose rapidly within 1h, and

the cells appear to be dividing normally (as at 37°C). This indicates that moderate cooling for a short period only temporarily reduces growth rate and is not detrimental to long-term cell growth. Cooling might act by blocking cell cycle progression at G2 or may have reduced the cell cycle in all checkpoints. Moreover, cooling may force reduction of metabolic activity of cells (compared to cells incubated at physiological temperature 37°C) (Si *et al.*, 1997).

#### **4.9.3 Time and temperature dependence of cytotoxic agent-induced cell cycle arrest and apoptosis under cooling conditions**

Treatment of HaCaTa cells with cytotoxic agents resulted in temperature dependent induction of cell cycle arrest and apoptosis. Intercalating drug doxorubicin at 37°C induced G2/M arrest progressively. Doxorubicin activates p53 and p21/Waf1, which leads to inhibition of G1/S cyclin CDK complex activity, thus cells were arrested in G1 phase. G1 arrest was relatively transient and the cells moved into S and G2 phase. However, cell arrest at the G2 checkpoint was permanent because of that cells accumulated in G2 Phase (Siu *et al.*, 1999).

One unanticipated finding in this study was that the cell cycle distribution at 22°C in cells treated with doxorubicin was similar to 37°C. Although changes in cell cycle distribution at 22°C started, albeit delayed in comparison to 37°C, both temperatures showed arrest at G2/M after 24h. Data on cell viability (Chapter 3), showed that biomass at 22°C was higher than at 37°C ~ 69.1% and 41.9% respectively. A possible explanation for these observations is that cooling reduced DNA damage induced by doxorubicin by a process called checkpoint recovery, and arrested cell cycle progression to allow time for DNA repair. After completion of DNA repair, checkpoint recovery activation is terminated, cell cycle progression can be restarted (Morii *et al.*, 2015); as a result, the cells recover and an increase in viability at 22°C observed. This may be supported by the low subG0/G1 levels at 22°C in comparison to 37°C, which means arrested cells have less damage DNA bypass to G2 and do not undergo apoptosis (although flow cytometry can only detect fragmented DNA). Furthermore, these data showed a strong relationship between temperature and cell cycle arrest, which was confirmed by the findings at 18°C, which showed a reduction in the percentage of cells in G2/M phase and the percentage of subG0/G1 (a hallmark of apoptosis), compared to control cells. Moreover, doxorubicin-mediated DNA damage, which leads to induction of apoptosis and cell cycle arrest is a dose- and time-dependent effects (Kim *et al.*, 2009; Lüpertz *et al.*, 2010).

Cells treated with docetaxel at 37°C exhibited a time-dependent cell cycle arrest in G2/M phase and induction of apoptosis (evident by a high subG0/G1 phase), with morphological changes characteristic of cells undergoing apoptosis. The protective effect of

cooling on docetaxel-treated cells was enhanced further by changing cooling conditions from 22°C to 18°C.

HaCaTa cells treated with 4-OH-CP showed accumulation of cells in S phase and induction of apoptotic cell death at 37°C, however, cell arrest was substantially reduced in cells treated at 22°C and completely prevented at 18°C. These findings are compatible with the hypothesis that cyclophosphamide induces DNA cross-links, as a result of which it causes cell cycle arrest, and this is inhibited by cooling. It should be though noted that cyclophosphamide is cell cycle non-specific and can target cells in all phases.

Moreover, we examined the responses of HaCaTa cells to 'starvation' as well as the well-characterised EGFR tyrosine kinase inhibitor PD153035 with and without treatment of chemotherapy drugs. The short-term starvation (by incubating cells without supplements) showed in a higher biomass compared with cells treated with complete KFSM medium (complete KFSM medium with supplements), which provided evidence that slowing cell growth rate correlates with protection from the cytotoxicity of the chemotherapy drugs. Although the short-term starvation protected HaCaTa cells against chemotherapy at 37°C, cooling alone showed better protection than short-term starvation, possibly because of the cellular stress caused by the starvation. On the other hand, pre-treatment with the EGFR inhibitor PD153035 remarkably protected from chemotherapy drug-mediated cytotoxicity for all drugs tested confirming that "protective pre-conditioning" (PPC) could improve protection from drug cytotoxicity.

PD153035 has been reported as being a specific inhibitor of the EGF receptor (Bos *et al.*, 1997; Fry *et al.*, 1994). HaCaTa cells that have been treated with lower inhibitor concentrations of PD153035, were shown to stimulate an overall increase in biomass (see Figure 4- 22), in comparison with the control samples (untreated cells with PD153035). Such a result is in accordance with those found in a previous report, in which the viability of H211 and H2373 cells that used the MTT assay were reduced only at a high concentration of PD153035. In contrast with this situation, at a reduced concentration of PD153035 cell viability was enhanced (Cole *et al.*, 2005).

An increase in cell growth when sub-lethal concentrations of otherwise cytotoxic drugs are used has been previously reported across an array of different cell types (Kayamba *et al.*, 2013; Paus *et al.*, 2013). Subthreshold cell damage that has been induced by cytotoxic agents may increase proliferative activity. However, this may only be a fleeting occurrence, seemingly just as a repair mechanism (Bodo *et al.*, 2007). These results are more likely as a consequence of the induction of the repair mechanisms through reduced PD153035 concentrations. Ultimately, this results in increased proliferative activity. Based on

these established results, it would of interest for future research to investigate gene expression responses to application of PD153035 treatment.

**CHAPTER 5: The effect of cooling on chemotherapy  
drug-mediated cell death induction, mitochondrial  
membrane potential disruption and Reactive Oxygen  
Species generation**

## 5.1 Background

Mitochondria play key roles in many fundamental biological processes and serve as the powerhouses of the cell. Their main task is to convert energy from nutrient molecules into ATP. Besides this, mitochondria can be involved in the induction of apoptosis and loss of the mitochondrial electrochemical potential gradient ( $\Delta\Psi$ ) is an early event of apoptosis (Fransson *et al.*, 2003). The intrinsic apoptosis pathway is mediated by the mitochondria (hence it is often referred to as the mitochondrial pathway) and is triggered by various intracellular stress signals, which include DNA damage such as due to treatment with chemotherapeutic agents, growth factor deprivation and reactive oxygen species (ROS). This results in mitochondrial outer membrane permeabilisation (MOMP) and a loss of mitochondrial membrane potential  $\Delta\Psi_m$  (Tait and Green, 2010) and in most cases triggers the caspase-dependent (caspase-9 and subsequently caspase-3) apoptosis pathway (Tait and Green, 2010).

Depolarisation of the mitochondrial membrane potential is accompanied by an increase in the release of ROS due to the fact that damaged mitochondria have a faulty electron transfer within the respiratory chain, and this produces ROS (Fulda *et al.*, 2010). This process can be stimulated by the substantial exogenous oxidisation of phospholipids that readily migrate to the mitochondria causing damage that is able to trigger the onset of the intrinsic apoptotic pathway (Chen *et al.*, 2007). So far, it is not completely clear how the mitochondrial energy and redox machinery, which can be activated by chemotherapy drugs, interacts with the apoptotic machinery (Liu *et al.*, 2013).

### 5.1.1 Reactive oxygen species

Reactive Oxygen Species (ROS) are produced during the cell's normal aerobic metabolism; these include hydroxyl radicals ( $\text{OH}\cdot$ ), superoxide anions ( $\text{O}_2^{\cdot-}$ ) and hydrogen peroxide ( $\text{H}_2\text{O}_2$ ) and are short-lived, highly-reactive harmful forms of oxygen ( $\text{O}_2$ ) that can easily oxidise other molecules, and they are normally removed by various antioxidant mechanisms inside cells. As mentioned earlier, the mitochondrial respiratory chain is the main source of ROS (Brand, 2010). Besides mediating cell and tissue damage, ROS has an important regulatory function in aerobic cells. ROS are continuously released during various metabolic processes in different compartments of the cell, and low concentrations of ROS can act as signalling molecules and stimulate the growth of cells. However, at higher concentrations, because of their reactivity, ROS cause oxidative modification of cellular components such as proteins, nucleic acids and lipids and can trigger cell death *via* either programmed cell death (apoptosis) or necrosis (Burdon, 1995; Samson, 1997).

ROS have short life span, and thus one way to improve the ROS competence is by co-localisation of their site of generation and their site of signalling role. In theory, the quantity of mitochondria within the cell has the ability to modify the quantity of ROS generated and, as a result modify their intracellular function. Mitochondrial biogenesis, which occurs by growth and division of pre-existing mitochondria, is regulated by PGC-1 $\alpha$  (peroxisome-proliferator-activated receptor  $\gamma$  co-activator-1 $\alpha$ ) (Ventura-Clapier *et al.*, 2008). Mitochondrial biogenesis is triggered by different stimuli such as cell division, in response to an oxidative stimulus, to exercise training, to an increase in the energy requirements of the cells, in certain mitochondrial diseases *etc.* (St-Pierre *et al.*, 2006; Valero, 2014). PGC-1 $\alpha$  has dual activities—stimulating mitochondrial biogenesis while suppressing ROS levels (St-Pierre *et al.*, 2006). The role of mitochondrial biogenesis as an antioxidant defence mechanism is well established. It has previously been shown that the increased production of mitochondria is a support mechanism that help maintain a satisfactory level of healthy mitochondria, which would be able to tolerate cellular energy needs in conditions when a large fraction of these mitochondria have suffered ROS-induced damage rendering them dysfunctional (Chou *et al.*, 2007; Yu, 2011). Previous studies have shown that mild hypothermia can regulate heat shock protein induction and mitochondrial biogenesis (Ning *et al.*, 1998; Tissier *et al.*, 2012).

### **5.1.2 Apoptosis mechanisms of HF under pathological conditions**

Application of chemotherapeutic drugs can trigger apoptosis in both *in vivo* and *in vitro* (Hasmall and Roberts, 1999). It is generally thought that chemotherapeutic drugs induce apoptosis *via* the intrinsic mitochondrial pathway by activation of pro-apoptotic factors. The intrinsic pathway is controlled by members of the Bcl-2 family, which act as inhibitors (e.g., Bcl-2) and promoters of apoptosis (such as Bak and Bax) (see Chapter 1 (Figure1-6)) (Korsmeyer, 1999; Petros *et al.*, 2004) and is associated with initiator caspase-9 activation (Schultz and Harrington Jr, 2003). Both the intrinsic (mitochondrial) and extrinsic (receptor-mediated) mechanisms can lead to the activation of effector caspases-3, 6 and 7, which in turn mediate cleavage of a variety of substrates, including deoxyribonuclease, which is responsible for the cleavage of nuclear DNA (Schultz and Harrington Jr, 2003; Van Gurp *et al.*, 2003).

The classical anticancer drugs have distinctly different mechanisms of action for instance, cyclophosphamide occurs through the alkylation of DNA and disruption of the nuclear DNA (Valeriote and Van Putten, 1975). DNA damage induces activation of the pro-apoptotic gene p53 (Botchkarev *et al.*, 2000; Botchkarev *et al.*, 2001) which migrates into the mitochondria and induces Bax and cytochrome c and apoptosis (Fulda *et al.*, 2010). A previous study has shown that 4-OH-CP, the activated form of cyclophosphamide, induced

cytotoxicity in 9L gliosarcoma cells by stimulating apoptosis resulting in induction of plasma membrane blebbing, DNA fragmentation and caspase-3/7 (Schwartz and Waxman, 2001).

Doxorubicin is an anthracycline that mainly acts *via* its intercalation into DNA, inducing ROS generation and DNA damage, which occurs *via* inhibition of topoisomerase II resulting in apoptosis (Sliwinska *et al.*, 2009). 5-Fluorouracil (5FU) also appears to act *via* p53-mediated apoptosis through the generation of ROS in the mitochondria (Ahrendt *et al.*, 2000; Hwang *et al.*, 2001). 5FU is an antimetabolite drug widely used in the treatment of cancer by suppressing essential biosynthetic processes through inhibition of thymidylate synthase and p53 activation (Longley *et al.*, 2003; Müller *et al.*, 1998).

Docetaxel interferes with microtubule stabilisation, which leads to accumulation of the cells in G2/M phase. Previous studies showed caspase-3 activation in cells treated with docetaxel and G2/M arrest using four human ovarian cell lines (A2780, H134, IGROV-1 and OVCAR-3) (Kofschoten *et al.*, 2002) and a clear connection exists between mitotic arrest and apoptosis in response to docetaxel (Morse *et al.*, 2005).

### **5.1.3 Measurement of intracellular ROS and mitochondrial membrane integrity**

To study the generation of ROS by chemotherapy drugs (and ultimately assess the effects of cooling), the fluorescent probe 2', 7'-dichlorofluorescein diacetate (H2DCFHDA) was used (Kalyanaraman *et al.*, 2012). After entry through the cell membrane, the acetyl groups of the stable non-polar non-fluorescent DCFH-DA are cleaved by intracellular esterase activity. The reduced non-fluorescent DCFH accumulates in the cell due to its polarity; in the presence of ROS (mainly H<sub>2</sub>O<sub>2</sub>) it is oxidised to green fluorescent DCF (Figure 5-1). The resulting fluorescence is proportional to the amount of active ROS and can be quantified by flow cytometry (Bass *et al.*, 1983).

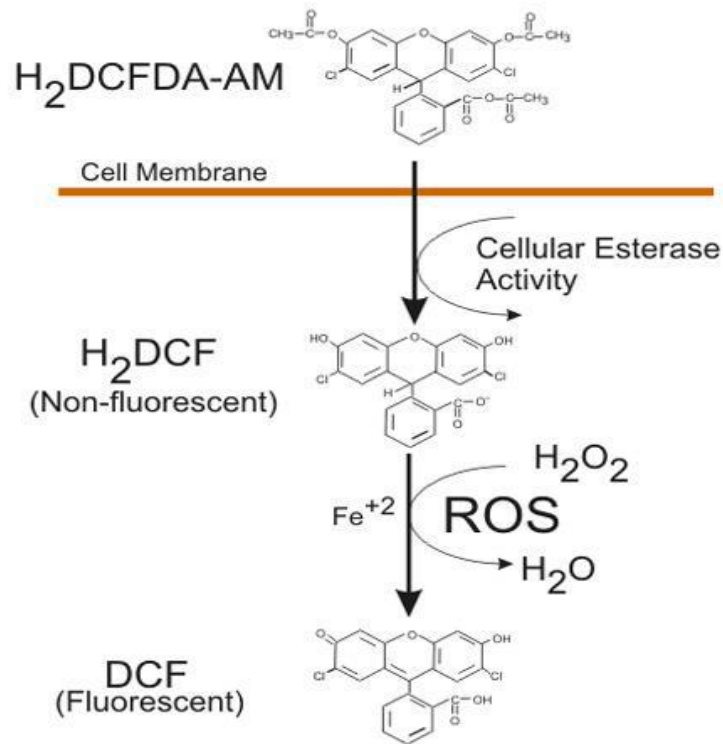


**Figure 5-1 The principle of ROS detection using H<sub>2</sub>DCFDA**

6-carboxy-2', 7'-dichlorodihydrofluorescein diacetate (H<sub>2</sub>DCFDA) is a derivative of reduced fluorescein that has cell permeability. The reduced forms of fluorescein lack any fluorescence until acetyl groups are removed by intracellular esterase(s) and oxidation is occurring within the cells. When this occurs, the charge of the molecules makes it much less likely to leave the cell and also emits detectable fluorescence. The levels of fluorescence intensity are therefore an indication of the intracellular concentration of ROS. Adapted from (Held, 2012).

#### 5.1.4 Use of JC-1 dye for mitochondrial membrane potential detection

Some of the most frequently used anticancer drugs in the clinic, for example doxorubicin, exert their cytotoxic effect *via* formation of ROS and direct intervention in the cell cycle machinery of the cells, as well as loss of mitochondrial membrane potential (Tsang *et al.*, 2003). Using the fluorescence dye 5,5- 6,6-tetrachloro-1,1- 3,3-tetraethylbenzimidazolyl carbocyaniniodid (JC-1) mitochondrial membrane potential in cells can be studied. The measurement of mitochondrial membrane depolarisation is particularly useful for the investigation of apoptosis. JC-1 is a cationic, membrane-permeable fluorescent dye that enters the mitochondria of living cells with intact membrane potential (membrane potential dependent) (Bortoletto *et al.*, 2004), where it forms red fluorescent aggregates. Events such as apoptosis, which lead to loss of mitochondrial membrane potential, prevent the accumulation of the JC-1 dye in the mitochondria. This leads to a diffuse distribution of the dye in the whole cell and to a shift of red fluorescence (JC-1 aggregates) to green fluorescence (JC-1 monomers) and this can be measured by fluorimetric analysis and subsequent calculation of the ratio (590 nm / 530 nm) using a plate reader or by direct detection of fluorescence changes using a flow cytometer (Figure 5-2) (Bortoletto *et al.*, 2004; Sakamuru *et al.*, 2012).

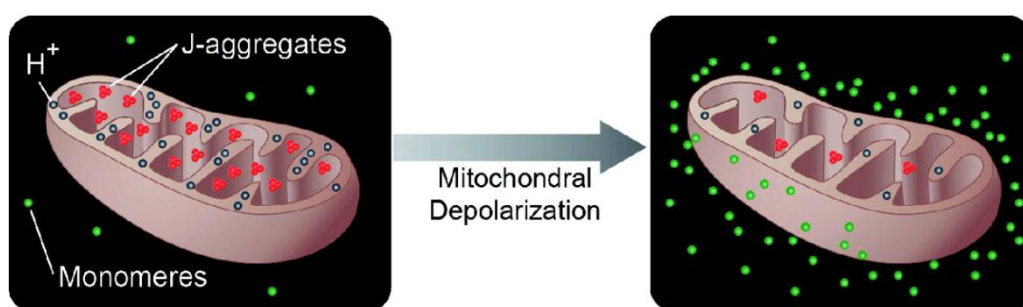


**Figure 5-2 The principle of the fluorescent JC-1 dye**

$\Delta\Psi_m$  is an important parameter of mitochondrial function used as an indicator of cell health. JC-1 can be used to study mitochondrial behaviour in a variety of conditions, including apoptosis. JC-1, a lipophilic dye, selectively enters mitochondria and reversibly changes colour from green to red with increasing membrane potential. In healthy cells with high mitochondrial  $\Delta\Psi_m$ , JC-1 spontaneously forms complexes known as J-aggregates with intense red fluorescence. However, in apoptotic cells or unhealthy low  $\Delta\Psi_m$ , JC-1 remains in the monomeric form, showing only green fluorescence (Sakamuru *et al.*, 2012).

## **5.2 Apoptosis assays for the detection of cell death induced by chemotherapeutic agents on human keratinocytes**

Most chemotherapeutic agents trigger apoptosis in dividing cells (Fabbri *et al.*, 2006). Because of the rapid division rate of hair matrix keratinocytes, the HF represents a target for many chemotherapeutic agents (Paus and Cotsarelis, 1999). Cells undergoing death can be detected by their morphological changes and biochemical changes which can be measured by different commercial assays. Previously published guidelines regarding the use of assays for detecting cell death (Galluzzi *et al.*, 2009) have recommended that at least two independent assays are utilised for the detection of cell apoptosis. The apoptosis assays used in this study to detect the cytotoxic effects of chemotherapeutic drugs at physiological temperature vs cooling conditions were the commercially available the CytoTox-Glo cytotoxicity assay, Sensolyte Homogenous Caspase-3/7 assay and the DNA fragmentation ELISA assay. In addition western blotting was used to explore the apoptotic pathways activated (Chapter 6).

### 5.3 Chapter Aims

In light of the cytotoxicity caused by chemotherapy drugs and effects of cooling in protecting from the deleterious effects of these drugs shown in previous chapters, the work described in this chapter was designed to examine mitochondrial trans-membrane potential and ROS production levels in human keratinocytes treated with chemotherapy drugs at physiological temperature (37°C) and at cooling conditions. The hypothesis was that chemotherapy drugs may induce MOMP and ROS release and the experiments investigated whether these changes might be altered by cooling, thus providing functional evidence for its cytoprotective ability. Moreover, a variety of well-characterised cell apoptosis assays were used to investigate the cytoprotective role of cooling against the cytotoxic effects of commonly used chemotherapeutic agents.

**Specifically the aims of the work in this chapter were to:**

- Investigate the effect of chemotherapy drugs doxorubicin, 4-OH-CP and docetaxel on the mitochondrial membrane potential ( $\Delta\Psi_m$ ) and the influence of cooling (temperatures 22°C, 18°C, and 14°C) was investigated for the first time using the JC-1 dye.
- Analyse the changes in ROS levels following chemotherapy drug administration, and an attempt was also undertaken to find out a correlation between ROS levels and culture temperature; the experiments involved use of H<sub>2</sub>DCFDA to quantify ROS induced by the chemotherapeutic drugs at 37°C and determine the effects of cooling on the accumulation of ROS after chemotherapy drug treatment.
- Use the luminescence-based CytoTox-Glo assay (which measures the release of a proprietary protease released by cells with compromised plasma membranes) as a surrogate marker of apoptosis.
- Investigate the activation of caspase-3/7 activity as an additional marker of apoptosis at 37°C compared with cells treated at cooling conditions.
- Detect chemotherapy drug-induced apoptosis by using a DNA fragmentation ELISA assay.

## 5.4 Optimisation of the JC-1 assay for the detection of changes in mitochondrial membrane potential ( $\Delta\Psi_m$ )

The first part of this chapter focused on the optimisation of the JC-1 fluorescent probe using flow cytometry for detecting JC-1 aggregates (red fluorescence) and monomeric (green fluorescence) in HaCaTa cells. HaCaTa cells were treated with 7.5  $\mu\text{g/mL}$  4-OH-CP (concentration used for optimisation experiments) for 2h at 37°C. Loss of mitochondrial membrane potential ( $\Delta\Psi_m$ ) is indicated by the reduced number of cells with red fluorescence and increases in the number of cells with green fluorescence. According to the manufacturer's instructions, the initial conditions for JC-1 assay may require modifications because of differences in cell types and culture conditions. Thus, the concentration of JC-1 was optimised and three concentrations were initially tested (1, 2, and 4  $\mu\text{M}$ ) to ensure that the JC-1 concentration used was sufficient for sensitive detection of  $\Delta\Psi_m$  loss (Figures 5-3 and 5-4). Data showed that the optimal concentration for JC-1 was 2  $\mu\text{M}$  compared to 1  $\mu\text{M}$ , which was less sensitive than 2  $\mu\text{M}$  on the other hand, there was no significant difference between 2 and 4  $\mu\text{M}$  of JC-1, therefore 2  $\mu\text{M}$  was used for all subsequent experiments. Also, as part of the optimisation, the time required for  $\Delta\Psi_m$  loss was investigated, and the time ranged from 6 to 48h (6 and 12h data are not shown as the induction of  $\Delta\Psi_m$  loss and the green fluorescence was very low compared to the positive control).

Three types of controls were used for all JC-1 experiments: 1) positive control for  $\Delta\Psi_m$  loss detection (positive green fluorescence control) in which the cells were treated in each experiment with carbonyl cyanide m-chlorophenyl (CCCP) hydrazone because it causes rapid mitochondrial membrane depolarisation, 2) negative control in which untreated cells were stained with JC-1, thus providing a pure red signals, 3) unstained cells as background control (without drug treatment and no JC-1 probe). Representative results with appropriate gating strategies are shown in Figures 5-3 and 5-4.

Following these initial experiments, the JC-1 assay was carried out in cells cultured under cooling conditions; to investigate the ability of cooling to protect against chemotherapy drugs-induced  $\Delta\Psi_m$  loss at 37°C and 18°C. When cells were examined after 24h treatment, there was a temperature dependent reduction of the red/green fluorescence (red = polarised mitochondria and green = depolarised mitochondria) with the mean value being ~38% and 19% at 37°C and 18°C respectively. After 36h, the values were ~70% and 27% at 37°C and 18°C respectively (Figures 5-5 and 5-6), clearly demonstrating that cooling significantly reduced chemotherapy drug-induced  $\Delta\Psi_m$  loss, i.e. prevented mitochondrial damage thereby rescuing HaCaTa cells from drug cytotoxicity.

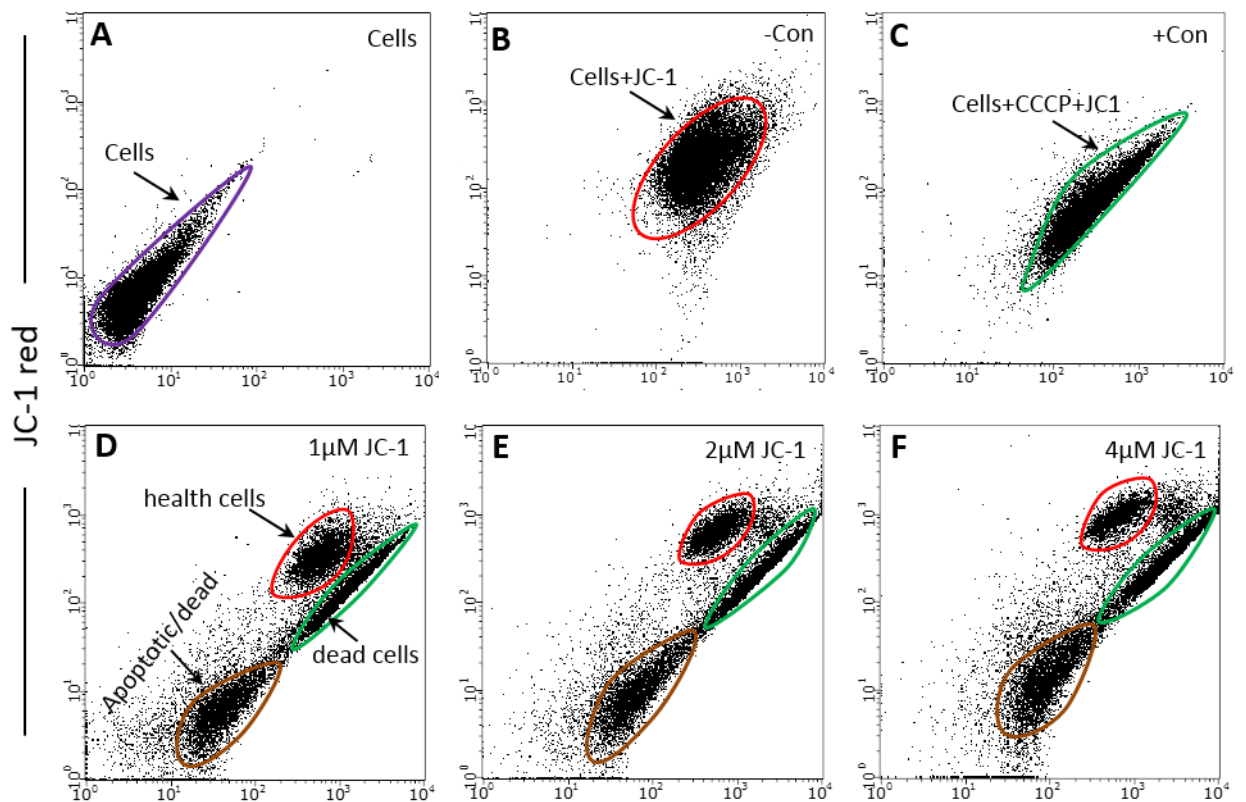


### Figure 5-3 Optimisation of JC-1 dye assay at 37°C

HaCaTa cells were seeded in 6-well plates at  $1.5 \times 10^5$  cells/well in KSFM medium and were incubated overnight at 37°C/ 5% CO<sub>2</sub>. Cells were then treated with 7.5 μg/mL 4-OH-CP for 2h at 37°C compared with vehicle control (cells treated with medium containing DMSO, in which the reagent was dissolved). The solvent represents the maximum amount of DMSO corresponding to the highest drug concentration). The drugs were then removed; wells were rinsed with PBS to remove any traces of drug before the cells were incubated in fresh medium. Both attached and floating cells were harvested 36h later and a total of 20,000 events were analysed.  $\Delta\Psi_m$  loss-related depolarisation of the JC-1 dye was monitored by FACS analysis. **A**) Cells alone (without JC-1 dye) are shown, hence only auto-fluorescence is detectable (purple colour gate, bottom left-hand corner). **B**) Control (untreated) cells labelled with 2μM JC-1 dye as a negative control (normal healthy cells, gated region (red) includes cells with intact mitochondrial membranes). **C**) Positive control cells treated with 1μM CCCP for 5 min and labelled with 2μM JC-1 (green gate includes cells with  $\Delta\Psi_m$  loss). **D**, **E** and **F**) Cells at 36h post-exposure to 7.5 μg/mL 4-OH-CP at 37°C and labelled with JC-1 dye (1, 2 and 4μM); red gate indicates healthy cells, green gate dead cells, and brown gate represents late apoptotic/dead cells. Data obtained from three independent biological experiments, each consisting of 2 technical replicates.

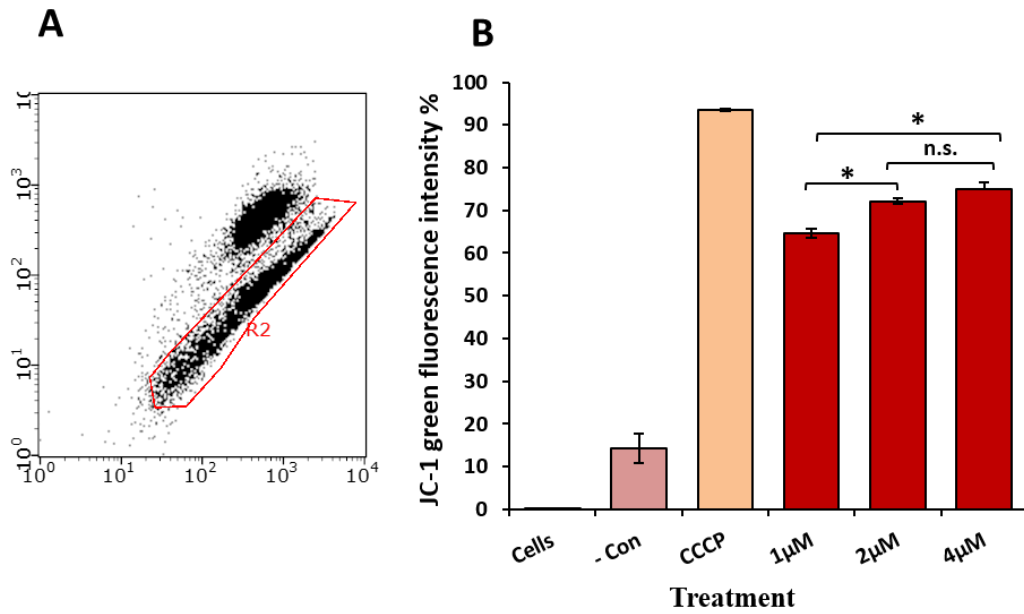


**Figure 5-4 Summary of optimisation of JC-1 concentration at 37°C**

The bar graph summarises  $\Delta\Psi_m$  loss (green fluorescence (R2 region) data obtained data obtained from as shown in Figure 5-3. Bars represent mean values of the percentage of cells ( $\pm$  S.E.M.). n.s., non-significant. \*,  $p < 0.05$ .

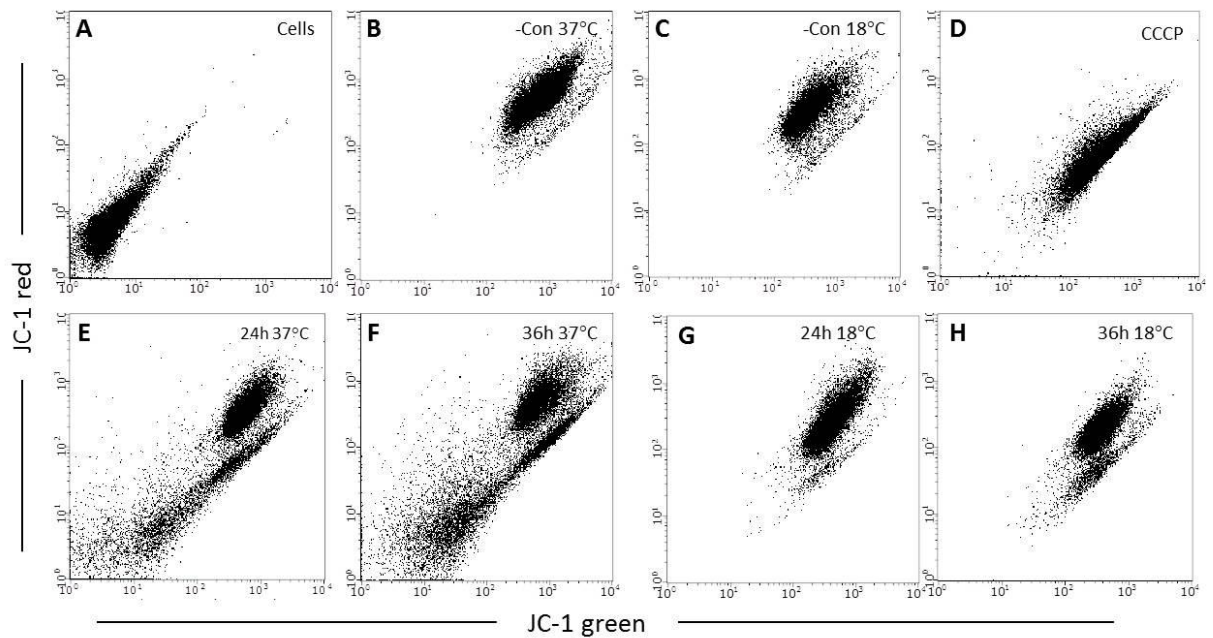


**Figure 5-5 Preliminary experiments on detection of chemotherapy drug-induced  $\Delta\Psi_m$  loss using JC-1 and the effect of cooling in HaCaTa cells**

HaCaTa cells were seeded in 6-well plates at  $1.5 \times 10^5$  cells/well in KFSM medium and were incubated overnight at 37°C/ 5% CO<sub>2</sub>. Cells were then treated with 7.5  $\mu\text{g}/\text{mL}$  4-OH-CP for 2h at 37°C and 18°C compared with vehicle control (cells treated with medium containing DMSO, in which the reagent was dissolved). The solvent represents the maximum amount of DMSO corresponding to the highest drug concentration). The drugs were then removed, wells were rinsed with PBS to remove any traces of drug before the cells were incubated in fresh medium. Both attached and floating cells were harvested 24h and 36h later and a total of 20,000 events were analysed.  $\Delta\Psi_m$  loss-related depolarisation of the JC-1 dye was monitored by FACS analysis. **A)** Cells alone (without JC-1 dye) are shown, hence only auto-fluorescence. **B)** Control (untreated) cells labelled with 2 $\mu\text{M}$  JC-1 dye as a negative control (normal healthy cells) incubated at 37°C. **C)** Control (untreated) cells labelled with 2 $\mu\text{M}$  JC-1 dye as a negative control (normal healthy cells) incubated at 18°C. **D)** Positive control cells treated with 1 $\mu\text{M}$  CCCP for 5 min and labelled with 2 $\mu\text{M}$  JC-1. **E)** Cells at 24h post-exposure, **F)** Cells at 36h post-exposure to 7.5  $\mu\text{g}/\text{mL}$  4-OH-CP at 37°C and labelled with 2 $\mu\text{M}$  JC-1 dye; red fluorescence indicates healthy cells, green fluorescence dead cells and late apoptotic/dead cells. **G)** Cells at 24h, **H)** Cells at 36h post-exposure to 7.5  $\mu\text{g}/\text{mL}$  4-OH-CP at 18°C and labelled with 2 $\mu\text{M}$  JC-1 dye; red fluorescence indicates healthy cells, green fluorescence dead cells and late apoptotic/dead cells. Data obtained from three independent biological experiments, each consisting of 2 technical replicates.

\*Gating was performed as in Figure 5-3 for the identification of green and red fluorescence and the calculation of % cells with  $\Delta\Psi_m$  loss.

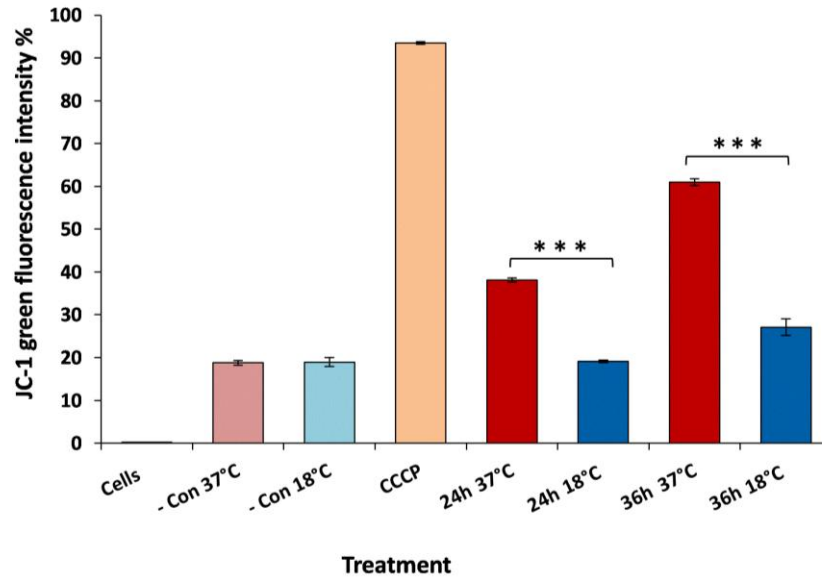


**Figure 5-6 Summary of replicate preliminary experiments on detection of chemotherapy drug-induced  $\Delta\Psi_m$  loss using JC-1 and the effect of cooling**

The bar graph shows summarises  $\Delta\Psi_m$  loss (green fluorescence (R2 region)) data obtained from three independent biological experiments, each consisting of 2 technical replicates. as shown in Figure 5-5. Bars represent mean values of % of cells ( $\pm$ S.E.M.). \*\*\*  $p < 0.001$ .

\*Gating was performed as in Figures 5-3 and 5-4 for the identification of green and red fluorescence and the calculation of percentage cells with  $\Delta\Psi_m$  loss.

## **5.5 Cytoprotective role of cooling against chemotherapy drug-induced $\Delta\Psi_m$ disruption in HaCaTa cells**

As mentioned above disruption of the  $\Delta\Psi_m$  can indicate mitochondrial dysfunction and it is a crucial stage in the mitochondrial death pathway induced by chemotherapy drugs (Charvat and Arrizabalaga, 2016). Therefore, modulation of the mitochondrial death pathway by cooling conditions was examined using the fluorogenic probe JC-1. In cells treated with chemotherapy drugs at 37°C a significant increase in green fluorescence of JC-1 monomers was detected indicating a reduction in  $\Delta\Psi_m$ . Treatment of HaCaTa cells with chemotherapy drugs under cooling conditions and the changes of the ratio of red/green fluorescence of the JC-1 probe were examined.

### **5.5.1 Effects of 4-OH-CP on $\Delta\Psi_m$ and role of cooling**

7.5  $\mu\text{g/mL}$  4-OH-CP at 37°C caused a  $\Delta\Psi_m$  loss evident by the reduced red, and increased green fluorescence, as shown in section 5.3. As shown in Figures 5-7 and 5-8, that cooling significantly reduced the 4-OH-CP-induced loss of  $\Delta\Psi_m$  and there was a strong correlation between  $\Delta\Psi_m$  loss of the cells and the temperature. A significant inhibition in green fluorescence was observed in HaCaTa cells at 36h post-exposure to 7.5  $\mu\text{g/mL}$  4-OH-CP and being 36.4% ( $\pm 2.4$ ), 22.6 ( $\pm 0.4$ ), and 16.1% ( $\pm 0.3$ ) at 22°C, 18°C, and 14°C respectively, compared to 62.6% ( $\pm 0.4$ ) at 37°C. Furthermore, 48h post-exposure to 7.5  $\mu\text{g/mL}$  4-OH-CP, green fluorescence at 37°C was 73.7% ( $\pm 0.9$ ) compared to 31.3% ( $\pm 1.3$ ), 27.7% ( $\pm 2$ ) and 13.9% ( $\pm 1.3$ ) at 22°C, 18°C, 14°C respectively. These data confirmed that cooling prevented mitochondrial damage thereby rescuing the HaCaTa cells from 4-OH-CP toxicity. Taken together, it can be concluded that cooling has anti-apoptotic effects and reduces the extent of cell death induced by 4-OH-CP in HaCaTa cells.

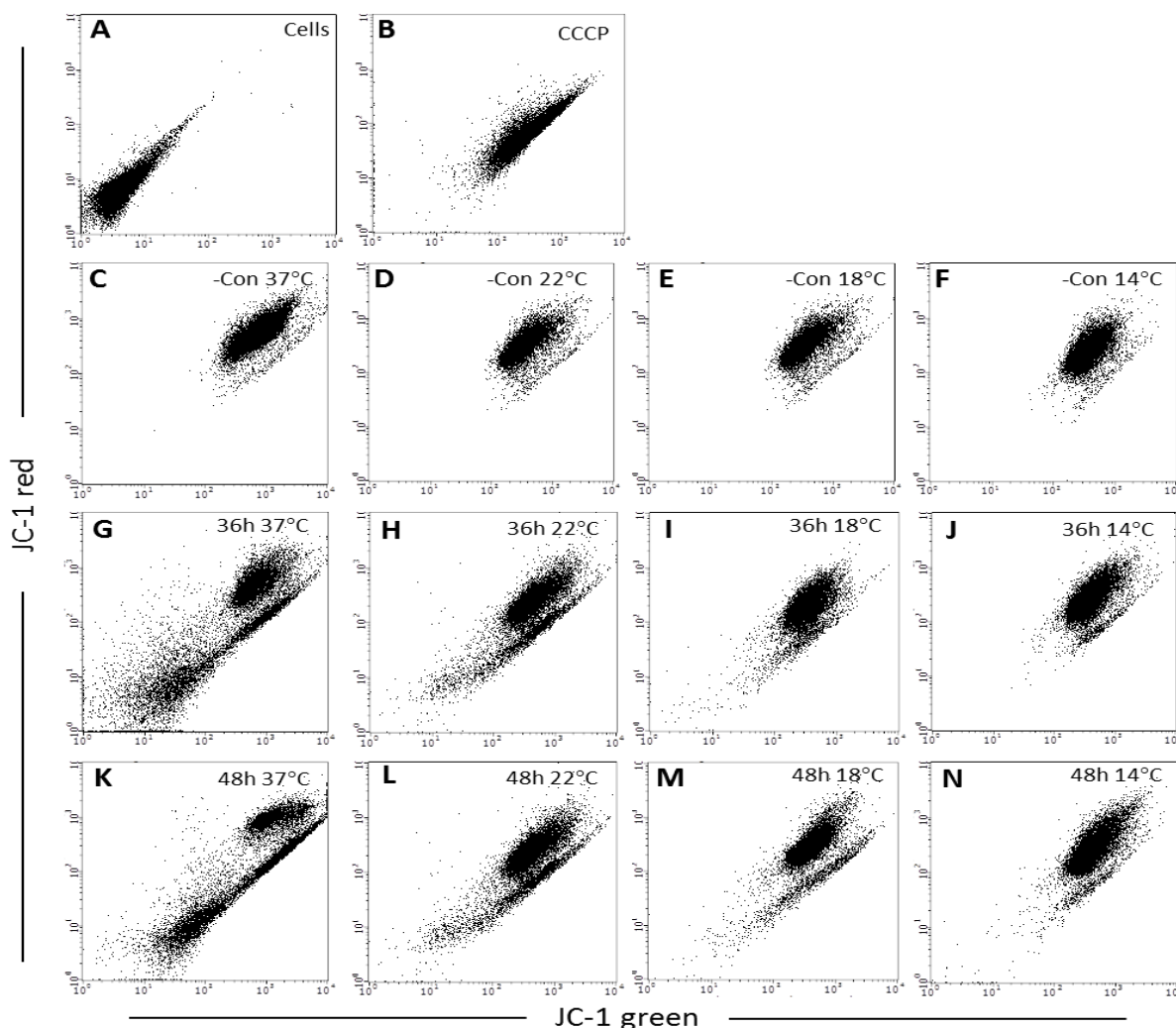


### Figure 5-7 Cooling inhibits 4-OH-CP- induced $\Delta\Psi_m$ loss in HaCaTa cells

HaCaTa cells were seeded in 6 well plates at  $1.5 \times 10^5$  cells/well in KFSM medium and were incubated overnight at 37°C/5% CO<sub>2</sub>. HaCaTa cells were treated with 7.5 μg/mL 4-OH-CP for 2h at 37°C 22°C, 18°C and 14°C compared with vehicle control (cells treated with medium containing DMSO, in which the reagent was dissolved). The solvent represents the maximum amount of DMSO corresponding to the highest drug concentration). The drugs were then removed, wells were rinsed with PBS to remove any traces of drug before the cells were incubated in fresh medium. Both attached and floating cells were harvested 36h and 48h later and a total of 20,000 events were analysed.  $\Delta\Psi_m$  loss-related depolarisation of the JC-1 dye was monitored by FACS analysis. **A**) Cells alone (without JC-1 dye) are shown, hence only auto-fluorescence. **B**) Positive control cells treated with 1μM CCCP for 5 min and labelled with 2μM JC-1. **C, D, E, and F**) Control (untreated) cells labelled with 2μM JC-1 dye as a negative control (normal healthy cells) incubated at 37°C, 22°C, 18°C and 14°C respectively. **G**) Cells at 36h, **K**) Cells at 48h post-exposure to 7.5g/mL 4-OH-CP at 37°C and labelled with 2μM JC-1 dye. **H**) Cells at 36h, **L**) Cells at 48h post-exposure to 7.5 μg/mL 4-OH-CP at 22°C and labelled with 2μM JC-1 dye. **I**) Cells at 36h, **M**) Cells at 48h post-exposure to 7.5 μg/mL 4-OH-CP at 18°C and labelled with 2μM JC-1 dye. **J**) Cells at 36h, **N**) Cells at 48h post-exposure to 7.5 μg/mL 4-OH-CP at 14°C and labelled with 2μM JC-1 dye. Data obtained from three independent biological experiments, each consisting of 2 technical replicates.

\*Gating was performed as in Figure 5-3 for the identification of green and red fluorescence and the calculation of percentage cells with  $\Delta\Psi_m$  loss.

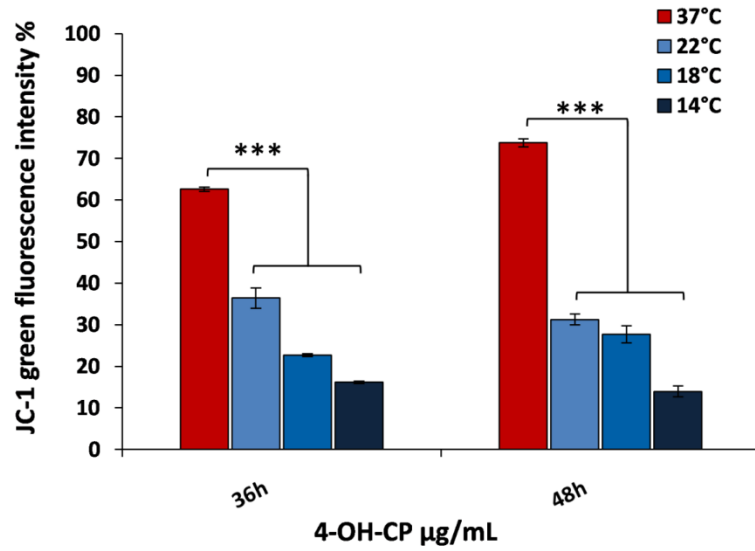


**Figure 5-8 Summary of independent replicate experiments on the role of cooling in 4-OH-CP-mediated disruption of  $\Delta\Psi_m$  in HaCaTa cells**

The bar graph shows summarises  $\Delta\Psi_m$  loss (green fluorescence (R2 region)) data obtained from three independent biological experiments, each consisting of 2 technical replicates as shown in Figure 5-7. Bars represent mean values of % of cells ( $\pm$ S.E.M.). \*\*\*  $p < 0.001$ .

\*Gating was performed as in Figure 5-4 for the identification of green and red fluorescence and the calculation of percentage cells with  $\Delta\Psi_m$  loss.

### 5.5.2 Effects of docetaxel on $\Delta\Psi_m$ and role of cooling

To determine the level of mitochondrial dysfunction after exposure to docetaxel, HaCaTa cells were treated with 0.01 $\mu$ g/mL docetaxel and  $\Delta\Psi_m$  measured at 36h and 48h post-exposure (Figures 5-9 and 5-10). Docetaxel treated cells showed a significantly greater collapse in  $\Delta\Psi_m$  with high green fluorescence percentage after 36h at 37°C and peaked at 48h at 37°C (Figure 5-9G and K). However, the effect of docetaxel was reduced remarkably by cooling and the percentage of green fluorescence was decreased significantly at 36h post-exposure to docetaxel was 24.6% ( $\pm$  0.7), 15.1% ( $\pm$  0.5), and 22.9% ( $\pm$  2.1) at 22°C, 18°C and 14°C respectively, compared with 59.1% ( $\pm$  3.3) at 37°C (Figure 5-10). The percentage of the green fluorescence associated cells (impaired  $\Delta\Psi_m$ ) steadily increased, reaching 70.6% ( $\pm$  2.5) at 37°C of cells 48h after treatment, compared with cells treated at cooling conditions being 25.4% ( $\pm$  2.1), 24.9% ( $\pm$  1.5), and 8% ( $\pm$  0.1) at 22°C, 18°C and 14°C respectively, compared with 70.6% ( $\pm$  2.5) at 37°C (Figure 5-10). These results suggest that the docetaxel-induced death of HaCaTa cells activates the mitochondrial pathway, and the cytoprotective effects of cooling relate to inhibition of the mitochondrial apoptosis pathway.

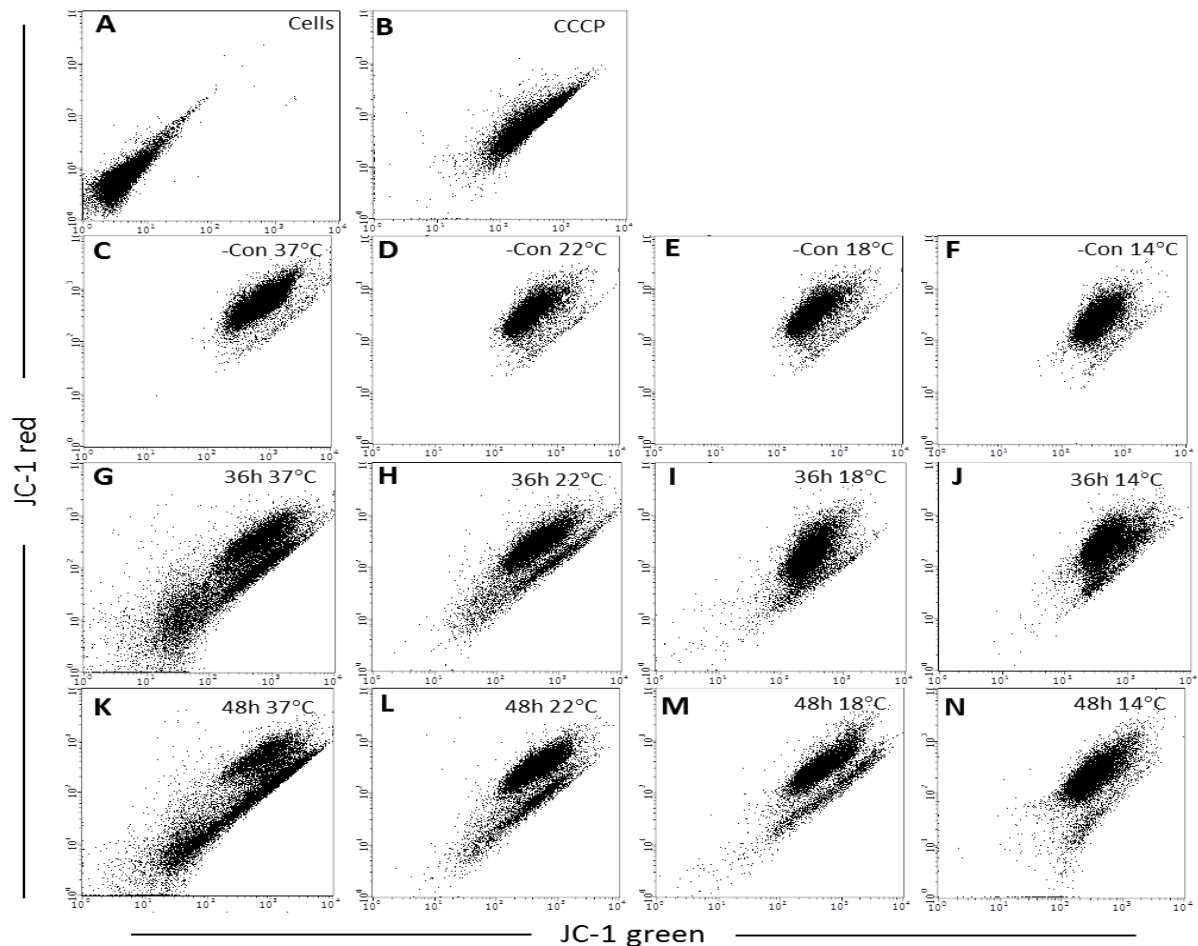


### Figure 5-9 Cooling inhibits docetaxel induced $\Delta\Psi_m$ loss in HaCaTa cells

HaCaTa cells were seeded in 6 well plates at  $1.5 \times 10^5$  cells/well in KSFM medium and were incubated overnight at 37°C/5% CO<sub>2</sub>. HaCaTa cells were treated with 0.01  $\mu\text{g}/\text{mL}$  docetaxel for 2h at 37°C, 22°C, 18°C and 14°C compared with vehicle control (cells treated with medium containing DMSO, in which the reagent was dissolved). The solvent represents the maximum amount of DMSO corresponding to the highest drug concentration). The drugs were then removed, wells were rinsed with PBS to remove any traces of drug before the cells were incubated in fresh medium. Both attached and floating cells were harvested 36h and 48h later and a total of 20,000 events were analysed.  $\Delta\Psi_m$  loss-related depolarisation of the JC-1 dye was monitored by FACS analysis. **A)** Cells alone (without JC-1 dye) are shown, hence only auto-fluorescence. **B)** Positive control cells treated with 1 $\mu\text{M}$  CCCP for 5 min and labelled with 2 $\mu\text{M}$  JC-1. **C, D, E, and F)** Control (untreated) cells labelled with 2 $\mu\text{M}$  JC-1 dye as a negative control (normal healthy cells) incubated at 37°C, 22°C, 18°C and 14°C respectively. **G)** Cells at 36h, **K)** Cells at 48h post-exposure to 0.01  $\mu\text{g}/\text{mL}$  docetaxel at 37°C and labelled with 2 $\mu\text{M}$  JC-1 dye. **H)** Cells at 36h, **L)** Cells at 48h post-exposure to 0.01  $\mu\text{g}/\text{mL}$  docetaxel at 22°C and labelled with 2 $\mu\text{M}$  JC-1 dye. **I)** Cells at 36h, **M)** Cells at 48h post-exposure to 0.01  $\mu\text{g}/\text{mL}$  docetaxel at 18°C and labelled with 2 $\mu\text{M}$  JC-1 dye. **J)** Cells at 36h, **N)** Cells at 48h post-exposure to 0.01  $\mu\text{g}/\text{mL}$  docetaxel at 14°C and labelled with 2 $\mu\text{M}$  JC-1 dye. Data obtained from three independent biological experiments, each consisting of 2 technical replicates.

\*Gating was performed as in Figure 5-3 for the identification of green and red fluorescence and the calculation of percentage cells with  $\Delta\Psi_m$  loss.

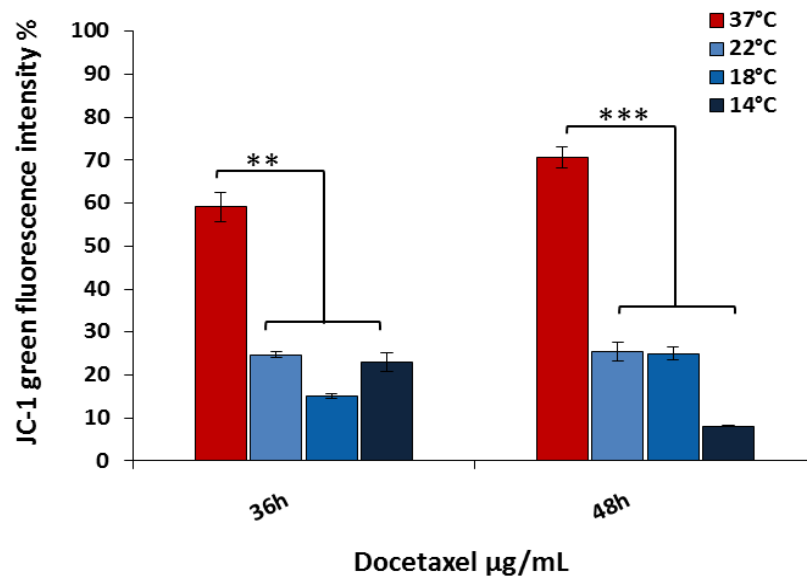


**Figure 5-10 Summary of independent replicates experiments the role of cooling in inhibits docetaxel disruption of the  $\Delta\Psi_m$  in HaCaTa cells**

The bar graph shows summarises  $\Delta\Psi_m$  loss (green fluorescence (R2 region)) data obtained from three independent biological experiments, each consisting of 2 technical replicates as shown in Figure 5-9. Bars represent mean values of % of cells ( $\pm$ S.E.M.). \*\*,  $p < 0.01$ ; \*\*\*,  $p < 0.001$ .

\*Gating was performed as in Figure 5-4 for the identification of green and red fluorescence and the calculation of percentage cells with  $\Delta\Psi_m$  loss.

### 5.5.3 Effects of doxorubicin on $\Delta\Psi_m$ and role of cooling

One of the primary targets of doxorubicin is mitochondria and it induces apoptosis through a mitochondrial pathway (Tomankova *et al.*, 2015). HaCaTa cells exposed to 0.5 $\mu$ g/mL doxorubicin for 2h at 37°C and then incubated in drug free media for 36h exhibited a collapse of  $\Delta\Psi_m$  (Figures 5-11 and 5-12). By contrast, when HaCaTa cells were exposed to 0.5 $\mu$ g/mL doxorubicin at 22°C, 18°C and 14°C, the  $\Delta\Psi_m$  was better maintained in a temperature dependent manner (Figure 5-11). The percentage of the green fluorescence (loss of  $\Delta\Psi_m$ ) after 36h was 38.8% ( $\pm$  1.7), 32.3% ( $\pm$  2.3), and 16.3% ( $\pm$  0.3) at 22°C, 18°C and 14°C respectively, compared with 59.2% ( $\pm$  0.9) at 37°C (Figure 5-12). After 48h at 37°C, the percentage of the green fluorescence associated cells increased significantly ~71.5% ( $\pm$  2.6); while at cooling conditions green fluorescence decreased significantly being 34.2% ( $\pm$  1.8), 29.6% ( $\pm$  2.4), and 13% ( $\pm$  0.6) at 22°C, 18°C and 14°C respectively (Figure 5-12). These results indicate that mitochondria fail to maintain their  $\Delta\Psi_m$  after treatment with doxorubicin, and cooling can inhibit doxorubicin-mediated reduction of  $\Delta\Psi_m$  of cells.

The data obtained with the JC-1 assay indicated that cooling protects from collapse of  $\Delta\Psi_m$  in cells exposed to doxorubicin, 4-OH-CP or docetaxel, which provides evidence that cooling can be an effective anti-apoptotic mediator. Collectively, these observations are in support of our data on cell viability / biomass (Chapter 3) and the cell cycle (Chapter 4), by not only demonstrating the cytoprotective role of cooling, but also providing further evidence that the lower the cooling temperature employed, the more significant the cytoprotective effect.

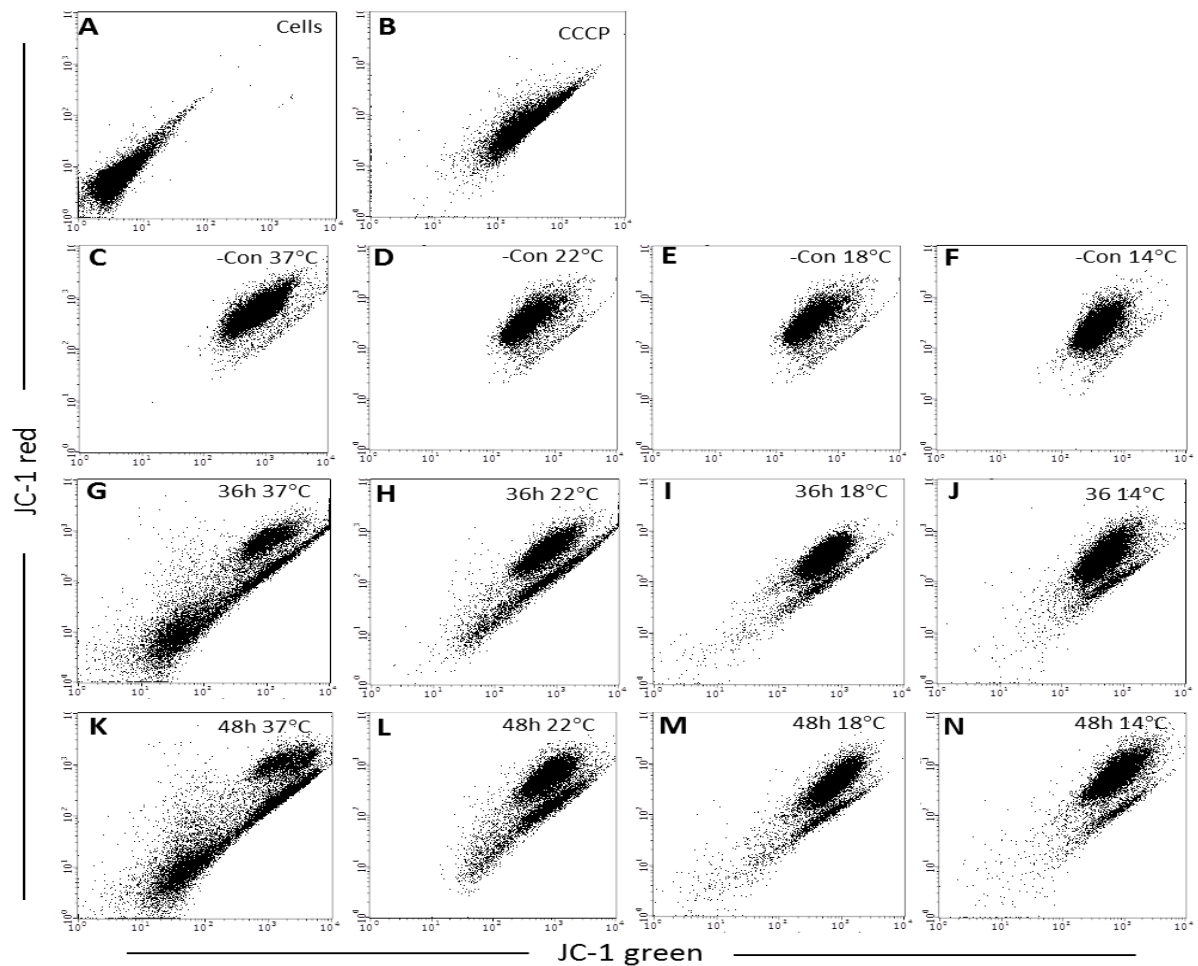


**Figure 5-11 Cooling inhibits doxorubicin induced  $\Delta\Psi_m$  loss in HaCaTa cells**

HaCaTa cells were seeded in 6 well plates at  $1.5 \times 10^5$  cells/well in KSFM medium and were incubated overnight at 37°C/5% CO<sub>2</sub>. HaCaTa cells were treated with 0.5 µg/mL doxorubicin for 2h at 37°C, 22°C, 18°C and 14°C compared with vehicle control (cells treated with medium containing DMSO, in which the reagent was dissolved). The solvent represents the maximum amount of DMSO corresponding to the highest drug concentration). The drugs were then removed, wells were rinsed with PBS to remove any traces of drug before the cells were incubated in fresh medium. Both attached and floating cells were harvested 36h and 48h later and a total of 20,000 events were analysed.  $\Delta\Psi_m$  loss-related depolarisation of the JC-1 dye was monitored by FACS analysis. **A)** Cells alone (without JC-1 dye) are shown, hence only auto-fluorescence. **B)** Positive control cells treated with 1µM CCCP for 5 min and labelled with 2µM JC-1. **C, D, E, and F)** Control (untreated) cells labelled with 2µM JC-1 dye as a negative control (normal healthy cells) incubated at 37°C, 22°C, 18°C and 14°C respectively. **G)** Cells at 36h, **K)** Cells at 48h post-exposure to 0.5 µg/mL doxorubicin at 37°C and labelled with 2µM JC-1 dye. **H)** Cells at 36h, **L)** Cells at 48h post-exposure to 0.5 µg/mL doxorubicin at 22°C and labelled with 2µM JC-1 dye. **I)** Cells at 36h, **M)** Cells at 48h post-exposure to 0.5 µg/mL doxorubicin at 18°C and labelled with 2µM JC-1 dye. **J)** Cells at 36h, **N)** Cells at 48h post-exposure to 0.5 µg/mL doxorubicin at 14°C and labelled with 2µM JC-1 dye. Data obtained from three independent biological experiments, each consisting of 2 technical replicates.

\*Gating was performed as in Figure 5-3 for the identification of green and red fluorescence and the calculation of percentage cells with  $\Delta\Psi_m$  loss.

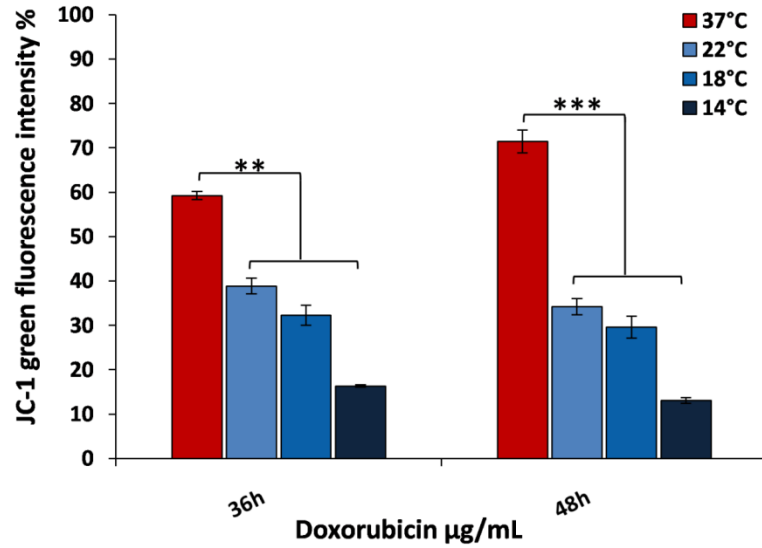


**Figure 5-12 Summary of independent replicates experiments the role of cooling in inhibits doxorubicin disruption of the  $\Delta\Psi_m$  in HaCaTa cells**

The bar graph shows summarises  $\Delta\Psi_m$  loss (green fluorescence (R2 region)) data obtained from three independent biological experiments, each consisting of 2 technical replicates as shown in Figure 5-11. Bars represent mean values of % of cells ( $\pm$ S.E.M.). \*\*,  $p < 0.01$ ; \*\*\*,  $p < 0.001$ .

\*Gating was performed as in Figures 5-3 and 5-4 for the identification of green and red fluorescence and the calculation of percentage cells with  $\Delta\Psi_m$  loss.

## 5.6 Cytoprotective role of cooling against chemotherapy drug-induced $\Delta\Psi_m$ disruption in NHEK cells

Following investigations in HaCaTa cells, for the first time the effect of chemotherapy drugs on  $\Delta\Psi_m$  of NHEKs was measured and the effect of cooling conditions was examined to confirm the validity of our results using HaCaTa cells as an *in vitro* model to study CIA.

NHEKs cells were treated with 4-OH-CP, docetaxel or doxorubicin at 37°C and compared with cells treated at 18°C. Based on the results in chapter 3, these cells appeared to be less sensitive than HaCaTa cells and higher drug concentrations of the drugs were used, i.e.: 10  $\mu\text{g}/\text{mL}$  4-OH-CP, 0.025  $\mu\text{g}/\text{mL}$  docetaxel, and 3  $\mu\text{g}/\text{mL}$  doxorubicin; doses which were confirmed to induce depolarisation ( $\Delta\Psi_m$  loss) (Figures 5-13 and 5-14). Importantly, cells treated at cooling conditions showed a significantly greater red and lower green fluorescence than cells treated at 37°C. More specifically, data showed that lower temperatures, protected from a loss of  $\Delta\Psi_m$  with the percentage of green fluorescence of cells after treatment with 4-OH-CP being 61.5% ( $\pm 2$ ) and 22.7% ( $\pm 3.8$ ) at 37°C and 18°C respectively (Figure 5-13E and F). In cells treated with docetaxel the values were 55.75% ( $\pm 4.3$ ) and 31.48% ( $\pm 1.8$ ) at 37°C and 18°C respectively (Figure 5-13G and H), and for doxorubicin 74.2% ( $\pm 2.1$ ) and 31.6% ( $\pm 1.2$ ) at 37°C and 18°C respectively (Figure 5-13 I and J). Therefore, despite the fact that they act *via* different molecular mechanisms, these drugs induced  $\Delta\Psi_m$  disruption and cooling consistently rescued cells from  $\Delta\Psi_m$  disruption for all three compounds in concordance with our observations with HaCaTa cells. The ability of cooling to protect from  $\Delta\Psi_m$  disruption was an indicator of the cytoprotective properties of cooling.

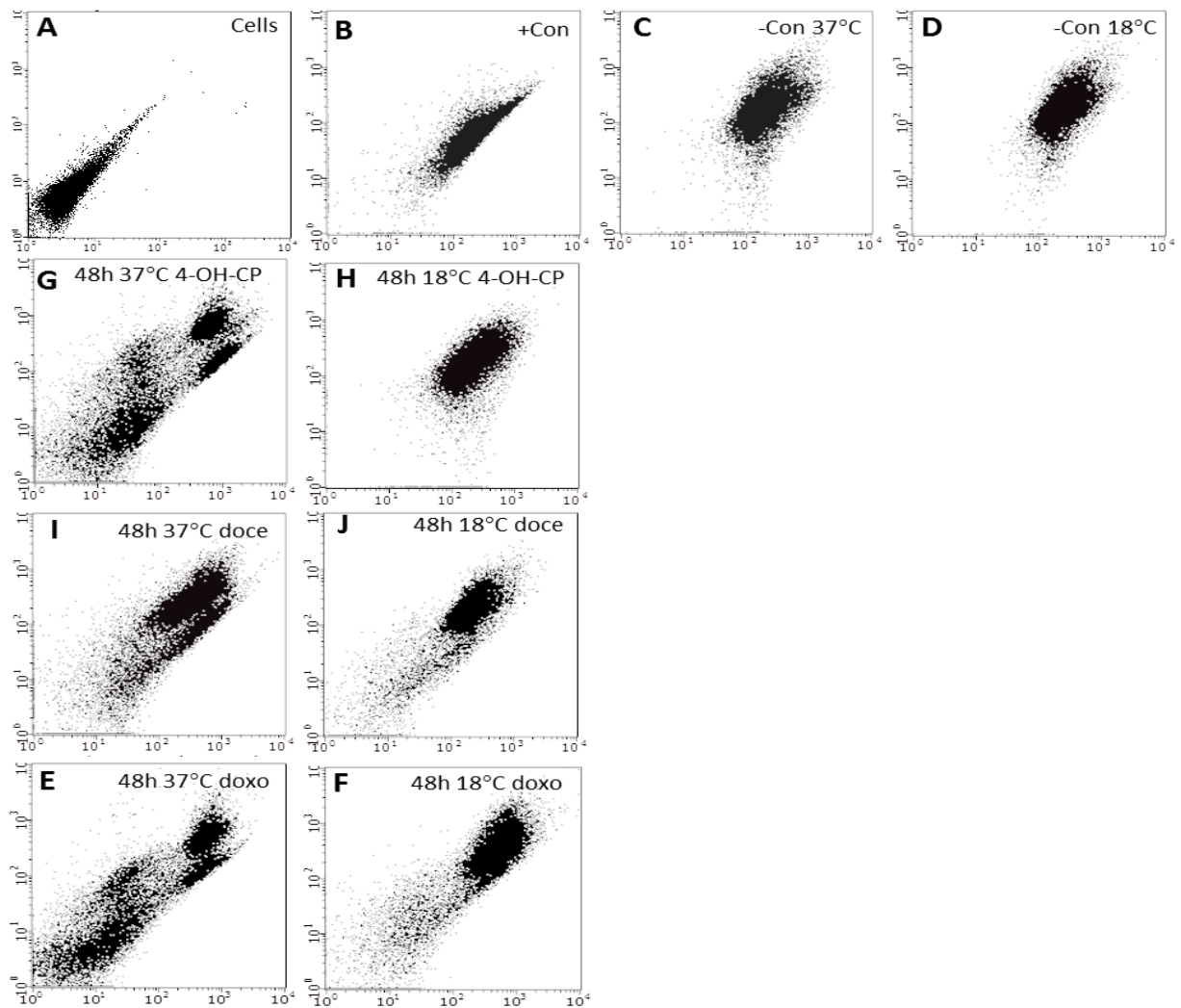


### Figure 5-13 Cooling inhibits chemotherapy drugs-induced $\Delta\Psi_m$ loss in NHEK cells

NHEK cells (passages 1–3) were seeded in 6 well plates at  $2.3 \times 10^5$  cells/well in KSMF medium and were incubated overnight at  $37^\circ\text{C}/5\% \text{CO}_2$ . NHEKs cells were treated with  $10\mu\text{g}/\text{mL}$  4-OH-CP;  $0.025\mu\text{g}/\text{mL}$  docetaxel (Doce); and  $3\mu\text{g}/\text{mL}$  doxorubicin (Doxo) for 2h at 37 and 18, compared with vehicle control (cells treated with medium containing DMSO, in which the reagent was dissolved). The solvent represents the maximum amount of DMSO corresponding to the highest drug concentration). The drugs were then removed; wells were rinsed with PBS to remove any traces of drug before the cells were incubated in fresh medium. Both attached and floating cells were harvested 48h later and a total of 20,000 events were analysed.  $\Delta\Psi_m$  loss-related depolarisation of the JC-1 dye was monitored by FACS analysis. **B)** Positive control cells treated with  $1\mu\text{M}$  CCCP for 5 min and labelled with  $2\mu\text{M}$  JC-1. **C, D)** Control (untreated) cells labelled with  $2\mu\text{M}$  JC-1 dye as a negative control (normal healthy cells) incubated at  $37^\circ\text{C}$  and  $18^\circ\text{C}$  respectively. **E, G, and I)** Cells at 48h post-exposure to 4-OH-CP; docetaxel; and doxorubicin respectively at  $37^\circ\text{C}$  and labelled with  $2\mu\text{M}$  JC-1 dye. **F, H, and J)** Cells at 48h post-exposure to 4-OH-CP; docetaxel; and respectively at  $18^\circ\text{C}$  and labelled with  $2\mu\text{M}$  JC-1 dye. Data obtained from three independent biological experiments, each consisting of 2 technical replicates.

\*Gating was performed as in Figure 5-3 for the identification of green and red fluorescence and the calculation of percentage cells with  $\Delta\Psi_m$  loss.

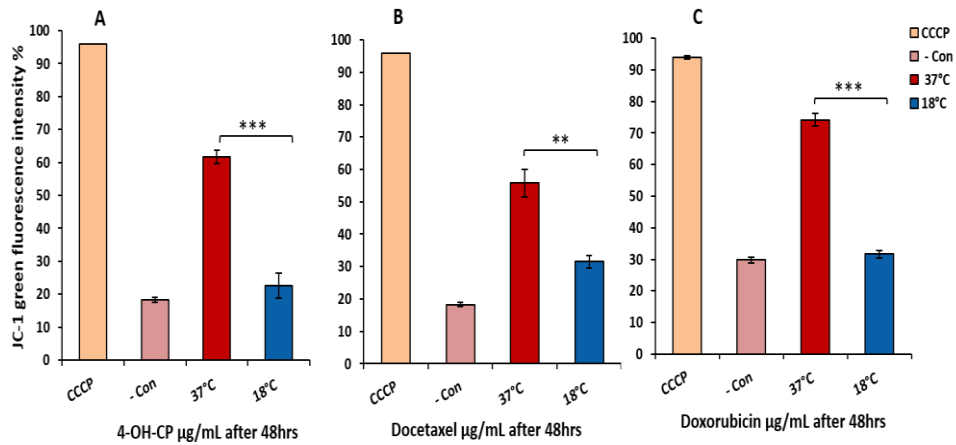


**Figure 5-14 Summary of independent replicates experiments the role of cooling in inhibits chemotherapy drugs disruption of the  $\Delta\Psi_m$  in NHEK cells**

The bar graph shows summarises  $\Delta\Psi_m$  loss (green fluorescence (R2 region)) data obtained from three independent biological experiments, each consisting of 2 technical replicates as shown in Figure 5-13. **A)** Cells treated with 4-OH-CP, **B)** cells treated with docetaxel **C)** cells treated with doxorubicin. Bars represent mean values of % of cells ( $\pm$ S.E.M.). \*\*,  $p < 0.01$ ; \*\*\*,  $p < 0.001$ .

\*Gating was performed as in Figure 5-4 for the identification of green and red fluorescence and the calculation of percentage cells with  $\Delta\Psi_m$  loss.

## 5.7 Cytoprotective role of cooling against chemotherapy drug-induced $\Delta\Psi_m$ disruption in HHFK cells

To further support our observations above in HaCaTa and NHEKs, HHFK cells, which are specifically isolated from the HF area, were used to investigate the effects of chemotherapy drugs on  $\Delta\Psi_m$ , as HHFK cells are a closer representative to the HF matrix keratinocytes. HHFK cells were treated with 4-OH-CP, docetaxel or doxorubicin at 37°C and compared with cells treated at 18°C. Similarly, to NHEKs, HHFK cells were treated with 10  $\mu\text{g}/\text{mL}$  4-OH-CP, 0.025  $\mu\text{g}/\text{mL}$  docetaxel, and 3  $\mu\text{g}/\text{mL}$  doxorubicin to induce depolarisation ( $\Delta\Psi_m$  loss) (Figure 5-15 and 5-16). Cells treated at cooling conditions showed a significantly greater red and lower green fluorescence than cells treated at 37°C. The percentage of cells demonstrating green fluorescence after treatment with 10  $\mu\text{g}/\text{mL}$  4-OH-CP was 67.6% ( $\pm 1.5$ ) and 29.5% ( $\pm 1.6$ ) at 37°C and 18°C respectively (Figure 5-15E and F), for cells treated with 0.025  $\mu\text{g}/\text{mL}$  docetaxel it was 64.6% ( $\pm 2.2$ ) and 29.2% ( $\pm 0.4$ ) at 37°C and 18°C respectively (Figure 5-15G and H), and for cells treated with 3  $\mu\text{g}/\text{mL}$  doxorubicin it was 74.2% ( $\pm 2$ ) and 31.6% ( $\pm 1.3$ ) at 37°C and 18°C respectively (Figure 5-15I and J).

These findings confirmed that cooling consistently rescued cells from  $\Delta\Psi_m$  disruption induced by the chemotherapy drugs. Moreover, these experiments further attested to our approach of using HaCaTa cells as a representative keratinocyte *in vitro* model.

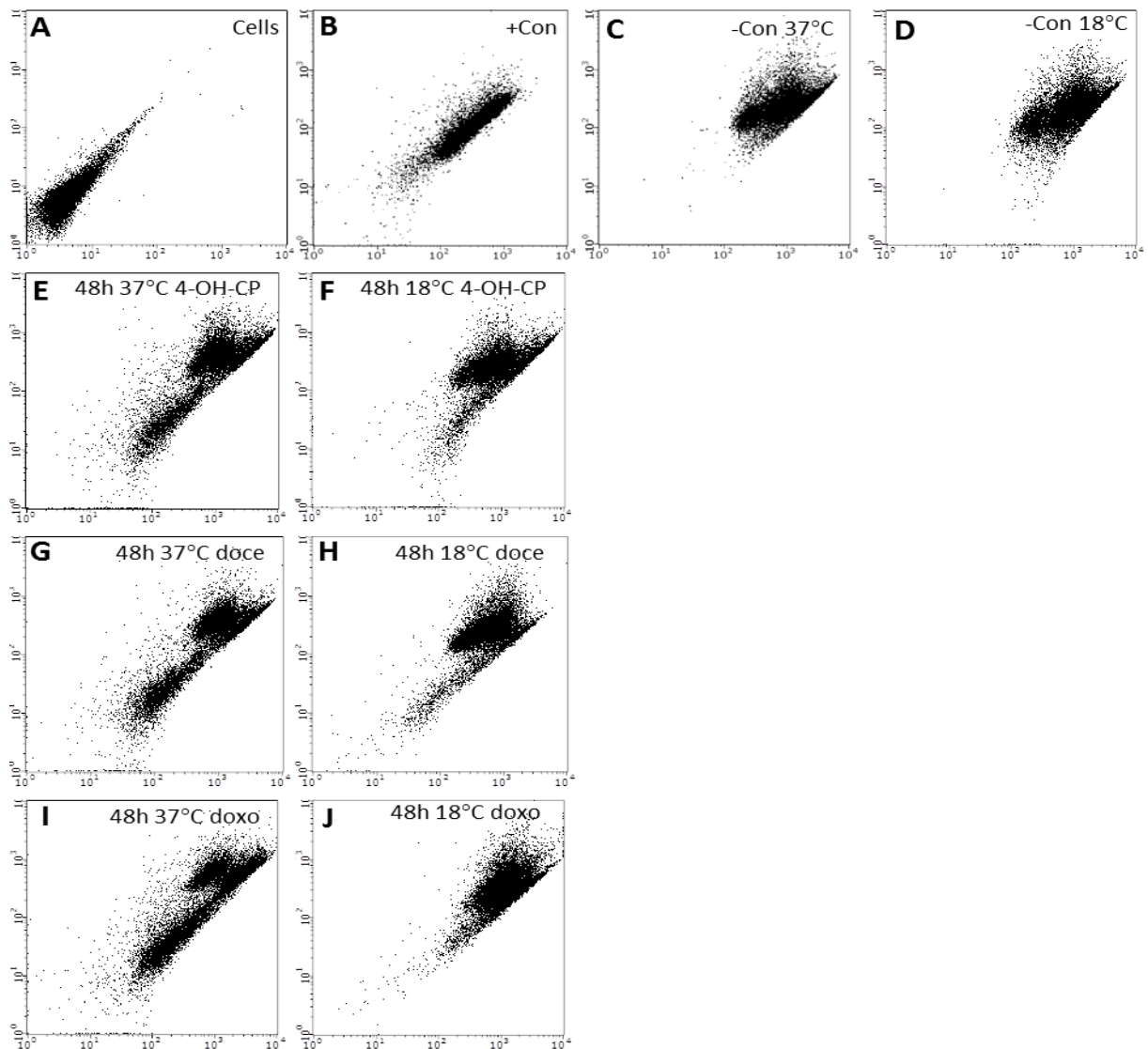


### Figure 5-15 Cooling inhibits chemotherapy drugs-induced $\Delta\Psi_m$ loss in HHFK cells

HHFK cells (passages 1–3) were seeded in 6 well plates at  $2.3 \times 10^5$  cells/well in KSM medium and were incubated overnight at  $37^\circ\text{C}/5\% \text{CO}_2$ . HHFK cells were treated with  $10\mu\text{g}/\text{mL}$  4-OH-CP;  $0.025\mu\text{g}/\text{mL}$  docetaxel (Doce); and  $3\mu\text{g}/\text{mL}$  doxorubicin (Doxo) for 2h at 37 and 18, compared with vehicle control (cells treated with medium containing DMSO, in which the reagent was dissolved). The solvent represents the maximum amount of DMSO corresponding to the highest drug concentration). The drugs were then removed, wells were rinsed with PBS to remove any traces of drug before the cells were incubated in fresh medium. Both attached and floating cells were harvested 48h later and a total of 20,000 events were analysed.  $\Delta\Psi_m$  loss-related depolarisation of the JC-1 dye was monitored by FACS analysis. **A)** Cells alone (without JC-1 dye) are shown, hence only auto-fluorescence. **B)** Positive control cells treated with  $1\mu\text{M}$  CCCP for 5 min and labelled with  $2\mu\text{M}$  JC-1. **C, D)** Control (untreated) cells labelled with  $2\mu\text{M}$  JC-1 dye as a negative control (normal healthy cells) incubated at  $37^\circ\text{C}$  and  $18^\circ\text{C}$  respectively. **E, G, and I)** Cells at 48h post-exposure to 4-OH-CP; docetaxel; and doxorubicin respectively at  $37^\circ\text{C}$  and labelled with  $2\mu\text{M}$  JC-1 dye. **F, H, and J)** Cells at 48h post-exposure to 4-OH-CP; docetaxel; and respectively at  $18^\circ\text{C}$  and labelled with  $2\mu\text{M}$  JC-1 dye. Data obtained from three independent biological experiments, each consisting of 2 technical replicates.

\*Gating was performed as in Figure 5-3 for the identification of green and red fluorescence and the calculation of % cells with  $\Delta\Psi_m$  loss.

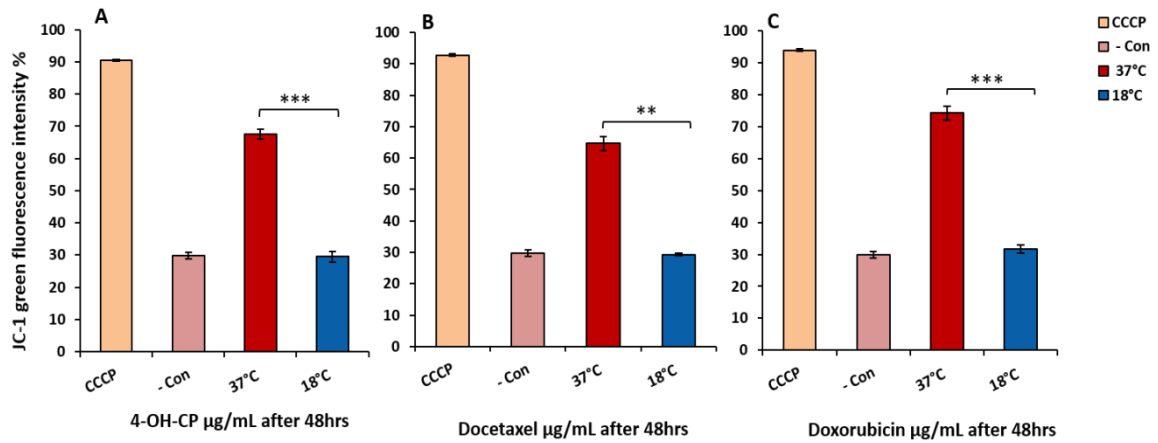


**Figure 5-16 Summary of independent replicates experiments the role of cooling in inhibits chemotherapy drugs, disruption of the  $\Delta\Psi_m$  in HHFK cells**

The bar graph shows summarises  $\Delta\Psi_m$  loss (green fluorescence (R2 region)) Data obtained from three independent biological experiments, each consisting of 2 technical replicates as shown in Figure 5-15. **A)** Cells treated with 4-OH-CP, **B)** cells treated with docetaxel **C)** cells treated with doxorubicin. Bars represent mean values of % of cells ( $\pm$ S.E.M.) \*\*,  $p < 0.01$ ; \*\*\*,  $p < 0.001$ .

\*Gating was performed as in Figures 5-3 and 5-4 for the identification of green and red fluorescence and the calculation of percentage cells with  $\Delta\Psi_m$  loss.

## 5.8 Optimization of the H2DCFDA assay for the detection of intracellular Reactive Oxygen Species

To investigate ROS production after treatment with chemotherapy drugs that induce CIA and the potential role of temperature, the H2DCFDA assay was optimised. To investigate ROS production the ROS-associated marker 6-carboxy-2',7'-dichlorodihydrofluorescein diacetate (H2DCFDA) was used. H2DCFDA is a non-fluorescent molecule, however, it fluoresces green when oxidised by intracellular ROS, and thus, the level of fluorescence is relative to the oxidative state of the cells (see Materials and Methods section 2.11.8).

In initial experiments, HaCaTa cells treated with (0–2.5 µg/mL) doxorubicin were used in conjunction with three concentrations of H2DCFDA (2.5, 5, and 10 µM) to determine the concentration that would sensitively determine levels of intracellular ROS, as a high reagent concentration can result in misleadingly high fluorescence levels in cells (Figure 5-17). Exposure to doxorubicin for 2h significantly increased ROS production above the control, as shown by microtiter plate analysis and spectrophotometric measurements. 5µM of H2DCFDA consistently discriminated between intracellular concentrations of ROS in cells treated with different concentrations of doxorubicin (Figure 5-17).

H2DCFDA can be measured using microtiter plate analysis (Takada *et al.*, 2002), flow cytometry, fluorescence microscopy (Yang *et al.*, 2005) or video microscopy (Leach *et al.*, 2001). In this study, following microtiter plate analysis above (Figure 5-17), flow cytometry was also used for the quantification of intracellular ROS, to allow direct comparison of ROS levels in HaCaTa cells exposed to doxorubicin, docetaxel and 4-OH-CP at 37°C and cooling conditions.

A series of titration experiments using flow cytometry were performed to optimise the assay conditions, including (a) H2DCFDA concentration; and (b) incubation periods, in order to determine not only the dose, but also equally importantly the optimal time-point for ROS measurement after treatment with each drug. It was found that the best time point for induction of ROS by doxorubicin was 30 min (Figure 5-18) and the concentration of 5µM H2DCFDA (Figures 5-19 and 5-20) sensitively and consistently discriminated between intracellular concentrations of ROS; these optimised methods for H2DCFDA-based ROS detection were applied for all experiments. Similar optimisations were then carried out for 4-OH-CP (Figures 5-21 and 5-22) and docetaxel (Figures 5-23 and 5-24) from 0 to 6h post-treatment.

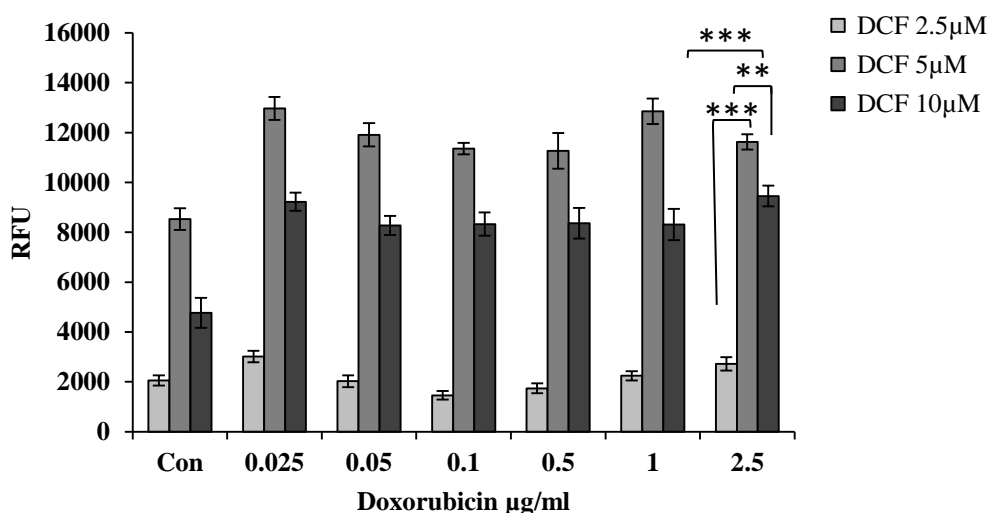


**Figure 5-17** Microtiter plate-based spectrophotometric detection of ROS levels after H2DCFDA staining in HaCaTa cells treated with doxorubicin

HaCaTa cells were seeded in 96 well plates at 5000 cells/well in KSM medium and were incubated overnight at 37°C/5% CO<sub>2</sub>. HaCaTa cells were treated for 2h with a range of concentrations of doxorubicin at 37°C, compared with vehicle control (cells treated with medium containing DMSO, in which the reagent was dissolved). The solvent represents the maximum amount of DMSO corresponding to the highest drug concentration). The drugs were then removed, wells were rinsed with PBS to remove any traces of drug and cultures incubated for a 30 min, after which H2DCFDA reagent (as a fluorescent probe) at different concentrations (2.5, 5, and 10µM) was added to the wells and plates were incubated at 37°C in 5% CO<sub>2</sub> for a 30 min. Fluorescence was measured at Excitation 485nm/Emission 520nm in the presence of PBS. Bars represent mean RFU values (±S.E.M) and results are representative of three independent experiments each consisting of 6–8 technical replicates. \*\*,  $p < 0.01$ ; \*\*\*,  $p < 0.001$ .

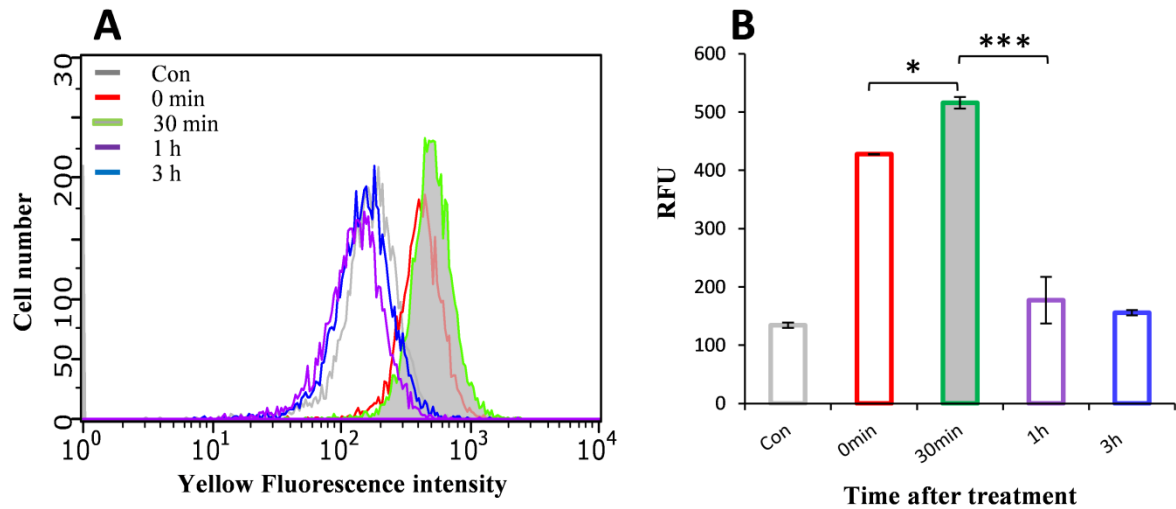


**Figure 5-18 Time-dependent ROS production measured by flow cytometry analysis using H2DCFDA after treatment with doxorubicin in HaCaTa cells**

HaCaTa cells were seeded in 6-well plates at  $1.5 \times 10^5$  cells/well in KSFM medium and were incubated overnight at  $37^\circ\text{C}/5\% \text{CO}_2$ . HaCaTa cells were treated for 2h with  $2.5 \mu\text{g}/\text{mL}$  doxorubicin (Doxo) at  $37^\circ\text{C}$ , compared with vehicle control (cells treated with medium containing DMSO, in which the reagent was dissolved). The solvent represents the maximum amount of DMSO corresponding to the highest drug concentration). The drugs were then removed, wells were rinsed with PBS to remove any traces of drug and cultures incubated for the indicated time points (0, 30min, 1h and 3h), and after which  $5 \mu\text{M}$  H2DCFDA reagent was added to the wells and plates were incubated at  $37^\circ\text{C}$  in  $5\% \text{CO}_2$  for 30 min. Cells were harvested by trypsinisation and ROS generation measured by flow cytometry. **A**) Representative flow cytometric histograms, **B**) bars represent median fluorescence intensity (MFI). Cells were acquired on a Guava EasyCyte flow cytometer and results analysed using GuavaSoft software. Bars show MFI ( $\pm$ S.E.M) for three independent biological experiments, each consisting of 2 technical replicates. \*,  $p < 0.05$ ; \*\*\*,  $p < 0.001$ .

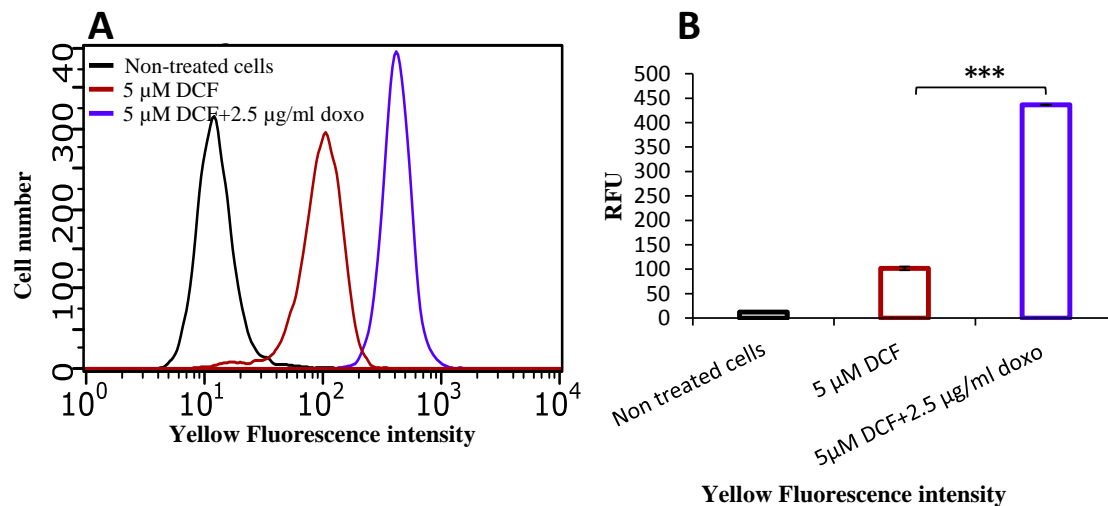


**Figure 5-19 ROS levels measured by flow cytometry analysis after drug treatment with and without H2DCFDA reagent in HaCaTa cells**

HaCaTa cells were seeded in 6-well plates at  $1.5 \times 10^5$  cells/well in KSFM medium and were incubated overnight at  $37^\circ\text{C}/5\% \text{CO}_2$ . HaCaTa cells were treated for 2h with  $2.5 \mu\text{g/mL}$  doxorubicin (Doxo) at  $37^\circ\text{C}$ , compared with vehicle control (cells treated with medium containing DMSO, in which the reagent was dissolved. The solvent represents the maximum amount of DMSO corresponding to the highest drug concentration). The drugs were then removed, wells were rinsed with PBS to remove any traces of drug and cultures incubated for a 30 min, after which  $5 \mu\text{M}$  H2DCFDA reagent was added to the wells and plates were incubated at  $37^\circ\text{C}$  in  $5\% \text{CO}_2$  for 30 min. Cells were harvested by trypsinisation ROS generation were analysed by flow cytometry using H2DCFDA as a fluorescent probe. **A**) Representative flow cytometric histograms, **B**) bars represent median fluorescence intensity (MFI). Cells were acquired on a Guava EasyCyte flow cytometer and results analysed using GuavaSoft software. Bars show MFI ( $\pm$ S.E.M) for three independent biological experiments, each consisting of 2 technical replicates. \*\*\*,  $p < 0.001$ .

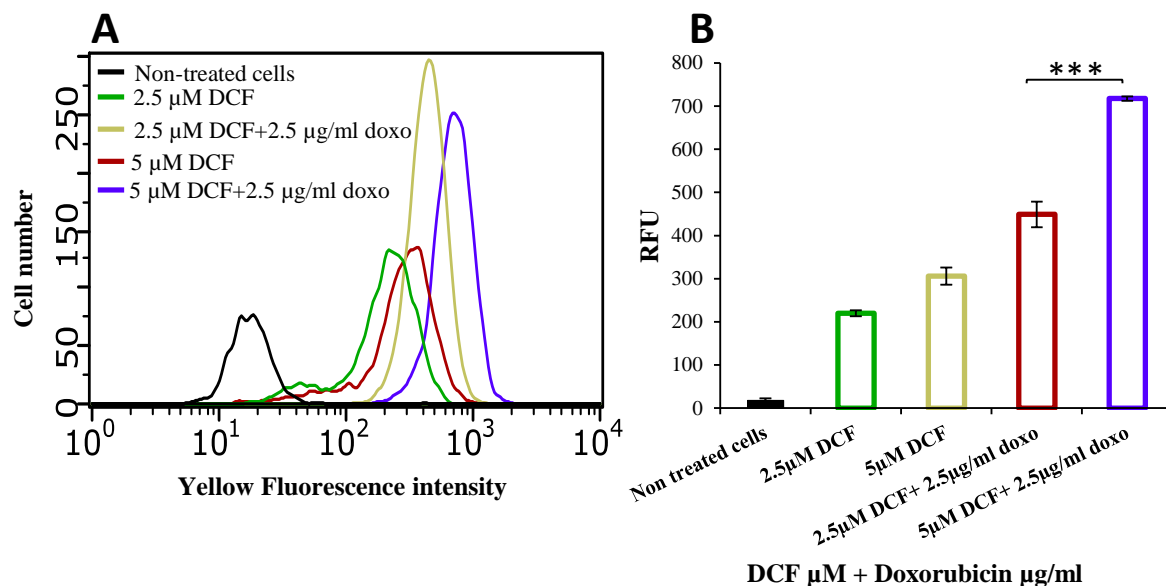


**Figure 5-20 ROS induction determined using 2.5 and 5  $\mu\text{M}$  [H2DCFDA] in HaCaTa Cells**  
 HaCaTa cells were seeded in 6 well plate at  $1.5 \times 10^5$  cells/well in KSFM medium and were incubated overnight at  $37^\circ\text{C}/5\% \text{CO}_2$ . HaCaTa cells were treated for 2h with 2.5  $\mu\text{g/ml}$  doxorubicin (Doxo) at  $37^\circ\text{C}$ , compared with vehicle control (cells treated with medium containing DMSO, in which the reagent was dissolved). The solvent represents the maximum amount of DMSO corresponding to the highest drug concentration). The drugs were then removed, wells were rinsed with PBS to remove any traces of drug and cultures incubated for a 30 min and after which (2.5 and 5  $\mu\text{M}$ ) H2DCFDA reagent were added to the wells and plates were incubated at  $37^\circ\text{C}$  in  $5\% \text{CO}_2$  for 30 min. Cells were harvested by trypsinisation ROS generation were analysed by flow cytometry using H2DCFDA as a fluorescent probe. **A)** Representative flow cytometric histograms, **B)** bars represent median fluorescence intensity (MFI). Cells were acquired on a Guava EasyCyte flow cytometer and results analysed using GuavaSoft software. Bars show MFI ( $\pm$ S.E.M) for three independent biological experiments, each consisting of 2 technical replicates. \*\*\*,  $p < 0.001$ .

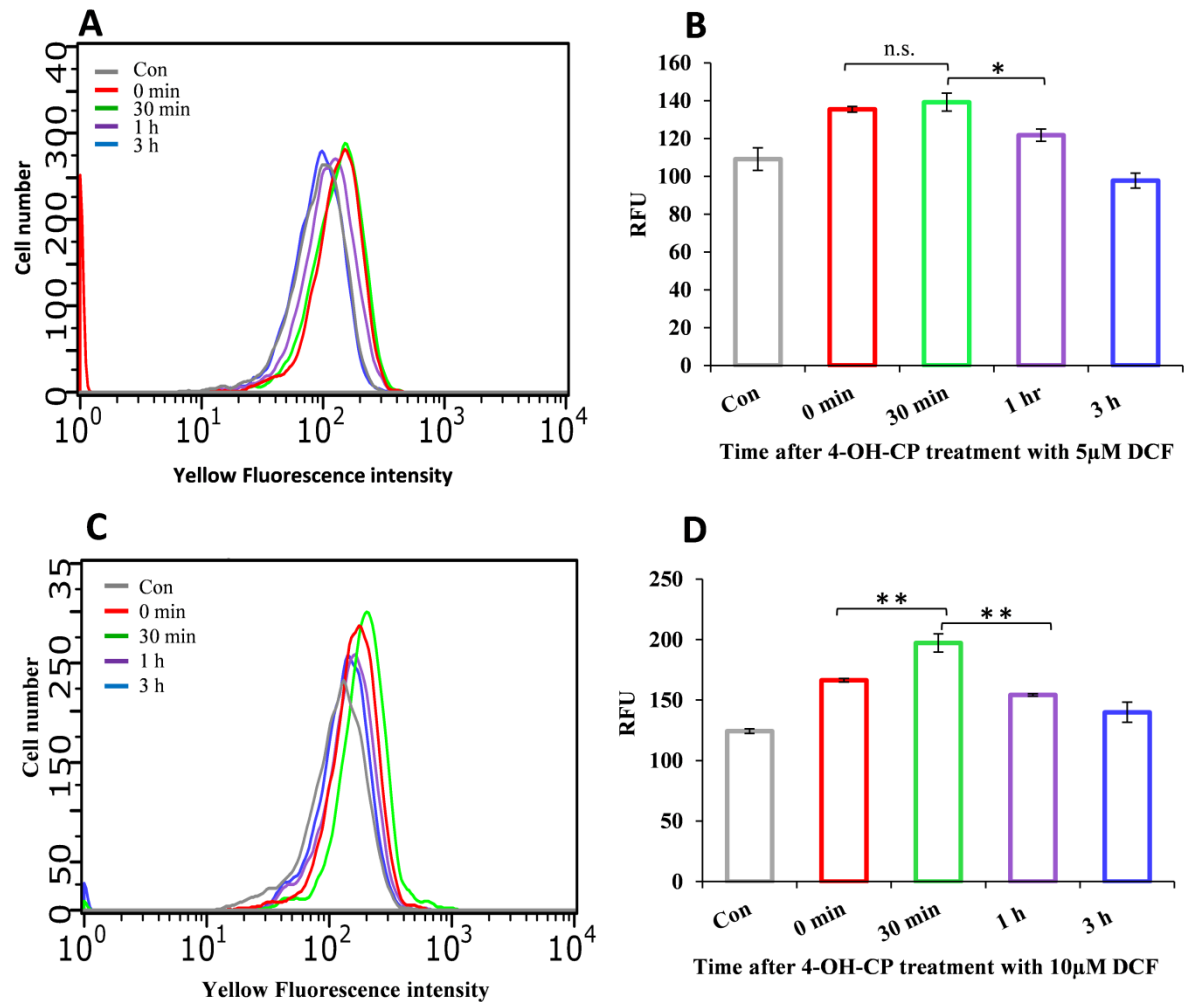


**Figure 5-21 Time-dependent reactive oxygen species (ROS) production measured by flow cytometry analysis after treatment with 4-OH-CP and 5 and 10  $\mu\text{M}$  [H2DCFDA] in HaCaTa cells**

HaCaTa cells were seeded in 6 well plate at  $1.5 \times 10^5$  cells/well in KFSM medium and were incubated overnight at  $37^\circ\text{C}/5\% \text{CO}_2$ . HaCaTa cells were treated for 2h with  $7.5 \mu\text{g}/\text{mL}$  4-OH-CP at  $37^\circ\text{C}$ , compared with vehicle control (cells treated with medium containing DMSO, in which the reagent was dissolved). The solvent represents the maximum amount of DMSO corresponding to the highest drug concentration). The drugs were then removed, wells were rinsed with PBS to remove any traces of drug and cultures incubated for a (0, 30 min, 1h and 3h and after which (5 and  $10 \mu\text{M}$ ) H2DCFDA reagent were added to the wells and plates were incubated at  $37^\circ\text{C}$  in  $5\% \text{CO}_2$  for 30 min. Cells were harvested by trypsinisation ROS generation were analysed by flow cytometry using H2DCFDA as a fluorescent probe. **A and C)** Representative flow cytometric histograms, **B and D)** bars represent median fluorescence intensity (MFI). Cells were acquired on a Guava EasyCyte flow cytometer and results analysed using GuavaSoft software. Bars show MFI ( $\pm$ S.E.M) for three independent biological experiments, each consisting of 2 technical replicates. n.s., non-significant; \*,  $p < 0.05$ ; \*\*,  $p < 0.01$ .

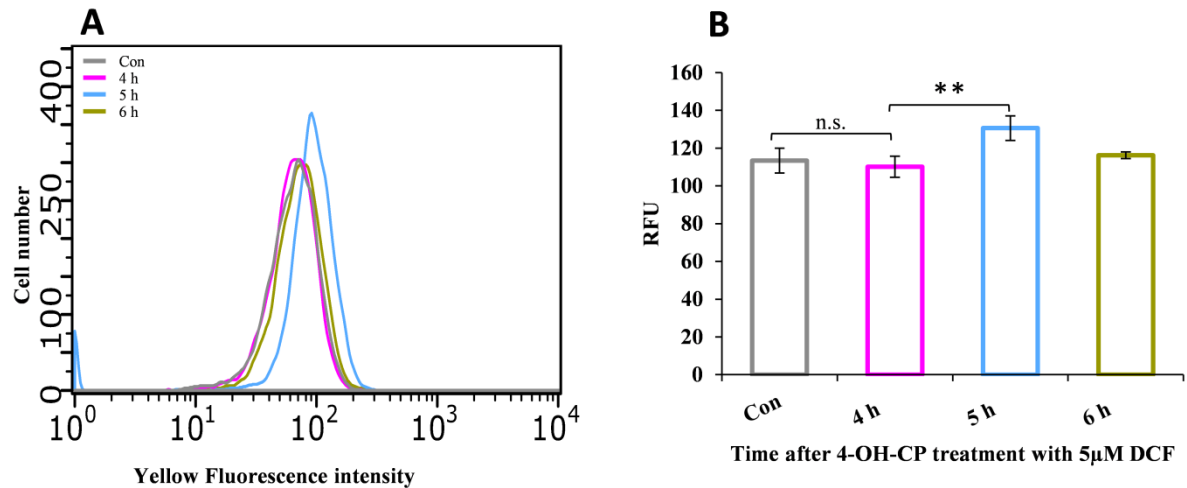


**Figure 5-22 Time-dependent reactive oxygen species (ROS) production measured by flow cytometry analysis after treatment with 4-OH-CP and 5 µM [H2DCFDA] in HaCaTa cells**

HaCaTa cells were seeded in 6 well plate at  $1.5 \times 10^5$  cells/well in KSFM medium and were incubated overnight at  $37^\circ\text{C}/5\% \text{CO}_2$ . HaCaTa cells were treated for 2h with  $7.5 \mu\text{g}/\text{mL}$  4-OH-CP at  $37^\circ\text{C}$ , compared with vehicle control (cells treated with medium containing DMSO, in which the reagent was dissolved). The solvent represents the maximum amount of DMSO corresponding to the highest drug concentration). The drugs were then removed, wells were rinsed with PBS to remove any traces of drug and cultures incubated for a (4, 5 and 6h) and after which (5 and  $10 \mu\text{M}$ ) H2DCFDA reagent were added to the wells and plates were incubated at  $37^\circ\text{C}$  in  $5\% \text{CO}_2$  for 30 min. Cells were harvested by trypsinisation ROS generation were analysed by flow cytometry using H2DCFDA as a fluorescent probe. **A)** Representative flow cytometric histograms, **B)** bars represent median fluorescence intensity (MFI). Cells were acquired on a Guava EasyCyte flow cytometer and results analysed using GuavaSoft software. Bars show MFI ( $\pm$  S.E.M.) for three independent biological experiments, each consisting of 2 technical replicates. n.s., non-significant; \*\*,  $p < 0.01$ .

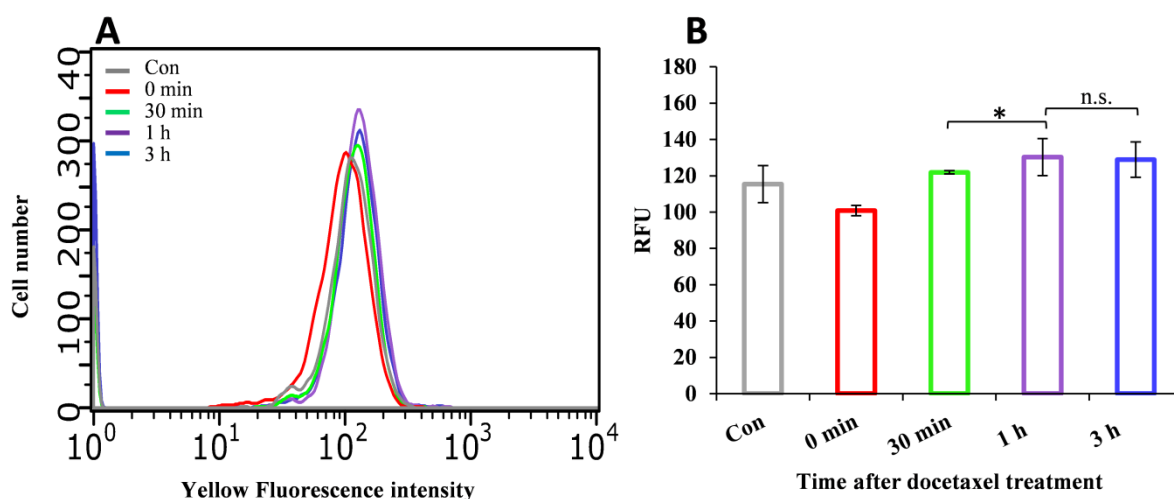


**Figure 5-23 Time-dependent reactive oxygen species (ROS) production measured by flow cytometry analysis after treatment with docetaxel and 5  $\mu$ M [H2DCFDA] in HaCaTa cells**

HaCaTa cells were seeded in 6 well plate at  $1.5 \times 10^5$  cells/well in KSM medium and were incubated overnight at 37°C/5% CO<sub>2</sub>. HaCaTa cells were treated for 2h with 0.01  $\mu$ g/mL docetaxel (Doce) at 37°C, compared with vehicle control (cells treated with medium containing DMSO, in which the reagent was dissolved. The solvent represents the maximum amount of DMSO corresponding to the highest drug concentration). The drugs were then removed, wells were rinsed with PBS to remove any traces of drug and cultures incubated for a (0, 30 min, 1h and 3h and after which 5 $\mu$ M H2DCFDA reagent were added to the wells and plates were incubated at 37°C in 5% CO<sub>2</sub> for 30 min. Cells were harvested by trypsinisation ROS generation were analysed by flow cytometry using H2DCFDA as a fluorescent probe. **A**) Representative flow cytometric histograms, **B**) bars represent median fluorescence intensity (MFI). Cells were acquired on a Guava EasyCyte flow cytometer and results analysed using GuavaSoft software. Bars show MFI ( $\pm$ S.E.M.) for three independent biological experiments, each consisting of 2 technical replicates. n.s., non-significant; \*,  $p < 0.05$ .

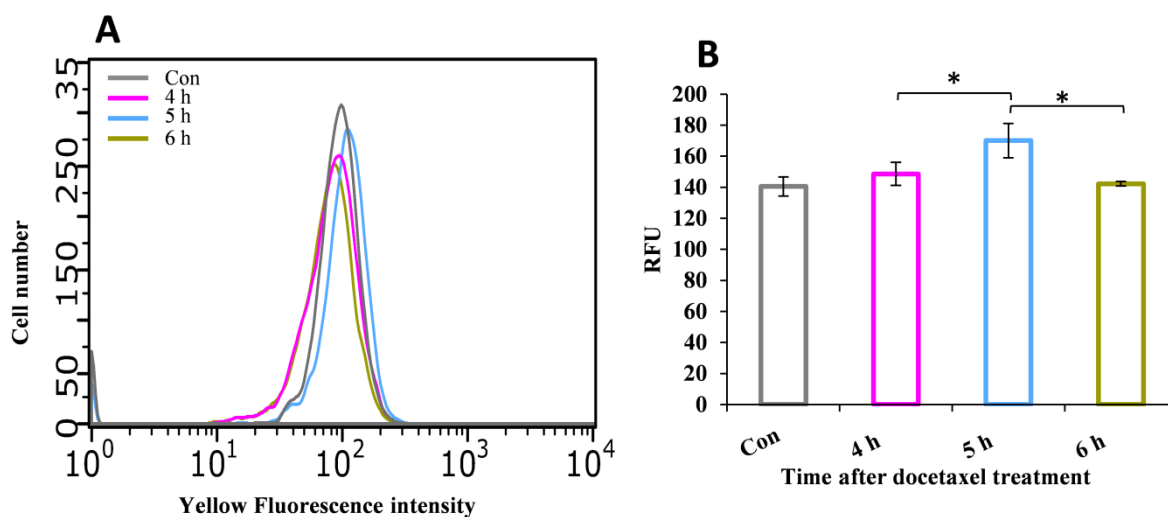


**Figure 5-24 Time-dependent reactive oxygen species (ROS) production measured by flow cytometry analysis after treatment with docetaxel and 5  $\mu$ M [H2DCFDA] in HaCaTa cells**

HaCaTa cells were seeded in 6 well plate at  $1.5 \times 10^5$  cells/well in KSFM medium and were incubated overnight at  $37^\circ\text{C}/5\% \text{CO}_2$ . HaCaTa cells were treated for 2h with  $0.01 \mu\text{g/mL}$  docetaxel (Doce) at  $37^\circ\text{C}$ , compared with vehicle control (cells treated with medium containing DMSO, in which the reagent was dissolved). The solvent represents the maximum amount of DMSO corresponding to the highest drug concentration). The drugs were then removed, wells were rinsed with PBS to remove any traces of drug and cultures incubated for a (4, 5 and 6h) and after which (5 and  $10\mu\text{M}$ ) H2DCFDA reagent were added to the wells and plates were incubated at  $37^\circ\text{C}$  in  $5\% \text{CO}_2$  for 30 min. Cells were harvested by trypsinisation ROS generation were analysed by flow cytometry using H2DCFDA as a fluorescent probe. **A)** Representative flow cytometric histograms, **B)** bars represent median fluorescence intensity (MFI). Cells were acquired on a Guava EasyCyte flow cytometer and results analysed using GuavaSoft software. Bars show MFI ( $\pm$ S.E.M.) for three independent biological experiments, each consisting of 2 technical replicates. \*,  $p < 0.05$

## **5.9 Effect of cooling on chemotherapy drug-induced ROS**

The ability of some chemotherapy drugs to trigger oxidative stress seems to play an important role in the anti-carcinogenic potential of these drugs, as is believed to be the case for one of the most frequently used drugs in the clinic, doxorubicin (Luanpitpong *et al.*, 2012). To further understand the mechanisms by which cooling protects from drug-induced cytotoxicity in HaCaTa cells, we measured intracellular ROS production at normal temperature and tested the effect of cooling on ROS production when cells were treated with doxorubicin (2.5 µg/mL), docetaxel (0.05 µg/mL) and 4-OH-CP (7.5 µg/mL).

### **5.9.1 Influence of temperature on ROS production induced by doxorubicin in HaCaTa cells**

It has been reported that hypothermia can reduce the level of intracellular ROS while hyperthermia may increase their production (Hsu *et al.*, 2011). Cellular ROS levels in HaCaTa cells 30 min after a 2h treatment with 2.5 µg/mL doxorubicin at 37°C or 22°C were assessed by H2DCF-DA labelling and flow cytometry. As shown in Figure 5-25 A and B, doxorubicin increased ROS generation and this was significantly reduced at 22°C. To further investigate the effect of temperature on ROS generation, cells were treated with doxorubicin at 18°C and (Figure 5-25C and D) and 14°C (Figure 5-25E and F). Results showed that the cellular ROS generation was further reduced at 18°C and almost abolished at 14°C indicating that ROS produced by cells in response to doxorubicin treatment are suppressed by cooling and that the lower the temperature the better the inhibition of ROS.

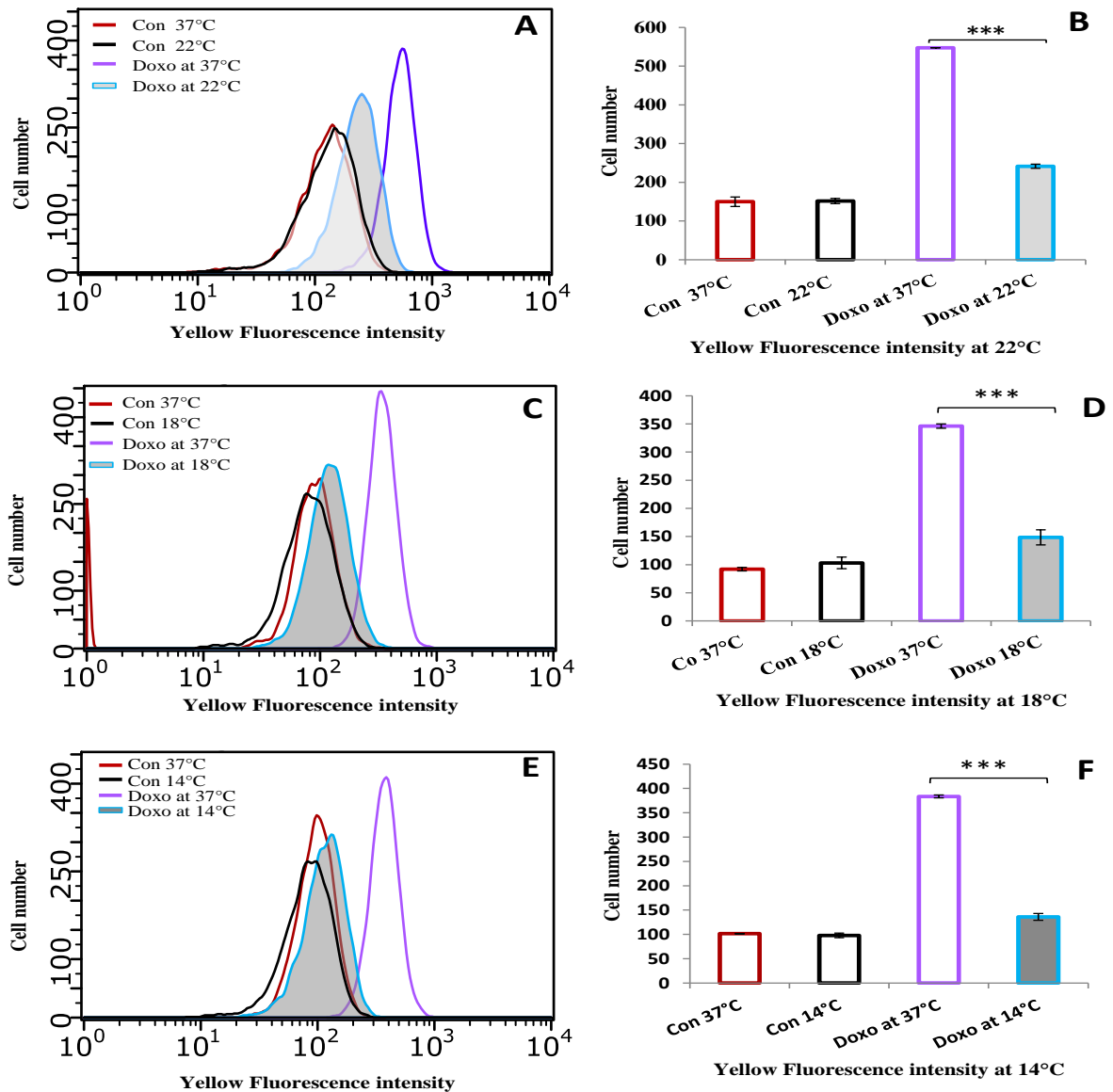


**Figure 5-25 Temperature-dependent reactive oxygen species (ROS) production after treatment with doxorubicin in HaCaTa cells**

HaCaTa cells were seeded in 6 well plate at  $1.5 \times 10^5$  cells/well in KFSM medium and were incubated overnight at 37°C/5% CO<sub>2</sub>. HaCaTa cells were treated for 2h with 2.5 µg/mL doxorubicin (Doxo) at 37°C, 22°C, 18°C, and 14°C compared with vehicle control (cells treated with medium containing DMSO, in which the reagent was dissolved). The solvent represents the maximum amount of DMSO corresponding to the highest drug concentration). The drugs were then removed, wells were rinsed with PBS to remove any traces of drug and cultures incubated for a 30 min and after which 5µM H<sub>2</sub>DCFDA reagent were added to the wells and plates were incubated at 37°C in 5% CO<sub>2</sub> for 30 min. Cells were harvested by trypsinisation ROS generation were analysed by flow cytometry using H<sub>2</sub>DCFDA as a fluorescent probe. **A, C and E**) Representative flow cytometric histograms at 22°C, 18°C, 14°C respectively, **B, D and F**) bars represent median fluorescence intensity (MFI) at 22°C, 18°C, and 14°C respectively. Cells were acquired on a Guava EasyCyte flow cytometer and results analysed using GuavaSoft software. Bars show MFI (±S.E.M.) for three independent biological experiments, each consisting of 2 technical replicates. \*\*\*,  $p < 0.001$ .

### 5.9.2 Influence of temperature on ROS production by 4-OH-CP in HaCaTa cells

It has been reported that cyclophosphamide can induce ROS generation (Gonzalez *et al.*, 2015; Sulkowska *et al.*, 1998); therefore the effect of cooling on oxidative stress was investigated to further understand the mechanism by which cyclophosphamide induces CIA and explain the protective effect of cooling. HaCaTa cells were treated with 7.5 µg/mL of 4-OH-CP and ROS levels determined as previously described after 30 min (as doxorubicin experiments in section 5.1.8 indicated that ROS elevation is rapid and short-lived). Results showed a slight increase in ROS generation was observed at 30 min after treatment at 37°C compared with the control (non-drug-treated cells). Hence, although 4-OH-CP does induce the generation of ROS it is lower than that induced by doxorubicin and furthermore the level of ROS at 22°C was higher than that at 37°C (Figure 5-26A and B).

To further investigate the effect of cooling on cyclophosphamide generation of intracellular ROS, temperature was further reduced to 18°C, and this decreased intracellular ROS compared with 22°C (Figure 5-26C and D). Moreover, 4-OH-CP-induced ROS generation at 14°C was investigated; surprisingly ROS generation at 14°C was higher than that at 18°C (Figure 5-26E and F).

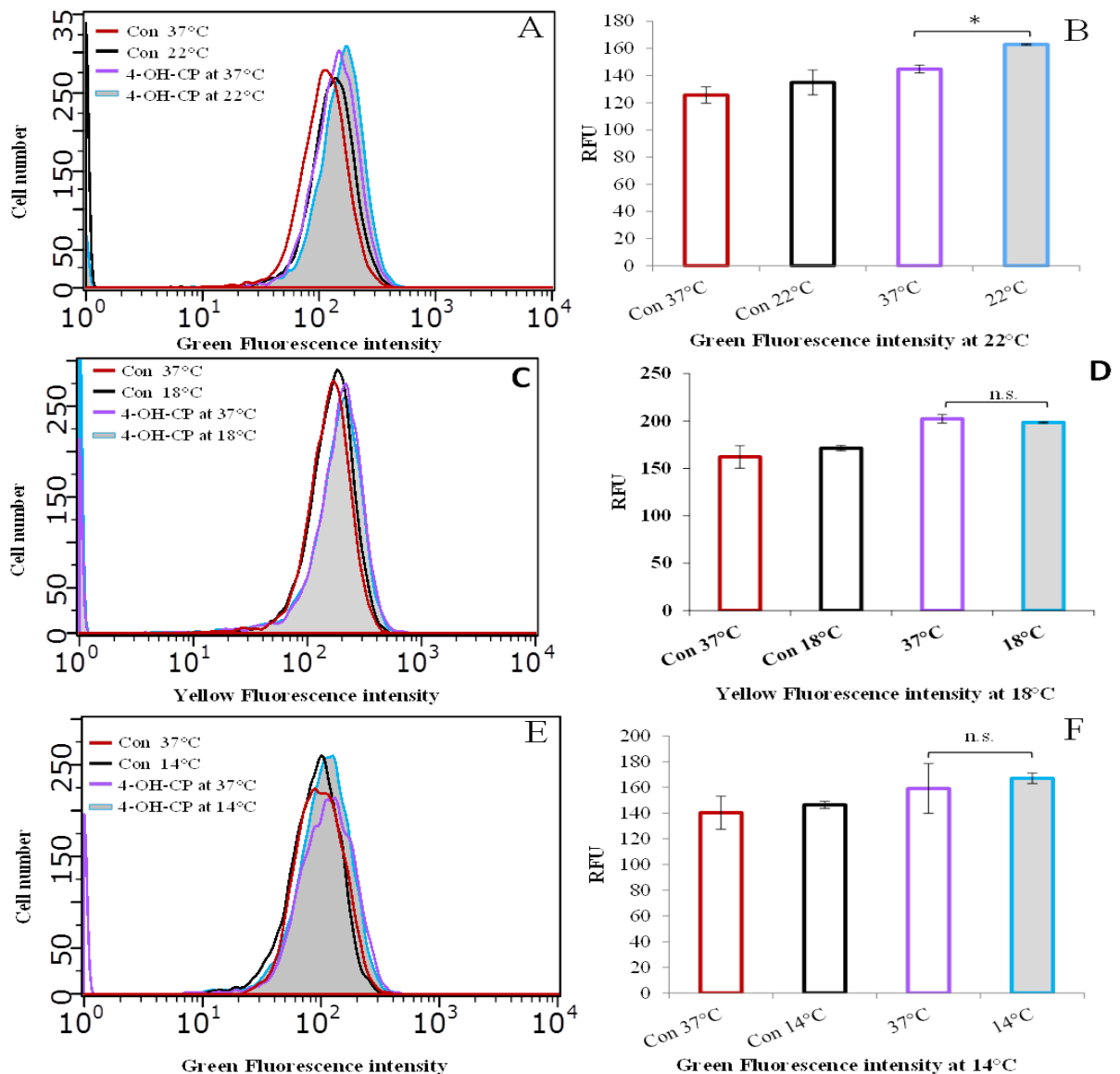


**Figure 5-26 Temperature-dependent reactive oxygen species (ROS) production after treatment with 4-OH-CP in HaCaTa cells**

HaCaTa cells were seeded in 6 well plate at  $1.5 \times 10^5$  cells/well in KSFM medium and were incubated overnight at 37°C/5% CO<sub>2</sub>. HaCaTa cells were treated for 2h with 7.5 µg/mL 4-OH-CP at 37°C, 22°C, 18°C, and 14°C compared with vehicle control (cells treated with medium containing DMSO, in which the reagent was dissolved). The solvent represents the maximum amount of DMSO corresponding to the highest drug concentration). The drugs were then removed, wells were rinsed with PBS to remove any traces of drug and cultures incubated for a 30 min and after which 5µM H2DCFDA reagent were added to the wells and plates were incubated at 37°C in 5% CO<sub>2</sub> for 30 min. Cells were harvested by trypsinisation ROS generation were analysed by flow cytometry using H2DCFDA as a fluorescent probe. **A, C and E)** Representative flow cytometric histograms at 22°C, 18°C, 14°C respectively, **B, D and F)** bars represent median fluorescence intensity (MFI) at 22°C, 18°C, and 14°C respectively. Cells were acquired on a Guava EasyCyte flow cytometer and results analysed using GuavaSoft software. Bars show MFI (±S.E.M.) for three independent biological experiments, each consisting of 2 technical replicates. n.s., non-significant; \*,  $p < 0.05$ .

### 5.9.3 ROS production mediated by docetaxel and effects of cooling

Next, ROS generation in HaCaTa cells treated with docetaxel and the effects of cooling were examined. As shown in Figure 5-27, treatment of 0.01  $\mu\text{g}/\text{mL}$  docetaxel and 5  $\mu\text{M}$  of H2DCFDA produced elevated levels of ROS at 14°C compared with cells treated at 37°C. These results suggested that docetaxel failed to affect the basal levels of ROS in HaCaTa cells.

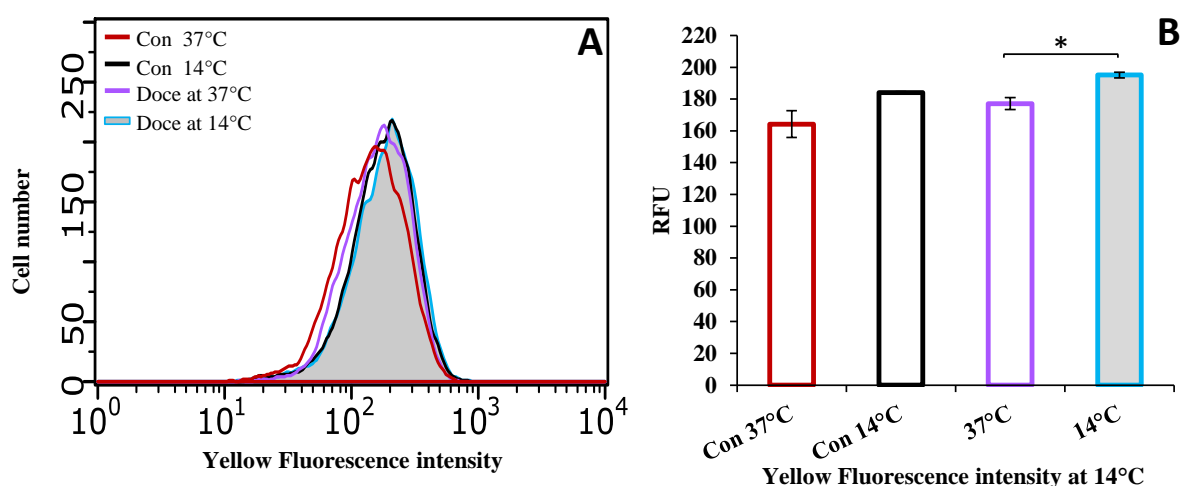


**Figure 5-27 Temperature-dependent reactive oxygen species (ROS) production after treatment with docetaxel in HaCaTa cells**

HaCaTa cells were seeded in 6 well plate at  $1.5 \times 10^5$  cells/well in KSFM medium and were incubated overnight at 37°C/5%  $\text{CO}_2$ . HaCaTa cells were treated for 2h with 0.01  $\mu\text{g}/\text{mL}$  docetaxel (Doce) at 37°C and 14°C compared with vehicle control (cells treated with medium containing DMSO, in which the reagent was dissolved). The solvent represents the maximum amount of DMSO corresponding to the highest drug concentration). The drugs were then removed, wells were rinsed with PBS to remove any traces of drug and cultures incubated for a 30 min and after which 5 $\mu\text{M}$  H2DCFDA reagent were added to the wells and plates were incubated at 37°C in 5%  $\text{CO}_2$  for 30 min. Cells were harvested by trypsinisation ROS generation were analysed by flow cytometry using H2DCFDA as a fluorescent probe. **A)** Representative flow cytometric histograms, **B)** bars represent median fluorescence intensity (MFI). Cells were acquired on a Guava EasyCyte flow cytometer and results analysed using GuavaSoft software. Bars show MFI ( $\pm$ S.E.M.) for three independent biological experiments, each consisting of 2 technical replicates. \*,  $p < 0.05$ .

As already described in this chapter, NHEK, HHFk, and HaCaTa cells treated with chemotherapeutic drugs showed a significant disruption in their mitochondrial membrane potential, and this was demonstrated using the JC-1 assay. The impairment of the integrity of the mitochondrial potential coincides with the decoupling of the respiratory chain and subsequently increased production of ROS, an effect that has been demonstrated for doxorubicin, which has been shown to induce ROS in HaCaT cells (Luanpitpong *et al.*, 2012). Disruption of mitochondrial function can have devastating consequences for the cell and led to death. The mitochondrial apoptosis pathway requires disruption of the  $\Delta\Psi_m$  and the release of mitochondrial proteins. To provide evidence for apoptosis induction and to confirm the protective roles of cooling against chemotherapy drugs induced cell death, assays that specifically detect cell death (apoptosis) were used.

## **5.10 Detection of chemotherapy drug mediated HaCaTa cell death using the CytoTox-Glo assay and assessment of the effect of cooling**

To determine the efficacy of cooling in the prevention from chemotherapy-induced cell death in HaCaTa cells, the CytoTox-Glo™ assay was conducted. Initially the effects of various concentrations of the drugs (doxorubicin, docetaxel, 4-OH-CP as well as 5-FU) were measured 24h after treatment at either 37°C or 18°C (Figure 5-28).

A significant increase in cell death occurred 24h after treatment with 0.5, 0.75 and 2.5 µg/mL doxorubicin and 0.005, 0.025, and 0.1 µg/mL docetaxel at 37°C compared with cells treated at 18°C. However, cells treated with 2.5, 5 and 10 µg/mL 4-OH-CP showed no significant effects (Figure 5-28). Data showed that using the CytoTox-Glo assay with the concentrations of drugs chosen was relatively modest effects after 24h. This indicated that a longer time period as well as higher concentrations of chemotherapy drugs might be necessary to observe a more significant cell death induction.

Therefore, a second protocol was followed in which cells were treated with 2.5 and 5 µg/mL doxorubicin, 0.025 and 0.1 µg/mL docetaxel and 10 and 30 µg/mL 4-OH-CP for 2h at 37°C and 18°C and cell death was assessed at 48h post treatment. A significantly greater cytotoxic effect was observed when the cells were exposed to the drugs at 37°C compared to cells treated at 18°C (Figure 5-29). Thus, the induction of apoptosis assessed with the CytoTox-Glo assay after 48h of treatment was far more marked compared to 24h. More importantly, although some protection was observed at 24h

(Figure 5-28), there was a more significant reduction of apoptosis in cells treated at cooling condition (18°C) at 48h, providing evidence that cooling could protect cells from cytotoxicity induced by chemotherapeutic drugs. Moreover, the cytotoxicity in HaCaTa cells treated with 10 and 25 µg/mL 5-FU was measured at 37°C and 18°C (Figure 5-30). The data showed that there was a significant decrease in cell death at 18°C compared to at 37°C. Taken together, these observations suggest that reduction in viability is due to active induction of cell death.

Since the CytoTox-Glo assay was not sensitive to detect cell death at low concentrations, in addition, CytoTox-Glo assay was not able to distinguish between cell death *via* apoptosis or necrosis develops, an alternative test system was used to investigate the extent chemotherapy drugs have a damaging effect. For this, the SensoLyte assay was used, where the activity of effector proteases programmed cell death *via* a special fluorescence detectable test substrate, which can measure caspase-3/7 activity.

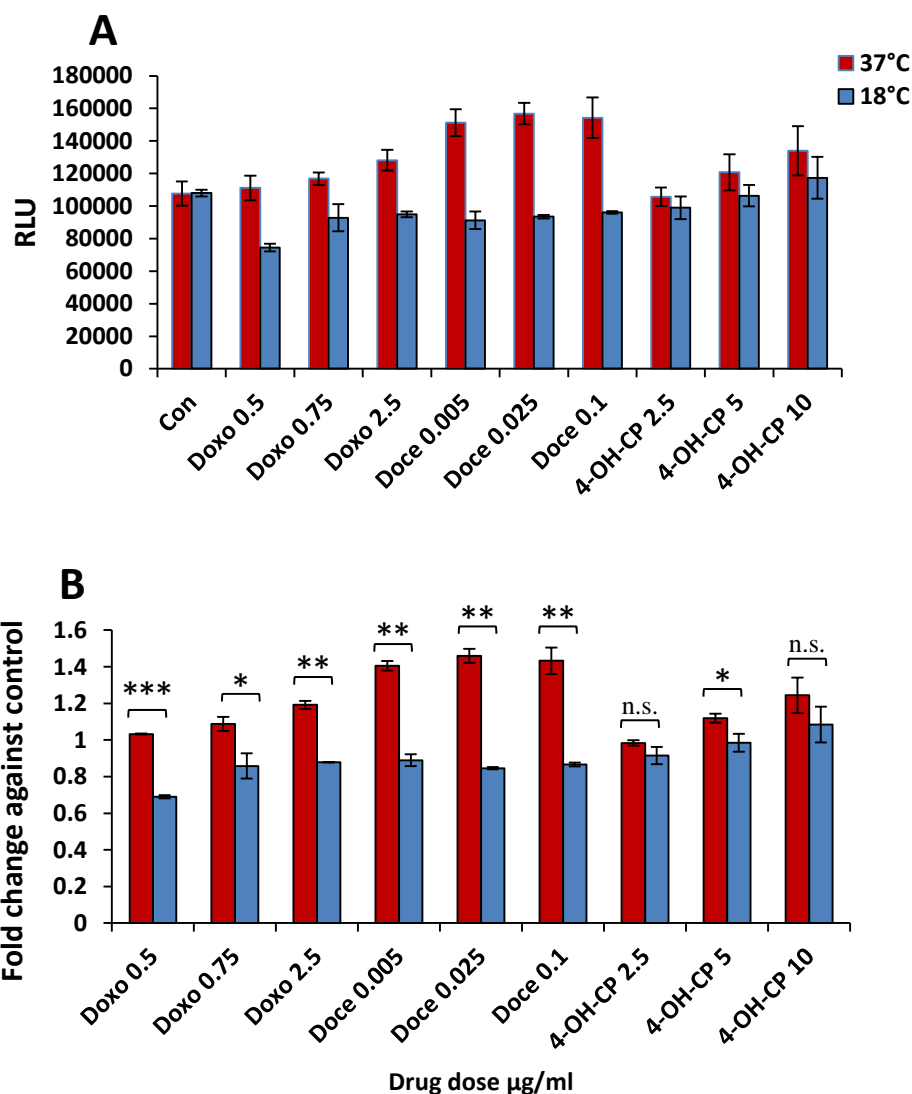


**Figure 5-28 Detection of the cytoprotective role of cooling against chemotherapy drug-mediated cell death in HaCaTa cells after 24h using CytoTox-Glo**

HaCaTa cells were seeded in 96 well plates at 5000 cells/well in KFSM complete medium and were incubated overnight at 37°C / 5% CO<sub>2</sub>. HaCaTa cells were treated for 2h with the indicated dose of doxorubicin (Doxo), docetaxel (Doce) and 4-OH-CP at 37°C and 18°C compared with vehicle control (cells treated with medium containing DMSO, in which the reagent was dissolved). The solvent represents the maximum amount of DMSO corresponding to the highest drug concentration). The drugs were then removed, wells were rinsed with PBS to remove any traces of drug and cultures incubated for a further 24h, after which 50 µL CytoTox-Glo substrate was added. After 15 min incubation at room temperature, luminescence was measured using a plate reader. RLU readings were deduced as described in Materials and Methods section 2.10.2. **A)** Results are plotted as raw luminescence data, **B)** Results are presented as fold change (from raw RLU data used in A) by comparing drug treated cells *versus* controls. Bars correspond to mean values of three technical replicates (±S.E.M.) for three independent biological experiments, each consisting of 6-8 technical replicates. n.s., non-significant; \*,  $p < 0.05$ ; \*\*,  $p < 0.01$ ; \*\*\*,  $p < 0.001$ .

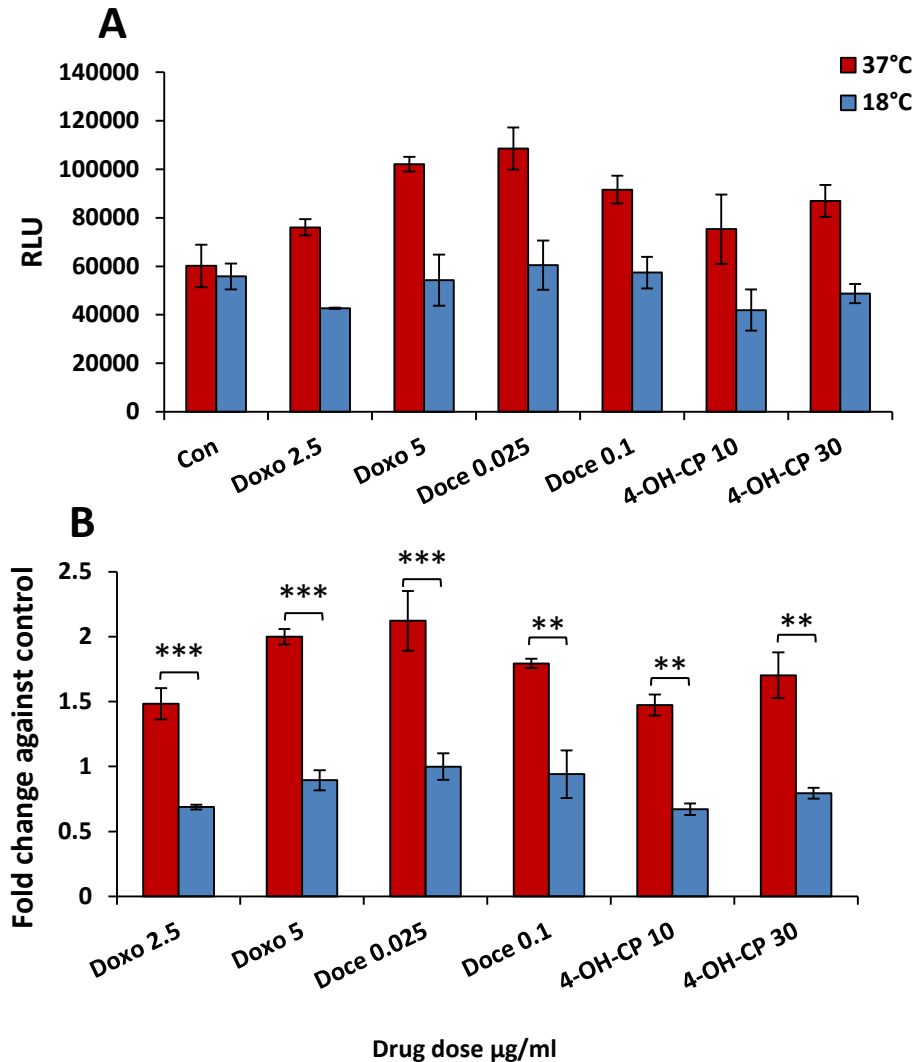


**Figure 5-29 Detection of the cytoprotective role of cooling against chemotherapy drug-mediated cell death in HaCaTa cells after 48h using CytoTox-Glo**

HaCaTa cells were seeded in 96 well plates at 5000 cells/well in KSFM complete medium and were incubated overnight at 37°C / 5% CO<sub>2</sub>. HaCaTa cells were treated for 2h with the indicated dose of doxorubicin (Doxo), docetaxel (Doce) and 4-OH-CP at 37°C and 18°C compared with vehicle control (cells treated with medium containing DMSO, in which the reagent was dissolved). The solvent represents the maximum amount of DMSO corresponding to the highest drug concentration). The drugs were then removed, wells were rinsed with PBS to remove any traces of drug and cultures incubated for a further 48h, after which 50 µL CytoTox-Glo substrate was added. After 15 min incubation at room temperature, luminescence was measured using a plate reader. RLU readings were deduced as described in Materials and Methods section 2.10.2. **A)** Results are plotted as raw luminescence data, **B)** Results are presented as fold change (from raw RLU data used in A) by comparing drug treated cells *versus* controls. Bars correspond to mean values of three technical replicates (±S.E.M.) for three independent biological experiments, each consisting of 6-8 technical replicates. \*\*,  $p < 0.01$ , \*\*\*,  $p < 0.001$ .

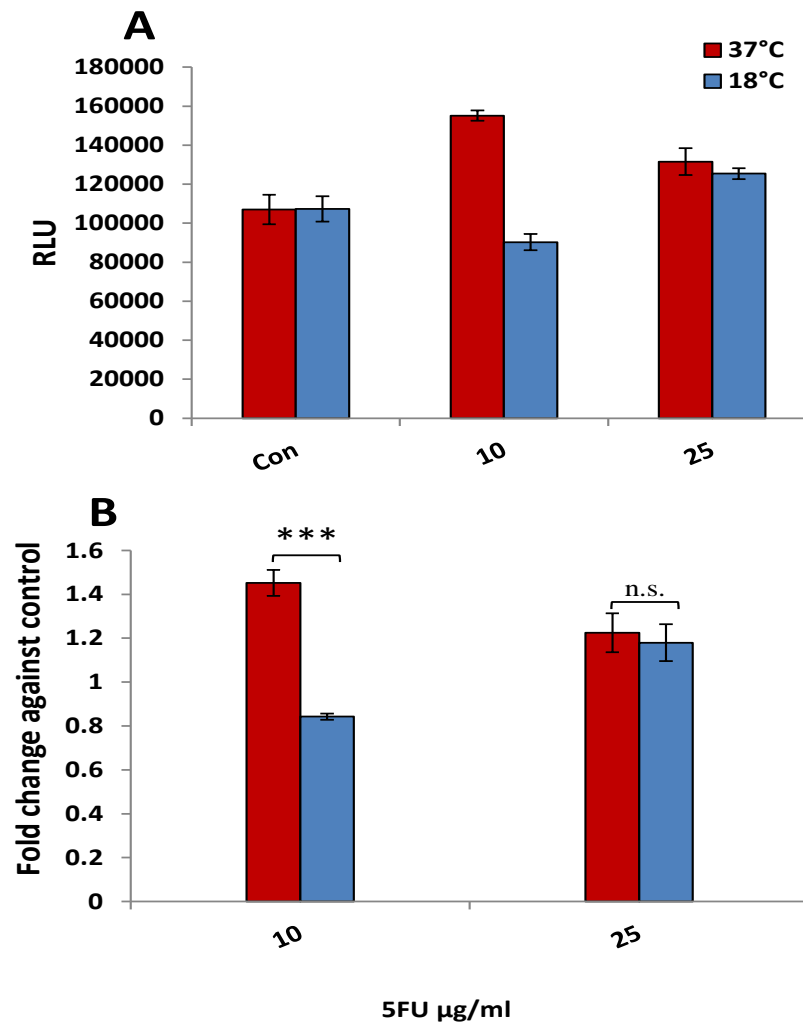


**Figure 5-30 Detection of cytoprotective role of cooling against 5-fluorouracil (5-FU)-mediated toxicity in HaCaTa cells after 48h using CytoTox-Glo**

HaCaTa cells were seeded in 96 well plates at 5000 cells/well in KSFM complete medium and were incubated overnight at 37°C / 5% CO<sub>2</sub>. HaCaTa cells were treated for 2h with the indicated dose of 5FU at 37°C and 18°C compared with vehicle control compared with vehicle control (cells treated with medium containing DMSO, in which the reagent was dissolved. The solvent represents the maximum amount of DMSO corresponding to the highest drug concentration). The drugs were then removed, wells were rinsed with PBS to remove any traces of drug and cultures incubated for a further 48h, after which 50 µL CytoTox-Glo substrate was added. After 15 min incubation at room temperature, luminescence was measured using a plate reader. RLU readings were deduced as described in Materials and Methods section 2.10.2. **A)** Results are plotted as raw luminescence data, **B)** Results are presented as fold change (from raw RLU data used in A) by comparing drug treated cells *versus* controls. Bars correspond to mean values of three technical replicates (±S.E.M.) for three independent biological experiments, each consisting of 6-8 technical replicates. n.s., non-significant; \*\*\*,  $p < 0.001$ .

## 5.11 Detection of chemotherapy drug-induced activation of caspases-3/7 using the SensoLyte assay and assessment of the effect of cooling

Caspases-3 and 7 have some similarities, but also some distinct roles in programmed cell death (apoptosis). They are both key effector (executioner) caspases and as a result are involved in both the extrinsic and intrinsic (mitochondrial) pathways (Lakhani *et al.*, 2006). Chemotherapeutic drugs often induce apoptosis *via* the intrinsic pathway by MOMP induction and subsequent caspase-3/7 activation (Scabini *et al.*, 2011). Caspase-3/7 are required for the execution phase of the apoptotic process, and their activities are commonly used as indicators (markers) of apoptosis (Jänicke *et al.*, 1998). Caspase-3 has an important role in driving DNA fragmentation and the morphological changes of apoptosis, while caspase-7 plays a minor role in these processes (Lakhani *et al.*, 2006). The SensoLyte caspase-3/7 assay was used for detection of caspase-3/7 activity in HaCaTa cells treated with doxorubicin, docetaxel and 4-OH-CP for 2h at 24 and 48h post-treatment.

A significant increase in caspase-3/7 activity occurred 24h after treatment with (0.5, 0.75 and 2.5 µg/mL) doxorubicin and (0.005, 0.025, and 0.1 µg/mL) docetaxel and (2.5, 5 and 10 µg/mL) 4-OH-CP at 37°C compared with cells treated at 18°C (Figure 5-31). Data showed that there was a correlation between doxorubicin concentration and caspase-3/7 activity and there was a significant rise in caspase-3/7 activity with the escalation of the concentration. Moreover, there was a significant increase in caspase-3/7 at 37°C compared to at 18°C (Figure 5-31).

The activity of caspase-3/7 was increased significantly in cells treated with docetaxel for nearly all concentrations tested at 37°C after 24h, compared with cells treated at 18°C (Figure 5-31). These data suggested that the cells treated with docetaxel even at low concentrations might induce high levels of active caspase-3/7 and apoptosis.

The results of HaCaTa cells 24h after treatment with different concentrations of 4-OH-CP at 37°C and 18°C, also showed a positive correlation between the caspase-3/7 activation and 4-OH-CP concentration for both temperatures, with a significant increase of caspase-3/7 activation compared with cells treated at 18°C where the activation was decreased significantly (Figure 5-31). Surprisingly, a lower level of caspase-3/7 activity was observed after the 48h incubation period (Figure 5-32), compared with that after 24h. These results are likely due to the effects of drugs, which is generally on cellular caspase-3 activation and this may occur in phases of the cell cycle earlier than 48h, as demonstrated in the cell cycle analysis.

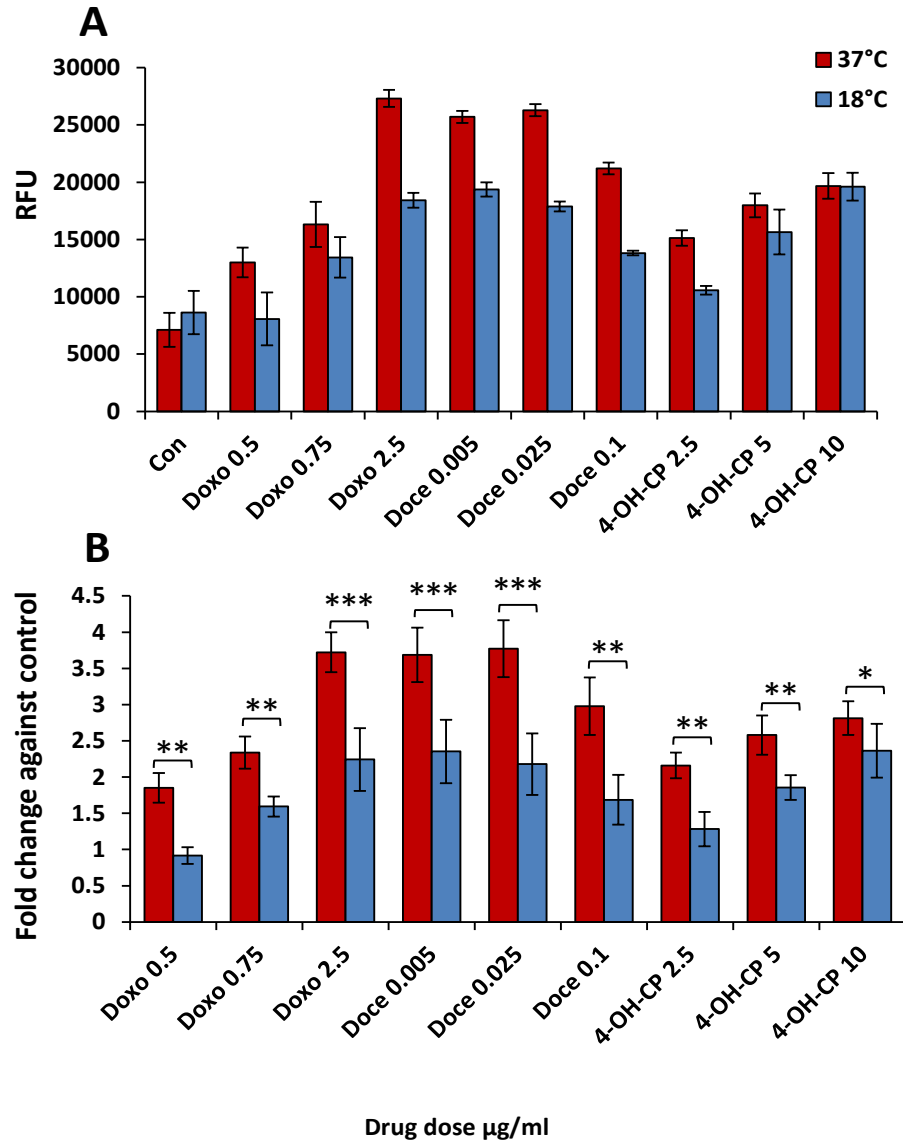


**Figure 5-31 The role of cooling in caspase-3/7 activation induced by chemotherapy drugs in HaCaTa cells after 24h using the Sensolyte assay**

HaCaTa cells were seeded in 96 well plates at 5000 cells/well in KFSM complete medium and were incubated overnight at 37°C / 5% CO<sub>2</sub>. HaCaTa cells were treated for 2h with the indicated dose of doxorubicin (Doxo), docetaxel (Doce) and 4-OH-CP at 37°C and 18°C compared with vehicle control (cells treated with medium containing DMSO, in which the reagent was dissolved). The solvent represents the maximum amount of DMSO corresponding to the highest drug concentration). The drugs were then removed, wells were rinsed with PBS to remove any traces of drug and cultures incubated for a further 24h, after which 50  $\mu\text{L}$  substrate of the Ansapec assay was added. After 60 min incubation in the dark at room temperature, fluorescence was measured using a plate reader. The Relative Fluorescence Units (RFU) readings were deduced as described in Materials and Methods section 2.10.3. **A**) Results are plotted as raw Fluorescence data; **B**) Results are presented as fold change (from raw RFU data used in A) by comparing drug treated cells *versus* controls. Bars correspond to mean values ( $\pm$ S.E.M.) for three independent biological experiments, each consisting of 6-8 technical replicates. \*,  $p < 0.05$ ; \*\*,  $p < 0.01$ , \*\*\*,  $p < 0.001$ .

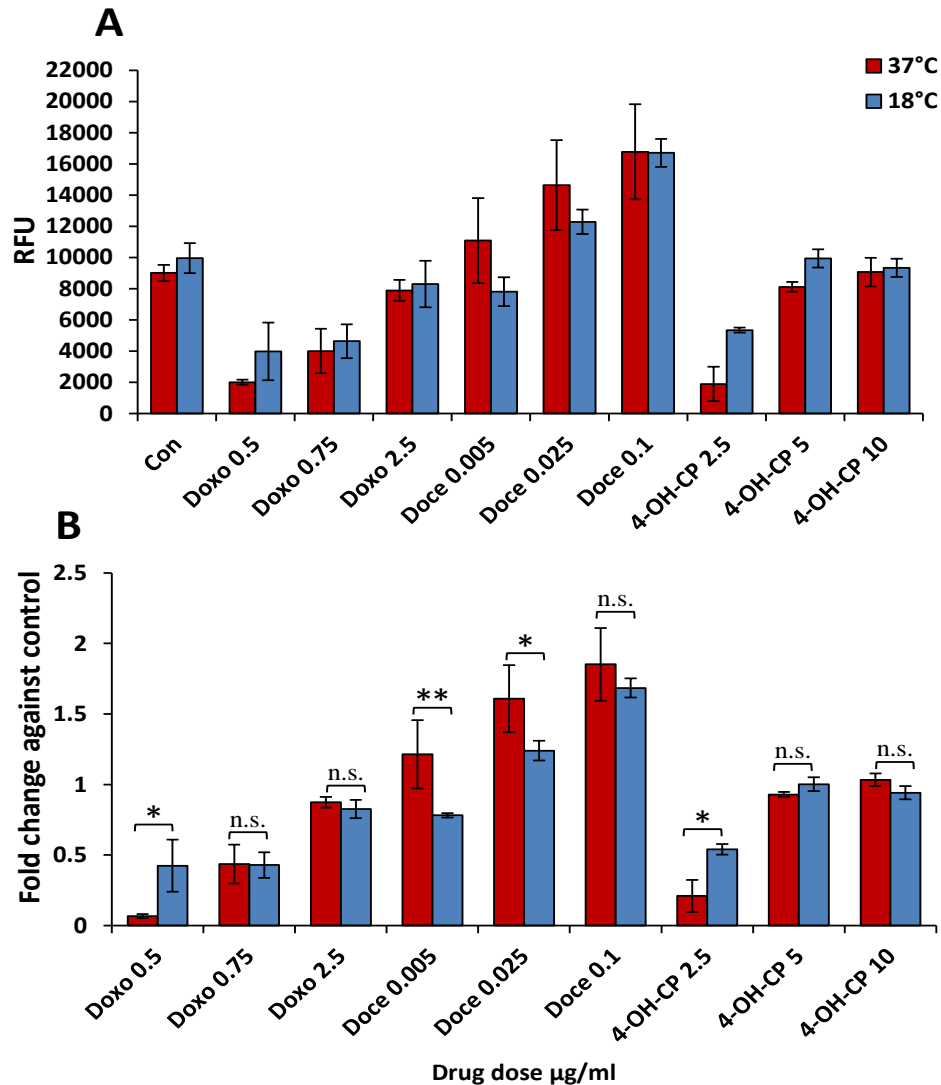


**Figure 5-32 The role of cooling in caspase-3/7 activation induced by chemotherapy drugs in HaCaTa cells after 48h using the Sensolyte assay**

HaCaTa cells were seeded in 96 well plates at 5000 cells/well in KSFM complete medium and were incubated overnight at 37°C / 5% CO<sub>2</sub>. HaCaTa cells were treated for 2h with the indicated dose of doxorubicin (Doxo), docetaxel (Doce) and 4-OH-CP at 37°C and 18°C compared with vehicle control (cells treated with medium containing DMSO, in which the reagent was dissolved). The solvent represents the maximum amount of DMSO corresponding to the highest drug concentration). The drugs were then removed, wells were rinsed with PBS to remove any traces of drug and cultures incubated for a further 48h, after which 50 µL substrate of the Ansapec assay was added. After 60 min incubation in the dark at room temperature, fluorescence was measured using a plate reader. The Relative Fluorescence Units (RFU) readings were deduced as described in Materials and Methods section 2.10.3. **A**) Results are plotted as raw Fluorescence data; **B**) Results are presented as fold change (from raw RFU data used in A) by comparing drug treated cells *versus* controls. Bars correspond to mean values (±S.E.M.) for three independent biological experiments, each consisting of 6-8 technical replicates. n.s., non-significant, \*,  $p < 0.05$ ; \*\*,  $p < 0.01$ .

## 5.12 Detection of DNA fragmentation after HaCaTa cell exposure to chemotherapeutic drugs and assessment of the role of cooling

In addition to the detection of apoptosis by Cytotox-Glo (as a surrogate marker of loss of membrane integrity) and SensoLyte/Anaspec (for the detection of caspase activity), cell death (apoptosis) was also measured by means of a DNA fragmentation ELISA assay (Materials and Methods section 2.10.4). DNA fragmentation detection can be a reliable, well characterised method to assess apoptotic cell death (Shaw *et al.*, 2005), as it detects one of the hallmarks of apoptosis. For the DNA fragmentation assay, staurosporine was used as a positive control. Staurosporine, which is derived from *Streptomyces staurosporeus*, inhibits a range of protein kinases essential for normal cell function and is often used as a positive control of apoptosis induction by the intrinsic apoptotic pathway (*via* MOMP) and leads to caspase-mediated cell death (Zhang *et al.*, 2004). Two types of controls were used in every experiment: positive control of apoptosis induction *via* treatment with 5 $\mu$ M staurosporine and negative control (untreated cells) for each temperature condition (normal *versus* cooling).

The DNA fragmentation assays were performed on HaCaTa cells treated for 2h with 0.5  $\mu$ g/mL doxorubicin, 0.005  $\mu$ g/mL docetaxel and 7.5  $\mu$ g/mL 4-OH-CP at 37°C and 18°C after 24 and 48h. There was a significant increase in DNA fragmentation in cells treated with doxorubicin and docetaxel (and staurosporine) compared to untreated controls, however, there was low level in DNA fragmentation in cells treated with 4-OH-CP at 37°C after 24h (Figure 5-33). Cell treated with doxorubicin showed higher DNA fragmentation than the positive control at 37°C at the same time point (Figure 5-33). The greatest DNA fragmentation was observed at 48h for doxorubicin, docetaxel, and staurosporine. 4-OH-CP, by contrast, induced only a very small increase in DNA fragmentation (Figures 5-33 and 5-34). To evaluate the effects of cooling on the DNA fragmentation cells were exposed to drugs at 18°C. As shown in Figures 5-33 and 5-34, cooling reduced DNA fragmentation significantly compared to cells treated at 37°C at both 24 and 48h.

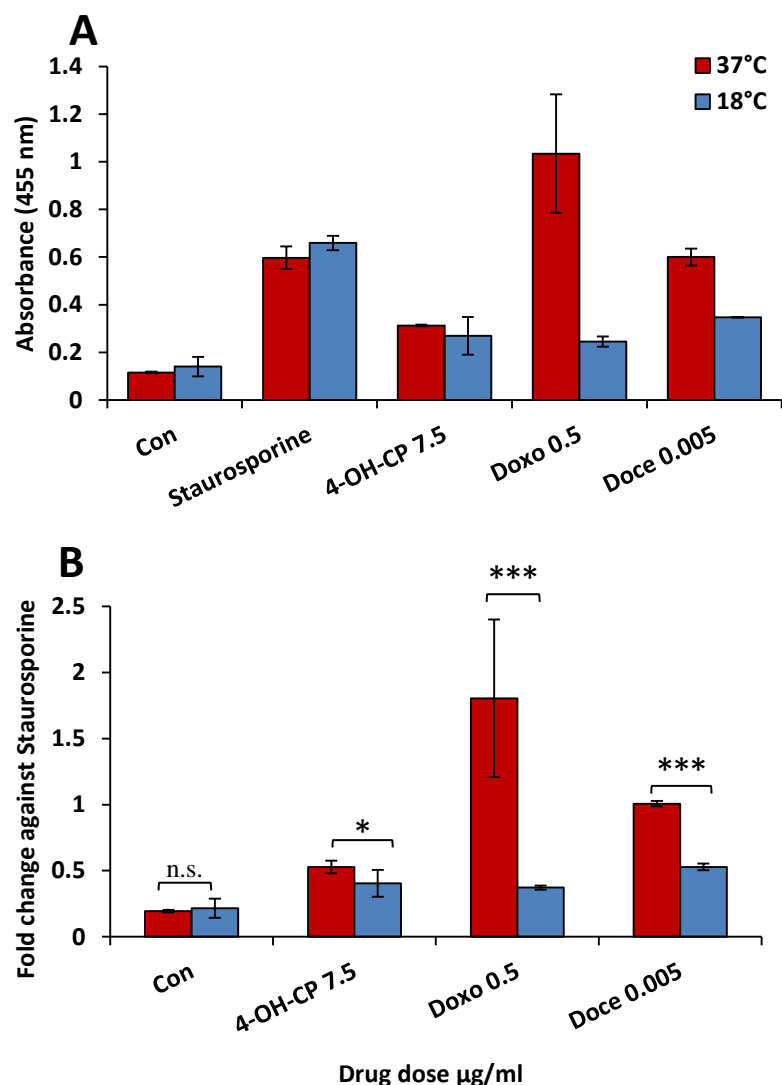


**Figure 5-33 The effect of cooling on DNA fragmentation induced by chemotherapy drugs in HaCaTa cells after 24h using the DNA fragmentation assay**

HaCaTa cells were seeded in 96 well plates at 5000 cells/well in KFSM complete medium and were incubated overnight at 37°C / 5% CO<sub>2</sub>. HaCaTa cells were treated for 2h with the indicated dose of doxorubicin (Doxo), docetaxel (Doce) and 4-OH-CP at 37°C and 18°C compared with vehicle control (cells treated with medium containing DMSO, in which the reagent was dissolved). The solvent represents the maximum amount of DMSO corresponding to the highest drug concentration) was used as negative control and cells were treated with 5 µM staurosporine (positive control). The drugs were then removed; wells were rinsed with PBS to remove any traces of drug. DNA fragmentations were measured after 24h absorbance (455nm) was measured by a plate reader and percentage was calculated as described in Materials and Methods section 2.10.4. **A**) Results are plotted as raw absorbance data, **B**) Result are also presented as fold change by comparing drug treated *versus* positive control. Bars correspond to mean values (±S.E.M.) for three independent biological experiments, each consisting of 3 technical replicates. n.s., non-significant; \*,  $p < 0.05$ ; \*\*\*,  $p < 0.001$ .

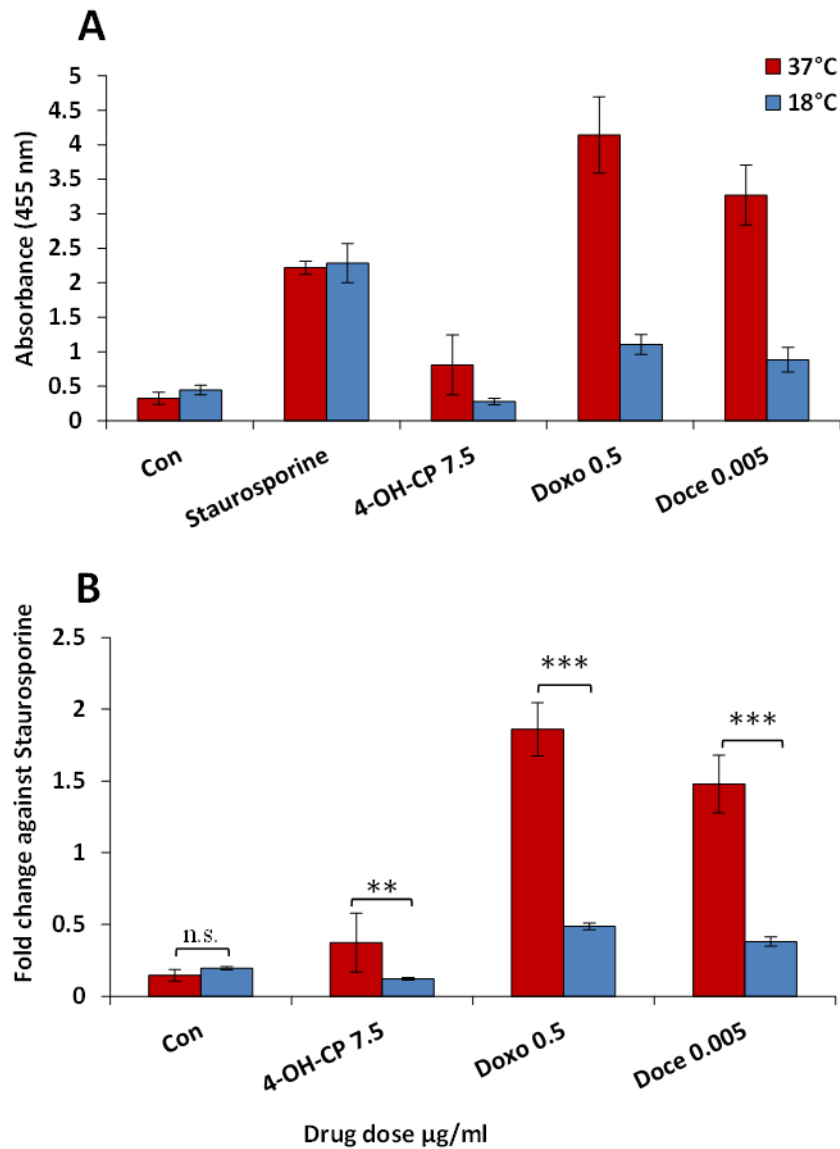


**Figure 5-34 The role of cooling in the inhibition of DNA fragmentation induced by chemotherapy drug in HaCaTa cells after 48h using the DNA fragmentation assay**

HaCaTa cells were seeded in 96 well plates at 5000 cells/well in KSFM complete medium and were incubated overnight at 37°C / 5% CO<sub>2</sub>. HaCaTa cells were treated for 2h with the indicated dose of doxorubicin (Doxo), docetaxel (Doce) and 4-OH-CP at 37°C and 18°C compared with vehicle control compared with vehicle control (cells treated with medium containing DMSO, in which the reagent was dissolved). The solvent represents the maximum amount of DMSO corresponding to the highest drug concentration) was used as negative control and cells were treated with 5 µM staurosporine (positive control). The drugs were then removed; wells were rinsed with PBS to remove any traces of drug. DNA fragmentations were measured after 48h absorbance (455nm) was measured by a plate reader and percentage was calculated as described in Materials and Methods section 2.10.4. **A)** Results are plotted as raw absorbance data, **B)** Result are also presented as fold change by comparing drug treated *versus* positive control. Bars correspond to mean values (±S.E.M.) for three independent biological experiments, each consisting of 3 technical replicates. n.s., non-significant; \*,  $p < 0.05$ ; \*\*\*,  $p < 0.001$ .

## 5.13 Summary

- One of the main objectives of this chapter was to examine the hypothesis that chemotherapy drugs may disrupt mitochondrial membrane potential ( $\Delta\Psi_m$ ) and induce MOMP as well as ROS release as part of their mechanism of cytotoxicity, and whether these changes are altered by cooling, to provide functional evidence for its cytoprotective effect. Moreover, a variety of well-characterised cell apoptosis assays were used to investigate the cytoprotective role of cooling against chemotherapy induced cytotoxicity.
- The cationic and lipophilic dye JC-1 was used to determine the changes in  $\Delta\Psi_m$ . The results showed that the optimal concentration of JC-1 was 2 $\mu$ M in HaCaTa cells treated with 4-OH-CP at 37°C compared with the positive control (cells treated with CCCP (carbonyl cyanide m-chlorophenylhydrazone)).
- 4-OH-CP caused a significant reduction of the red / green ratio (red = polarized mitochondria, green = depolarized mitochondria) in cells at 37°C after 24-48h post treatment.
- Data showed that alterations in mitochondrial membrane potential ( $\Delta\Psi_m$ ) in HaCaTa, NHEK and HHFK cells at physiological temperature (37°C) on the challenge with cytotoxic drugs were significantly reduced when the cells were treated at cooling conditions (22°C and 18°C) during drug exposure. This is the first study showing that cooling provides protection from the change in  $\Delta\Psi_m$  induced by three routinely used chemotherapy drugs.
- HaCaTa cells were more sensitive to the cytotoxic drugs than NHEK and HHFK. For this reason the concentrations of chemotherapy drugs used to treat NHEK and HHFK cells were higher than that used to treat HaCaTa cells.
- Using H2DCFDA as a ROS-detection probe, ROS generation was explored by flow cytometry. The data in this study provide evidence that ROS is a key mediator of doxorubicin induced apoptosis through the mitochondrial pathway in HaCaTa cells. Time-course measurements showed that the maximum response was 30 min after a 2h doxorubicin exposure. However, ROS induced by doxorubicin was inhibited by cooling and this also inhibited apoptosis induced by doxorubicin and thus this further supported the role of ROS in apoptosis. In addition, further cooling of cells to 14°C incrementally reduced further ROS production.
- Results showed that HaCaTa cells treated with 4-OH-CP did not proportionally cause increases in ROS generation after treatment (0-6h). This is not in

accordance with published observations that have reported cyclophosphamide-mediated ROS generation and apoptosis (Abraham and Kanakasabapathy, 2008; Karbowski *et al.*, 1999). It is possible that further experiments might be required to detect ROS increases by 4-OH-CP in keratinocytes (perhaps due to the extremely short ROS life span that could not be detected by H2DCFDA probe).

- Although previous studies reported that docetaxel increased mitochondrial generation of ROS (Mizumachi *et al.*, 2008; Taniguchi *et al.*, 2005); in this study, data did not show a significant induction of ROS apart from a slight increase after 5h post exposure to docetaxel in HaCaTa cells at 37°C.
- Results revealed doxorubicin, docetaxel, 4-OH-CP and 5-FU-mediated cytotoxicity and apoptosis in HaCaTa cells in a dose- and time-dependent manner. No significant increase in cell death was found after 24h in cells treated with doxorubicin, docetaxel, and 4-OH-CP. However, a significant increase of cytotoxicity occurred after 48h at high concentrations of doxorubicin and 4-OH-CP, while cells treated with docetaxel showed high cell death even at low concentrations. This demonstrated cell death occurs after 48h, and that there was a clear dose-response relationship between doxorubicin and 4-OH-CP concentration and number of dead cells.
- The results indicated for the first time that cooling protects from cytotoxicity, reduced caspase-3/7 activity and reduced DNA fragmentation. Doxorubicin showed the highest DNA fragmentation at 37°C after 24 and 48h compared to docetaxel and 4-OH-CP. By contrast, 4-OH-CP showed relatively to the other drugs the least cytotoxicity.
- Overall, the results in this chapter have thus provided a more mechanistic explanation for the cytoprotective effects of cooling (based on biomass detection) reported in previous chapters.

## 5.14 Discussion

### 5.14.1 Cytoprotective properties of cooling against chemotherapy drug-induced mitochondrial damage

The main aim of this work was to the establishment of a model system for the study of pathobiology and management of CIA processed by cooling. A stable mitochondrial membrane potential is essential for mitochondrial function. Lowered membrane potential means less polarization of the mitochondrial membrane and thus an obstacle to the functioning of the respiratory chain and ATP formation. In our study, for the first time we determined that cooling reduced the effects of chemotherapy drugs, by protecting from  $\Delta\Psi_m$  changes and thus increased viability of cells after drug treatment, thus subsequently protecting keratinocytes from apoptosis *in vitro*. Previous reports have demonstrated that, following induction of DNA damage, doxorubicin can cause a collapse of  $\Delta\Psi_m$  and apoptosis in a p53 dependent fashion in cardiac myocytes (L'ecuyer *et al.*, 2006).

Mitochondrial damage results in activation of downstream caspases and apoptosis. The state of the mitochondrial membrane potential ( $\Delta\Psi_m$ ) was measured by the fluorescent cationic dye JC-1 and flow cytometry. Mitochondrial depolarisation is considered an irreversible step in the apoptosis process, which leads to release of apoptogenic factors (Kluck *et al.*, 1997). JC-1 staining measures whether mitochondrial membrane is polarized (viable cells) or depolarized (apoptotic cells) (for an example see (Perry *et al.*, 2011)). The results obtained by JC-1 staining and other apoptosis determination methods were closely similar, supporting the reliability of this method (Salvioli *et al.*, 1997). For these studies, three types of cells were used (HaCaTa, NHEK, and HHFK) at different time points and treated with 4-OH-CP, docetaxel, and doxorubicin to identify the specific changes in the  $\Delta\Psi_m$ .

The present results in keratinocytes showed that the toxicity of chemotherapy drugs at clinically relevant concentrations *in vitro* induced alteration of mitochondrial membrane potential followed by apoptosis. These processes would involve the formation of Bak/Bax channels in the outer mitochondrial membrane (OMM), release of cytochrome c and finally activation of caspases. So far, little is known concerning the molecular mechanism involved in signal transduction and apoptosis at low temperature on chemotherapy treated cells. A previous study showed that treatment with doxorubicin at 32°C in human HeLa cells, and U-2 OS cells, provided protection from doxorubicin-mediated cytotoxicity by suppressing caspase-9 activation and mitochondrial-mediated apoptosis. However, the exact mechanism has not been fully understood (Sakurai *et al.*, 2005). Our data showed a decrease in  $\Delta\Psi_m$  following 24h drug exposure, a further decrease after 36h and maximum MOMP following

48h at 37°C. However, cooling at 22°C showed protection from the  $\Delta\Psi_m$  in HaCaTa cells. Interestingly, cooling at 18°C and even more so at 14°C resulted in better protection from mitochondria  $\Delta\Psi_m$  loss.

The effects of cooling on  $\Delta\Psi_m$  loss induced by 4-OH-CP at 36h and 48h post treatment in HaCaTa, NHEK, and HHFK cells were investigated. The data showed that cooling caused inhibition of 4-OH-CP-mediated  $\Delta\Psi_m$  loss and the maximum levels of restoration of  $\Delta\Psi_m$  were after 48h post treatment at 22°C, 18°C and 14°C. The obtained results indicate that cooling inhibits 4-OH-CP. NHEK and HHFK cells treated with 4-OH-CP at 37°C and 18°C at 48h post-treatment showed essentially the same results as shown in HaCaTa cells. These observations provide molecular evidence for the cytoprotective role of cooling as well as attesting to the fact that HaCaTa cells are a good model to study the cytotoxic effects of drugs clinically associated with CIA *in vitro*.

Apoptosis induced by docetaxel can proceed *via* the mitochondrial pathway, evident by changes in  $\Delta\Psi_m$  as reported elsewhere (Mhaidat *et al.*, 2007). The triggering mechanism is believed to involve changes in the expression of anti- and pro-apoptotic members of the Bcl-2 family (Rowinsky *et al.*, 1992). Analysis of changes in the  $\Delta\Psi_m$  by JC-1 labelling and flow cytometry in HaCaTa cells at 37°C after 36 and 48h post treatment with docetaxel showed that the drug induced loss of  $\Delta\Psi_m$ , as HaCaTa cells treated with docetaxel at 22°C showed a decrease in the percentage of the green cells and an increase in red fluorescence compared to 37°C. Moreover, when cells were treated at 18°C and 14°C they exhibited a significant reduction of green fluorescence, suggesting that cooling protects from mitochondrial 'rupture' induced by docetaxel. These data provided evidence that docetaxel-induced death in HaCaTa, NHEK and HHFK cells involved activation of the mitochondrial pathway, and the cytoprotective effect of cooling relates to its ability to reduce the level of cell death induced by docetaxel.

The observation of the ability of doxorubicin to cause changes in the mitochondrial membrane potential are in agreement with its ability to cause mitochondrial membrane permeability, release of cytochrome c, cell death and ultimately cytotoxicity in keratinocytes (Bedard and Krause, 2007; Fu *et al.*, 2010; Tsang *et al.*, 2003), findings that were confirmed here in chapter 3. Of note, it is clear that there is a correlation between temperature and doxorubicin stimulated intracellular peroxide production (Figure 5-26). Moreover, doxorubicin has been shown to down-regulate Bcl-2 and up-regulate Bax and PUMA as well as causing rupture of mitochondrial membrane, and activation of caspase-9 and 3 (Liu *et al.*, 2008; Nithipongvanitch *et al.*, 2007). In addition, doxorubicin has been shown to simultaneously increase p53 and collapse  $\Delta\Psi_m$ . Our data clearly suggest that cooling significantly reduced

chemotherapy drug-induced  $\Delta\Psi_m$  loss, i.e. it efficiently prevented mitochondrial damage thereby rescuing HaCaTa, NHEK and HHFk cells from drug cytotoxicity.

#### **5.14.2 Effects of cooling on chemotherapy drug-induced ROS generation in HaCaTa cells**

Chemotherapy drugs, such as doxorubicin, are intended to increase ROS levels to induce irreparable damage to cancer cells subsequently resulting in apoptosis (Korkmaz *et al.*, 2007; Wang *et al.*, 2004). As the majority of the drugs tested in this study have been reported to induce oxidative stress in the form of ROS, the hypothesis examined was that an increase in ROS levels would be caused following drug treatment in keratinocytes. The level and timing of ROS production were measured using spectrophotometry and flow cytometry and utilising the oxidation of the detection reagent dichlorofluorescein diacetate (H2DCFDA). It should be noted that the H2DCFDA is a non-specific indicator of ROS levels (Kalyanaraman *et al.*, 2012) and more specific reagents for the detection of individual types of ROS (such as hydrogen peroxide, hydroxyl radicals *etc.*) are commercially available.

In this study, we demonstrated that induction of apoptosis by doxorubicin in HaCaTa cells is mediated *via* mitochondrial death pathway and in association with ROS-generation, a change that could be reduced significantly by cooling. The role of ROS in doxorubicin toxicity was previously reported in several studies including for instance neonatal mouse primary cardiomyocyte cultures (Fu *et al.*, 2010). However, the effects of cooling on doxorubicin-induced ROS generation have not been investigated before. Here for the first time we found that there is a correlation between ROS induced by doxorubicin and cooling. These results support the hypothesis that cooling reduces the intracellular ROS generation in HaCaTa cells. Interestingly, ROS induction by doxorubicin was higher than ROS induced by docetaxel and 4-OH-CP. Furthermore, ROS generation was rapid and the highest level of ROS was observed within 30 min after a 2h treatment with doxorubicin (Figure 5-10).

Many chemotherapy drugs have been shown to produce ROS, yet anthracyclines (e.g., doxorubicin, epirubicin and daunorubicin) generate the highest levels of ROS (Conklin, 2004). Furthermore, a number of reports supported the role of ROS as a mediator of apoptosis and caspase-3 activation (Chung *et al.*, 2003; Yuan *et al.*, 2001). The Bcl-2 family of proteins can regulate the generation of ROS with their elimination from the scavenging system or by preventing the generation of ROS (Chung *et al.*, 2003).

Previous studies suggested that docetaxel induces ROS production (Hung *et al.*, 2015), however, in this study, this induction was very low. This may be due to dose dependent generation and more concentrations might need to be tested. Furthermore, ROS

has a short life span and more optimization might be required to determine the optimal time point of induction. So far, it is not clear what the role of ROS in apoptosis induced by docetaxel is (Cao *et al.*, 2004). Interestingly, cooling at 14°C increased ROS generation compared with at 37°C, which might indicate a stress response evident by the induction of ROS levels. This would be in complete accordance with the induction of p53 activation and up-regulation of p21 demonstrated in this study (see subsequent parts of this Discussion).

Although previous studies showed that cyclophosphamide induced the generation of ROS (Abraham and Kanakasabapathy, 2008; Karbowski *et al.*, 1999), this study showed that 4-OH-CP did not consistently cause increases in ROS generation (Figure 5-25). A slight increase in ROS generation was evident at 30 min after drug treatment at 37°C, however, at 22°C was slightly higher than at 37°C. Further research should be undertaken to investigate the effect of the cooling on ROS generation by 4-OH-CP. The temperature of 18°C was tested and the results showed at 18°C the level of ROS was slightly reduced compared with at 22°C, however, this was not statistically significantly different than the ROS levels at 37°C. The lack of marked ROS induction is in agreement with the observations on docetaxel. Interestingly, once again, at 14°C, the level of ROS generation was higher than at 18°C, perhaps again indicating a stress response to cooling this data suggesting that ROS at cooling samples works as the messenger to induce growth.

Although not all drugs tested showed significant ROS induction, more recent studies in our laboratory have provided evidence that 4-OH-CP can induce ROS in HaCaTa cells (Dunnill and Georgopoulos, unpublished observations produced during the preparation of this thesis). The induction of ROS in human keratinocytes by drugs such doxorubicin and 4-OH-CP could be important in the understanding of CIA and more importantly may provide novel complimentary cytoprotective approaches to treat and prevent chemotherapy-induced hair loss (see subsequent sections).

#### **5.14.3 Chemotherapy drug-induced apoptosis in HaCaTa cells is attenuated by cooling**

Doxorubicin, docetaxel, and cyclophosphamide are chemotherapeutic drugs commonly used for treating metastatic breast cancer (Ho and Mackey, 2014) and they work through different mechanisms (Payne and Miles, 2008). In this study, these drugs were shown to induce varying degrees of cell death in HaCaTa cells. Studying the effect of cooling on drug-mediated apoptosis was important in order to further characterise the molecular mechanisms of cooling-mediated cytoprotection.

This study has extensively used the CellTiter assay, which is based on the same principle as the traditional MTT assay, to assess cell viability. However, it is important to consider that CellTiter assay is based on cellular metabolic activity (Quent *et al.*, 2010) or appropriately reflect induction of cell death in particular. Therefore, in addition to assessing cell viability using CellTiter in keratinocyte cells treated with different chemotherapy drugs, a number of cell death detection assays in particular CytoTox-Glo, a caspase detection assay and DNA fragmentation, were used to assess the cytotoxic effects of chemotherapy drugs on keratinocytes.

Using the CytoTox-Glo assay, we showed that there was a substantial increase in cell death 24h post-exposure to doxorubicin and docetaxel at 37°C; however, this was significantly reduced under cooling conditions (18°C). Initial experiments with cells treated with 2.5, 5 and 10 µg/mL 4-OH-CP showed no significant effects (Figure 5-28) at both temperatures compared with doxorubicin and docetaxel. However, when the protocol was revised and we tested higher 4-OH-CP doses (10 and 30 µg/mL) after 48h post-exposure, a significantly greater cytotoxic effect at 37°C was observed and cooling at 18°C rescued from cell death. These findings provided more evidence that cooling protects cells from cytotoxicity induced by chemotherapeutic drugs by preventing induction of cell death. These observations were extended to 5-FU where cooling caused significant reduction in cell death induced by 5-FU.

Many chemotherapeutic drugs have been developed to control cancer by triggering apoptosis *via* caspases because they play crucial roles in apoptosis. The measurement of caspase activation in cells helps in the understanding of the molecular mechanisms of apoptosis, in addition to the evaluation of the effect of anticancer drugs on apoptotic pathways (Sha *et al.*, 2012). Previous studies have shown that doxorubicin (Luanpitpong *et al.*, 2012), docetaxel (Kolfshoten *et al.*, 2002), and cyclophosphamide (Schwartz and Waxman, 2001) can induce cleavage of executioner caspase-3.

As mentioned in previous sections, apoptotic pathways dependent on caspase inducing apoptosis pathway-specific proteases, associated with the intrinsic and extrinsic pathway, the latter mainly engaging initiator caspase-8 (Hengartner, 2000); these two pathways can often converge downstream of initiator caspases to joint activation of effector caspases (specific executors of apoptosis), in particular caspase-3, as well as caspases-6 and -7 (Green and Kroemer, 1998). The BH3-only protein Bid provides the link between the two pathways, which is activated after caspase-8-mediated cleavage of Bid to tBid (Winter *et al.*, 2014). In this study, tBID was detected after chemotherapy drug treatment in HaCaTa cells (see subsequent sections). The intrinsic apoptotic pathway is the principal pathway of

chemotherapy-induced cell death triggered by formation of the apoptosome (cytochrome c/Apaf-1/caspase-9), which triggers the activation of caspase-3 (Ditsworth *et al.*, 2003; Ricci and Zong, 2006).

Therefore, in addition to the CytoTox-Glo assay, the SensoLyte caspase-3/7 assay was used to further understand drug mediated apoptosis. Activation of caspase-3/7 in HaCaTa cells over a range of drug treatments and the effect of cooling were examined. For the first time caspase-3/7 activation was detected in HaCaTa cells at 37°C, 24h after treatment with chemotherapy drugs. However, under cooling conditions (18°C) there was a significant reduction in caspase-3/7 activation, particularly in the case of doxorubicin and docetaxel. Interestingly the level of caspase-3/7 activation differed between 24 and 48h post treatment, suggesting that the assay more sensitively detected caspase activation at earlier time points, and diminished as cells became late apoptotic / necrotic later on during cell death. Activation of caspase-3/7 occurs after proteolytic cleavage, which leads to a cascade of activation that may occur even earlier than disruption of mitochondria because this process does not require transcription/translation related regulation (Cullen and Martin, 2009) which is in agreement with the observation that caspase-3/7 activation after 48h at 37°C was lower. Importantly, at 18°C less caspase-3/7 activation occurs which is in agreement with the cytoprotective effect of cooling thus resulting in higher cell survival.

Previous studies showed that doxorubicin triggers the intrinsic apoptotic pathway in human keratinocytes and is associated with caspase-9 activation, as shown after treatment of HaCaT cells with doxorubicin, with caspase-9 and caspase-3/7 activation reported (Cullen and Martin, 2009; Luanpitpong *et al.*, 2012). Another study showed that doxorubicin induced caspase-3 in a dose-dependent manner after 24h in HaCaT cells (Sauter *et al.*, 2010). In this study, cooling inhibited doxorubicin-induced apoptosis in HaCaTa cells as demonstrated by the reduction of the activity of caspase-3/7 after 24h post treatment compared with cells treated at 37°C.

Moreover, in HaCaTa cells treated with docetaxel, there was caspase-3/7 activation that was higher than that observed for doxorubicin and 4-OH-CP (Figure 6-4 and 6-5). This relates closely to our findings from experiments where HaCaTa cells were investigated upon exposure to docetaxel for 2h, and docetaxel induced arrest in G2/M and a significantly higher subG0/G1 population (compared to HaCaTa cells treated with doxorubicin and 4-OH-CP), whilst apoptosis induction was evidenced by a decrease of mitochondrial membrane potential. As expected the low concentrations show low activation of caspase-3/7 activation at 18°C compared to 37°C. These results therefore confirmed data from CellTiter and JC-1 assays that cooling protects from cytotoxicity. These findings suggest that docetaxel-

mediated apoptosis occurs *via* a caspase-dependent, although more specific functional experiments (e.g. involving use of caspase inhibitors or RNA interference) would be required to address this.

Our 4-OH-CP results are in agreement with a previous study on cyclophosphamide-induced apoptosis reporting that caspase-9 may be the initiating caspase triggering apoptosis and had an important role in the apoptotic cascade, utilising a caspase-3-dependent pathway (Schwartz and Waxman, 2001). This study showed activation of caspase-3/7 after treatment with 4-OH-CP, which correlated with drug concentration and was attenuated by cooling.

Another hallmark of apoptosis is the induction of DNA fragmentation. Previous studies have shown that doxorubicin can induce DNA fragmentation and cell death after 24h in the breast cancer MCF7 cells (Kim *et al.*, 2006b; Li *et al.*, 2007). Furthermore, it has been previously shown that cyclophosphamide induced caspase-3 activation and DNA fragmentation in murine vascular endothelial cell (Ohtani *et al.*, 2006). To confirm apoptosis induction in HaCaTa cells following drug treatment, DNA fragmentation was detected using a DNA fragmentation ELISA. A higher level of DNA fragmentation was induced by doxorubicin and docetaxel in comparison with 4-OH-CP as detected using this assay, however cooling significantly reduced DNA fragmentation. The lack of significant DNA fragmentation observed here is in agreement with previous studies in MCF-7 cells demonstrating that although morphological apoptotic features were observed following cell treatment with cyclophosphamide, cell death caused by cyclophosphamide (and 5-FU) did not involve DNA-fragmentation (Kugawa *et al.*, 2004). Our findings agree with the result in the above report and thus suggest that death induced by cyclophosphamide might be characterised by a mixture of apoptotic and non-apoptotic features.

Collectively, our CytoTox-Glo assay, caspase-3/7 assay and the DNA fragmentation test data provided clear and consistent evidence that cooling protects cells from drug cytotoxicity apoptosis. This study therefore increased our understanding of the mechanisms *via* which cooling may protect against chemotherapy induced cell damage.

**CHAPTER 6: Investigations on the effects of cooling on  
the activation and functional involvement of key  
intracellular mediators in chemotherapy drug-mediated  
apoptosis in human keratinocytes**

## 6.1 The selective induction of apoptosis as a therapeutic strategy

Most chemotherapy drugs act by inducing apoptosis in treated cells without selectivity. When DNA is damaged by UV irradiation or by chemotherapeutic drugs, the p53 protein is activated and performs a critical role, which includes transcriptional regulation of a wide range of genes. Such p53-responsive genes include the gene *WAF1/CIP1/p21*, which is a classical cyclin-dependent kinase inhibitor, thus capable of blocking the cell cycle to allow the cell to repair its DNA (Bai and Zhu, 2006). If the DNA damage exceeds the ability of cellular repair mechanisms, apoptosis is induced as a result of the up-regulation and subsequent activation of apoptosis-associated signalling proteins; in this case, active (phosphorylated) p53 activates the mitochondrial pathway of apoptosis which leads to "suicide" of the cell experiencing genotoxic damage (Bai and Zhu, 2006).

## 6.2 Control of DNA damage responses by p53: regulation of cell cycle and induction of apoptosis

As the "guardian of the genome", the transcription factor p53 has a critical role in controlling the integrity of the genome prior to (and after) DNA replication. The level of p53 protein is low in normal cells, owing to the very short half-life of the protein and expression of p53 is monitored continuously by the MDM2 protein, which is an ubiquitin ligase that binds to p53 and leads to its degradation by the proteasome (Sakurai *et al.*, 2005). When the genome undergoes alterations, the binding between p53 and MDM2 is inhibited by different post-translational mechanisms and p53 accumulates, inducing expression of its target genes (Slee *et al.*, 2004). p53 levels within cells rise dramatically in response to stress signals, such as the application of chemotherapy drugs. p53-inducible genes can be generally placed into two groups: a) those induced rapidly after low levels of stress (generally cell-cycle arrest) such as p21; b) those that are induced by higher levels of p53/stress, such as the pro-apoptotic genes whose promoters contain p53-binding sites (generally apoptotic targets) such as Bax, DR5, Fas, PUMA, and Noxa. Stopping the cycle permits DNA repair and repression of p53 (Sablina *et al.*, 2005; Slee *et al.*, 2004). Apoptosis is triggered when, for instance, Bax, PUMA, and Noxa localize to the mitochondria and promote the loss of  $\Delta\Psi_m$  (MOMP) and release of cytochrome c, resulting in the formation of the apoptosome complex (Bai and Zhu, 2006; Nakano and Vousden, 2001) and subsequent activation of initiator caspase-9. Moreover, induced ROS production subsequently caused mitochondrial dysfunction and initiate apoptosis (Polyak *et al.*, 1997). Previous studies showed that mouse embryo fibroblasts lacking Noxa or PUMA are resistant to apoptotic death in response to

DNA damage, a process known to be mediated by p53 (Shibue *et al.*, 2003; Yu and Zhang, 2003).

### 6.3 Mechanisms of action of the Bcl-2 family members

The Bcl-2 family of proteins regulate MOMP (i.e. permeabilization of the OMM) and are critical regulators of apoptosis and each protein has a role to play in the apoptotic process (Billen *et al.*, 2008). The Bcl-2 family is subdivided to anti-apoptotic, such as Bcl-XL and Bcl-w, containing four regions of homology with Bcl-2 (BH regions 1–4) and the pro-apoptotic Bcl-2 family proteins. The pro-apoptotic proteins can be divided into the multi-BH-domain (BH regions 1–3 proteins), such as Bax and Bak, and the activator BH3-only proteins such as Bid, Bim and Puma, which can directly induce Bax/Bak to cause MOMP (Kim *et al.*, 2006a) and these proteins can be seized by anti-apoptotic proteins. The second subgroup, which is termed sensitizer BH3-only proteins, such as Bad, Noxa, Bmf, Hrk, as they induce apoptosis by binding to anti-apoptotic proteins to release the activator BH3-only proteins (Letai *et al.*, 2002) or activated Bax and Bak (Willis *et al.*, 2005). Of note, the death receptor-mediated apoptosis pathway can also be regulated by p53, as p53 can induce expression of DR5 (TRAIL receptor 1), Fas and PIDD (Takimoto and El-Deiry, 2000). Previous studies demonstrated that p53 activation is essential in chemotherapy-induced alopecia (CIA) in mice (Botchkarev *et al.*, 2000). Also *in vivo* studies showed that a chemical inhibitor of p53 decreased the toxicity of chemotherapy drugs (Komarov *et al.*, 1999). These findings suggest that local pharmacological inhibition of p53 may be useful in preventing CIA.

Bcl-2 family members interact with each other, forming homodimers or heterodimers. The relative amount of each protein in the cell determines the sensitivity to a death signal (Adams and Cory, 1998). A large majority of members of this protein family contains a hydrophobic carboxy-terminal domain, which is predicted to allow them to anchor to a variety of cell membranes such as to the cytoplasmic face of the outer mitochondrial membrane (OMM), the endoplasmic reticulum (ER) and nuclear membranes (Torrecillas *et al.*, 2007). The pattern of membrane localization differs among the anti- and pro-apoptotic proteins. For example, Bax is kept inactive in the cytosol of healthy cells by association with 14-3-3 proteins and Ku-70, and only anchored to the outer membrane of the mitochondria (OMM) upon activation (Petros *et al.*, 2004; Tsuruta *et al.*, 2004). By contrast, Bak is located in the OMM where it is maintained in an inactive monomeric state *via* its interaction with VDAC2 protein (Cheng *et al.*, 2003; Willis *et al.*, 2005). Moreover each of BH3-only proteins resides in a distinct cellular compartment and meets a specific apoptotic stimulus (Lomonosova and Chinnadurai, 2008; Opferman and Korsmeyer, 2003). Following an apoptotic stress, they head to the mitochondria where they interact with multi-BH-domain proteins (BH regions 1–3

proteins). Some BH3 proteins interact with proapoptotic proteins Bax and Bak to activate, others with anti-apoptotic proteins Bcl-2 and Bcl-x L to inactivate, and some would be able to interact with pro- and anti-apoptotic members (Strasser, 2005).

## 6.4 Hypothesis and Specific Aims

Clinical application of scalp cooling during chemotherapy drug administration can show good efficacy in the clinic (Breed *et al.*, 2011) and results in this study have shown that cooling can protect cells from cytotoxicity of chemotherapy drugs *in vitro*. However, the molecular mechanisms underlying the protective effects of cooling remain unknown, as no such studies have been performed *in vitro*. For this purpose, the mechanism of doxorubicin, docetaxel, and 4-OH-CP-induced apoptosis was investigated in normal and cooling conditions. Previous reports have demonstrated that chemotherapy drugs stimulate apoptosis in the HFs (Botchkarev, 2003; Botchkarev *et al.*, 2000), whilst a number of cell cycle arrest- and apoptosis-associated genes induced by genotoxic signals are up-regulated by p53. Thus, the work in this chapter aimed to investigate whether p53 itself and p53-regulated proteins are induced by the panel of chemotherapy drugs tested in this study and whether cooling may interfere with this process, in order to understand a) the mechanisms of drug cytotoxicity and b) provide a molecular explanation for the cytoprotective effect of cooling.

To study such intracellular mediators, the work employed immunoblotting (Western blotting) following preparation of whole cell lysates. This was a challenge as it required a high number of cells for the preparation of such lysates, hence it was particularly challenging in the case of studying primary cells NHEK and HHFk as a model (due to their limited life-span only limited amounts of cell lysate could be prepared). Therefore, although lysates from NHEK and particularly HHFk cells were tested for confirmatory purposes, for most of the experiments HaCaTa cells were used for investigating the effect of chemotherapy-induced cytotoxicity and the effect of cooling on the expression of these proteins. Moreover, as it was essential to ensure that equal loading could be achieved for both 37°C and for cooling conditions, as a loading control, the housekeeping protein  $\beta$ -actin was used.

The experiments examined the levels of intracellular signalling mediators and pro-apoptotic protein expression following treatment with 5  $\mu$ g/mL 4-OH-CP, 0.5  $\mu$ g/mL doxorubicin, and 0.01  $\mu$ g/mL docetaxel at 37°C and under cooling conditions (22°C, 18°C, and 14°C) at different time points post drug treatment. Controls involved keratinocyte cultures after 24h of seeding and incubation in drug-free medium.

**The specific objectives of this chapter were to study:**

- The molecular mechanisms underlying cell cytotoxicity and the effects of cooling in keratinocyte lines HaCaTa (mainly), NHEK and HHFK
- p53 regulation after exposure of keratinocytes to doxorubicin, docetaxel, and 4-OH-CP at 37°C and if cooling had an effect on this regulation at different time points
- Cooling effects on p53 target genes involved in chemotherapy-induced cell cycle arrest or apoptosis such as p21 and the pro-apoptotic proteins PUMA, Noxa, Bax, Bak, tBid, TRAIL, and FasL.
- To employ a specific blocking monoclonal antibody for blockade of the FasL (CD95 ligand) to determine if p53-dependent apoptosis after DNA damage is mediated by CD95 signalling.
- To utilise the small-molecule pharmacological inhibitor pifithrin- $\alpha$  (PFT- $\alpha$ ) to inhibit p53 function and whether it might be useful in preventing or at least reducing the toxicity triggered by the chemotherapy drugs.

## 6.5 Regulation of p53 activation in human keratinocytes after chemotherapy drug treatment at 37°C and the effect of cooling

This is the first study to explore the effects of cooling on the expression of intracellular signalling proteins following chemotherapy drug treatment in human keratinocytes. In response to DNA damage, accumulation of activated, i.e. phosphorylated-p53 (which from here onwards will be denoted P-p53) is often detected, as part of the well-established relation between DNA damage and p53 activation.

To clarify the molecular mechanism underlying chemotherapy drug-induced keratinocyte death, HaCaTa cells were used and immunoblotting experiments performed to assess whether functional p53 is up-regulated after 5 µg/mL 4-OH-CP, 0.5 µg/mL doxorubicin and 0.01 µg/mL docetaxel treatment at 37°C. To determine the effects of cooling on drug-mediated p53 activation, cells were treated with chemotherapy drugs at 22°C, 18°C, and 14°C. Protein expression was measured at different time-points (6, 12, and 24h) by Western blotting and results shown in Figures 6-1 to 6-4. The concentrations of chemotherapy drugs chosen for treatment were those which showed a correlation with reducing the temperature, as the biomass was increased with further reduction of temperature; as shown in HaCaTa cells treated with 4-OH-CP, doxorubicin and docetaxel, cell biomass increased with decreasing temperature. The drug concentration chosen was the one that demonstrated optimal protection in correlation with decreasing temperature conditions (see Appendix V).

The results showed that activated P-p53 protein expression was low in untreated cells (controls) at all temperature conditions (Figure 6-1). On the other hand, 5 µg/mL 4-OH-CP-treated HaCaTa cells exhibited a strong induction of P-p53 which was rapid (already evident at 6h after treatment) compared with controls and continued to rise up to the 24h time point. p53 activation was visualised by detection of its phosphorylation at residue Ser-15 (Iyer *et al.*, 2004). P-p53 levels dramatically decreased in cells treated under cooling conditions, especially after 24h compared to p53 level at 37°C. Strikingly, the response appeared to be incremental and temperature-dependent, as the levels of P-p53 decreased proportionally to and in parallel with the gradual reduction of the temperature, as decreasing the temperature from 22°C to 14°C caused a gradual decrease of P-p53 protein levels (see Figure 6-1A, B and C).

For confirmatory purposes and to determine whether the effects of 4-OH-CP demonstrated in HaCaTa cells also occur in NHEK and HHFK primary cells, such cultures were also treated with 4-OH-CP. However, the concentration of 4-OH-CP used to treat

primary cells was 10 µg/mL, thus higher than the doses used in HaCaTa cells (as mentioned previously, HaCaTa cells were more sensitive to 4-OH-CP than NHEK and HHFK cells (Chapter 3). Cell cultures incubated at 37°C were compared with 18°C as representative cooling conditions. As shown in Figure 6-2A the expression of P-p53 in NHEK was up-regulated as early as 6h following treatment with 4-OH-CP and continued to rise up to the 24h time point, which was similar to our observations in HaCaTa cells. Next, the effect of 4-OH-CP in HHFK was assessed using the same drug concentrations used with NHEK cells; the results showed that P-p53 levels at 37°C were higher than 18°C, with the most prominent down-modulation of P-p53 expression, as in both HaCaTa and NHEK, being observed after 12h of exposure to 4-OH-CP (Figure 6-2B).

To extend the above observations, we then investigated p53 activation in HaCaTa cells treated with 0.5 µg/mL doxorubicin. As seen in Figure 6-3, doxorubicin induced P-p53 at 37°C compared with control untreated cells, however, the level of P-p53 was reduced at 22°C (compared to 37°C) and a similar result was shown at 18°C. However, there was no substantial reduction at 18°C in comparison to 22°C (Figure 6-3A and B). The most striking effect was observed when cells were treated at 14°C as they showed a dramatic reduction in P-p53 levels at all-time points and particularly after 12h (Figure 6-3C).

In order to evaluate the possibility of docetaxel-mediated induction of P-p53, HaCaTa cells were exposed to 0.01 µg/mL of docetaxel in similar time-course experiments. As shown in Figure 6-4, there was an induction in P-p53 levels at 37°C in comparison to controls, but cooling at 22°C, 18°C, or 14°C down-modulated expression, with 14°C showing the lowest level of P-p53 after 12h and 24h compared with all other temperatures.

These results show that all three chemotherapy drugs (whether classical genotoxic agents, such as doxorubicin and 4-OH-CP, or an anti-mitotic compound, docetaxel) initiated a DNA damage response evident by the activation of p53 and that cooling inhibited this in a temperature-dependent fashion.

**4-OH-CP**  
**HaCaTa cells**

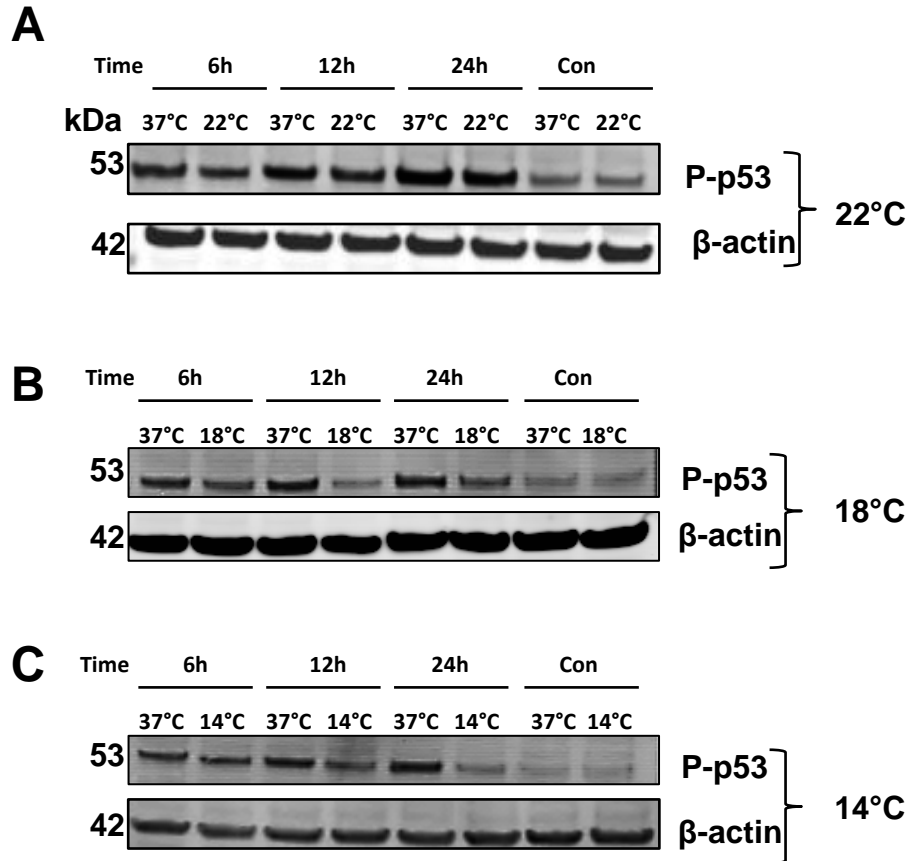


**Figure 6-1 The role of temperature on the regulation of P-p53 expression in response to 4-OH-CP in HaCaTa cells**

$9 \times 10^5$  HaCaTa cells were seeded in 10 cm<sup>2</sup> culture dishes in KSFM complete medium and the cells were incubated overnight in 37°C/5% CO<sub>2</sub>. Cells were treated with 5 µg/mL 4-OH-CP at 37°C as well as 22°C, 18°C and 14°C. 6, 12, and 24h after treatment, the cells were lysed 2X SDS-lysis buffer. 20 µg/well of lysate was separated by SDS-PAGE using 4-12% (W/V) Bis Tris gels and blotted onto a PVDF membrane. The membrane was probed overnight with an anti-P-p53 antibody in TBS Tween 0.1% (1:1000 dilution). Following that, the membrane was incubated for 1h with Goat anti-Rabbit IgG IRDye 800nm (1:10000 dilution). β-actin (AC-15-A5441) was used as specificity and loading control, the membrane was incubated with the antibody (1:50000 dilution) and secondary antibody Goat anti-Mouse IgG Alexa 680 (1:10000 dilution). Membranes were scanned at 700nm and 800nm on a Licor Odyssey Infra-Red Imaging system and images are shown in black and white. Cells were treated at **A**) 37°C and 22°C, **B**) 37°C and 18°C, **C**) 37°C and 14°C. Data obtained from two independent biological experiments.

## 4-OH-CP

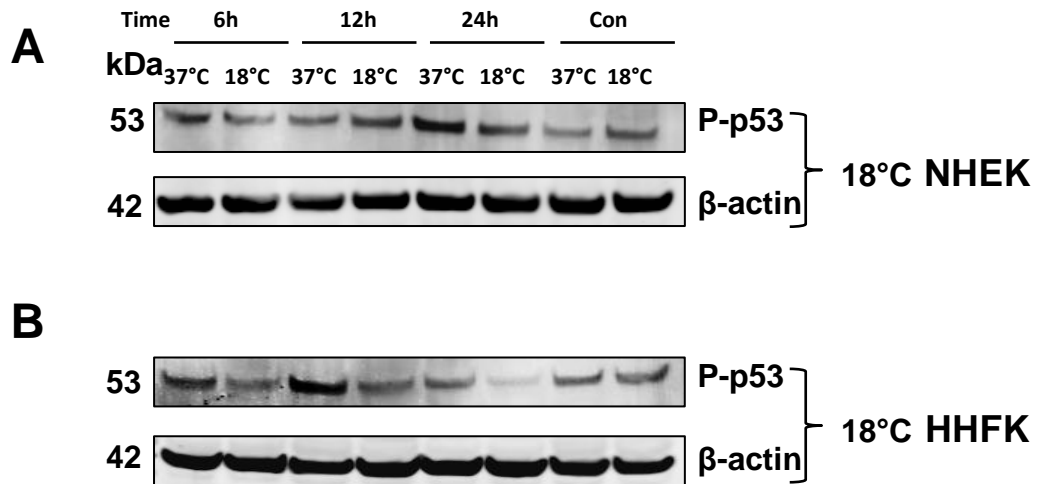


**Figure 6-2 The role of temperature on the regulation of P-p53 expression in response to 4-OH-CP in primary keratinocytes**

9x10<sup>5</sup> HHFK and NHEK cells (passages 1–3) were seeded in 10 cm<sup>2</sup> culture dishes in KSFM medium and the cells were incubated overnight in 37°C/5% CO<sub>2</sub>. NHEK and HHFK cells were treated with a 10 µg/mL 4-OH-CP at 37°C and 18°C. 6, 12, and 24h after treatment, the cells were lysed 2X SDS-lysis buffer. The total protein loading 20 µg/well of lysate was separated by SDS-PAGE using 4-12% (W/V) Bis Tris gels and immunoblotted onto a PVDF membrane. The membrane was probed overnight with an anti-P-p53 antibody in TBS Tween 0.1% (1:1000 dilution). The membrane was incubated for one hour with Goat anti-Rabbit IgG IRDye 800nm (1:10000 dilution). β-actin (AC-15-A5441) was used as specificity and loading control, the membrane was incubated with the antibody diluted at 1:50000 and secondary antibody goat-anti mouse IgG Alexa 680 diluted 1:10000. Membranes were scanned at 700nm and 800nm on Licor Odyssey Infra-Red Imaging system and images are shown in black and white. **A**) NHEK cells were treated at 37°C and 18°C, **B**) HHFK cells were treated at 37°C and 18°C. Data obtained from two independent biological experiments.

**Doxorubicin  
HaCaTa cells**

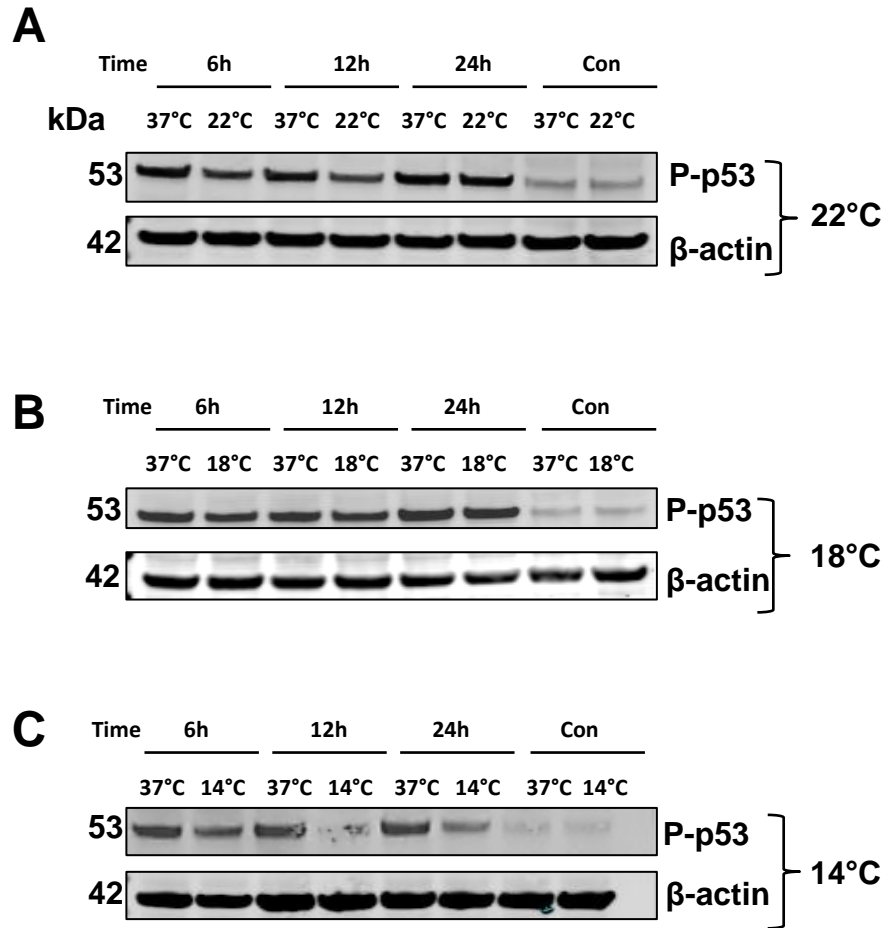


**Figure 6-3 The role of temperature on the regulation of P-p53 expression in response to doxorubicin in HaCaTa cells**

$9 \times 10^5$  HaCaTa cells were seeded in 10 cm<sup>2</sup> culture dishes in KSM complete medium and the cells were incubated overnight in 37°C/5% CO<sub>2</sub>. Cells were treated with 0.5 µg/mL doxorubicin at 37°C as well as 22°C, 18°C and 14°C. 6, 12, and 24h after treatment, the cells were lysed 2X SDS-lysis buffer. 20 µg/well of lysate was separated by SDS-PAGE using 4-12% (W/V) Bis Tris gels and blotted onto a PVDF membrane. The membrane was probed overnight with an anti-P-p53 antibody in TBS Tween 0.1% (1:1000 dilution). Following that, the membrane was incubated for 1h with Goat anti-Rabbit IgG IRDye 800nm (1:10000 dilution). β-actin (AC-15-A5441) was used as specificity and loading control, the membrane was incubated with the antibody (1:50000 dilution) and secondary antibody Goat anti-Mouse IgG Alexa 680 (1:10000 dilution). Membranes were scanned at 700nm and 800nm on a Licor Odyssey Infra-Red Imaging system and images are shown in black and white. Cells were treated at **A**) 37°C and 22°C, **B**) 37°C and 18°C, **C**) 37°C and 14°C. Data obtained from two independent biological experiments.

**Docetaxel  
HaCaTa cells**

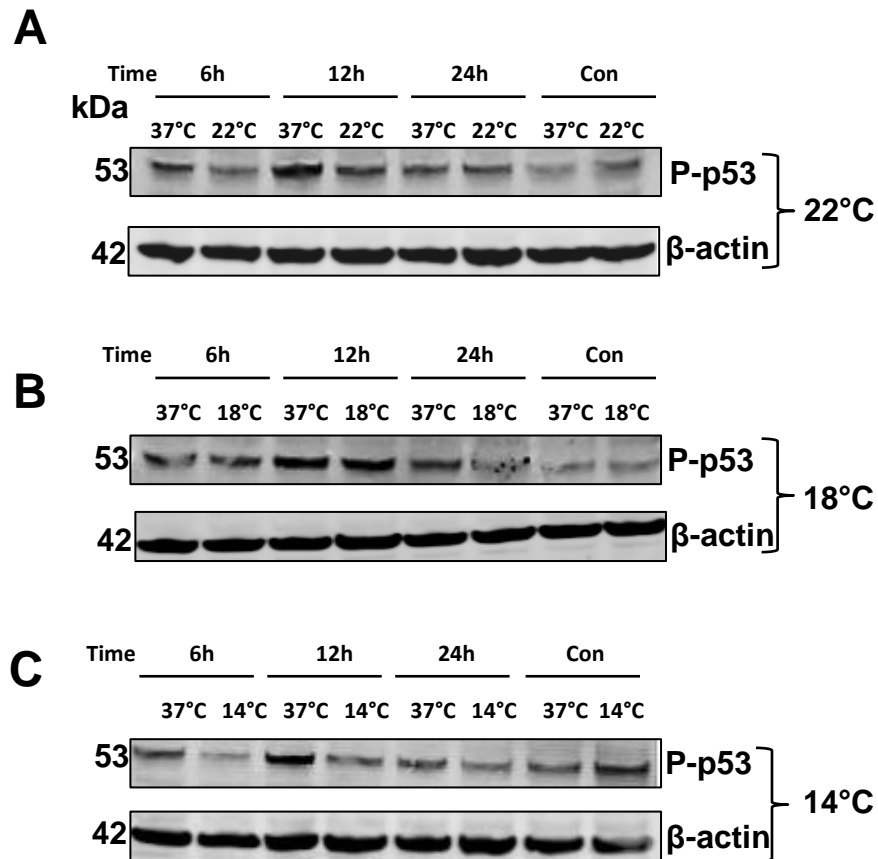


**Figure 6-4 The role of temperature on the regulation of P-p53 expression in response to docetaxel in HaCaTa cells**

$9 \times 10^5$  HaCaTa cells were seeded in 10 cm<sup>2</sup> culture dishes in KSFM complete medium and the cells were incubated overnight in 37°C/5% CO<sub>2</sub>. Cells were treated with 0.01 µg/mL docetaxel at 37°C as well as 22°C, 18°C and 14°C. 6, 12, and 24h after treatment, the cells were lysed 2X SDS-lysis buffer. 20 µg/well of lysate was separated by SDS-PAGE using 4-12% (W/V) Bis Tris gels and blotted onto a PVDF membrane. The membrane was probed overnight with an anti-P-p53 antibody in TBS Tween 0.1% (1:1000 dilution). Following that, the membrane was incubated for 1h with Goat anti-Rabbit IgG IRDye 800nm (1:10000 dilution). β-actin (AC-15-A5441) was used as specificity and loading control, the membrane was incubated with the antibody (1:50000 dilution) and secondary antibody Goat anti-Mouse IgG Alexa 680 (1:10000 dilution). Membranes were scanned at 700nm and 800nm on a Licor Odyssey Infra-Red Imaging system and images are shown in black and white. Cells were treated at **A**) 37°C and 22°C, **B**) 37°C and 18°C, **C**) 37°C and 14°C. Data obtained from two independent biological experiments.

## 6.6 The p53 inhibitor pifithrin- $\alpha$ (PFT- $\alpha$ )

Previous studies have shown that PFT- $\alpha$  is a compound that inhibits the translocation of p53 to mitochondria and the nucleus, as a result of which it inhibits the binding of p53 to specific DNA sites and also suppresses the apoptotic cascade (Chou *et al.*, 2011; Culmsee *et al.*, 2001). To support a direct role of p53 activation in the cytotoxic responses observed after treatment with chemotherapeutic agents at 37°C and in response to cooling conditions, p53 function was blocked using the specific p53 inhibitor PFT- $\alpha$ . The aim was to determine whether p53 mitochondrial function blockade could help reduce the effects of chemotherapy drug treatment and also, ultimately, if we could improve the function of cooling for some drugs which poorly respond to cooling-mediated protection and whether improvement could be achieved also for combinations of drugs. To determine the optimal concentration of PFT- $\alpha$ , pre-titration experiments were performed; HaCaTa cells were treated with different concentrations of PFT- $\alpha$  at 37°C (Figure 6-5). These experiments showed that there was a slight toxicity in cells treated with PFT- $\alpha$  at concentration over 15-20  $\mu\text{g/mL}$  compared with untreated cells (controls).

The ability of PFT- $\alpha$  to protect keratinocytes from cytotoxicity caused by 4-OH-CP (1 and 2.5  $\mu\text{g/mL}$ ) was then investigated and p53 was blocked with the protective effect of PFT- $\alpha$  concentrations (0.5 and 1  $\mu\text{g/mL}$ ). As shown in Figure 6-6, there was increased biomass (and hence cytoprotection) in cells treated with 4-OH-CP in the presence of PFT- $\alpha$  compared with controls. However, the cytoprotective effects were relatively modest and PFT- $\alpha$  did not fully block cytotoxicity, yet previous studies have reported that PFT- $\alpha$  can completely block the cytotoxic effects of UV and a range of cytotoxic drugs in HCT116 cells (Sohn *et al.*, 2009). To exclude the possibility that lack of complete blockade of cytotoxicity was not because the concentrations used were not enough (in comparison to other studies), with a small range of concentrations PFT- $\alpha$  concentrations was assessed and 0-20  $\mu\text{g/mL}$  PFT- $\alpha$  concentrations were tested against 1  $\mu\text{g/mL}$  of 4-OH-CP. The result showed there was a slight increase in biomass for cells treated with PFT- $\alpha$  compared with cells treated with 4-OH-CP alone (Figure 6-7).

To extend our observations to more chemotherapy drugs, the possibility that PFT- $\alpha$  may protect from cytotoxicity induced by doxorubicin was investigated. However, surprisingly, the result showed that PFT- $\alpha$  did not block yet instead increased doxorubicin-induced cytotoxicity (Figure 6-8) or caused no detectable protection for lower drug doses (Figure 6-9). These findings suggest that p53 inhibition by PFT- $\alpha$  might not represent an adequately efficient (or even at all appropriate) tool to enhance the protective effect of cooling against cytotoxic drugs.

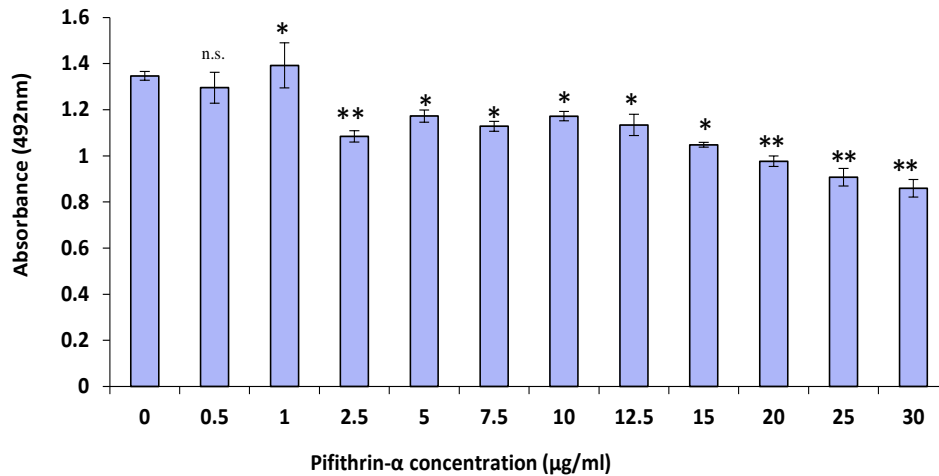


**Figure 6-5 Viability of HaCaTa cells after incubation with Pifithrin-  $\alpha$  (PFT- $\alpha$ )**

HaCaTa cells were seeded in 96 well plates at 5000 cells/well in KSFM medium and were incubated overnight at 37°C/ 5% CO<sub>2</sub>. HaCaTa cells were incubated with a range of concentrations of the PFT- $\alpha$ , compared with vehicle control (cells treated with medium containing DMSO, in which the reagent was dissolved. The solvent represents the maximum amount of DMSO corresponding to the highest drug concentration). The drugs were then removed, wells were rinsed with PBS to remove any traces of drug and cultures incubated for a further 72h, and after which 20  $\mu\text{L}$  of CellTiter 96® AQueous One solution was added to the wells and plates were incubated at 37°C in 5% CO<sub>2</sub> for a total of four hours. Bars correspond to mean absorbance at 492 nm ( $\pm$ S.E.M.) for three independent biological experiments, each consisting of 6–8 technical replicates. n.s., non-significant; \*,  $p < 0.05$ ; \*\*,  $p < 0.01$ .

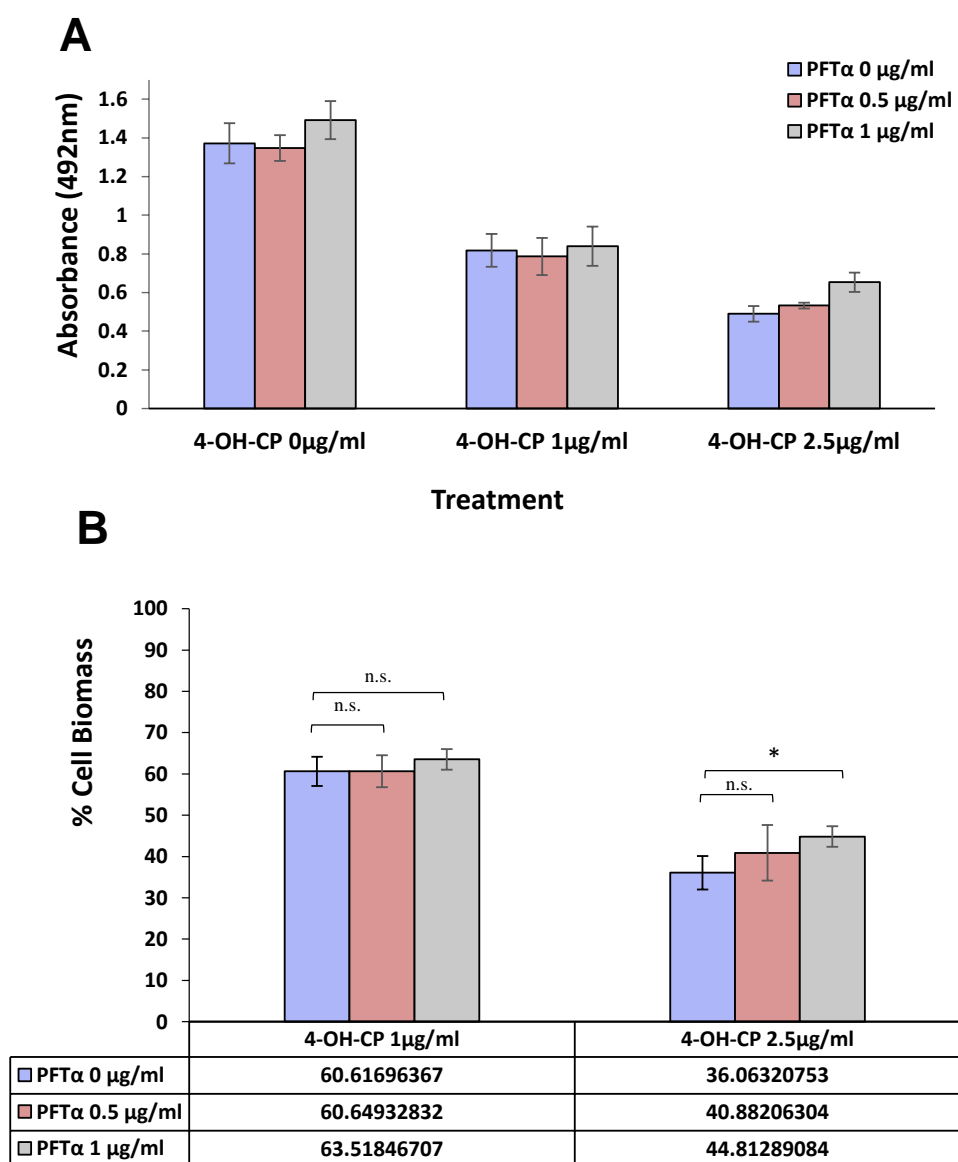


**Figure 6-6 Protection against 4-OH-CP drug cytotoxicity by lower concentrations of PFT- $\alpha$  in HaCaTa**

HaCaTa cells were seeded in 96 well plates at 5000 cells/well in KSFM medium and were incubated overnight at 37°C/ 5% CO<sub>2</sub>. HaCaTa cells were pre-treated with and without 0-1 µg/mL PFT- $\alpha$  for 30 min at 37°C. HaCaTa cells were treated for 2h with 1 and 2 µg/mL 4-OH-CP with and without PFT- $\alpha$  at 37°C compared with vehicle control (cells treated with medium containing DMSO, in which the reagent was dissolved). The solvent represents the maximum amount of DMSO corresponding to the highest drug concentration). The drugs were then removed, wells were rinsed with PBS to remove any traces of drug and cultures incubated for a further 72h, and after which 20 µL of CellTiter 96® AQueous One solution was added to the wells and plates were incubated at 37°C in 5% CO<sub>2</sub> for a total of four hours. Data is presented as **A**) Absorbance (raw data) **B**) % cell biomass shown in a bar graph. Data points correspond to mean % cell biomass ( $\pm$ S.E.M.) for three independent biological experiments, each consisting of 6–8 technical replicates. n.s., non-significant; \*,  $p < 0.05$ .

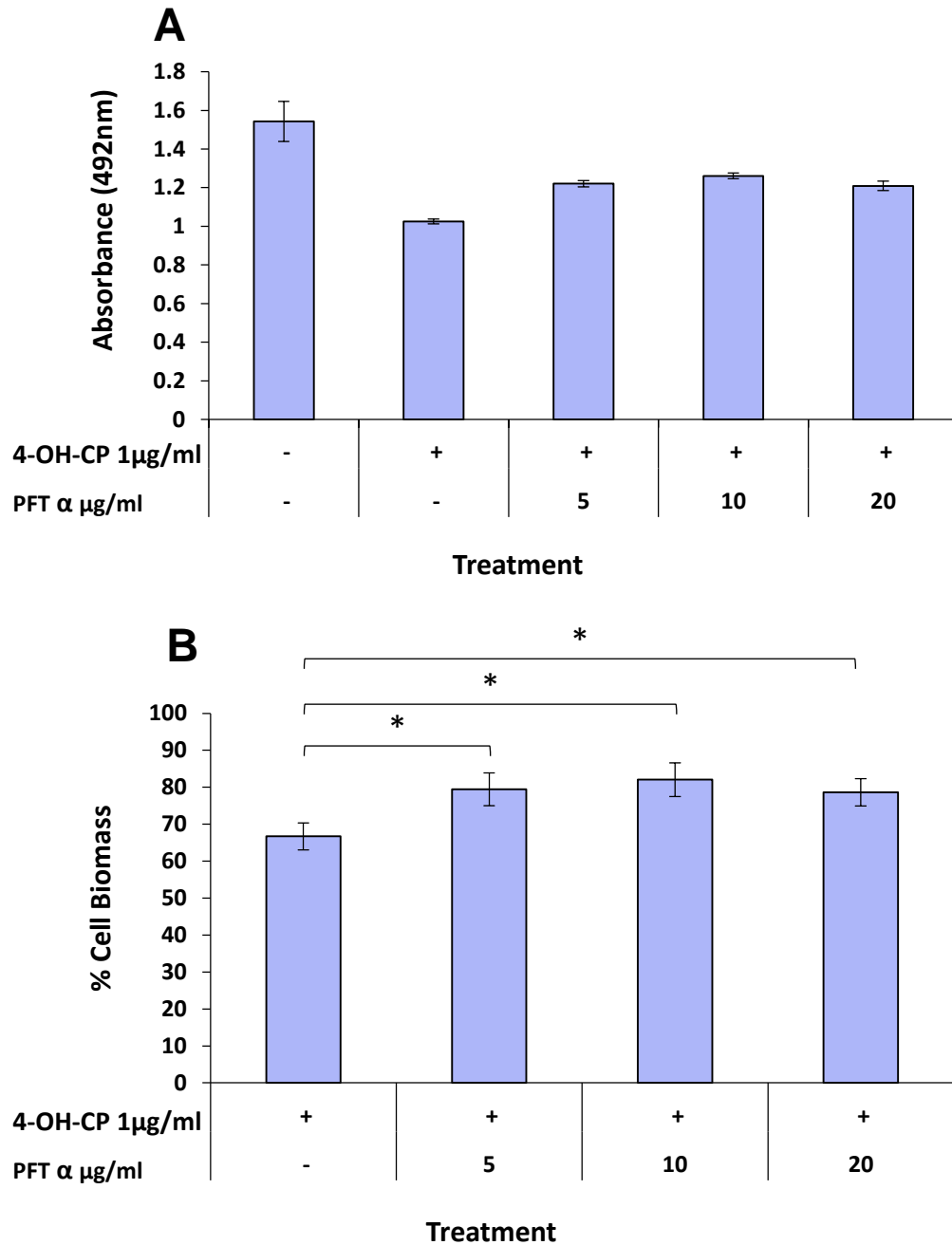


**Figure 6-7 : Protection against 4-OH-CP drug cytotoxicity by PFT-α in HaCaTa cells**

HaCaTa cells were seeded in 96 well plates at 5000 cells/well in KSFM medium and were incubated overnight at 37°C/ 5% CO<sub>2</sub>. HaCaTa cells were pre-treated with and without 0-20 μg/mL PFT-α for 30 min at 37°C. HaCaTa cells were treated for 2h with 1 μg/mL 4-OH-CP with and without PFT-α at 37°C compared with vehicle control (cells treated with medium containing DMSO, in which the reagent was dissolved). The solvent represents the maximum amount of DMSO corresponding to the highest drug concentration). The drugs were then removed, wells were rinsed with PBS to remove any traces of drug and cultures incubated for a further 72h, and after which 20 μL of CellTiter 96® AQueous One solution was added to the wells and plates were incubated at 37°C in 5% CO<sub>2</sub> for a total of four hours. Data is presented as **A**) Absorbance (raw data) **B**) % cell biomass shown in bar graph. Data points correspond to mean % cell biomass (±S.E.M.) for three independent biological experiments, each consisting of 6–8 technical replicates. \*, *p* < 0.05.

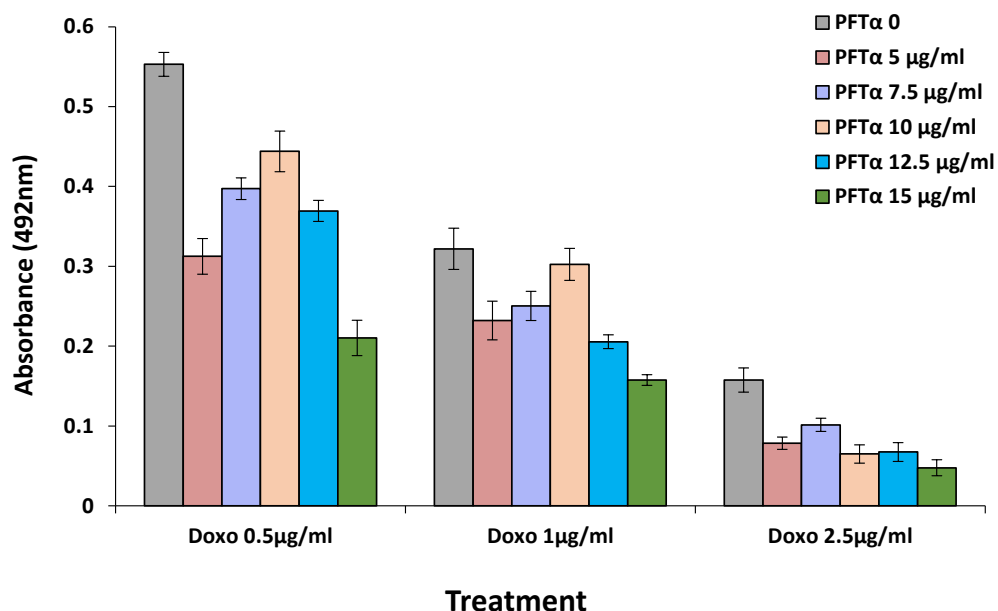


**Figure 6-8 Protection against doxorubicin drug cytotoxicity by PFT- $\alpha$  in HaCaTa cells**  
 HaCaTa cells were seeded in 96 well plates at 5000 cells/well in KSFM medium and were incubated overnight at 37°C/ 5% CO<sub>2</sub>. HaCaTa cells were pre-treated with and without 0-15 µg/mL PFT- $\alpha$  for 30 min at 37°C. HaCaTa cells were treated for 2h with 0.5-2.5 µg/mL doxorubicin (Doxo) with and without PFT- $\alpha$  at 37°C compared with vehicle control (cells treated with medium containing DMSO, in which the reagent was dissolved. The solvent represents the maximum amount of DMSO corresponding to the highest drug concentration). The drugs were then removed, wells were rinsed with PBS to remove any traces of drug and cultures incubated for a further 72h, and after which 20 µL of CellTiter 96® Aqueous One solution was added to the wells and plates were incubated at 37°C in 5% CO<sub>2</sub> for a total of four hours. Data is presented as % cell biomass shown in bar graph. Data points correspond to mean % cell biomass ( $\pm$ S.E.M.) Data points correspond to mean % cell biomass ( $\pm$ S.E.M.) for three independent biological experiments, each consisting of 6–8 technical replicates.

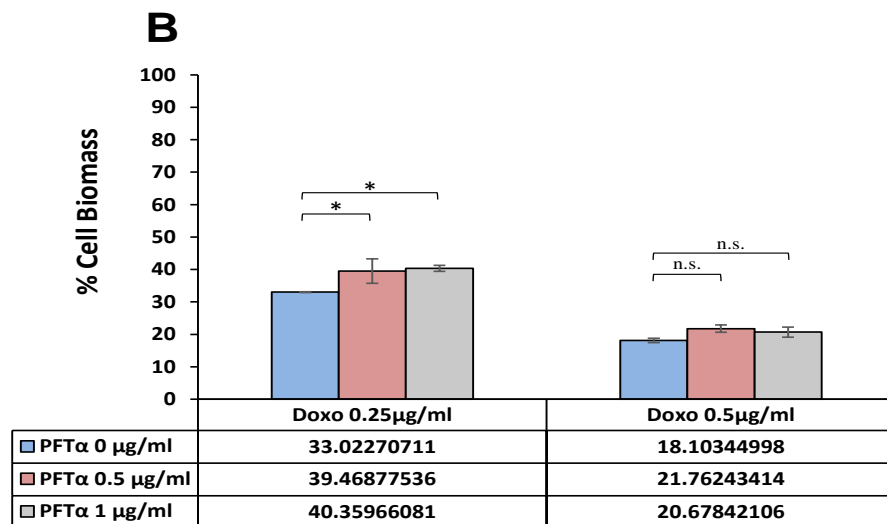
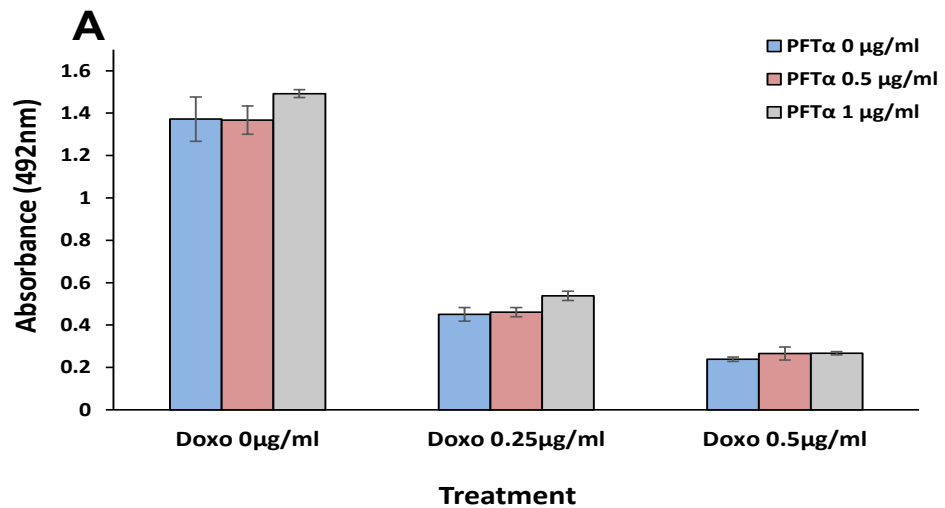


**Figure 6-9 Protection against doxorubicin drug cytotoxicity by lower concentrations of PFT-α in HaCaTa cells**

HaCaTa cells were seeded in 96 well plates at 5000 cells/well in KSFM medium and were incubated overnight at 37°C/ 5% CO<sub>2</sub>. HaCaTa cells were pre-treated with and without (0-1) μg/mL PFT-α for 30 min at 37°C. HaCaTa cells were treated for 2h with 0.25-0.5 μg/mL doxorubicin (Doxo) with and without PFT-α at 37°C compared with vehicle control (cells treated with medium containing DMSO, in which the reagent was dissolved). The solvent represents the maximum amount of DMSO corresponding to the highest drug concentration). The drugs were then removed, wells were rinsed with PBS to remove any traces of drug and cultures incubated for a further 72h, and after which 20μL of CellTiter 96® Aqueous One solution was added to the wells and plates were incubated at 37°C in 5% CO<sub>2</sub> for a total of four hours. Data is presented as % cell biomass shown in bar graph. Data points correspond to mean % cell biomass (±S.E.M.) Data points correspond to mean % cell biomass (±S.E.M.) for three independent biological experiments, each consisting of 6–8 technical replicates. n.s., non-significant; \*,  $p < 0.05$ .

## 6.7 Regulation of p21 in response to chemotherapy drug treatment and the effects of cooling

Work described in previous chapters showed by flow cytometry based analysis that 4-OH-CP treatment appeared to arrest keratinocytes in the S phase and doxorubicin arrested cells in G2/M, whilst docetaxel induced a high subG0/G1 population (characteristic of apoptosis) and arrest in G2/M.

The expression of p21 in response to treatment with 4-OH-CP, doxorubicin and docetaxel was investigated in HaCaTa cells to provide evidence on p53-mediated transcriptional activity and to assess whether cooling could affect p21 up-regulation. The p21 protein is a major target of p53, as p53 acts as the “instructor” and p21 the “executioner” in cell cycle arrest induction, for which p21 activation is largely responsible (Waldmann *et al.*, 1992). Moreover, both p21 and p53 are critical in maintaining cell cycle control in response to chemotherapy-induced DNA damage (Ahrendt *et al.*, 2000). Therefore, p21 protein expression was analysed by Western blotting using cell lysates from HaCaTa, NHEK and HHFK cells.

Following treatment of HaCaTa cells with 4-OH-CP at 37°C, 6h later an increase in the expression of p21 was observed and cooling appeared to down-modulate p21, which was particularly evident for the 18°C cooling conditions (Figure 6-10). However, it became obvious that extensive cooling alone was progressively causing some induction of p21 (see controls) and as a result after 12h of treatment, p21 levels at 37°C actually were lower than p21 levels at cooling temperatures (particularly 14°C) (Figure 6-10). Therefore, although cooling mediated down-modulation of p21 to an extent, it is possible that extensive (24h) or extreme (14°C) cooling might independently also trigger a p21-related “stress” response.

To extend these observations, NHEK cells were treated with 4-OH-CP and the results were similar to those observed in HaCaTa cells (Figure 6-11). However, when similar experiments were carried out in HHFK cells, the response observed was slightly different, as enhanced reduction in p21 expression was observed at 18°C. Although the reasons for these discrepancies remain unknown, future investigation into additional cooling conditions (temperatures other than 18°C) could address these disparities.

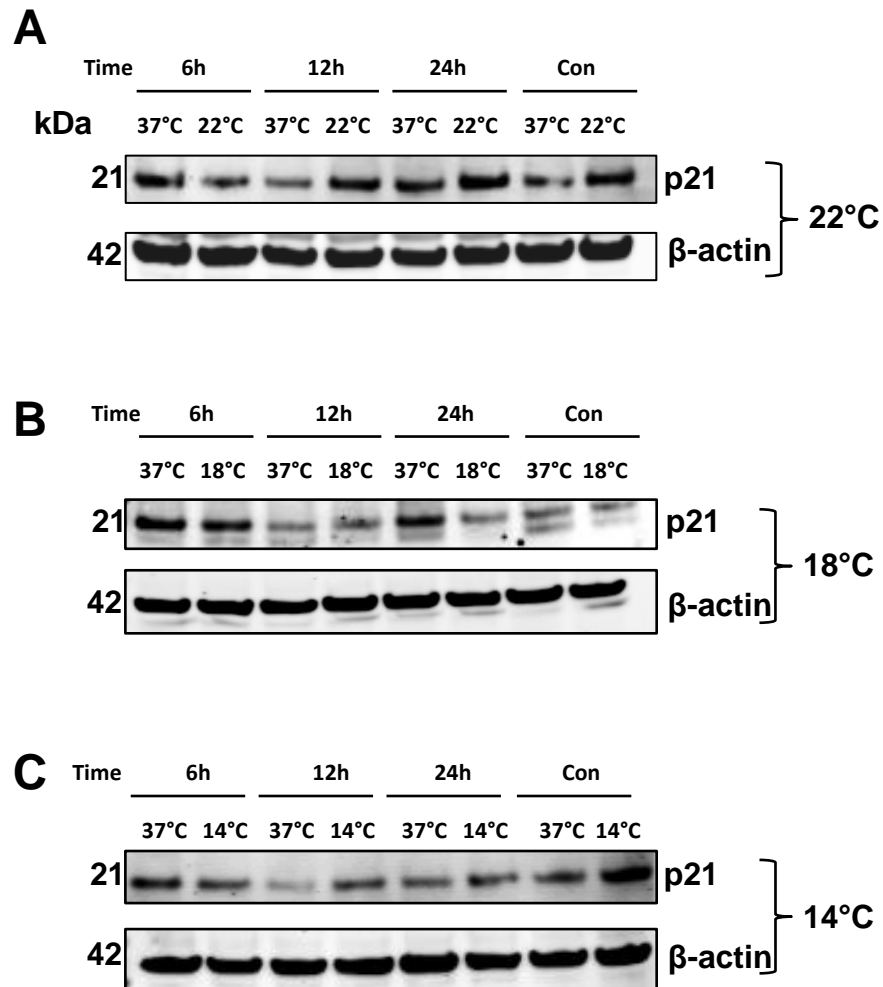
The expression of p21 in response to doxorubicin was investigated in HaCaTa cells to assess whether cooling at different temperatures could have an effect on p21 expression. The results showed that doxorubicin induced an increase in p21 levels after 24h at all the temperatures tested and cooling appeared to down-modulate p21 expression (as seen in

Figure 6-12), with 14°C showing the lowest p21 expression level compared with other temperatures tested (Figure 6-12C).

The ability of cooling to down-modulate p21 was even more evident in experiments where the expression of p21 in response to docetaxel was investigated in HaCaTa cells, where particularly at 24h cooling significantly reduced p21 expression (Figure 6-13). The induction of p21 by docetaxel suggests that p53 is most likely involved in the apoptosis induction (evident by the subG0/G1 peak) and that p21 protein plays a role in docetaxel-induced cell cycle arrest observed (Chapter 4).

The study of p21 and its regulation has allowed us to successfully demonstrate an increase in p21 expression when cells were treated with different chemotherapy drugs, consistent with the observed p53 activation (phosphorylation), as well as the confirmation that cooling, *via* the evident inhibition of P-p53, attenuates subsequent p21 induction. However, as noted above, untreated cells exhibited p21 bands particularly following extensive (24h) or extreme (14°C) cooling, which might reflect a p21-related “stress” response and subsequent p21-mediated arrest, which is in accordance with our observation that cooling arrested cells in G1 (cell cycle analysis) and this mechanism (ability to take cells out of cycle) might be a contributory factor to its cytoprotective effect.

**4-OH-CP**  
**HaCaTa cells**



**Figure 6-10 The role of temperature on the regulation of p21 expression in response to 4-OH-CP in HaCaTa cells**

$9 \times 10^5$  HaCaTa cells were seeded in 10 cm<sup>2</sup> culture dishes in KSFM complete medium and the cells were incubated overnight in 37°C/5% CO<sub>2</sub>. Cells were treated with 5 µg/mL 4-OH-CP at 37°C as well as 22°C, 18°C and 14°C. 6, 12, and 24h after treatment, the cells were lysed 2X SDS-lysis buffer. 20 µg/well of lysate was separated by SDS-PAGE using 4-12% (W/V) Bis Tris gels and blotted onto a PVDF membrane. The membrane was probed overnight with an anti-p21 antibody in TBS Tween 0.1% (1:1000 dilution). Following that, the membrane was incubated for one hour with goat-anti mouse IgG Alexa 680 (1:10000 dilution). β-actin (AC-15-A5441) was used as specificity and loading control, the membrane was incubated with the antibody (1:50000 dilution) and secondary antibody Goat anti-Mouse IgG Alexa 680 (1:10000 dilution). Membranes were scanned at 700nm and 800nm on a Licor Odyssey Infra-Red Imaging system and images are shown in black and white. Cells were treated at **A**) 37°C and 22°C, **B**) 37°C and 18°C, **C**) 37°C and 14°C. Data obtained from two independent biological experiments.

## 4-OH-CP

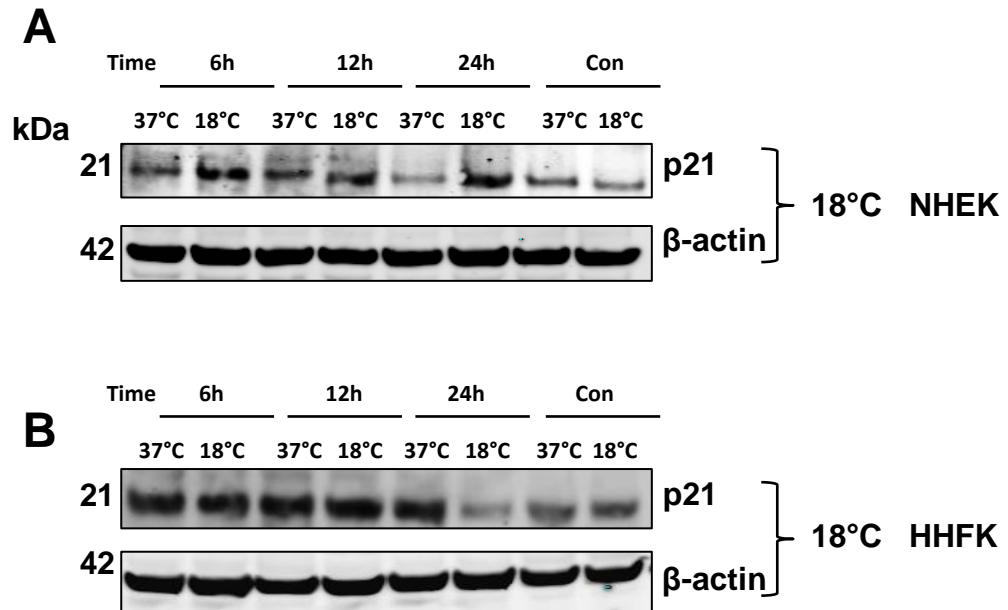


**Figure 6-11 The role of temperature on the regulation of p21 expression in response to 4-OH-CP in primary keratinocytes**

$9 \times 10^5$  HHFK and NHEK cells (passages 1–3) were seeded in  $10 \text{ cm}^2$  culture dishes in KFSM medium and the cells were incubated overnight in  $37^\circ\text{C}/5\% \text{ CO}_2$ . NHEK and HHFK cells were treated with a  $10 \mu\text{g}/\text{mL}$  4-OH-CP at  $37^\circ\text{C}$  and  $18^\circ\text{C}$ . 6, 12, and 24h after treatment, the cells were lysed 2X SDS-lysis buffer. The total protein loading  $20 \mu\text{g}/\text{well}$  of lysate was separated by SDS-PAGE using 4-12% (W/V) Bis Tris gels and immunoblotted onto a PVDF membrane. The membrane was probed overnight with an anti-p21 antibody in TBS Tween 0.1% (1:1000 dilution). Following that, the membrane was incubated for one hour with goat-anti mouse IgG Alexa 680 (1:10000 dilution).  $\beta$ -actin (AC-15-A5441) was used as specificity and loading control, the membrane was incubated with the antibody (1:50000 dilution) and secondary antibody Goat anti-Mouse IgG Alexa 680 (1:10000 dilution). Membranes were scanned at 700nm and 800nm on a Licor Odyssey Infra-Red Imaging system and images are shown in black and white. **A)** NHEK cells were treated at  $37^\circ\text{C}$  and  $18^\circ\text{C}$ , **B)** HHFK cells were treated at  $37^\circ\text{C}$  and  $18^\circ\text{C}$ . Data obtained from two independent biological experiments.

**Doxorubicin  
HaCaTa cells**

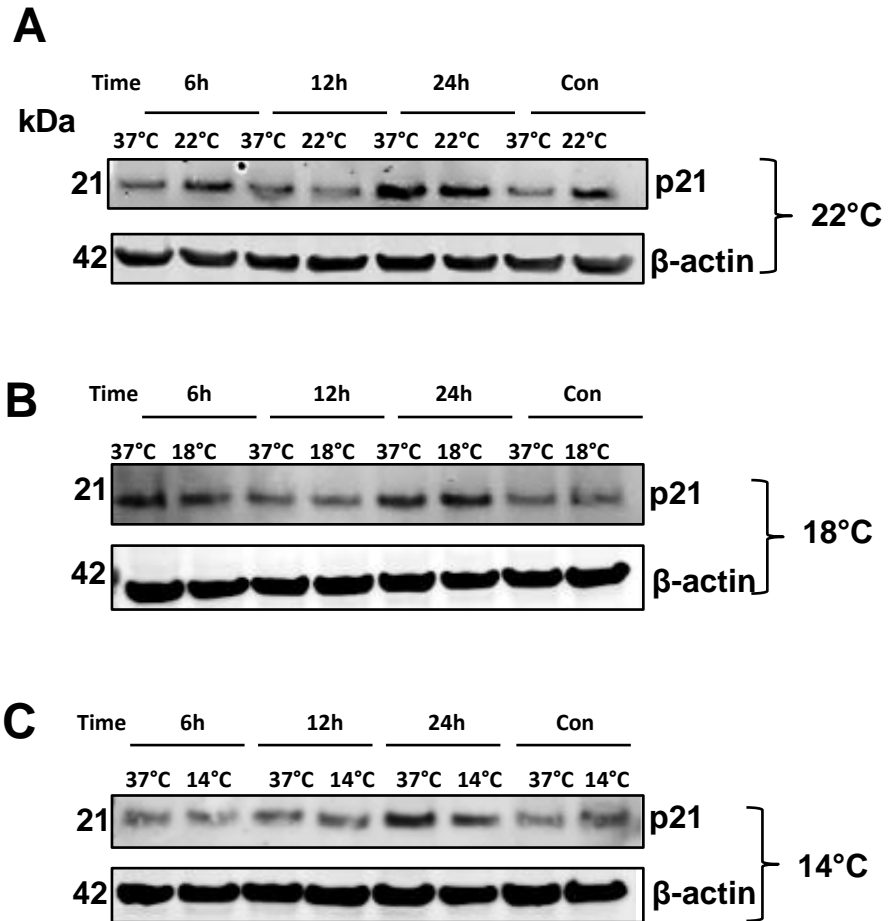


**Figure 6-12 The role of temperature on the regulation of p21 expression in response to doxorubicin in HaCaTa cells**

$9 \times 10^5$  HaCaTa cells were seeded in 10 cm<sup>2</sup> culture dishes in KSFM complete medium and the cells were incubated overnight in 37°C/5% CO<sub>2</sub>. Cells were treated with 0.5 µg/mL doxorubicin at 37°C as well as 22°C, 18°C and 14°C. 6, 12, and 24h after treatment, the cells were lysed 2X SDS-lysis buffer. 20 µg/well of lysate was separated by SDS-PAGE using 4-12% (W/V) Bis Tris gels and blotted onto a PVDF membrane. The membrane was probed overnight with an anti-p21 antibody in TBS Tween 0.1% (1:1000 dilution). Following that, the membrane was incubated for one hour with goat-anti mouse IgG Alexa 680 (1:10000 dilution). β-actin (AC-15-A5441) was used as specificity and loading control, the membrane was incubated with the antibody (1:50000 dilution) and secondary antibody Goat anti-Mouse IgG Alexa 680 (1:10000 dilution). Membranes were scanned at 700nm and 800nm on a Licor Odyssey Infra-Red Imaging system and images are shown in black and white. Cells were treated at **A**) 37°C and 22°C, **B**) 37°C and 18°C, **C**) 37°C and 14°C. Data obtained from two independent biological experiments.

**Docetaxel  
HaCaTa cells**

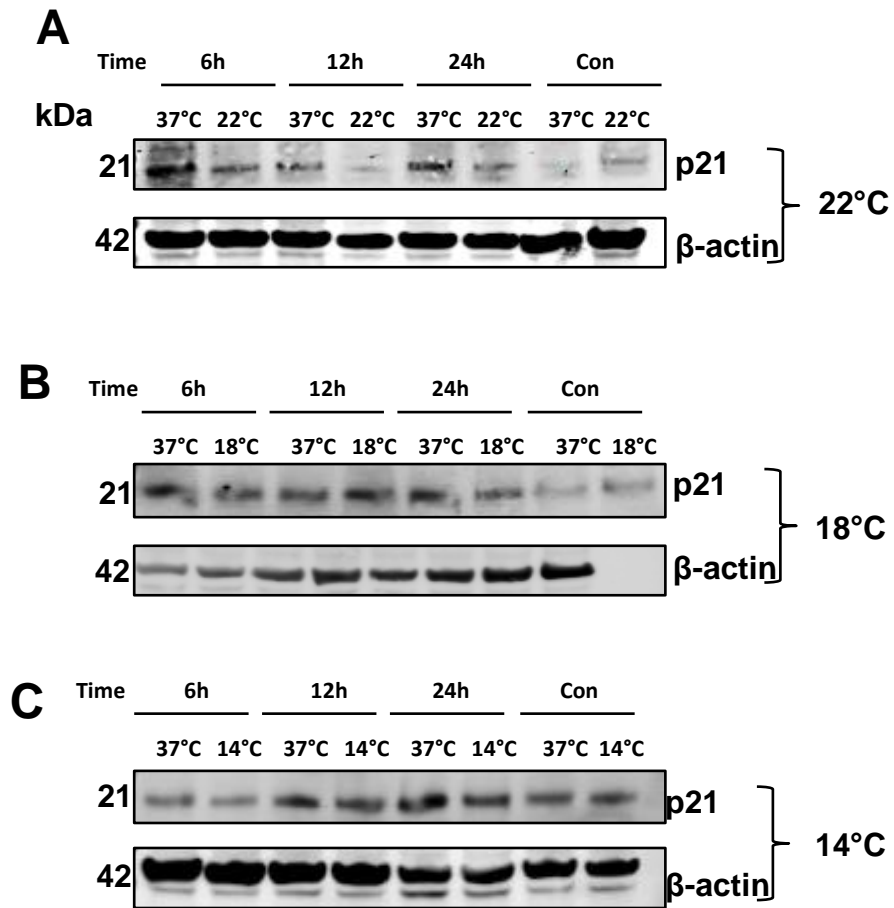


**Figure 6-13 The role of temperature on the regulation of p21 expression in response to docetaxel in HaCaTa cells**

$9 \times 10^5$  HaCaTa cells were seeded in 10 cm<sup>2</sup> culture dishes in KSFM complete medium and the cells were incubated overnight in 37°C/5% CO<sub>2</sub>. Cells were treated with 0.01 µg/mL docetaxel at 37°C as well as 22°C, 18°C and 14°C. 6, 12, and 24h after treatment, the cells were lysed 2X SDS-lysis buffer. 20 µg/well of lysate was separated by SDS-PAGE using 4-12% (W/V) Bis Tris gels and blotted onto a PVDF membrane. The membrane was probed overnight with an anti-p21 antibody in TBS Tween 0.1% (1:1000 dilution). Following that, the membrane was incubated for one hour with goat-anti mouse IgG Alexa 680 (1:10000 dilution). β-actin (AC-15-A5441) was used as specificity and loading control, the membrane was incubated with the antibody (1:50000 dilution) and secondary antibody Goat anti-Mouse IgG Alexa 680 (1:10000 dilution). Membranes were scanned at 700nm and 800nm on a Licor Odyssey Infra-Red Imaging system and images are shown in black and white. Cells were treated at **A**) 37°C and 22°C, **B**) 37°C and 18°C, **C**) 37°C and 14°C. Data obtained from two independent biological experiments.

## 6.8 Regulation of PUMA protein in response to chemotherapy drug treatment and the effects of cooling

PUMA, was identified in 2001 by three groups by the method of double hybrid with Bcl-2 as a gene that may be activated by p53 in cells where apoptosis is induced by p53 (Han *et al.*, 2001). PUMA plays a critical role in p53-mediated apoptosis, it has a very high affinity for the anti-apoptotic Bcl-2 proteins (Jeffers *et al.*, 2003; Shen and White, 2001). To determine whether following p53 activation there was an increase in PUMA protein expression. HaCaTa cells were treated with 5 µg/mL 4-OH-CP and PUMA expression detected by immunoblotting. The most noticeable changes in PUMA expression in HaCaTa cells were observed at 6h post-treatment with 4-OH-CP, where there was a consistent induction of PUMA which was down-modulated by cooling at all temperatures. PUMA levels peaked during the first 6h of drug treatment, followed by a progressive decline towards basal levels after 24h (Figure 6-14). When similar experiments were performed in NHEK cells treated with 4-OH-CP, PUMA expression patterns observed were similar to those in HaCaTa cells (Figure 6-15). Furthermore, immunoblotting showed that PUMA was induced in HaCaTa cells as early as 6h following treatment with doxorubicin (Figure 6-16) and docetaxel (Figure 6-17) and the results were relatively similar to those obtained in cells treated with 4-OH-CP.

Of note, however, untreated cells exhibited PUMA-specific bands, indicating basal expression of the PUMA protein, whilst interestingly, and in agreement with our p21 observations, untreated cells (no drug treatment controls) at cooling temperatures showed higher PUMA levels compared to control at 37°C (Figures 6-14 to 6-17) indicating a cooling related response.

**4-OH-CP**  
**HaCaTa cells**

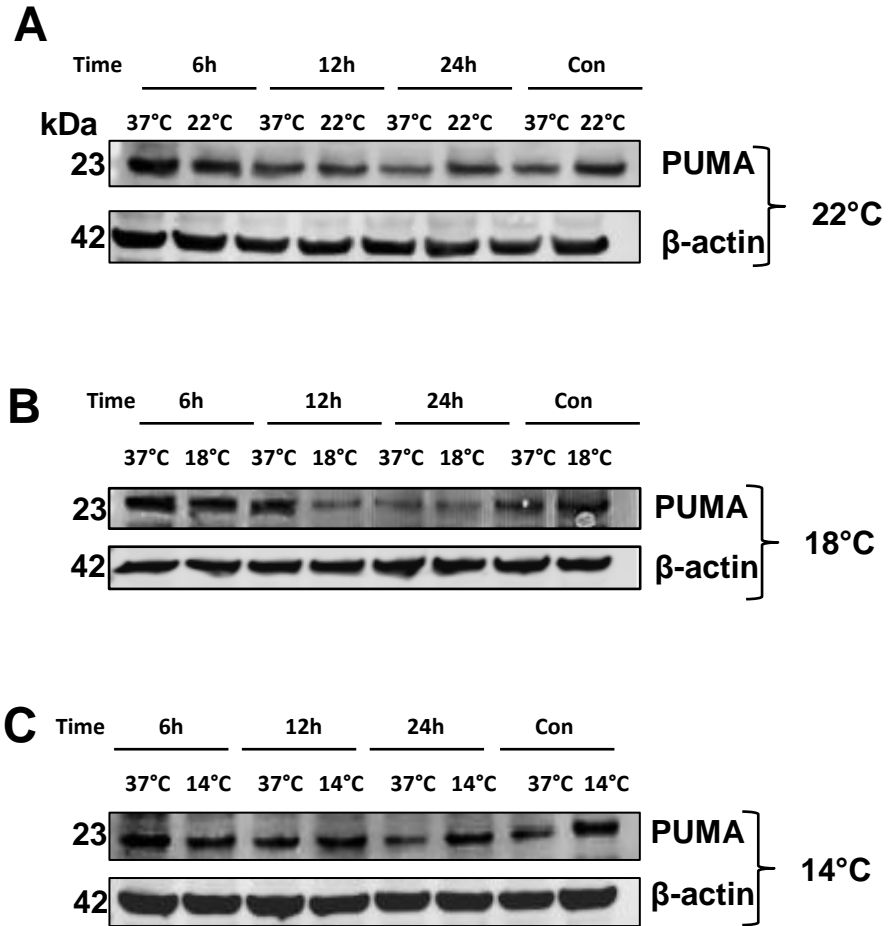


**Figure 6-14 The role of temperature on the regulation of PUMA expression in response to 4-OH-CP in HaCaTa cells**

$9 \times 10^5$  HaCaTa cells were seeded in  $10 \text{ cm}^2$  culture dishes in KSFM complete medium and the cells were incubated overnight in  $37^\circ\text{C}/5\% \text{ CO}_2$ . Cells were treated with  $5 \mu\text{g}/\text{mL}$  4-OH-CP at  $37^\circ\text{C}$  as well as  $22^\circ\text{C}$ ,  $18^\circ\text{C}$  and  $14^\circ\text{C}$ . 6, 12, and 24h after treatment, the cells were lysed 2X SDS-lysis buffer.  $20 \mu\text{g}/\text{well}$  of lysate was separated by SDS-PAGE using 4-12% (W/V) Bis Tris gels and blotted onto a PVDF membrane. The membrane was probed overnight with an anti-PUMA antibody in TBS Tween 0.1% (1:1000 dilution). Following that, the membrane was incubated for one hour with Goat anti-Rabbit IgG IRDye 800nm (1:10000 dilution).  $\beta$ -actin (AC-15-A5441) was used as specificity and loading control, the membrane was incubated with the antibody (1:50000 dilution) and secondary antibody Goat anti-Mouse IgG Alexa 680 (1:10000 dilution). Membranes were scanned at 700nm and 800nm on a Licor Odyssey Infra-Red Imaging system and images are shown in black and white. Cells were treated at **A)**  $37^\circ\text{C}$  and  $22^\circ\text{C}$ , **B)**  $37^\circ\text{C}$  and  $18^\circ\text{C}$ , **C)**  $37^\circ\text{C}$  and  $14^\circ\text{C}$ . Data obtained from two independent biological experiments.

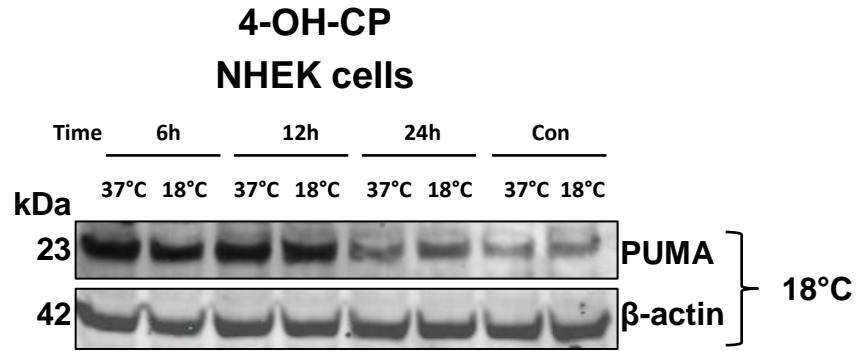


**Figure 6-15 The role of temperature on the regulation of PUMA expression in response to 4-OH-CP in NHEK cells**

9x10<sup>5</sup> NHEK cells (passages 1–3) were seeded in 10 cm<sup>2</sup> culture dishes in KSFM medium and the cells were incubated overnight in 37°C/5% CO<sub>2</sub>. NHEK cells were treated with a 10 µg/mL 4-OH-CP at 37°C and 18°C. 6, 12, and 24h after treatment, the cells were lysed 2X SDS-lysis buffer. The total protein loading 20 µg/well of lysate was separated by SDS-PAGE using 4-12% (W/V) Bis Tris gels and immunoblotted onto a PVDF membrane. The membrane was probed overnight with an anti-PUMA antibody in TBS Tween 0.1% (1:1000 dilution). The membrane was incubated for one hour with Goat anti-Rabbit IgG IRDye 800nm (1:10000 dilution). β-actin (AC-15-A5441) was used as specificity and loading control, the membrane was incubated with the antibody diluted at 1:50000 and secondary antibody goat-anti mouse IgG Alexa 680 diluted 1:10000. Membranes were scanned at 700nm and 800nm on Licor Odyssey Infra-Red Imaging system and images are shown in black and white. Data obtained from two independent biological experiments.

**Doxorubicin  
HaCaTa cells**

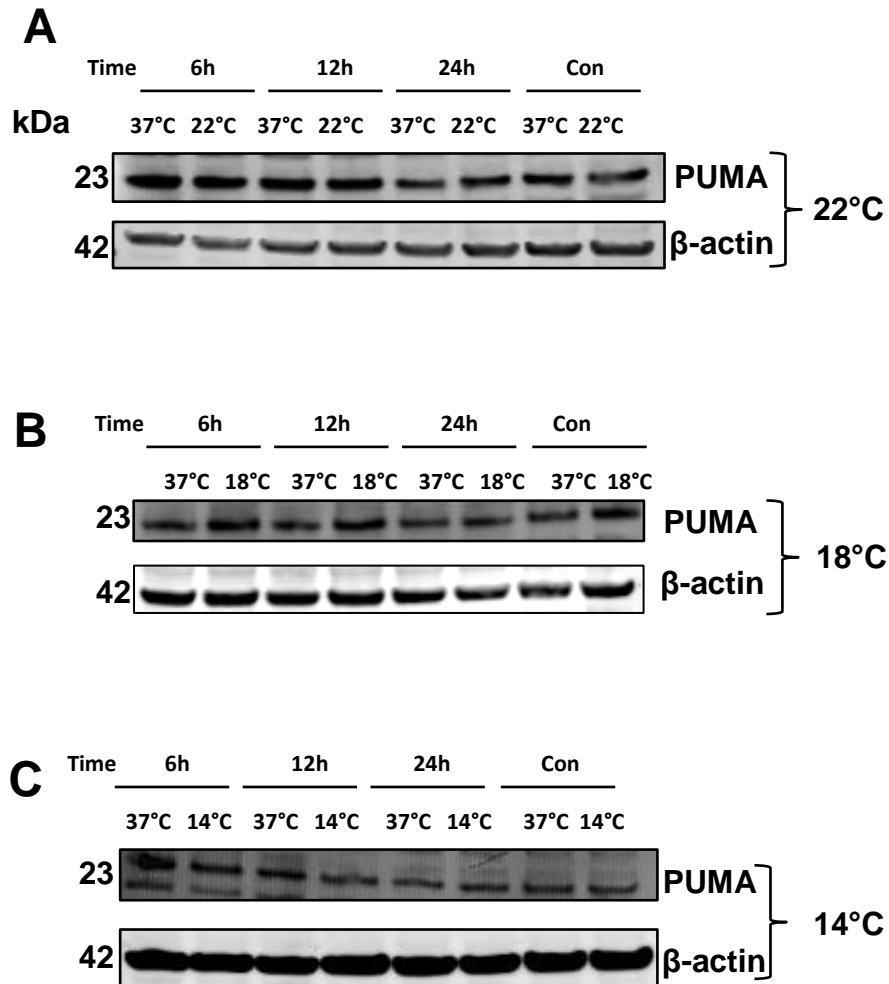


**Figure 6-16 The role of temperature on the regulation of PUMA expression in response to doxorubicin in HaCaTa cells**

$9 \times 10^5$  HaCaTa cells were seeded in 10 cm<sup>2</sup> culture dishes in KFSM complete medium and the cells were incubated overnight in 37°C/5% CO<sub>2</sub>. Cells were treated with 0.5 µg/mL doxorubicin at 37°C as well as 22°C, 18°C and 14°C. 6, 12, and 24h after treatment, the cells were lysed 2X SDS-lysis buffer. 20 µg/well of lysate was separated by SDS-PAGE using 4-12% (W/V) Bis Tris gels and blotted onto a PVDF membrane. The membrane was probed overnight with an anti-PUMA antibody in TBS Tween 0.1% (1:1000 dilution). Following that, the membrane was incubated for one hour with Goat anti-Rabbit IgG IRDye 800nm (1:10000 dilution). β-actin (AC-15-A5441) was used as specificity and loading control, the membrane was incubated with the antibody (1:50000 dilution) and secondary antibody Goat anti-Mouse IgG Alexa 680 (1:10000 dilution). Membranes were scanned at 700nm and 800nm on a Licor Odyssey Infra-Red Imaging system and images are shown in black and white. Cells were treated at **A**) 37°C and 22°C, **B**) 37°C and 18°C, **C**) 37°C and 14°C. Data obtained from two independent biological experiments.

**Docetaxel**  
**HaCaTa cells**

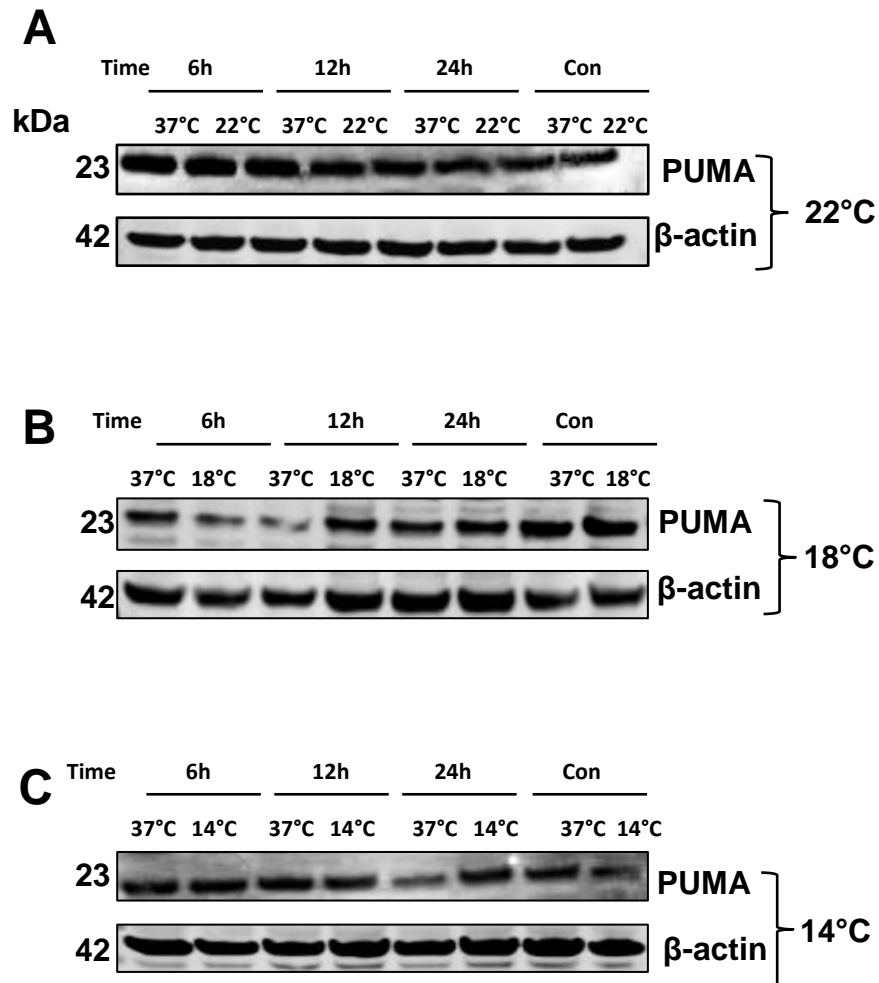


**Figure 6-17 The role of temperature on the regulation of PUMA expression in response to docetaxel in HaCaTa cells**

9x10<sup>5</sup> HaCaTa cells were seeded in 10 cm<sup>2</sup> culture dishes in KSFM complete medium and the cells were incubated overnight in 37°C/5% CO<sub>2</sub>. Cells were treated with 0.01 µg/mL docetaxel at 37°C as well as 22°C, 18°C and 14°C. 6, 12, and 24h after treatment, the cells were lysed 2X SDS-lysis buffer. 20 µg/well of lysate was separated by SDS-PAGE using 4-12% (W/V) Bis Tris gels and blotted onto a PVDF membrane. The membrane was probed overnight with an anti-PUMA antibody in TBS Tween 0.1% (1:1000 dilution). Following that, the membrane was incubated for one hour with Goat anti-Rabbit IgG IRDye 800nm (1:10000 dilution). β-actin (AC-15-A5441) was used as specificity and loading control, the membrane was incubated with the antibody (1:50000 dilution) and secondary antibody Goat anti-Mouse IgG Alexa 680 (1:10000 dilution). Membranes were scanned at 700nm and 800nm on a Licor Odyssey Infra-Red Imaging system and images are shown in black and white. Cells were treated at **A**) 37°C and 22°C, **B**) 37°C and 18°C, **C**) 37°C and 14°C. Data obtained from two independent biological experiments.

## **6.9 Regulation of Noxa protein expression in response to chemotherapy drug treatment and the effects of cooling**

In addition to PUMA, the expression of BH3-only Bcl-2 family member Noxa was also investigated to assess its regulation following treatment with chemotherapy drugs at different temperatures and at different time points as above. Noxa is the smallest known BH3-only protein with an approximate size of ~10 kDa.

Immunoblotting analysis revealed increased protein expression of Noxa in HaCaTa cells treated with 4-OH-CP at 37°C (Figure 6-18). Treatment with 4-OH-CP resulted in up-regulation of Noxa as quickly as 6h; however, the levels of Noxa declined progressively until 24h. Importantly, cooling consistently down-regulated Noxa expression when it was at its peak (6h), however, no significant reduction in Noxa was observed after 6h, although this might be due to the decline of Noxa protein expression at 37°C (Figure 6-18). Interestingly, these results are consistent with the findings on the expression of the related (and similarly p53-regulated pro-apoptotic PUMA, above), thus suggesting similarities in the regulation of these two proteins.

The effect of doxorubicin treatment on pro-apoptotic Noxa protein expression was then tested. Noxa expression was substantially induced after 6h at 37°C and markedly reduced by cooling at 22°C and particularly at 14°C (yet it should be noted that for unknown reasons the observations differed at 18°C as for that condition no such reduction was observed) (Figure 6-19). Finally, expression of Noxa following treatment with docetaxel was investigated, and the results indicate that the level of Noxa did not decline as it did for 4-OH-CP and doxorubicin and the level kept increasing. However interestingly, at 14°C there was a significant reduction in Noxa expression (Figure 6-20).

Collectively, in addition to the observation that PUMA and Noxa demonstrated similar patterns of expression in response to chemotherapy drugs and cooling appeared to have similar effects on both proteins, also our results indicate that in both cases cooling alone resulted in PUMA and Noxa protein expression indicating a cooling related response. Interestingly, also, although the mechanisms by which these drugs (4-OH-CP, doxorubicin, and docetaxel) induce cytotoxicity/apoptosis differ significantly, a similar trend was observed in the regulation of both PUMA and Noxa after treatment with these drugs and cooling appeared to regulate expression of these proteins in a similar fashion.

**4-OH-CP**  
**HaCaTa cells**

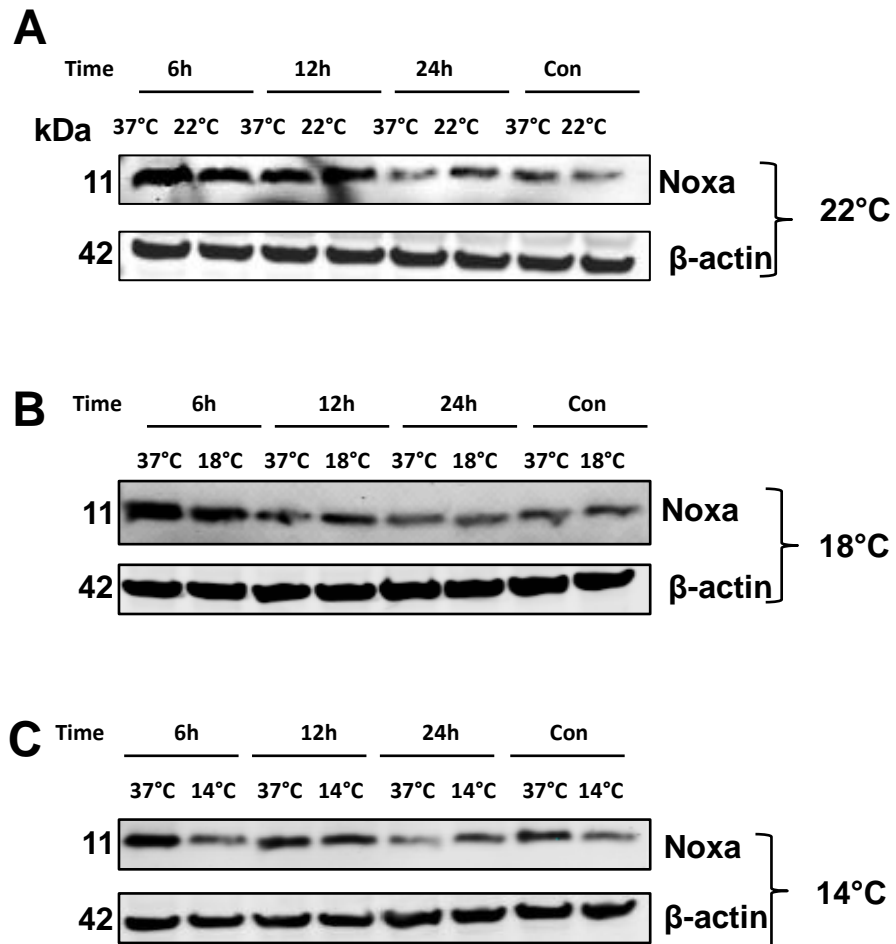


**Figure 6-18 The role of temperature on the regulation of Noxa expression in response to 4-OH-CP in HaCaTa cells**

$9 \times 10^5$  HaCaTa cells were seeded in 10 cm<sup>2</sup> culture dishes in KFSM complete medium and the cells were incubated overnight in 37°C/5% CO<sub>2</sub>. Cells were treated with 5 µg/mL 4-OH-CP at 37°C as well as 22°C, 18°C and 14°C. 6, 12, and 24h after treatment, the cells were lysed 2X SDS-lysis buffer. 20 µg/well of lysate was separated by SDS-PAGE using 4-12% (W/V) Bis Tris gels and blotted onto a PVDF membrane. The membrane was probed overnight with an anti-Noxa antibody in TBS Tween 0.1% (1:1000 dilution). Following that, the membrane was incubated for one hour with goat-anti mouse IgG Alexa 680 (1:10000 dilution). β-actin (AC-15-A5441) was used as specificity and loading control, the membrane was incubated with the antibody (1:50000 dilution) and secondary antibody Goat anti-Mouse IgG Alexa 680 (1:10000 dilution). Membranes were scanned at 700nm and 800nm on a Licor Odyssey Infra-Red Imaging system and images are shown in black and white. Cells were treated at **A**) 37°C and 22°C, **B**) 37°C and 18°C, **C**) 37°C and 14°C. Data obtained from two independent biological experiments.

**Doxorubicin  
HaCaTa cells**

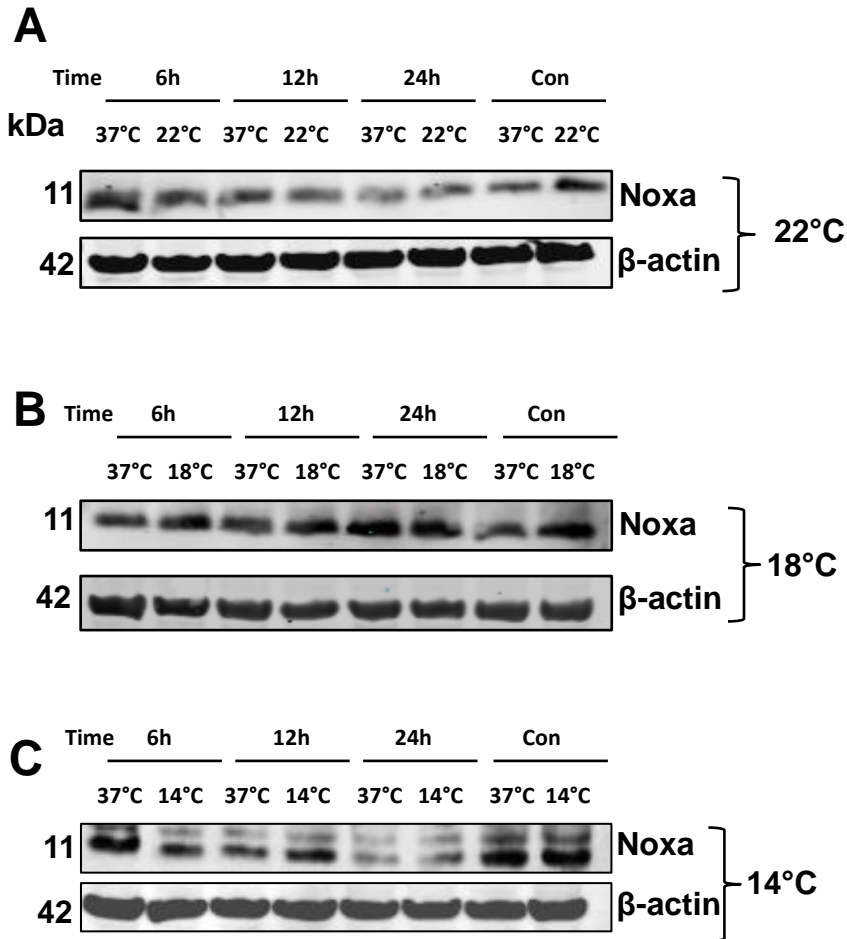


**Figure 6-19 The role of temperature on the regulation of Noxa expression in response to doxorubicin in HaCaTa cells**

$9 \times 10^5$  HaCaTa cells were seeded in 10 cm<sup>2</sup> culture dishes in KSFM complete medium and the cells were incubated overnight in 37°C/5% CO<sub>2</sub>. Cells were treated with 0.5 µg/mL doxorubicin at 37°C as well as 22°C, 18°C and 14°C. 6, 12, and 24h after treatment, the cells were lysed 2X SDS-lysis buffer. 20 µg/well of lysate was separated by SDS-PAGE using 4-12% (W/V) Bis Tris gels and blotted onto a PVDF membrane. The membrane was probed overnight with an anti-Noxa antibody in TBS Tween 0.1% (1:1000 dilution). Following that, the membrane was incubated for one hour with goat-anti mouse IgG Alexa 680 (1:10000 dilution). β-actin (AC-15-A5441) was used as specificity and loading control, the membrane was incubated with the antibody (1:50000 dilution) and secondary antibody Goat anti-Mouse IgG Alexa 680 (1:10000 dilution). Membranes were scanned at 700nm and 800nm on a Licor Odyssey Infra-Red Imaging system and images are shown in black and white. Cells were treated at **A**) 37°C and 22°C, **B**) 37°C and 18°C, **C**) 37°C and 14°C. Data obtained from two independent biological experiments.

**Docetaxel  
HaCaTa cells**

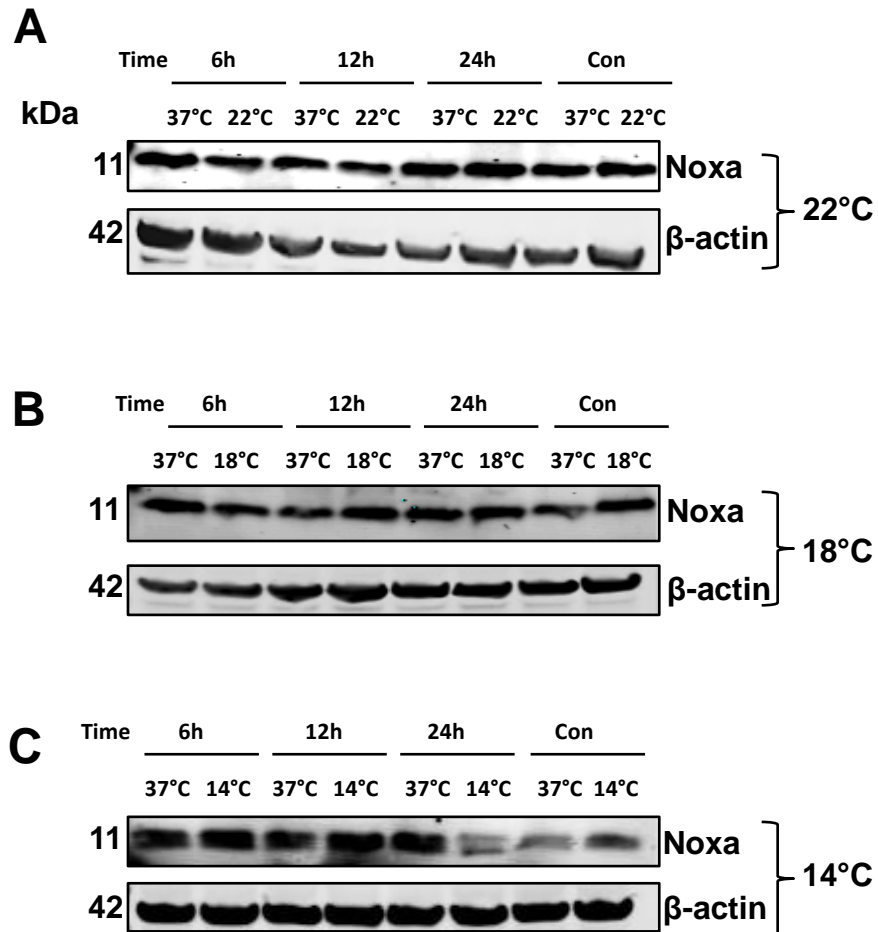


**Figure 6-20 The role of temperature on the regulation of Noxa expression in response to docetaxel in HaCaTa cells**

$9 \times 10^5$  HaCaTa cells were seeded in 10 cm<sup>2</sup> culture dishes in KSM complete medium and the cells were incubated overnight in 37°C/5% CO<sub>2</sub>. Cells were treated with 0.01 µg/mL docetaxel at 37°C as well as 22°C, 18°C and 14°C. 6, 12, and 24h after treatment, the cells were lysed 2X SDS-lysis buffer. 20 µg/well of lysate was separated by SDS-PAGE using 4-12% (W/V) Bis Tris gels and blotted onto a PVDF membrane. The membrane was probed overnight with an anti-Noxa antibody in TBS Tween 0.1% (1:1000 dilution). Following that, the membrane was incubated for one hour with goat-anti mouse IgG Alexa 680 (1:10000 dilution). β-actin (AC-15-A5441) was used as specificity and loading control, the membrane was incubated with the antibody (1:50000 dilution) and secondary antibody Goat anti-Mouse IgG Alexa 680 (1:10000 dilution). Membranes were scanned at 700nm and 800nm on a Licor Odyssey Infra-Red Imaging system and images are shown in black and white. Cells were treated at **A**) 37°C and 22°C, **B**) 37°C and 18°C, **C**) 37°C and 14°C. Data obtained from two independent biological experiments.

## 6.10 Regulation of pro-apoptotic Bak protein in response to chemotherapy drug treatment and the effects of cooling

The two main pro-apoptotic proteins of the Bcl-2 family, Bax and Bak are important inducers of the mitochondrial apoptotic pathway. Loss of function of these proteins (e.g. genetic deletion) inhibits the release of cytochrome c from the mitochondria and apoptosis (Cheng *et al.*, 2003; Wei *et al.*, 2001). The three chemotherapy drugs used in this study have all been reported to induce mitochondrial apoptosis pathway *via* activation of Bax and Bak (Panaretakis *et al.*, 2002; Strauss *et al.*, 2008).

In order to investigate the importance of Bak in our study, an antibody that recognizes the active conformation of Bak was used to detect the ~26 kDa protein. HaCaTa, NHEK and HHFK cells were treated for 2h with 4-OH-CP and expression assessed at 37°C *versus* cooling conditions (at 22°C, 18°C and 14°C). Although a basal level of Bak expression was detectable in HaCaTa cells, 6h of treatment with 4-OH-CP the level of Bak expression increased significantly. Importantly, under cooling conditions, and depending on the exact temperature, there was a remarkable reduction in Bak expression, and in some cases drug-mediated Bak induction was completely attenuated by cooling (Figure 6-21). The most consistent down-modulation of Bak by cooling was observed at 24h post-treatment (Figure 6-21). However, as indicated by the results obtained at 14°C at 12 and 24h, although cooling protects from cytotoxic drugs, very low temperature (extreme cooling, such as 14°C) might induce some level of “stress” on the cells. To strengthen these observations, similar investigations were performed for NHEK and HHFK cultured after treatment with 10 µg/mL 4-OH-CP at 37°C and 18°C and the level of Bak protein was analysed. Bak protein expression levels in NHEK and HHFK showed a similar pattern of up-regulation to that observed for HaCaTa cells, particularly at 6h. However, in the case of HHFK cells some inconsistency was observed at 12h in comparison to HaCaTa and NHEK cells (Figure 6-22).

When the effect of doxorubicin was assessed, a rapid induction of Bak was observed at 6h at 37°C and cooling could down-modulate this induction particularly at 18°C and to a lesser extent at 14°C; however, the levels of Bak gradually declined with time and the level of the protein was evidently reduced for all the groups by 24h (Figure 6-23). Similar results were observed following HaCaTa cell treatment with docetaxel shown in Figure 6-24, however, for unknown reasons, there was an increase in Bak expression at cooling conditions in drug treated cells in comparison to treatment at 37°C (Figure 6-24).

These results indicated that Bak protein is induced during apoptosis induction by the three drugs used in this study and cooling can down-regulate Bak levels significantly, particularly in the case of 4-OH-CP.

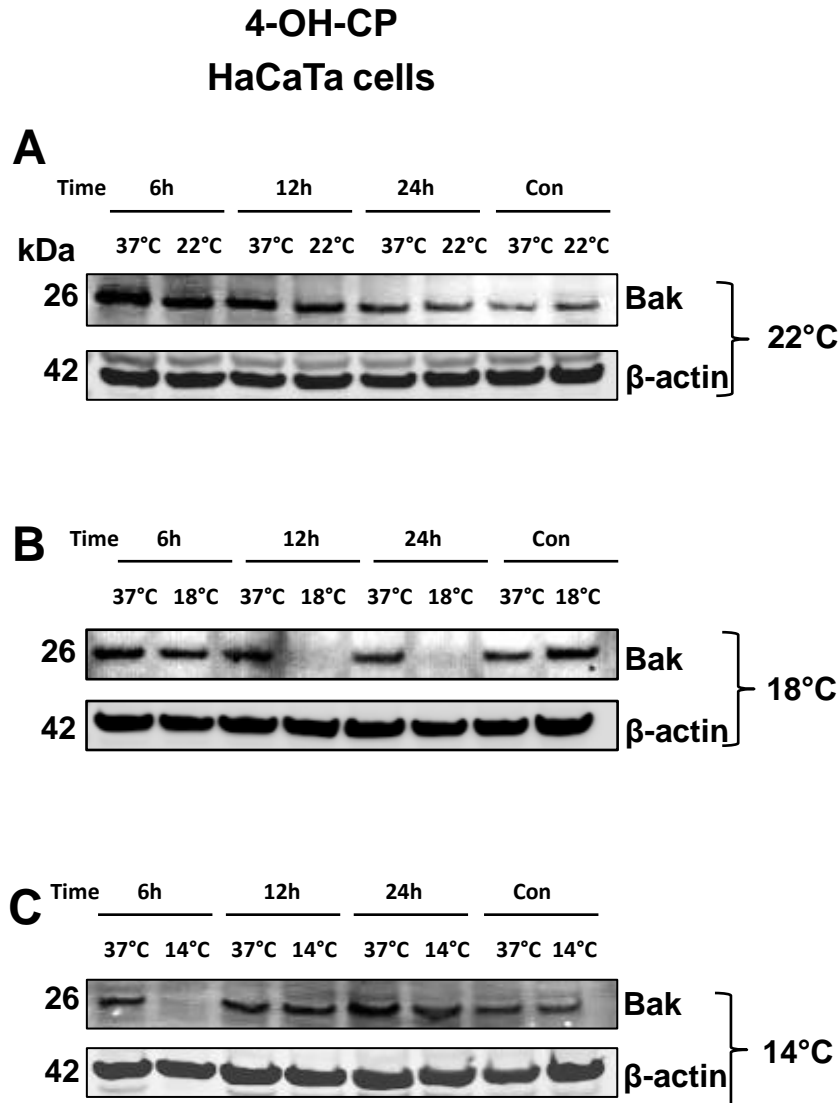


**Figure 6-21 The role of temperature on the regulation of Bak expression in response to 4-OH-CP in HaCaTa cells**

9x10<sup>5</sup> HaCaTa cells were seeded in 10 cm<sup>2</sup> culture dishes in KSFM complete medium and the cells were incubated overnight in 37°C/5% CO<sub>2</sub>. Cells were treated with 5 µg/mL 4-OH-CP at 37°C as well as 22°C, 18°C and 14°C. 6, 12, and 24h after treatment, the cells were lysed 2X SDS-lysis buffer. 20 µg/well of lysate was separated by SDS-PAGE using 4-12% (W/V) Bis Tris gels and blotted onto a PVDF membrane. The membrane was probed overnight with an anti-Bak antibody in TBS Tween 0.1% (1:1000 dilution). Following that, the membrane was incubated for one hour with Goat anti-Rabbit IgG IRDye 800nm (1:10000 dilution). β-actin (AC-15-A5441) was used as specificity and loading control, the membrane was incubated with the antibody (1:50000 dilution) and secondary antibody Goat anti-Mouse IgG Alexa 680 (1:10000 dilution). Membranes were scanned at 700nm and 800nm on a Licor Odyssey Infra-Red Imaging system and images are shown in black and white. Cells were treated at **A**) 37°C and 22°C, **B**) 37°C and 18°C, **C**) 37°C and 14°C. Data obtained from two independent biological experiments.

## 4-OH-CP

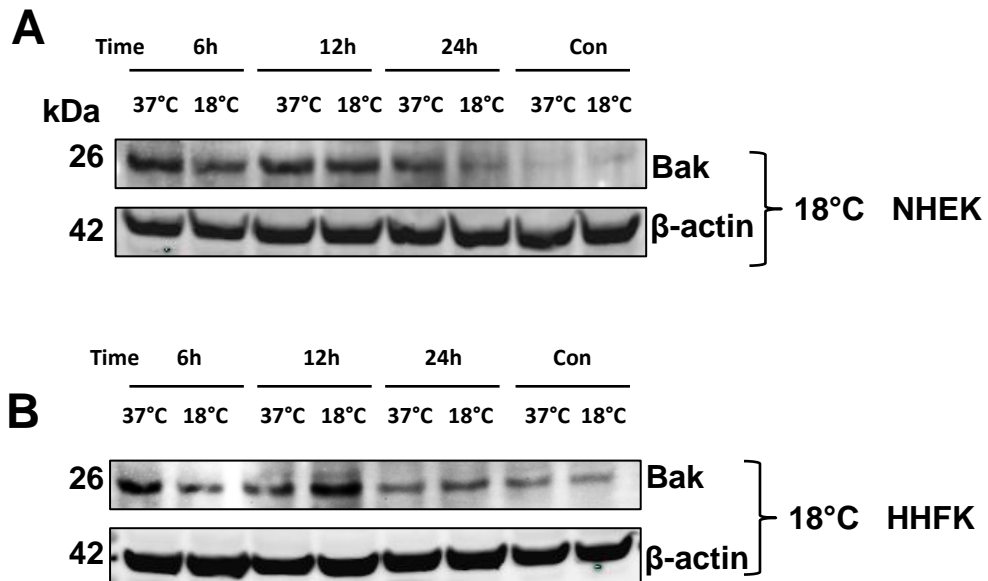


**Figure 6-22 The role of temperature on the regulation of Bak expression in response to 4-OH-CP in primary keratinocytes**

$9 \times 10^5$  HHFK and NHEK cells (passages 1–3) were seeded in  $10 \text{ cm}^2$  culture dishes in KSM medium and the cells were incubated overnight in  $37^\circ\text{C}/5\% \text{ CO}_2$ . NHEK and HHFK cells were treated with a  $10 \mu\text{g}/\text{mL}$  4-OH-CP at  $37^\circ\text{C}$  and  $18^\circ\text{C}$ . 6, 12, and 24h after treatment, the cells were lysed 2X SDS-lysis buffer. The total protein loading  $20 \mu\text{g}/\text{well}$  of lysate was separated by SDS-PAGE using 4-12% (W/V) Bis Tris gels and immunoblotted onto a PVDF membrane. The membrane was probed overnight with an anti-Bak antibody in TBS Tween 0.1% (1:1000 dilution). The membrane was incubated for one hour with Goat anti-Rabbit IgG IRDye 800nm (1:10000 dilution).  $\beta$ -actin (AC-15-A5441) was used as specificity and loading control, the membrane was incubated with the antibody diluted at 1:50000 and secondary antibody goat-anti mouse IgG Alexa 680 diluted 1:10000. Membranes were scanned at 700nm and 800nm on Licor Odyssey Infra-Red Imaging system and images are shown in black and white. **A)** NHEK cells were treated at  $37^\circ\text{C}$  and  $18^\circ\text{C}$ , **B)** HHFK cells were treated at  $37^\circ\text{C}$  and  $18^\circ\text{C}$ . Data obtained from two independent biological experiments.

## Doxorubicin HaCaTa cells

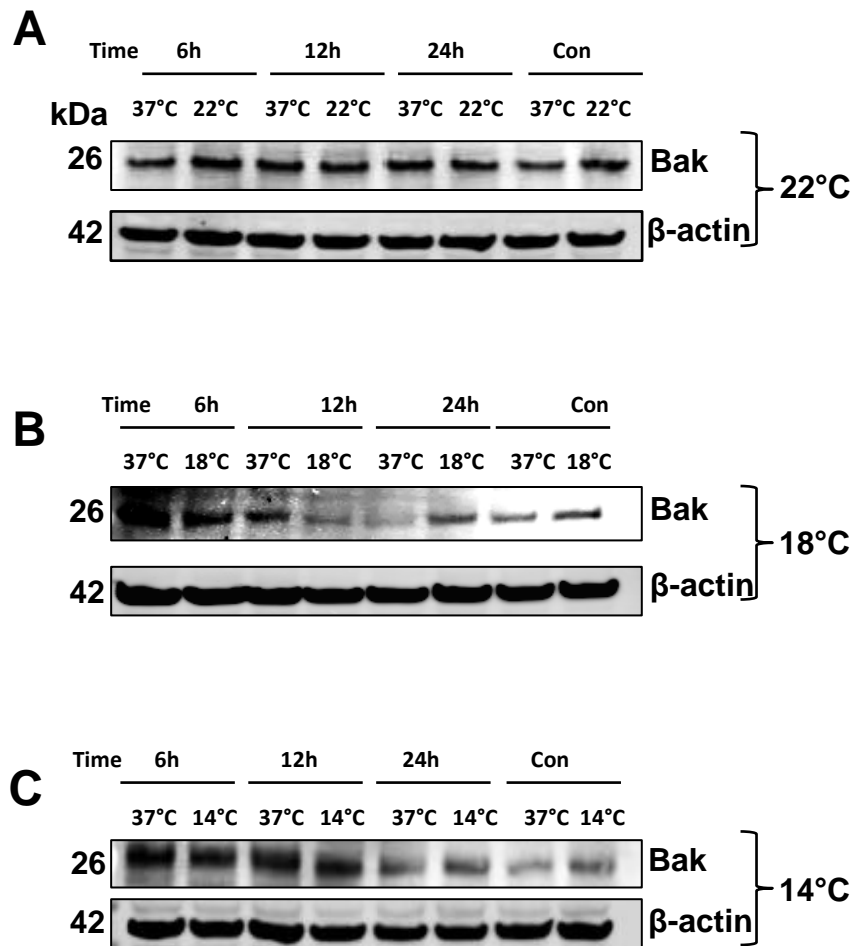
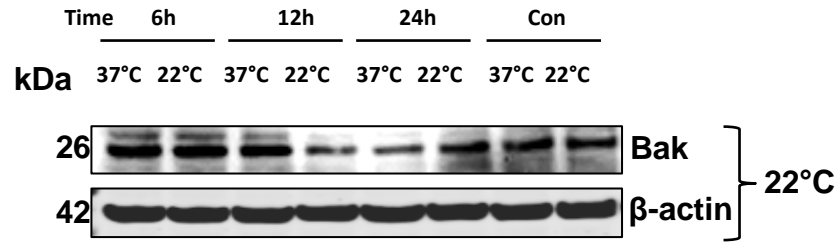


**Figure 6-23 The role of temperature on the regulation of Bak expression in response to doxorubicin in HaCaTa cells**

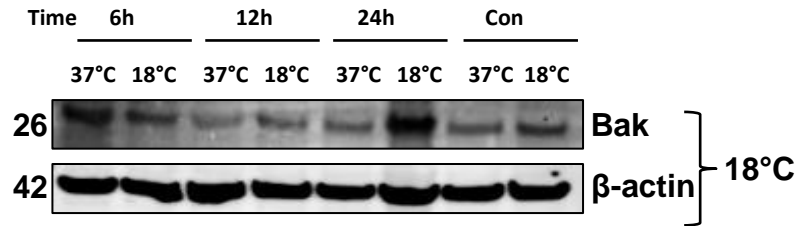
$9 \times 10^5$  HaCaTa cells were seeded in 10 cm<sup>2</sup> culture dishes in KSFM complete medium and the cells were incubated overnight in 37°C/5% CO<sub>2</sub>. Cells were treated with 0.5 µg/mL doxorubicin at 37°C as well as 22°C, 18°C and 14°C. 6, 12, and 24h after treatment, the cells were lysed 2X SDS-lysis buffer. 20 µg/well of lysate was separated by SDS-PAGE using 4-12% (W/V) Bis Tris gels and blotted onto a PVDF membrane. The membrane was probed overnight with an anti-Bak antibody in TBS Tween 0.1% (1:1000 dilution). Following that, the membrane was incubated for one hour with Goat anti-Rabbit IgG IRDye 800nm (1:10000 dilution). β-actin (AC-15-A5441) was used as specificity and loading control, the membrane was incubated with the antibody (1:50000 dilution) and secondary antibody Goat anti-Mouse IgG Alexa 680 (1:10000 dilution). Membranes were scanned at 700nm and 800nm on a Licor Odyssey Infra-Red Imaging system and images are shown in black and white. Cells were treated at **A**) 37°C and 22°C, **B**) 37°C and 18°C, **C**) 37°C and 14°C. Data obtained from two independent biological experiments.

**Docetaxel  
HaCaTa cells**

**A**



**B**



**C**

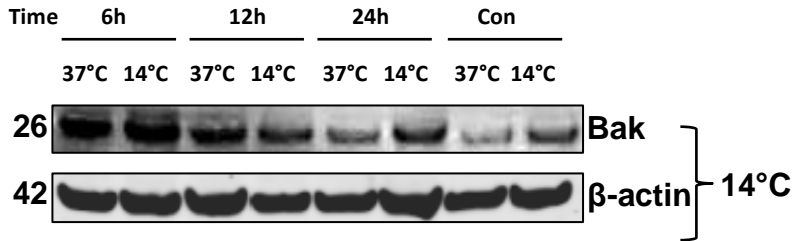


**Figure 6-24 The role of temperature on the regulation of Bak expression in response to docetaxel in HaCaTa cells**

$9 \times 10^5$  HaCaTa cells were seeded in  $10 \text{ cm}^2$  culture dishes in KSFM complete medium and the cells were incubated overnight in  $37^\circ\text{C}/5\% \text{ CO}_2$ . Cells were treated with  $0.01 \text{ }\mu\text{g/mL}$  docetaxel at  $37^\circ\text{C}$  as well as  $22^\circ\text{C}$ ,  $18^\circ\text{C}$  and  $14^\circ\text{C}$ . 6, 12, and 24h after treatment, the cells were lysed 2X SDS-lysis buffer.  $20 \text{ }\mu\text{g/well}$  of lysate was separated by SDS-PAGE using 4-12% (W/V) Bis Tris gels and blotted onto a PVDF membrane. The membrane was probed overnight with an anti-Bak antibody in TBS Tween 0.1% (1:1000 dilution). Following that, the membrane was incubated for one hour with Goat anti-Rabbit IgG IRDye 800nm (1:10000 dilution).  $\beta$ -actin (AC-15-A5441) was used as specificity and loading control, the membrane was incubated with the antibody (1:50000 dilution) and secondary antibody Goat anti-Mouse IgG Alexa 680 (1:10000 dilution). Membranes were scanned at 700nm and 800nm on a Licor Odyssey Infra-Red Imaging system and images are shown in black and white. Cells were treated at **A**)  $37^\circ\text{C}$  and  $22^\circ\text{C}$ , **B**)  $37^\circ\text{C}$  and  $18^\circ\text{C}$ , **C**)  $37^\circ\text{C}$  and  $14^\circ\text{C}$ . Data obtained from two independent biological experiments.

## 6.11 Changes in Bax protein expression following chemotherapy drug treatment and the effects of cooling

Following investigations on Bak activation, the role of cooling in Bax regulation following drug treatment was investigated as above. HaCaTa cells were treated with the panel of chemotherapy drugs at 37°C or at cooling conditions (22°C, 18°C, and 14), and Bax expression analysed by immunoblotting to detect the ~21 kDa protein.

When HaCaTa cells were tested by immunoblotting there was clearly a high level of Bax expression and treatment with 4-OH-CP caused only minor up-regulation of Bax at 37°C *versus* cooling conditions. Interestingly, Bax levels diminished at 18°C however, this appeared to be unique for that specific temperature, as no similar trend was noted for other conditions (Figure 6-25). Similar expression patterns were observed in experiments where the effect of doxorubicin on Bax was assessed. In such experiments, though some changes were noted in Bax protein levels, they were clearly non-significant and no clear differences were observed (Figure 6-26). By contrast, as shown in Figure 6-27, an induction in Bax expression was observed at 37°C at 6h in docetaxel-treated HaCaTa cells. However, for all the groups after 12h and 24h treatment with docetaxel Bax levels appeared to exhibit little if any difference from basal levels.

Therefore, unlike our observation on Bak (previous section) where clear Bak induction by chemotherapy drugs was observed and cooling appeared to modulate Bak expression, no such pattern was observed for Bax; this might be because either Bax might not be involved in apoptosis in these cells, or due to the already high basal expression levels of Bax protein in HaCaTa cells, which made comparisons between conditions difficult. It is possible that rather than absolute proteins levels measured here, the exact localisation pattern of proteins such as Bax, might provide a better idea of its role in cytotoxicity and its regulation by cooling.

**4-OH-CP**  
**HaCaTa cells**

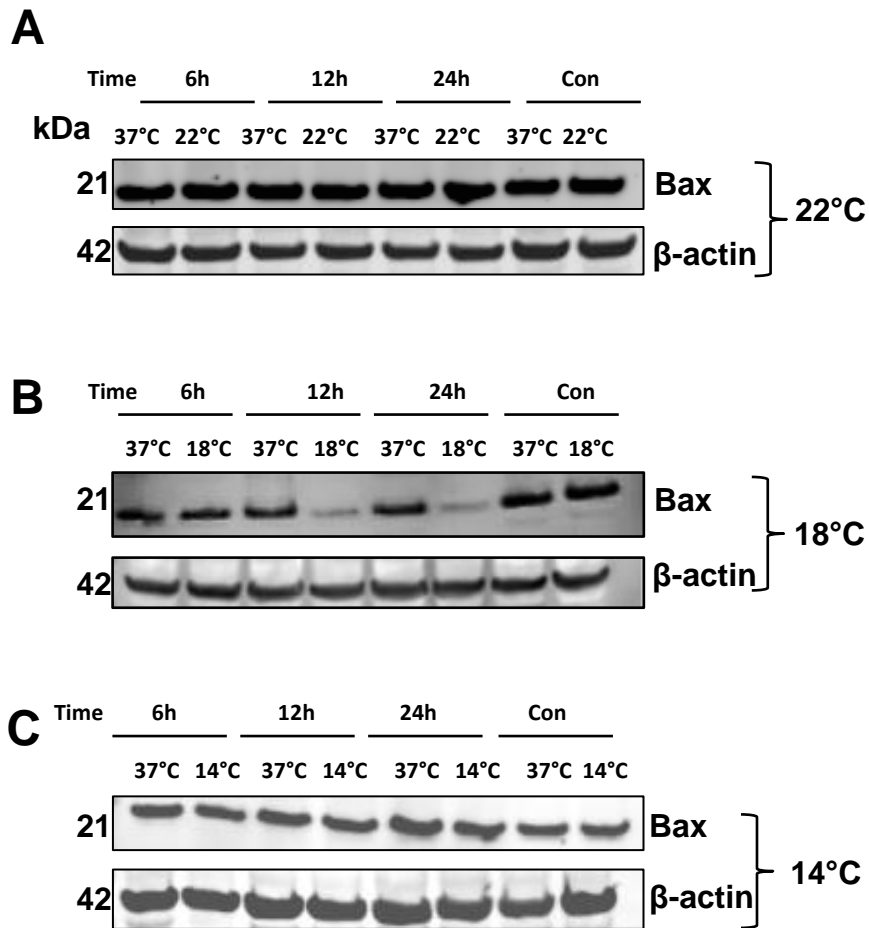


**Figure 6-25 The role of temperature on the regulation of Bax expression in response to 4-OH-CP in HaCaTa cells**

$9 \times 10^5$  HaCaTa cells were seeded in 10 cm<sup>2</sup> culture dishes in KSM complete medium and the cells were incubated overnight in 37°C/5% CO<sub>2</sub>. Cells were treated with 5 µg/mL 4-OH-CP at 37°C as well as 22°C, 18°C and 14°C. 6, 12, and 24h after treatment, the cells were lysed 2X SDS-lysis buffer. 20 µg/well of lysate was separated by SDS-PAGE using 4-12% (W/V) Bis Tris gels and blotted onto a PVDF membrane. The membrane was probed overnight with an anti-Bax antibody in TBS Tween 0.1% (1:1000 dilution). Following that, the membrane was incubated for one hour with goat-anti mouse IgG Alexa 680 (1:10000 dilution). β-actin (AC-15-A5441) was used as specificity and loading control, the membrane was incubated with the antibody (1:50000 dilution) and secondary antibody Goat anti-Mouse IgG Alexa 680 (1:10000 dilution). Membranes were scanned at 700nm and 800nm on a Licor Odyssey Infra-Red Imaging system and images are shown in black and white. Cells were treated at **A**) 37°C and 22°C, **B**) 37°C and 18°C, **C**) 37°C and 14°C. Data obtained from two independent biological experiments.

**Doxorubicin  
HaCaTa cells**

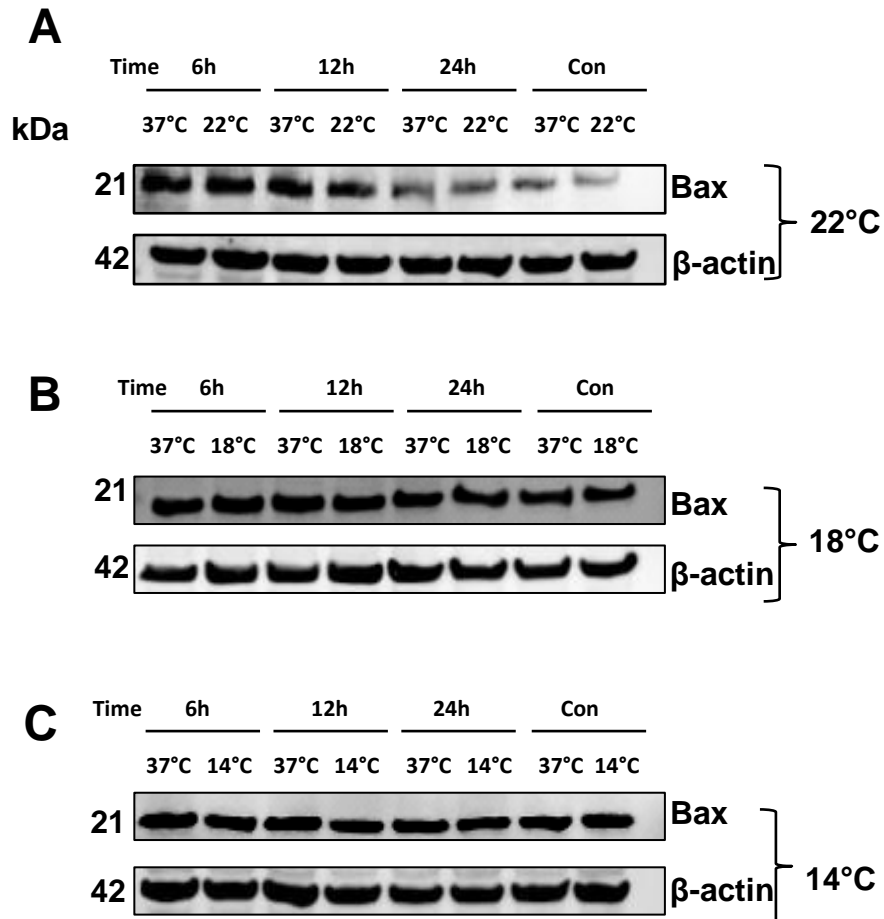


**Figure 6-26 The role of temperature on the regulation of Bax expression in response to doxorubicin in HaCaTa cells**

$9 \times 10^5$  HaCaTa cells were seeded in  $10 \text{ cm}^2$  culture dishes in KSFM complete medium and the cells were incubated overnight in  $37^\circ\text{C}/5\% \text{ CO}_2$ . Cells were treated with  $0.5 \mu\text{g}/\text{mL}$  doxorubicin at  $37^\circ\text{C}$  as well as  $22^\circ\text{C}$ ,  $18^\circ\text{C}$  and  $14^\circ\text{C}$ . 6, 12, and 24h after treatment, the cells were lysed 2X SDS-lysis buffer.  $20 \mu\text{g}/\text{well}$  of lysate was separated by SDS-PAGE using 4-12% (W/V) Bis Tris gels and blotted onto a PVDF membrane. The membrane was probed overnight with an anti-Bax antibody in TBS Tween 0.1% (1:1000 dilution). Following that, the membrane was incubated for one hour with goat-anti mouse IgG Alexa 680 (1:10000 dilution).  $\beta$ -actin (AC-15-A5441) was used as specificity and loading control, the membrane was incubated with the antibody (1:50000 dilution) and secondary antibody Goat anti-Mouse IgG Alexa 680 (1:10000 dilution). Membranes were scanned at 700nm and 800nm on a Licor Odyssey Infra-Red Imaging system and images are shown in black and white. Cells were treated at **A)**  $37^\circ\text{C}$  and  $22^\circ\text{C}$ , **B)**  $37^\circ\text{C}$  and  $18^\circ\text{C}$ , **C)**  $37^\circ\text{C}$  and  $14^\circ\text{C}$ . Data obtained from two independent biological experiments.

**Docetaxel  
HaCaTa cells**

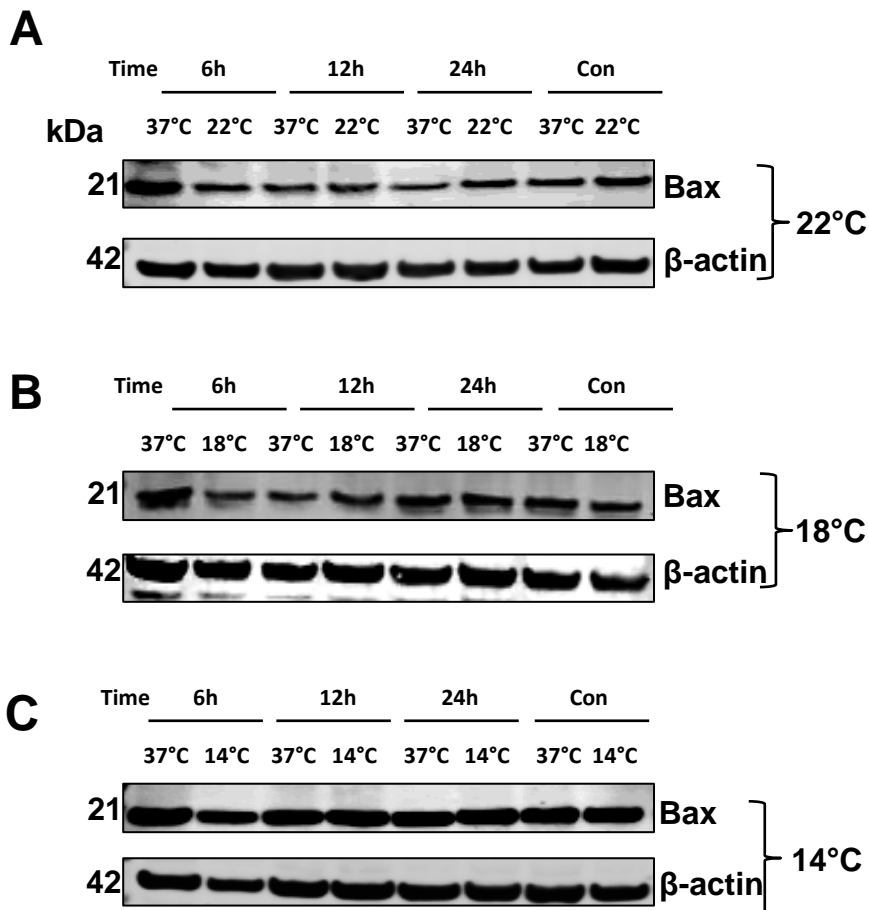


**Figure 6-27 The role of temperature on the regulation of Bax expression in response to docetaxel in HaCaTa cells**

$9 \times 10^5$  HaCaTa cells were seeded in 10 cm<sup>2</sup> culture dishes in KSM complete medium and the cells were incubated overnight in 37°C/5% CO<sub>2</sub>. Cells were treated with 0.01 µg/mL docetaxel at 37°C as well as 22°C, 18°C and 14°C. 6, 12, and 24h after treatment, the cells were lysed 2X SDS-lysis buffer. 20 µg/well of lysate was separated by SDS-PAGE using 4-12% (W/V) Bis Tris gels and blotted onto a PVDF membrane. The membrane was probed overnight with an anti-Bax antibody in TBS Tween 0.1% (1:1000 dilution). Following that, the membrane was incubated for one hour with goat-anti mouse IgG Alexa 680 (1:10000 dilution). β-actin (AC-15-A5441) was used as specificity and loading control, the membrane was incubated with the antibody (1:50000 dilution) and secondary antibody Goat anti-Mouse IgG Alexa 680 (1:10000 dilution). Membranes were scanned at 700nm and 800nm on a Licor Odyssey Infra-Red Imaging system and images are shown in black and white. Cells were treated at **A**) 37°C and 22°C, **B**) 37°C and 18°C, **C**) 37°C and 14°C. Data obtained from two independent biological experiments.

## 6.12 Regulation of Fas ligand (FasL) in response to chemotherapy drug treatment and the effects of cooling

In addition to the induction of the intrinsic apoptotic cell death pathway, which can be triggered by stimuli such as chemotherapy drugs and UV irradiation, several studies have suggested that the extrinsic (receptor-mediated) pathway, for instance CD95/APO-1/Fas receptor activation or TNF-alpha-mediated apoptosis, may also participate in chemotherapy drug induced-DNA damage (Friesen *et al.*, 1996; Poulaki *et al.*, 2001). Keratinocytes cells carry on their surface the Fas receptor, which is activated by its natural ligand, FasL, and induces apoptosis in the cell (Aragane *et al.*, 1998). Previous studies demonstrated p53-mediated induction of Fas in cyclophosphamide-induced apoptosis in the HFs of C57BL/6 mice (Botchkarev *et al.*, 2000). Chemotherapy drugs such as doxorubicin, cyclophosphamide, etoposide, cisplatin, mitoxantrone, and 5-fluorouracil have been shown to trigger nuclear accumulation of p53 (Müller *et al.*, 1997). As shown in (Section 6.5) 4-OH-CP, doxorubicin and docetaxel caused activation of p53 at 37°C and cooling regulated the level of active p53.

As p53 is activated in human keratinocytes following treatment with the panel of chemotherapy drugs tested in this study, we hypothesised that the apoptotic pathway may also be associated with p53-mediated induction of death ligands. Therefore, experiments were carried out to investigate whether these drugs induce the Fas/FasL system to mediate their cytotoxic effects as part of p53-mediated apoptosis and to examine the effect of cooling in this context. HaCaTa were treated with the chemotherapy drugs as above at 37°C and compared with cells treated under cooling conditions (22°C, 18°C and 14°C), and the level of FasL protein was analysed by immunoblotting (Figure 6-28 to Figure 6-30). Results showed that there was some basal expression of FasL in controls (untreated cells). On the other hand, 4-OH-CP-treated HaCaTa cells exhibited a strong induction of FasL which was rapid (already evident at 6h after treatment) compared with controls. Interestingly, FasL levels dramatically decreased in cells treated at 14°C and 18°C after 24h compared to 37°C (Figure 6-28). In addition, the results showed that both doxorubicin and docetaxel induced an increase in FasL levels after 6h at all the temperatures tested and cooling appeared to down-modulate FasL expression.

Treatment of HaCaTa cells with all three drugs 4-OH-CP, doxorubicin and docetaxel, though these drugs have distinct mechanisms of action, resulted in FasL up-regulation in all cases. Importantly, FasL induction was significantly attenuated in most cases by cooling, particularly at 22°C and 18°C (and to a lesser extent at 14°C). These findings suggested that

as part of the apoptotic response, and in addition to activation of p53 targets such as p21 or pro-apoptotic mediators such as PUMA/Noxa, the classical pro-apoptotic TNF ligand FasL is also induced; yet cooling can attenuate the induction of FasL.

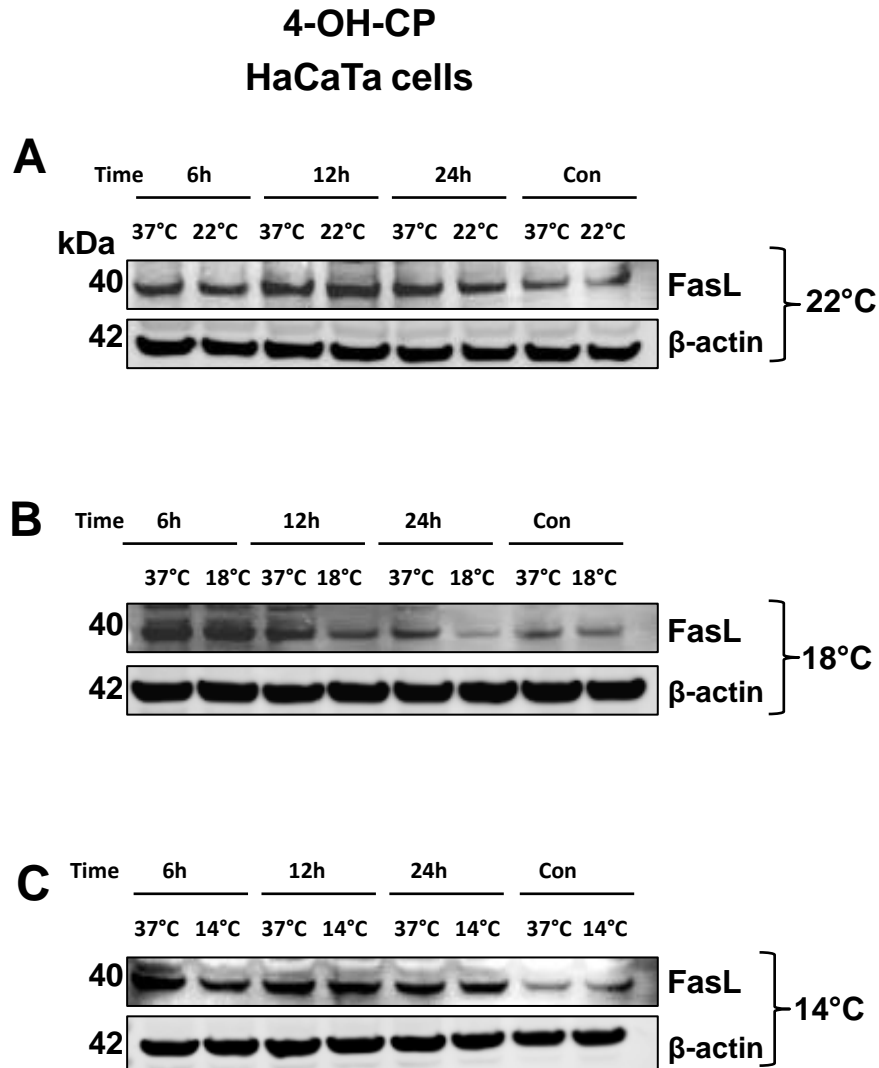


**Figure 6-28 The role of temperature on the regulation of FasL expression in response to 4-OH-CP in HaCaTa cells**

$9 \times 10^5$  HaCaTa cells were seeded in 10 cm<sup>2</sup> culture dishes in KSFM complete medium and the cells were incubated overnight in 37°C/5% CO<sub>2</sub>. Cells were treated with 5 µg/mL 4-OH-CP at 37°C as well as 22°C, 18°C and 14°C. 6, 12, and 24h after treatment, the cells were lysed 2X SDS-lysis buffer. 20 µg/well of lysate was separated by SDS-PAGE using 4-12% (W/V) Bis Tris gels and blotted onto a PVDF membrane. The membrane was probed overnight with an anti-FasL antibody in TBS Tween 0.1% (1:1000 dilution). Following that, the membrane was incubated for one hour with Goat anti-Rabbit IgG IRDye 800nm (1:10000 dilution). β-actin (AC-15-A5441) was used as specificity and loading control, the membrane was incubated with the antibody (1:50000 dilution) and secondary antibody Goat anti-Mouse IgG Alexa 680 (1:10000 dilution). Membranes were scanned at 700nm and 800nm on a Licor Odyssey Infra-Red Imaging system and images are shown in black and white. Cells were treated at **A**) 37°C and 22°C, **B**) 37°C and 18°C, **C**) 37°C and 14°C. Data obtained from two independent biological experiments.

**Doxorubicin  
HaCaTa cells**

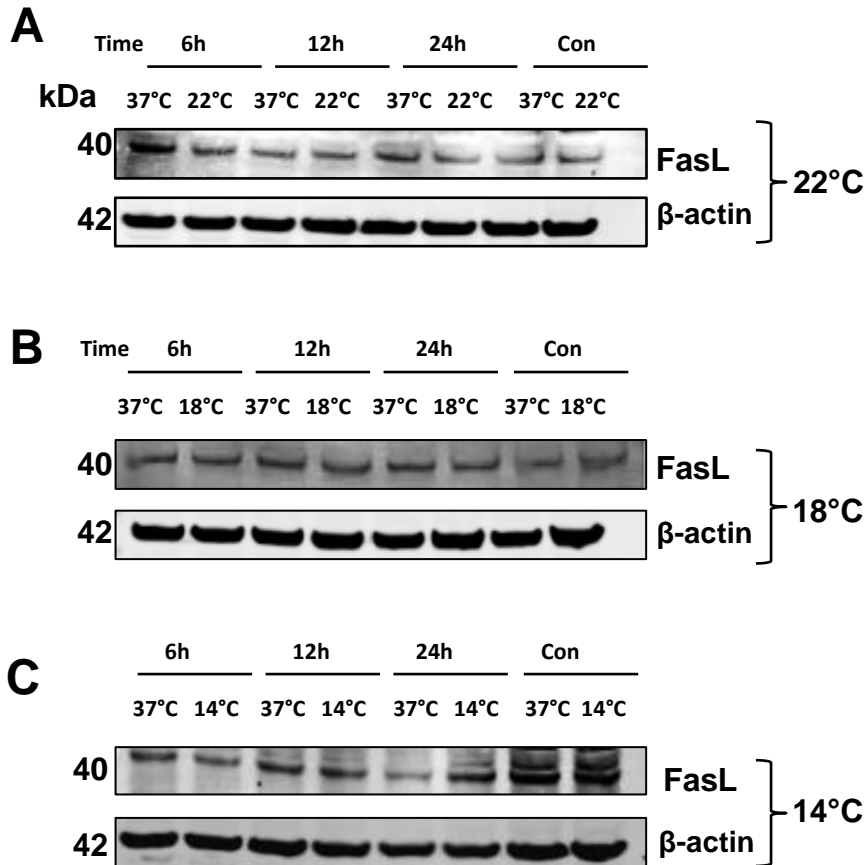


**Figure 6-29 The role of temperature on the regulation of FasL expression in response to doxorubicin in HaCaTa cells**

$9 \times 10^5$  HaCaTa cells were seeded in  $10 \text{ cm}^2$  culture dishes in KFSM complete medium and the cells were incubated overnight in  $37^\circ\text{C}/5\% \text{ CO}_2$ . Cells were treated with  $0.5 \text{ }\mu\text{g/mL}$  doxorubicin at  $37^\circ\text{C}$  as well as  $22^\circ\text{C}$ ,  $18^\circ\text{C}$  and  $14^\circ\text{C}$ . 6, 12, and 24h after treatment, the cells were lysed 2X SDS-lysis buffer.  $20 \text{ }\mu\text{g/well}$  of lysate was separated by SDS-PAGE using 4-12% (W/V) Bis Tris gels and blotted onto a PVDF membrane. The membrane was probed overnight with an anti-FasL antibody in TBS Tween 0.1% (1:1000 dilution). Following that, the membrane was incubated for one hour with Goat anti-Rabbit IgG IRDye 800nm (1:10000 dilution).  $\beta$ -actin (AC-15-A5441) was used as specificity and loading control, the membrane was incubated with the antibody (1:50000 dilution) and secondary antibody Goat anti-Mouse IgG Alexa 680 (1:10000 dilution). Membranes were scanned at 700nm and 800nm on a Licor Odyssey Infra-Red Imaging system and images are shown in black and white. Cells were treated at **A**)  $37^\circ\text{C}$  and  $22^\circ\text{C}$ , **B**)  $37^\circ\text{C}$  and  $18^\circ\text{C}$ , **C**)  $37^\circ\text{C}$  and  $14^\circ\text{C}$ . Data obtained from two independent biological experiments.

**Docetaxel  
HaCaTa cells**

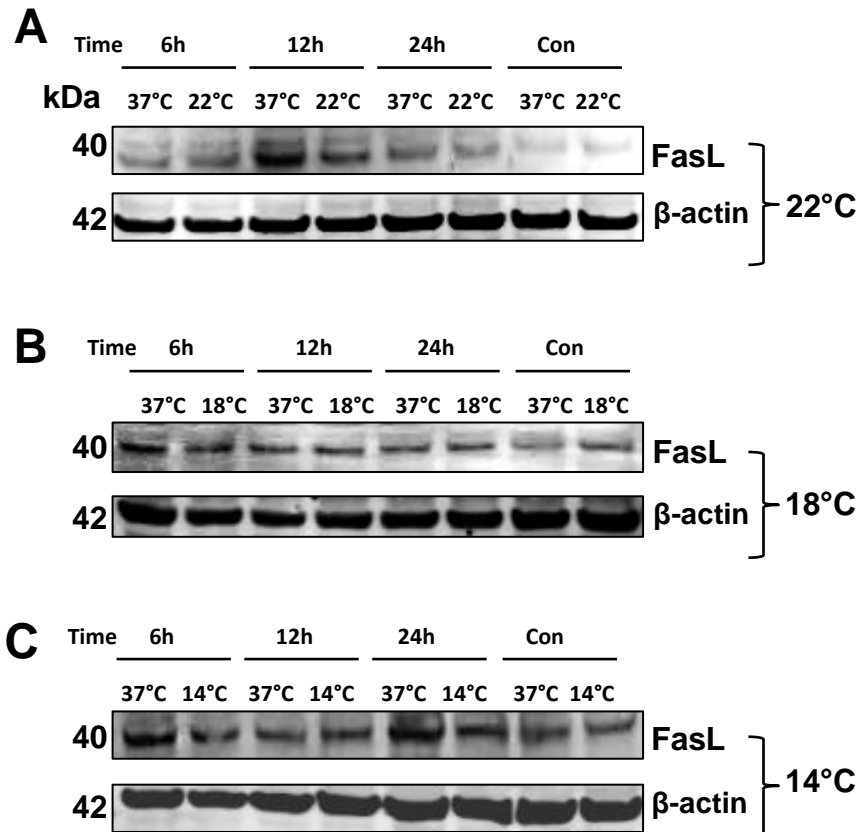


**Figure 6-30 The role of temperature on the regulation of FasL expression in response to docetaxel in HaCaTa cells**

$9 \times 10^5$  HaCaTa cells were seeded in 10 cm<sup>2</sup> culture dishes in KFSM complete medium and the cells were incubated overnight in 37°C/5% CO<sub>2</sub>. Cells were treated with 0.01 µg/mL docetaxel at 37°C as well as 22°C, 18°C and 14°C. 6, 12, and 24h after treatment, the cells were lysed 2X SDS-lysis buffer. 20 µg/well of lysate was separated by SDS-PAGE using 4-12% (W/V) Bis Tris gels and blotted onto a PVDF membrane. The membrane was probed overnight with an anti-FasL antibody in TBS Tween 0.1% (1:1000 dilution). Following that, the membrane was incubated for one hour with Goat anti-Rabbit IgG IRDye 800nm (1:10000 dilution). β-actin (AC-15-A5441) was used as specificity and loading control, the membrane was incubated with the antibody (1:50000 dilution) and secondary antibody Goat anti-Mouse IgG Alexa 680 (1:10000 dilution). Membranes were scanned at 700nm and 800nm on a Licor Odyssey Infra-Red Imaging system and images are shown in black and white. Cells were treated at **A**) 37°C and 22°C, **B**) 37°C and 18°C, **C**) 37°C and 14°C. Data obtained from two independent biological experiments.

### **6.13 Effect of functional blockade of FasL/Fas interaction on drug-mediated apoptosis in HaCaTa cells**

As FasL was detected to be up-regulated in HaCaTa cells, its functional implication in chemotherapy drugs-mediated apoptosis was addressed. For this purpose, HaCaTa cells were treated with 4-OH-CP and doxorubicin in the presence of the classical antagonistic antibody NOK-1, which blocks FasL and thus inhibits FasL/CD95 mediated signalling and apoptosis. The NOK-1 mAb specifically binds to the region of FasL (CD178) that normally interacts with the Fas receptor (CD95) (Kayagaki *et al.*, 1995). As shown in Figure 6-31, the blocking antibody had no effect on cytotoxic drug-induced apoptosis. Although this appears unexpected, it is possible that FasL might remain functional. As previous studies from our laboratory have demonstrated, death ligands, such as FasL, may be expressed and be functional *via* intracellular compartments (Steele *et al.*, 2006). In other words, during chemotherapy drug-mediated apoptosis, FasL may exert its effect not by paracrine or juxtacrine presentation but by intracellular signalling, thus different approaches (such as siRNA-mediated knockdown would be necessary to address such hypotheses).

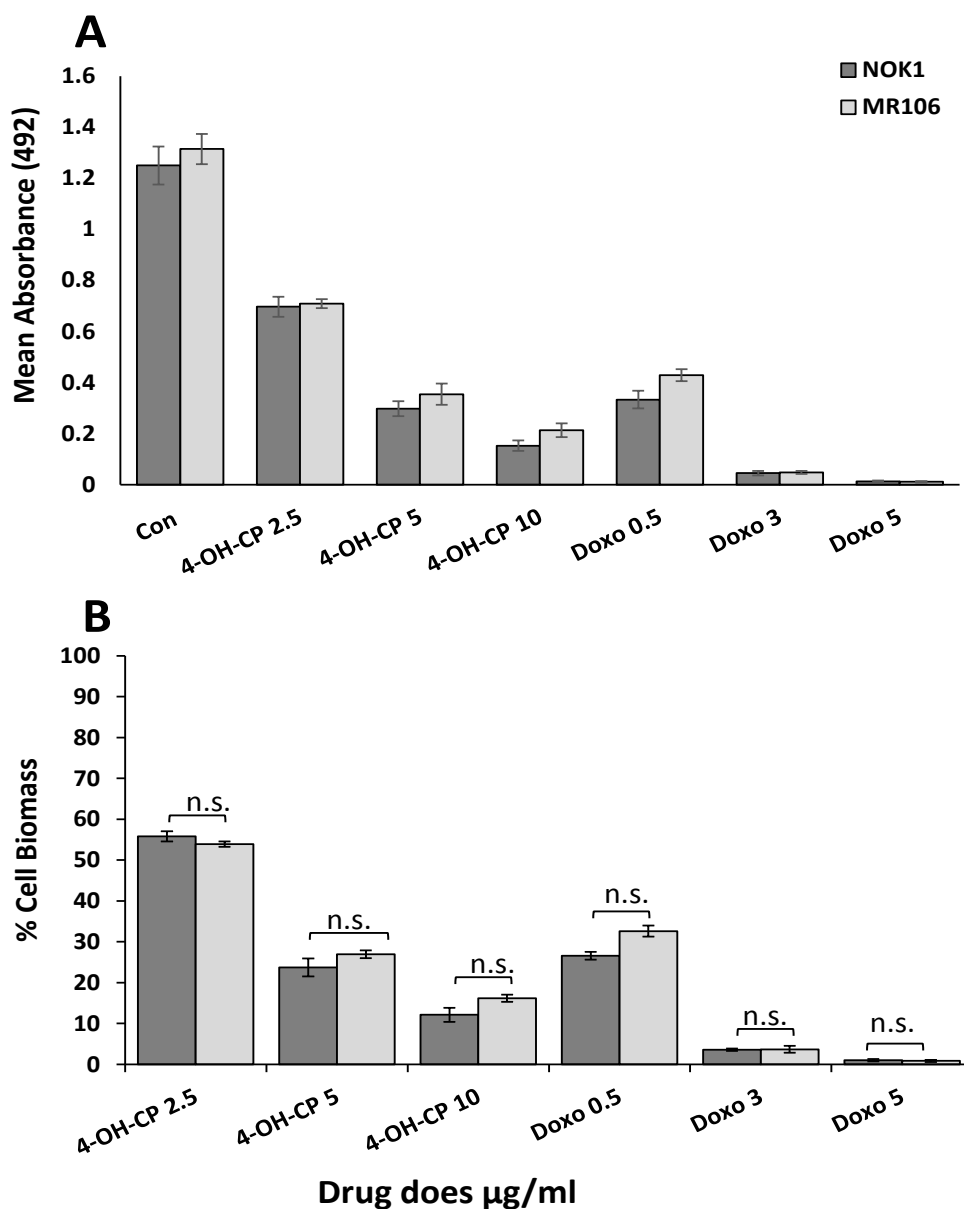


**Figure 6-31 Effect of the blocking anti-FasL antibody NOK1 on drug-mediated apoptosis**

HaCaTa cells were seeded in 96-well plates at 5000 cells/well in KSFM complete medium and were incubated overnight at 37°C/ 5% CO<sub>2</sub>. HaCaTa cells were pre-treated with ± 10 µg/mL of the NOK1 (monoclonal antibody (mAb) to block FasL for 1h at 37°C (as well as the isotype control mAb MR106). HaCaTa cells were treated for 2h with the indicated dose of doxorubicin (Doxo), and 4-OH-CP at 37°C compared with vehicle control (cells treated with medium containing DMSO, in which the reagent was dissolved). The solvent represents the maximum amount of DMSO corresponding to the highest drug concentration). The drugs were then removed, wells were rinsed with PBS to remove any traces of drug and cultures incubated for a further 72h, and after which 20 µL of CellTiter 96® AQueous One solution was added to the wells and plates were incubated at 37°C in 5% CO<sub>2</sub> for a total of four hours. Absorbance was measured spectrophotometrically at a wavelength of 492nm and % cell biomass was calculated as described in Materials and Methods (Chapter 2). Data is presented as **A**) Absorbance (raw data) **B**) % cell biomass shown in bar graph. Data points correspond to mean % cell biomass (±S.E.M.) for three independent biological experiments, each consisting of 6–8 technical replicates. n.s., non-significant.

## 6.14 Expression of TRAIL ligand in response to chemotherapy drug treatment and the effects of cooling

Sharova *et al.*, (2014) suggested that the Tumour necrosis factor (TNF)-related apoptosis-inducing ligand (TRAIL) signalling plays an important role in doxorubicin mediating -induced hair loss. A study on microarray gene expression analysis, using human scalp HFs cultures treated with doxorubicin showed changes in expression of 504 genes in doxorubicin-treated HF *versus* the controls, among these genes Fas and TRAIL receptors were up-regulated (Sharova *et al.*, 2014). Based on this previously published evidence, and having demonstrated that chemotherapy drugs induced FasL expression and cooling could modulate expression of this pro-apoptotic ligand, we investigated whether these chemotherapy drugs induced TRAIL expression to exert their cytotoxic effects and whether cooling had any effect on TRAIL expression. When HaCaTa cells were treated with each of the three drugs (4-OH-CP, doxorubicin, and docetaxel), no TRAIL protein expression was detected using two different antibodies (results for one of these antibodies are shown in Figure 6-32). As expected based on the lack of TRAIL expression at 37°C, cooling at 22°C had no effect on the levels of TRAIL in the cells.

## HaCaTa cells

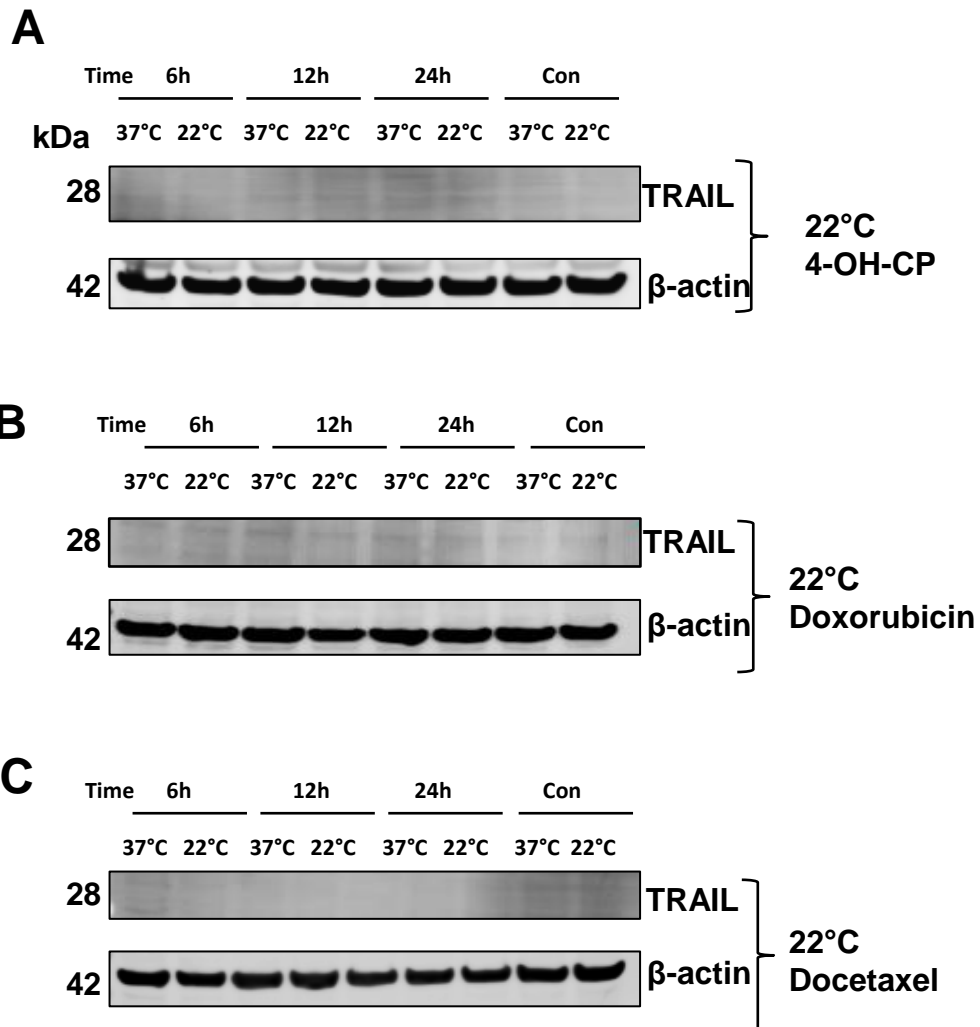


**Figure 6-32 The role of temperature on the regulation of TRAIL expression in response to chemotherapy drugs in HaCaTa cells**

$9 \times 10^5$  HaCaTa cells were seeded in  $10 \text{ cm}^2$  culture dishes in KFSM complete medium and the cells were incubated overnight in  $37^\circ\text{C}/5\% \text{ CO}_2$ . Cells were treated with  $5 \mu\text{g}/\text{mL}$  4-OH-CP at  $37^\circ\text{C}$  as well as  $22^\circ\text{C}$ ,  $18^\circ\text{C}$  and  $14^\circ\text{C}$ . 6, 12, and 24h after treatment, the cells were lysed 2X SDS-lysis buffer.  $20 \mu\text{g}/\text{well}$  of lysate was separated by SDS-PAGE using 4-12% (W/V) Bis Tris gels and blotted onto a PVDF membrane. The membrane was probed overnight with an anti-TRAIL antibody in TBS Tween 0.1% (1:1000 dilution). Following that, the membrane was incubated for one hour with Goat anti-Rabbit IgG IRDye 800nm (1:10000 dilution).  $\beta$ -actin (AC-15-A5441) was used as specificity and loading control, the membrane was incubated with the antibody (1:50000 dilution) and secondary antibody Goat anti-Mouse IgG Alexa 680 (1:10000 dilution). Membranes were scanned at 700nm and 800nm on a Licor Odyssey Infra-Red Imaging system and images are shown in black and white. Cells were treated at **A**)  $37^\circ\text{C}$  and  $22^\circ\text{C}$ , **B**)  $37^\circ\text{C}$  and  $18^\circ\text{C}$ , **C**)  $37^\circ\text{C}$  and  $14^\circ\text{C}$ . Data obtained from two independent biological experiments.

## 6.15 Changes in Bid protein in response to chemotherapy drugs treatment and the effects of cooling

Bid, is a pro-apoptotic Bcl-2 family member, capable of binding to pro-apoptotic Bax, and it is a key intracellular protein that acts as the point of cross-talk between the extrinsic and intrinsic (mitochondrial) apoptotic pathways. Bid is cleaved mainly by caspase-8 during death receptor-mediated signalling (such as signalling triggered by FasL and TRAIL). Protease-cleaved Bid migrates to mitochondria where it induces MOMP that is dependent on the pro-apoptotic proteins Bax and/or Bak, and thus Bid acts as a sentinel for protease-mediated death signals. During apoptosis, Bid ~21 kDa is proteolytically cleaved to tBid (~15 kDa), thus is inserted into the mitochondrial membrane and allows the activation of the mitochondrial apoptosis pathway (Billen *et al.*, 2008).

We therefore examined the possibility that the activation of FasL might represent a mechanism of cross-talk *via* which chemotherapy drugs induce apoptosis in HaCaTa cells by assessing drug-induced cleavage of Bid to its active form tBid. Treatment of HaCaTa cells with 4-OH-CP induced a small degree of Bid cleavage was seen after 6h and 12h, and a modest reduction in tBid levels at 18°C (Figure 6-33B) and 14°C (Figure 6-33C) was observed. By contrast, a far more marked induction of Bid cleavage was observed following HaCaTa treatment with doxorubicin (Figure 6-34) and docetaxel (Figure 6-35) and cooling at various temperatures attenuated Bid cleavage at most time points investigated. This observation is quite striking, as it coincides with the FasL expression data (previous section), where doxorubicin and docetaxel caused more significant induction of FasL than did 4-OH-CP. Therefore, the pattern of FasL expression and its regulation by cooling closely mirrors the pattern of Bid cleavage and the effects of cooling in its formation.

**4-OH-CP**  
**HaCaTa cells**

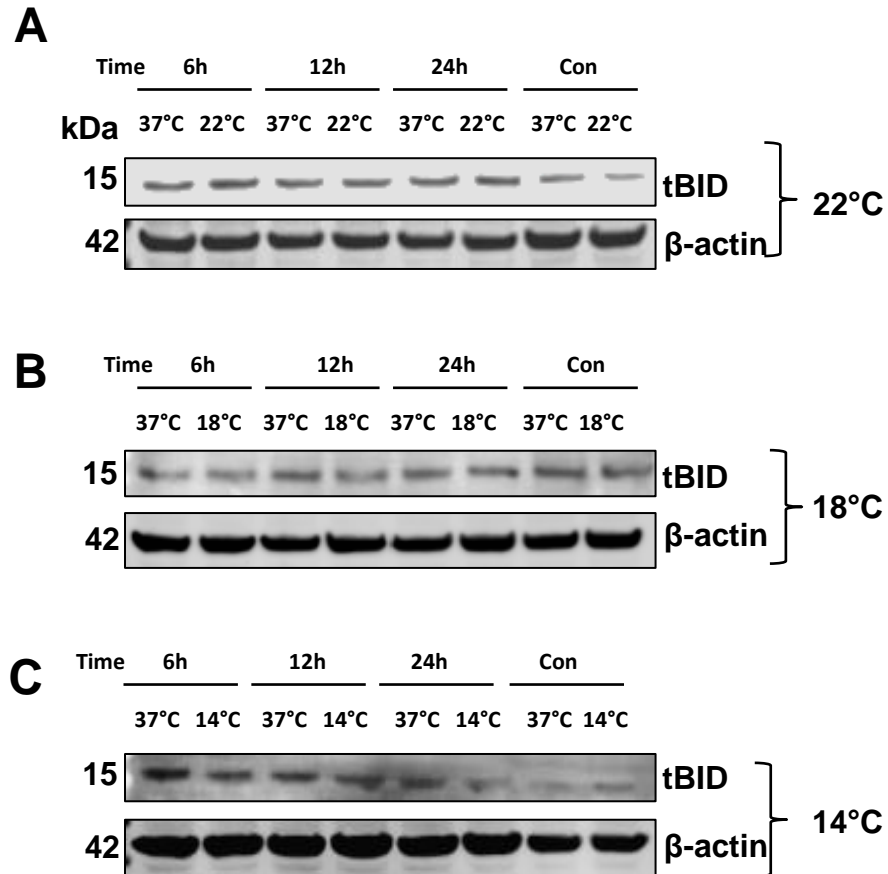


**Figure 6-33 The role of cooling on Bid cleavage (tBid formation) in response to 4-OH-CP in HaCaTa cells**

9x10<sup>5</sup> HaCaTa cells were seeded in 10 cm<sup>2</sup> culture dishes in KSFM complete medium and the cells were incubated overnight in 37°C/5% CO<sub>2</sub>. Cells were treated with 5 µg/mL 4-OH-CP at 37°C as well as 22°C, 18°C and 14°C. 6, 12, and 24h after treatment, the cells were lysed 2X SDS-lysis buffer. 20 µg/well of lysate was separated by SDS-PAGE using 4-12% (W/V) Bis Tris gels and blotted onto a PVDF membrane. The membrane was probed overnight with an anti-BID antibody in TBS Tween 0.1% (1:1000 dilution). Following that, the membrane was incubated for one hour with Goat anti-Rabbit IgG IRDye 800nm (1:10000 dilution). β-actin (AC-15-A5441) was used as specificity and loading control, the membrane was incubated with the antibody (1:50000 dilution) and secondary antibody Goat anti-Mouse IgG Alexa 680 (1:10000 dilution). Membranes were scanned at 700nm and 800nm on a Licor Odyssey Infra-Red Imaging system and images are shown in black and white. Cells were treated at **A**) 37°C and 22°C, **B**) 37°C and 18°C, **C**) 37°C and 14°C. Data obtained from two independent biological experiments.

**Doxorubicin  
HaCaTa cells**

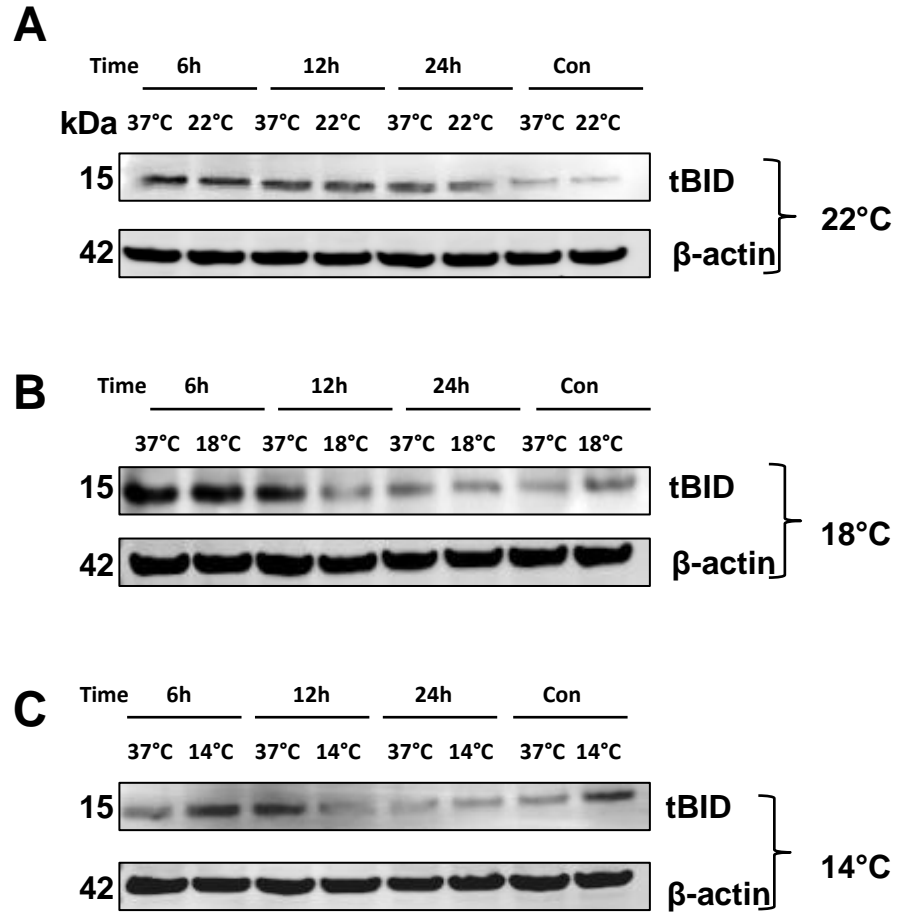


**Figure 6-34 The role of cooling on Bid cleavage (tBid formation) in response to doxorubicin in HaCaTa cells**

$9 \times 10^5$  HaCaTa cells were seeded in 10 cm<sup>2</sup> culture dishes in KSFM complete medium and the cells were incubated overnight in 37°C/5% CO<sub>2</sub>. Cells were treated with 0.5 µg/mL docetaxel at 37°C as well as 22°C, 18°C and 14°C. 6, 12, and 24h after treatment, the cells were lysed 2X SDS-lysis buffer. 20 µg/well of lysate was separated by SDS-PAGE using 4-12% (W/V) Bis Tris gels and blotted onto a PVDF membrane. The membrane was probed overnight with an anti-BID antibody in TBS Tween 0.1% (1:1000 dilution). Following that, the membrane was incubated for one hour with Goat anti-Rabbit IgG IRDye 800nm (1:10000 dilution). β-actin (AC-15-A5441) was used as specificity and loading control, the membrane was incubated with the antibody (1:50000 dilution) and secondary antibody Goat anti-Mouse IgG Alexa 680 (1:10000 dilution). Membranes were scanned at 700nm and 800nm on a Licor Odyssey Infra-Red Imaging system and images are shown in black and white. Cells were treated at **A**) 37°C and 22°C, **B**) 37°C and 18°C, **C**) 37°C and 14°C. Data obtained from two independent biological experiments.

**Docetaxel  
HaCaTa cells**

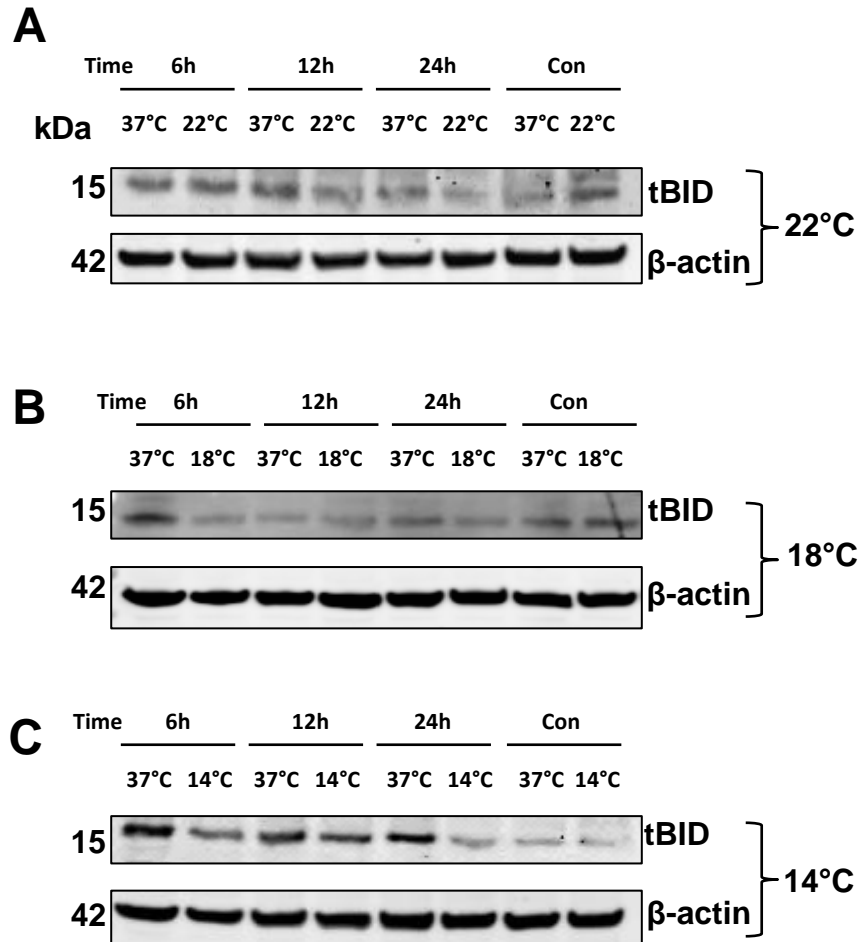


**Figure 6-35 The role of cooling on Bid cleavage (tBid formation) in response to docetaxel in HaCaTa cells**

9x10<sup>5</sup> HaCaTa cells were seeded in 10 cm<sup>2</sup> culture dishes in KSFM complete medium and the cells were incubated overnight in 37°C/5% CO<sub>2</sub>. Cells were treated with 0.01 µg/mL docetaxel at 37°C as well as 22°C, 18°C and 14°C. 6, 12, and 24h after treatment, the cells were lysed 2X SDS-lysis buffer. 20 µg/well of lysate was separated by SDS-PAGE using 4-12% (W/V) Bis Tris gels and blotted onto a PVDF membrane. The membrane was probed overnight with an anti-BID antibody in TBS Tween 0.1% (1:1000 dilution). Following that, the membrane was incubated for one hour with Goat anti-Rabbit IgG IRDye 800nm (1:10000 dilution). β-actin (AC-15-A5441) was used as specificity and loading control, the membrane was incubated with the antibody (1:50000 dilution) and secondary antibody Goat anti-Mouse IgG Alexa 680 (1:10000 dilution). Membranes were scanned at 700nm and 800nm on a Licor Odyssey Infra-Red Imaging system and images are shown in black and white. Cells were treated at **A**) 37°C and 22°C, **B**) 37°C and 18°C, **C**) 37°C and 14°C. Data obtained from two independent biological experiments.

## 6.16 Summary

- The main objective of this chapter was to investigate the intracellular signalling mediators involved in chemotherapy-induced toxicity and their regulation by cooling in NHEK, HHFK, and HaCaTa cells. Interestingly, for most of the proteins investigated in this study rapid changes were observed as early as 6h post treatment.
- Western blotting results demonstrated dramatic and rapid increase in the level of P-p53 at 37°C and maximal expression was occurred 24h post treatment with cytotoxic agents. However, the level P-p53 was reduced significantly by cooling and in some cases completely attenuated.
- The expression of P-p53 in NHEK cells treated with 4-OH-CP was up-regulated as early as 6h following treatment and continued to rise up 24h, which was similar to the expression of P-p53 in HaCaTa cells. Similar results were observed in HHFK cells, where there was a prominent down-modulation of P-p53 expression, as was the case in HaCaTa and NHEK, being observed after 12h post exposure to 4-OH-CP.
- There was a marked reduction in P-p53 levels at all-time points and particularly after 12h in HaCaTa cells treated with doxorubicin under cooling conditions compared with at 37°C. Interestingly, there was also reduction in P-p53 levels in cells treated with docetaxel under cooling conditions compared with cells treated at 37°C, indicating that all three chemotherapy drugs (whether classical genotoxic agents, such as doxorubicin and 4-OH-CP, or an anti-mitotic compound, docetaxel) initiated a DNA damage response evident by the activation of p53 and that cooling inhibited this in a temperature-dependent fashion.
- The small chemical p53 inhibitor, PFT- $\alpha$ , only slightly inhibited or reduced drug-mediated apoptosis after treatment with 4-OH-CP, and there was no effect after treated with doxorubicin. The low concentrations of PFT- $\alpha$  were not sufficient to significantly inhibit cell death, whilst high concentrations exhibited toxic effects.
- p21 induction at 37°C was observed at 6h and this up-regulation was reduced by cooling and in particularly evident for the 18°C after exposure to 4-OH-CP in HaCaTa cells. Furthermore, p21 levels in NHEK cells treated with 4-OH-CP showed similar results with those observed in HaCaTa cells. Interestingly, extensive cooling alone was progressively causing some induction of p21 in untreated cells (controls) and as a result after 12h of treatment, p21 levels at 37°C

were lower than p21 levels at cooling temperatures (particularly 14°C). These results suggested that, although cooling mediated down-modulation of p21 to an extent, it is possible that extensive (24h) or extreme (14°C) cooling might independently also trigger a p21-related “stress” response.

- Western blot experiments demonstrated increases in the level of pro-apoptotic protein PUMA in HaCaTa and NHEK cells at 6h post-treatment with 4-OH-CP, however, PUMA levels progressively declined towards basal levels after 24h. PUMA induction was down-modulated by cooling at all temperatures.
- Of note, PUMA-specific bands were observed in untreated cells, indicating basal expression of the PUMA protein, and these bands at cooling temperatures showed higher PUMA levels compared to control at 37°C indicating a cooling related response.
- Interestingly, the p53-regulated pro-apoptotic Noxa and PUMA both showed the same trend of expression after 4-OH-CP treatment. These results suggested similarities in the regulation of these two proteins. In HaCaTa cells treated with doxorubicin the results showed that Noxa expression was substantially induced after 6h at 37°C and markedly reduced by cooling at 22°C and particularly 14°C, however, at 18°C there was no such reduction in Noxa level. Furthermore, there was no decline in Noxa levels and the level kept increasing in HaCaTa cells treated with docetaxel at 22°C and 18°C, but there was a significant reduction in expression at 14°C.
- In untreated HaCaTa cells, basal Bak expression was detected. Following treatment with 4-OH-CP, the level of Bak expression increased significantly as early as 6h post treatment, and under cooling conditions there was a remarkable reduction in Bak expression. This regulation was temperature-dependent and the greatest down-modulation of Bak by cooling was observed at 24h post-treatment. Interestingly the results obtained at 14°C showed a significant reduction at 12 and 24h. Moreover, Bak protein expression levels in NHEK and HHFK showed a similar pattern of up-regulation to that observed for HaCaTa cells, particularly at 6h.
- The results showed that the expression of Bak protein in HaCaTa cells treated with doxorubicin was up-regulated 6h after treatment at 37°C and cooling down-regulated Bak induction particularly at 18°C and 14°C. However, for unknown reasons there was an increase in Bak expression in HaCaTa cells treated with docetaxel at cooling conditions compared to cells treated at 37°C. Overall, our

results showed that there was clear induction of Bak protein and cooling successfully appeared to modulate this expression.

- In Bax expression investigations, though some changes were noted in Bax protein levels, they were clearly non-significant and no clear differences were observed. Although an induction in Bax expression was observed at 37°C at 6h in docetaxel-treated HaCaTa cells, for all treatment groups after 12h and 24h treatment with docetaxel Bax levels appeared to exhibit little if any difference from basal levels.
- Thus, overall, no clear Bax induction was observed in this work; one main reason was the high basal expression levels of Bax protein in HaCaTa cells, which made comparisons between conditions difficult or, perhaps, unlike Bak, Bax might not be involved in apoptosis in these cells. It is however important to consider that rather than absolute protein levels, the exact localisation pattern of proteins such as Bax, might provide a better idea of its role in cytotoxicity and its regulation by cooling.
- FasL expression was investigated in HaCaTa cells treated with 4-OH-CP, doxorubicin and docetaxel; although there was some basal expression of FasL in untreated cells, HaCaTa cells treated with 4-OH-CP, doxorubicin and docetaxel exhibited a strong induction of FasL at 6h post treatment compared with controls. Interestingly, cooling (14°C and 18°C) dramatically decreased FasL levels. These findings suggest activation of p53-induced target proteins such as p21, proapoptotic mediators such as PUMA/Noxa, and the classical pro-apoptotic ligand FasL are all induced in drug-mediated apoptosis and, cooling can reduce their induction.
- However the classical antagonistic antibody NOK-1, which specifically binds to the region of FasL that normally interacts with the Fas receptor (CD95), did not show any effect on viability in cells treated with chemotherapy drugs; these data suggested that FasL may exert its effect not *via* paracrine or juxtacrine presentation but *via* intracellular signalling.
- TRAIL expression was also investigated, however no TRAIL protein expression was observed after treatment at any temperature tested (at all time points).
- A small degree of Bid cleavage was seen after 6h and 12h, and a modest reduction in tBid levels at 18°C and 14°C in HaCaTa cells treated with 4-OH-CP. However, HaCaTa treated with doxorubicin and docetaxel showed a far more marked induction of Bid cleavage than 4-OH-CP, and cooling conditions attenuated Bid cleavage at most time points tested.

- Interestingly, the pattern of FasL expression and its regulation by cooling closely mirrored the pattern of Bid cleavage and the effects of cooling in its formation, thus providing strong evidence for the existence of a cross talk with an extrinsic apoptotic pathway (although more studies would be necessary to provide a clear functional link). This observation was quite striking, as tBid expression coincides with FasL expression data, were doxorubicin and docetaxel caused more significant induction of FasL than did 4-OH-CP.

## 6.17 Discussion

### 6.17.1 Cooling reduces p53 activation and subsequent p21 induction triggered by chemotherapy drug treatment

To provide a more detailed understanding of the precise mechanisms underpinning the cytoprotective role of cooling against chemotherapy drug-mediated toxicity at the molecular level, this work for the first time examined the expression and activation patterns of important intracellular signalling mediators that could be critical in cell cycle arrest, cytotoxicity and more specifically apoptosis induction.

As discussed above, most anticancer drugs used clinically to date have been able to induce apoptosis in rapidly dividing cancer cells *in vitro* and *in vivo*. Apoptotic pathways initiated by anti-cancer treatments are multiple and can differ depending on the type of drug used and the cell type. Any such agent that can induce damage of nuclear DNA is capable of activating p53 and its turn induce apoptosis (Henseleit *et al.*, 1997; Payne and Miles, 2008), although under some circumstances genotoxic drugs can also induce apoptotic pathways independent of p53. The key role of p53 in the intrinsic apoptotic pathway is well established (Henseleit *et al.*, 1997).

The present work demonstrated the up-regulation of P-p53 by all three well-known chemotherapeutic drugs doxorubicin, cyclophosphamide, and docetaxel in HaCaTa, NHEK, and HHFK cells. Moreover, this study showed that cooling could completely abrogate the induction of p53 activation in a temperature dependent fashion (with gradually reduced P-p53 at temperature values 22°C, 18°C and 14°C).

More specifically, using an antibody that recognizes specifically p53 phosphorylated at Ser-15, a very low basal level of P-p53 in untreated keratinocytes was detected; however P-p53 protein was rapidly induced in HaCaTa cells as early as 6h following exposure to doxorubicin, 4-OH-CP and docetaxel, suggesting an important role for p53 in cell cycle control and apoptosis in response to drug treatment 37°C. The levels of P-p53 was reduced dramatically at cooling conditions, and was particularly striking as the temperature was reduced further from 22°C to 14°C 24h post exposure to 4-OH-CP. Importantly, the same or very similar results were obtained in NHEK and HHFK primary cells after treatment with 4-OH-CP at 18°C (as representative cooling conditions). Also cooling showed reduced P-p53 expression after doxorubicin treatment especially at 14°C after 12h post-treatment. Similar observation were made for doxorubicin and docetaxel at 14°C particularly after 12h post treatment, in agreement with the accumulation of cells in subG0/G1 phase at 37°C and the significant inhibition of this population by cooling after 24h of treatment.

Inactive p53 is localized predominantly in the cytoplasm; in response to DNA damage, p53 is activated and migrates to the nucleus to regulate the expression of pro-apoptotic genes, such as PUMA, Noxa, Bax and Bak (Sakurai *et al.*, 2005). MDM2 controls the activity of p53; it acts by blocking the function of p53 as a transcription factor and accelerates its degradation. Interestingly, previous studies reported that MDM2 mRNA levels were nearly double when BALB c/3T3 cells were cultured at 32°C, whilst increases in p53 degradation and nuclear export of p53 were observed (Sakurai *et al.*, 2005).

To provide functional evidence for the involvement of p53 in triggering cell cycle arrest or particularly cytotoxicity by the chemotherapy drugs, the p53 inhibitor Pifithrin- $\alpha$  (PFT- $\alpha$ ) was exploited. Several reports have shown that PFT- $\alpha$  is a reversible inhibitor of p53-dependent gene transcription and p53-mediated apoptosis (Hoagland *et al.*, 2005; Sohn *et al.*, 2009). The mechanism of action of PFT- $\alpha$  is still unknown; it is only known; that it blocks the transcriptional activity of p53 and the nuclear transport interrupts which inhibits the p53-dependent apoptosis (Sohn *et al.*, 2009; Walton *et al.*, 2005). PFT- $\alpha$  slightly reduced the viability rate in chemotherapy drug-untreated HaCaTa cells, which is probably due to the significant cytotoxicity of PFT- $\alpha$ . Co-administered PFT- $\alpha$  and 4-OH-CP showed a very slight increase in cell biomass compared to only 4-OH-CP; however, co-administered PFT- $\alpha$  and doxorubicin showed a reduction in viability compared with cells only treated with doxorubicin. These findings are in accordance with a previous report showing that PFT- $\alpha$  is unstable in media and converted to PFT- $\beta$  and both forms exhibited cytotoxic effects (Walton *et al.*, 2005). It would be important for future studies to investigate the functional role of p53 in these responses, e.g. by functional inactivation (Shaw *et al.*, 2005) or RNA interference, and more importantly the precise mechanisms involved in cooling mediated regulation of p53 activation.

The p53 protein has the ability to interrupt cell cycle and thus cell proliferation to prevent a suspect or genomics degenerate cell, to allow the cell time to repair DNA damage. p53 transcriptionally up-regulates the p21 protein, which is a potent cyclin dependent kinase (CDK) inhibitor. Because p21 can block most cyclin-cdk complexes, the cell cycle can be stopped in most phases depending on the specific trigger. Also a previous study showed that ROS regulate the expression and activity of p21 (Qiu *et al.*, 1996). Cell cycle analysis (Chapter 4) showed that the growth rate of untreated keratinocytes (controls that were not a chemotherapy drug treated) incubated at cooling conditions was reduced. Western blotting showed p21 induction in response to chemotherapy drug treatment in HaCaTa cells, thus providing evidence on p53-mediated transcriptional activity.

There was a marked increase in the level of p21 at 37°C after exposure to 4-OH-CP, and cooling seemed to down-modulate p21, mainly at 18°C. Interestingly, there was an induction of p21 in untreated cells at 14°C compared to normal temperature after 24h exposure to cooling alone. It is possible that extreme cooling (14°C) might independently trigger a p21-related “stress” response. Importantly, normal keratinocytes (NHEKs) showed similar results with HaCaTa cells after 4-OH-CP exposure, providing more evidence that HaCaTa cells are a suitable keratinocyte cell line model for investigating chemotherapy drug induced toxicity relating to CIA. The above analysis does not enable us to determine whether cell growth arrest was p21 dependent and functional experiments would be necessary. Moreover, the extreme cooling associated p21 induction is very interesting and merits further investigation. Also, other p53 targets could be investigated, such as such as p27.

Keratinocytes treated with doxorubicin showed increased levels of p21 at 37°C compared with cooling conditions, with the lowest level of p21 seen at 14°C. Doxorubicin induced p21 expression as early as 6h post-treatment, consistent with previous work in HCT116 and HT29 cells treated with doxorubicin (Ravizza *et al.*, 2004). Doxorubicin can lead to p53 accumulation (Bender *et al.*, 2011), stabilisation and activation (Oren, 1999); it is possible that the sensitivity of cells to doxorubicin is associated with an increase of p21. Finally, there was marked p21 induction after docetaxel treatment in HaCaTa cells, however, cooling significantly reduced p21 expression particularly at 24h post treatment. As docetaxel caused significant SubG0/G1 peak, also induction of P-p53 and p21, collectively these data suggest that p53 is most probably involved in the apoptosis induction (evident by the subG0/G1 peak) and that p21 protein may play an important role in the docetaxel-induced cell cycle arrest observed.

Results showed that the role of p53 in apoptosis in HaCaTa cells induced by doxorubicin, 4-OH-CP, and docetaxel is different. The role of cooling in proteins, which were involved in this work, is still poorly determined and merits further study. For this, two experiments will be carried out: firstly, block the expression of p53 in our lines and secondly, work with a p53 deficient control line.

## **6.18 Cooling attenuates induction of p53-dependent pro-apoptotic BH3-only proteins PUMA and Noxa**

One major finding in this study was that cooling progressively and in a temperature-dependent fashion blocked the activation of p53-dependent pro-apoptotic signalling pathways in human keratinocytes. As activation of p53 leads to induction of downstream pro-apoptotic “BH3-only” proteins such as PUMA and Noxa, these proteins were investigated, as

they represent major signalling players contributing to apoptosis. A main role of the pro-apoptotic members of the BH3-only family is to control anti-apoptotic Bcl-2 proteins. Bravo-Cuellar *et al* have previously shown that doxorubicin induced both Noxa and PUMA in HaCaT cells (Boccellino *et al.*, 2010; Bravo-Cuellar *et al.*, 2010), consistent with other studies showing that 4-OH-CP induced PUMA and Noxa in E $\mu$ -Myc cell lines (Happo *et al.*, 2010), as well as docetaxel in MCF-7 (Kontos *et al.*, 2014).

Up-regulation of PUMA was observed 6h post-treatment with chemotherapy drugs 4-OH-CP, doxorubicin and docetaxel. PUMA expression was down-modulated by cooling at all temperatures; PUMA levels peaked during the first 6h, followed by a progressive decline towards basal levels after 24h in both HaCaTa and NHEK cells. One interesting finding in this work was that both PUMA and p21 exhibited detectable bands in untreated (control) cells and higher protein levels were detected at later time points compared to controls at 37°C, suggesting that cooling alone might be modulating expression. In HaCaTa cells after treatment with 4-OH-CP the pattern of Noxa protein expression was similar to that of PUMA protein and Noxa was up-regulated as quickly as 6h, however the levels of Noxa declined progressively during the course of 24h. It would be appropriate for future studies to identify the functional role of PUMA or Noxa (by RNAi) and to determine their importance in apoptosis after treatment with chemotherapeutic drugs.

Noxa and PUMA are direct targets of the transcriptional control of p53; however, in this work the relationship between p53 activity and Noxa / PUMA proteins was not investigated and therefore represents an interesting topic for future study. Generation of cells with inactive or absent p53 would permit investigations as to whether in such cells PUMA and Noxa are induced by chemotherapy drugs. Importantly, however, p53 activation is suppressed by cooling and in turn, PUMA and Noxa expression is attenuated.

### **6.18.1 Effects of cooling on the expression of pro-apoptotic proteins Bax and Bak**

Bax and Bak proteins play central roles in the induction of the mitochondrial apoptotic pathway; since the deletion of these proteins inhibits the release of cytochrome c from the mitochondria (Wei *et al.*, 2001). Bak is located in the outer membrane of the mitochondria where it is maintained in an inactive monomeric state *via* its interaction with the protein VDAC2 (Cheng *et al.*, 2003). Bax was the first member of this group shown to be induced by p53 (Thornborrow *et al.*, 2002). Bax is itself kept inactive in the cytosol of healthy cells by association with 14-3-3 and Ku-70 proteins (Thornborrow *et al.*, 2002; Tsuruta *et al.*, 2004). Triggered by an apoptotic stress signal, Bax is activated and translocates to the OMM where

it forms multimeric complexes that can serve as pores for cytochrome c release (Basañez *et al.*, 2002). Several mechanisms could be responsible for the activation of Bax. p53 protein associates with Bax to induce a conformational change and result in its activation (Chipuk *et al.*, 2004). The BH3-only proteins Bid, Bim, Noxa, and PUMA are also capable of inducing activation of Bax (Cartron *et al.*, 2004).

Investigations in HaCaTa, NHEK and HHFK cells treated with 4-OH-CP showed that Bak was detectable and induced 6h after exposure to 4-OH-CP; the level of Bak was significantly high in HaCaTa cells at 37°C. Importantly, under cooling conditions, and depending on the precise temperature, there was a significant reduction in Bak expression and the lowest down-modulation of Bak by cooling mostly was observed at 24h post-treatment at 18°C. However, at 14°C although there was protection against drug cytotoxicity the level of the protein was higher than at 18°C. These data indicate that extreme cooling, such as 14°C, might induce some level of “stress” on the cells, an observation in line with our findings on p21 and PUMA expression. An important finding of this work was that a similar pattern of up-regulation of Bak was observed in primary NHEK cells, too, in similarity to what was observed for HaCaTa cells at 18°C after exposure to 4-OH-CP. Moreover, Bak expression increased after doxorubicin treatment and cooling down-modulated this induction particularly at 18°C (and to a lesser extent at 14°C). These data strongly suggested that cooling modulated Bak, which is significant as Bak represents a critical regulator of the mitochondrial pathway and interfere with this pathway provides further evidence for its ability to confer protection against chemotherapy drugs induced cytotoxicity.

Our findings on the role of 4-OH-CP and doxorubicin in Bax expression and its regulation by cooling were more difficult to interpret due to the high basal level of Bax in these cells. Thus, it was impossible to distinguish between 37°C and 22°C conditions. It is possible that despite our observation for p53 activation, Bax will not be transcriptionally induced in our system. Cytosolic p53 can promote apoptosis directly by inducing the oligomerization and activation of pro-apoptotic Bax (Chipuk *et al.*, 2004) and transcription-dependent and independent pathways of p53-mediated apoptosis do exist (Chipuk and Green, 2004; Chipuk *et al.*, 2004). Future studies should address these possibilities.

### **6.18.2 Investigation on possible cell death signalling cross-talk in apoptosis induction and the effects of cooling**

Increased p53 activity leads to HF damage by up-regulation of Fas (Lindner *et al.*, 1997; Sharov *et al.*, 2004). The up-regulation of FasL and receptors and a reduction of Bcl-2 / Bax ratio has a pro-apoptotic effect in HFs during the catagen phase of the hair cycle

(Lindner *et al.*, 1997). It is believed that FasL and receptors are also important in the process of dystrophic restructuring of HF during CIA (Sharov *et al.*, 2004). Chemotherapy drugs such as etoposide, cytarabine, cisplatin, methotrexate and doxorubicin have been shown to activate the Fas / FasL system and induce apoptosis by both intrinsic and extrinsic pathways (Harris, 1996; Müller *et al.*, 1998). To determine the potential role of the Fas/FasL system in chemotherapy drug-mediated keratinocyte death and assess the possible role of cooling, Western blotting analysis was performed and showed marked up-regulation of FasL induced by doxorubicin, 4-OH-CP, and docetaxel.

Death domain-containing receptors such as TNF-R1, Fas (CD95) or TRAIL (TNF-Related Apoptosis Inducing Ligand) receptors activate signalling pathways leading to cell death by apoptosis (Micheau and Tschopp, 2003). Previous studies showed that the ligand TRAIL represents one p53 transcriptional target gene after treatment of HCT116 cells with 5-Fluorouracil (5FU) (Kuribayashi *et al.*, 2008). More relevant to this work, Sharova *et al.*, (2014), based on work utilising *ex vivo* cultured human HFs, suggested that the Tumour necrosis factor (TNF)-related apoptosis-inducing ligand (TRAIL) signalling plays an important role in doxorubicin-induced hair loss (Sharova *et al.*, 2014).

No TRAIL was detected following treatment with doxorubicin, 4-OH-CP and docetaxel in drug treated HaCaTa cells (and no basal activity was detectable in untreated control cells). Therefore, at least in HaCaTa cells, TRAIL does not appear to be induced suggesting lack of involvement in cytotoxicity. Collectively, our findings suggest that the Fas/FasL system, but not TRAIL-R/TRAIL system might be critical in apoptosis induction and regulation of FasL expression has added another piece of evidence for the ability of cooling to protect from drug-mediated cytotoxicity. This is in agreement with previous studies demonstrated p53-mediated induction of Fas in cyclophosphamide-induced apoptosis in the HFs of C57BL/6 mice (Botchkarev *et al.*, 2000). HaCaTa cells treated with 4-OH-CP, doxorubicin and docetaxel exhibited a strong induction of FasL at early time point post treatment, however, cooling dramatically decreased FasL levels. These findings suggest activation of p53-induced target proteins such as p21, pro-apoptotic mediators such as PUMA/Noxa, and the classical pro-apoptotic ligand FasL are all induced in drug-mediated apoptosis and, cooling can reduce their induction.

The majority of studies on BH3-only protein Bid demonstrate that cleavage of this protein by caspase-8 is required to initiate, in functional association with Bax, the release of cytochrome c from the mitochondria to the cytoplasm (Roy and Nicholson, 2000; Tang *et al.*, 2000). Bid cleavage evident by the generation of tBid was detected following treatment with cytotoxic drugs in HaCaTa cells with a different pattern for each drug. A small degree of

Bid cleavage was seen after 6h and 12h, and a modest reduction in tBid levels at 18°C and 14°C in HaCaTa cells treated with 4-OH-CP. By contrast, HaCaTa cells treated with doxorubicin and docetaxel showed a far more marked induction of Bid cleavage than 4-OH-CP, and cooling conditions attenuated Bid cleavage at most time points tested. These findings suggest a signalling cross-talk between extrinsic and intrinsic apoptosis pathways in HaCaTa cells post drug treatment and cooling appears to suppress this pathway.

The role of tBid has mostly been described in the context of cell death triggered by death receptors (Roy and Nicholson, 2000). It seems that Bid is induced during apoptosis triggered by doxorubicin and docetaxel in particular in HaCaTa cells; it is possible that Bid might play a role *via* direct association with Bax to increase mitochondrial permeability (Wei *et al.*, 2000) which are hypotheses that could form the basis for future studies. Moreover, tBid formation tends to be mediated by caspase-8 of the extrinsic pathway or caspase-2 (Lassus *et al.*, 2002). Interestingly, previous studies showed that docetaxel induced apoptosis *via* activation of caspase-2 (Mhaidat *et al.*, 2007); it would be interesting to investigate the induction of caspase-2 and the effects of cooling on its induction. Notably, the pattern of FasL expression and its regulation by cooling closely mirrored the pattern of Bid cleavage and the effects of cooling in its formation. This provides strong evidence for the existence of cross talk with an extrinsic apoptotic pathway (although more studies would be necessary to provide a clear functional link). This observation was quite striking, as tBid expression coincides with FasL expression data, where doxorubicin and docetaxel caused more significant induction of FasL than 4-OH-CP. Data in this work provides strong evidence for the existence of a cross talk with an extrinsic apoptotic pathway (although more studies would be necessary to provide a clear functional link). This observation was quite striking, as tBid expression coincides with FasL expression data, where doxorubicin and docetaxel caused more significant induction of FasL than did 4-OH-CP.

**CHAPTER 7: The effect of antioxidant-mediated  
blockade of ROS in cooling-induced cytoprotection:  
combinatorial treatment with N-acetyl-cysteine (NAC)  
and cooling protects against chemotherapy drug  
cytotoxicity**

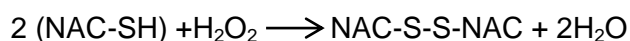
## 7.1 Oxidative stress and cellular antioxidant mechanisms

Oxidative stress refers to a state in which highly reactive molecules (such as reactive oxygen species, ROS) occur at high levels in cells, which can have a damaging effect on these cells. ROS, as mentioned previously in chapter 5, are constantly formed in an organism, and they are not merely metabolic by-products but can also perform physiological functions, and there are different enzymes to degrade (detoxify) them. However, once the generation of ROS reaches beyond the capacity of the redox-regulating mechanisms in the cell, proteins and DNA (as well as other structures such as lipids) are damaged, and once the damage is beyond repair, cell death is induced (Simon *et al.*, 2000; Yu, 1994).

In order to cope with oxidative stress, mammalian cells have developed a very complex system of cytoprotective mechanisms against such stress. These include non-enzymatic antioxidants such as a glutathione (or GSH) (Atkuri *et al.*, 2007). GSH is a molecule that the body makes from various nutrients, including the amino acid cysteine (Sprietsma, 1999). GSH is the main line of defence against such harmful substances, and plays several physiological roles including signal transduction, regulation, intracellular defences against oxidative stress and other important functions in the neoplastic process (Schumacker, 2015). Effective regulation of the cellular balance between oxidation and anti-oxidation (reduction) is physiologically vital, hence, for instance, when GSH levels drop below baseline, this can disrupt the functioning of immune cells and make the body more sensitive to the toxic effects of certain drugs (Kerksick and Willoughby, 2005).

## 7.2 N-acetyl-cysteine (NAC) and its antioxidant properties

Radical scavengers such as N-acetylcysteine (NAC), ascorbate (vitamin C), Trolox (vitamin E) and folate (vitamin B12) can cause a decrease in the intracellular accumulation of ROS (Huang *et al.*, 2002). NAC is a relatively low-molecular weight compound (MW = 163.20) with chemical formula  $C_5H_9NO_3S$  (Prasad *et al.*, 2012). NAC is a derivative of the amino acid L-cysteine, which is a source of sulfhydryl (SH) groups, and is converted into metabolites capable of stimulating glutathione (GSH) synthesis (Atkuri *et al.*, 2007; Kelly, 1998). The SH groups in NAC can easily be oxidised, which form a disulfide bond to give a compound of two linked NAC molecules, by targeting ROS radicals, NAC causes these to be simultaneously reduced, and thus lose their damaging effect. NAC reduces such species in a way quite similar to glutathione, and shows preference for hydrogen peroxide ( $H_2O_2$ ) and hydroxyl radicals ( $OH\bullet$ ) (Jaworska *et al.*, 1995). Below is a representation of the reaction of NAC with hydrogen peroxide:



Due to its efficient antioxidant properties, NAC constitutes a compound with an impressive array of protective mechanisms, as it can protect against DNA damage and is thus its anti-carcinogenic effects (both linked directly to its antioxidant activity), whilst mediating modulation of metabolism, detoxification, DNA repair, it has anti-inflammatory activity and related immunological effects (De Flora *et al.*, 2001). NAC has an influence on cell cycle progression, and in the context of cancer, it causes inhibition of invasion and metastasis. Moreover, by directly inactivating ROS, it can protect towards the adverse effects of cancer chemotherapeutic agents (De Flora *et al.*, 2001).

Several studies showed evidence that NAC has anti-apoptotic activity, for instance, in beta-nerve cells and pancreatic cells (Luanpitpong *et al.*, 2011; Luanpitpong *et al.*, 2012; Savion *et al.*, 2014) and more recent work in our laboratory has confirmed the strong anti-apoptotic capacity of NAC. It is believed that NAC is capable of impairing the apoptotic program, which might be due to its antioxidant activity, and more specifically due to its role as a precursor to GSH thus can protect cell membranes against lipid peroxidation and protein oxidation (Yan *et al.*, 1995), whilst GSH can regulate the activity of some pro-apoptotic proteins such as JNK. Previous studies also showed that NAC has a protective effect against chemotherapy drug cytotoxicity and its protective function was demonstrated by *in vivo* and *in vitro* experiments, which showed that NAC reduces the antitumor activity of paclitaxel (Alexandre *et al.*, 2006).

### 7.3 Chapter Aims

Work in previous chapters demonstrated that cancer chemotherapy drugs induce death and engage critical mediators of the intrinsic (mitochondrial) apoptosis pathway in human keratinocytes. As part of this response, in addition to mitochondrial MOMP we also observed rapid increases in ROS levels. Due to the importance of ROS in the induction of apoptosis as demonstrated previously and more recently in our laboratory (Dunnill, *et al.*, In Press), we hypothesised that ROS are critical in mediating the cytotoxic effects of these chemotherapy drugs.

This study also showed that cooling could have a strong cytoprotective effect against chemotherapy drug-induced cytotoxicity. Yet, notably, the *in vitro* work demonstrated that the temperature during cell cooling is critical in determining the strength of the cytoprotective capacity of cooling, as temperatures in the region of 22°C are moderately cytoprotective, however, reduction of temperature by an additional 4°C (18°C) can have a significant impact and renders cooling significantly more cytoprotective. Strikingly, these findings are supported by recently published clinical studies demonstrating that the efficacy of scalp cooling during chemotherapy is temperature dependent and the best results appear to be obtained when the scalp temperature decreases to or below 18°C (Komen *et al.*, 2016).

As it is clear that the scalp temperature reached during scalp cooling varies amongst individuals (Komen *et al.*, 2013b; Van Den Hurk *et al.*, 2012b), in some patients scalp cooling might not be efficient at reducing the temperature of the scalp adequately to provide cytoprotection, as only sub-optimal cooling conditions might be achieved in such individuals. Therefore, collectively, we hypothesised that it may be possible to compensate for such sub-optimal temperatures by combination of cooling with treatment with an antioxidant, as part of a possible therapeutic intervention of cooling plus topical treatment with an antioxidant compound to prevent CIA without compromising the anticancer effects of chemotherapy.

#### **Specifically the aims of the work in this chapter were to:**

- Examine the effects of N-acetylcysteine (NAC) during chemotherapy drug-treatment of human keratinocytes.
- Test the effects of combination of cooling and NAC treatment on cell viability in order to understand whether NAC could further enhance the cytoprotective effects of cooling.
- Test the efficacy of “sub-optimal temperature conditions” in protecting from cytotoxicity and, more importantly, examine for the first time the possibility that

treatment with antioxidant NAC may compensate for the inability of “sub-optimal” cooling to protect cells from drug-mediated toxicity.

## 7.4 Optimisation (titration) of NAC

In order to assess the cytoprotective effects of NAC, whether alone or in combination with cooling, HaCaTa cells were treated with NAC (0-20 mM) as part of initial pre-titration experiments (and viability was determined by the CellTiter assay after 72h of exposure, see Materials and Method section 2.2.3). Interestingly, a significant difference in cell viability arose in cultures and there was a dramatic increase in viability (as indicated by the rise in absorbance) in cells treated with NAC in comparison with controls (cells cultured in medium only without the addition of NAC). The highest increase in cell viability was observed at 5 mM. NAC alone after 72h of incubation showed cytotoxicity only at very high concentrations (20mM) (Figure 7-1).

The potential of NAC alone to directly protect from chemotherapy drug-mediated cytotoxicity was assessed in HaCaTa cells using the lower range concentrations of NAC (0.625 and 1.25 mM), as those were the doses with the weakest effect on cell viability. Cells were pre-treated with 0.625 and 1.25 mM NAC for 30 min, before being treated with 0.5, 0.75, and 2.5 µg/mL doxorubicin, 0.005, 0.025, and 0.1 µg/mL docetaxel and 2.5, 5, and 10 µg/mL 4-OH-CP. The data showed that cells treated with 0.625 mM NAC showed a significant increase in viability and thus were rescued significantly from drug cytotoxicity compared to cells treated without NAC; interestingly, a better protection from the cytotoxicity was observed with the lower NAC concentration than with 1.25 mM NAC. The most dramatic protection was observed with 4-OH-CP and in particular for the lower drug dose, “drug + NAC” treated cells showed a significant increase in biomass >20% compared to cells without NAC (Figure 7-2). Overall, notably, in cells treated with 1.25 mM NAC for all three drugs tested, the viability was lower in the presence of NAC compared with drug-treated cells treated without NAC (Figure 7-2). Based on these data, the 0.625 mM dose was selected for all subsequent experiments.

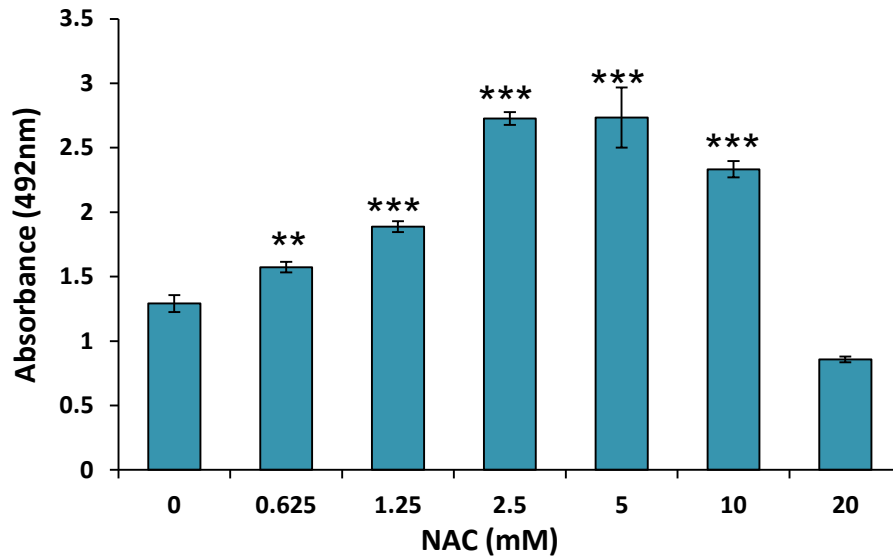


**Figure 7-1 Titration of NAC on HaCaTa cells**

HaCaTa cells were seeded in 96-well plates at 5000 cells/well in KSFM complete medium and were incubated overnight at 37°C/ 5% CO<sub>2</sub>. HaCaTa cells were treated with a range of concentrations of NAC and 72h post-treatment the culture medium was removed and fresh medium added. 20 µL of CellTiter 96® AQueous One solution was added to the wells and plates were incubated at 37°C in 5% CO<sub>2</sub> for a total of four hours. Absorbance was measured spectrophotometrically at a wavelength of 492nm. Bars correspond to mean absorbance values (± S.E.M.) of three independent biological experiments, each consisting of 6–8 technical replicates. \*\*,  $p < 0.01$ ; \*\*\*,  $p < 0.001$ .

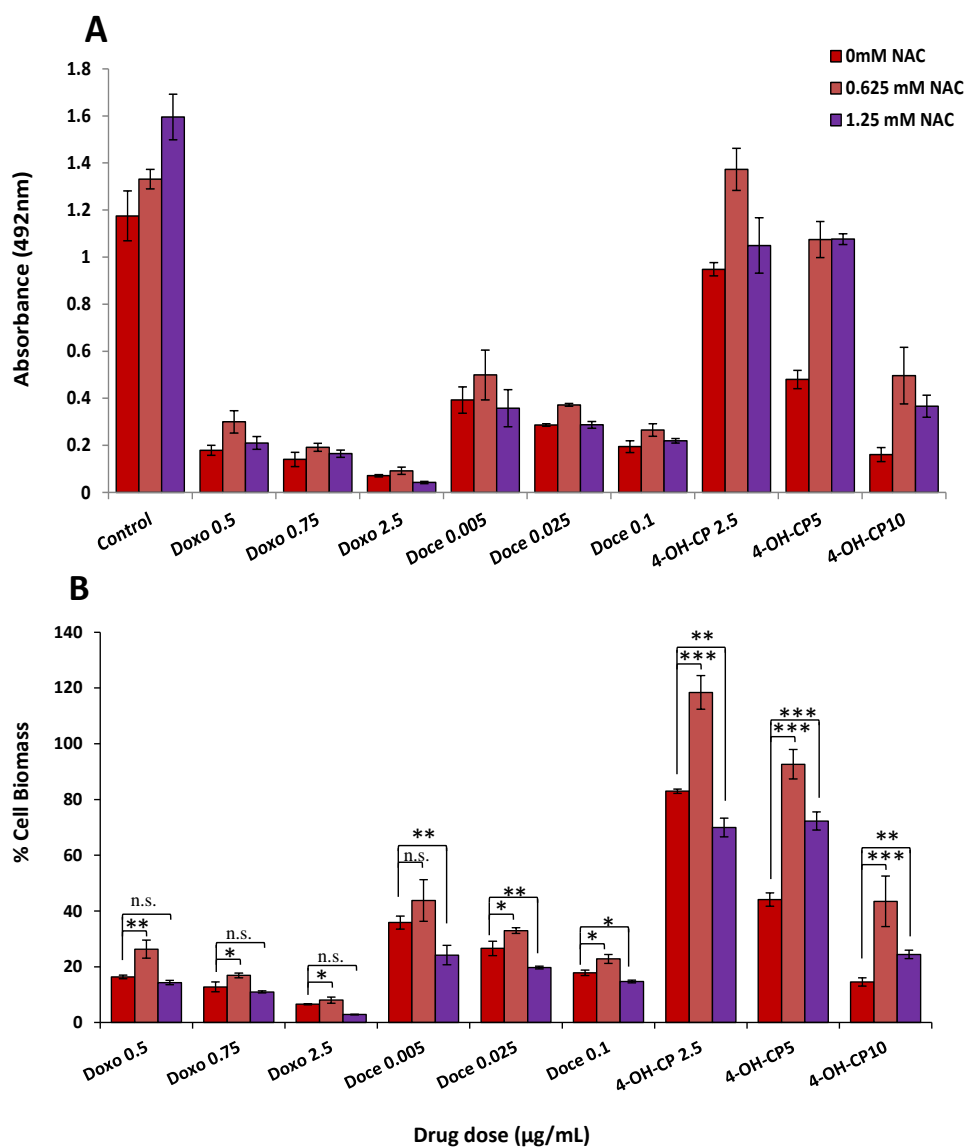


**Figure 7-2 Protection against chemotherapy drug cytotoxicity by NAC**

HaCaTa cells were seeded in 96 well plates at 5000 cells/well in KSM medium and were incubated overnight at 37°C/ 5% CO<sub>2</sub>. HaCaTa cells were pre-treated with and without 0.625 and 0.125 mM NAC for 30 min at 37°C. HaCaTa cells were treated for 2h with the indicated dose of doxorubicin (Doxo), docetaxel (Doce) and 4-OH-CP with and without NAC at 37°C compared with vehicle control (cells treated with medium containing DMSO, in which the reagent was dissolved). The solvent represents the maximum amount of DMSO corresponding to the highest drug concentration). The drugs were then removed, wells were rinsed with PBS to remove any traces of drug and cultures incubated for a further 72h, after which the culture medium was removed and fresh medium added then 20 µL of CellTiter 96® AQueous One solution was added to the wells and plates were incubated at 37°C in 5% CO<sub>2</sub> for a total of four hours. Absorbance was measured spectrophotometrically at a wavelength of 492nm and % cell biomass was calculated as described in Materials and Methods (Chapter 2). Data is presented as **A**) Absorbance (raw data) **B**) % cell biomass shown in bar graph. Data points correspond to mean % cell biomass (±S.E.M.) for three independent biological experiments, each consisting of 6–8 technical replicates. n.s., non-significant; \*,  $p < 0.05$ ; \*\*,  $p < 0.01$ ; \*\*\*,  $p < 0.001$ .

## 7.5 Determining the efficacy of combination of cooling and NAC in protecting from chemotherapy drug-mediated cytotoxicity

Our findings on the ability of NAC to reduce chemotherapy drug-mediated cytotoxicity are in agreement with a previous study which showed that NAC has chemoprotective activity (Muldoon *et al.*, 2001), however, for the first time these effects were tested for a range of drugs and on human keratinocytes. To understand whether NAC could further enhance the significant cytoprotective effects of cooling as shown in previous chapters (Chapter 3), the effect of combination of cooling and NAC treatment on cell viability was investigated. HaCaTa cells were pre-incubated with and without 0.625 mM of NAC 30 min prior to exposure to doxorubicin, docetaxel, and 4-OH-CP for 2h at 37°C *versus* 22°C and 18°C and cytotoxicity was assessed after 72h by cell viability assays. Notably, the results showed significant increases in biomass (thus indicating cytoprotection) in cells treated with cooling in the presence of NAC compared with cells without NAC (Figures 7-3 and 7-4) and the positive impact of NAC was detectable for both 22°C and 18°C cooling conditions. Interestingly, these drugs act *via* different molecular mechanisms, yet there was a significant increase in biomass in cells treated with NAC under cooling conditions in all cases, thus providing evidence for the first time that NAC can significantly enhance the cytoprotective effects of cooling against a variety of drugs.

As the doses of 4-OH-CP employed in the studies described above were relatively lower in comparison to those used in chapter 3 a wider range of doses was investigated, cytoprotection by combinatorial treatment of cooling and NAC against higher concentrations of 4-OH-CP was investigated. HaCaTa cells were treated with 5, 10, 30, and 50 µg/mL 4-OH-CP at 37°C and 22°C. As shown in Figure 7-5, a remarkable protection against all concentrations was observed, particularly with very high drug concentrations 30 and 50 µg/mL 4-OH-CP. The cytotoxicity was clearly further reduced in cells treated with cooling and NAC over the cytoprotection levels reached with cooling alone; the percentage of biomass increased from 35 to 70% and from 10 to 50% in cells treated with 30 and 50 µg/mL with cooling plus NAC, respectively (Figure 7-5). Although not as dramatic, marked increases in cell viability were also observed in the case of doxorubicin treatments.

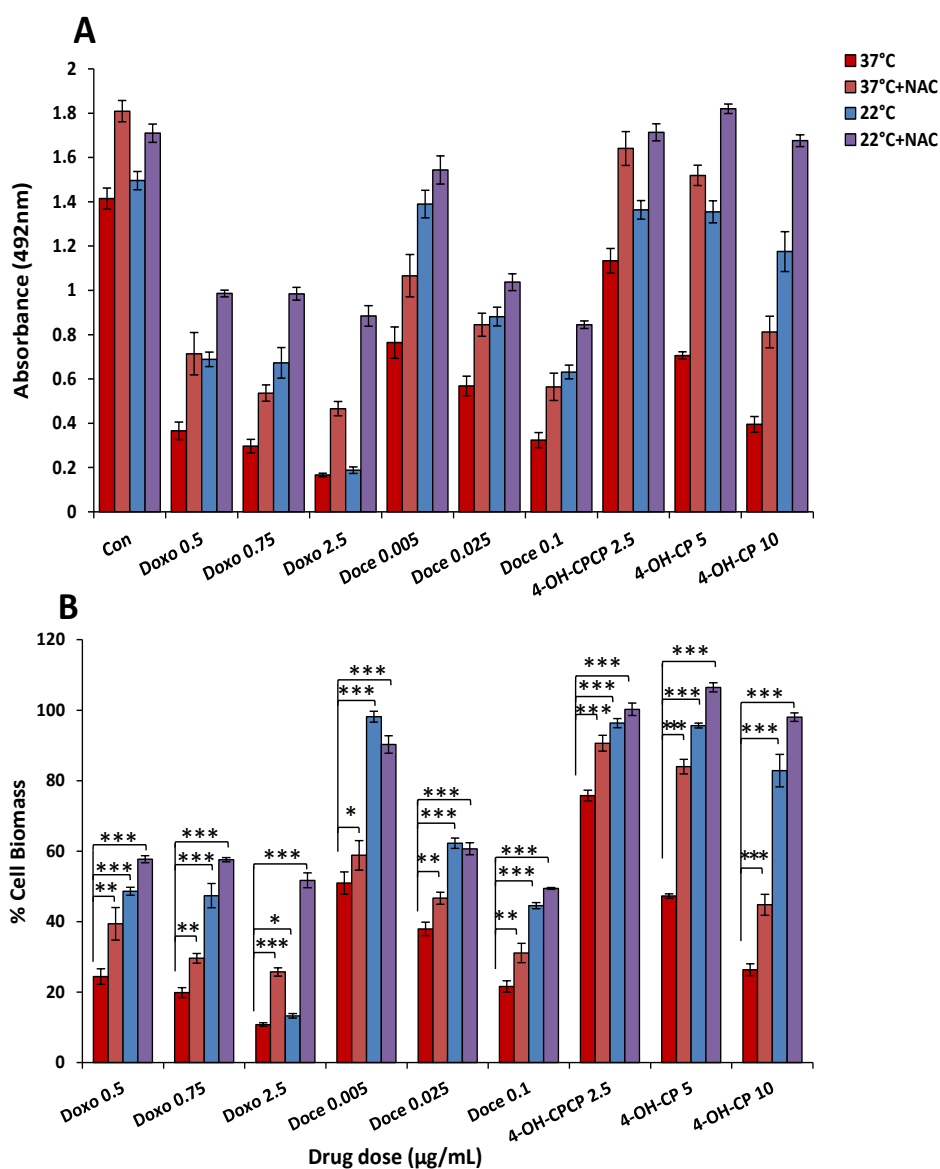


**Figure 7-3 Cytoprotective role of combination of cooling and NAC treatment against chemotherapy drug-mediated toxicity in HaCaTa cells at 37°C and 22°C**

HaCaTa cells were seeded in 96 well plates at 5000 cells/well in KSFM medium and were incubated overnight at 37°C/ 5% CO<sub>2</sub>. HaCaTa cells were pre-treated with and without 0.625 mM NAC for 30 min at 37°C. HaCaTa cells were treated for 2h with the indicated dose of doxorubicin (Doxo), docetaxel (Doce) and 4-OH-CP with and without NAC at 37°C and 22°C compared with vehicle control (cells treated with medium containing DMSO, in which the reagent was dissolved). The solvent represents the maximum amount of DMSO corresponding to the highest drug concentration). The drugs were then removed, wells were rinsed with PBS to remove any traces of drug and cultures incubated for a further 72h, after which the culture medium was removed and fresh medium added then 20 μL of CellTiter 96® Aqueous One solution was added to the wells and plates were incubated at 37°C in 5% CO<sub>2</sub> for a total of four hours. Absorbance was measured spectrophotometrically at a wavelength of 492nm and % cell biomass was calculated as described in Materials and Methods (Chapter 2). Data is presented as **A**) Absorbance (raw data) **B**) % cell biomass shown in bar graph form. Data points correspond to mean % cell biomass (±S.E.M.) for three independent biological experiments, each consisting of 6–8 technical replicates. \*,  $p < 0.05$ ; \*\*,  $p < 0.01$ ; \*\*\*,  $p < 0.001$ .

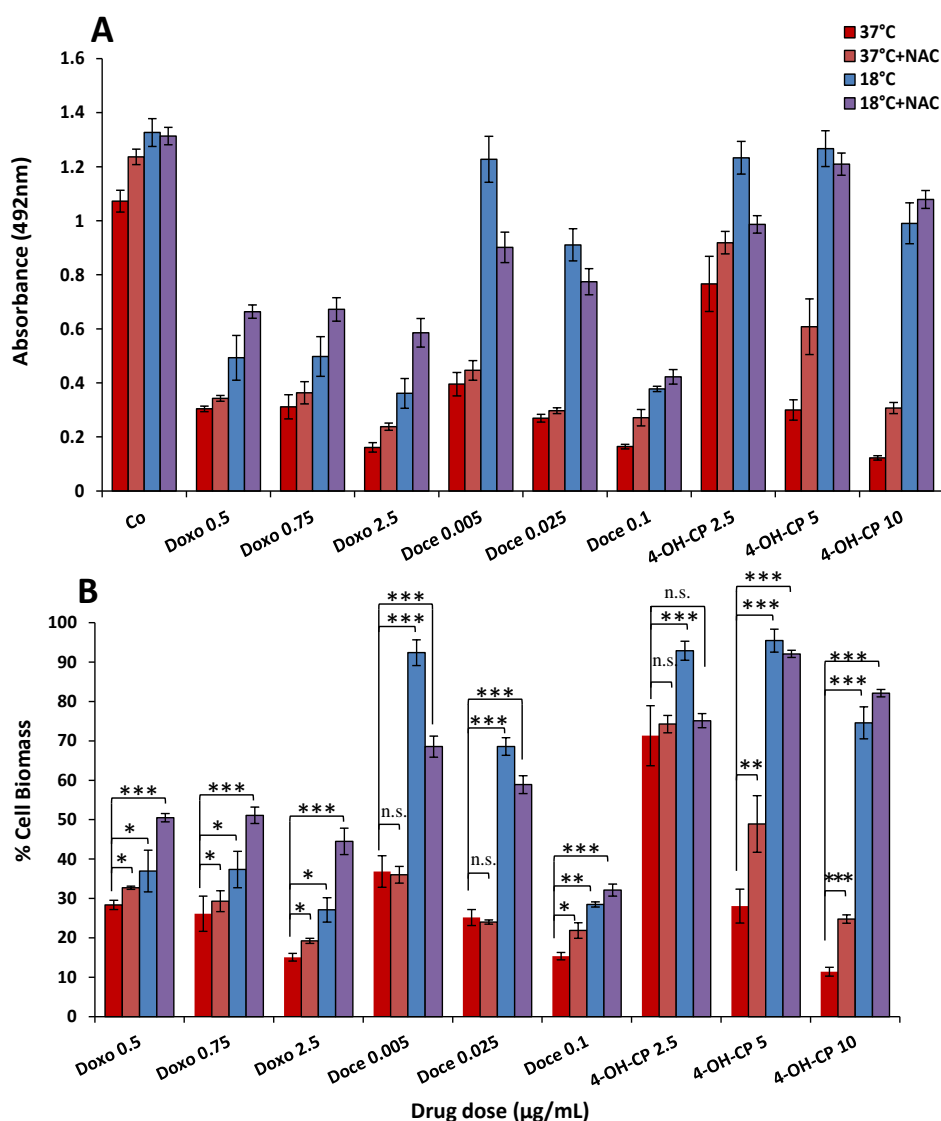


**Figure 7-4 Cytoprotective role of combination of cooling and NAC treatment against chemotherapy drug-mediated toxicity in HaCaTa cells at 37°C and 18°C**

HaCaTa cells were seeded in 96 well plates at 5000 cells/well in KFSM medium and were incubated overnight at 37°C/ 5% CO<sub>2</sub>. HaCaTa cells were pre-treated with and without 0.625 mM NAC for 30 min at 37°C. HaCaTa cells were treated for 2h with the indicated dose of doxorubicin (Doxo), docetaxel (Doce) and 4-OH-CP with and without NAC at 37°C and 18°C compared with vehicle control (cells treated with medium containing DMSO, in which the reagent was dissolved). The solvent represents the maximum amount of DMSO corresponding to the highest drug concentration). The drugs were then removed, wells were rinsed with PBS to remove any traces of drug and cultures incubated for a further 72h, after which the culture medium was removed and fresh medium added then 20 µL of CellTiter 96® Aqueous One solution was added to the wells and plates were incubated at 37°C in 5% CO<sub>2</sub> for a total of four hours. Absorbance was measured spectrophotometrically at a wavelength of 492nm and % cell biomass was calculated as described in Materials and Methods (Chapter 2). Data is presented as **A**) Absorbance (raw data) **B**) % cell biomass shown in bar graph form. Data points correspond to mean % cell biomass (±S.E.M.) for three independent biological experiments, each consisting of 6–8 technical replicates. n.s., non-significant; \*,  $p < 0.05$ ; \*\*,  $p < 0.01$ ; \*\*\*,  $p < 0.001$ .

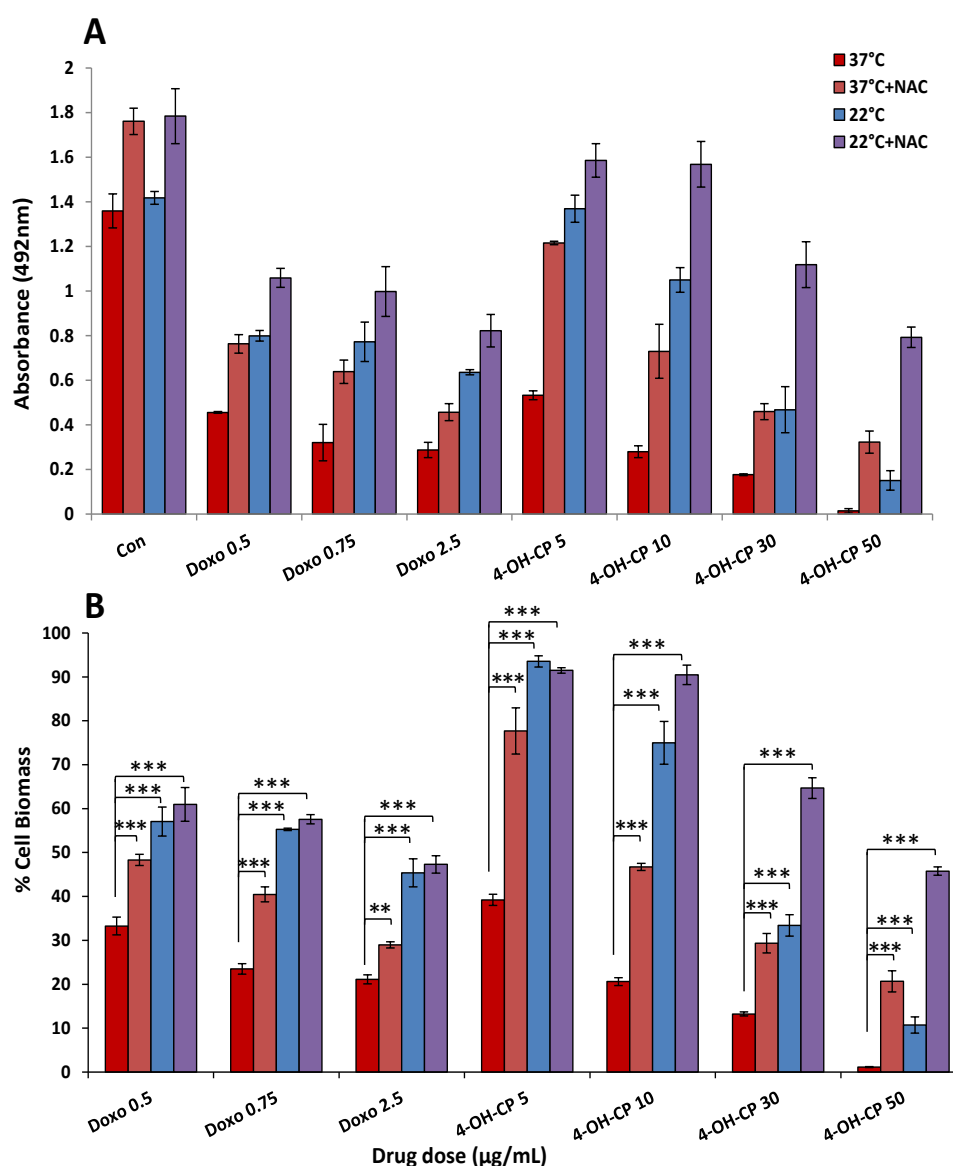


**Figure 7-5 Cytoprotective role of combination of cooling and NAC treatment against high concentrations of 4-OH-CP at 37°C and 22°C**

HaCaTa cells were seeded in 96 well plates at 5000 cells/well in KSFM medium and were incubated overnight at 37°C/ 5% CO<sub>2</sub>. HaCaTa cells were pre-treated with and without 0.625 mM NAC for 30 min at 37°C. HaCaTa cells were treated for 2h with the indicated dose of doxorubicin (Doxo), and 4-OH-CP with and without NAC at 37°C and 22°C compared with vehicle control (cells treated with medium containing DMSO, in which the reagent was dissolved). The solvent represents the maximum amount of DMSO corresponding to the highest drug concentration). The drugs were then removed, wells were rinsed with PBS to remove any traces of drug and cultures incubated for a further 72h, after which the culture medium was removed and fresh medium added then 20 µL of CellTiter 96® Aqueous One solution was added to the wells and plates were incubated at 37°C in 5% CO<sub>2</sub> for a total of four hours. Absorbance was measured spectrophotometrically at a wavelength of 492nm and % cell biomass was calculated as described in Materials and Methods (Chapter 2). Data is presented as **A**) Absorbance (raw data) **B**) % cell biomass shown in bar graph form. Data points correspond to mean % cell biomass (±S.E.M.) for three independent biological experiments, each consisting of 6–8 technical replicates. \*\*,  $p < 0.01$ ; \*\*\*,  $p < 0.001$ .

## **7.6 Investigations on the ability of NAC to enhance protection from chemotherapy drug-mediated cytotoxicity under sub-optimal cooling conditions**

Previous studies in our laboratory, involving the use of Paxman cooling caps and infra-red camera measurements to determine scalp temperature during cooling on healthy volunteers, demonstrated that the temperature of the scalp for certain individuals did not reach optimal values, i.e. temperatures of 22°C or below – in some cases only temperatures ranging from 25-27°C were actually reached (unpublished observations). Although it was an important observation that NAC could enhance the cytoprotective effect of optimal cooling conditions (i.e. temperature values that offered significant cytoprotection), it was equally important to investigate the cytoprotective capacity of cooling in combination with NAC at sub-optimal conditions (i.e. at temperature values higher than 22°C such as 24°C and 26°C where less protection would be expected).

HaCaTa cells were pre-treated with and without 0.625 mM NAC for 30 min before incubation with a range of doxorubicin and 4-OH-CP doses at 37°C and 26°C. Results showed that HaCaTa biomass increased significantly in cells treated with NAC compared with cells treated without NAC (Figure 7-6). These data provided strong evidence for enhanced cytoprotective effects mediated by addition of NAC at sub-optimal cooling conditions. Furthermore, additional experiments were performed to assess the effects of the combinatorial treatment (sub-optimal cooling and NAC) against doxorubicin over a wider range of drug concentrations. Interestingly, there was a clear and significant rescue from cytotoxicity for all doxorubicin concentrations in cells treated with a combination of NAC and cooling compared with cooling alone, even at very high drug concentrations, as biomass increased from 10% to nearly 65% (Figure 7-7). Finally, to expand the above observations on the ability of NAC to enhance cooling mediated cytoprotection, further experiments were performed, where cells were treated at 24°C to represent sub-optimal cooling conditions. As shown in Figure 7-8, NAC in combination with sub-optimal cooling provided a significant enhancement in protection when compared to cooling alone for cells treated with 4-OH-CP and doxorubicin. It remains unknown, however, why cells treated with doxorubicin exposed to NAC and cooling at 26°C showed better protection than at 24°C.

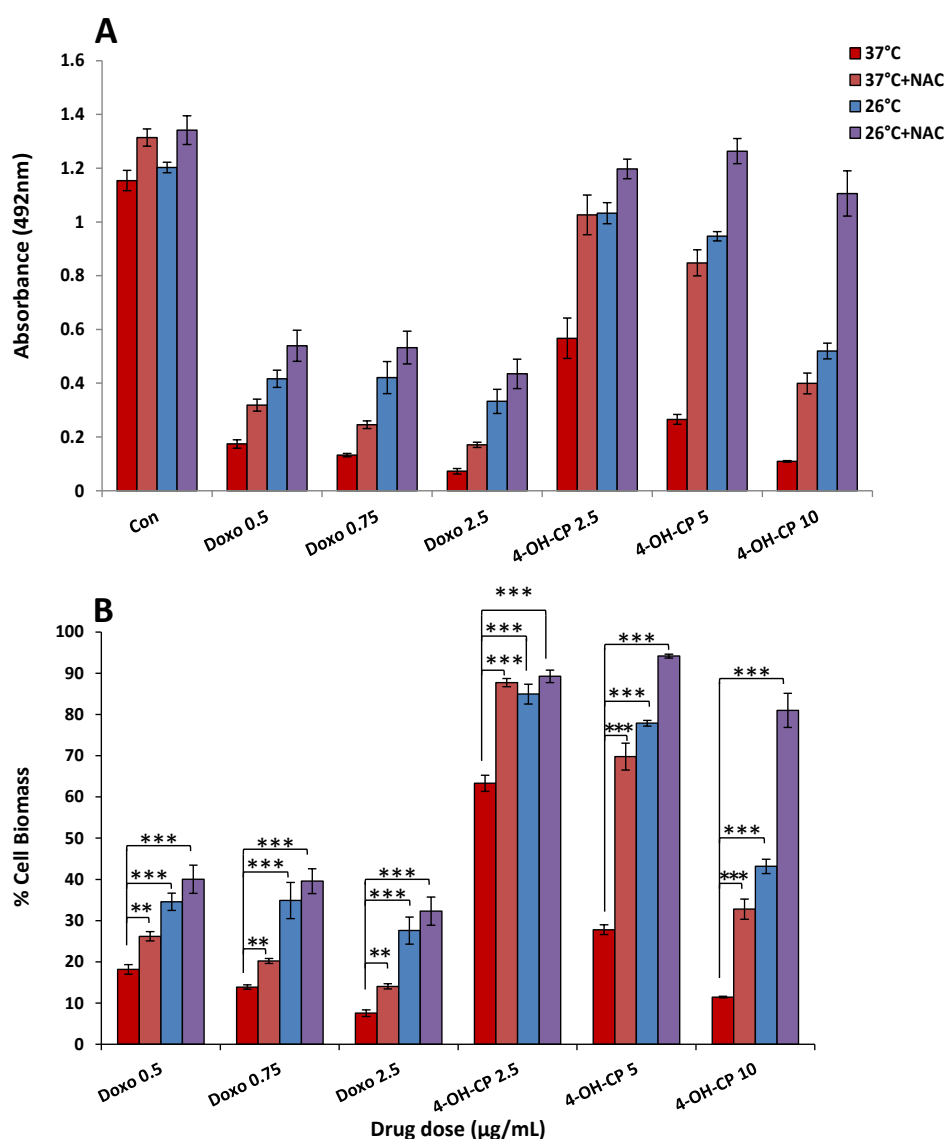


**Figure 7-6 Cytoprotective role of combination of cooling and NAC against chemotherapy drug-mediated toxicity in HaCaTa cells at 37°C and 26°C**

HaCaTa cells were seeded in 96 well plates at 5000 cells/well in KSFM medium and were incubated overnight at 37°C/ 5% CO<sub>2</sub>. HaCaTa cells were pre-treated with and without 0.625 mM NAC for 30 min at 37°C. HaCaTa cells were treated for 2h with the indicated dose of doxorubicin (Doxo), docetaxel (Doce) and 4-OH-CP with and without NAC at 37°C and 26°C compared with vehicle control (cells treated with medium containing DMSO, in which the reagent was dissolved). The solvent represents the maximum amount of DMSO corresponding to the highest drug concentration). The drugs were then removed, wells were rinsed with PBS to remove any traces of drug and cultures incubated for a further 72h, after which the culture medium was removed and fresh medium added then 20 µL of CellTiter 96® Aqueous One solution was added to the wells and plates were incubated at 37°C in 5% CO<sub>2</sub> for a total of four hours. Absorbance was measured spectrophotometrically at a wavelength of 492nm and % cell biomass was calculated as described in Materials and Methods (Chapter 2). Data is presented as **A**) Absorbance (raw data) **B**) % cell biomass shown in bar graph. Data points correspond to mean % cell biomass (±S.E.M.) for three independent biological experiments, each consisting of 6–8 technical replicates. \*\*,  $p < 0.01$ ; \*\*\*,  $p < 0.001$ .

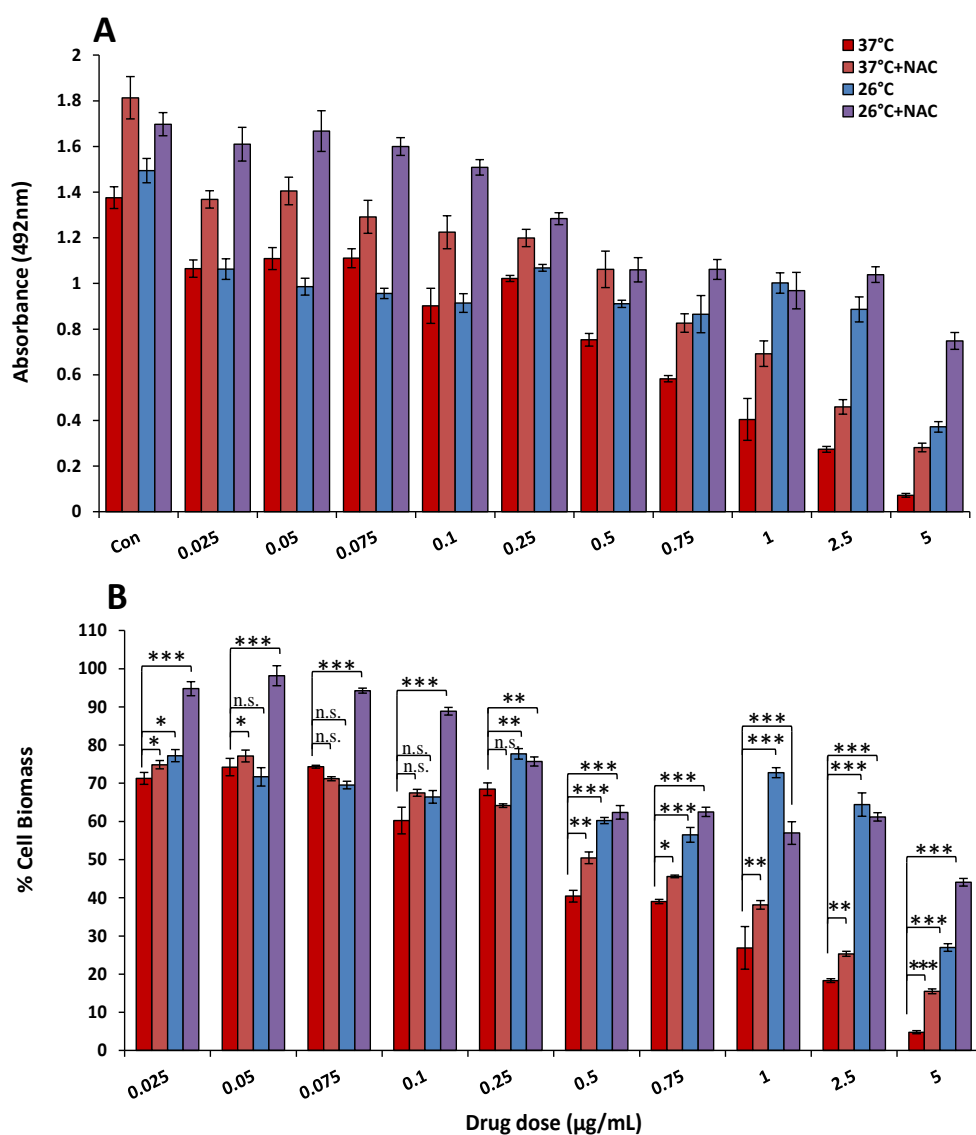


**Figure 7-7 Cytoprotective role of combination of cooling and NAC against doxorubicin-mediated toxicity in HaCaTa cells at 37°C and 26°C**

HaCaTa cells were seeded in 96 well plates at 5000 cells/well in KSFM medium and were incubated overnight at 37°C/ 5% CO<sub>2</sub>. HaCaTa cells were pre-treated with and without 0.625 mM NAC for 30 min at 37°C. HaCaTa cells were treated for 2h with the indicated dose of doxorubicin (Doxo), docetaxel (Doce) and 4-OH-CP with and without NAC at 37°C and 26°C compared with vehicle control (cells treated with medium containing DMSO, in which the reagent was dissolved). The solvent represents the maximum amount of DMSO corresponding to the highest drug concentration). The drugs were then removed, wells were rinsed with PBS to remove any traces of drug and cultures incubated for a further 72h, after which the culture medium was removed and fresh medium added then 20 µL of CellTiter 96® Aqueous One solution was added to the wells and plates were incubated at 37°C in 5% CO<sub>2</sub> for a total of four hours. Absorbance was measured spectrophotometrically at a wavelength of 492nm and % cell biomass was calculated as described in Materials and Methods (Chapter 2). Data is presented as **A**) Absorbance (raw data) **B**) % cell biomass shown in bar graph. Data points correspond to mean % cell biomass (±S.E.M.) for three independent biological experiments, each consisting of 6–8 technical replicates. n.s., non-significant; \*,  $p < 0.05$ ; \*\*,  $p < 0.01$ ; \*\*\*,  $p < 0.001$ .

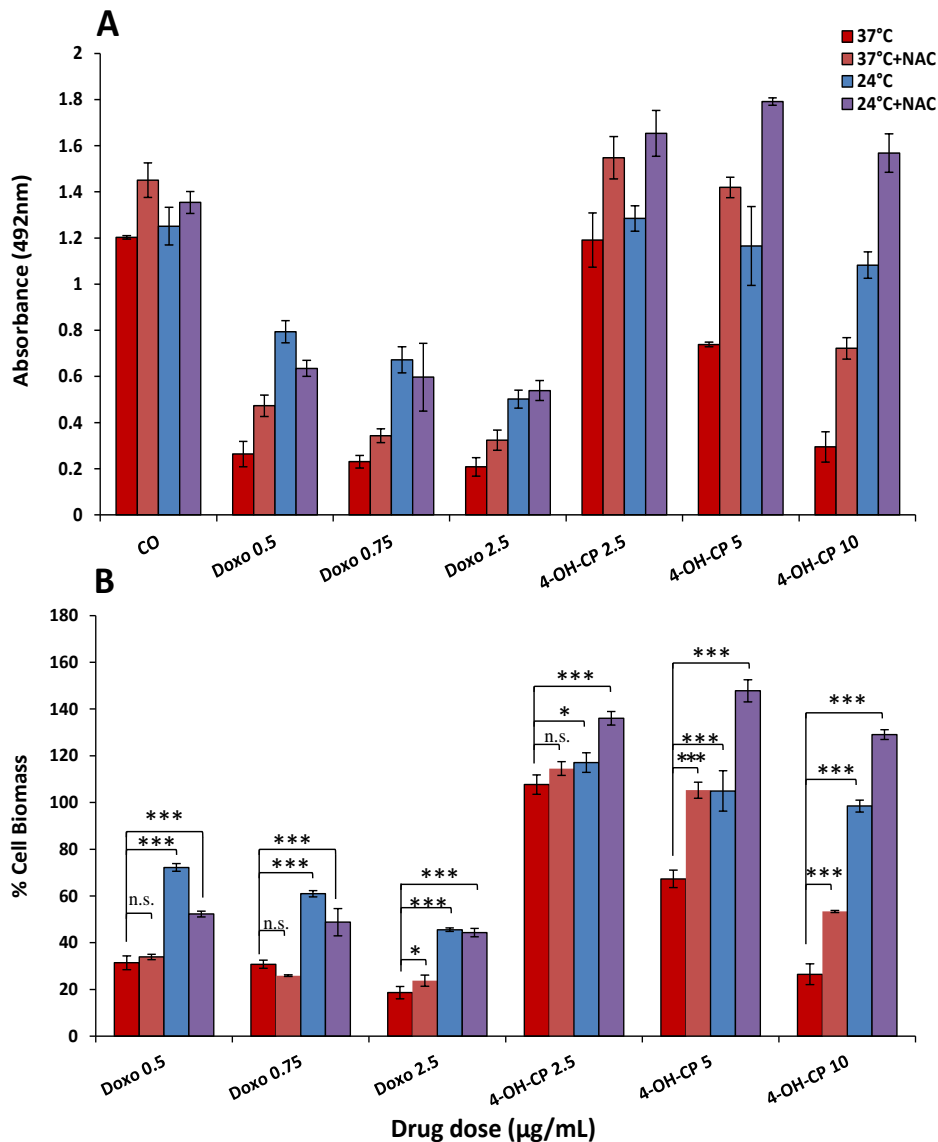


**Figure 7-8 Cytoprotective role of combination of cooling and NAC against chemotherapy drug-mediated toxicity in HaCaTa cells at 37°C and 24°C**

HaCaTa cells were seeded in 96 well plates at 5000 cells/well in KSFM medium and were incubated overnight at 37°C/ 5% CO<sub>2</sub>. HaCaTa cells were pre-treated with and without 0.625 mM NAC for 30 min at 37°C. HaCaTa cells were treated for 2h with the indicated dose of doxorubicin (Doxo), docetaxel (Doce) and 4-OH-CP with and without NAC at 37°C and 24°C compared with vehicle control (cells treated with medium containing DMSO, in which the reagent was dissolved). The solvent represents the maximum amount of DMSO corresponding to the highest drug concentration). The drugs were then removed, wells were rinsed with PBS to remove any traces of drug and cultures incubated for a further 72h, after which the culture medium was removed and fresh medium added then 20 µL of CellTiter 96® AQueous One solution was added to the wells and plates were incubated at 37°C in 5% CO<sub>2</sub> for a total of four hours. Absorbance was measured spectrophotometrically at a wavelength of 492nm and % cell biomass was calculated as described in Materials and Methods (Chapter 2). Data is presented as **A**) Absorbance (raw data) **B**) % cell biomass shown in bar graph. Data points correspond to mean % cell biomass (±S.E.M.) for three independent biological experiments, each consisting of 6–8 technical replicates. n.s., non-significant; \*,  $p < 0.05$ ; \*\*,  $p < 0.01$ ; \*\*\*,  $p < 0.001$ .

## **7.7 Effect of combination of cooling and NAC treatment on AC and TAC-mediated cytotoxicity in HaCaTa cells**

Work presented in chapter 3 demonstrated that although cooling can protect human keratinocytes substantially (in some cases 100%) and rescue from single drug treatments, it was less effective at protecting from combinatorial drug treatment and in particular from TAC (Chapter 3). Therefore, the ability of combinatorial treatment with cooling and NAC to protect from the cytotoxic effects of the AC (doxorubicin/cyclophosphamide) and TAC regimes at different temperatures was assessed.

For the AC regimen, cells were treated with doxorubicin (A) followed by 4-OH-CP (C) with 10% of the doxorubicin dose (denoted 'AC (+10%)') at 37°C *versus* 22°C, 18°C and the sub-optimal temperature 26°C as detailed in Materials and Methods section 2.7.3. The results showed consistently improved, though relatively modest, degrees of cytoprotection at 22°C (Figure 7-9), 18°C (Figure 7-10), and 26°C (Figure 7-11) when cooling was combined with NAC, in comparison to treatment with cooling alone (without NAC co-treatment). The TAC regimen at 26°C on HaCaTa cells was also tested and based on the previous studies in chapter 3 regimen 'TAC (+10%)' was followed and the drug concentrations chosen were doses that corresponded to the maximal observed cytoprotection upon cooling in HaCaTa cells (Figure 7-12). Collectively, these results showed that in addition to the cytoprotection by cooling observed against combinatorial drug treatments, cells co-treated with NAC during cooling showed higher viability than cells treated without NAC at all temperatures, which indicates that NAC can have a positive, though modest for AC and TAC, influence on cooling-mediated chemoprotection against such combinatorial drug regimes.

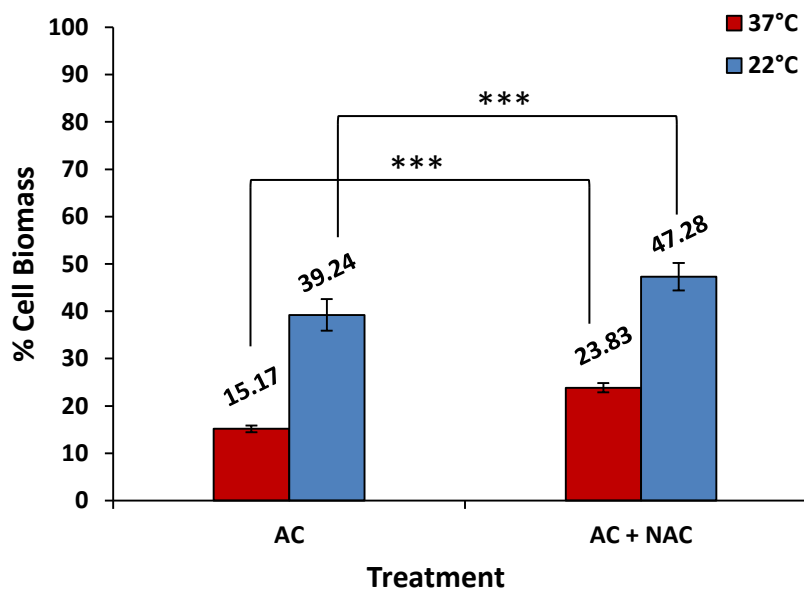


**Figure 7-9 Effect of combination of cooling and NAC on AC-mediated cytotoxicity in HaCaTa cells at 37°C and 22°C**

HaCaTa cells were seeded in 96 well plates at 5000 cells/well in KSFM medium and were incubated overnight at 37°C/ 5% CO<sub>2</sub>. HaCaTa cells were pre-treated with and without 0.625 mM NAC for 30 min at 37°C. Cells were treated with the combinatorial drug protocols 'AC (+10%)' with and without NAC at 37°C and 22°C compared with vehicle control (cells treated with medium containing DMSO, in which the reagent was dissolved. The solvent represents the maximum amount of DMSO corresponding to the highest drug concentration) as detailed in section 2.7.3. The drugs were then removed, wells were rinsed with PBS to remove any traces of drug and cultures incubated for a further 72h, after which the culture medium was removed and fresh medium added then 20 µL of CellTiter 96® AQueous One solution was added to the wells and plates were incubated at 37°C in 5% CO<sub>2</sub> for a total of four hours. Absorbance was measured spectrophotometrically at a wavelength of 492nm and % cell biomass was calculated as described in Materials and Methods section 2.7.3. Data points correspond to mean % cell biomass (±S.E.M.) for three independent biological experiments, each consisting of 6–8 technical replicates. \*\*,  $p < 0.01$ ; \*\*\*,  $p < 0.001$ .

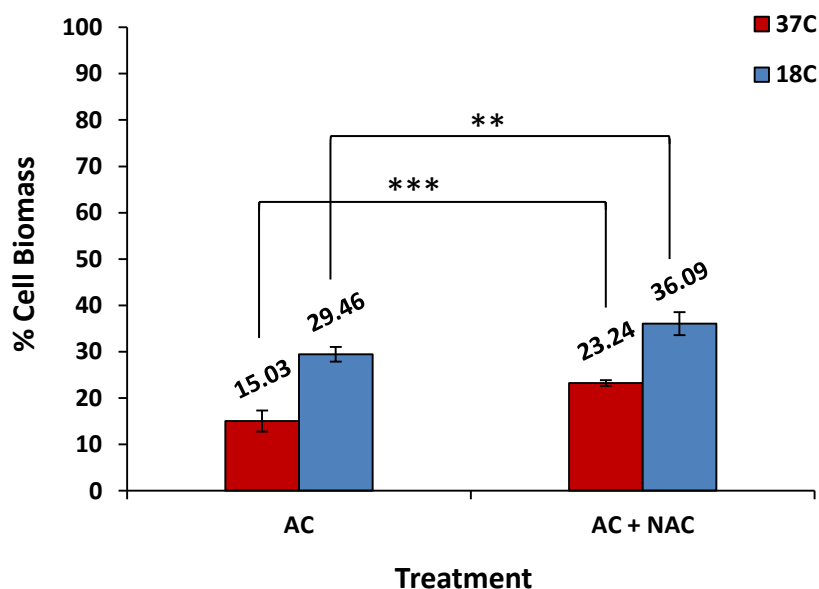


**Figure 7-10 Effect of combination of cooling and NAC on AC-mediated cytotoxicity in HaCaTa cells at 37°C and 18°C**

HaCaTa cells were seeded in 96 well plates at 5000 cells/well in KSFM medium and were incubated overnight at 37°C/ 5% CO<sub>2</sub>. HaCaTa cells were pre-treated with and without 0.625 mM NAC for 30 min at 37°C. Cells were treated with the combinatorial drug protocols 'AC (+10%)' with and without NAC at 37°C and 18°C compared with vehicle control (cells treated with medium containing DMSO, in which the reagent was dissolved. The solvent represents the maximum amount of DMSO corresponding to the highest drug concentration) as detailed in section 2.7.3. The drugs were then removed, wells were rinsed with PBS to remove any traces of drug and cultures incubated for a further 72h, after which the culture medium was removed and fresh medium added then 20 µL of CellTiter 96® AQueous One solution was added to the wells and plates were incubated at 37°C in 5% CO<sub>2</sub> for a total of four hours. Absorbance was measured spectrophotometrically at a wavelength of 492nm and % cell biomass was calculated as described in Materials and Methods section 2.7.3. Data points correspond to mean % cell biomass (±S.E.M.) for three independent biological experiments, each consisting of 6–8 technical replicates. \*\*,  $p < 0.01$ ; \*\*\*,  $p < 0.001$ .

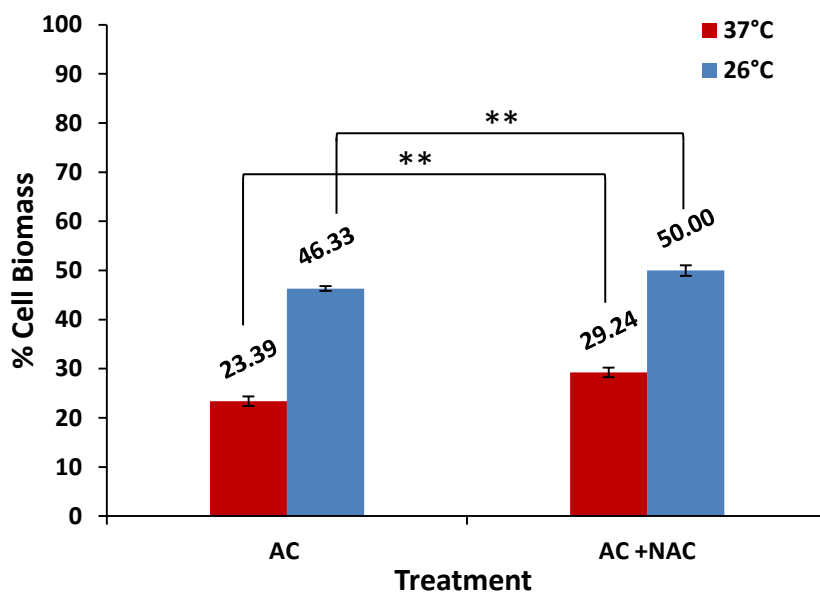


**Figure 7-11 Effect of combination of cooling and NAC on AC-mediated cytotoxicity in HaCaTa cells at 37°C and 26°C**

HaCaTa cells were seeded in 96 well plates at 5000 cells/well in KSFM medium and were incubated overnight at 37°C/ 5% CO<sub>2</sub>. HaCaTa cells were pre-treated with and without 0.625 mM NAC for 30 min at 37°C. Cells were treated with the combinatorial drug protocols 'AC (+10%)' with and without NAC at 37°C and 18°C compared with vehicle control (cells treated with medium containing DMSO, in which the reagent was dissolved. The solvent represents the maximum amount of DMSO corresponding to the highest drug concentration) as detailed in section 2.7.3. The drugs were then removed, wells were rinsed with PBS to remove any traces of drug and cultures incubated for a further 72h, after which the culture medium was removed and fresh medium added then 20 µL of CellTiter 96® AQueous One solution was added to the wells and plates were incubated at 37°C in 5% CO<sub>2</sub> for a total of four hours. Absorbance was measured spectrophotometrically at a wavelength of 492nm and % cell biomass was calculated as described in Materials and Methods section 2.7.3. Data points correspond to mean % cell biomass (±S.E.M.) for three independent biological experiments, each consisting of 6–8 technical replicates. \*\*,  $p < 0.01$ .

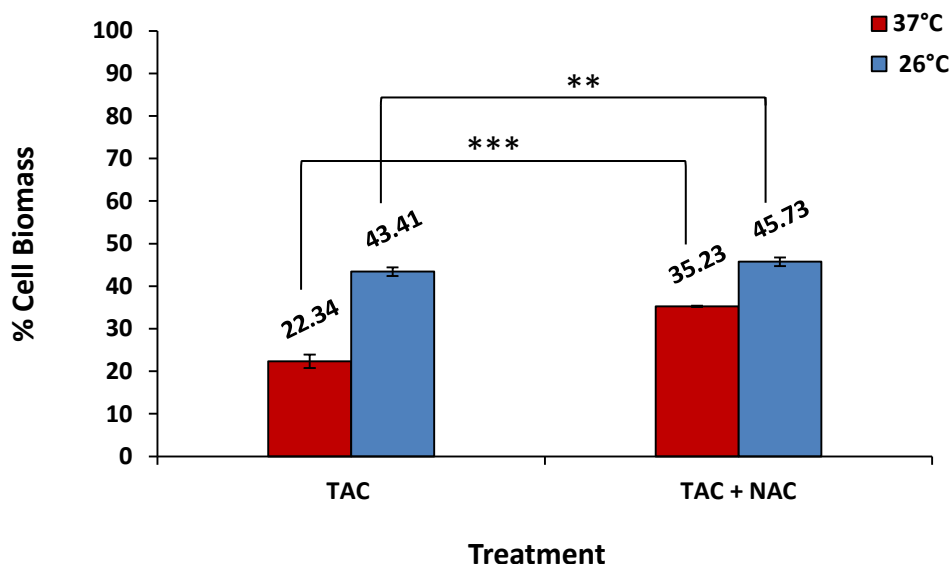


**Figure 7-12 Effect of combination of cooling and NAC on TAC-mediated cytotoxicity in HaCaTa cells at 37°C and 26°C**

HaCaTa cells were seeded in 96 well plates at 5000 cells/well in KSFM medium were incubated overnight at 37°C/ 5% CO<sub>2</sub>. HaCaTa cells were pre-treated with and without 0.625 mM NAC for 30 min at 37°C. Cells were treated with the combinatorial drug protocols 'TAC (+10%)' with and without NAC at 37°C and 18°C compared with vehicle control (cells treated with medium containing DMSO, in which the reagent was dissolved. The solvent represents the maximum amount of DMSO corresponding to the highest drug concentration) as detailed in section 2.7.3. The drugs were then removed, wells were rinsed with PBS to remove any traces of drug and cultures incubated for a further 72h, after which the culture medium was removed and fresh medium added then 20 µL of CellTiter 96® AQueous One solution was added to the wells and plates were incubated at 37°C in 5% CO<sub>2</sub> for a total of four hours. Absorbance was measured spectrophotometrically at a wavelength of 492nm and % cell biomass was calculated as described in Materials and Methods section 2.7.3. Data points correspond to mean % cell biomass (±S.E.M.) for three independent biological experiments, each consisting of 6–8 technical replicates. \*\*,  $p < 0.01$ ; \*\*\*,  $p < 0.001$ .

## 7.8 Summary

- The objective of this chapter was to investigate for the first time the hypothesis that cooling combined with the antioxidant N-acetylcysteine (NAC) may enhance the cytoprotective effect of cooling, and particularly for sub-optimal cooling conditions, as a potential novel therapeutic intervention.
- Initial pre-titration experiments allowed the determination of an optimal concentration of NAC, according to these experiments the optimal concentration of NAC was 0.625 mM.
- HaCaTa cells were pre-treated with NAC for 30 min, then co-treated with chemotherapy drugs (doxorubicin, docetaxel, and 4-OH-CP) at 37°C. The results showed that NAC significantly protected from drug-mediated cytotoxicity for all compounds tested, and rescued cells from drug toxicity. Furthermore, 4-OH-CP showed the best results in comparison with doxorubicin and docetaxel.
- NAC not only showed protection from chemotherapy drugs that act through the production of ROS to induce apoptosis such as doxorubicin, but also against docetaxel, which interferes with microtubule stabilisation in cells. Furthermore, data in this work showed that 4-OH-CP did not induce ROS generation (Chapter 4). However, in this chapter NAC showed protection from 4-OH-CP-induced cytotoxicity in HaCaTa cells, these results suggested that NAC might act independently of ROS.
- Combination of NAC and cooling during chemotherapy drug treatment provided significant protection from drug-mediated cytotoxicity for nearly all concentrations tested for doxorubicin, docetaxel and 4-OH-CP. NAC was effective at reducing drug toxicity even at high drug doses such as 50 µg/mL of 4-OH-CP and the toxicity was reduced from 10% to 65%.
- Significantly, when experiments were carried out to investigate the efficacy of cooling at sub-optimal conditions (24°C and 26°C) in combination with NAC, the combination significantly protected against a range of doxorubicin and 4-OH-CP doses at 37°C and 26°C with cells treated without NAC. These data provided strong evidence for enhanced cytoprotective effects against chemotherapy drugs by combination of NAC and sub-optimal cooling conditions.
- Interestingly the result showed that there was a significant rescue from cytotoxicity in HaCaTa cells treated with the combinatorial treatment 26°C and NAC against a wider range of doxorubicin concentrations compared with cells treated without

NAC. Furthermore, the results showed that when HaCaTa cells were treated with combinatorial treatment 24°C and NAC there was an enhancement in protection for cells treated with 4-OH-CP and doxorubicin in comparison to cooling alone. Strangely, NAC and cooling at 26°C showed better protection than at 24°C.

- The chemoprotective effects of combinatorial treatment of cooling and NAC against the AC (doxorubicin/cyclophosphamide) and TAC regimes at different temperatures was also assessed. The results showed consistently enhanced, though relatively modest, degrees of cytoprotection at 22°C, 18°C, and 26°C in cells co-treated with NAC, in comparison to treatment with cooling alone. HaCaTa cells treated with TAC at with NAC and cooling at 26°C, showed improved, though relatively modest, cell viability.
- An important and interesting finding is that NAC could not fully protect from drug induced toxicity, although a range of NAC concentrations should be investigated in future studies. Yet, in combination with cooling it showed significant enhancement of the cytoprotective effects of cooling.
- Of note, although NAC showed effective chemoprotection, the molecular mechanisms underlying the cytoprotective effect of NAC and cooling have not been fully established here and must form the basis of future studies.
- Nevertheless, the fact that antioxidant NAC enhances the chemoprotective effects of cooling at both sub-optimal (24°C and 26°C), moderately efficient (22°C) and optimal (18°C) cooling conditions, supports the promise of the combinatorial treatment as a strategy to improve the efficacy of scalp cooling which is currently, overall, 50% in cancer patients.

## 7.9 Discussion

### 7.9.1 The chemoprotective agent and antioxidant N-acetylcysteine (NAC) blocks chemotherapy drug-induced cell death and enhances the cytoprotective effect of cooling

The main aim of this study was to understand the pathway of cytotoxicity with the long-term aim to design new and more effective strategies to complement or improve the efficacy of scalp cooling. Ideally, the aim would be to design of a topical treatment to help protect from CIA without affecting chemotherapy treatment efficacy. Despite the fact that cooling can be effective against CIA, against the combined treatment (TAC) and monotherapies such as docetaxel at high concentrations, cooling shows limited efficacy. Furthermore, in some patients scalp cooling might not be efficient at reducing the temperature of the scalp effectively to provide cytoprotection, as only sub-optimal cooling conditions might be achieved in such individuals. In fact, the findings of this study have clearly demonstrated that even a small number of degrees in temperature difference may be significant in rescuing from drug-mediated cytotoxicity.

As ROS appeared to be induced by chemotherapy drugs and these molecules are often central in mitochondrial apoptosis pathways, the hypothesis raised was that the cytoprotective effect of cooling might be enhanced *via* co-treatment with the antioxidant NAC. The idea behind this combinatorial treatment of “cooling plus NAC”, was that a) for drug regimes where cooling shows limited efficacy NAC may improve the cytoprotective effect, and b) NAC could enhance cytoprotection for patients where scalp cooling devices might not reduce the scalp temperature adequately, i.e. only achieve sub-optimal scalp temperatures (such as 24°C and 26°C). The aim was to test a possible therapeutic intervention of cooling plus topical treatment with antioxidant NAC to prevent CIA without compromising the anticancer effects of chemotherapy.

The effectiveness of NAC has been shown experimentally as reported using *in vitro* and *in vivo* studies; it is clinically proven in humans to inhibit ROS, protect against DNA damage and carcinogenesis (De Flora *et al.*, 2001). Other studies have demonstrated that the NAC can reduce the invasive and metastatic potential of the melanoma and fibrosarcoma cells (Tosetti *et al.*, 2002). Moreover, a number of experimental studies reported the effects of NAC on different models, pre or post treatment, in various fields of toxicology or pharmacology. NAC protection of deleterious effects during the administration of anticancer drugs adriamycin, bleomycin, cisplatin (and its derivatives), doxorubicin, ifosfamide, methotrexate, or antimicrobials (amphotericin, vancomycin); these effects (but not all) appear

to be related to its ability to reduce oxidative stress (De Flora *et al.*, 2001; Wu *et al.*, 2005). Moreover, in several biological studies, NAC has been used as a tool for investigating ROS (Zafarullah *et al.*, 2003) and more recently in studies in our laboratory have shown that NAC can rescue from apoptosis by members of the TNF receptor family that engage the mitochondrial pathway.

This study for the first time examined a range of concentrations of doxorubicin, docetaxel and 4-OH-CP with and without NAC in HaCaTa cells and investigated the possible influence of NAC and temperature on drug-mediated cytotoxicity. NAC was able to prevent cell death induced by doxorubicin, docetaxel, and 4-OH-CP and caused increases in cell viability compared with cells treated without NAC. The improvement by NAC was particularly evident as sub-optimal cooling conditions. Despite the fact that doxorubicin, docetaxel and 4-OH-CP act *via* different molecular mechanisms, the cytoprotective effect of NAC was significant and evident for all drugs tested, particularly 4-OH-CP.

ROS are continually released during various metabolic processes in the cell and it has long been known that reactive oxygen species in the form of oxidative stress are involved in pathogenic processes. ROS also act as signalling intermediates in physiological regulatory mechanisms recognized for their involvement in the control of cell division (Luanpitpong *et al.*, 2011; Schulze-Osthoff *et al.*, 1996). Yet, extensive ROS induction is associated with toxicity and induction of apoptosis. Doxorubicin exerts its anti-cancer effect *via* the formation of oxygen radicals and direct interference with the cell cycle (Luanpitpong *et al.*, 2012). Doxorubicin-mediated cytotoxicity appears to be dependent on ROS generation (Luanpitpong *et al.*, 2011; Luanpitpong *et al.*, 2012), however, cyclophosphamide in our study did not show induction of ROS whilst the mechanism of action of docetaxel is different and induces cell death *via* microtubule de-stabilisation (Bhardwaj *et al.*, 2014). However, the observation that NAC caused a protection from all these three chemotherapy drugs suggests that NAC might also act independently of ROS and might have direct effects on these drugs.

ROS are involved in the activation of JNK in response to stress, whilst activation of JNK and apoptosis induced by cisplatin is inhibited by NAC, but potentiated by the addition of hydrogen peroxide (Benhar *et al.*, 2001). The role of oxidative stress in activation of JNK was also demonstrated after treatment with a topoisomerase inhibitor (Shiah *et al.*, 1999). ERK pathways can also be activated by NAC to promote cell survival and prevent apoptosis, which lead to cell growth (Li *et al.*, 2000b; Wung *et al.*, 1999). NAC can block the induction of several DNA alterations in rat lung cells (Izzotti *et al.*, 1999; Marnett, 2000).

Finally, when the response to combinatorial therapies AC and TAC with and without NAC and cooling were examined, despite extensive toxicity in HaCaTa cell at 37°C, cooling

plus NAC showed that cooling-mediated cytoprotection improved consistently. This was particularly evident at 26°C, which showed better protection for both AC and TAC compared with all other temperatures tested in this study. However, it must be noted that the improvement achieved was relatively modest in comparison to monotherapies.

However, recent work in our laboratory that took place during the preparation of this thesis, in collaboration with Paxman Coolers (Dunnill and Georgopoulos, unpublished observations), has investigated additional antioxidant compounds that alone as well in combination with NAC significantly improved the ability of cooling to cytoprotect. In particular, compounds such as quercetin have now been demonstrated to significantly enhance the cytoprotective effect of cooling when combined with NAC, particularly against combinatorial treatment AC, which is responsible for significant levels of CIA in the clinic.

This more recent data, combined with the findings presented here, confirm that cooling protects from cytotoxicity induced by chemotherapy drugs, and the combination of cooling with antioxidants can rescue from drug-mediated cytotoxicity better than cooling alone. As a result, this more recent work has led to the submission of European patent application (Georgopoulos NT and Paxman Coolers) relating to the co-treatment of patients with cooling plus combinations of antioxidants to reduce or protect from chemotherapy induced hair loss.

## CHAPTER 8: Concluding remarks

The main aim of this work was to establish human keratinocyte models for the study of the cellular effects of cancer chemotherapy drugs in order to assess the ability of cooling to protect from drug-induced cytotoxicity and to determine the underpinning mechanisms of cytoprotection. By providing several novel observations, the findings presented in this thesis have enhanced both our understanding of the effects of chemotherapy drugs on keratinocyte cell growth and also the mechanisms of cooling-mediated cytoprotection. Figure 8.2 provides a summary of the mechanisms of cooling-mediated cytoprotection demonstrated in this study.

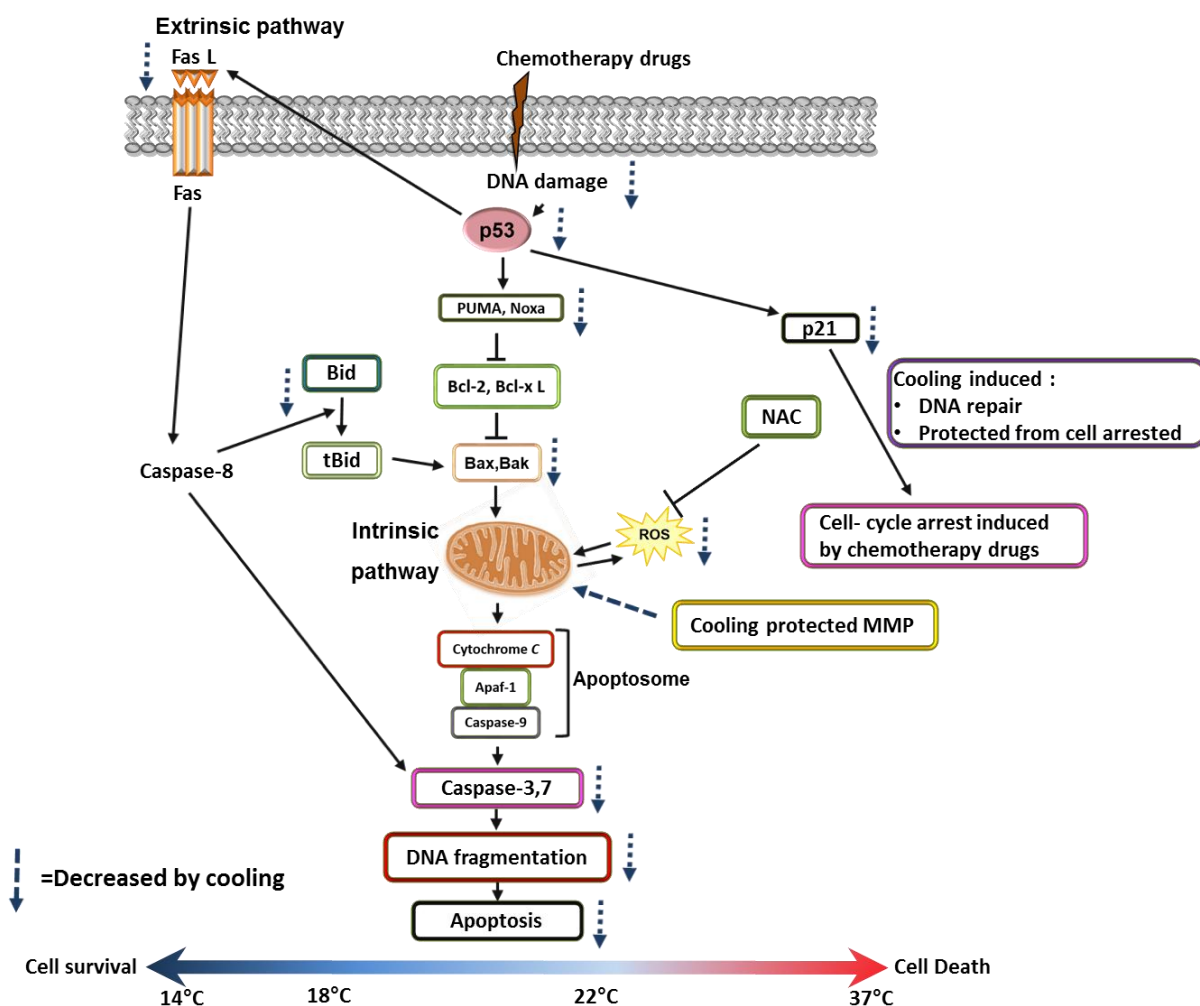


**Figure 8-1 Molecular mechanisms of cooling mediated cytoprotection against chemotherapy drug-mediated toxicity**

## 8.1 Future work

There are many avenues of future study that could be pursued, for instance:

- One of the hypothesis mentioned above is that the rate of drug diffusion across a plasma membrane may be reduced by cooling, thus lowering the 'effective' drug dose entering the cells. Future studies should determine the effects of cooling on cellular drug uptake. Preliminary work in our laboratory has provided some evidence that cooling may alter the amount of cellular drug uptake. However, cooling conditions that fully block cytotoxicity (shown in the present study) did not fully prevent drug uptake. This indicates that combination of both prevention of drug uptake as well as direct cellular effects are triggered by cooling.
- This study has provided evidence that cooling decreased the level of cellular metabolic activity; by showing that human keratinocytes are exiting the cell cycle; the study has suggested reduced metabolic activity. Future studies should involve measuring the metabolic activity of cells as described elsewhere (Zhang *et al.*, 2012) using different techniques, for example the cytometric quantification of cellular fluorescence upon cleavage of fluorescein diacetate.
- It would be interesting to determine the relationship between chemotherapy-induced cell arrest and the checkpoint recovery induced by cooling using western blotting assay in order to understand the proteins involved.
- To fully elucidate the role of p53, knockdown/knockout of p53 protein (by RNAi or CRISPR-Cas9 technologies) could be employed to investigate effects of chemotherapy drugs with and without cooling. Moreover, measurements of the levels of MDM2 in cells at different temperature would be important in understanding the mechanisms underpinning cooling effects.
- The release of Cyto-c from mitochondria is a critical event in the activation of caspase-9, and as Bid is cleaved, it would be interesting to understand whether activation of caspase-8 mediated tBid production and downstream apoptosome formation; moreover, detection of the localisation of pro-apoptotic Bax by microscopy would allow a better understanding of its involvement and whether cooling regulates its localisation and activation.
- The ability of cooling to protect from chemotherapy drug-mediated increases in ROS and loss of mitochondrial integrity in HaCaTa cells has generated an interesting avenue that would involve investigation on the nature of ROS involved in cytotoxicity and whether the exact types of ROS are altered by ROS.

- In response to chemotherapy drugs in this work, we detected P-p53 and p21 and apoptotic proteins, Bax, Bak, PUMA and Noxa; although cooling led to down-regulation of these proteins, protein levels were detected at several time points following chemotherapy drug treatment and at different cooling conditions. Yet, the observation that extreme cooling alone or extended (24h) cooling caused induction of some of these important signalling mediators will form the basis of novel studies that might provide a better explanation for the cytoprotective effects of cooling.
- To provide a better understanding of how antioxidants like NAC enhance the cytoprotective effect cooling against cytotoxic agents, the apoptotic signalling pathways could be investigated by detection of proteins involved in cell arrest and apoptosis (such as p53, p21, Bak, and FasL).

# Appendix I

## List of Suppliers

Supplier	Webpage/Address
Alpha labs	<a href="http://www.alphalabs.co.uk">www.alphalabs.co.uk</a>
Bio-Rad Laboratories Ltd	<a href="http://www.bio-rad.com">www.bio-rad.com</a>
Biosera	<a href="http://www.biosera.com">www.biosera.com</a>
Calbiochem	Supplied by Merck
Cambridge Bioscience	<a href="http://www.bioscience.co.uk">www.bioscience.co.uk</a>
ENZO	<a href="http://www.enzolifesciences.com">www.enzolifesciences.com</a>
Falcon	Supplied by VWR
Fisher Scientific UK Ltd	<a href="http://www.fisher.co.uk">www.fisher.co.uk</a>
Greiner Bio-one Ltd	<a href="http://www.greinerbioone.com/en/england/start/">www.greinerbioone.com/en/england/start/</a>
Insight Biotechnology Ltd	<a href="http://www.insightbio.com">www.insightbio.com</a>
Invitrogen Ltd	<a href="http://www.invitrogen.com">www.invitrogen.com</a>
Invivogen	<a href="http://www.invivogen.com">www.invivogen.com</a>
Li-Cor Biosciences UK Ltd	<a href="http://www.licor.com">www.licor.com</a>
Merck	<a href="http://www.merck.co.uk">www.merck.co.uk</a>
Microsoft Corporation	<a href="http://www.microsoft.com">www.microsoft.com</a>
Millipore	<a href="http://www.merckmillipore.co.uk">www.merckmillipore.co.uk</a>
Molecular Probes	Supplied by Invitrogen
Nalgene Europe Ltd	Supplied by Fisher Scientific
New England Biolabs (UK) Ltd	<a href="http://www.neb.uk.com">www.neb.uk.com</a>
Promega UK Ltd	<a href="http://www.promega.com">www.promega.com</a>
Qiagen Ltd	<a href="http://www.qiagen.com">www.qiagen.com</a>
Roche Diagnostics Ltd	<a href="http://www.roche.co.uk/portal/uk/diagnostics">www.roche.co.uk/portal/uk/diagnostics</a>
Santa Cruz Biotechnology	Supplied by Insight Biotechnology Ltd
Sigma-Aldrich Company Ltd	<a href="http://www.sigmaaldrich.com">www.sigmaaldrich.com</a>
Starstedt Ltd	<a href="http://www.sarstedt.com">www.sarstedt.com</a>
Statebourne Cryogenics Ltd	<a href="http://www.statebourne.com">www.statebourne.com</a>
Sterilin Ltd	Supplied by Fisher
Tebu-bio	<a href="http://www.tebu-bio.co.uk">www.tebu-bio.co.uk</a>
ThermoFisher Scientific Inc	<a href="http://www.fisher.com">www.fisher.com</a>
VWR international	<a href="http://www.vwr.com">www.vwr.com</a>

## Appendix II

### Reagents

#### Phosphate Buffer Saline (PBS) (Invitrogen 14200-67)

Compound	Concentration
137 mM	Sodium Chloride NaCl
2.7 mM	Potassium Chloride KCl
3.2 mM	Disodium hydrogen phosphate Na <sub>2</sub> HPO <sub>4</sub>
147 mM	Potassium hydrogen phosphate KH <sub>2</sub> PO <sub>4</sub>
pH 7.2 dissolved in autoclaved dH <sub>2</sub> O. Prepared from 10X solution	

#### 2x SDS lysis buffer:

Amount(volume or mass)	Material
10 mL (2% W/V)	Glycerol (Sigma)
1 gram (2% W/V)	SDS
6.25 mL (Stock 1M)	Tris-HCl
0.42g /200 mM	Sodium fluoride (NaF)(Sigma)
0.446g	Sodium pyrophosphate tetrabasic
2 mM	Sodium Orthovanadate
Up to total volume of 50mL	Deionised water

Chemicals used in preparation of SDS sample buffer. All chemicals were dissolved using magnetic heat block and then store at -20C in 2.5mL or aliquots.

#### Standards: Cat# PN23208

Standards	Concentrations µg/mL BSA/ volume
bovine serum albumin (BSA)	125, 250, 500, 750, 1000, 1500, 2000/ 3.5mL each
Diluted in 0.9% saline and preserved with 0.05% sodium azide	

### Tris Buffered Saline (TBS)

Volume or Weight	Chemical
1.21g	Tris (Hydroxy methyl amino methan)
8.18g	Sodium hydrochloride (NaCl) (Sigma)
Made up to 1L by deionised water pH 7.4	

### TBS-Tween

Volume or Weight	Chemical
1.21g	Tris (Hydroxy methyl amino methane)
8.18g	Sodium hydrochloride (NaCl) (Sigma)
Made up to 1L by deionised water, and pH was adjusted (pH 7.4) then 1mL of Tween-20 was added.	

### Transfer Buffer

Volume or Weight	Chemicals
1.45 g	Tris( 12 mM)
7.2 g	Glycine(96 mM)
200 mL	Methanol (20%)
Make up to 1L by deionised water (*made fresh on day of use*)	

### The CellTiter 96® Cell proliferation assay

Volume	Chemicals
100mL CellTiter 96	Cell Proliferation Assay 5,000 assays CellTiter 96® AQueous One Solution
Ready to use / 20 µL/well- store the reagent at -20C for long term storage or for short up to 6 week at 4C protected from the light.	

([www.promega.com](http://www.promega.com))

### Caspase-3/7 activity reagents

Components	Volume	Store components
Caspase-3/7 substrate	270 µL	-20 °C
AFC, Fluorescence reference standard	20 µL (in 10mM DMSO)	-20 °C
Ac-DEVD-CHO a known caspase-3/7 inhibitor	5 mM DMSO solution 15 µL	-20 °C
Assay buffer	30mL	4 °C
DTT	1mL	-20 °C
Lysis buffer	20mL	4 °C

The chemical compound used in the measurement of caspase-3/7 activity.  
([www.anaspec.com](http://www.anaspec.com))

### CytoTox-Glo™ Cytotoxicity reagents

Component	Bottle/Size	Storage	Cat #
Assay Buffer	5 x10mL	-20 °C	G9291
AAF-Glo™ substrate(Alanyle alanyl-phenylal alanyl-amino luciferin	5 bottles		
Digitonin	175 µL		

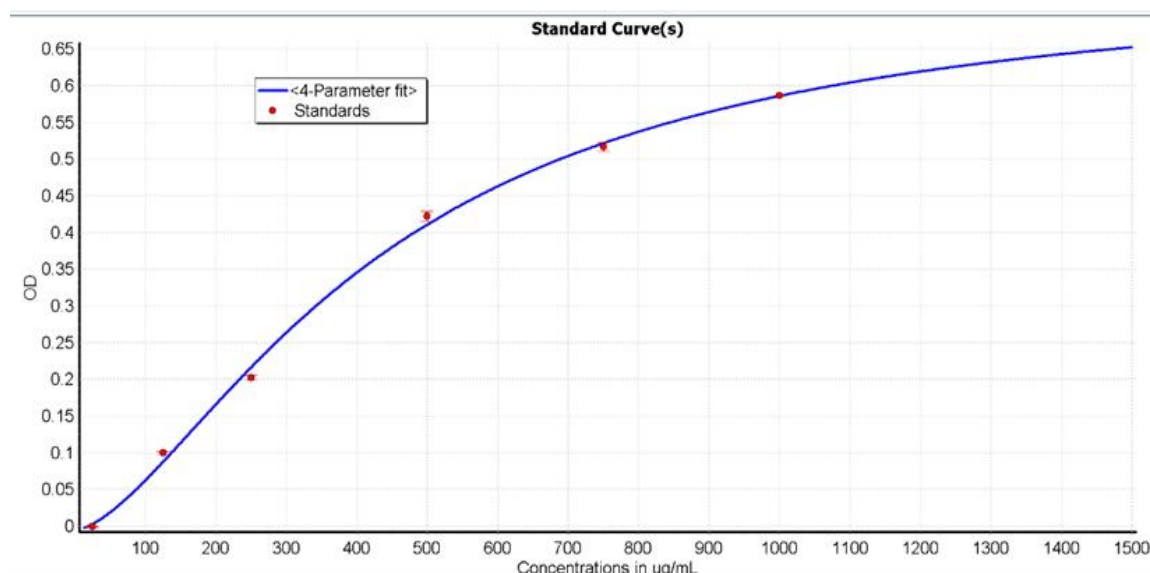
([www.promega.com](http://www.promega.com))

## Appendix III

The concentrations of protein for all lysates; (HaCaTa, NHKE and HHFK cell line) at different time point (6h, 12h, 24h and controls) at different temperature (37°C vs 22°C, 18°C, and 14°C. The concentrations of protein for HaCaTa cell line at 37°C vs 22°C lysate are shown in the Table.

	6h		12h		24h		Con	
	37°C	22°C	37°C	22°C	37°C	22°C	37°C	22°C
<b>µg/mL</b>	3117.3	4056.8	2805.7	3746.2	2788.6	2725.6	2880.5	2266.4
<b>µg/µL</b>	3.1	4.1	2.8	3.7	2.8	2.7	2.9	2.3
<b>Volume with 20 µg</b>	6.42	4.93	7.13	5.34	7.17	7.34	6.94	8.82
<b>dH<sub>2</sub>O</b>	6.58	8.07	5.87	7.66	5.83	5.66	6.06	4.18
<b>Sample volume</b>	13	13	13	13	13	13	13	13
<b>Reducing Agent</b>	2	2	2	2	2	2	2	2
<b>LDS sample buffer</b>	5	5	5	5	5	5	5	5
<b>Total (µL)</b>	20	20	20	20	20	20	20	20

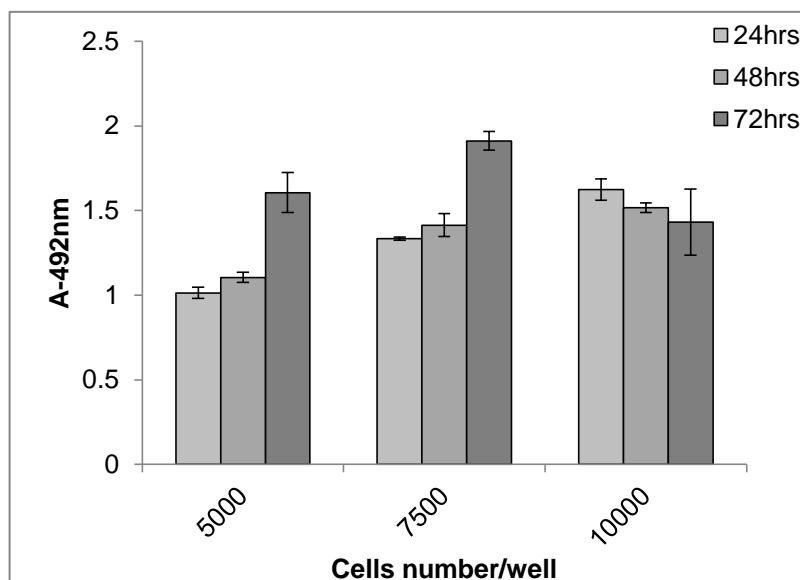
**Protein concentration in different cell lysates. The table also indicates the amount of other reagents added to the lysates preparation for western blotting.**



Standard curve 4-parameter-fit to measure protein concentration

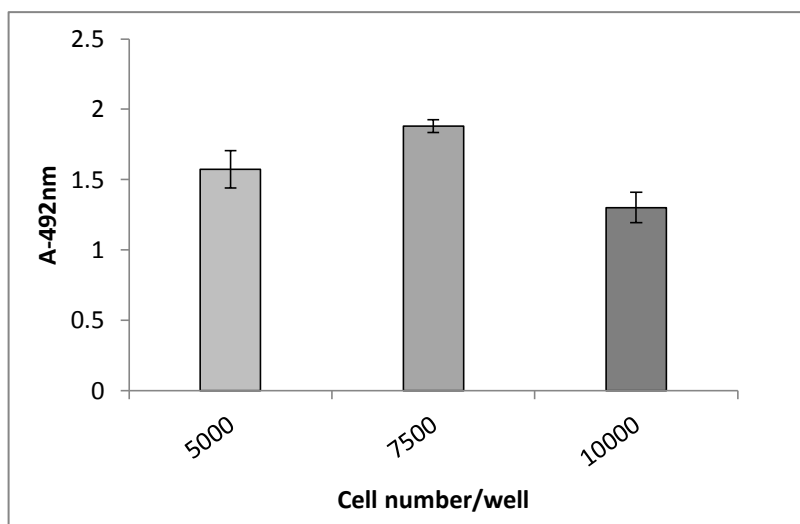
## Appendix IV

### Proliferation assay for NHEKs and HHFK



### Viability assay for NHK cell line

Cell viability percentage was estimated by CellTiter 96® AQueous One Solution in 96-well plates following 24, 48 and 72h. NHEK cells at increasing cell densities ('Low', 'Medium' and 'High') under routine culture conditions ('Cell number' represents number of cells seeded per well). Bars correspond to mean absorbance at 492 nm ( $\pm$ SD) for three independent biological experiments, each consisting of 6 technical replicates.



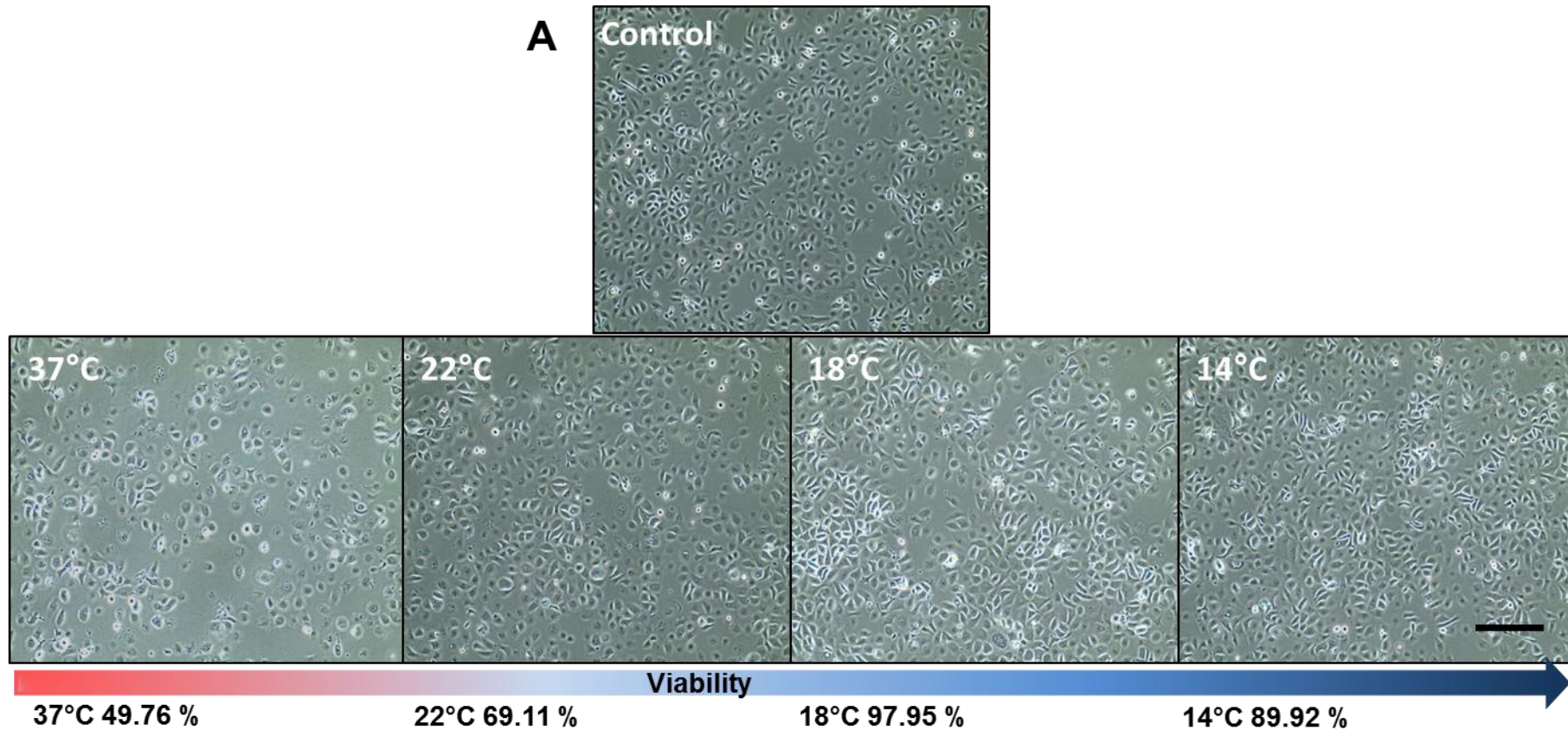
### Viability assay for HHFK cell line

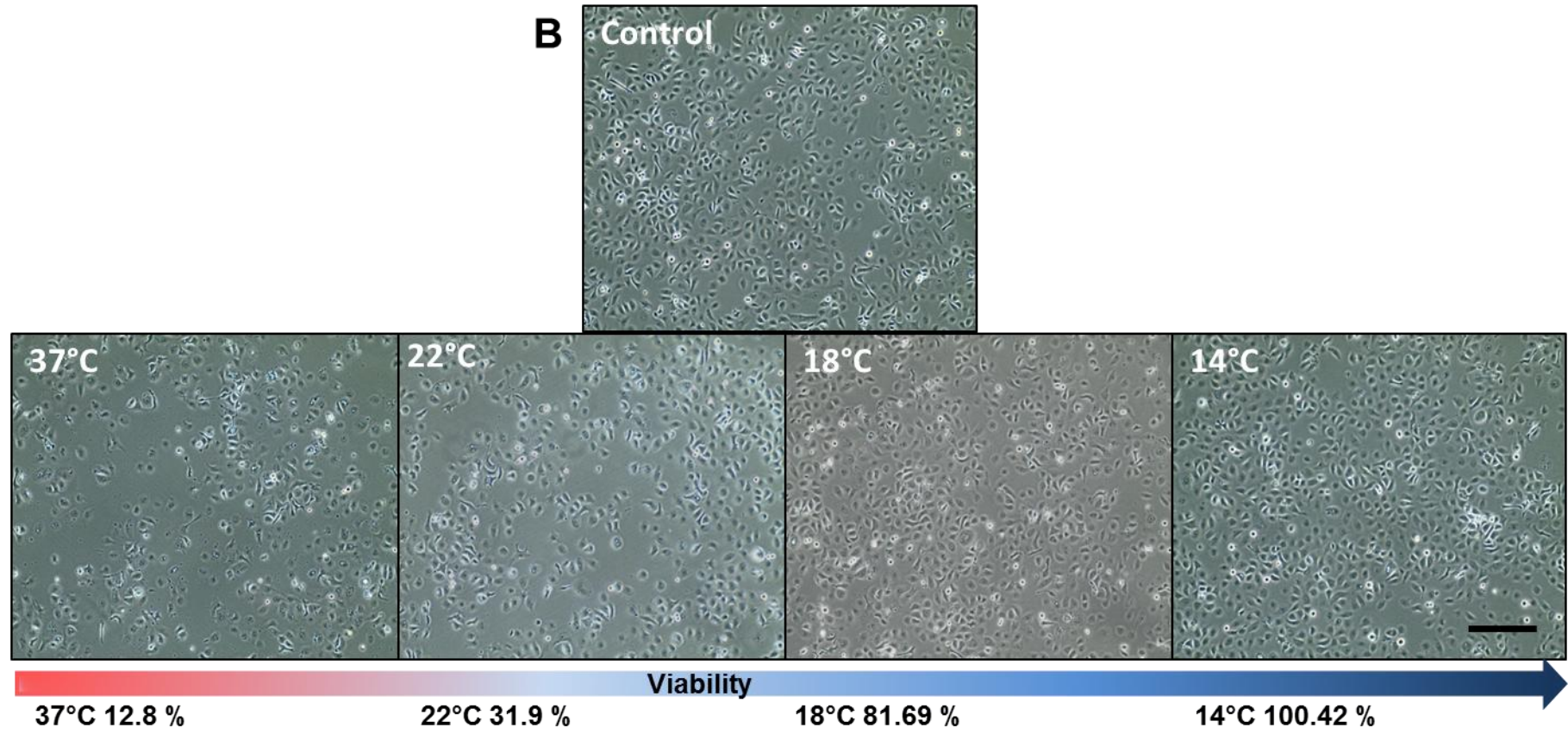
Cell viability percentage was estimated by CellTiter 96® AQueous One Solution in 96-well plates following 72h. HHFK cells at increasing cell densities ('Low', 'Medium' and 'High') under routine culture conditions ('Cell number' represents number of cells seeded per well). Bars correspond to mean absorbance at 492 nm ( $\pm$ SD) for three independent biological. Experiments, each consisting of 6 technical replicates.

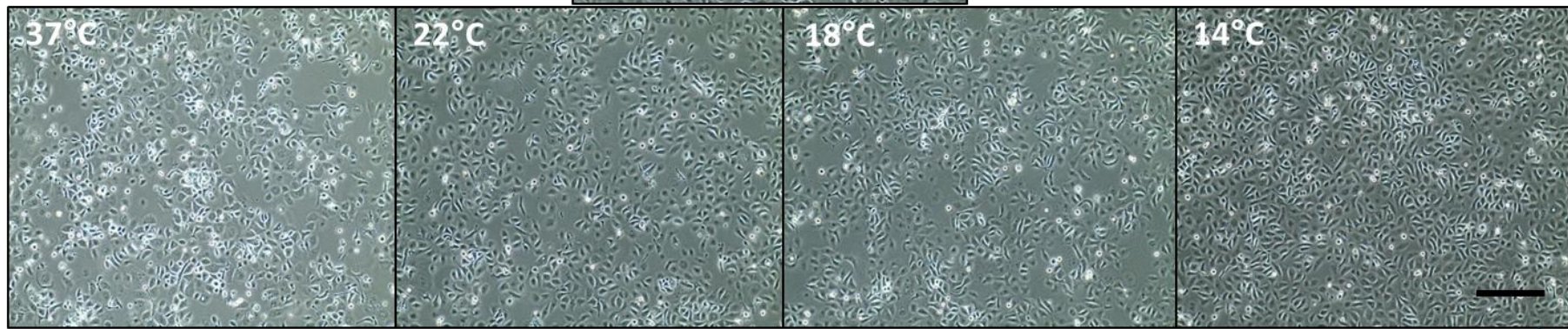
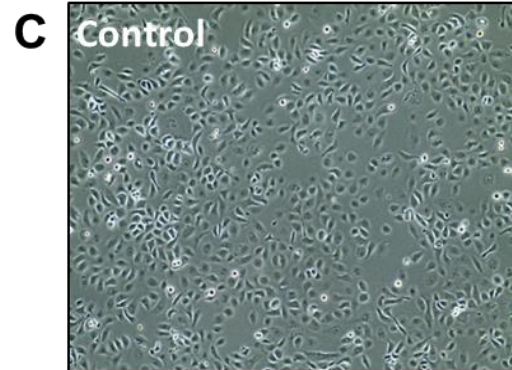
## Appendix V

### Microscopic observation of cooling-mediated cytoprotection of HaCaT cells from chemotherapy drug-mediated toxicity

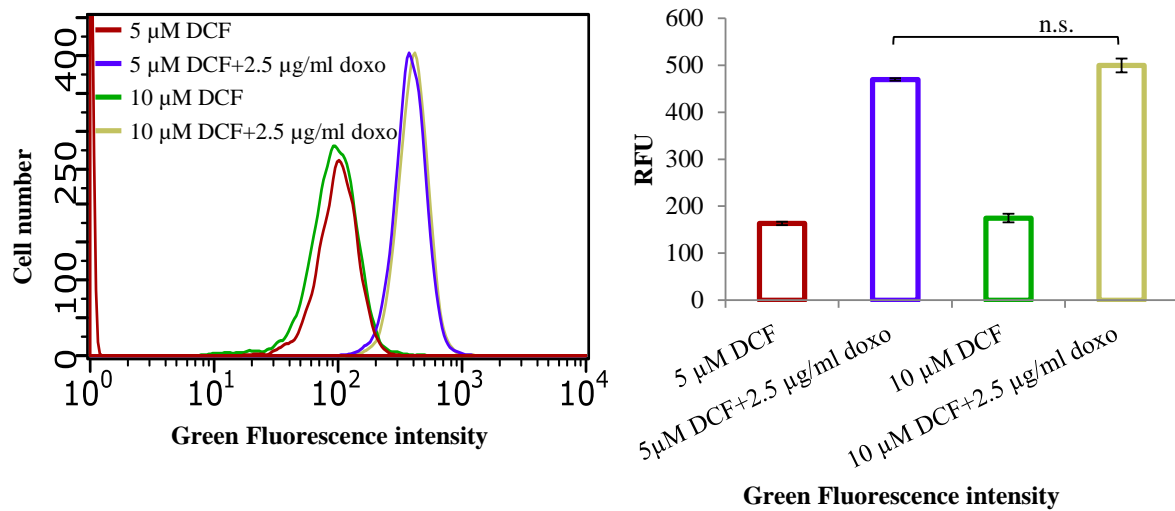
HaCaT cells were treated with the indicated doses of 0.5  $\mu\text{g}/\text{mL}$  doxorubicin (A), 5  $\mu\text{g}/\text{mL}$  4-OH-CP (B) and 0.01  $\mu\text{g}/\text{mL}$  docetaxel (C) at 37°C and 22°C. Solvent alone-treated (Control) HaCaT cultures served as negative controls. Phase contrast light microscopy was used to assess the viability of control and drug-treated cultures and representative photomicrographs are provided from two independent series of experiments. The presence of non-adherent, phase-bright cells following drug treatment was indicative of drug-mediated cytotoxicity. Phase contrast images were obtained using an EVOS XL core inverted microscope and at x100 magnification.







## Appendix V



### ROS levels measured by flow cytometry analysis after treatment with doxorubicin and H2DCFDA(5 and 10 $\mu$ M) in HaCaTa cells

HaCaTa cells were seeded in 6 well plate at  $1.5 \times 10^5$  cells/well in KSFM medium and were incubated overnight at  $37^\circ\text{C}/5\% \text{CO}_2$ . HaCaTa cells were treated for 2h with  $2.5 \mu\text{g/mL}$  doxorubicin at  $37^\circ\text{C}$ , compared with vehicle control (cells treated with medium containing the solvent in which the reagent was dissolved). The drugs were then removed, wells were rinsed with PBS to remove any traces of drug and cultures incubated for a 30 min and after which (5 and  $10 \mu\text{M}$ ) H2DCFDA reagent were added to the wells and plates were incubated at  $37^\circ\text{C}$  in  $5\% \text{CO}_2$  for 30 min. Cells were harvested by trypsinisation ROS generation were analysed by flow cytometry using H2DCFDA as a fluorescent probe. A) Representative flow cytometric histograms, B) bars represent median fluorescence intensity (MFI). Cells were acquired on a Guava EasyCyte flow cytometer and results analysed using GuavaSoft software. Bars show  $\text{MFI} \pm \text{S.E.M}$  for 3 technical replicates. \*\*\*,  $p < 0.001$ .

## References

- Abraham, P., Kanakasabapathy, I., 2008. Alterations in antioxidant enzyme activities and increased oxidative stress in cyclophosphamide-induced hemorrhagic cystitis in the rat. *Cancer Therapy* 16, 563-570.
- Adams, J. M., Cory, S., 1998. The Bcl-2 protein family: arbiters of cell survival. *Science* 281, 1322-1326.
- Ahrendt, S. A., Brown, H. M., Komorowski, R. A., Zhu, Y.-R., Wilson, S. D., Erickson, B. A., Ritch, P. S., Pitt, H. A., Demeure, M. J., 2000. p21 WAF1 expression is associated with improved survival after adjuvant chemoradiation for pancreatic cancer. *Surgery* 128, 520-530.
- Al-Tameemi, W., Dunnill, C., Hussain, O., Komen, M. M., Van Den Hurk, C. J., Collett, A., Georgopoulos, N. T., 2014. Use of *in vitro* human keratinocyte models to study the effect of cooling on chemotherapy drug-induced cytotoxicity. *Toxicology in Vitro* 28, 1366-1376.
- Alexandre, J., Batteux, F., Nicco, C., Chéreau, C., Laurent, A., Guillevin, L., Weill, B., Goldwasser, F., 2006. Accumulation of hydrogen peroxide is an early and crucial step for paclitaxel-induced cancer cell death both *in vitro* and *in vivo*. *International Journal of Cancer* 119, 41-48.
- Alkan, F. U., Anlas, C., Cinar, S., Yildirim, F., Ustuner, O., Bakirel, T., Gurel, A., 2014. Effects of curcumin in combination with cyclophosphamide on canine mammary tumour cell lines. *Veterinari Medicina* 59, 553-572.
- Amoh, Y., Li, L., Katsuoka, K., Hoffman, R. M., 2007. Chemotherapy targets the hair-follicle vascular network but not the stem cells. *Journal of Investigative Dermatology* 127, 11-15.
- Anderson, J. E., Hunt, J. M., Smith, I. E., 1981. Prevention of doxorubicin-induced alopecia by scalp cooling in patients with advanced breast cancer. *British Medical Journal* 282, 423-424.
- Apisarnthanarax, N., Duvic, M. M., 2003. *Dermatologic Complications of Cancer Chemotherapy*. BC Decker, Hamilton, London 559-570.
- Aragane, Y., Kulms, D., Metze, D., Wilkes, G., Pöppelmann, B., Luger, T. A., Schwarz, T., 1998. Ultraviolet light induces apoptosis *via* direct activation of CD95 (Fas/APO-1) independently of its ligand CD95L. *The Journal of Cell Biology* 140, 171-182.
- Ashkenazi, A., Dixit, V. M., 1998. Death receptors: signaling and modulation. *Science* 281, 1305-1308.
- Atkuri, K. R., Mantovani, J. J., Herzenberg, L. A., Herzenberg, L. A., 2007. N-Acetylcysteine—a safe antidote for cysteine/glutathione deficiency. *Current Opinion in Pharmacology* 7, 355-359.
- Aurelian, L., 2005. Cross talk of signaling and apoptotic cascades in the CNS: Target for virus modulation. *Frontiers in Bioscience* 10, 2776-2787.
- Auvinen, P. K., Mahonen, U. A., Soininen, K. M., Paananen, P. K., Ranta-Koponen, P. H., Saavalainen, I. E., Johansson, R. T., 2010. The effectiveness of a scalp cooling cap in preventing chemotherapy-induced alopecia. *Journal of Tumor* 96, 271-275.
- Bai, L., Zhu, W.-G., 2006. p53: structure, function and therapeutic applications. *Journal of Cancer Molecules* 2, 141-153.

- Balsari, A., Morelli, D., Menard, S., Veronesi, U., Colnaghi, M., 1994. Protection against doxorubicin-induced alopecia in rats by liposome-entrapped monoclonal antibodies. *The Federation of American Societies for Experimental Biology* 8, 226-230.
- Barlogie, B., Drewinko, B., Johnston, D. A., Freireich, E. J., 1976. The effect of adriamycin on the cell cycle traverse of a human lymphoid cell line. *Cancer Research* 36, 1975-1979.
- Basañez, G., Sharpe, J. C., Galanis, J., Brandt, T. B., Hardwick, J. M., Zimmerberg, J., 2002. Bax-type apoptotic proteins porate pure lipid bilayers through a mechanism sensitive to intrinsic monolayer curvature. *Journal of Biological Chemistry* 277, 49360-49365.
- Bass, D., Parce, J. W., Dechatelet, L. R., Szejda, P., Seeds, M., Thomas, M., 1983. Flow cytometric studies of oxidative product formation by neutrophils: a graded response to membrane stimulation. *The Journal of Immunology* 130, 1910-1917.
- Batchelor, D., 2001. Hair and cancer chemotherapy: consequences and nursing care – a literature study. *European Journal of Cancer Care* 10, 147-163.
- Bedard, K., Krause, K.-H., 2007. The NOX family of ROS-generating NADPH oxidases: physiology and pathophysiology. *Physiological Reviews* 87, 245-313.
- Bender, A., Opel, D., Naumann, I., Kappler, R., Friedman, L., Von Schweinitz, D., Debatin, K., Fulda, S., 2011. PI3K inhibitors prime neuroblastoma cells for chemotherapy by shifting the balance towards pro-apoptotic Bcl-2 proteins and enhanced mitochondrial apoptosis. *Oncogene* 30, 494-503.
- Benhar, M., Dalyot, I., Engelberg, D., Levitzki, A., 2001. Enhanced ROS production in oncogenically transformed cells potentiates c-Jun N-terminal kinase and p38 mitogen-activated protein kinase activation and sensitization to genotoxic stress. *Molecular and Cellular Biology* 21, 6913-6926.
- Bhardwaj, A., Srivastava, S. K., Singh, S., Arora, S., Tyagi, N., Andrews, J., McClellan, S., Carter, J. E., Singh, A. P., 2014. CXCL12/CXCR4 signaling counteracts docetaxel-induced microtubule stabilization *via* p21-activated kinase 4-dependent activation of LIM domain kinase 1. *Oncotarget* 5, 11490-11500.
- Bichsel, K. J., Gogia, N., Malouff, T., Pena, Z., Forney, E., Hammiller, B., Watson, P., Hansen, L. A., 2013. Role for the epidermal growth factor receptor in chemotherapy-induced alopecia. *PloS One* 8 (7): e69368.
- Billen, L., Shamas-Din, A., Andrews, D., 2008. Bid: a Bax-like BH3 protein. *Oncogene* 27, 93-104.
- Blanpain, C., Lowry, W. E., Geoghegan, A., Polak, L., Fuchs, E., 2004. Self-renewal, multipotency, and the existence of two cell populations within an epithelial stem cell niche. *Cell* 118, 635-648.
- Blume-Peytavi, U., Whiting, D. A., Trüeb, R. M., 2008. Hair growth and disorders. Springer Berlin 124, 21–28.
- Boatright, K. M., Salvesen, G. S., 2003. Mechanisms of caspase activation. *Current Opinion in Cell Biology* 15, 725-731.
- Boccellino, M., Pedata, P., Castiglia, L., La Porta, R., Pieri, M., Quagliuolo, L., Acampora, A., Sannolo, N., Miraglia, N., 2010. Doxorubicin can penetrate nitrile gloves and induces apoptosis in keratinocytes cell lines. *Toxicology letters* 197, 61-68.
- Bodo, E., Tobin, D. J., Kamenisch, Y., Biro, T., Berneburg, M., Funk, W., Paus, R., 2007. Dissecting the impact of chemotherapy on the human hair follicle: a pragmatic *in vitro* assay for studying the pathogenesis and potential management of hair follicle dystrophy. *American Journal of Pathology* 171, 1153-67.

- Bodo, E., Van Beek, N., Naumann, V., Ohnemus, U., Brzoska, T., Abels, C., Paus, R., 2009. Modulation of chemotherapy-induced human hair follicle damage by 17-beta estradiol and prednisolone: potential stimulators of normal hair regrowth by "dystrophic catagen" promotion. *Journal of Investigative Dermatology* 129, 506-9.
- Boelsma, E., Verhoeven, M. C., Ponc, M., 1999. Reconstruction of a human skin equivalent using a spontaneously transformed keratinocyte cell line (HaCaT). *Journal of Investigative Dermatology* 112, 489-498.
- Bortoletto, R., Silva, N. D., Zangaro, R., Pacheco, M., Da Matta, R., Pacheco-Soares, C., 2004. Mitochondrial membrane potential after low-power laser irradiation. *Lasers in Medical Science* 18, 204-206.
- Bos, M., Mendelsohn, J., Kim, Y.-M., Albanell, J., Fry, D. W., Baselga, J., 1997. PD153035, a tyrosine kinase inhibitor, prevents epidermal growth factor receptor activation and inhibits growth of cancer cells in a receptor number-dependent manner. *Clinical Cancer Research* 3, 2099-2106.
- Botchkarev, V. A., Komarova, E. A., Siebenhaar, F., Botchkareva, N. V., Komarov, P. G., Maurer, M., Gilchrest, B. A., Gudkov, A. V., 2000. p53 is essential for chemotherapy-induced hair loss. *Cancer Research* 60, 5002-5006.
- Botchkarev, V. A., Komarova, E. A., Siebenhaar, F., Botchkareva, N. V., Sharov, A. A., Komarov, P. G., Maurer, M., Gudkov, A. V., Gilchrest, B. A., 2001. p53 Involvement in the control of murine hair follicle regression. *The American Journal of Pathology* 158, 1913-1919.
- Botchkarev, V. A., 2003. Molecular mechanisms of chemotherapy-induced hair loss. *Journal of Investigative Dermatology Symposium Proceedings* 8, 72-75.
- Botchkarev, V. A., Kishimoto, J., 2003. Molecular control of epithelial–mesenchymal interactions during hair follicle cycling. *Journal of Investigative Dermatology Symposium Proceedings* 8, 46-55.
- Botchkareva, N. V., Khlgatian, M., Longley, B. J., Botchkarev, V. A., Gilchrest, B. A., 2001. SCF/c-kit signaling is required for cyclic regeneration of the hair pigmentation unit. *The Federation of American Societies for Experimental Biology* 15, 645-658.
- Botchkareva, N. V., Ahluwalia, G., Shander, D., 2006a. Apoptosis in the hair follicle. *Journal of Investigative Dermatology* 126, 258-264.
- Botchkareva, N. V., Kahn, M., Ahluwalia, G., Shander, D., 2006b. Survivin in the human hair follicle. *Journal of Investigative Dermatology* 127, 479-482.
- Boukamp, P., Petrussevska, R. T., Breitkreutz, D., Hornung, J., Markham, A., Fusenig, N. E., 1988. Normal keratinization in a spontaneously immortalized aneuploid human keratinocyte cell line. *The Journal of Cell Biology* 106, 761-771.
- Bowden, P. E., Hainey, S. D., Parker, G., Jones, D. O., Zimonjic, D., Popescu, N., Hodgins, M. B., 1998. Characterization and chromosomal localization of human hair-specific keratin genes and comparative expression during the hair growth cycle. *Journal of Investigative Dermatology* 110, 158-164.
- Brajac, I., Tkalčić, M., Dragojević, D. M., Gruber, F., 2003. Roles of stress, stress perception and trait-anxiety in the onset and course of alopecia areata. *The Journal of Dermatology* 30, 871-878.
- Brand, M. D., 2010. The sites and topology of mitochondrial superoxide production. *Experimental Gerontology* 45, 466-472.
- Bravo-Cuellar, A., Ortiz-Lazareno, P. C., Lerma-Diaz, J. M., Dominguez-Rodriguez, J. R., Jave-Suarez, L. F., Aguilar-Lemarroy, A., Del Toro-Arreola, S., De Celis-Carrillo, R., Sahagun-Flores, J. E., De Alba-Garcia, J. E. G., 2010. Sensitization of cervix cancer

- cells to Adriamycin by Pentoxifylline induces an increase in apoptosis and decrease senescence. *Molecular Cancer* 9, 1.
- Braylan, R. C., Diamond, L. W., Powell, M. L., Harty-Golder, B., 1980. Percentage of cells in the S phase of the cell cycle in human lymphoma determined by flow cytometry. Correlation with labeling index and patient survival. *Cytometry* 1, 171-174.
- Breed, W. P., Van Den Hurk, C. J., Peerbooms, M., 2011. Presentation, impact and prevention of chemotherapy-induced hair loss: scalp cooling potentials and limitations. *Expert Review of Dermatology* 6, 109-25.
- Brunsvig, P. F., Andersen, A., Aamdal, S., Kristensen, V., Olsen, H., 2007. Pharmacokinetic analysis of two different docetaxel dose levels in patients with non-small cell lung cancer treated with docetaxel as monotherapy or with concurrent radiotherapy. *BMC Cancer* 7, 197-205.
- Bülow, J., Friberg, L., Gaardsting, O., Hansen, M., 1985. Frontal subcutaneous blood flow, and epi-and subcutaneous temperatures during scalp cooling in normal man. *Scandinavian Journal of Clinical and Laboratory Investigation* 45, 505-508.
- Burdon, R. H., 1995. Superoxide and hydrogen peroxide in relation to mammalian cell proliferation. *Free Radical Biology and Medicine* 18, 775-794.
- Buyukhatipoglu, H., Babacan, T., Kertmen, N., Balakan, O., Suner, A., Ates, O., Sarici, F., Aslan, A., Diker, O., Tasdemir, V., 2015. A retrospective analysis of adjuvant CAF, AC-T and TAC regimens in triple negative early stage breast cancer. *Journal of the Balkan Union of Oncology* 20, 22-77.
- Cao, D.-X., Qiao, B., Ge, Z.-Q., Yuan, Y.-J., 2004. Comparison of burst of reactive oxygen species and activation of caspase-3 in apoptosis of K562 and HL-60 cells induced by docetaxel. *Cancer Letters* 214, 103-113.
- Cartron, P.-F., Gallenne, T., Bougras, G., Gautier, F., Manero, F., Vusio, P., Meflah, K., Vallette, F. M., Juin, P., 2004. The first  $\alpha$  helix of Bax plays a necessary role in its ligand-induced activation by the BH3-only proteins Bid and PUMA. *Molecular Cell* 16, 807-818.
- Chansky, K., Benedetti, J., Macdonald, J. S., 2005. Differences in toxicity between men and women treated with 5-fluorouracil therapy for colorectal carcinoma. *Cancer* 103, 1165-1171.
- Charvat, R. A., Arrizabalaga, G., 2016. Oxidative stress generated during monensin treatment contributes to altered *Toxoplasma gondii* mitochondrial function. *Scientific Reports* 15(6):22997.
- Chen, R., Yang, L., McIntyre, T. M., 2007. Cytotoxic phospholipid oxidation products cell death from mitochondrial damage and the intrinsic caspase cascade. *Journal of Biological Chemistry* 282, 24842-24850.
- Cheng, E. H.-Y., Sheiko, T. V., Fisher, J. K., Craigen, W. J., Korsmeyer, S. J., 2003. VDAC2 inhibits BAK activation and mitochondrial apoptosis. *Science* 301, 513-517.
- Chevremont, S., Chevremont, M., 1956. Action de températures subnormales suivies de rechauffement sur l'activité mitotique en culture de tissus-contribution à l'étude de la préparation à la mitose. *Comptes Rendus Des Seances De La Société De Biologie Et De Ses Filiales* 150, 1046-1049.
- Chipuk, J. E., Green, D. R., 2004. Cytoplasmic p53: bax and forward. *Cell Cycle* 3, 427-429.
- Chipuk, J. E., Kuwana, T., Bouchier-Hayes, L., Droin, N. M., Newmeyer, D. D., Schuler, M., Green, D. R., 2004. Direct activation of Bax by p53 mediates mitochondrial membrane permeabilization and apoptosis. *Science* 303, 1010-1014.

- Chou, J., Greig, N., Reiner, D., Hoffer, B., Wang, Y., 2011. Enhanced survival of dopaminergic neuronal transplants in hemiparkinsonian rats by the p53 inactivator PFT- $\alpha$ . *Cell Transplantation* 20, 1351-1359.
- Chou, Y.-F., Yu, C.-C., Huang, R.-F. S., 2007. Changes in mitochondrial DNA deletion, content, and biogenesis in folate-deficient tissues of young rats depend on mitochondrial folate and oxidative DNA injuries. *The Journal of Nutrition* 137, 2036-2042.
- Chung, Y. M., Bae, Y. S., Lee, S. Y., 2003. Molecular ordering of ROS production, mitochondrial changes, and caspase activation during sodium salicylate-induced apoptosis. *Free Radical Biology and Medicine* 34, 434-442.
- Cline, B. W., 1984. Prevention of chemotherapy-induced alopecia: a review of the literature. *Cancer Nursing* 7, 221-228.
- Gold, V., Loening, K., McNaught, A., & Shemi, P. 2nd ed (1997). *IUPAC Compendium of Chemical Terminology (the "Gold Book")*: Blackwell Science, Oxford.
- Cole, G. W., Alleva, A. M., Reddy, R. M., Maxhimer, J. B., Zuo, J., Schrumpp, D. S., Nguyen, D. M., 2005. The selective epidermal growth factor receptor tyrosine kinase inhibitor PD153035 suppresses expression of prometastasis phenotypes in malignant pleural mesothelioma cells *in vitro*. *The Journal of Thoracic and Cardiovascular Surgery* 129, 1010-1017.
- Conklin, K. A., 2004. Chemotherapy-associated oxidative stress: impact on chemotherapeutic effectiveness. *Integrative Cancer Therapies* 3, 294-300.
- Cossarizza, A., Baccaranicontri, M., Kalashnikova, G., Franceschi, C., 1993. A new method for the cytofluorometric analysis of mitochondrial membrane potential using the J-aggregate forming lipophilic cation 5, 5', 6, 6'-tetrachloro-1, 1', 3, 3'-tetraethylbenzimidazolcarbocyanine iodide (JC-1). *Biochemical and Biophysical Research Communications* 197, 40-45.
- Cotsarelis, G., Sun, T.-T., Lavker, R. M., 1990. Label-retaining cells reside in the bulge area of pilosebaceous unit: implications for follicular stem cells, hair cycle, and skin carcinogenesis. *Cell* 61, 1329-1337.
- Cotsarelis, G., 2006. Epithelial stem cells: a folliculocentric view. *Journal of Investigative Dermatology* 126, 1459-1468.
- Couchman, J. R., Gibson, W. T., 1985. Expression of basement membrane components through morphological changes in the hair growth cycle. *Developmental Biology* 108, 290-298.
- Cullen, S., Martin, S., 2009. Caspase activation pathways: some recent progress. *Cell Death and Differentiation* 16, 935-938.
- Culmsee, C., Zhu, X., Yu, Q. S., Chan, S. L., Camandola, S., Guo, Z., Greig, N. H., Mattson, M. P., 2001. A synthetic inhibitor of p53 protects neurons against death induced by ischemic and excitotoxic insults, and amyloid  $\beta$ -peptide. *Journal of Neurochemistry* 77, 220-228.
- Daniel, N. N., Korsmeyer, S. J., 2004. Cell death: critical control points. *Cell* 116, 205-219.
- Davis, S. T., Benson, B. G., Bramson, H. N., Chapman, D. E., Dickerson, S. H., Dold, K. M., Eberwein, D. J., Edelstein, M., Frye, S. V., Gampe, R. T., 2001. Prevention of chemotherapy-induced alopecia in rats by CDK inhibitors. *Science* 291, 134-137.
- De Flora, S., Izzotti, A., D'agostini, F., Balansky, R. M., 2001. Mechanisms of N-acetylcysteine in the prevention of DNA damage and cancer, with special reference to smoking-related end-points. *Carcinogenesis* 22, 999-1013.

- Dean, J. C., 1979. Prevention of doxorubicin-induced hair loss with scalp hypothermia. *The New England Journal of Medicine* 301, 1427-9.
- Dewey, D., 1987. Cycle reset in a melanoma cell line caused by cooling. *Cell Proliferation* 20, 603-609.
- Deyrieux, A. F., Wilson, V. G., 2007. *In vitro* culture conditions to study keratinocyte differentiation using the HaCaT cell line. *Cytotechnology* 54, 77-83.
- Deyrieux, A. F., Rosas-Acosta, G., Ozbun, M. A., Wilson, V. G., 2007. Sumoylation dynamics during keratinocyte differentiation. *Journal of Cell Science* 120, 125-136.
- Di Leonardo, A., Linke, S. P., Clarkin, K., Wahl, G. M., 1994. DNA damage triggers a prolonged p53-dependent G1 arrest and long-term induction of Cip1 in normal human fibroblasts. *Genes and Development* 8, 2540-2551.
- Diana, D., Anp, Vahdat, L. T., 2008. Etoposides: clinical update and future directions. *Oncology* 22, 408.
- Ditsworth, D., Priestley, M. A., Loepke, A. W., Ramamoorthy, C., Mccann, J., Staple, L., Kurth, C. D., 2003. Apoptotic neuronal death following deep hypothermic circulatory arrest in piglets. *The Journal of the American Society of Anesthesiologists* 98, 1119-1127.
- Domashenko, A., Gupta, S., Cotsarelis, G., 2000. Efficient delivery of transgenes to human hair follicle progenitor cells using topical lipoplex. *Nature Biotechnology* 18, 420-423.
- Dorr, V. J., 1998. A practitioner's guide to cancer-related alopecia. *Seminars in Oncology* 25, 562-570.
- Douglas, M., Anderson A., 2004. *Mosby's Medical, Nursing, and Allied Health Dictionary*, New York: Piccin.
- Duvic, M., Lemak, N. A., Valero, V., Hymes, S. R., Farmer, K. L., Hortobagyi, G. N., Trancik, R. J., Bandstra, B. A., Compton, L. D., 1996. A randomized trial of minoxidil in chemotherapy-induced alopecia. *Journal of the American Academy of Dermatology* 35, 74-78.
- Ekert, P. G., Vaux, D. L., 2005. The mitochondrial death squad: hardened killers or innocent bystanders. *Current Opinion in Cell Biology* 17, 626-630.
- Epstein Jr, E. H., Lutzner, M. A., 1969. Folliculitis induced by actinomycin D. *New England Journal of Medicine* 281, 1094-1096.
- Espinosa, E., Zamora, P., Feliu, J., González Barón, M., 2003. Classification of anticancer drugs—a new system based on therapeutic targets. *Cancer Treatment Reviews* 29, 515-523.
- Evan, G. I., Vousden, K. H., 2001. Proliferation, cell cycle and apoptosis in cancer. *Nature* 411, 342-348.
- Fabbri, F., Carloni, S., Briigliadori, G., Zoli, W., Lapalombella, R., Marini, M., 2006. Sequential events of apoptosis involving docetaxel, a microtubule-interfering agent: a cytometric study. *BMC Cell Biology* 7, 74-78.
- Fink, S. L., Cookson, B. T., 2005. Apoptosis, pyroptosis, and necrosis: mechanistic description of dead and dying eukaryotic cells. *Infection and Immunity* 73, 1907-1916.
- Forrest, G., Plumb, C., Ziebland, S., Stein, A., 2006. Breast cancer in the family—children's perceptions of their mother's cancer and its initial treatment: qualitative study. *British Medical Journal* 332, 998-1003.

- Fransson, Å., Ruusala, A., Aspenström, P., 2003. Atypical Rho GTPases have roles in mitochondrial homeostasis and apoptosis. *Journal of Biological Chemistry* 278, 6495-6502.
- Fridman, J. S., Lowe, S. W., 2003. Control of apoptosis by p53. *Oncogene* 22, 9030-9040.
- Friesen, C., Herr, I., Krammer, P. H., Debatin, K.-M., 1996. Involvement of the CD95 (APO-1/Fas) receptor/ligand system in drug-induced apoptosis in leukemia cells. *Nature Medicine* 2, 574-577.
- Fry, D. W., Kraker, A. J., Mcmichael, A., Ambroso, L. A., Nelson, J. M., Leopold, W. R., Connors, R., Bridges, A. J., 1994. A specific inhibitor of the epidermal growth factor receptor tyrosine kinase. *Science-New York Then Washington*, 1093-1093.
- Fu, Z., Guo, J., Jing, L., Li, R., Zhang, T., Peng, S., 2010. Enhanced toxicity and ROS generation by doxorubicin in primary cultures of cardiomyocytes from neonatal metallothionein-I/II null mice. *Toxicology in Vitro* 24, 1584-1591.
- Fulda, S., Galluzzi, L., Kroemer, G., 2010. Targeting mitochondria for cancer therapy. *Nature Reviews Drug Discovery* 9, 447-464.
- Galluzzi, L., Aaronson, S. A., Abrams, J., Alnemri, E. S., Andrews, D. W., Baehrecke, E. H., Bazan, N. G., Blagosklonny, M. V., Blomgren, K., Borner, C., 2009. Guidelines for the use and interpretation of assays for monitoring cell death in higher eukaryotes. *Cell Death and Differentiation* 16, 1093-1107.
- Ge, H., Liu, H., Fu, Z., Sun, Z., 2012. Therapeutic and preventive effects of an epidermal growth factor receptor inhibitor on oral squamous cell carcinoma. *Journal of International Medical Research* 40, 455-466.
- Georgopoulos, N. T., Kirkwood, L. A., Walker, D. C., Southgate, J., 2010. Differential regulation of growth-promoting signalling pathways by E-cadherin. *PloS One* 5, e13621.
- Georgopoulos, N. T., Kirkwood, L. A., Southgate, J., 2014. A novel bidirectional positive-feedback loop between Wnt- $\beta$ -catenin and EGFR-ERK plays a role in context-specific modulation of epithelial tissue regeneration. *Journal of Cell Science* 127, 2967-2982.
- Geraghty, R., Capes-Davis, A., Davis, J., Downward, J., Freshney, R., Knezevic, I., Lovell-Badge, R., Masters, J., Meredith, J., Stacey, G., 2014. Guidelines for the use of cell lines in biomedical research. *British Journal of Cancer* 111, 1021-1046.
- Geras, A., 1990. *Dermatology: a medical artist's interpretation 1990*. Basel: WR 100, G356.
- Gligorov, J., Lotz, J. P., 2004. Preclinical pharmacology of the taxanes: implications of the differences. *The Oncologist* 9, 3-8.
- Gonzalez, E. J., Peterson, A., Malley, S., Daniel, M., Lambert, D., Kosofsky, M., Vizzard, M. A., 2015. The effects of tempol on cyclophosphamide-induced oxidative stress in rat micturition reflexes. *The Scientific World Journal* 5, 45-48.
- Gottlieb, E., Oren, M., 1998. p53 facilitates pRb cleavage in IL-3-deprived cells: novel proapoptotic activity of p53. *The EMBO Journal* 17, 3587-3596.
- Green, D., Kroemer, G., 1998. The central executioners of apoptosis: caspases or mitochondria. *Trends in Cell Biology* 8, 267-271.
- Gregory, R., Cooke, T., Middleton, J., Buchanan, R., Williams, C., 1982. Prevention of doxorubicin-induced alopecia by scalp hypothermia: relation to degree of cooling. *British Medical Journal (Clinical Research Ed.)* 284, 1674.
- Grevelman, E. G., Breed, W. P., 2005. Prevention of chemotherapy-induced hair loss by scalp cooling. *Annals of Oncology* 16, 352-358.

- Grunt, T. W., Tomek, K., Wagner, R., Puckmair, K., Zielinski, C. C., 2007. The DNA-binding epidermal growth factor-receptor inhibitor PD153035 and other DNA-intercalating cytotoxic drugs reactivate the expression of the retinoic acid receptor- $\beta$  tumor-suppressor gene in breast cancer cells. *Differentiation* 75, 883-890.
- Guy, R., Parker, H., Shah, S., Geddes, D., 1982. Scalp cooling by thermocirculator. *The Lancet* 319, 937-938.
- Halliwell, B., 2014. Cell culture, oxidative stress, and antioxidants: avoiding pitfalls. *Biomedical journal* 37, 99.
- Han, J.-W., Flemington, C., Houghton, A. B., Gu, Z., Zambetti, G. P., Lutz, R. J., Zhu, L., Chittenden, T., 2001. Expression of *bbc3*, a pro-apoptotic BH3-only gene, is regulated by diverse cell death and survival signals. *Proceedings of the National Academy of Sciences* 98, 11318-11323.
- Hansen, L. A., Alexander, N., Hogan, M. E., Sundberg, J. P., Dlugosz, A., Threadgill, D. W., Magnuson, T., Yuspa, S. H., 1997. Genetically null mice reveal a central role for epidermal growth factor receptor in the differentiation of the hair follicle and normal hair development. *The American Journal of Pathology* 150, 1959.
- Happo, L., Cragg, M. S., Phipson, B., Haga, J. M., Jansen, E. S., Herold, M. J., Dewson, G., Michalak, E. M., Vandenberg, C. J., Smyth, G. K., 2010. Maximal killing of lymphoma cells by DNA damage-inducing therapy requires not only the p53 targets Puma and Noxa, but also Bim. *Blood* 116, 5256-5267.
- Hardy, M. H., 1992. The secret life of the hair follicle. *Trends in Genetics* 8, 55-61.
- Harris, C. C., 1996. Structure and function of the p53 tumour suppressor gene: clues for rational cancer therapeutic strategies. *Journal of the National Cancer Institute* 88, 1442-1455.
- Hartwell, L. H., Kastan, M. B., 1994. Cell cycle control and cancer. *Science* 266, 1821-1828.
- Hasmall, S. C., Roberts, R. A., 1999. The perturbation of apoptosis and mitosis by drugs and xenobiotics. *Pharmacology and Therapeutics* 82, 63-70.
- Held, P., 2012. An introduction to reactive oxygen species-measurement of ROS in cells. White Paper. BioTek Instruments, Winooski.
- Hengartner, M. O., 2000. The biochemistry of apoptosis. *Nature* 407, 770-776.
- Henseleit, U., Zhang, J., Wanner, R., Haase, I., Kolde, G., Rosenbach, T., 1997. Role of p53 in UVB-induced apoptosis in human HaCaT keratinocytes. *Journal of Investigative Dermatology* 109, 722-727.
- Hernández-Vargas, H., Palacios, J., Moreno-Bueno, G., 2007. Molecular profiling of docetaxel cytotoxicity in breast cancer cells: uncoupling of aberrant mitosis and apoptosis. *Oncogene* 26, 2902-2913.
- Hesketh, P. J., Batchelor, D., Golant, M., Lyman, G. H., Rhodes, N., Yardley, D., 2004. Chemotherapy-induced alopecia: psychosocial impact and therapeutic approaches. *Supportive Care in Cancer* 12, 543-549.
- Higgins, C. A., Westgate, G. E., Jahoda, C. A., 2009. From telogen to exogen: mechanisms underlying formation and subsequent loss of the hair club fibre. *Journal of Investigative Dermatology* 129, 2100-2108.
- Hilton, S., Hunt, K., Emslie, C., Salinas, M., Ziebland, S., 2008. Have men been overlooked? A comparison of young men and women's experiences of chemotherapy-induced alopecia. *Physical Oncology* 17, 577-583.
- Ho, M. Y., Mackey, J. R., 2014. Presentation and management of docetaxel-related adverse effects in patients with breast cancer. *Cancer Management and Research* 6, 253-258.

- Hoagland, M. S., Hoagland, E. M., Swanson, H. I., 2005. The p53 inhibitor pifithrin- $\alpha$  is a potent agonist of the aryl hydrocarbon receptor. *Journal of Pharmacology and Experimental Therapeutics* 314, 603-610.
- Hoffman, D. M., Grossano, D. D., Damin, L., & Woodcock, T. M. (1979). Stability of refrigerated and frozen solutions of doxorubicin hydrochloride. *American Journal of Health-System Pharmacy*, 36 (11), 1536-1538.
- Hsu, Y.-L., Yu, H.-S., Lin, H.-C., Wu, K.-Y., Yang, R.-C., Kuo, P.-L., 2011. Heat shock induces apoptosis through reactive oxygen species involving mitochondrial and death receptor pathways in corneal cells. *Experimental Eye Research* 93, 405-412.
- Huang, R.-F. S., Huang, S.-M., Lin, B.-S., Hung, C.-Y., Lu, H.-T., 2002. N-Acetylcysteine, vitamin C and vitamin E diminish homocysteine thiolactone-induced apoptosis in human promyeloid HL-60 cells. *The Journal of Nutrition* 132, 2151-2156.
- Hung, C.-H., Chan, S.-H., Chu, P.-M., Tsai, K.-L., 2015. Docetaxel facilitates endothelial dysfunction through oxidative stress *via* modulation of protein kinase C beta: the protective effects of Sotrastaurin. *Toxicological Sciences* 145, 59-67.
- Hussein, A. M., Jimenez, J. J., Mccall, C. A., Yunis, A. A., 1990. Protection from chemotherapy-induced alopecia in a rat model. *Science* 249, 1564-1566.
- Hussein, A. M., 1993. Chemotherapy-induced alopecia: new developments. *Southern Medical Journal* 86, 489-496.
- Hussein, A. M., 1995. Protection against cytosine arabinoside-induced alopecia by minoxidil in a rat animal model. *International Journal of Dermatology* 34, 470-473.
- Hussein, A., Stuart, A., Peters, W., 2009. Protection against chemotherapy-induced alopecia by cyclosporin A in the newborn rat animal model. *Dermatology* 190, 192-196.
- Hwang, P. M., Bunz, F., Yu, J., Rago, C., Chan, T. A., Murphy, M. P., Kelso, G. F., Smith, R. A., Kinzler, K. W., Vogelstein, B., 2001. Ferredoxin reductase affects p53-dependent, 5-fluorouracil-induced apoptosis in colorectal cancer cells. *Nature Medicine* 7, 1111-1117.
- <http://www.niomech.com/>.
- Inui, S., Itami, S., Pan, H.-J., Chang, C., 2000. Lack of androgen receptor transcriptional activity in human keratinocytes. *Journal of Dermatological Science* 23, 87-92.
- Istomin, Y., Zhavrid, E., Alexandrova, E., Sergeyeva, O., Petrovich, S., 2008. Dose enhancement effect of anticancer drugs associated with increased temperature *in vitro*. *Experimental oncology* 30, 56-59.
- Itami, S., Kurata, S., Takayasu, S., 1995. Androgen induction of follicular epithelial cell growth is mediated *via* insulin-like growth factor-I from dermal papilla cells. *Biochemical and Biophysical Research Communications* 212, 988-994.
- Itoh, K., Sasaki, Y., Fujii, H., Minami, H., Ohtsu, T., Wakita, H., Igarashi, T., Watanabe, Y., Onozawa, Y., Kashimura, M., Ohashi, Y., 2000. Study of dose escalation and sequence switching of administration of the combination of docetaxel and doxorubicin in advanced breast cancer. *Clinical Cancer Research* 6, 4082-90.
- Iyer, N. G., Chin, S.-F., Ozdag, H., Daigo, Y., Hu, D.-E., Cariati, M., Brindle, K., Aparicio, S., Caldas, C., 2004. p300 regulates p53-dependent apoptosis after DNA damage in colorectal cancer cells by modulation of PUMA/p21 levels. *Proceedings of the National Academy of Sciences of the United States of America* 101, 7386-7391.
- Izzotti, A., Cartiglia, C., Taningher, M., De Flora, S., Balansky, R., 1999. Age-related increases of 8-hydroxy-2'-deoxyguanosine and DNA-protein crosslinks in mouse

- organs. *Mutation Research/Genetic Toxicology and Environmental Mutagenesis* 446, 215-223.
- Jaeschke, H., Lemasters, J. J., 2003. Apoptosis *versus* oncotic necrosis in hepatic ischemia/reperfusion injury. *Gastroenterology* 125, 1246-1257.
- Jahoda, C., Mauger, A., Bard, S., Sengel, P., 1992. Changes in fibronectin, laminin and type IV collagen distribution relate to basement membrane restructuring during the rat vibrissa follicle hair growth cycle. *Journal of Anatomy* 181, 47-51.
- Jänicke, R. U., Sprengart, M. L., Wati, M. R., Porter, A. G., 1998. Caspase-3 is required for DNA fragmentation and morphological changes associated with apoptosis. *Journal of Biological Chemistry* 273, 9357-9360.
- Janssen, F., Van Leeuwen, G., Van Steenhoven, A., 2005. Modelling of temperature and perfusion during scalp cooling. *Physics in Medicine and Biology* 50, 4065-4069.
- Janssen, F. P., Rajan, V., Steenbergen, W., Van Leeuwen, G. M., Van Steenhoven, A. A., 2007. The relationship between local scalp skin temperature and cutaneous perfusion during scalp cooling. *Physiological Measurement* 28, 829-39.
- Janssen, F. P., Bouten, C. V., Van Leeuwen, G. M., Van Steenhoven, A. A., 2008. Effects of temperature and doxorubicin exposure on keratinocyte damage *in vitro*. *In Vitro Cellular and Developmental Biology - Animal* 44, 81-86.
- Jaworska, M., Gillissen, A., Schärting, B., Wickenburg, D., Schultze-Werninghaus, G., 1995. N-acetylcysteine: a functional oxygen radical scavenger *in vitro* and *ex vivo* in monocytes and neutrophilic granulocytes of patients with COPD. *Pneumologie (Stuttgart, Germany)* 49, 539-545.
- Jeffers, J. R., Parganas, E., Lee, Y., Yang, C., Wang, J., Brennan, J., Maclean, K. H., Han, J., Chittenden, T., Ihle, J. N., 2003. Puma is an essential mediator of p53-dependent and-independent apoptotic pathways. *Cancer Cell* 4, 321-328.
- Jimenez, J. J., Yunis, A. A., 1992a. Protection from 1- $\beta$ -d-arabinofuranosylcytosine-induced alopecia by epidermal growth factor and fibroblast growth factor in the rat model. *Cancer Research* 52, 413-415.
- Jimenez, J. J., Yunis, A. A., 1992b. Protection from chemotherapy-induced alopecia by 1, 25-dihydroxyvitamin D3. *Cancer Research* 52, 5123-5125.
- Jimenez, J. J., Huang, H.-S., Yunis, A. A., 1992. Treatment with ImuVert/JV-Acetylcysteine protects rats from cyclophosphamide/cytarabine-induced alopecia. *Cancer Investigation* 10, 271-276.
- Johansen, L. V., 1985. Scalp hypothermia in the prevention of chemotherapy-induced alopecia. *Acta Oncologica* 24, 113-116.
- Jordan, M. A., Wilson, L., 2004. Microtubules as a target for anticancer drugs. *Nature Reviews Cancer* 4, 253-265.
- Joshi, R. S., 2011. The inner root sheath and the men associated with it eponymically. *International Journal of Trichology* 3, 57-61.
- Joss, R., Kiser, J., Weston, S., Brunner, K., 1988. Fighting alopecia in cancer chemotherapy. *Supportive Care in Cancer Patients*. Springer 25, 117-126.
- Kaina, B., 2003. DNA damage-triggered apoptosis: critical role of DNA repair, double-strand breaks, cell proliferation and signalling. *Biochemical Pharmacology* 66, 1547-1554.
- Kajstura, M., Halicka, H. D., Pryjma, J., Darzynkiewicz, Z., 2007. Discontinuous fragmentation of nuclear DNA during apoptosis revealed by discrete "sub-G1" peaks on DNA content histograms. *Cytometry Part A* 71, 125-131.

- Kaltschmidt, B., Kaltschmidt, C., Hofmann, T. G., Hehner, S. P., Dröge, W., & Schmitz, M. L. (2000). The pro-or anti-apoptotic function of NF- $\kappa$ B is determined by the nature of the apoptotic stimulus. *European Journal of Biochemistry*, 267 (12), 3828-3835.
- Kalyanaraman, B., Darley-Usmar, V., Davies, K. J., Dennery, P. A., Forman, H. J., Grisham, M. B., Mann, G. E., Moore, K., Roberts, L. J., Ischiropoulos, H., 2012. Measuring reactive oxygen and nitrogen species with fluorescent probes: challenges and limitations. *Free Radical Biology and Medicine* 52, 1-6.
- Karbowski, M., Kurono, C., Wozniak, M., Ostrowski, M., Teranishi, M., Soji, T., Wakabayashi, T., 1999. Cycloheximide and 4-OH-TEMPO suppress chloramphenicol-induced apoptosis in RL-34 cells *via* the suppression of the formation of megamitochondria. *Biochimica et Biophysica Acta (BBA)-Molecular Cell Research* 1449, 25-40.
- Katsimbri, P., Bamias, A., Pavlidis, N., 2000. Prevention of chemotherapy-induced alopecia using an effective scalp cooling system. *European Journal of Cancer* 36, 766-771.
- Kayagaki, N., Kawasaki, A., Ebata, T., Ohmoto, H., Ikeda, S., Inoue, S., Yoshino, K., Okumura, K., Yagita, H., 1995. Metalloproteinase-mediated release of human Fas ligand. *The Journal of Experimental Medicine* 182, 1777-1783.
- Kayamba, F., Dunnill, C., Hamnett, D. J., Rodríguez, A., Georgopoulos, N. T., Moran, W. J., 2013. Piperolein B, isopiperolein B and piperamide C9: 1 (8E): total synthesis and cytotoxicities. *Royal Society of Chemistry* 3, 16681-16685.
- Kelly, G. S., 1998. Clinical applications of N-acetylcysteine. *Alternative Medicine Review: a Journal of Clinical Therapeutic* 3, 114-127.
- Kerksick, C., Willoughby, D., 2005. The antioxidant role of glutathione and N-acetyl-cysteine supplements and exercise-induced oxidative stress. *Journal of the International Society of Sports Nutrition* 2, 1-5.
- Kim, H., Rafiuddin-Shah, M., Tu, H.-C., Jeffers, J. R., Zambetti, G. P., Hsieh, J. J.-D., Cheng, E. H.-Y., 2006a. Hierarchical regulation of mitochondrion-dependent apoptosis by BCL-2 subfamilies. *Nature Cell Biology* 8, 1348-1358.
- Kim, S. J., Park, K. M., Kim, N., Yeom, Y. I., 2006b. Doxorubicin prevents endoplasmic reticulum stress-induced apoptosis. *Biochemical and Biophysical Research Communications* 339, 463-468.
- Kim, H.-S., Lee, Y.-S., Kim, D.-K., 2009. Doxorubicin exerts cytotoxic effects through cell cycle arrest and Fas-mediated cell death. *Pharmacology* 84, 300-309.
- Kligman, A. M., 1961. Pathologic dynamics of human hair loss: Telogen effluvium. *Archives of Dermatology* 83, 175-198.
- Kluck, R. M., Bossy-Wetzell, E., Green, D. R., Newmeyer, D. D., 1997. The release of cytochrome c from mitochondria: a primary site for Bcl-2 regulation of apoptosis. *Science* 275, 1132-1136.
- Kluger, N., Jacot, W., Frouin, E., Rigau, V., Pujol, S., Dereure, O., Guillot, B., Romieu, G., Bessis, D., 2012. Permanent scalp alopecia related to breast cancer chemotherapy by sequential fluorouracil/epirubicin/cyclophosphamide (FEC) and docetaxel: a prospective study of 20 patients. *Annals of Oncology* 23, 2879-2884.
- Kobayashi, T., Okumura, H., Hashimoto, K., Asada, H., Inui, S., Yoshikawa, K., 1998. Synchronization of normal human keratinocyte in culture: its application to the analysis of 1, 25-dihydroxyvitamin D<sub>3</sub> effects on cell cycle. *Journal of Dermatological Science* 17, 108-114.
- Kolfschoten, G. M., Hulscher, T. M., Duyndam, M. C., Pinedo, H. M., Boven, E., 2002. Variation in the kinetics of caspase-3 activation, Bcl-2 phosphorylation and apoptotic

- morphology in unselected human ovarian cancer cell lines as a response to docetaxel. *Biochemical Pharmacology* 63, 733-743.
- Komarov, P. G., Komarova, E. A., Kondratov, R. V., Christov-Tselkov, K., Coon, J. S., Chernov, M. V., Gudkov, A. V., 1999. A chemical inhibitor of p53 that protects mice from the side effects of cancer therapy. *Science* 285, 1733-1737.
- Komen, M., Smorenburg, C. H., Van Den Hurk, C., Nortier, J., 2013a. Factors Influencing the Effectiveness of Scalp Cooling in the Prevention of Chemotherapy-Induced Alopecia. *The Oncologist* 18, 885-891.
- Komen, M. M., Smorenburg, C. H., Van Den Hurk, C. J., Nortier, J. W., 2013b. Factors influencing the effectiveness of scalp cooling in the prevention of chemotherapy-induced alopecia. *The Oncologist* 18, 885-891.
- Komen, M. M., Breed, W. P., Smorenburg, C. H., Van Der Ploeg, T., Goey, S., Van Der Hoeven, J. J., Nortier, J. W., Van Den Hurk, C. J., 2016. Results of 20-versus 45-min post-infusion scalp cooling time in the prevention of docetaxel-induced alopecia. *Supportive Care in Cancer* 24, 2735-2741.
- Kontos, C., Christodoulou, M.-I., Scorilas, A., 2014. Apoptosis-related BCL2-family members: Key players in chemotherapy. *Anti-Cancer Agents in Medicinal Chemistry* 14, 353-374.
- Korkmaz, A., Topal, T., Oter, S., 2007. Pathophysiological aspects of cyclophosphamide and ifosfamide induced hemorrhagic cystitis; implication of reactive oxygen and nitrogen species as well as PARP activation. *Cell Biology and Toxicology* 23, 303-312.
- Korsmeyer, S. J., 1999. BCL-2 gene family and the regulation of programmed cell death. *Cancer Research* 59, 1693-1700.
- Krajewski, S., Krajewska, M., Shabaik, A., Miyashita, T., Wang, H. G., Reed, J. C., 1994. Immunohistochemical determination of *in vivo* distribution of Bax, a dominant inhibitor of Bcl-2. *The American Journal of Pathology* 145, 1323-1328.
- Krause, K., Foitzik, K., 2006. Biology of the hair follicle: the basics. *Seminars in Cutaneous Medicine and Surgery* 25, 2-10.
- Kroemer, G., Galluzzi, L., Vandenabeele, P., Abrams, J., Alnemri, E., Baehrecke, E., Blagosklonny, M., El-Deiry, W., Golstein, P., Green, D., 2009. Classification of cell death: recommendations of the Nomenclature Committee on Cell Death 2009. *Cell Death and Differentiation* 16, 3-11.
- Kugawa, F., Ueno, A., Kawasaki, M., Aoki, M., 2004. Evaluation of cell death caused by CDF (cyclophosphamide, doxorubicin, 5-fluorouracil) multi-drug administration in the human breast cancer cell line MCF-7. *Biological and Pharmaceutical Bulletin* 27, 392-398.
- Kuribayashi, K., Krigsfeld, G., Wang, W., Xu, J., Mayes, P. A., Dicker, D. T., Wu, G. S., El-Deiry, W. S., 2008. TNFSF10 (TRAIL), a p53 target gene that mediates p53-dependent cell death. *Cancer Biology and Therapy* 7, 2034-2038.
- Kyoizumi, S., Suzuki, T., Teraoka, S., Seyama, T., 1998. Radiation sensitivity of human hair follicles in SCID-hu mice. *Radiation Research* 149, 11-18.
- L'ecuyer, T., Sanjeev, S., Thomas, R., Novak, R., Das, L., Campbell, W., Vander Heide, R., 2006. DNA damage is an early event in doxorubicin-induced cardiac myocyte death. *American Journal of Physiology-Heart and Circulatory Physiology* 291, 1273-1280.
- Lakhani, S. A., Masud, A., Kuida, K., Porter, G. A., Booth, C. J., Mehal, W. Z., Inayat, I., Flavell, R. A., 2006. Caspases 3 and 7: key mediators of mitochondrial events of apoptosis. *Science* 311, 847-851.

- Land, S. R., Kopec, J. A., Yothers, G., Anderson, S., Day, R., Tang, G., Ganz, P. A., Fisher, B., Wolmark, N., 2004. Health-related quality of life in axillary node-negative, estrogen receptor-negative breast cancer patients undergoing AC *versus* CMF chemotherapy: findings from the National Surgical Adjuvant Breast and Bowel Project B-23. *Breast Cancer Research and Treatment* 86, 153-164.
- Lane, P., Vichi, P., Bain, D. L., Tritton, T. R., 1987. Temperature dependence studies of adriamycin uptake and cytotoxicity. *Cancer Research* 47, 4038-4042.
- Lassus, P., Opitz-Araya, X., Lazebnik, Y., 2002. Requirement for caspase-2 in stress-induced apoptosis before mitochondrial permeabilization. *Science* 297, 1352-1354.
- Lavrik, I. N., Golks, A., Krammer, P. H., 2005. Caspases: pharmacological manipulation of cell death. *The Journal of Clinical Investigation* 115, 2665-2672.
- Leach, J. K., Van Tuyle, G., Lin, P.-S., Schmidt-Ullrich, R., Mikkelsen, R. B., 2001. Ionizing radiation-induced, mitochondria-dependent generation of reactive oxygen/nitrogen. *Cancer Research* 61, 3894-3901.
- Legué, E., Nicolas, J.-F., 2005. Hair follicle renewal: organization of stem cells in the matrix and the role of stereotyped lineages and behaviours. *Development* 132, 4143-4154.
- Lehman, T. A., Modali, R., Boukamp, P., Stanek, J., Bennett, W. P., Welsh, J. A., Metcalf, R. A., Stampfer, M. R., Fusenig, N., Rogan, E. M., 1993. p53 mutations in human immortalized epithelial cell lines. *Carcinogenesis* 14, 833-839.
- Lemenager, M., Lecomte, S., Bonnetterre, M. E., Bessa, E., Dauba, J., Bonnetterre, J., 1997. Effectiveness of cold cap in the prevention of docetaxel-induced alopecia. *European Journal of Cancer* 33, 297-300.
- Lemieux, J., Amireault, C., Provencher, L., Maunsell, E., 2009. Incidence of scalp metastases in breast cancer: a retrospective cohort study in women who were offered scalp cooling. *Breast Cancer Research and Treatment* 118, 547-552.
- Lemieux, J., Desbiens, C., Hogue, J. C., 2011. Breast cancer scalp metastasis as first metastatic site after scalp cooling: two cases of occurrence after 7- and 9-year follow-up. *Breast Cancer Research and Treatment* 128, 563-566.
- Lemieux, J., 2012. Reducing chemotherapy-induced alopecia with scalp cooling. *Clinical Advances in Hematology and Oncology* 10, 681-682.
- Lemieux, J., Provencher, L., Perron, L., Brisson, J., Amireault, C., Blanchette, C., Maunsell, E., 2015. No effect of scalp cooling on survival among women with breast cancer. *Breast Cancer Research and Treatment* 149, 263-268.
- Letai, A., Bassik, M. C., Walensky, L. D., Sorcinelli, M. D., Weiler, S., Korsmeyer, S. J., 2002. Distinct BH3 domains either sensitize or activate mitochondrial apoptosis, serving as prototype cancer therapeutics. *Cancer Cell* 2, 183-192.
- Li, H., Kolluri, S. K., Gu, J., Dawson, M. I., Cao, X., Hobbs, P. D., Lin, B., Chen, G.-Q., Lu, J.-S., Lin, F., 2000a. Cytochrome c release and apoptosis induced by mitochondrial targeting of nuclear orphan receptor TR3. *Science* 289, 1159-1164.
- Li, S., Zhou, Y., Wang, R., Zhang, H., Dong, Y., Ip, C., 2007. Selenium sensitizes MCF-7 breast cancer cells to doxorubicin-induced apoptosis through modulation of phospho-Akt and its downstream substrates. *Molecular Cancer Therapeutics* 6, 1031-1038.
- Li, W. Q., Dehnade, F., Zafarullah, M., 2000b. Thiol antioxidant, N-acetylcysteine, activates extracellular signal-regulated kinase signalling pathway in articular chondrocytes. *Biochemical and Biophysical Research Communications* 275, 789-794.
- Liebermann, D. A., Hoffman, B., Steinman, R. A., 1995. Molecular controls of growth arrest and apoptosis: p53-dependent and independent pathways. *Oncogene* 11, 199-210.

- Lilenbaum, R. C., Herndon, J. E., List, M. A., Desch, C., Watson, D. M., Miller, A. A., Graziano, S. L., Perry, M. C., Saville, W., Chahinian, P., 2005. Single-agent *versus* combination chemotherapy in advanced non-small-cell lung cancer: The Cancer and Leukemia Group B (study 9730). *Journal of Clinical Oncology* 23, 190-196.
- Lindner, G., Botchkarev, V. A., Botchkareva, N. V., Ling, G., Van Der Veen, C., Paus, R., 1997. Analysis of apoptosis during hair follicle regression (catagen). *The American Journal of Pathology* 151, 1601.
- Liu, J., Mao, W., Ding, B., Liang, C.-S., 2008. ERKs/p53 signal transduction pathway is involved in doxorubicin-induced apoptosis in H9c2 cells and cardiomyocytes. *American Journal of Physiology-Heart and Circulatory Physiology* 295, 1956-1963.
- Liu, L., Xie, H., Chen, X., Shi, W., Xiao, X., Lei, D., Li, J., 2012. Differential response of normal human epidermal keratinocytes and HaCaT cells to hydrogen peroxide-induced oxidative stress. *Clinical and Experimental Dermatology* 37, 772-780.
- Liu, Q., Harvey, C. T., Geng, H., Xue, C., Chen, V., Beer, T. M., Qian, D. Z., 2013. Malate dehydrogenase 2 confers docetaxel resistance *via* regulations of JNK signaling and oxidative metabolism. *The Prostate* 73, 1028-1037.
- Lockshin, R. A., Zakeri, Z., 2004. Apoptosis, autophagy, and more. *The International Journal of Biochemistry and Cell Biology* 36, 2405-2419.
- Lomonosova, E., Chinnadurai, G., 2008. BH3-only proteins in apoptosis and beyond: an overview. *Oncogene* 27, 2-19.
- Longley, D. B., Harkin, D. P., Johnston, P. G., 2003. 5-fluorouracil: mechanisms of action and clinical strategies. *Nature Reviews Cancer* 3, 330-338.
- Luanpitpong, S., Nimmannit, U., Chanvorachote, P., Leonard, S., Pongrakhananon, V., Wang, L., Rojanasakul, Y., 2011. Hydroxyl radical mediates cisplatin-induced apoptosis in human hair follicle dermal papilla cells and keratinocytes through Bcl-2-dependent mechanism. *Apoptosis* 16, 769-782.
- Luanpitpong, S., Rojanasakul, Y., 2012a. Chemotherapy-Induced Alopecia. *Clinical and Experimental Dermatology* 37, 760-769.
- Luanpitpong, S., Chanvorachote, P., Nimmannit, U., Leonard, S. S., Stehlik, C., Wang, L., Rojanasakul, Y., 2012b. Mitochondrial superoxide mediates doxorubicin-induced keratinocyte apoptosis through oxidative modification of ERK and Bcl-2 ubiquitination. *Biochemical Pharmacology* 83, 1643-1654.
- Lüpertz, R., Wätjen, W., Kahl, R., Chovolou, Y., 2010. Dose- and time-dependent effects of doxorubicin on cytotoxicity, cell cycle and apoptotic cell death in human colon cancer cells. *Toxicology* 271, 115-121.
- Magerl, M., Tobin, D. J., Müller-Röver, S., Hagen, E., Lindner, G., McKay, I. A., Paus, R., 2001. Patterns of proliferation and apoptosis during murine hair follicle morphogenesis. *Journal of Investigative Dermatology* 116, 947-955.
- Majno, G., Joris, I., 1995. Apoptosis, oncosis, and necrosis. An overview of cell death. *The American Journal of Pathology* 146, 3.
- Manning, D. D., Reed, N. D., Shaffer, C. F., 1973. Maintenance of skin xenografts of widely divergent phylogenetic origin on congenitally athymic (nude) mice. *The Journal of Experimental Medicine* 138, 488-494.
- Marnett, L. J., 2000. Oxyradicals and DNA damage. *Carcinogenesis* 21, 361-370.
- Massey, C. S., 2004. A multicentre study to determine the efficacy and patient acceptability of the Paxman Scalp Cooler to prevent hair loss in patients receiving chemotherapy. *European Journal of Oncology Nursing* 8, 121-30.

- Matijasevic, Z., 2001. Selective protection of non-cancer cells by hypothermia. *Anticancer Research* 22, 3267-3272.
- Maxwell, M. B., 1980. Scalp tourniquets for chemotherapy-induced alopecia. *The American Journal of Nursing* 80, 900-902.
- Mccredie, K. B., Ho, D. H. W., Freireich, E. J., 1973. L-asparaginase for the treatment of cancer. *Cancer Journal for Clinicians* 23, 220-227.
- Mcelwee, K., Hoffmann, R., 2000. Growth factors in early hair follicle morphogenesis. *European Journal of Dermatology* 10, 341-50.
- Mcgregor, J. M., Berkhout, R. J., Rozycka, M., Ter Schegget, J., 1997. p53 mutations implicate sunlight in post-transplant skin cancer irrespective of human papillomavirus status. *Oncogene* 15, 1737-1740.
- Mhaidat, N. M., Wang, Y., Kiejda, K. A., Zhang, X. D., Hersey, P., 2007. Docetaxel-induced apoptosis in melanoma cells is dependent on activation of caspase-2. *Molecular Cancer Therapeutics* 6, 752-761.
- Micheau, O., Tschopp, J., 2003. Induction of TNF receptor I-mediated apoptosis *via* two sequential signaling complexes. *Cell* 114, 181-190.
- Mihm, M. C., Soter N. A., 1976. "The structure of normal skin and the morphology of atopic eczema." *Journal of Investigative Dermatology* 67 (3): 305-312.
- Millar, S. E., 2002. Molecular mechanisms regulating hair follicle development. *Journal of Investigative Dermatology* 118, 216-225.
- Milner, Y., Sudnik, J., Filippi, M., Kizoulis, M., Kashgarian, M., Stenn, K., 2002. Exogen, shedding phase of the hair growth cycle: characterization of a mouse model. *Journal of Investigative Dermatology* 119, 639-644.
- Mizumachi, T., Suzuki, S., Naito, A., Carcel-Trullols, J., Evans, T., Spring, P., Oridate, N., Furuta, Y., Fukuda, S., Higuchi, M., 2008. Increased mitochondrial DNA induces acquired docetaxel resistance in head and neck cancer cells. *Oncogene* 27, 831-838.
- Moll, U. M., Petrenko, O., 2003. The MDM2-p53 interaction. *Molecular Cancer Research* 1, 1001-1008.
- Mooberry, S. L., 2011. Microtubules as a target for anticancer drugs. *New Frontiers and Treatment Paradigms for Metastatic Breast Cancer* 28, 7-9.
- Morgan, G., 2003. Chemotherapy and the cell cycle. *Cancer Nursing Practice* 2, 27-30.
- Morii, M., Fukumoto, Y., Kubota, S., Yamaguchi, N., Nakayama, Y., Yamaguchi, N., 2015. Imatinib inhibits inactivation of the ATM/ATR signaling pathway and recovery from adriamycin/doxorubicin-induced DNA damage checkpoint arrest. *Cell Biology International* 39, 923-932.
- Morse, D. L., Gray, H., Payne, C. M., Gillies, R. J., 2005. Docetaxel induces cell death through mitotic catastrophe in human breast cancer cells. *Molecular Cancer Therapeutics* 4, 1495-1504.
- Muldoon, L. L., Walker-Rosenfeld, S. L., Hale, C., Purcell, S. E., Bennett, L. C., Neuwelt, E. A., 2001. Rescue from enhanced alkylator-induced cell death with low molecular weight sulfur-containing chemoprotectants. *Journal of Pharmacology and Experimental Therapeutics* 296, 797-805.
- Müller-Röver, S., Handjiski, B., Van Der Veen, C., Eichmüller, S., Foitzik, K., McKay, I. A., Stenn, K. S., Paus, R., 2001. A comprehensive guide for the accurate classification of murine hair follicles in distinct hair cycle stages. *Journal of Investigative Dermatology* 117, 3-15.

- Müller, M., Strand, S., Hug, H., Heinemann, E.-M., Walczak, H., Hofmann, W. J., Stremmel, W., Krammer, P. H., Galle, P. R., 1997. Drug-induced apoptosis in hepatoma cells is mediated by the CD95 (APO-1/Fas) receptor/ligand system and involves activation of wild-type p53. *Journal of Clinical Investigation* 99, 403-408.
- Müller, M., Wilder, S., Bannasch, D., Israeli, D., Lehlbach, K., Li-Weber, M., Friedman, S. L., Galle, P. R., Stremmel, W., Oren, M., 1998. p53 activates the CD95 (APO-1/Fas) gene in response to DNA damage by anticancer drugs. *The Journal of Experimental Medicine* 188, 2033-2045.
- Münstedt, K., Manthey, N., Sachsse, S., Vahon, H., 1997. Changes in self-concept and body image during alopecia induced cancer chemotherapy. *Supportive Care in Cancer* 5, 139-143.
- Nabholtz, J. M., Mackey, J. R., Smylie, M., Paterson, A., Noel, D. R., Al-Tweigeri, T., Tonkin, K., North, S., Azli, N., Riva, A., 2001. Phase II study of docetaxel, doxorubicin, and cyclophosphamide as first-line chemotherapy for metastatic breast cancer. *Journal of Clinical Oncology* 19, 314-21.
- Nakano, K., Vousden, K. H., 2001. Puma, a Novel Proapoptotic Gene, Is Induced by p53. *Molecular Cell* 7, 683-694.
- Neste, D., Brouwer, B., Dumortier, M., 1991. Reduced linear hair growth rates of vellus and of terminal hairs produced by human balding scalp grafted onto nude mice. *Annals of the New York Academy of Sciences* 642, 480-482.
- Nicoletti, I., Migliorati, G., Pagliacci, M., Grignani, F., Riccardi, C., 1991. A rapid and simple method for measuring thymocyte apoptosis by propidium iodide staining and flow cytometry. *Journal of Immunological Methods* 139, 271-279.
- Nicolson, G. L., Conklin, K. A., 2008. Molecular Replacement in Cancer Therapy: Reversing Cancer Metabolic and Mitochondrial Dysfunction, Fatigue and the Adverse Effects of Cancer Therapy. *Current Cancer Therapy Reviews* 4, 66-76.
- Ning, X.-H., Xu, C.-S., Song, Y. C., Xiao, Y., Hu, Y.-J., Lupinetti, F. M., Portman, M. A., 1998. Hypothermia preserves function and signaling for mitochondrial biogenesis during subsequent ischemia. *American Journal of Physiology-Heart and Circulatory Physiology* 274, 786-793.
- Nithipongvanitch, R., Ittarat, W., Cole, M. P., Tangpong, J., Clair, D. K. S., Oberley, T. D., 2007. Mitochondrial and nuclear p53 localization in cardiomyocytes: redox modulation by doxorubicin (Adriamycin). *Antioxidants and Redox Signalling* 9, 1001-1008.
- O'Brien, R., Zelson, J. H., Schwartz, A. D., Pearson, H. A., 1970. Scalp tourniquet to lessen alopecia after vincristine. *The New England Journal of Medicine* 283, 1469-1469.
- Odland, G. F., 1991. "Structure of the skin." *Physiology, biochemistry, and molecular biology of the skin*. Oxford University Press, New York pp 205-236.
- Oh, H.-S., Smart, R. C., 1996. An estrogen receptor pathway regulates the telogen-anagen hair follicle transition and influences epidermal cell proliferation. *Proceedings of the National Academy of Sciences* 93, 12525-12530.
- Ohtani, T., Nakamura, T., Toda, K.-I., Furukawa, F., 2006. Cyclophosphamide enhances TNF- $\alpha$ -induced apoptotic cell death in murine vascular endothelial cell. *Federation of European Biochemical Societies* 580, 1597-1600.
- Olsen, E. A., 2011. Chemotherapy-induced alopecia: overview and methodology for characterizing hair changes and regrowth. *The MASCC Textbook of Cancer Supportive Care and Survivorship*. Springer, pp. 381-386.
- Oltvai, Z. N., Korsmeyer, S. J., 1994. Checkpoints of dueling dimers foil death wishes. *Cell* 79, 189-192.

- Opferman, J. T., Korsmeyer, S. J., 2003. Apoptosis in the development and maintenance of the immune system. *Nature Immunology* 4, 410-415.
- Oren, M., 1999. Regulation of the p53 tumour suppressor protein. *Journal of Biological Chemistry* 274, 36031-36034.
- Organization, W. H., 1979. WHO handbook for reporting results of cancer treatment.
- Oshima, H., Rochat, A., Kedzia, C., Kobayashi, K., Barrandon, Y., 2001. Morphogenesis and renewal of hair follicles from adult multipotent stem cells. *Cell* 104, 233-245.
- Panaretakis, T., Pokrovskaja, K., Shoshan, M. C., Grandér, D., 2002. Activation of Bak, Bax, and BH3-only proteins in the apoptotic response to doxorubicin. *Journal of Biological Chemistry* 277, 44317-44326.
- Pardee, A. B., 1989. G1 events and regulation of cell proliferation. *Science* 246, 603-608.
- Pardi, G., Ferrari, M. M., Iorio, F., Acocella, F., Boero, V., Berlanda, N., Monaco, A., Reato, C., Santoro, F., Cetin, I., 2004. The effect of maternal hypothermic cardiopulmonary bypass on fetal lamb temperature, hemodynamics, oxygenation, and acid-base balance. *The Journal of Thoracic and Cardiovascular Surgery* 127, 1728-1734.
- Parish, L. C., 2011. "Andrews' Diseases of the Skin: Clinical Dermatology. *The Journal of the American Medical Association* 306 (2), 213-213.
- Partridge, A. H., Burstein, H. J., Winer, E. P., 2001. Side effects of chemotherapy and combined chemohormonal therapy in women with early-stage breast cancer. *Journal of the National Cancer Institute*, 30, 135-142
- Patel, S., & Tosti, A. (2014). An overview of management of drug-induced hair and nail disorders. *Clinical Practice*, 11 (3), 327-339.
- Patel, S., Sharma, V., Chauhan, N. S., Dixit, V. K., 2014. A study on the extracts of *Cuscuta reflexa* Roxb. in treatment of cyclophosphamide induced alopecia. *Journal of Pharmaceutical Sciences* 22, 7-12.
- Paus, R., 2006. Therapeutic strategies for treating hair loss. *Drug Discovery Today: Therapeutic Strategies* 3, 101-110.
- Paus, R. 2011. A neuroendocrinological perspective on human hair follicle pigmentation. *Pigment Cell and Melanoma Research*, 24 (1), 89-106.
- Paus, R., Cotsarelis, G., 1999. The biology of hair follicles. *The New England Journal of Medicine* 341, 491-497.
- Paus, R., Foitzik, K., 2004. In search of the "hair cycle clock": a guided tour. *Differentiation* 72, 489-511.
- Paus, R., Handjiski, B., Eichmüller, S., Czarnetzki, B. M., 1994. Chemotherapy-induced alopecia in mice. Induction by cyclophosphamide, inhibition by cyclosporine A, and modulation by dexamethasone. *The American Journal of Pathology* 144 (4), 719-734.
- Paus, R., Haslam, I. S., Sharov, A. A., Botchkarev, V. A., 2013. Pathobiology of chemotherapy-induced hair loss. *The Lancet Oncology* 14, 50-59.
- Paus, R., Müller-Röver, S., Van Der Veen, C., Maurer, M., Eichmüller, S., Ling, G., Hofmann, U., Foitzik, K., Mecklenburg, L., Handjiski, B., 1999. A comprehensive guide for the recognition and classification of distinct stages of hair follicle morphogenesis. *Journal of Investigative Dermatology* 113, 523-532.
- Paus, R., Rosenbach, T., Haas, N., Czarnetzki, B. M., 1993. Patterns of cell death: the significance of apoptosis for dermatology. *Experimental Dermatology* 2, 3-10.

- Paus, R., Schilli, M. B., Handjiski, B., Menrad, A., Henz, B. M., Plonka, P., 1996. Topical calcitriol enhances normal hair regrowth but does not prevent chemotherapy-induced alopecia in mice. *Cancer Research* 56, 4438-4443.
- Payne, A. S., James, W. D., Weiss, R. B., 2006. Dermatologic toxicity of chemotherapeutic agents. *Seminars in Oncology*. Elsevier 33, 86-97.
- Payne, S., Miles, D., 2008. Mechanisms of anticancer drugs. *Scott-Brown's Otorhinolaryngology: Head and Neck Surgery 7Ed*: 3 volume set, 134.
- Perelman, A., Wachtel, C., Cohen, M., Haupt, S., Shapiro, H., Tzur, A., 2012. JC-1: alternative excitation wavelengths facilitate mitochondrial membrane potential cytometry. *Cell Death and Disease* 3, 430-437.
- Perry, S. W., Norman, J. P., Barbieri, J., Brown, E. B., Gelbard, H. A., 2011. Mitochondrial membrane potential probes and the proton gradient: a practical usage guide. *Biotechniques* 50, 98-105.
- Peters, E. M., Hansen, M. G., Overall, R. W., Nakamura, M., Pertile, P., Klapp, B. F., Arck, P. C., Paus, R., 2005. Control of human hair growth by neurotrophins: brain-derived neurotrophic factor inhibits hair shaft elongation, induces catagen, and stimulates follicular transforming growth factor  $\beta$ 2 expression. *Journal of Investigative Dermatology* 124, 675-685.
- Petros, A. M., Olejniczak, E. T., Fesik, S. W., 2004. Structural biology of the Bcl-2 family of proteins. *Biochimica Biophysica Acta (BBA)-Molecular Cell Research* 1644, 83-94.
- Phillips, J., Smith, S., Storer, J., 1986. Hair loss. Common congenital and acquired causes. *Postgraduate Medicine* 79, 207-215.
- Pickard-Holley, S., 1995. The symptom experience of alopecia. *Seminars in oncology nursing*. Elsevier 11, 235-238.
- Piérard, G. E., Clemmensen, O. J., Hainau, B., Hansted, B., 1991. The ultrastructure of the transition zone between specialized cells ("Flugelzellen") of Huxley's layer of the inner root sheath and cells of the outer root sheath of the human hair follicle. *The American Journal of Dermatopathology* 13, 264-270.
- Pinedo, H. M., Schornagel, J. H., 1996. Platinum and other metal coordination compounds in cancer chemotherapy 2. Springer Science and Business Media. (Howell SB ed) pp. 151–159, Plenum Press, New York.
- Pispa, J., Thesleff, I., 2003. Mechanisms of ectodermal organogenesis. *Developmental Biology* 262, 195-205.
- Polyak, K., Xia, Y., Zweier, J. L., Kinzler, K. W., Vogelstein, B., 1997. A model for p53-induced apoptosis. *Nature* 389, 300-305.
- Poulaki, V., Mitsiades, C. S., Mitsiades, N., 2001. The role of Fas and FasL as mediators of anticancer chemotherapy. *Drug Resistance Updates* 4, 233-242.
- Prasad, L. G., Krishnakumar, V., Nagalakshmi, R., 2012. Growth and nonlinear optical studies of N-acetyl-L-cysteine crystal. *The European Physical Journal Applied Physics* 57, 10201- 10208.
- Prevezas, C., Matard, B., Piquier, L., Reygagne, P., 2009. Irreversible and severe alopecia following docetaxel or paclitaxel cytotoxic therapy for breast cancer. *British Journal of Dermatology* 160, 883-885.
- Protiere, C., Evans, K., Camerlo, J., D'ingrado, M. P., Macquart-Moulin, G., Viens, P., Maraninchi, D., Genre, D., 2002. Efficacy and tolerance of a scalp-cooling system for prevention of hair loss and the experience of breast cancer patients treated by adjuvant chemotherapy. *Support Care Cancer* 10, 529-37.

- Qiu, X., Forman, H. J., Schönthal, A. H., Cadenas, E., 1996. Induction of p21 mediated by reactive oxygen species formed during the metabolism of aziridinybenzoquinones by HCT116 cells. *Journal of Biological Chemistry* 271, 31915-31921.
- Quent, V., Loessner, D., Friis, T., Reichert, J. C., Hutmacher, D. W., 2010. Discrepancies between metabolic activity and DNA content as tool to assess cell proliferation in cancer research. *Journal of Cellular and Molecular Medicine* 14, 1003-1013.
- Raffaghello, L., Lee, C., Safdie, F. M., Wei, M., Madia, F., Bianchi, G., Longo, V. D., 2008. Starvation-dependent differential stress resistance protects normal but not cancer cells against high-dose chemotherapy. *Proceedings of the National Academy of Sciences* 105, 8215-8220.
- Raj, D., Brash, D. E., Grossman, D., 2006. Keratinocyte apoptosis in epidermal development and disease. *Journal of Investigative Dermatology* 126, 243-257.
- Ramirez, O. T., Mutharasan, R., 1990. Cell cycle-and growth phase-dependent variations in size distribution, antibody productivity, and oxygen demand in hybridoma cultures. *Biotechnology and Bioengineering* 36, 839-848.
- Randall, V. A., Botchkareva, N. V., 2008. The biology of hair growth. *Cosmetic Applications of Laser and Light Based Systems*. Norwich, NY: William Andrew, 3-35.
- Rao, P. N., Engelberg, J., 1965. HeLa cells: effects of temperature on the life cycle. *Science* 148, 1092-1094.
- Ravizza, R., Gariboldi, M. B., Passarelli, L., Monti, E., 2004. The Role of the p53/p21 system in the response of human colon carcinoma cells to doxorubicin. *BMC cancer* 4, 92-98.
- Reed, J., 1997. Bcl-2 family proteins: role in dysregulation of apoptosis and chemoresistance. *Apoptosis and Cancer*, Karger Landes Systems, Basel, 65-72.
- Remesh, A, 2012. Toxicities of anticancer drugs and its management. *International Journal of Basic and Clinical Pharmacology*, 1(1): 2-12.
- Riccardi, C., Nicoletti, I., 2006. Analysis of apoptosis by propidium iodide staining and flow cytometry. *Nature Protocols* 1, 1458-1461.
- Ricci, M. S., Zong, W.-X., 2006. Chemotherapeutic approaches for targeting cell death pathways. *The Oncologist* 11, 342-357.
- Rieder, C. L., Cole, R. W., 2002. Cold-shock and the Mammalian cell cycle. *Cell Cycle* 1, 168-174.
- Roh, C., Tao, Q., Photopoulos, C., Lyle, S., 2005. *In vitro* differences between keratinocyte stem cells and transit-amplifying cells of the human hair follicle. *Journal of Investigative Dermatology* 125, 1099-105.
- Ronald, S., Paul, R., Michael, M., 2004. Hair Transplantation. Revised and Expanded, Unger and Shapiro. International Standard Book Number-13: 978-1-4200-3035-8
- Rowinsky, E. K., Onetto, N., Canetta, R. M., Arbusk, S. G., 1992. Taxol: the first of the taxanes, an important new class of antitumor agents. *Seminars in Oncology*, 19, 646-662.
- Rowinsky, E. K., Citardi, M. J., Noe, D. A., Donehower, R. C., 1993. Sequence-dependent cytotoxic effects due to combinations of cisplatin and the antimicrotubule agents taxol and vincristine. *Journal of Cancer Research and Clinical Oncology* 119, 727-733.
- Roy, S., Nicholson, D. W., 2000. Cross-talk in cell death signaling. *The Journal of Experimental Medicine* 192, 21-26.
- Rozengurt, E., 1986. Early signals in the mitogenic response. *Science* 234, 161-166.

- Rudman, S. M., Philpott, M. P., Thomas, G. A., Kealey, T., 1997. The role of IGF-I in human skin and its appendages: morphogen as well as mitogen. *Journal of Investigative Dermatology* 109, 770-777.
- Ryan, O. S., Christiano, A. M., 2004. Inherited disorders of the skin in human and mouse: from development to differentiation. *International Journal of Developmental Biology* 48, 171-180.
- Sablina, A. A., Budanov, A. V., Ilyinskaya, G. V., Agapova, L. S., Kravchenko, J. E., Chumakov, P. M., 2005. The antioxidant function of the p53 tumour suppressor. *Nature Medicine* 11, 1306-1313.
- Safdie, F. M., Dorff, T., Quinn, D., Fontana, L., Wei, M., Lee, C., Cohen, P., Longo, V. D., 2009. Fasting and cancer treatment in humans: A case series report. *Aging Revolutionizing Gerontology by Abolishing Dogmas* 1, 988-1007.
- Sakamuru, S., Li, X., Attene-Ramos, M. S., Huang, R., Lu, J., Shou, L., Shen, M., Tice, R. R., Austin, C. P., Xia, M., 2012. Application of a homogenous membrane potential assay to assess mitochondrial function. *Physiological Genomics* 44, 495-503.
- Sakurai, T., Itoh, K., Liu, Y., Higashitsuji, H., Sumitomo, Y., Sakamaki, K., Fujita, J., 2005. Low temperature protects mammalian cells from apoptosis initiated by various stimuli *in vitro*. *Experimental Cell Research* 309, 264-272.
- Salvioli, S., Ardizzoni, A., Franceschi, C., Cossarizza, A., 1997. JC-1, but not DiOC 6 (3) or rhodamine 123, is a reliable fluorescent probe to assess  $\Delta\Psi$  changes in intact cells: implications for studies on mitochondrial functionality during apoptosis. *The Federation of European Biochemical Societies* 411, 77-82.
- Samson, F. E., 1997. Oxygen, gene expression, and cellular function. *Shock* 8, 389-395.
- Sauter, K. A., Magun, E. A., Iordanov, M. S., Magun, B. E., 2010. ZAK is required for doxorubicin, a novel ribotoxic stressor, to induce SAPK activation and apoptosis in HaCaT cells. *Cancer Biology and Therapy* 10, 258-266.
- Savion, N., Izigov, N., Morein, M., Pri-Chen, S., Kotev-Emeth, S., 2014. S-Allylmercapto-N-acetylcysteine (ASSNAC) protects cultured nerve cells from oxidative stress and attenuates experimental autoimmune encephalomyelitis. *Neuroscience Letters* 583, 108-113.
- Scabini, M., Stellari, F., Cappella, P., Rizzitano, S., Texido, G., Pesenti, E., 2011. *In vivo* imaging of early stage apoptosis by measuring real-time caspase-3/7 activation. *Apoptosis* 16, 198-207.
- Schilli, M. B., Paus, R., Menrad, A., 1998. Reduction of intrafollicular apoptosis in chemotherapy-induced alopecia by topical calcitriol-analogs. *Journal of Investigative Dermatology* 111, 598-604.
- Schmidt-Ullrich, R., Paus, R., 2005. Molecular principles of hair follicle induction and morphogenesis. *Bioessays* 27, 247-261.
- Schmidt, J. B., 1994. Hormonal basis of male and female androgenic alopecia: clinical relevance. *Skin Pharmacology and Physiology* 7, 61-66.
- Schneider, M. R., Schmidt-Ullrich, R., Paus, R., 2009. The hair follicle as a dynamic miniorgan. *Current Biology* 19, 132-142.
- Schultz, D. R., Harrington Jr, W. J., 2003. Apoptosis: programmed cell death at a molecular level. *Seminars in Arthritis and Rheumatism, Elsevier* 32, 345-369.
- Schulze-Osthoff, K., Bauer, M., Vogt, M., Wesselborg, S., 1996. Oxidative stress and signal transduction. *International journal for vitamin and nutrition research. International Journal for Vitamin and Nutrition Research* 67, 336-342.

- Schumacker, P. T., 2015. Reactive oxygen species in cancer: a dance with the devil. *Cancer Cell* 27, 156-157.
- Schwartz, P. S., Waxman, D. J., 2001. Cyclophosphamide induces caspase 9-dependent apoptosis in 9L tumor cells. *Molecular Pharmacology* 60, 1268-1279.
- Selleri, S., Arnaboldi, F., Vizzotto, L., Balsari, A., Rumio, C., 2004. Epithelium–mesenchyme compartment interaction and oncosis on chemotherapy-induced hair damage. *Laboratory Investigation* 84, 1404-1417.
- Senderowicz, A. M., 2002. The cell cycle as a target for cancer therapy: basic and clinical findings with the small molecule inhibitors flavopiridol and UCN-01. *The Oncologist* 7, 12-19.
- Sevadjan, C. M., 1985. Pustular contact hypersensitivity to fluorouracil with rosacealike sequelae. *Archives of Dermatology* 121, 240-242.
- Sha, S., Jin, H., Li, X., Yang, J., Ai, R., Lu, J., 2012. Comparison of caspase-3 activation in tumor cells upon treatment of chemotherapeutic drugs using capillary electrophoresis. *Protein and Cell* 3, 392-399.
- Sharov, A. A., Li, G.-Z., Palkina, T. N., Sharova, T. Y., Gilchrest, B. A., Botchkarev, V. A., 2003. Fas and c-kit are involved in the control of hair follicle melanocyte apoptosis and migration in chemotherapy-induced hair loss. *Journal of Investigative Dermatology* 120, 27-35.
- Sharov, A. A., Siebenhaar, F., Sharova, T. Y., Botchkareva, N. V., Gilchrest, B. A., Botchkarev, V. A., 2004. Fas signalling is involved in the control of hair follicle response to chemotherapy. *Cancer Research* 64, 6266-6270.
- Sharova, T. Y., Poterlowicz, K., Botchkareva, N. V., Kondratiev, N. A., Aziz, A., Spiegel, J. H., Botchkarev, V. A., Sharov, A. A., 2014. Complex changes in the apoptotic and cell differentiation programs during initiation of the hair follicle response to chemotherapy. *Journal of Investigative Dermatology* 134, 2873-2882.
- Shaw, N. J., Georgopoulos, N. T., Southgate, J., Trejdosiewicz, L. K., 2005. Effects of loss of p53 and p16 function on life span and survival of human urothelial cells. *International Journal of Cancer* 116, 634-639.
- Shen, Y., White, E., 2001. p53-dependent apoptosis pathways. *Advances in Cancer Research* 82, 55-84.
- Shiah, S.-G., Chuang, S.-E., Chau, Y.-P., Shen, S.-C., Kuo, M.-L., 1999. Activation of c-Jun NH2-terminal kinase and subsequent CPP32/Yama during topoisomerase inhibitor  $\beta$ -lapachone-induced apoptosis through an oxidation-dependent pathway. *Cancer Research* 59, 391-398.
- Shibano, T., Morimoto, Y., Kemmotsu, O., Shikama, H., Hisano, K., Hua, Y., 2002. Effects of mild and moderate hypothermia on apoptosis in neuronal PC12 cells. *British Journal of Anaesthesia* 89, 301-305.
- Shibue, T., Takeda, K., Oda, E., Tanaka, H., Murasawa, H., Takaoka, A., Morishita, Y., Akira, S., Taniguchi, T., Tanaka, N., 2003. Integral role of Noxa in p53-mediated apoptotic response. *Genes and Development* 17, 2233-2238.
- Si, Q.-S., Nakamura, Y., Kataoka, K., 1997. Hypothermic suppression of microglial activation in culture: inhibition of cell proliferation and production of nitric oxide and superoxide. *Neuroscience* 81, 223-229.
- Simon, H.-U., Haj-Yehia, A., Levi-Schaffer, F., 2000. Role of reactive oxygen species (ROS) in apoptosis induction. *Apoptosis* 5, 415-418.

- Siu, W. Y., Yam, C. H., Poon, R. Y., 1999. G1 *versus* G2 cell cycle arrest after adriamycin-induced damage in mouse Swiss3T3 cells. *Federation of European Biochemical Societies* 461, 299-305.
- Skeel, R. T., Khleif, S. N., 2011. *Handbook of cancer chemotherapy*. Wolters Kluwer Health.
- Slee, E. A., O'connor, D. J., Lu, X., 2004. To die or not to die: how does p53 decide. *Oncogene* 23, 2809-2818.
- Sliwiska, M. A., Mosieniak, G., Wolanin, K., Babik, A., Piwocka, K., Magalska, A., Szczepanowska, J., Fronk, J., Sikora, E., 2009. Induction of senescence with doxorubicin leads to increased genomic instability of HCT116 cells. *Mechanisms of Ageing and Development* 130, 24-32.
- Slominski, A., Wortsman, J., Plonka, P. M., Schallreuter, K. U., Paus, R., Tobin, D. J., 2005. Hair follicle pigmentation. *Journal of Investigative Dermatology* 124, 13-21.
- Smiley, S. T., Reers, M., Mottola-Hartshorn, C., Lin, M., Chen, A., Smith, T. W., Steele, G., Chen, L. B., 1991. Intracellular heterogeneity in mitochondrial membrane potentials revealed by a J-aggregate-forming lipophilic cation JC-1. *Proceedings of the National Academy of Sciences* 88, 3671-3675.
- Smith PJ, Yue E (Editors) (2006). *CDK Inhibitors of Cyclin-Dependent Kinases as Anti-Tumor Agents*. Monographs on Enzyme Inhibitors. CRC Press, Taylor & Francis: Boca Raton, FL, 2, 448.
- Sohn, D., Graupner, V., Neise, D., Essmann, F., Schulze-Osthoff, K., Jänicke, R., 2009. Pifithrin- $\alpha$  protects against DNA damage-induced apoptosis downstream of mitochondria independent of p53. *Cell Death & Differentiation* 16, 869-878.
- Soma, T., Ogo, M., Suzuki, J., Takahashi, T., Hibino, T., 1998. Analysis of apoptotic cell death in human hair follicles *in vivo* and *in vitro*. *Journal of Investigative Dermatology* 111, 948-954.
- Spencer, L. V., Callen, J. P., 1987. Hair loss in systemic disease. *Dermatologic Clinics* 5, 565-570.
- Spiegel, D., Giese-Davis, J., 2003. Depression and cancer: mechanisms and disease progression. *Biological Psychiatry*.
- Sprietsma, J., 1999. Cysteine, glutathione (GSH) and zinc and copper ions together are effective, natural, intracellular inhibitors of (AIDS) viruses. *Medical Hypotheses* 52, 529-538.
- Sredni, B., Xu, R. H., Albeck, M., Gafter, U., Gal, R., Shani, A., Tichler, T., Shapira, J., Bruderman, I., Catane, R., 1996. The protective role of the immunomodulator AS101 against chemotherapy-induced alopecia studies on human and animal models. *International Journal of Cancer* 65, 97-103.
- St-Pierre, J., Drori, S., Uldry, M., Silvaggi, J. M., Rhee, J., Jäger, S., Handschin, C., Zheng, K., Lin, J., Yang, W., 2006. Suppression of reactive oxygen species and neurodegeneration by the PGC-1 transcriptional coactivators. *Cell* 127, 397-408.
- Steele, L. P., Georgopoulos, N. T., Southgate, J., Selby, P. J., Trejdosiewicz, L. K., 2006. Differential susceptibility to TRAIL of normal *versus* malignant human urothelial cells. *Cell Death and Differentiation* 13, 1564-1576.
- Steffen, C., 2001. The Man Behind the Eponym: Jacob Henle-Henle's Layer of the Internal Root Sheath. *The American Journal of Dermatopathology* 23, 549-551.
- Stenn, K., Parimoo, S., Prouty, S., 1998. Growth of the hair follicle: a cycling and regenerating biological system. *Molecular Basis of Epithelial Appendage Morphogenesis* 20, 111-130.

- Stenn, K., Paus, R., 2001. Controls of hair follicle cycling. *Physiological Reviews* 81, 449-494.
- Strasser, A., 2005. The role of BH3-only proteins in the immune system. *Nature Reviews Immunology* 5, 189-200.
- Strauss, G., Westhoff, M., Fischer-Posovszky, P., Fulda, S., Schanbacher, M., Eckhoff, S., Stahnke, K., Vahsen, N., Kroemer, G., Debatin, K., 2008. 4-hydroperoxy-cyclophosphamide mediates caspase-independent T-cell apoptosis involving oxidative stress-induced nuclear relocation of mitochondrial apoptogenic factors AIF and EndoG. *Cell Death and Differentiation* 15, 332-343.
- Sulkowska, M., Sulkowski, S., Skrzydlewska, E., Farbiszewski, R., 1998. Cyclophosphamide-induced generation of reactive oxygen species. Comparison with morphological changes in type II alveolar epithelial cells and lung capillaries. *Experimental and Toxicologic Pathology* 50, 209-220.
- Sunley, K., Butler, M., 2010. Strategies for the enhancement of recombinant protein production from mammalian cells by growth arrest. *Biotechnology Advances* 28, 385-394.
- Swift, L. P., Rephaeli, A., Nudelman, A., Phillips, D. R., Cutts, S. M., 2006. Doxorubicin-DNA adducts induce a non-topoisomerase II-mediated form of cell death. *Cancer Research* 66, 4863-4871.
- Symonds, R., Foweraker, K., 2006. Principles of chemotherapy and radiotherapy. *Current Obstetrics and Gynaecology* 16, 100-106.
- Tait, S. W., Green, D. R., 2010. Mitochondria and cell death: outer membrane permeabilization and beyond. *Nature Reviews Molecular Cell Biology* 11, 621-632.
- Takada, Y., Hachiya, M., Park, S.-H., Osawa, Y., Ozawa, T., Akashi, M., 2002. Role of Reactive Oxygen Species in cells overexpressing manganese superoxide dismutase mechanism for induction of radioresistance 1. *Molecular Cancer Research* 1, 137-146.
- Takimoto, C. H., Calvo, E., 2008. Principles of oncologic pharmacotherapy. *Cancer Management: A Multidisciplinary Approach* 11. R. Pazdur, L. D. Wagman, K. A. Camphausen, and W. J. Hoskins, Eds., 11th edition.
- Takimoto, R., El-Deiry, W., 2000. Wild-type p53 transactivates the KILLER/DR5 gene through an intronic sequence-specific DNA-binding site. *Oncogene* 19, 1735-1743.
- Tallon, B., Blanchard, E., Goldberg, L. J., 2010. Permanent chemotherapy-induced alopecia: case report and review of the literature. *Journal of the American Academy of Dermatology* 63, 333-336.
- Tang, D., Lahti, J. M., Kidd, V. J., 2000. Caspase-8 activation and bid cleavage contribute to MCF7 cellular execution in a caspase-3-dependent manner during staurosporine-mediated apoptosis. *Journal of Biological Chemistry* 275, 9303-9307.
- Taniguchi, T., Takahashi, M., Shinohara, F., Sato, T., Echigo, S., Rikiishi, H., 2005. Involvement of NF- $\kappa$ B and mitochondrial pathways in docetaxel-induced apoptosis of human oral squamous cell carcinoma. *International Journal of Molecular Medicine* 15, 667-673.
- Tannock, I. F., Hill, R. P., 1998. The basic science of oncology. New York: McGraw-Hill.
- Taylor, M., Ashcroft, A. T., Messenger, A. G., 1993. Cyclosporin A prolongs human hair growth *in vitro*. *Journal of Investigative Dermatology* 100, 237-239.

- Thibaut, S., De Becker, E., Caisey, L., Baras, D., Karatas, S., Jammayrac, O., Bernard, B., 2010. Human eyelash characterization. *British Journal of Dermatology*, 162 (2), 304-310.
- Thornborrow, E. C., Patel, S., Mastropietro, A. E., Schwartzfarb, E. M., Manfredi, J. J., 2002. A conserved intronic response element mediates direct p53-dependent transcriptional activation of both the human and murine bax genes. *Oncogene* 21, 990-999.
- Tierney, A. J., Taylor, J., Closs, S. J., 1992. Knowledge, expectations and experiences of patients receiving chemotherapy for breast cancer. *Scandinavian Journal of Caring Sciences* 6, 75-80.
- Tissier, R., Ghaleh, B., Cohen, M. V., Downey, J. M., Berdeaux, A., 2012. Myocardial protection with mild hypothermia. *Cardiovascular Research* 94, 217-225.
- Tobin, D. J., Gunin, A., Magerl, M., Handijski, B., Paus, R., 2003. Plasticity and cytokinetic dynamics of the hair follicle mesenchyme: implications for hair growth control. *Journal of Investigative Dermatology* 120, 895-904.
- Tobin, D. J., Foitzik, K., Reinheckel, T., Mecklenburg, L., Botchkarev, V. A., Peters, C., Paus, R., 2002. The lysosomal protease cathepsin L is an important regulator of keratinocyte and melanocyte differentiation during hair follicle morphogenesis and cycling. *The American Journal of Pathology* 160, 1807-1821.
- Tollenaar, R., Liefers, G., Van Driel, O., Van De Velde, C., 1994. Scalp cooling has no place in the prevention of alopecia in adjuvant chemotherapy for breast cancer. *European Journal of Cancer* 30, 1448-1453.
- Tomankova, K., Polakova, K., Pizova, K., Binder, S., Havrdova, M., Kolarova, M., Kriegova, E., Zapletalova, J., Malina, L., Horakova, J., 2015. *In vitro* cytotoxicity analysis of doxorubicin-loaded/superparamagnetic iron oxide colloidal nanoassemblies on McF7 and NIH3T3 cell lines. *International Journal of Nanomedicine* 10, 949.
- Torrecillas, A., Martínez-Senac, M. M., Ausili, A., Corbalán-García, S., Gómez-Fernández, J. C., 2007. Interaction of the C-terminal domain of Bcl-2 family proteins with model membranes. *Biochimica et Biophysica Acta (BBA)-Biomembranes* 1768, 2931-2939.
- Tosetti, F., Ferrari, N., De Flora, S., Albini, A., 2002. 'Angioprevention': angiogenesis is a common and key target for cancer chemopreventive agents. *The Federation of American Societies for Experimental Biology* 16, 2-14.
- Tosti, A., Piraccini, B., Vincenzi, C., Misciali, C., 2005. Permanent alopecia after busulfan chemotherapy. *British Journal of Dermatology* 152, 1056-1058.
- Tran, D., Sinclair, R., Schwarzer, A., Chow, C., 2000. Permanent alopecia following chemotherapy and bone marrow transplantation. *Australasian Journal of Dermatology* 41, 106-108.
- Trigg, M. E., Flanigan-Minnick, A., 2011. Mechanisms of action of commonly used drugs to treat cancer. *Community Oncology* 8, 357-369.
- Trüeb, R. M., 2003. Association between smoking and hair loss: another opportunity for health education against smoking. *Dermatology* 206, 189-191.
- Trüeb, R. M., 2009a. Chemotherapy-induced alopecia. *Current Opinion in Supportive and Palliative Care* 4, 281-284.
- Trüeb, R. M., 2009b. Chemotherapy-induced alopecia. *Seminars in Cutaneous Medicine and Surgery*. Elsevier 28, 11-14.
- Trüeb, R. M., 2010. Chemotherapy-induced hair loss. *Skin Therapy Letter* 15, 5-7.

- Tsang, W., Chau, S. P., Kong, S., Fung, K., Kwok, T., 2003. Reactive oxygen species mediate doxorubicin induced p53-independent apoptosis. *Life Sciences* 73, 2047-2058.
- Tsuruta, F., Sunayama, J., Mori, Y., Hattori, S., Shimizu, S., Tsujimoto, Y., Yoshioka, K., Masuyama, N., Gotoh, Y., 2004. JNK promotes Bax translocation to mitochondria through phosphorylation of 14-3-3 proteins. *The European Molecular Biology Organization* 23, 1889-1899.
- Tumbar, T., Guasch, G., Greco, V., Blanpain, C., Lowry, W. E., Rendl, M., Fuchs, E., 2004. Defining the epithelial stem cell niche in skin. *Science* 303, 359-363.
- Tyagi, A. K., Singh, R. P., Agarwal, C., Chan, D. C., Agarwal, R., 2002. Silibinin strongly synergizes human prostate carcinoma DU145 cells to doxorubicin-induced growth inhibition, G2-M arrest, and apoptosis. *Clinical Cancer Research* 8, 3512-3519.
- Valeriotte, F., Van Putten, L., 1975. Proliferation-dependent cytotoxicity of anticancer agents: a review. *Cancer Research* 35, 2619-2630.
- Valeyrie-Allanore, L., Sassolas, B., & Roujeau, J.-C. 2007. Drug-induced skin, nail and hair disorders. *Drug Safety*, 30 (11), 1011-1030.
- Valero, T., 2014. Editorial (Thematic issue: mitochondrial biogenesis: pharmacological approaches). *Current Pharmaceutical Design* 20, 5507-5509.
- Van Den Hurk, C. J., Breed, W. P., Nortier, J. W., 2012a. Short post-infusion scalp cooling time in the prevention of docetaxel-induced alopecia. *Support Care Cancer* 20, 3255-3260.
- Van Den Hurk, C. J., Peerbooms, M., Van De Poll-Franse, L. V., Nortier, J. W., Coebergh, J. W. W., Breed, W. P., 2012b. Scalp cooling for hair preservation and associated characteristics in 1411 chemotherapy patients-results of the Dutch Scalp Cooling Registry. *Acta Oncologica* 51, 497-504.
- Van Den Hurk, C., Van De Poll-Franse, L., Breed, W., Coebergh, J., Nortier, J., 2013. Scalp cooling to prevent alopecia after chemotherapy can be considered safe in patients with breast cancer. *The Breast* 22, 1001-1004.
- Van Gorp, M., Festjens, N., Van Loo, G., Saelens, X., Vandenabeele, P., 2003. Mitochondrial intermembrane proteins in cell death. *Biochemical and Biophysical Research Communications* 304, 487-497.
- Ventura-Clapier, R., Garnier, A., Veksler, V., 2008. Transcriptional control of mitochondrial biogenesis: the central role of PGC-1 $\alpha$ . *Cardiovascular Research* 79, 208-217.
- Vichi, P., Robison, S., Tritton, T. R., 1989. Temperature dependence of adriamycin-induced DNA damage in L1210 cells. *Cancer Research* 49, 5575-5580.
- Von Bubnoff, A., Cho, K. W., 2001. Intracellular BMP signalling regulation in vertebrates: pathway or network. *Developmental Biology* 239, 1-14.
- Wagner, L., Bye, M. G., 1979. Body image and patients experiencing alopecia as a result of cancer chemotherapy. *Cancer Nursing* 2, 365-370.
- Walton, M. I., Wilson, S. C., Hardcastle, I. R., Mirza, A. R., Workman, P., 2005. An evaluation of the ability of pifithrin- $\alpha$  and - $\beta$  to inhibit p53 function in two wild-type p53 human tumor cell lines. *Molecular Cancer Therapeutics* 4, 1369-1377.
- Wang, J., Lu, Z., Au, J. L., 2006. Protection against chemotherapy-induced alopecia. *Journal of Pharmacy Research* 23, 2505-14.
- Wang, S., Konorev, E. A., Kotamraju, S., Joseph, J., Kalivendi, S., Kalyanaraman, B., 2004. Doxorubicin induces apoptosis in normal and tumour cells *via* distinct different

- mechanisms. intermediacy of H<sub>2</sub>O<sub>2</sub>- and p53-dependent pathways. *J Biol Chem* 279, 25535-25543.
- Watanabe, I., Okada, S., 1967. Effects of temperature on growth rate of cultured mammalian cells (L5178Y). *The Journal of Cell Biology* 32, 309-323.
- Wei, M. C., Lindsten, T., Mootha, V. K., Weiler, S., Gross, A., Ashiya, M., Thompson, C. B., Korsmeyer, S. J., 2000. tBID, a membrane-targeted death ligand, oligomerizes BAK to release cytochrome c. *Genes and Development* 14, 2060-2071.
- Wei, M. C., Zong, W.-X., Cheng, E. H.-Y., Lindsten, T., Panoutsakopoulou, V., Ross, A. J., Roth, K. A., Macgregor, G. R., Thompson, C. B., Korsmeyer, S. J., 2001. Proapoptotic BAX and BAK: a requisite gateway to mitochondrial dysfunction and death. *Science* 292, 727-730.
- Whiting, D. A., 2004. The structure of the human hair follicle. Light microscopy of vertical and horizontal sections of scalp biopsies. *Cell* 75, 855-862.
- Widelitz, R. B., Baker, R. E., Plikus, M., Lin, C. M., Maini, P. K., Paus, R., Chuong, C. M., 2006. Distinct mechanisms underlie pattern formation in the skin and skin appendages. *Birth Defects Research Part C: Embryo Today: Reviews* 78, 280-291.
- Wikramanayake, T., Amini, S., Simon, J., Mauro, L., Elgart, G., Schachner, L., Jimenez, J., 2012. A novel rat model for chemotherapy-induced alopecia. *Clinical and Experimental Dermatology* 37, 284-289.
- Wilkes, G. M., 1996. Potential Toxicities and Nursing Management. *Cancer Chemotherapy: a Nursing Process Approach*, 97.
- Willis, S. N., Chen, L., Dewson, G., Wei, A., Naik, E., Fletcher, J. I., Adams, J. M., Huang, D. C., 2005. Proapoptotic Bak is sequestered by Mcl-1 and Bcl-xL, but not Bcl-2, until displaced by BH3-only proteins. *Genes and Development* 19, 1294-1305.
- Wilson, C., Cotsarelis, G., Wei, Z. G., Fryer, E., Margolis-Fryer, J., Ostead, M., Tokarek, R., Sun, T. T., Lavker, R. M., 1994. Cells within the bulge region of mouse hair follicle transiently proliferate during early anagen: heterogeneity and functional differences of various hair cycles. *Differentiation* 55, 127-136.
- Winter, E., Chiaradia, L. D., Silva, A. H., Nunes, R. J., Yunes, R. A., Creczynski-Pasa, T. B., 2014. Involvement of extrinsic and intrinsic apoptotic pathways together with endoplasmic reticulum stress in cell death induced by naphthylchalcones in a leukemic cell line: Advantages of multi-target action. *Toxicology in Vitro* 28, 769-777.
- Winters, Z., 2002. p53 pathways involving G2 checkpoint regulators and the role of their subcellular localisation. *Journal of the Royal College of Surgeons of Edinburgh* 47, 591-598.
- Woodworth, C. D., Michael, E., Marker, D., Allen, S., Smith, L., and Nees, M. (2005). Inhibition of the epidermal growth factor receptor increases expression of genes that stimulate inflammation, apoptosis, and cell attachment. *Molecular Cancer Therapeutics*, 4 (4), 650-658.
- Wu, Y. J., Muldoon, L. L., Neuwelt, E. A., 2005. The chemoprotective agent N-acetylcysteine blocks cisplatin-induced apoptosis through caspase signaling pathway. *Journal of Pharmacology and Experimental Therapeutics* 312, 424-431.
- Wung, B., Cheng, J., Chao, Y., Hsieh, H., Wang, D., 1999. Modulation of Ras/Raf/extracellular signal-regulated kinase pathway by reactive oxygen species is involved in cyclic strain-induced early growth response-1 gene expression in endothelial cells. *Circulation Research* 84, 804-812.

- Yan, C. Y. I., Ferrari, G., Greene, L. A., 1995. N-acetylcysteine-promoted survival of PC12 cells is glutathione-independent but transcription-dependent. *Journal of Biological Chemistry* 270, 26827-26832.
- Yang, H., Asaad, N., Held, K. D., 2005. Medium-mediated intercellular communication is involved in bystander responses of X-ray-irradiated normal human fibroblasts. *Oncogene* 24, 2096-2103.
- Yeager, C. E., Olsen, E. A., 2011. Treatment of chemotherapy-induced alopecia. *Dermatology and Therapy* 24, 432-42.
- Young, R., 1980. Morphological and ultrastructural aspects of the dermal papilla during the growth cycle of the vibrissal follicle in the rat. *Journal of Anatomy* 131, 355-360.
- Yu, B. P., 1994. Cellular defenses against damage from reactive oxygen species. *Physiological Reviews* 74, 139-162.
- Yu, J., Zhang, L., 2003. No PUMA, no death: implications for p53-dependent apoptosis. *Cancer Cell* 4, 248-249.
- Yu, M., 2011. Generation, function and diagnostic value of mitochondrial DNA copy number alterations in human cancers. *Life Sciences* 89, 65-71.
- Yuan, Y.-J., Li, C., Hu, Z.-D., Wu, J.-C., 2001. Signal transduction pathway for oxidative burst and taxol production in suspension cultures of *Taxus chinensis* var. *mairei* induced by oligosaccharide from *Fusarium oxysprum*. *Enzyme and Microbial Technology* 29, 372-379.
- Yun, S. J., Kim, S.-J., 2007. Hair loss pattern due to chemotherapy-induced anagen effluvium: a cross-sectional observation. *Dermatology* 215, 36-40.
- Zafarullah, M., Li, W., Sylvester, J., Ahmad, M., 2003. Molecular mechanisms of N-acetylcysteine actions. *Cellular and Molecular Life Sciences* 60, 6-20.
- Zakeri, Z., Lockshin, R. A., 2002. Cell death during development. *Journal of Immunological Methods* 265, 3-20.
- Zamzami, N., Marchetti, P., Castedo, M., Zanin, C., Vayssiere, J.-L., Petit, P. X., Kroemer, G., 1995. Reduction in mitochondrial potential constitutes an early irreversible step of programmed lymphocyte death *in vivo*. *The Journal of Experimental Medicine* 181, 1661-1672.
- Zeng, S., Zu Chen, Y., Fu, L., Johnson, K. R., Fan, W., 2000. *In vitro* evaluation of schedule-dependent interactions between docetaxel and doxorubicin against human breast and ovarian cancer cells. *Clinical Cancer Research* 6, 3766-3773.
- Zhang, J., Nuebel, E., Wisidagama, D. R., Setoguchi, K., Hong, J. S., Van Horn, C. M., Imam, S. S., Vergnes, L., Malone, C. S., Koehler, C. M., 2012. Measuring energy metabolism in cultured cells, including human pluripotent stem cells and differentiated cells. *Nature Protocols* 7, 1068-1085.
- Zhang, X. D., Gillespie, S. K., Hersey, P., 2004. Staurosporine induces apoptosis of melanoma by both caspase-dependent and-independent apoptotic pathways. *Molecular Cancer Therapeutics* 3, 187-197.
- Zillikens, D., 2010. Thyroid hormones are direct modulators of human hair follicle growth and pigmentation. *Clinical Endocrinology and Metabolism* 93 (11), 4381-4388.